Structures and Dynamics of Asphaltenes

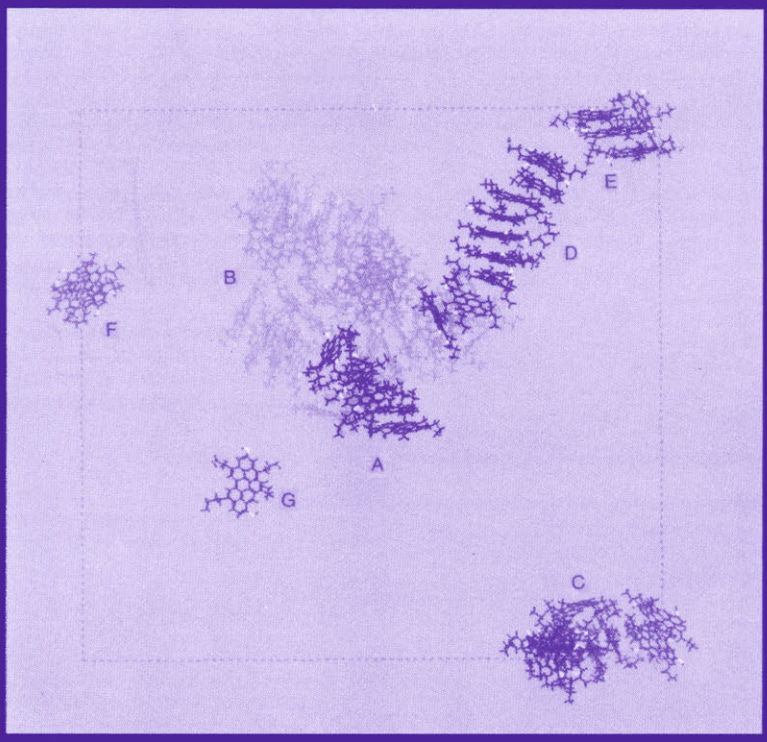

Edited by
Oliver C. Mullins and
Eric Y. Sheu

Structures and Dynamics of Asphaltenes

Structures and Dynamics of Asphaltenes

Edited by

Oliver C. Mullins

Schlumberger–Doll Research
Ridgefield, Connecticut

and

Eric Y. Sheu

Texaco, Inc.
Beacon, New York

Springer Science+Business Media, LLC

Library of Congress Cataloging in Publication Data

Structures and dynamics of asphaltenes / edited by Oliver C. Mullins and Eric Y. Sheu.
p. cm.
"Proceedings of the International Symposium on Asphaltenes, held during the Fine Particle Society Meeting, August 23–24, 1995, in Chicago, Illinois and a Symposium on Asphaltene and Resid Characterization, sponsored jointly by the Fuel and Petroleum divisions of the American Chemical Society, held April 13–17, 1998, in San Francisco, California"—T.p. verso.
Includes bibliographical references and index.
ISBN 978-1-4899-1617-4
1. Asphaltene—Congresses. I. Mullins, Oliver C. II. Sheu, Eric Y. III. Fine Particle Society. Meeting (1995: Chicago, Ill.) IV. American Chemical Society. V. International Symposium on Asphaltenes (1995: Chicago, Ill.) VI. Symposium on Asphaltene and Resid Characterization (1998: San Francisco, Calif.)
QD305.H7S68 1998 98-39452
665.5'388—dc21 CIP

Proceedings of the International Symposium on Asphaltenes, held during the Fine Particle Society Meeting, August 23–24, 1995, in Chicago, Illinois, and a Symposium on Asphaltene and Resid Characterization, sponsored jointly by the Fuel and Petroleum Divisions of the American Chemical Society, held April 13–17, 1998, in San Francisco, California

ISBN 978-1-4899-1617-4 ISBN 978-1-4899-1615-0 (eBook)
DOI 10.1007/978-1-4899-1615-0

Originally published by Plenum Press, New York in 1998
Softcover reprint of the hardcover 1st edition 1998

10 9 8 7 6 5 4 3 2 1

To Cynthia,
Olivia, Stephanie, and Clinton,

— OCM

To Julie,
Jonathan and Anthony

— EYS

PREFACE

The investigative assault upon the enigmatic asphaltenes has recently resulted in significant advances in many varied disciplines. Taken individually, each discipline exposes certain facets of asphaltenes, but each, alone, can never reveal asphaltenes from all vantages. Even seemingly narrowly focused issues such as the molecular structures of asphaltenes, or the colloidal structures of asphaltenes require a confluence of many lines of investigation to yield an understanding which differs from truth by diminishing uncertainty. An holistic treatment of the asphaltenes is a powerful approach to evolve further their understanding. For example, examination of asphaltenes at the highest resolution yields molecular structure. A slight increase in scale probes asphaltene colloidal structure. Weaving together asphaltene studies performed at different length scales results in a fabric which envelops an encompassing vision of asphaltenes. At the same time, the interfaces of these hierarchical studies provide additional constraints on imagination, more than investigations at individual length scales alone. These considerations shaped the timing, format, and the content of our book. The editors are very appreciative of the diligence and hard work manifest in each of the contributed chapters herein. We thank the contributing authors for making this project a success.

Oliver C. Mullins
Eric Y. Sheu

CONTENTS

I. Asphaltenes: Types and Sources 1
Teh Fu Yen

II. Optical Interrogation of Aromatic Moieties in Crude Oils and Asphaltenes 21
Oliver C. Mullins

III. Molecular Structure and Intermolecular Interaction of Asphaltenes by FT-IR, NMR, EPR 79
R. Scotti and L. Montanari

IV. Self-Association of Asphaltenes: Structure and Molecular Packing 115
Eric Y. Sheu

V. Colloidal Structural Evolution from Stable to Flocculated State of Asphaltene Solutions and Heavy Crudes 145
D. Espinat, E. Rosenberg, M. Scarsella, L. Barre, D. Fenistein, and D. Broseta

VI. Molecular and Colloidal Structure of Coal Asphaltenes and Other Heavy Solvent Soluble Components 203
Masashi Iino and Toshimasa Takanohashi

VII. Characterization and Phase Behavior of Asphaltenic Crude Oils 227
Kevin A. Ferworn and William Y. Svrcek

VIII. Conductivity of Asphaltenes 247
Per Fotland and Hilde Anfindsen

IX. A New Suspension Viscosity Model and Its Application to Asphaltene Association Thermodynamics and Structures 267
Moon-Sun Lin, J. M. Chaffin, R. R. Davison, C. J. Glover, and J. A. Bullin

X. Characterization of Asphaltenes and Heavy Oils Using Hydrodynamic Property Measurements 303
Ruth E. Baltus

XI. Asphaltene and Resin Stabilized Crude Oil Emulsions: Experimental Characterization and Destabilization 337
Johan Sjöblom, Øystein Sæther, Øivind Midttun, Marit-Helen Ese, Olav Urdahl, and Harald Førdedal

XII. The Role of Petroleum Asphaltenes in the Stabilization of Water-in-Oil Emulsions 377
Joseph D. McLean, P. Matthew Spiecker, Andrew P. Sullivan, and Peter K. Kilpatrick

Index 423

Chapter I

ASPHALTENES

Types and Sources

Teh Fu Yen

School of Engineering
University of Southern California
Los Angeles, California 90089-2531

INTRODUCTION

What will be stated in the following is that asphaltenes are not limited to petroleum origins. Asphaltenes can be derived from any fossil fuel sources. These sources include the virgin component, all the intermediates leading to a finished commodity, and to the processed products. A few of the fossil fuel derived asphaltenes are: virgin petroleum, refining bottoms, coal liquids, tar sands, bitumens, oil shale extracts, shale oils, coal extracts, and a great number of naturally-occurring asphaltoids, asphaltites, and asphalts. In order to explore the role of asphaltene in these different sources or types, the unique properties of asphaltenes must be discussed here.

The properties and behavior of asphalts and bitumens are critically dependent on the nature of the constituents. Chemically these constituents consist of hydrocarbons and heterocyclic or nitrogen-, sulfur-, and oxygen-containing compounds. Separation of the various fractions of asphalt or bitumen is usually based on their different boiling point ranges, molecular weights, and solubilities in solvents of different polarities. Techniques for obtaining narrow fractions include vacuum distillation, solvent extraction, thermal diffusion, crystallization, and others, individually or in combination, followed by chromatographic separation. Often the topped crude and the asphalt are fractionated by solvent partitioning, selective absorption-desorption, and chemical precipitation. The principal classes of constituents are gas oil, asphaltene, resin, carboid, carbene and mesophase.

All fossil based oils contain some asphaltics, ranging from 0.1–50 percent; however, heavy oil has the highest asphaltene content. The amount and the types of asphaltene will greatly influence the constitution and properties of a particular oil. The following Table 1 illustrates the principle that asphaltenes derived from petroleum, shale oil, and coal liquid are widely different if characterized by even a few structural parameters. The fine structure of a

Table 1. Ranges of value as expressed by structural parameters of various asphaltenes derived from different sources

Parameter*	Petroleum	Shale	Coal
f_a	0.2-0.5	0.4	0.6-0.7
L_a(A)	10-15	7-12	7-14
L_c(A)	20	15	10
σ	0.5-0.7	0.5-0.6	0.3-0.5
$H_{aru}/C_{ar}(H_I/C_A)$	0.3-0.5	0.8-0.9	0.6-0.8
n	4-6	2-3	1-2

*f_a, aromaticity; L_a, layer diameter; L_c, cluster height; σ, degree of substitution; H_{aru}/C_{ar}, degree of ring condensation; n, average chain length.

given asphaltene often can be elucidated by a number of structural parameters. At this time, it should be pointed out that although there are distinctive differences among asphaltenes, generally speaking they are very similar when compared in infrared or NMR spectra.

SEPARATION OF ASPHALTENE FROM SOURCE MATERIAL

Separation of components usually can be achieved by distillation. When a solution of a binary liquid has partially vaporized that component with the higher partial vapor pressure tends to concentrate in the vapor. This vapor may be condensed, and the vapor resulting from the heating of this condensate is still further enriched in the more volatile component. This process of separation based on successive vaporization and condensation is fractional distillation. The separation factor is based on relative volatility. Multicomponent distillation is possible at minimum reflux.

Average virgin heavy crudes contain a certain portion of volatiles. It is not advisable to use the conventional method of characterizing crude by simple distillation at atmospheric pressure up to 275 °C or even higher, since some thermal cracking reactions start above 200 °C. The best way is to "top" the volatile portion from the residue by vacuum distillation at very low pressure [1] and to keep the pot temperature below 150 °C. In this manner, the heat-sensitive portion of these fractions will be preserved [2]. In most distillation procedures, the bottom of the pot—the heavy fractions—have been severely thermally altered due to cumulative effects. An empirical method to approximate the boiling point of most compounds has been based on the boiling point number (BPN), and BPN can be computed from the structural component of a given compound [3]:

$$bP = 230.14(BPN)^{1/3} - 543$$

The segregation of individual components from a mixture can be accomplished by adsorption chromatography. The adsorbent is either packed in an open tube (column chromatography) or shaped in the form of a sheet (thin layer chromatography, TLC) [4,5]. Solvent is used to elute from the bed, and the resolution for a two-component system can be expressed as:

$$R_s = 1/4\left[(K_1/K_2) - 1\right]N^{1/2}\left\{K_2\left[(V^0/W) + K_2\right]\right\}$$

The first product deals with K_1/K_2, a ratio of the adsorption coefficients of the two components, which refers to the selectivity of the adsorption system. The sample adsorption distribution coefficient can be correlated to the sample adsorption energy, which in turn can be predicted from the group contribution of the free energy adsorption. A change of a given solvent will alter the sample's adsorption distribution coefficient greatly. For different solvents, the solvent strength parameter, ε^0, becomes an indicator. The second product in the above equation deals with N, the number of theoretical plates in the bed. For a larger K_2 value, this product is constant and is equal to one. V^0 is the free space and W is the weight of the adsorbent [6].

Duffy [7] was able to further fractionate the hexane-insoluble heavy fractions by spreading on Teflon and eluting with increasingly polar solvents: n-hexane, cyclohexane, ether, MEK, benzene, and chloroform. Asphaltene can further be purified from the SARA (saturated, aromatic, resin, asphaltene) column as developed by Jewell [8]. The SARA column is made from packed layers of cationic and anionic exchange resins, as well as ferric chloride on clay. This has become the ASTM D4124 method and is used widely. Recently, Lian et al. [5] used a thin-layer Chromatotron for preparative collection of the SARA fractions. Another chromatographic method is based on the polarity, and the heavy fraction can be separated into three fractions, I, II, III, and IV [9]. In this case, there will be no SARA fractions and asphaltene is dispersed in I, II, and III.

The solubility parameters concept is the basis of solvent fractionation. The basic assumption in the "solubility parameter" concept is that there is a correlation between the cohesive-energy density (potential energy per unit volume) and mutual miscibility. The cohesive-energy density, C, is defined as:

$$C = \frac{\Delta U^V}{V^L}$$

where ΔU^V is the energy change for complete isothermal vaporization of the saturated liquid to the ideal gas state and V^L is the molar volume of the liquid. The "solubility parameter," δ, is defined as the positive square root of the cohesive-energy density:

$$\delta = \left[\frac{\Delta U^V}{V^L}\right]^{1/2}$$

The dimensions of the "solubility parameter" in cgs units are $cal^{1/2}cm^{-3/2}$ or "hildebrands." In SI units the nearest equivalent is the square root of the megapascal, $Mpa^{1/2}$, because 1 MPA = 10^6 J m^{-3} = 1J cm^{-3}. To convert from hildebrands to $Mpa^{1/2}$, multiply by

$$\sqrt{4.187} = 2.046$$

For a material to dissolve in a solvent, the free energy change, ΔG_m, of the process must be negative, $\Delta G_m = \Delta H_m - T\Delta S_m$. Since the entropy change, ΔS_m, is always positive, the heat of mixing, ΔH_m, determines whether dissolution will occur or not. Experimentally, it has been found that, for most polymer systems, the heat of mixing is either positive or zero. According to the Hildebrand and Scott and Scatchard theory, the heat of mixing is given by

$$\Delta H_m = V_m(\delta_1 - \delta_2)^2 \phi_1 \phi_2$$

where V_m is the total volume of the mixture, ϕ_1, ϕ_2 are the volume fractions, and δ_1, δ_2 are the "solubility parameters" of the solvent and solute, respectively. Therefore, the heat of mixing will be small or zero and the free energy change negative when $\delta_1 \cong \delta_2$. The assumptions in the above are: (1) forces of attraction are due primarily to dispersion of forces, (2) molar volumes of the solute and the solvent are not significantly different, (3) no volume change occurs on mixing, and (4) mixing is random. These assumptions are not generally valid, and many more sophisticated theories have been developed. However, the relation produced is a simple one and is easy to use as a rough guide.

Solvent fractionation adopted by Yen in most of his work for a number of fossil fuel derived liquids can be easily designated by solubility parameter (Figure 1). Actually, the separation of asphaltene can proceed from both directions of the extractability curve as either side of the solubility parameter scale, e.g., asphaltene can be from n-pentane insoluble and benzene soluble (left side of curve, between 7–9 hildebrands) or from ethanol insoluble and benzene soluble (right side of curve between 12.5 and 9 hildebrands). (Figure 2) [10,11].

The analytical scheme is shown in Figure 3. In this manner, asphalt or bitumen or topped crude can be separated into six major fractions (see Table 2). Using the asphaltene as a standard scale, there are fractions related to asphaltene as indicated by the upper and lower entries, for example, gas oil and resin are above and carbene, carboid, and mesophase are below. Gas oil can be further separated to saturates and aromatics. These related materials are termed asphaltics, which are considered to be the allied substances to asphaltene.

ASPHALTICS OR ALLIED SUBSTANCES TO ASPHALTENES

In this manner, the principal classes of constituents are given in Table 2. Mesophase can be generated by heat treatment and is seldomly found in ordinary asphalt. These

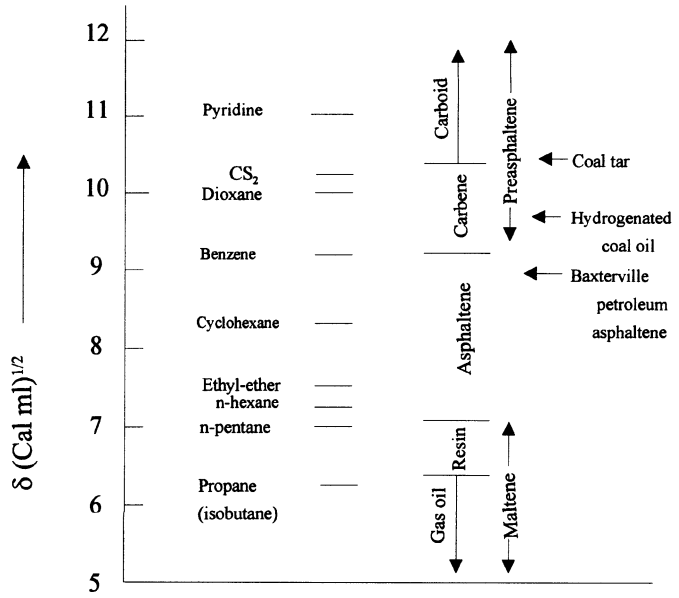

Figure 1. Separation of major heavy fractions based on solubility parameters of solvent system.

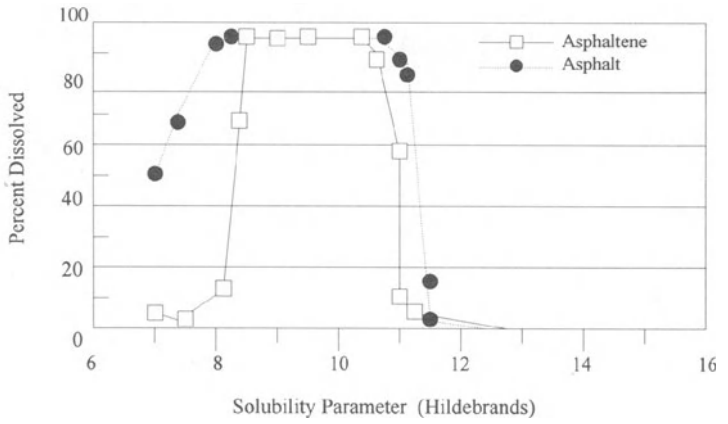

Figure 2. The solubility parameter spectra from West Texas Intermediate/West Sour. a) asphaltene and b) asphalt. Notice precipitation can originate from the shoulder of 6–8 (left hand side, conventional) or 12–11 (right side).

classes can be clearly defined by the solubility parameter range. The designations "petrolene" and "maltene" are often used in the asphalt literature.

In some cases, the fractions obtained by different conventional methods of separation constitute portions of the same component. For example, the polar aromatic constituents in Corbett's scheme and the related acid compounds (acid-affins) determined in Rostler's test are actually portions of resin components.

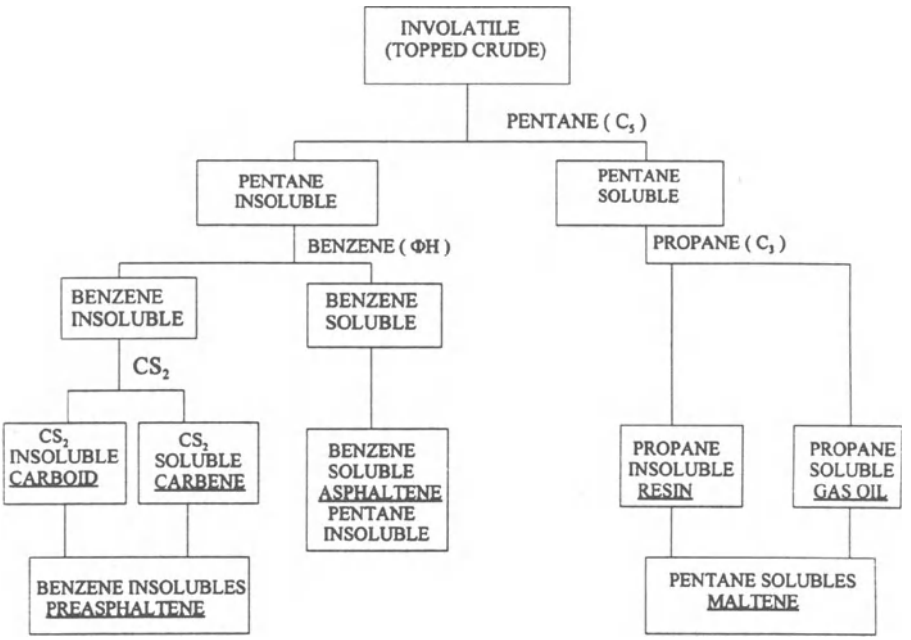

Figure 3. Analytical scheme of the isolation of asphaltene fraction.

Table 2. Solvent fractions of asphalt and related carbonaceous material[a]

Fraction			Solubility parameter	
Number	Designation	Solubility	δ in hildebrands[b]	Remarks
1	gas oil	propane soluble	below 6	saturated and aromatic hydrocarbons
2	resin	propane insoluble pentane soluble	6-7	combined 1 and2 are also called maltene or petrolene
3	asphaltene	pentane insoluble benzene soluble	7-9	ASTM uses CCl_4 instead of benzene
4	carbene	benzene insoluble CS_2 soluble[c]	9-10	ASTM uses CCl_4 instead of benzene
5	carboid	CS_2 insoluble[c] pyridine soluble	10-11	combined 4 and 5 are referred to as preasphaltene or asphaltol
6	mesophase	pyridine insoluble	above 11	

[a]Volatile-free basis.
[b]1 hildebrand = 2.04 $J^{1/2}/cm^{3/2}$ = 1 $cal^{1/2}/cm^{3/2}$.
[c]Because of the flammability of CS_2, pyridine is preferred; fractions 4 and 5 can be combined.

Asphaltenes

Asphaltenes are obtained by precipitation in nonpolar solvents such as low-boiling naphthas, petroleum ether, pentane, isopentane, and hexane. They are soluble in liquids of high surface tension such as pyridine, carbon disulfide, and carbon tetrachloride, but are insoluble in petroleum gases such as methane, ethane, and propane, in which they are precipitated. Commercially, propane is used to separate asphaltenes from other asphaltic residues.

In terms of chemically fine structure, asphaltene is a multipolymer system containing a great variety of building blocks. The statistically average molecule contains a flat sheet of condensed aromatic systems that may be interconnected by sulfide, ether, aliphatic chains, or naphthenic ring linkages. Gaps and holes in the aromatic system with heterocyclic atoms coordinated to transition metals such as vanadium, nickel, and iron are most likely caused by free radicals. The compactness of the aromatic system varies widely as a function of source and temperature.

The basic unit sheet of asphaltene usually has a molecular weight of 1000–4000 which may contain oligomers of up to eight units.

Based on the functional groups and acid-based properties, asphaltenes can be further separated into acids and bases as well as amphoteric and neutral compounds [12].

Resins

Resins are soluble in the liquids that precipitate asphaltenes and can be separated from the residua in the maltene mixture by chromatography. They are coprecipitated with asphaltenes in propane deasphalting processes and are strongly adsorbed onto the asphaltenes. Resins can be released from asphaltene by exhaustive extraction with n-pentane. They are usually separated from the residue by desorption with chloroform after chromatography through a silica gel column containing methylcylcohexane as solvent.

Resins are considered smaller analogues of asphaltenes with a much lower molecular weight. For this reason, the bulk of the resins can be preparatively separated by gel permeation chromatography as well as by centrifugal thin layer chromatography. The res-

ins contain aromatic compounds substituted with longer alkyls and a higher number of side chains attached to the rings than asphaltenes. The combination of the saturated and the aromatic characteristics of the resins stabilizes the colloidal nature of the asphaltenes in the oil medium.

Gas Oils

Gas oils are the lowest molecular weight fraction of the asphalt and serve as the dispersion medium for the peptized asphaltenes. They are soluble in petroleum ether, propane, and most other organic solvents, and may be separated into saturated, aromatic, and other hydrocarbon types through column chromatography employing solvents of varying polarity. In this manner, resins contain different values of hydrophile lipophile balance (HLB) which are useful in surfactants.

Molecular weights of the gas oils range below 800; most are in the region of 360–500. Structurally, gas oils consist mostly of naphthenic-aromatic nuclei with a greater proportion of side chains than the resins. Alkyl naphthenes predominate and straight chain alkanes are rarely present. The naphthenic content is 15–50%, with naphthenics containing 2 to 5 nuclei per molecule.

High aromaticity in the maltenes indicates good solvency for asphaltenes, and the overlap of hydrocarbons comprising the gas oils, resins, and asphaltenes is the basis for true asphaltene dispersion.

In all three main fractions, gas oil, resin, and asphaltene, the quantitative distribution of the fractions is important to the consistency and compatibility of asphalt, as well as the distribution pattern of individual homologous molecules within each fraction.

Naturally occurring interfacial active agents such as inorganic salts of long chain carboxylic acids, alcohols, waxes, mercaptans, and acidic hydrogen-bearing molecules, and other metallo-chelates or complexes, such as porphyrins, concentrate in trace amounts in the asphaltene and resin [12]. These substances have an important influence on the properties of asphalt as indicated in the following.

ASPHALTENE AND METALS

Metals are known to concentrate in the asphaltene fraction. The major metals found in oils are vanadium, nickel, and iron (which ranges from a few parts per million to a few hundred thousand parts per million). [13] Two forms of bonding are essential. The first is chelation, or complexing, which is illustrated by metalloporphyrins. The other is characterized by the bonding of metal ions directly to the defect centers, the "gaps" or "holes", of an imperfect aromatic sheet. [14]

The association of a metallo-complex to asphaltene is similar to the self-association of the aromatic sheets for the asphaltene clusters. The activation energy for such bonding has been approximated by the interconversion of the anisotropic and isotropic vanadium ESR spectroscopy by the doping of known vanadyl complexes to asphaltenes. They range in value from 14–20 kcal/ mole.

The uptake and concentration capacity of metal to asphaltene has been used for dispersion or recycling of effective catalysts and for the retrieval of excess, or spent, catalysts, which sometimes are used in the slurry process for residua and in the SRC-II recycle process. Many minerals, such as FeS, contained in the freshly-separated coal asphaltene, may prove to be valuable in-situ catalysts for processing.

The origin of porphyrin and non-porphyrin vanadium and nickel in asphaltene has been known [15]. Namely, the porphyrin skeleton is from the fossilized geoporphyrin of blue-green algae. The non-porphyrin type may be derived either from the porphyrin-transferred or degraded products or other ligands present in petroleum. The latter may be involved in pick up and addition processes later during geological times.

ASPHALTENE AND SULFUR

Among all the heteroatoms, sulfur is the most important in petroleum-derived asphaltenes. The sulfur distribution in asphaltenes is essentially in sulfide form. The thioether linkage should be easy to cleave; the difficulty with hydrosulfurization results from the location of sulfur in a hindered position, well protected by the association and clustering nature. Mass transfer of reacting species is greatly hampered.

Sulfur may be very essential in the generation of asphaltene, which is colloidal in nature and consists of micelles. The formation of micelles in two nonmiscible liquids may start with the emulsion polymerization of an associated locus. In such polymerization processes, the sulfide or mercaptan radical is a useful and necessary chain-transfer agent. The edge group of thioether in asphaltene cluster is essential, since, during diagenesis, these sulfurs may control the size of the micelle.

In conventional hydrodesulfurization, with the use of cobalt or nickel-molybdenum supported on SiO_2-Al_2O_3 applications, the sulfiding step will involve polysulfide formation. The Aurabon process (licensed by UOP), whether the use of added VS_X or of the VS_X formed *in-situ*, has to rely on the polysulfide groups to reach within the micelle of petroleum feeds to cause hydrocracking.

The heteroatoms S, N, and O are also essential in the control of the asphaltene derived from source material. For example, sulfur is essential for petroleum origin, oxygen is essential for coal origin, and nitrogen is essential for oil shale origin. The amount of heteroatoms in a given asphaltene can be used as a correlation guide for reparation of coal and non-coal origin, e.g., use of ESR parameter of g-tensor [16]. Recently, the sulfur types can be evaluated by XANES method [17]. The origins of the sulfur in asphaltene may also be an addition process during geochemical time [18].

ASPHALTENE AS A GEOLOGICAL MATURATION INDICATOR

One can conclude that gas and oil originate from kerogen decomposition. The intermediate is asphaltic (involatile components of crude oil) through the sequence:

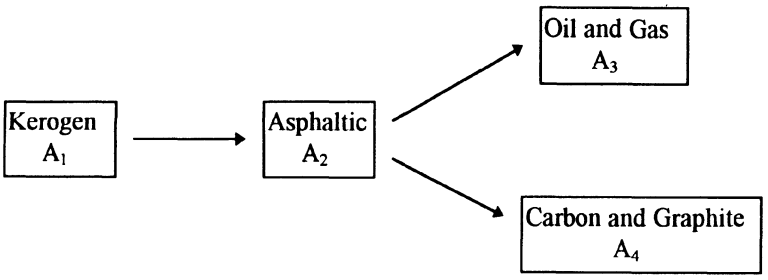

Table 3. Structural parameters of Green River asphaltenes

	Temperature (°C)		
Structural Parameter	250	425	500
Aromaticity (f_a)	0.24	0.51	0.60
Degree of Substitution (σ)	0.73	0.53	0.51
Average Chain length (n)	4.2	2.4	2.0
Degree of Ring Condensation (H_I/C_A)	0.99	0.75	0.66

Asphaltene and other asphaltic components such as gas oil, resin, carbene, carboid, etc. are components of a typical asphaltic. In many cases asphaltic (A_2) is contaminated with oil and gas (A_3) and may be produced concurrently from a reservoir. Also, under other situations, kerogen (A_1) and bitumen (A_2) are in one source (e.g., Green River Oil Shale). An example can be found in the oil fields in Ceylon in which the gas and carbon (graphite) can be coproduced. One must view the mechanism as consecutive and parallel reaction kinetics with temperature and time scale as a trade-off.

Asphaltenes isolated at various temperatures in a pyrolysis chamber from oil shale exhibit a wider range of structural differences. Not only the aromaticity values, but also the average chain length, extent of ring condensation, etc. are quite different as shown in Table 3.

ASPHALTENE AND SOURCES MIGRATION AND OCCURRENCE

Through catagenesis, the bitumen may convert to heavy oil via pyrobitumen and may eventually end up as graphite. The other route may yield light oil and other gaseous hydrocarbons and finally result in methane. In this manner the fluid portion of petroleum will migrate (multiphase flow) according to the potential of a given environment, e.g., buoyancy degree, capillary pressure, hydrodynamic flow of contact water, etc. Migration through faults, fractures, fissures, permeability channels, nonuniformities, and intrusions such as mud diapirs, piercement salt domes and igneous blockages will finally result in traps for various forms of natural bitumens.

Table 4 shows many native bitumens studied [19]. The heading of this table is still classified according to Abraham's scheme. As indicated by the asphaltic contents, namely percentages of resin, asphaltene and preasphaltene (benzene-insoluble), Abraham's scheme may not be correct. For example, the coorongite does not belong to elaterite; thus, it is not an asphaltoid (see Table 5). It is also true that grahamite should not be an asphaltite, but an asphaltoid. This can be verified easily by a ternary diagram (see Figure 4).

ASPHALTENE AS GEOLOGICAL CLOCK

It is known that a study of the nature of the associated porphyrins in asphaltene can roughly indicate the geological age of that petroleum. For example, the series ratio of the

Table 4. Distribution of asphaltic fractions in native bitumens (% by weight)

	Resin	Asphaltene	Preasphaltene
Mineral Wax			
Ozokerite	93	7	0
Seeps			
Rozel point	77	23	0
Oil Sand			
Athabasca (Mildrel Lake)	78	22	0
Asphalt			
Tabbyite	16	84	0
Pyrobitumen			
Ragusa	73	27	0
Asphaltites			
Grahamite	7	21.5	71.5
Gilsonite	14	62	24
Manjak	30	62	8
Asphaltoids			
Coorongite	94	6	0
Albertite	3	1	96
Ingramite	2	1	96
Wurtzilite	3	0	97
Anthraxolite	0	0	100

deoxophyllo - erythroetioporphyrin (DPEP) to the alkylporphyrin (etio) varies with the geological age of the crude as well as burial depth. One positive correlation of asphaltene with depth is that of the molecular weight, especially the average particle weight. For example, the particle weight as determined from the vapor pressure osmometry with benzene and tetrahydrofuran is approximately a function of the burial depth (see Figure 5) [20].

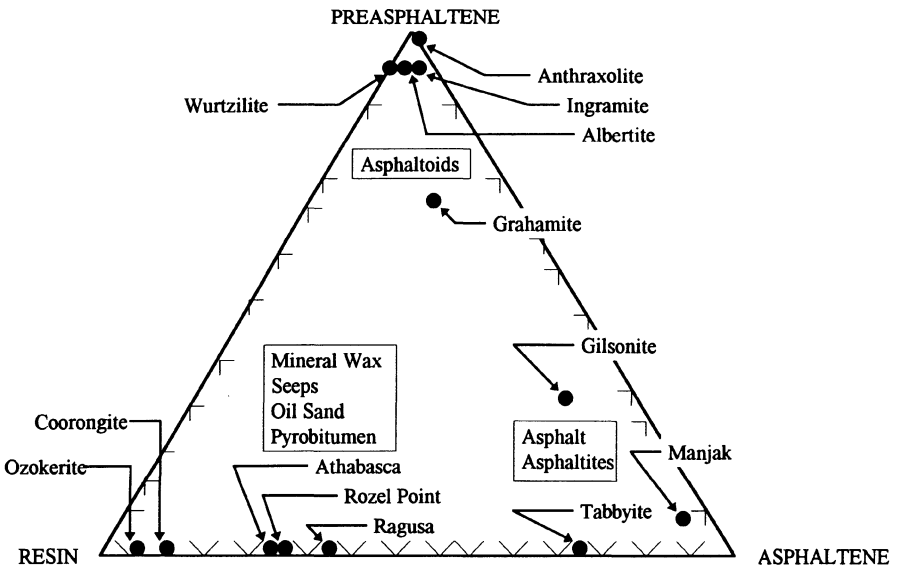

Figure 4. Ternary diagram of a number of asphaltoids, asphaltites, and other bitumens.

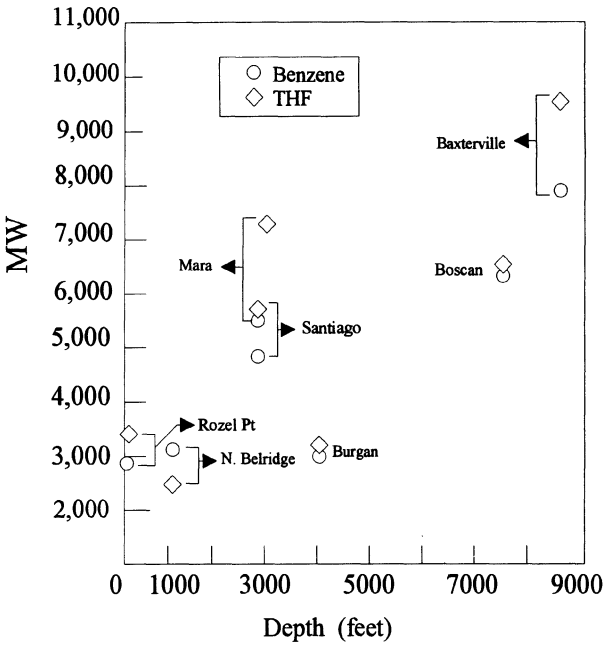

Figure 5. Molecular weight vs. depth of burial.

ASPHALTENE AND UPGRADING

Thermal and hydrocracking processes are largely used for upgrading asphaltics in heavy oil to useful oil. Chemically speaking, the conversion of asphaltene to lighter ends may involve a combination of the following: the hydrogenation of aromatics, transalkylation, cracking, hydrogen transfer, or hydrogenolysis. The first step, the penetration of the micelle, is in the realm of colloidal science approach. Next is the separation of stacks in asphaltene clusters and the support of atomic hydrogen at a surface. Overcoming the thermal energy at elevated temperatures, by complexing with a stronger π-system (to form another stack by donor-acceptance interaction), by forming a charge-transfer complex with halide or Lewis acid (such as a stable iodine complex), or by obtaining a new and smaller sandwich compound is the final step.

The above illustrations are plentiful; for example, the massive halide catalysts used for hydrogenation of coal-derived asphaltene. Coordinated molecules for the sheets are spread apart so that hydrogen and solvents can gain access for hydrogenation. The explanation is also valid for the zinc chloride coal conversion process. The clean products resulting from hydrocracking of Athabasca bitumen by using ferric chloride may be explained similarly. (For example, the following case of blown asphalt may be a simple one to comprehend.) The air-blowing process is essentially a free radical mechanism. Being an effective radical inhibitor, asphaltene will strongly retard this reaction. The only way to combat this retardation is to modify the structure of asphaltene by forming a complex. In this manner, the sheet in the cluster will be transformed into a new substance similar to met-cars, e.g., M_8C_{12} without the spin excitation from associated sheets. The most efficient catalyst for the

airblowing of asphalt is the Lewis acid type metal halide, which allows an increase of penetration value and a decrease in curing time. The mechanism is to render an inert free radical to become a new substance for the free radical type of air-oxidation.

ASPHALTENE AND CHEMICAL REACTIVITY

The polarity of an asphaltene is quite important in reactions such as hydrogen-bonding of the acid-base or the donor-acceptor nature of a given type of asphaltene. Hydrogen bonding is essential to the viscosity behavior. Association through polar groups may form the basis for the lamella structure, so that the order of a large micelle may be established. The inter- and intra-cluster property is controlled by the polar functional groups of the asphaltenes.

Reactions such as nitration, halogenation, and Friedel-Craft's can occur if the percent-substitution sites in the periphery of the aromatic sheet remain available. This is the reason why coal-derived asphaltene is more reactive than petroleum-derived asphaltene. This behavior is essential in the applications of storage stability and processing inertness among others.

Excessive peri-condensed systems, in general, will result in localized double bonds and the reactive conjugated diene system. In such a system, the Diels-Alder reaction can occur. A simple diagnostic tool is the occurrence of caged molecules in a typical crude.

ASPHALTENE AND COLLOIDAL NATURE

Asphalt or bitumen is a colloidal system similar to petroleum, the difference being that the lighter molecules have been removed. In crude oil, asphaltene micelles are present as discrete or colloidally dispersed particles in the oily phase. As the various low boiling and intermediate petroleum oils are removed during the distilling process, the particles of asphaltene micelles are massed together to form larger particles. Thus, asphalts or bitumen are colloidal dispersions of high molecular weight non-hydrocarbons or asphaltenes in a dispersion medium of gas oil (primarily alkanes and naphthenics) and resin. Although the asphaltenes themselves are insoluble in gas oil, they can exist as fine or coarse dispersions, depending on the resin content. The resins are part of the oily medium but have a polarity higher than gas oil. This property enables the molecules to be easily adsorbed into the asphaltene micelles. Here, they act by charge neutralization as the peptizing agent of the colloid stabilizer.

In its native state, asphaltene exists in an oil-external (Winsor's terminology) or reversed micelle. The polar groups are oriented towards the center, which can be water, silica (or clay), or metals (V, Ni, Fe, etc.). The driving force of the polar groups assembled toward the center originates from hydrogen-bonding charge transfer, or even salt formation. This oil external micelle system can be reversed to an oil-internal, water external micelle system (usually called Hartley micelles).

An aggregate of asphaltene particles with adsorbed resins is termed a supermicelle (aggregates or assemblages). In this case, resin acts as a peptizing agent which can be modified by amphiphiles. Sometimes gas oil may be occluded between supermicelles and it then behaves as an intermicellar medium. Asphalts or bitumen can be treated as a colloidal system. Micellar structures are predominant in asphalts with a high asphaltene content. Structural orders of asphaltenes would explain various properties existing in heavy crude and tar sand bitumens. The sizes of asphaltene increase due to association and aggregation are as follows (numbers in parentheses are distances in nm):

Unit sheet	→	Stacks	→	Aggregates	→	Assemblages	→	Cluster	→	Flocs and spherules
(1.2–2.0)		(3.0)		(5.0)		(10–15)		(200–2000)		(1×10^3 to 20×10^3)

The application of amphiphatic molecules (surface active agents) can modify the arrangement of asphaltene units in the micelles and vesicles, thus altering the solubility parameter. The addition of amphiphiles to different asphaltenes have been evaluated and it has been found that the peptization of asphaltene by pentane or hexane can be reduced [21]. This principle can be extended to the appropriate reinjection of resin fractions for improved oil recovery (IOR), since resin is an excellent amphiphile.

ASPHALTENE AND IMPROVED OIL RECOVERY

First, the nature of caustic flooding hinges on the ultra low surface tension properties of the alkaline-water-oil system. The fact is that the alkaline metals can replace all replaceable hydrogen atoms in the petroleum component. This activity depends on polar molecules with heteroatom functional groups, largely derived from the resin fractions, and sometimes also the asphaltenes. Table 5 summarizes the resin and asphaltene content of the recovery from Huntington Beach Oilfield. As a rule, after the secondary recovery the resin decreases and the asphaltene content increases. Since the interfacial activity ties more with the resin fraction than the asphaltene, for the three petroleum zones in Huntington Beach Oilfield, the Upper Main Zone is more prone to alkaline flooding, followed by the Upper Jones Zone. The Lower Main Zone will be the last choice due to its lowest resin and asphaltene content of the three wells.

Furthermore, some of the reactive (or replaceable hydrogen) groups are hidden in the asphaltene (either through inter- or intra- hydrogen bonding or ester formation). These can only be released by subsequent acid hydrolysis after the alkaline treatment. Thus, the injection sequence formulated with intermittent slugs of hydrochloric acid will help to boost the recovery efficiency.

Many amphiphatic molecules can be isolated from the asphaltene-resin fractions. In the simplest case, that for tar sands in the presence of aqueous sodium orthosilicates, a wide variety of surfactants can be recovered. In many instances, this crude surfactant mixture can be used for further recovery of bitumen from sands or even to clean oil-contaminated soils. It is feasible to install well-site units for the continuous injection of this type of surfactant as the oil or bitumen portion is recovered.

There are advantages for the application of mixed surfactants: for example, the range of hydrophile-lipophile balance (HLB) would be wide, and accordingly it would have a broad favorable salinity response. Surfactant flooding has traditionally been used in IOR. The performance characteristics of the surfactant used are critical micelle concen-

Table 5. Resin and asphaltene contents in Huntington Beach Oilfield (Upper Miocene series)

Production zones	Well no.	Recovery stage	Depth (ft)	% Resin	% Asphaltene
Upper Jones	UJ-225	water	3500 (Delmontian)	0	12.3
Upper main	426-104	primary	4500 (Upper Mohnian)	14.3	3.6
Lower main	S-47	water	4800 (Upper Mohnian)	0.7	7.9

tration (CMC), cloud point, adsorption, foam volume, and interfacial tension, which is dependent on the surfactant used related to HLB, the salinity and temperature. A two-component or three-component system is used in conjunction with a cosolvent. These wide salt response systems will tend to reduce gel- and liquid-crystalline phase separation. In this context, the concept of compatibility must be interpreted as the approximate equality of the internal energy of molecules of all concerns. For example, the equivalence alkane carbon number (EACN) of substrate and host molecules is similar.

Furthermore, the asphaltene can be viewed as an internal polymer in reservoirs. Naturally it can be easily modified to gain compatibility to the injected polymer and for this reason it can behave as a sacrificing agent. Since the organic structure of asphaltene indicated that a number of functional groups can be introduced to the molecular matrix, different reactions have been conducted with asphaltenes and it has been found that they proceeded with relative ease. The asphaltene-resin fractions after separation from the well head can be chemically modified, e.g., sulfonation, and reinjected back to the production zone for use. One such example is that a hybrid surfactant-polymer dual combination can be obtained from an asphaltene-resin fraction and modified to proper hydrophobically associated, interpolymer complexes for better mobility ratio and profile control application.

Synthetically, it is possible to import water-soluble groups into the reacted asphaltene. A hydrophobically modified polyacrylamide terpolymer can increase the apparent viscosity tremendously in oil-brine solution. Similarly, the multimer systems of a chemically modified asphaltene can be tailor-made to meet the requirements of a specific oil-in-place for IOR. Almost all the currently used synthetic water-soluble polymers can be included in Table 6. All of these types of polymers can also be prepared based on asphaltenes since it inherently can be constructed with infinite architecture and design in asphaltene single units and multiples. It is also important to point out that resin represents a small analog of asphaltene in structural consideration.

ASPHALTENE AND MESOPHASE MATERIAL

Asphaltenes are known to be precursors leading to specialty cokes, manufactured carbons and graphites. The relation between asphaltene and mesophase was discussed. Certain asphaltenes can give coarse deformed structures with Brooks-Taylor spherules while others

Table 6. Synthetic water soluble polymers

Nonionic polymers
Polar, nonionic functional groups on backbone (e.g., PAM)
Polyelectrolytes (charged polymers)
Charges along or pendent to backbone
anionic
cationic
Amphoteric polymers
polybetanes
polyampholytes
interpolymer complexes
Hydrophobically modified polymers
intrachain liaisons on homopolymers
copolymer with minor content of a comonomer
cosolute binding systems

do not. The key to mesophase growth seems to be the formation of a preasphaltene intermediate that can condense to form the pre-order and be incorporated into the mesophase. The requirement for a precursor of asphaltene origin is that the oxygen content should be less than 6%,and the aromaticity values between $f_a = 0.75–0.90$. Petroleum pitch and semi-coke have been useful as precursors for high-quality carbons and graphites, or carbon fibers. Asphaltene behaves differently if heated to 500°C and 600°C (mesophase temperature). For example, the FMC-COED asphaltene forms a fine isotropic structure and is completely transformed at 420°C, whereas both Synthoil and Catalytic Inc.-SRC asphaltenes exhibit coarse and deformed structures with Brooks-Taylor spherules [22]. Studies have been carried out for the feasibility evaluation of making carbon fibers from oil shale [23]. The asphaltic portion of shale oil can produce coarse deformed patterns.

ASPHALTENE IN OIL TRANSPORTATION AND SPILLAGES

The asphaltic contents and constituents strongly effect the thixotropic pseudo-plastic nature of heavy oils. Flow properties of these crudes can be modified so that efficient pumpability and pipe-line transportability may be obtained. Some of the modifications such as heat treatment, solvent addition, additives of p-inhibitors, drag reduction polymers, water bed transport, etc. will definitely hinge on the macrostructure changes of the asphaltics [24].

Accidental spillage of heavy oil on land and sea would result in fast evaporation of the volatiles and oxidation (weathering) of the gas oil and resin into asphaltene and the interconversion of asphaltene into pre-asphaltene (carbene and carboid). The relation of asphaltene to the Blokker constants for spilled oil can be approximated. In reality, a study of the origin of tar balls floating off the Southern California coastline has to rely on the properties of their asphaltene fractions. Figure 6 is a plot of the vanadium content vs. the

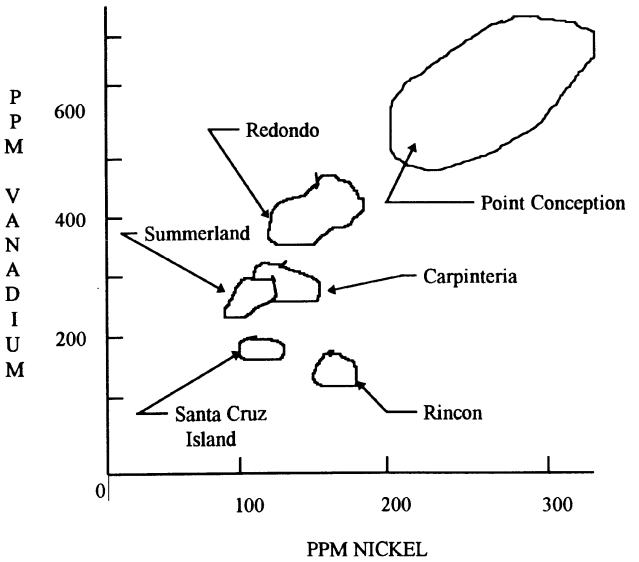

Figure 6. The vanadium and nickel constants of a number of tar balls.

nickel content, both analyzed from their asphaltene fraction. In this manner different zones can be mapped for tracing to the origins. For example, the seeps from Point Conception are widely different from those of Santa Cruz Island (Figure 6). In Figure 6 a source identification can readily be made.

Due to the deposition of asphaltene/wax, the transportation of petroleum is affected by flocculation and deposition of the solids in reservoir tabulors, pumps, storage vessels, transfer pipelines, dewater units, etc. The abatement is the proper addition of appropriate collectors for the elimination of fouling and blockage. As indicated by the flotation principle, on solving the combined Young's equation and Dupré relation, the work for dispersion must be lower than the work of cohesion which is brought out by the collector (again a surfactant).

Blockage and fouling also can come from both barium sulfate and asphaltene. Together, additives and dissolvers can be introduced to chelate the barium to facilitate the dissolution of the plugging solid. In many practices the technology involves physical treatment such as exposure to a certain magnetic field.

ASPHALTENES ISOLATED FROM VARIOUS SOURCES

Using the concept of solubility parameter approach for solvent fractions, a great variety of asphaltenes were isolated from different carbonaceous sources. Because the method is the same, the properties of each asphaltene can be used for comparisons with each other. There are definite trends within each of the sources. They are:

- well head sample is different from storage sample
- native petroleum sample is different from refining sample
- sample exposed to plowing condition is different from original sample
- asphaltene isolated from bitumens of oil shale rock is different from that of retorted oil shale
- asphaltene isolated from original coal sample is different from the coal liquid
- conversion by a number of chemical and physical processes)
- asphaltene exposed to UV light or air can alter the structure of original asphaltene and so are the differences

Even for asphaltenes that were isolated from the major sources, the structural parameters obtained are different. For example, coal derived asphaltenes have been separated from coal liquids by the following processes:

- PERC – Synthetic oil process
- HRI – H Coal Process
- FMC – COED process
- PAMCO, Fort Lewis, WA – solvent refined coal process
- Catalytic Inc., Wilsonville, AL – solvent refined coal process

Asphaltenes isolated from the above five coal liquids were all different [25]. In general, there are structural differences between asphaltenes isolated from petroleum and those isolated from coal liquids [26]. For petroleum samples, the asphaltenes are different in refinery products (such as paving asphalts), in native petroleums, and in non-petroleum asphalts (these are asphaltides or asphaltoids). However, their dependence of aromaticity to H/C atomic ratio are quite close (see Figure 7 and Table 7) [27].

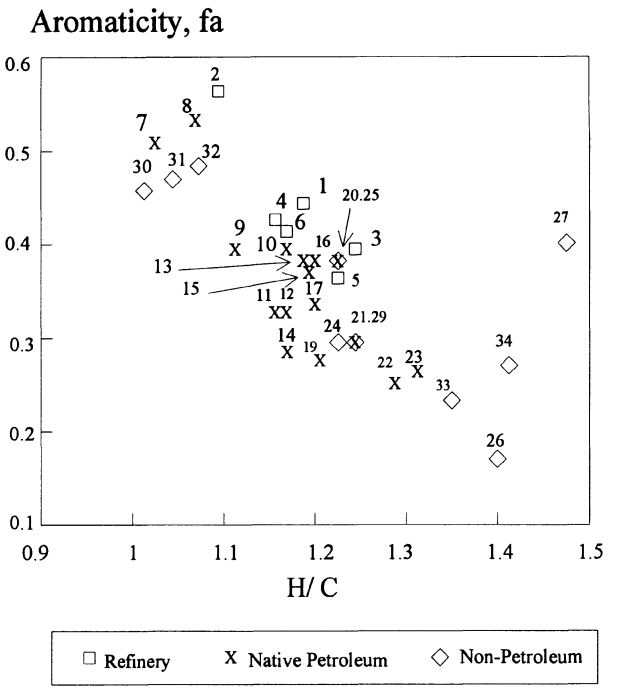

Figure 7. The plot of asphaltene aromaticity vs. H/C ratio from various asphalt sources.

For example, the major differences between petroleum asphaltene and coal-liquid asphaltene are:

- The aromaticity of petroleum-derived asphaltene (f_a = 0.2–0.5) is lower than that of coal-derived asphaltene (f_a = 0.6–0.7).
- The aromatic ring systems within petroleum-derived asphaltene are much more condensed (H_{aru}/C_{ar} = 0.3–0.5, which is peri) than those of coal-derived asphaltene (H_{aru}/C_{ar} = 0.5–0.7, which is kata).
- The substituents of the petroleum-derived asphaltenes are longer (n = 4–6) than those of coal-derived asphaltenes (n =1–2).
- The aromatic system of the petroleum-derived asphaltenes is extensively substituted (50%-70%) whereas the coal-derived asphaltene is sparingly substituted (30%-50%).
- The molecular weight of petroleum-derived asphaltene is about three times higher than that of coal-derived asphaltene. Unit molecular weight of coal asphaltene is 400–600 whereas that of petroleum asphaltene is 800–2500.
- Petroleum-derived asphaltene is more highly associated (Me = 5–7) than is coal-derived asphaltene (Me = 2–4); this will be reflected in the ease of processing.
- The aromatic system in coal derived asphaltene is small (L_a = 7–14 Å), compared with that of petroleum (L_a = 10–15 Å)
- Petroleum-derived asphaltene is less polar than coal-derived asphaltene (X/C for coal-derived asphaltene is about 0.08, and for petroleum-derived asphaltene is about 0.05).

Table 7. The asphaltene H/C ratio and aromaticity from different sources

No.	Asphaltene	H/C	f_a
Refinery Asphalt			
1	AAA-1	1.15	0.44
2	AAB-1	1.06	0.57
3	AAD-1	1.23	0.39
4	AAG-1	1.12	0.43
5	AAK-1	1.21	0.36
6	AAM-1	1.13	0.42
Native Petroleum			
7	Baxterville (a)	1.02	0.51
8	Baxterville (b)	1.05	0.53
9	Bachaquero	1.08	0.41
10	Lagunillas	1.13	0.41
11	Boscan (a)	1.15	0.35
12	Boscan (b)	1.16	0.35
13	Burgan (Kuwait)	1.17	0.38
14	Raudhatain	1.17	0.32
15	Wafra No. A-1	1.18	0.37
16	Melones	1.18	0.38
17	Mara	1.19	0.35
18	Wafra No. 17	1.19	0.35
19	Belridge	1.19	0.30
20	Yorba Linda	1.21	0.38
21	Santiago	1.22	0.31
22	Libya	1.25	0.25
23	Ragusa	1.29	0.26
Non-Petroleum			
24	Athabasca (a)	1.21	0.31
25	Athabasca (b)	1.21	0.38
26	Rozel Point	1.40	0.18
27	Coorongite	1.49	0.41
28	Tabbyite	0.92	0.15
29	Grahamite (BS)	1.22	0.31
30	Grahamite (BI)	1.01	0.46
31	Mavjak (BS)	1.04	0.47
32	Mavjak (BI)	1.06	0.48
33	Gilsonite (BS)	1.36	0.21
34	Gilsonite (BI)	1.41	0.29

- Coal-derived asphaltene contains more hydroxyl and pyrrolic groups in addition to ether-oxygen or basic nitrogen functions.
- The high polarity and low association of coal-derived asphaltenes can be used to explain the nature (hydrogen-bonding) and reactivity of coal conversion.
- The charge-transfer nature of donor-acceptor properties of petroleum asphaltenes can influence the processing of petroleum.

There are two types of asphaltene derived from oil shale. One is from oil shale extraction and the other is from retorted oil. The former has an aromaticity value of 0.1, but the latter reaches 0.5 [27]. In summary, please see Table 8 for the differences among asphaltene isolated from the major sources.

Table 8. Nature of aromatic systems of different asphaltenes

	Structural parameters*					
	f_a	L_a	σ	H_I/C_A	n	N
Native crude oil	0.2-0.5	10-15	0.5-0.7	0.3-0.5	4-6	4
Refinery bottoms	0.5-0.6	8-9	0.5	0.6	2-3	–
Oil shale (Green River)	0.4	7-12	0.5-0.6	0.8-0.9	3-4	1
Oil shale (Devonian)	0.6-0.7	–	0.5	0.6	2	–
Coal	0.6-0.7	7-14	0.3-0.5	0.6-0.8	1-2	2

*L_a, layer dimension; N, oligomer number.

Laboratory experiments have documented the extracts from a number of ancient shales, namely, Chattanooga Shale, Appalachian Shale, Nonesuch Shale, Gunflint Shale, etc. Furthermore, structurally the kerogen portion of many rock samples as well as retigens from meteorites (organic) have been evaluated.

REFERENCES

1. P.A. Farmanian, N. Davis, J.K. Kwan, R.M. Weinbrandt, and T.F. Yen, "Precipitation of Selective Native Petroleum Fractions in Lowering Interfacial Tensions of Aqueous Alkane Systems" in *Chemistry of Oil Recovery* (R.T. Johanson and R.L. Berg, ed) ACS Symposium Series 91, 103–114 (1979).
2. T.F. Yen and P.A. Farmanian, Petroleum Recovery Process Using Native Petroleum Surfactant, US Patent 4, 232, 738, (1980).
3. H.F. Herbrandon and F.C. Nachod in *Determination of Organic Structures by Physical Metals* (E.A. Brande and F.C. Nachod ed.) Academic Press, 10, (1955).
4. Y.Y. Wang and T.F. Yen, "Rapid Differentiation and Characterization of Fossil Fuels by Thin-Layer Chromatography," *J. Planar Chromatography*, Heidelberg *3*, 376–380, (1990).
5. H. Lian, C.Z.H. Lee, Y.Y. Wang and T.F. Yen, "Characterization of Asphalt by Preparative Chromatotron," *J. Planar Chromatography*, Heidelberg *5*, 263–266, (1992).
6. L.R. Snyder, *Principles of Adsorption Chromatography*, Macel Dekker, New York, (1968).
7. L. Duffy, *Characterization of Heavy Fraction of Petroleum*, API Research Project 60, Rept. No. 13, (1973).
8. D.M. Jewell, *ACS Div. Petroleum Chem., Reprint, 17(4)*, F81-F91, (1972).
9. K.M. Sadeghi, M.-A. Sadeghi, W.H. Wu and T.F. Yen, *Fractionation of Various Heavy Oils and Bitumen for Characterization Based on Polarity, Fuel, 68*, 782–787 (1989).
10. J.R. Lin and T.F. Yen, "The Study of Molecular Attractions in the Asphalt Particles" in *Fossil Fuel Exploration, Recovery, Refining, and Petroleum Processes*, Plenum Press, New York, 171–182, (1994).
11. V.L. Weinberg and T.F. Yen, "Solubility Parameters in Coal Liquefaction Products," *Fuel 59*, 287–289 (1970).
12. T.F. Yen, "Multiple Structure Orders of Asphaltenes" in *Asphaltenes and Asphalts*, Vol. 1, Elsevier, Amsterdam, 111–123 (1994).
13. T.F. Yen, *The Role of Trace Metal in Petroleum*, Ann Arbor Science, (1975).
14. T.F. Yen, J.G. Erdman and A.J. Saraceno, "Investigating the Nature of Free Radicals in Petroleum Asphaltene and Related Substances by Electron Spin Resonance," *Anal. Chem., 34*, 694–700 (1962).
15. T.W. Baker, T.F. Yen, J.P. Dickie, R.E. Rhodes and L.F. Clark," Mass Spectrometry of Porphyrins, II. Characterization of Petroporphyrins, *JACS 89* 3631–3639 (1967).
16. T.F. Yen and S.R. Sprang, "Contribution of ESR Analysis to Diagenic Mechanisms in Bituminous Deposits," *Geochem. Cosmochim. Acta 41(8)*, 1007–1018 (1977).
17. O.C. Mullins, "Sulfur and Nitrogen Structures in Asphaltenes and Related Materials Quantified by XANES Spectroscopy, " in *Asphaltenes*, Plenum, New York (1995).
18. T.F. Yen, "The Realms and Definitions of Asphaltenes," *Asphaltenes and Asphalts*, Vol. 2, Elsevier Sci. Publishers, (1998).

19. T.F. Yen, "The Nature of Asphaltene in Heavy Oil," *Proc. 1st Pan Pacific Synfuel Conferences*, Vol. II, pp. 547–557 (1982).
20. T.F. Yen and G.V. Chilingar, "Structural Parameters from Asphaltenes and their Geochemical Significance," in *Asphaltenes and Asphalts*, Vol. 1, 159–178 (1994).
21. H. Lian, J.-R. Lin and T.F. Yen, "Peptization Studies of Asphaltene and Solubility Parameter Spectra," *Fuel*, *73*, 423–428 (1994).
22. V.A. Weinberg and T.F. Yen, "Mesophase Formation in Coal Liquid Solvent Fractions," *Carbon*, *21* 39–45 (1983).
23. M.A. Sadeghi, K.M. Sadeghi and T.F. Yen, "Formation of Mesophase Using Precursors from Shale Oil," *Energy Sources*, *15* 391–401 (1993).
24. T.F. Yen and R. McDavid, "Chemical Aspect of Improving the Flow Characteristics of Heavy Crudes," NATO International Institute of Advanced Studies, Caracas, Venezuela (1982).
25. I. Schwager and T.F. Yen, "Coal Liquefaction Products from Major Demonstration Process 1. Separation and Analysis." *Fuel*, *57* 100–104 (1978).
26. T.F. Yen, "Structural Difference between Asphaltenes Isolated from Petroleum and from Coal Liquid," *ACS Adv. Chem. Series 195*, 39–45 (1981).
27. H.J. Lian and T.F. Yen, "Classification of Asphalt Types by Asphaltenes," *Asphaltic Particles in Fossil Fuel Exploration, Reforming and Production Processes*, Plenum, 63–80 (1994).

Chapter II

OPTICAL INTERROGATION OF AROMATIC MOIETIES IN CRUDE OILS AND ASPHALTENES

Oliver C. Mullins

Schlumberger-Doll Research
Ridgefield, Connecticut 06877

1. INTRODUCTION

1.1. Overview

Optical spectroscopy provides an extremely powerful methodology to investigate molecular structure and molecular dynamics. Molecular structures are governed by favorable energetics of the spatial arrangement of constituent atoms and valence electrons. The energy of optical photons correlates with the excitation of valence electrons to higher energy orbitals thereby yielding a direct probe of molecular structure. Molecular dynamics are also amenable to investigation via optical spectroscopy. Pump-probe experiments, where the first photon excites the molecule into an evolving state and the second photon of known time delay interrogates the evolution of the molecule, have been applied to dynamics such as molecular dissociation at the femtosecond (10^{-15} sec) time scale. Intermolecular interactions in solutions are readily studied using optical fluorescence measurements. Typical fluorescence lifetimes are on the order of nanoseconds (10^{-9} sec) and can be used to probe a temporal range of diffusion-mediated intermolecular interactions.

In additional to yielding fundamental information about molecules, optical spectroscopy has been employed in wide ranging applications. Chemical reactions and processes are often monitored by comparing absorption spectra of reaction solutions with known spectra of reactants and products. The presence or absence of particular analytes is routinely monitored by optical absorption or fluorescence detection such as in chromatographic flowstreams and in ground water samples. In the oil field, fluorescence detection of crude oil shows in rock cuttings has been employed at well sites for 60 years. Recently, optical spectroscopy has been introduced in the borehole commercially to provide characterization of crude oils during well logging.[1] Whenever the characterization of materials is important, one obvious candidate technique is optical spectroscopy. Here, the optical spectral range is defined to correspond to the excitation of valence electrons, thus,

includes the ultra-violet (UV), visible and into the near-infrared (NIR). The spectral study of molecular vibrations corresponds to infrared spectroscopy and is another very powerful spectral technique. Infrared spectroscopy relies on different molecular physics and is considered in Chapter 3 of this book.

The utilization of optical spectroscopic techniques has had a long history in the oil field, due to the strong optical fluorescence of crude oils. During the drilling of oil wells, rock cuttings are carried to the surface. One method to check whether an oil-bearing zone has been penetrated by the drill string, is to illuminate the rock cuttings with UV to check for visible fluorescence. In a similar manner, whole cores, or side-wall cores from oil wells are illuminated with UV to check for crude oil fluorescence. The intensity and color of the fluorescence are noted, and provide qualitative information about the oil saturation and oil type. Certain minerals fluoresce, but if the fluorescence is extractable from the cuttings, then crude oil is the likely origin of the fluorescence. Various more sophisticated fluorescence measurements have been performed in the oil field during the drilling of oil wells. One procedure utilizes solvent extraction of the crude oil from the cuttings and a spectrometer is employed producing quantification of the results.[2–4] A novel continuous wireline fluorescence logging technique for the direct detection of crude oil relies on establishing optical contact with the borehole wall to perform excitation fluorescence spectroscopy.[5] These new techniques are improving the effectiveness of finding oil-bearing formations.

Optical techniques have been employed routinely in the characterization of carbonaceous materials related to crude oils and asphaltenes. For example, components of coals and coal-derived materials are often characterized through the use of fluorescence.[6–8] Kerogen properties such as maturation can be investigated through fluorescence methods.[9–11] Higher maturations correspond to decreased fluorescence and greater fluorescence red-shifts. Petroleum inclusions in minerals are most readily studied by fluorescence.[12,13] Limestone fluorescence, which is an important issue in oil field applications, can be traced to the fluorescence of limestone organic components.[14,15] Furthermore, a variety of environmental applications related to carbonaceous materials utilize fluorescence. The detection of crude and refined oil contaminants using remote fiber optics sensing[16] can be accomplished with fluorescence measurements. Coupling fiber optics with cone penetrometers allows direct sampling of the subsurface.[17] In environmental monitoring, fluorescence lifetime measurements as well as spectral measurements are applicable.[18–20] In spite of the utility of fluorescence, particularly associated with carbonaceous materials, systematic studies of the optical properties of crude oils and related materials have only recently been performed.

The general characterization of crude oils and asphaltenes has been a major objective in the oil industry since its origin.[9,21–24] Different crude oils exhibit an enormous range of properties impacting all phases of exploitation of this resource. The properties of a heavy tar are inordinately different from a gas condensate (or natural gas); thereby leading to different methods of resource production, transportation, processing, and utilization. For example, the production of a light crude oil with a large gas fraction mandates surface facilities which can treat large volumes of high pressure gas. Medium weight crude oils can flocculate asphaltenes in production tubing with the reduction of pressure necessitating special considerations. Consequently, precise characterization of various crude oil properties allows optimization of economic objectives. The quantity of asphaltenes contained in the hydrocarbon resource is a particularly important issue due to their dramatic and generally negative effects on all aspects of resource exploitation. In addition, the properties of asphalts and asphaltenes become critical when utilizing asphalt-rich hydrocarbon resources; related difficulties can be mitigated with proper accounting of asphaltene chemistry and physics.

Asphalts with their constituent asphaltenes are utilized in a range of applications. Enormous volumes of asphalts are used for road pavement. Asphalts are also widely used for durable, protective coatings and for encapsulation. Understanding the chemical and physical properties of asphalts and asphaltenes looms important especially when balancing desired asphalt performance with environmental extremes to which asphalts are subjected.

Asphaltenes exhibit a narrower range of properties than, say, crude oils, reducing the importance of gathering wide-ranging samples; nevertheless, comparison of asphaltenes from different source materials must proceed with caution. Asphaltenes are inherently very complex chemically, thereby motivating investigative assault via a plethora of technical approaches. In addition to the utilitarian approach to asphaltene and crude oil science, these materials represent interesting scientific puzzles, related to their chemical composition, and to their formation. In the larger picture, crude oils and asphaltenes result from the diagenesis of organic constituents of sedimentary materials; models describing geological evolution of sedimentary formations must be consistent with observed organic diagenesis.

Crude oils have been subjected to extensive chromatographic and mass spectral analyses, where individual molecular components are isolated.[9,25] These analyses are particularly adept at providing extensive information about the light and medium weight fractions and the saturated fractions of crude oils and have proven very fruitful in the analysis of biomarkers, which, for example, correlate between source rock and crude oil.[26] Chromatography is routinely employed to find evidence of biodegradation of crude oil. Unicellular organisms preferentially consume n-alkanes, which are predominant in an unaltered crude oil. Asphaltenes are less amenable to chromatographic analysis due to their large molecular weights coupled with their aromaticity and polarity. Nevertheless, large numbers of individual components, particularly lighter components, can be resolved to advantage, especially with regard to probing specific types of compounds, such as biomarkers. In general, analytic methods which rely on the separation of individual molecular components of high molecular weight materials such as asphaltenes, can experience difficulty because the resolving power is diminished for similar, massive molecules, and because the largest fraction may be inaccessible to analysis by particular techniques. Furthermore, for materials such as asphaltenes with the tremendous number of individual molecular components, general chemical trends can be obscured by the appearance of a huge number of individual peaks, precluding a simple view of the "forest."

Bulk analyses of asphaltenes have proven very powerful in elucidating general chemical properties. Traditional spectroscopic analyses of asphaltenes, such as Infrared (IR) and Nuclear Magnetic Resonance (NMR) studies of asphaltenes have been critical in characterizing the chemical properties of asphaltenes.[9,21] For instance, C13 NMR has shown that the carbon fraction of petroleum asphaltenes are approximately 40% aromatic with the remainder saturated,[22] while proton NMR and IR indicate that approximately 90% of the hydrogen population resides on saturated carbon atoms.[22] These results constrain proposed molecular structures of asphaltenes. Chapter 3 in this book provides the latest NMR and IR results on asphaltenes and, in addition, describes Electron Paramagnetic Resonance (EPR) results on asphaltenes. Novel techniques such as x-ray absorption near edge structure (XANES) have provided an excellent view of the heteroatom molecular structures in asphaltenes and related materials.[27] Essentially, all of asphaltene nitrogen is aromatic with pyrrolic forms dominating pyridinic forms; asphaltene sulfur is predominantly thiophenic (aromatic), with some sulfidic (aliphatic equivalent), but some sulfoxide can also be present.

In recent years, optical techniques have advanced the elucidation of fundamental properties of crude oils and asphaltenes. Asphaltene precipitation has been investigated

thorough optical techniques. Light scattering methods have been used to follow the kinetics of asphaltene flocculation and sedimentation.[28] Asphaltene aggregate formation has been reported using fluorescence depolarization.[29] The role of solvent polarizability in the precipitation of asphaltenes has been investigated via index-of-refraction methods.[30] For crude oil components, optical spectroscopy corresponds predominantly to the excitation of π electrons. The energy of the π transitions are related in a general sense to the physical size of the aromatic ring system; the larger the size, the lower the transition energy.[31] All but the lightest crude oils possess a huge number of aromatic molecules, thereby exhibiting optical absorption from electronic transitions across the UV, visible and, for many crudes, even into the NIR. In spite of the complications of many overlapping absorption bands in crude oil spectra, simplifying features of individual spectra, coupled with the underlying uniformity observed in all crude oil spectra have permitted broad conclusions. The lowest energy electronic transitions for the saturated components correspond to the vacuum ultraviolet; the large number of saturated components in crude oils with their absorption bands at nearly the same energy has precluded this line of investigation.

1.2. Scope of Chapter

In this chapter, optical spectral methods are used as a direct probe of the aromatic components of crude oils and asphaltenes. The tremendous spectral range of absorption and emission thresholds for different aromatic molecules yields the ability to select a particular aromatic fraction for investigation within a complex mixture of aromatics. This feature makes optical spectroscopy eminently suitable for the investigation of crude oils and asphaltenes. The rough correlation between aromatic ring size and threshold absorption and emission wavelengths facilitates analysis. In fact, the largest molecules in asphaltenes and crude oils, which are difficult to analyze by other methods, produce electronic absorption at the longest wavelengths, where no other molecules produce absorption. Thus, using absorption spectroscopy, the clearest picture is obtain of the normally intractable, heaviest fraction. The electronic absorption of all crude oils and asphaltenes exhibit systematics which are characteristic of broad ranging systems including semiconductors as well as organics. In crude oils, an exponential decrease of increasingly larger chromophores is found. However, the exact molecular size range for this exponential decrease depends on the crude oil; for light crude oils, the exponential decrease is found for small aromatics, for asphaltenes, big aromatics.

Fluorescence spectroscopy provides a powerful probe of the chromophores of crude oils. Fluorescence is initiated by optical absorption, as such, complements absorption analyses. Fluorescence naturally yields intensity as a function of two experimental variables, excitation and emission wavelength. In addition, fluorescence emission is relatively slow ($\sim 10^{-8}$ sec), so dynamic processes can be explored. The independent measurements of fluorescence lifetimes, quantum yields and spectra provide stringent tests for models of chromophore and fluorophore populations and interactions. Intermolecular interactions such as energy quenching and energy transfer are much more rapid than fluorescence emission, given suitable molecular configurations. Quenching yields reduced optical emission, while energy transfer affects fluorescence spectra; both processes reduce fluorescence lifetimes. Diffusion is generally required to bring potentially interacting molecules sufficiently close, so concentration and type of crude oil become relevant variables. With so many measurement variables, and contributing processes, fluorescence spectroscopy offers hope of unraveling the complexities of the chromophore distributions and dynamics in asphaltenes and crude oils.

Crude oils provide an excellent and uncommon example of a generally expected photophysical rule, the Energy Gap Law. A single set of simple, governing processes along with population distributions of crude oil chromophores are found to account for a large variety of data. The smallest aromatics fluoresce in the short wavelength UV, where no other ring systems can fluoresce. Thus, in asphaltenes, the smallest rings, which are often obscured from view by the large chromophores, can readily be investigated. At first glance, one might anticipate that the aromatic components of crude oils are too complex to allow systematic characterization. Instead, a more accurate description is that the huge number of aromatic components of crude oils act as a statistical ensemble with well-defined behavior. The underlying similarities of the geophysical and geochemical processes which give rise to different crude oils apparently impose rather strict limits on the populations and resulting properties of these aromatic components of crude oils.

2. EXPERIMENTAL SECTION

Approximately 30 crude oils have been used here from locations all over the world and ranging greatly in many physical properties. n-Heptane asphaltenes have been used here; n-heptane was added to the crude oil (40cc/g) and the solution was stirred for 24 hours. The precipitate was collected by filtration and the precipitate was washed with warm n-heptane until the solvent wash was colorless.

Optical absorption experiments were performed using a Cary 5 UV-visible-NIR spectrometer. Some fluorescence spectra and some fluorescence lifetimes were determined using a PTI LS-100 fluorescence spectrometer. For lifetime data collection, the PTI LS-100 fluorescence spectrometer employs a nitrogen lamp. This line source provides output at a few discrete wavelengths and is of low intensity. Typical spectral widths were 6 nm for the source and 12 nm for the emission. Fluorescence lifetime and spectral measurements were performed in the front surface mode for neat (undiluted) crude oils and for highly concentrated solutions of crude oils and in the transmission mode for dilute solutions. Front surface and transmission measurements performed on the same solution for both lifetime and spectral measurements showed no significant differences. Samples which were used for fluorescence lifetime determinations were de-aerated using nitrogen gas typically for 12 minutes. A GC septum was used as a stopper on the sample cuvette and two GC needles were used to inject and vent the nitrogen. The effectiveness of de-aeration was determined using pyrene solutions; without de-aeration, our measured fluorescence lifetime of pyrene in heptane was 25 ns, and with de-aeration, 495 ns.

Fluorescence lifetime data were also collected using beamline U9B of the National Synchrotron Light Source of Brookhaven National Laboratory. This UV-visible beamline allowed selection of desired excitation and emission wavelengths and provides very high source power. As our lifetimes are fairly long, data collection could proceed only when the synchrotron was operated in the single bunch mode. The short time duration (1 ns) of the synchrotron pulse obviated the need for pulse deconvolution of the data. A comparison of the data collected at Brookhaven and with our spectrometer showed excellent agreement.

Quantum yield measurements and fluorescence spectra were performed for both dilute and neat crude oil solutions, and for several dyes. Figure 1 shows the configuration for collection of fluorescence spectra and optical power for both front surface and transmission geometries using several laser sources. This system allowed sensitive detection of fluorescence spectra to wavelengths as large as one micron, well beyond the limits of photomultipliers employed in fluorescence spectrometers. Different laser sources were

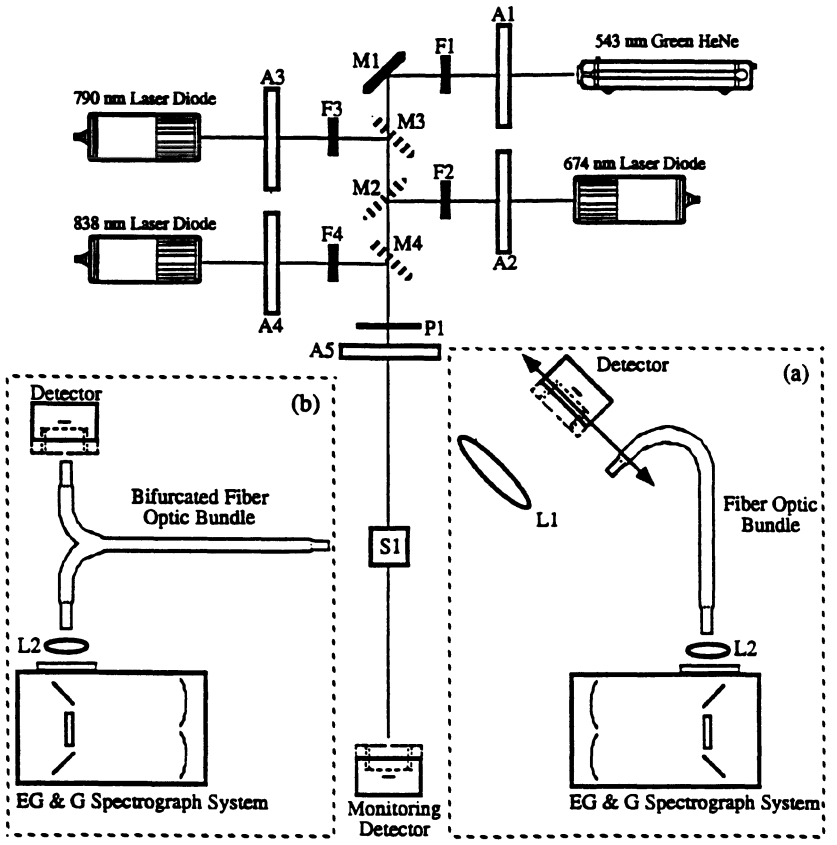

Figure 1. Schematic of system for fluorescence spectral and power measurements. Front surface (a) and dilute solutions (b) can be used. A single laser source, four are shown, is selected for excitation. Fluorescence optical power is measured with a power meter. Fluorescence spectra are measured using a spectrograph with a CCD detector.

used for fluorescence excitation. A polarized HeCd laser, Liconix Model 4207NB, was used for excitation at 325 nm (4 mW) and 442 nm (15 mW). A 0.3 mW Melles Griot GreNe, (Model 05SGR871), with polarizing filter was used for excitation at 543 nm and a polarized laser diode, 5 mW Melles Griot laser diode (Model 06DLL601) was used for excitation at 674 nm. A 30 mW Melles Griot 790 nm laser diode (model 06DLL401) and a 40 mW Melles Griot 838 nm laser diode (model 06DLL503) were used.

For dilute solutions, optical densities were kept near 0.1 and were matched for the reference and experimental samples. To measure quantum yields, the sample (or reference) was placed in a 10 mm cuvette and the optical power emitted transverse to the incident beam direction was collected by a bifurcated, randomized fiber optic made with high OH, silica-silica fiber, avoiding fiber fluorescence.[32] The source power and sample fluorescence power were measured using two Newport optical power meters (Model 838) with 1.13 cm diameter silicon detectors (Model 818UV). As shown in Figure 1, the spectrum of fluorescence plus any spurious scattered light was measured by coupling one arm of the fiber optic into the source slit of a 0.275 m focal length Acton spectrograph with an EG&G

512×512 CCD detector. This allowed correction for the scattered light inadvertently collected with fluorescence. This correction is significant only for long wavelength excitation where quantum yields are low.

For determination of quantum yields of dilute solutions at 674 nm, 790 nm, and 838 nm excitation, sample fluorescence was compared to Rayleigh scattered light from an aqueous suspension of 107 nm polystyrene-polyvinylstyrene spheres (Duke Scientific).[33,34] The cross section was verified to depend on the fourth power of wavelength. For excitation at shorter wavelengths, standard dye solutions were used as the reference.[33,34] Quantum yields of neat oil samples were measured referenced against scattering from concentrated solutions of the 107 nm spheres. The emission from the oils and the scattering from the spheres was unpolarized and had a Lambertian profile.[33] Again, the spectrum of the fluorescence was measured allowing removal of effects from scattered source light.

For quantum yields of dilute solutions, the following equation was used.[34]

$$\phi_o = K\left(\frac{\Delta I_o}{\Delta I_R}\right)\left(\frac{P_o(\lambda_o)}{P_R(\lambda_R)}\right)\left(\frac{\lambda_o}{\lambda_R}\right)\left(\frac{n_o^2}{n_R^2}\right)\left(\frac{S_o - S_s}{S_o}\right)\phi_R \tag{1}$$

where (ΔI_i) is the change in intensity in solution i at the exciting wavelength. Subscripts o and R refer to the oil of unknown quantum yield and the reference solution, respectively. $P_i(\lambda_i)$ is the power reading of the power meter at wavelength λ_i. The quantum yield of the power meter varies appreciably in the short wavelength range used here, so the power meter reading was adjusted for the wavelength of emission; the power ratio is converted into the photon ratio using the ratio of wavelengths. n_i is the index of refraction of solution i. The next to last term corrects for scattered light collected in the fluorescence spectrum; S_s is the excess area under the excitation band, S_0 is the total area under the fluorescence spectrum, and ϕ is the reference quantum yield. When fluorescent dyes of known quantum yield are used, K=1. For a reference scattering solution, K is a correction factor accounting for differences in the angular distribution between the scattered light (dipolar) and the fluorescence (isotropic). Ideally, K is 1.5 for the source light polarized perpendicular to the plane of incidence and detection. A corrected value for K of 1.43 was found from an analysis of the experimental setup by including factors such as actual source and fiber bundle sizes.

Quantum yields for concentrated solutions for each of our source wavelengths were determined using the following equation.[34]

$$\phi_o = \left(\frac{P_o(\lambda_o)}{P_R(\lambda_R)}\right)\left(\frac{\lambda_o}{\lambda_R}\right)\left(\frac{n_o^2}{n_R^2}\right)\left(\frac{S_o - S_S}{S_o}\right)(1 + R_\alpha) \tag{2}$$

The emission from these optically dense samples is randomly polarized so no polarization term is included. Self absorption effects in the front surface geometry are accounted for with the factor $(1+R_\alpha)$, where R_α is the ratio of extinction coefficients at the fluorescence and the excitation wavelengths, respectively.[33] For each of the excitation wavelengths, the mean red-shift can be determined from the spectra; values for the excitation wavelength and mean red-shift of the fluorescence are 325 nm, 100 nm; 442 nm, 90 nm; 543 nm, 87 nm; 674 nm, 66 nm; 790 nm, 55 nm; 838 nm, 40 nm. Using the universal exponential decay constant for crude oil absorption spectra, 2162 cm^{-1}, the values of R_α can be approximated for each excitation wavelength.[35] The values of R_α are 0.04 for 325 nm, 0.17 for 442 nm, 0.31 for 543 nm, 0.54 for 674 nm, 0.68 for 790 nm and 0.77 for 838 nm.

3. OPTICAL TRANSITIONS OF MOLECULES

3.1. Theory

Within the Born-Oppenheimer approximation, molecular wavefunctions can be factored into three constituents, electronic (e), vibrational (v) and rotational (Ro); $\Psi=\psi_e(\mathbf{r},\mathbf{R})\psi_v(\mathbf{R})\psi_{Ro}(\mathbf{R})$ where **r** and **R** represent electronic and nuclear position vectors, respectively.[36] Excitation of valence electrons from the ground state to excited states typically corresponds to an energy of several electron volts (eV), although in crude oils and asphaltenes, the largest molecules exhibit electronic transitions in the near-infrared, at ~1/2 eV which is quite low. Inner shell electronic transitions are at much higher energies, corresponding to x-rays and are not of interest here.

The π electrons in aromatic molecules are delocalized; the larger the aromatic molecule, the greater the delocalization. In accord with the principles of the quantum particle in a box, the greater extent of electronic delocalization, the lower energy the electronic transitions. For instance, the lowest allowed transition in benzene is at ~260 nm; naphthalene (two rings), ~290 nm; anthracene (three rings), ~380 nm; and graphite (∞ rings) is a zero-bandgap semiconductor. Of course, details of molecular structure, such as the location of rings, chemical substitution, and heteroatom content can significantly affect transition energies. Nevertheless, the general trend of lower energy transitions for larger aromatics allows direct correlation of spectra and populations, particularly for crude oils and asphaltenes, where aromatic molecular structures are systematic and constrained in type.

Vibrational frequencies are proportional to $(k/\mu)^{1/2}$, where k is the force constant of the vibrational mode, and μ is the corresponding reduced mass of the mode. Fundamental vibrational excitations of highest energy occur at about 3000 cm^{-1} and involve bonds containing hydrogen, which have the smallest reduced masses. Aromatic ring stretching modes, with their strong bonds and large force constants, appear at approximately 1600 cm^{-1}. Overtone and combination bands of these high frequency modes occur in the NIR which are forbidden, consequently are relatively weak.[36] Higher harmonics are progressively weaker in transition strength, or, equivalently in peak height. Rotational bands, which are typically in the microwave range, are quantized for molecules in field free space, but rotational lines merge in solution; that is, in solution, rotational transitions are not quantized due to asymmetric and variable intermolecular interactions. Rotational transitions are not evident and are not of concern here, although hindered rotations, called librations, are evident in some NIR spectra.

Several different units are used for photon energy, all have their conveniences. 1 eV equals 8065.7 cm^{-1} (or wavenumber). Wavenumber is a convenient energy unit as it is the inverse of the wavelength, e.g. 10,000 cm^{-1} corresponds to light of 1 micron wavelength (λ). $\lambda\nu=c$, so the product of c and the photon wavenumber gives the frequency, ν. Thus, electronic transitions of several eV correspond to ~10^{15} hertz (sec^{-1}).

Figure 2 schematically depicts ground and excited electronic states of a diatomic molecule, where molecular potential energy wells are plotted as a function of interatomic distance. At very large distances, the (ground or excited) neutral atoms are noninteracting, so the energy is not a function of position. At very short distances, the inner core electrons of the two atoms repel, resulting in high energy configurations. At intermediate distances, valence electron density resides preferentially between the two cores resulting in bonding. Orthogonal electron potential energy curves can be generated (within the Born-Oppenheimer approximation) by solving the Schroedinger equation for each internuclear distance. The resulting electron energy curves are then used to provide the boundary conditions for nuclear motion yielding vibrational states (see fig. 2).

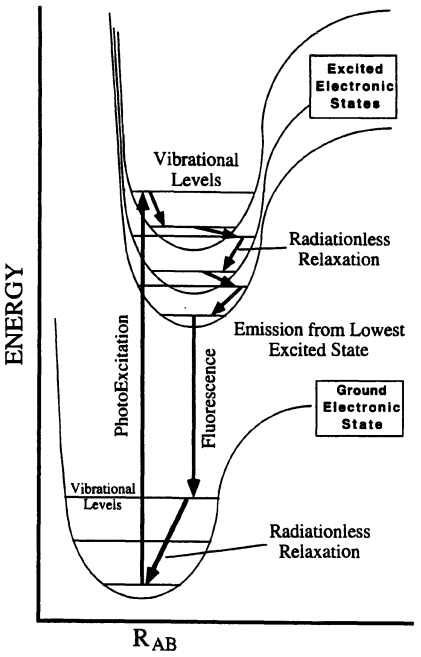

Figure 2. Schematic of photoexcitation and fluorescence emission. Photoexcitation can populate various excited states. Fluorescence emission typically occurs from the lowest excited state, excess energy is deposited in vibrational modes and ultimately in the solvent bath. Excitation of the first excited state yields small fluorescence red-shifts from the excitation wavelength, excitation of high-lying states produces large red-shifts. The large energy gap for small aromatic molecules and the small energy gap for large aromatic molecules produce the spectral identity of the fluorophores.

Electronic absorption corresponds to the excitation from the ground electronic state to an excited electronic state, while fluorescence emission corresponds to the reverse process, radiative de-excitation of typically the lowest excited state to the ground state. The photon is a one electron operator **r**, and the cross-section σ for excitation to the excited state denoted by * is given by

$$\sigma = | < \Psi^*_e(\mathbf{r},\mathbf{R})\, \Psi^*_v(\mathbf{R}) | \mathbf{r} | \Psi_e(\mathbf{r},\mathbf{R}) \Psi_v(\mathbf{R}) > |^2 \quad (3)$$

Using the Franck-Condon Principle, this integral separates as

$$\sigma = | < \Psi^*_e(\mathbf{r}) | \mathbf{r} | \Psi_e(\mathbf{r}) > < \Psi^*_v(\mathbf{R}) | \Psi_v(\mathbf{R}) > |^2 \quad (4)$$

where the first factor is the electronic excitation integral and the second factor is the projection of the initial vibrational state onto the final vibrational states. The square of the second factor is called the Franck-Condon factor. This projection is simply the δ function if the ground and excited states have identical molecular potentials but vertically displaced (in Figure 2).

3.2. Optical Spectra of Simple Aromatic Compounds

Figure 3 shows the absorption spectrum of anthracene (three fused benzene rings). The overall envelope corresponds to a single electronic transition involving the lowest excited state, the electronic integral of Eq. 4. The individual peaks correspond to the excitation of a series of vibrational states within this electronic transition, through the vibrational state projection integral of Eq. 4. As depicted in Figure 2, the absorption spectrum, at higher energy (on the left in Figure 3) shows excitation from predominantly the

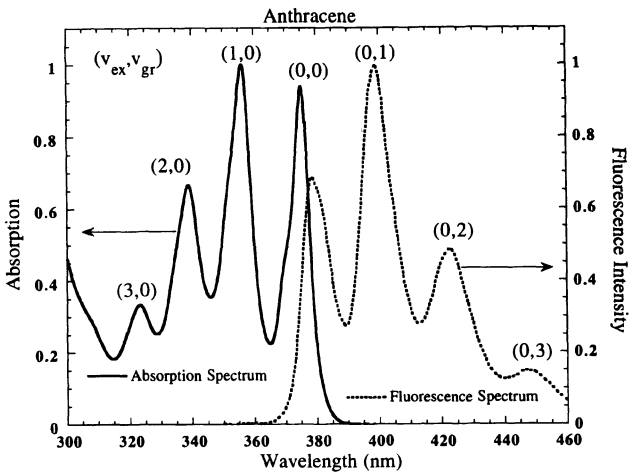

Figure 3. Optical absorption spectrum (solid line) and fluorescence emission spectrum (dotted line) of anthracene. A single electronic transition envelope with vibrational structure is shown. In the absorption spectrum, the individual bands correspond to excitation of the lowest vibrational state of the ground electronic state to different vibrational states of the lowest excited electronic state. The emission spectrum shows emission from the lowest vibrational state of the lowest excited electronic state to different vibrational levels of the ground electronic state. Pairs of vibrational quanta are shown for each peak, the left entry refers to the excited electronic state, right, ground electronic state. Due to the similarity of vibrational state projection operators in absorption and emission, the corresponding spectra are often mirror images of each other.

single, lowest vibrational state (of a particular mode) of the ground electronic state, to a series of vibrational states in the lowest excited electronic state. The fluorescence emission spectrum shows emission predominantly from the single, lowest vibrational state in the lowest excited electronic state to a series of vibrational states of the ground electronic state. The absorption and emission curves are nearly mirror images of each other implying $\langle\psi^*_v(\mathbf{R})|\psi_0(\mathbf{R})\rangle \sim \langle\psi^*_0(\mathbf{R})|\psi_v(\mathbf{R})\rangle$ for relevant v.

The vibrational energy spacing measured in Figure 3 of roughly 1400 cm^{-1} corresponds to the aromatic ring stretching mode. Promotion of a π electron from a bonding orbital to an antibonding orbital influences this mode. Thus, the ground vibrational state will overlap with several, not one, vibrational states of the excited electronic state and the vibrational state projection in Eq. 4 is not a δ function. The relative population of the ground vibrational state for this vibrational mode is given by the Boltzmann factor, $\exp(-\Delta E/kT)$. For room temperature, and for ΔE=1400 cm^{-1}, the Boltzmann factor is ~10^{-3}, thus only the ground vibrational state has significant population. Other vibrational modes, not affected by the π electron excitation, give δ functions for the vibrational state projection in Eq. 4.

One can identify the vibrational states involved in each of the vibrational transitions, they are marked in the figure. The first number in the parenthesis corresponds to the vibrational state of the excited electronic state, the second to the vibrational state of the ground electronic state. The 0–0 band is at a slightly higher energy in the absorption spectrum than the emission spectrum. Prior to the act of photoexcitation, the solvent is oriented in a favorable energy configuration for the ground electronic state. Once photoabsorption takes place, the solvent is no longer optimally configured, and must reorient to accommodate the excited state. Thus, initially the excited state molecule is in a high energy solvent cage, and this energy is supplied by the photon. Likewise, when the excited molecule undergoes

photoemission, the solvent cage which has been oriented for the excited state must reconfigure for the ground electronic state. This again costs energy which is unavailable for photoemission. Thus, the 0–0 emission photon is of a lower energy than the 0–0 excitation photon; this difference is refered to as the Stokes shift. Solvents of higher polarity exhibit a larger Stokes shift, here the solvent is n-heptane and the Stokes shift is small (25 cm^{-1}).[37]

The emission spectrum of anthracene is independent of which vibrational band is excited. Thermalization of the vibrational states (10^{-12} sec) occurs much more rapidly than photoemission (10^{-8} sec). Thus, even if higher vibrational levels are excited in the photoabsorption process, the Boltzmann distribution of vibrational levels is established by rapid intermolecular collisional relaxation and by intramolecular energy redistribution long before photoemission can occur. Furthermore, even if higher lying electronic states are photoexcited, emission will occur only from the lowest lying electronic state. The reason this occurs is because the 2nd, 3rd and higher excited electronic states will relax to the 1st electronic excited state. This general rule, Kasha's rule, is only occasionally violated for a few particular compounds for which photoemission also occurs from the 2nd electronic excited state. The reason this occurs is related to the spacing of electronic states.

It is instructive to recall the Rydberg equation which gives the energy E as a function of the principal quantum number n of electronic states of the hydrogen atom.

$$E_n = \frac{R}{n^2} \tag{5}$$

where R is the Rydberg constant, 13.6 eV. Energy equals zero ($n = \infty$) corresponds to the electron and proton separated by infinite distance and with zero kinetic energy. The ground state of hydrogen has an energy of R, its ionization or binding energy. The 1st excited state has an energy of R/4. The energy gap between the ground and first excited state is 3/4 of the ionization energy, and thus much larger than any other energy gap between adjacent states. In fact, an infinite number of electronic states are compressed in the 1/4 R energy gap between the first excited state and the continuum. Although the Rydberg equation is accurate only for hydrogen, the governing principles still apply for other atoms and for molecules. The energy gap between the ground and first excited state for molecules is also typically an appreciable fraction of the ionization energy, and is typically the largest energy gap between any adjacent electronic states (within a given spin manifold). These energy considerations account for the dramatic difference in de-excitation of higher lying excited states vs the first excited state.

Radiationless relaxation of the excited state can occur by electronic-vibrational coupling. Figure 4 depicts the relevant vibrational wavefunctions indicating the importance of the energy gap. Closely spaced electronic states have similar vibrational wavefunctions at a given total energy so the corresponding overlap integral is large; radiationless relaxation for these states is rapid. For the first excited state and ground state, there is typically a very large electronic energy gap producing very different vibrational wavefunctions for the two electronic states. Figure 4 depicts the slowly varying vibrational state of the upper electronic state vs. the highly oscillatory (large kinetic energy) vibrational state of the lower electronic state. Radiationless relaxation is inhibited by the small vibrational state overlap integral allowing the relatively slow process of radiative relaxation to occur. Typical radiative (fluorescence) lifetimes are nanoseconds. Radiative electronic relaxation couples nearly equivalent vibrational states yielding large overlap integrals (see Figure 4). These general guiding principles of chromophores explain why fluorescence spectra of typical chromophores are independent of excitation wavelength. Furthermore, these con-

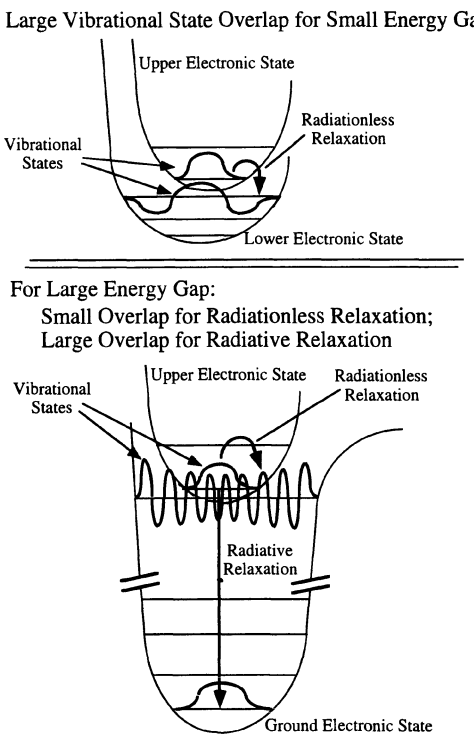

Figure 4. The importance of the vibrational state overlap is depicted. For a small energy separation between two electronic states, the vibrational overlap integral is large for radiationless relaxation. For a large energy gap, typical for the ground and first excited state, the vibrational states of the same energy for the two electronic states are very different, so radiationless relaxation is suppressed. Radiative relaxation can then occur. These considerations relate to the Energy Gap Law described later in this chapter.

siderations provide the framework for understanding the dependence of quantum yield on the energy gap. The Energy Gap Law will be treated explicitly in the Quantum Yield Section of this chapter.

Consequently, the energy gap between the ground and first excited state (within a given spin manifold) is of considerable importance and is called the HO-LU gap, (**H**ighest **O**ccupied molecular orbital—**L**owest **U**noccupied molecular orbital energy gap). The HO-LU gap is directly analogous to the bandgap in solid state physics. For organic molecules without heavy atoms, spin-orbit coupling is generally weak, yielding allowed optical transitions only within a given spin manifold, justifying the focus on individual spin manifolds.

4. ABSORPTION SPECTRA AND CHROMOPHORE DISTRIBUTIONS OF CRUDE OILS AND ASPHALTENES

4.1. Absorption Spectra

Figure 5 shows the optical absorption (optical density) vs. wavelength for many crude oils for a 2 mm pathlength.[35] Each spectrum consists of a series of decreasing absorption peaks with increasing energy, superimposed on a structureless profile with increasing absorption at shorter wavelengths. The series of peaks seen in Figure 5 corresponds to combination and overtone bands of primarily saturated CH_2 and CH_3 groups[38] and are seen to be very similar for all crude oils including the heaviest oils. These peak energies are the 4350 cm^{-1} (stretch+bend), 5800 cm^{-1} (two-stretch), 7200 cm^{-1} (two-

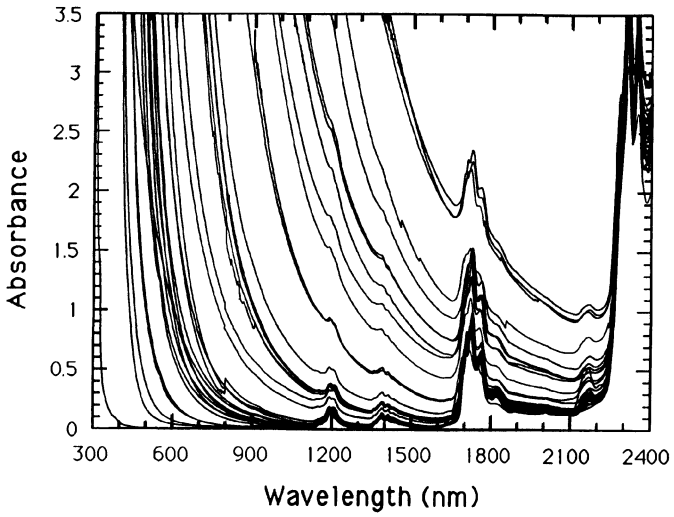

Figure 5. Optical absorption spectra for a series of crude oils. The vibrational absorption peaks are regularly spaced, and become smaller at higher energy. These bands are nearly the same for all crude oils due to the similarity of their bulk, saturated hydrocarbons. Crude oils possess continuous, electronic absorption at different spectral locations which grows in magnitude at shorter wavelength. This absorption is due to the aromatic component of crude oils.

stretch+bend), 8400 cm^{-1} (three-stretch), 9800 cm^{-1} (three-stretch+bend) and 10900 cm^{-1} (four-stretch). The Mid-IR and NIR vibrational bands of asphaltenes are quite informative. For example, the spectra indicate that the hydrogen is substituted predominantly on saturated, not aromatic carbon. (The two-stretch overtone of aromatic CH, which occurs at ~5980 cm^{-1}, has roughly the same oscillator strength as the saturated CH per hydrogen, yet the aromatic overtone remains small even for asphaltenes). Nevertheless, in this Chapter, we are concerned primarily with the electronic transitions of aromatic hydrocarbons, so we will not discuss further these overtone and combination bands.

The broad, increasing absorption profile corresponds to the absorption edge of electronic excitation. Previous work has shown that, even in the NIR, absorption rather than scattering from dispersed (not flocculated) asphaltene particles produces this optical density of crude oils.[39] Of course, if the crude oil has an insoluble wax phase or flocculated asphaltene then scattering becomes appreciable and the spectrum of the two-phase crude oil will be highly altered. For crude oils, the wavelength range of increasing absorption is much broader than the absorption bands of individual molecules and is due to the overlapping spectra of many molecular components. The spectral location of the absorption edge varies considerably and almost continuously for the different crude oils. The darkest crude oils, which are tar-like, show appreciable electronic absorption in the near-infrared; the lightest oil, a gas condensate, barely absorbs any light in the visible.

A certain similarity is evident in the absorption spectra of the crude oils. For instance, Figure 5 shows the absorption spectra of two crude oils usually do not cross unless the spectra are nearly identical at all wavelengths. Figure 6 shows the same absorption spectra as Figure 5 except the optical density (OD) is plotted on a logarithm scale against photon energy instead of on a linear scale against wavelength. (OD equals absorption (A)

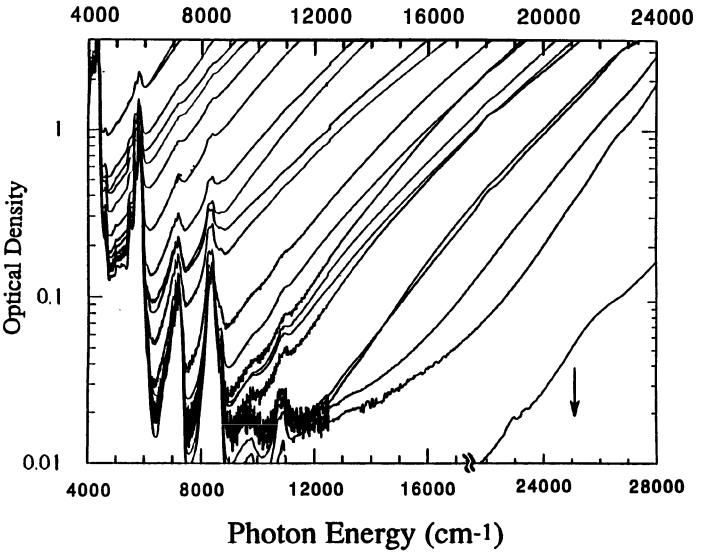

Figure 6. Optical absorption spectra of 22 crude oils. The absorbance is plotted on a logarithm scale vs photon energy yielding straight line spectra of nearly the same slope for all crude oils, from the heaviest tar to the lightest gas condensate. The surprising regularity of the optical spectra relates to the similar regularities of the population distributions of aromatic molecules in all crude oils.

plus scattering, if there is no scattering then OD=A.) The similarities in the absorption spectra are much more striking in this figure. All crude oils, from the heaviest tar to the lightest gas condensate, are seen to exhibit the same slope in the electronic absorption edge. This remarkable result establishes that the population of aromatic molecules of all crude oils are related in some sense, as will be described.[35] The straight lines in Figure 6 mean that the absorption tails of crude oils decay exponentially with photon energy; the uniformity of the slopes in Figure 6 means that the exponential decay widths of optical absorption for all crude oils are nearly the same.

Figure 7 shows similar optical absorption spectra for four asphaltenes, with absorption plotted on a logarithm scale, vs photon energy.[40] Asphaltenes uniformly have their electronic absorption edge in the NIR. The lack of individual absorption peaks signifies contributions from a large number of chromophores. Due to their intense electronic absorption, the vibrational overtones of asphaltenes appear small. Figure 7 shows that the monotonic increase of absorption with wavelength for asphaltenes extends over several orders of magnitude in absorption. This figure was obtained by splicing spectra for solutions of different asphaltene concentrations in order to get the large range in optical density. Similarly, no optical absorption peaks are seen for asphaltenes separated by GPC, with the exception of the possible appearance of the Soret band in the lowest molecular weight fraction.[41] In the absorption edge of asphaltenes, where the absorption is smallest, the spectral profile becomes linear on the log plot; that is, the absorption exponentially decreases with lower photon energy. Figure 8 shows the same type of plot with five crude oils and one asphaltene; generally absorption peaks are absent (except for the occasional appearance of the porphyrin Soret band at ~25,000 cm^{-1}). These absorption spectra are very different than that observed for anthracene, where well resolved electronic and even vibrational bands are seen (in Figure 3). These spectral profiles clearly indicate that crude oils and asphaltenes contain a huge

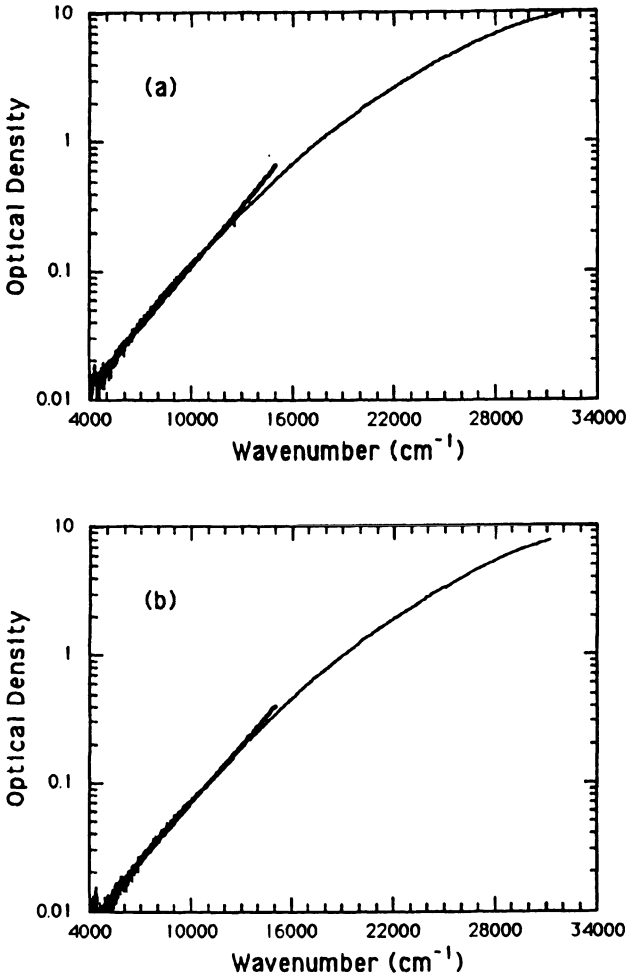

Figure 7. Absorption spectra of four asphaltenes in CCl_4 (0.26mg/cc). The asphaltenes exhibit monotonically increasing optical absorption towards shorter wavelength, over several orders of magnitude. (Spectra were spliced to obtain these composite spectra.) As with crude oils, the edge of the electronic absorption of asphaltenes produces straight line of similar slopes, when absorption is plotted on a log scale vs photon energy. Straight lines are included in the spectra to guide the eye.

number of chromophores with overlapping spectra. One might expect that such a huge, even continuous population of chromophores precludes analysis of absorption spectra. Indeed, this would be the case for random collections of chromophores; however, the chromophore populations of crude oils and asphaltenes are highly constrained by nature and their systematic behavior is very amenable to analysis.

4.2. The Urbach Tail

The constant decay widths of the electronic absorption edge for crude oils and asphaltenes recall the Urbach phenomenon, first observed in inorganic solids. In 1953, Urbach re-

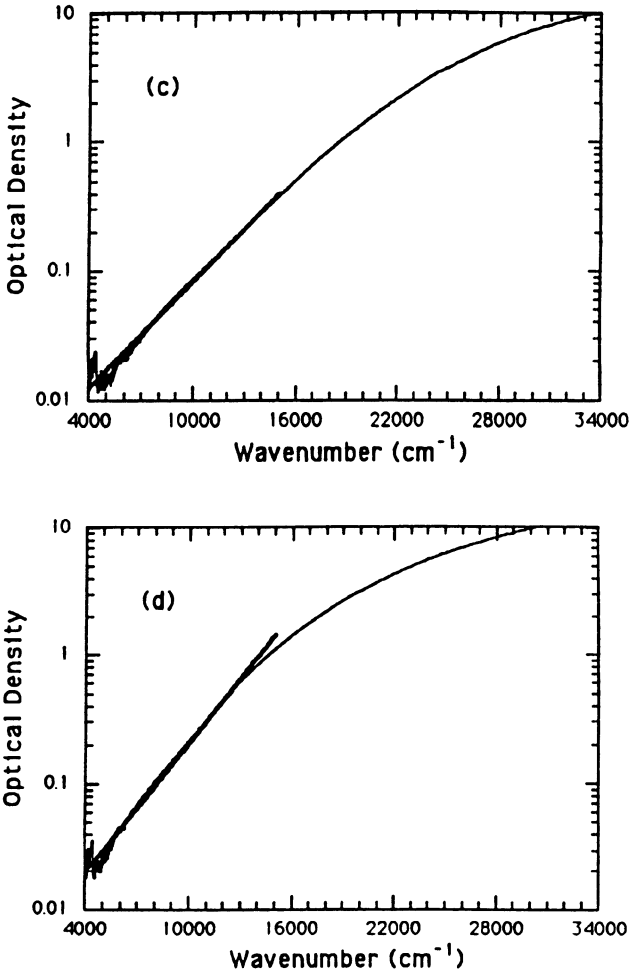

Figure 7. *(Continued)*

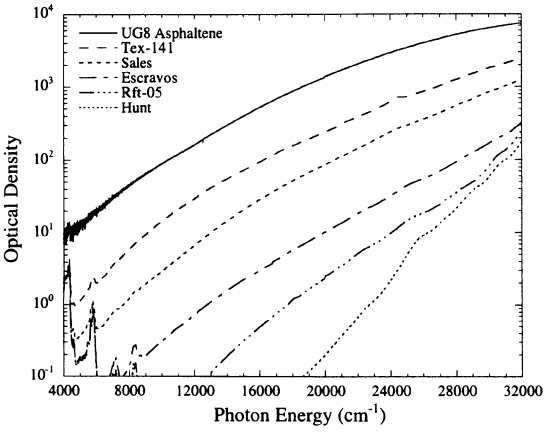

Figure 8. Optical absorption spectra of five crude oils and an asphaltene showing monotonically increasing absorption with decreasing wavelength. The Urbach region corresponds to the lowest optical densities were the spectra are straight lines. At larger optical densities, the slopes of the spectra decrease. Each spectrum consists of spliced spectra of the neat crude oil and corresponding dilute samples.

ported measurements of the low energy tail of electronic absorption for alkali halides.[42] He found that the tail in the optical absorption coefficient α was exponential in form

$$\alpha = \alpha_0 \exp\left(\frac{h\nu}{E_0}\right) \tag{6}$$

where hν is the photon energy and E_0 is the Urbach width. The pre-exponential factor is weakly dependent on photon energy. Furthermore, Urbach found that roughly $E_0 = kT$ (T is temperature). Since then many materials have been shown to possess the "Urbach" tail in electronic absorption. Many amorphous semiconductors exhibit the Urbach tail over one or more decades in the electronic absorption coefficient.[43] The tail results from thermal excitation of individual absorber sites, where the bandgap is reduced by the excitation energy. For some glassy materials the width of the Urbach tail is characterized roughly by the glass transition temperature; the thermal disorder is frozen into the glass, and the disorder correspondingly affects the bandgap.[43] In hydrogenated amorphous silicon, the width of the Urbach tail was found to exceed significantly thermal widths, the large tail width was found to be dominated by structural rather than thermal disorder.[44] General theoretical formalisms of the Urbach phenomenon have been developed[45] providing a basis for plausible expectation that thermally excited absorbers possess a thermal width in the absorption spectrum. Solutions of organic dyes such as coumarin[46] and rhodamine[47] also exhibit the Urbach tail in long wavelength absorption and long wavelength emission and where the width parameters are thermal.

The Urbach behavior in the absorption edge of Figures 6 and 7 corresponds to the linear spectral section at the smallest optical densities. The mean and standard deviations for the decay widths (E_0 of Eq. 6) of crude oils are 2162 ± 260 cm^{-1}; for asphaltenes, 2840 ± 245 cm^{-1}. At larger absorbances, the spectra show a smaller increase in the absorbances than expected based on extrapolation of the Urbach decay width. That is, at larger absorbances, the absorbance grows less rapidly than exponential. Figure 6 shows that the absorption edge of each crude oil exhibits the same slope independent of spectral position of the absorption edge. Figure 8 confirms this observation, but also shows that the similar slopes are confined only to the edge region; the absorption spectra of different crude oils and asphaltenes in a given spectral region exhibit different slopes, depending on the mag-

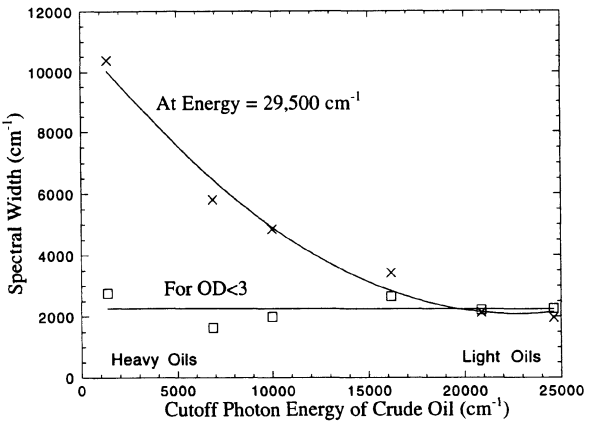

Figure 9. Decay width of the curves in Figure 8 determined for OD < 3 and at energy = 29,500 cm^{-1} vs the cutoff wavelength (where the OD = 3) for different crude oils and an asphaltene. The similar widths for different crude oils at OD < 3 corresponds to the Urbach tail while increasing widths for darker crude oils at higher photon energies correspond to increasing deviations from the Urbach tail. The cutoff wavelength (inverse of cutoff photon energy) is a measure of crude oil weight, heavy oils have larger cutoff wavelength.

nitude of the absorption strength. In Figure 9, the decay width determined at OD < 3, the absorption edge, is plotted vs the cutoff wavelength. The cutoff wavelength is defined to be the wavelength where the OD = 3 for the absorption curves in Figure 5 and is analogous terminology to optical edge filters. Heavy crude oils have large cutoff wavelengths thus small cutoff photon energies. Also plotted in Figure 9 is the decay width determined at one energy, 29,500 cm^{-1} (any large value of energy would suffice). This decay width is the inverse of the slope at 29,500 cm^{-1} of the absorption curves. For the light crude oils, the decay width at 29,500 cm^{-1} remains within the Urbach tail. That is, the width is exponential down to small absorbances. For the heavy crude oils, the slope at 29,500 cm^{-1} is small compared to the slope of the absorption tail; the decay is not strictly exponential from 29,500 cm^{-1} down to small absorbances; absorption at 29,500 cm^{-1} is not represented by the Urbach description for the heavy crude oils. This important result shows that the Urbach tail is not a function of the particular chromophores which absorb at some spectral location; rather, the Urbach tail corresponds to the population of chromophores in the low absorption tail of a crude oil.

Crude oils and asphaltenes exhibit exponential tails of nearly the same decay width but the decay width is much larger (×10) than thermal widths. Furthermore, this decay width is far larger than would be expected if the maturation temperature of the crude oil resulted in the decay width of the asphaltenes, analogous to glass transition temperatures of glassy materials. Initially, it may seem strange that a complex mixture such as asphaltenes has any relation in their electronic absorption profile to amorphous semiconductors. However, upon further reflection similarities become apparent. Single component systems such as amorphous semiconductors have absorber sites differing in their thermal activation, each site with its own absorption characteristics. Crude oils and asphaltenes have a distribution of chromophores (absorbers) produced in a thermally activated (maturation) process; each chromophore has its own absorption characteristics. The width of the asphaltene absorption spectrum is not due to thermal excitation of individual molecules; rather, the spectral widths are characteristic of the chromophore population distribution which results from a thermally activated process. Thus, the decay widths are not given by kT. The similarity of the diagenetic (thermal) process which gives rise to different crude oils is responsible for their uniform Urbach tails. The absorption edge corresponds to the smallest energies of excitation which in turn, correspond to the largest aromatics. Thus, the Urbach tail relates to the population distribution of the largest chromophores in crude oils and asphaltenes.

4.3. Fluorescence Properties within the Urbach Tail

Fluorescence spectroscopy is quite useful in unraveling the complexities of the optical properties of crude oils. Here, fluorescence analysis of crude oils and asphaltenes is

Figure 10. Fluorescence emission spectra for dilute samples of (top) Hunt, a light crude oil; (middle) Texaco, a heavy crude oil; and (bottom) an asphaltene. With long wavelength excitation, all emission peaks have small widths and small red-shifts. With short wavelength excitation, only the light crude oil exhibits small widths and red-shifts indicating that, for light crude oils, absorption is dominated by lowest energy electronic transitions throughout the visible. This requires an increasing population of chromophores with larger HO-LU energy gaps; that is, the population of blue-absorbing molecules is much larger than that of red-absorbing molecules. The heavier samples exhibit large widths and large red-shifts with short wavelength excitation indicating higher energy electronic transitions account for absorption here. Thus, the population of blue-absorbing molecules is not much larger than that of red-absorbing molecules.

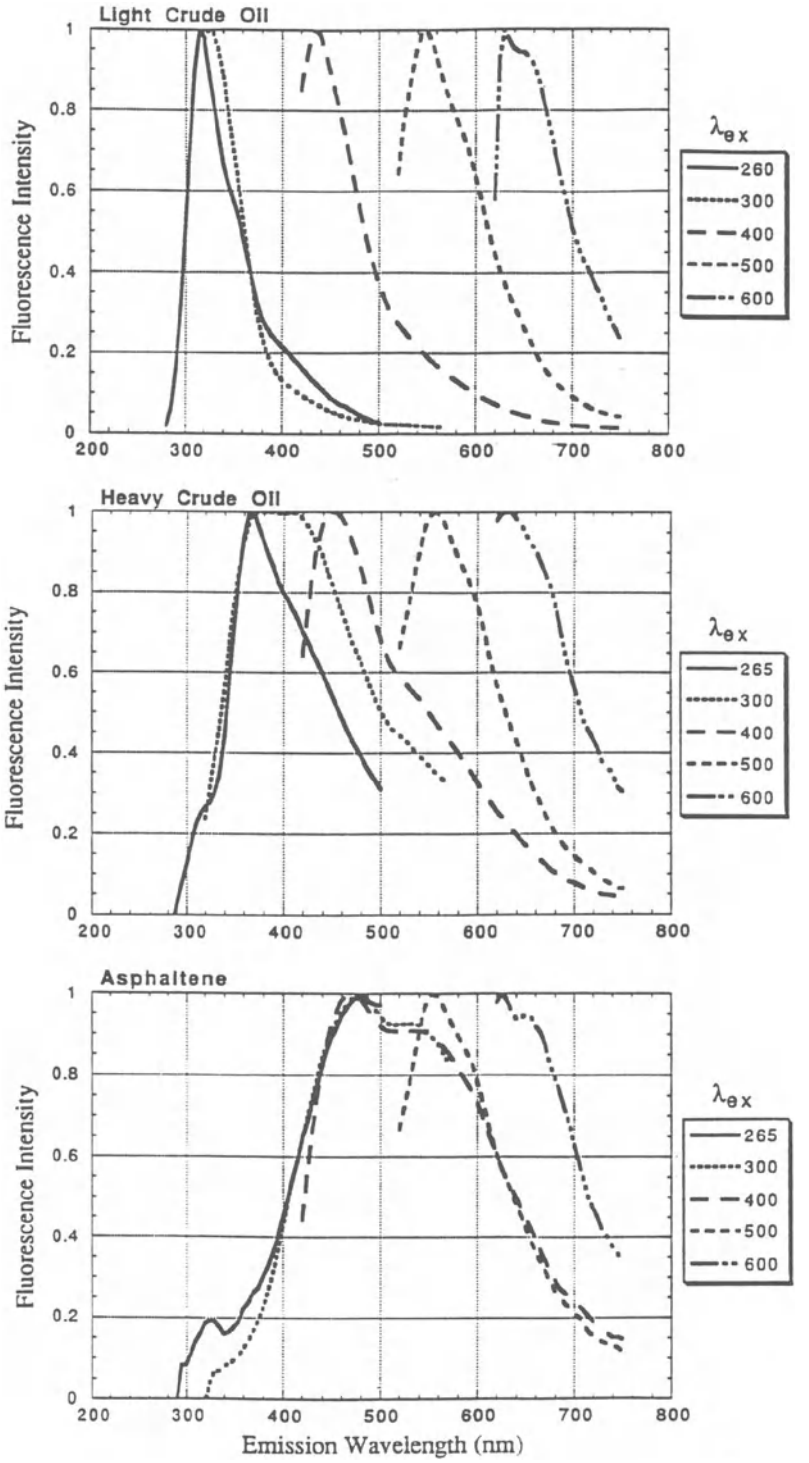
Light Crude Oil
Heavy Crude Oil
Asphaltene
Fluorescence Intensity
Emission Wavelength (nm)
λex
260
265
300
400
500
600
0
0.2
0.4
0.6
0.8
1
200
300
400
500
600
700
800

used to explore spectral regions where the Urbach behavior is obeyed and violated. Figure 10 shows several fluorescence emission spectra with various excitation wavelengths for Hunt, a light crude oil, Texaco, a heavy crude oil and an asphaltene. These spectra were obtained on dilute solutions with low absorbance. For the light crude oil Hunt, the fluorescence emission peaks are narrow (~70 nm) with a small red-shift from the excitation wavelength. These spectral characteristics imply that for each excitation wavelength, absorption is dominated by lowest energy electronic transitions. The number of chromophores with lowest energy absorption in the blue far exceed those in the red as determined by the exponential increase in absorption at higher energies. Thus, the contribution to blue-absorption by high energy transitions of large (red-absorbing) chromophores is small compared to the absorption corresponding to lowest energy electronic transitions of blue-absorbing chromophores. For this Hunt crude oil, the Urbach tail spans the spectral range down to 300 nm (see Figure 8).

Figure 10 shows for a heavy crude oil Texaco the fluorescence emission peak widths and red-shifts are small for long wavelength excitation but increase for short wavelength excitation. In contrast to the light crude oil, blue-absorption for the heavy crude oil is due in part to high energy transitions of red-absorbing molecules. Figure 10 also shows that for an asphaltene, only the reddest excitation produces small peak widths and shifts. For heavy crude oils and asphaltenes, the blue-absorbing chromophores are lacking relative to the red-absorbing chromophores. The relative lack of blue chromophores in the heavy crude oils results in the loss of blue fluorescence. This lack also results in smaller blue-absorption than predicted based on the Urbach tail (deviation from the Urbach behavior), which predicts exponentially increasing absorption at shorter wavelengths. Lowest energy electronic transitions dominate absorption when the Urbach behavior applies while higher energy transitions are significant when the Urbach behavior breaks down. An exponentially increasing population with decreasing chromophore size within in the Urbach tail region is consistent with these observations.

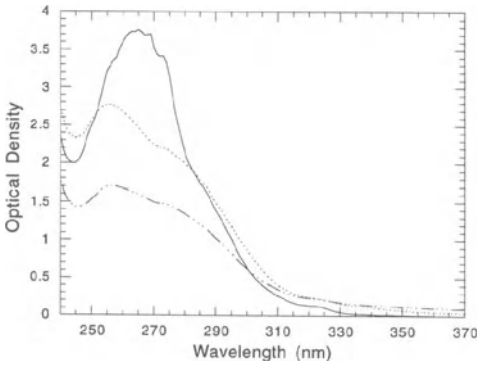

Figure 11. Absorption spectra of several n-heptane solutions of light crude oils in the range where one- and two-ring aromatics absorb. Fluorescence emission spectra with 260 nm excitation show small red-shifts and widths indicating that these peaks correspond to lowest energy transitions of small aromatic molecules. These absorption peaks which occur near the Urbach tail for these crude oils confirm that absorption in (near) the Urbach region is dominated by lowest energy electronic transitions, not by transitions to higher lying states of red-absorbing chromophores. Heavy crude oils do not exhibit these peaks, absorption by heavy oils at 260 nm is due to excitation of high-lying electronic states of multi-ring chromophores.

Figure 11 shows the absorption spectra of three light crude oils diluted with n-heptane; in this spectral range, small aromatic molecules have their lowest energy transitions. Individual peaks at ~260 nm are resolvable in the crude oil spectra corresponding to single ring aromatics. Here, the bulk of optical absorption is by molecules with their HO-LU gap at this photon energy. The continuum population of aromatic chromophores cannot apply for the smallest ring systems, where relative ring-size differences are large. For light crude oils, this spectral range is close to the Urbach absorption tail region. Figure 10 (top) shows the fluorescence emission spectrum of one of these light crude oils. The small red-shift and small peak width of the fluorescence emission with 260 nm excitation implies that the 260 nm peak in the absorption spectrum is indeed due to the lowest energy transition of small molecules (one- and two-ring aromatics), not some high energy transition of a large molecule. These data support the concept that the absorption tail is dominated by lowest energy electronic transitions.

Figure 12 shows normalized fluorescence emission spectra for four different excitation wavelengths for different crude oils and asphaltenes. The crude oils are listed from lightest to heaviest with the two asphaltenes being comparable. With excitation at 600 nm and 500 nm, the longest wave excitation, all crude oils exhibit similar spectra with small red-shifts and narrow peaks. With decreasing wavelength, the light crude oils still exhibit small fluorescence emission red-shifts with narrow peaks, while the heavier crude oils and asphaltenes exhibit increasing red-shifts and peak widths. The light crude oils exhibit fluorescence spectra at each excitation wavelength which suggest that absorption excites the lowest energy electronic state. For the heavy crude oils, lowest energy transitions dominate only in the red spectral range. With short wave excitation of heavy crude oils and asphaltenes, significant red-shifts are observed; excitation occurs to higher energy electronic states with considerable radiationless relaxation before fluorescence emission.

For heavier crude oils, the Urbach tail region shifts to lower energy; thus, larger fluorescence red-shifts and widths correlate with deviations from the Urbach behavior. Figure 13 illustrates this point where the fluorescence peak shift (with excitation at 300 nm) is plotted against the absorption decay width at 29,500 cm^{-1} for a series of crude oils. The absorption decay width is defined as the exponential decay width determined for a small spectral range at 29,500 cm^{-1}; that is, the absorption decay width is simply the inverse of the slope at 29,500 cm^{-1} of the absorption curves shown in Figure 8. Larger decay widths correspond to large deviations from the Urbach tail. Increasing deviation from the Urbach behavior is seen to correlate with increasing fluorescence peak red-shifts. When the absorption at short wavelengths is smaller than predicted from an extrapolation of the Urbach tail, the relative population of blue-absorbing chromophores is less, so the fluorescence emission spectra show less blue fluorescence and relatively greater red fluorescence.

4.4. Population Distributions of Large Chromophores in Crude Oils and Asphaltenes

The Urbach phenomenology describes the absorption spectral profile of crude oils and asphaltenes when absorption is dominated by lowest energy transitions. The absorption spectral profile, therefore, provides a measure of the population distribution of molecules. The monotonically decreasing absorption at longer wavelengths indicates a monotonically decreasing population of larger chromophores. If we make the approximation that the oscillator strengths of sets of chromophores with their lowest energy transition in different spectral regions are the same, then the Urbach region of the spectrum directly gives the population distribution. Individual oscillator strengths will vary appreciably, but averages over sets of molecules make this approximation more reasonable.

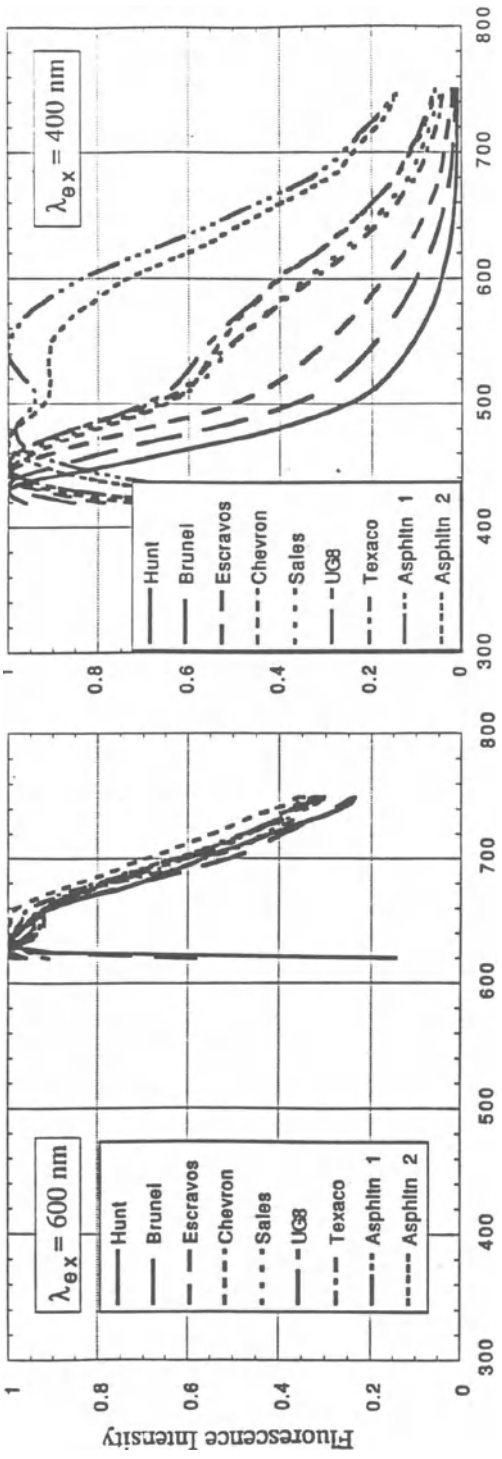

Figure 12. Fluorescence emission spectra for seven crude oils (listed light to heavy) and of two asphaltenes. With all excitation wavelengths, the light crude oils show small red-shifts and small fluorescence peak widths. Thus, optical absorption in the electronic (Urbach) tail, which is in the visible for light crude oils, is dominated by lowest energy electronic transitions. With shorter wavelength excitation, heavier crude oils increasingly show larger red-shifts and larger widths; visible excitation is to high-lying electronic states.

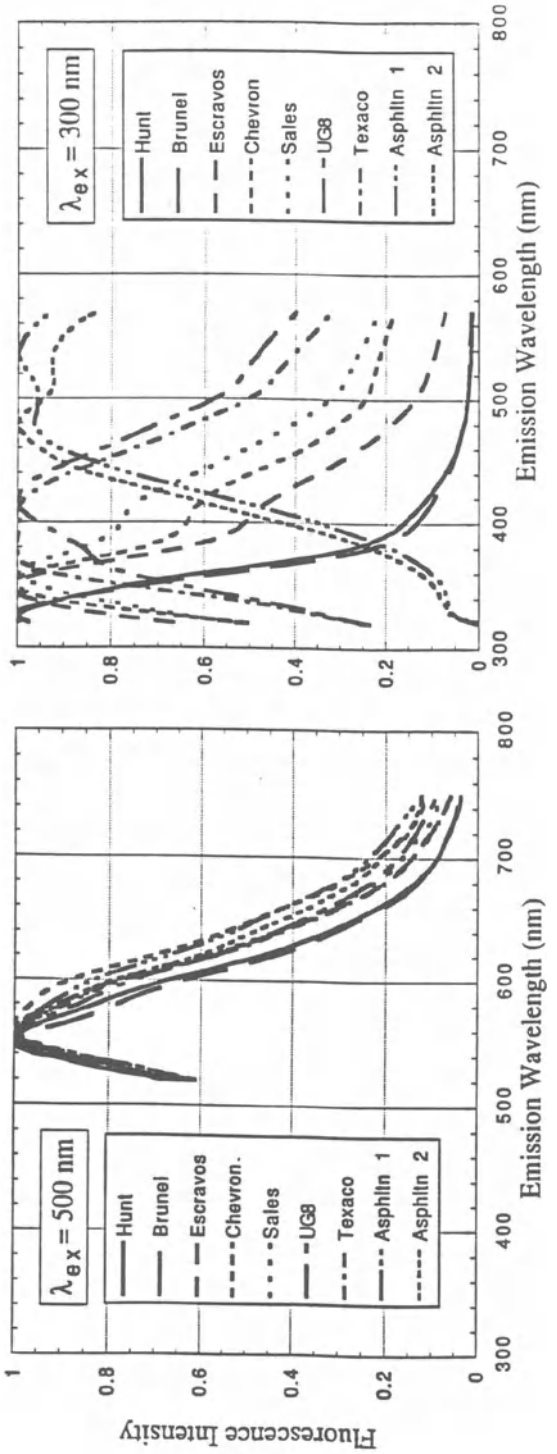

Figure 12. (*Continued*)

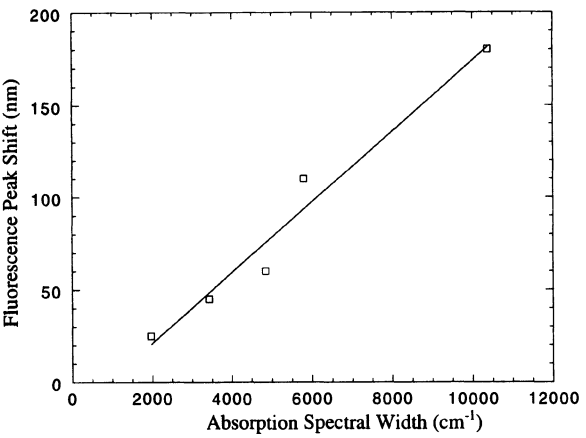

Figure 13. Fluorescence emission red-shifts with excitation at 300 nm vs *absorption* spectral width measured at 29,500 cm^{-1}. Decay widths larger than ~2000 cm^{-1} indicate deviations from the Urbach tail. Large fluorescence red-shifts result from excitation to higher energy electronic states and correlate with deviations from the Urbach behavior.

With this approximation, the population distribution of increasingly larger absorbers exponentially declines in crude oils and asphaltenes. Asphaltenes include a set of molecules constrained by this population ratio. It is always tempting to draw individual molecular structures for asphaltenes which are compatible with the large number of bulk chemical constraints imposed by various experimental techniques. In reality, it is important to understand that the physical and chemical properties of asphaltenes are determined in part by the existence of the set of molecules where the properties of the set are constrained.

A plausible explanation for this decreasing population of larger chromophores is that in the in-situ thermal processing of the source material and crude oil, larger chromophores are produced from smaller chromophores and the production is rate limited. This process would imply that the largest chromophores are least abundant. With continuing thermal alteration increasingly large chromophores would be produced thereby moving the electronic absorption edge to lower energies. Increasing thermal maturation also cracks alkyl chains off aromatics producing insoluble pyrobitumen. The loss of heavy end aromatics also contributes to the aromatic population distribution. The maturation processes for different crude oils are similar in nature but the extent of thermal alteration for different crude oils varies, producing similar Urbach widths at different spectral locations.

Figure 14 shows a schematic representation of the population distribution of the chromophores of crude oils and asphaltenes. The population of largest chromophores (for a particular sample) diminish exponentially, giving rise to the Urbach tail. Within the Urbach spectral tail region, the optical absorption at any wavelength is dominated by those molecules with their HO-LU gap at that wavelength. At energies larger than those corresponding to the Urbach tail, the population of smaller chromophores no longer increases exponential with decreasing size. The corresponding optical absorption is due in part to small molecules (non-Urbach region in Figure 14), but also has a significant component due higher energy transitions of larger molecules.

5. FLUORESCENCE AND INTERMOLECULAR INTERACTIONS

Fluorescence is an excellent probe of the dynamics of chromophores in crude oils and asphaltenes, due to the long fluorescence lifetimes compared to solution dynamics.

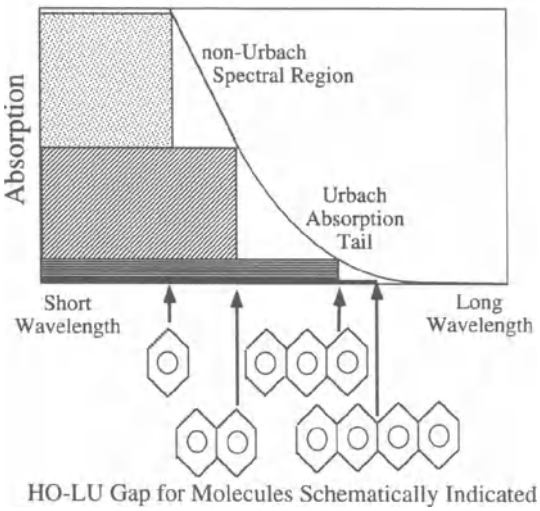

Figure 14. Schematic representation of population distributions of large chromophores in crude oils and asphaltenes. In the Urbach absorption tail, the population of larger chromophores decreases exponentially, yielding exponentially decreasing absorption. In the Urbach tail, absorption is dominated by molecules with their HO-LU gap at the selected wavelength. In the non-Urbach region, smaller chromophores no longer exponentially increase, yielding less than predicted absorption. Here, absorption occurs both due to lowest energy electronic transitions (benzene as depicted here) and due to higher-lying excited states of other chromophores (naphthalene as depicted here). This produces large fluorescence red-shifts and peak widths. For asphaltenes and heavy crude oils, the Urbach tail occurs in the near-infrared, so larger chromophores are involved.

Simple models of the structure and dynamics of chromophores of crude oils can generate predictions of their fluorescence properties. Stringent tests of these models can be developed; variables include crude oil type and isolated components, concentration and temperature; measurement parameters include excitation and emission wavelength, fluorescence spectra, lifetimes and quantum yields, along with optical absorption. A robust framework for understanding these chromophores can be developed and can be used to probe asphaltene chromophores in ways inaccessible by other methods.

5.1. Unifying Model of Molecular Interaction in Crude Oils

Intermolecular interactions can have significant effects on fluorescence properties, particularly for complex mixtures such as crude oils. Consider the outcome of the absorption of an optical photon by a fluorescent molecule in such a mixture. In the absence of intermolecular interactions, the fluorophore will radiate with its intrinsic spectrum, its intrinsic lifetime and its intrinsic quantum yield. (These intrinsic properties are influenced by solvent; the saturated hydrocarbon "solvent" of crude oils tends to be relatively noninteracting, resulting in minimal solvent effects.) However, if the excited molecule collides with or interacts with another chromophore, then one of several processes can take place. Energy transfer to a second fluorophore, necessarily with a smaller HO-LU gap, can result in longer wavelength emission. Thus, the fluorescence spectrum is altered. Quenching which can result from interaction of the excited fluorophore with a second chromophore reduces the quantum yield. Finally, due to the additional de-excitation processes of energy

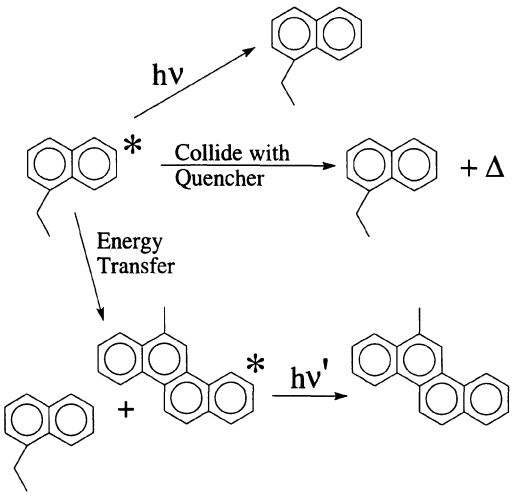

Figure 15. Schematic representation of the evolution of electronic excitation energy. The excited molecule can radiate (top process), collide with a quencher thermalizing the energy (middle process), or transfer the excitation energy to a second fluorophore of small HO-LU gap. Quenching reduces fluorescence quantum yields and lifetimes. Energy transfer produces a red-shifted fluorescence spectrum and also reduces the lifetime of the originally excited molecule. These intermolecular processes are readily investigated using measurements of lifetimes, spectra, and quantum yields as a function of concentration.

transfer and quenching, the excited state lifetime is reduced; thus the measured fluorescence lifetime of the initially excited molecule is reduced. Intermolecular interactions can result from diffusional processes; thus concentration is correspondingly a critical parameter. Eqs. 7–11 list several processes which are relevant to crude oils and asphaltenes. Figure 15 depicts these processes schematically.

$A + h\nu_A \rightarrow A^*$	:Electronic Photoexcitation	(7)
$A^* \rightarrow A + h\nu$	:Fluorescence Emission, Rate is k_F. If no competing process, Rate is k_{Fo}	(8)
$A^* + B \rightarrow A + B^* + \delta$	:Energy Transfer, Rate is $k_{ET}[B]$,	(9)
$B^* \rightarrow B + h\nu'$	:Fluorescence following Energy Transfer	(10)
$A^* + Q \rightarrow A + Q + \Delta$	:Quenching, Rate is $k_Q[Q]$	(11)

where A and B are fluorophores, Q is a chromophore capable of quenching an excited fluorophore, and hν is a photon, δ and Δ are small and large quantities of heat, respectively. Eq. 7 corresponds to photoexcitation, and Eq. 8, fluorescence emission. The emission photon of A*, hν is at a lower energy than that of the photoabsorption, $h\nu_A$, due to solvent effects (see Figure 2). Eq. 9 shows energy transfer; here it is implicitly assumed that energy transfer results in fluorescence emission. The photoemission from B*, hν', depicted in Eq. 10, is at a lower energy than from A* due to the small thermal energy release associated with energy transfer. Eq. 11 shows quenching, or thermalization of the energy

of the excited state. When intermolecular interactions are suppressed, say by low concentration, the fluorescence decay rate is intrinsic. If additional decay channels are active, the lifetime of A* is reduced below the intrinsic value. For energy transfer and quenching interactions, we do not differentiate between the long-range Coulomb interaction and the short-range exchange interaction. We use the term 'collision' to refer to both processes.

Eqs. 7–11 do not explicitly treat the effects of molecular complex formation. For room temperature solutions of moderate concentrations, small aromatics are not expected to have much of a tendency to form complexes. However, larger aromatics in concentrated solutions are expected to form complexes. Complexes can produce concentration-dependent fluorescence quenching, and as such, contribute to Eq 11. Optical measurements of the temperature dependence of fluorescence in crude oils have exhibited very small but definite effects from complex formation.[48] Asphaltenes are known to have strong associative tendencies. Nevertheless, as we shall see, lifetime measurements are consistent with greater significance of diffusional intermolecular interactions over complex-mediated intermolecular interactions for low concentrations relevant to work reported here. At the end of this chapter, fluorescence properties are used to probe asphaltene structure; careful examination of intramolecular effects or intra-complex effects is performed.

5.2. Fluorescence Lifetimes

Initial measurements of crude oils showed that their fluorescence lifetimes are sufficiently long to be influenced by chromophore interactions.[49] A single decay width was determined by use of phase sensitive detection methods for several crude oils; heavier crude oils were found to have shorter lifetimes, presumably due to increased decay rates from quenching processes depicted in Eq. 11 above.[49] Single-photon-counting methods have also been used to measure crude oil fluorescence lifetimes. Figure 16 shows a typical fluorescence decay curve for crude oil.[50] Because the decay curve is not linear in this logarithm plot, the data fitting requires more than a single exponential decay. Only a few of the decay curves of crude oils could be accurately fit using a single decay width. In all cases, a fit using two exponential decays could reproduce the data; thereby providing a long and a short decay component.[50] Of course, crude oils are complex mixtures and the corresponding fluorescence decay curves may consist of three or more decay components. However, these data are not sufficient to obtain more than two components from a fit. Simple computational modeling shows that a two component analysis of a multicompo-

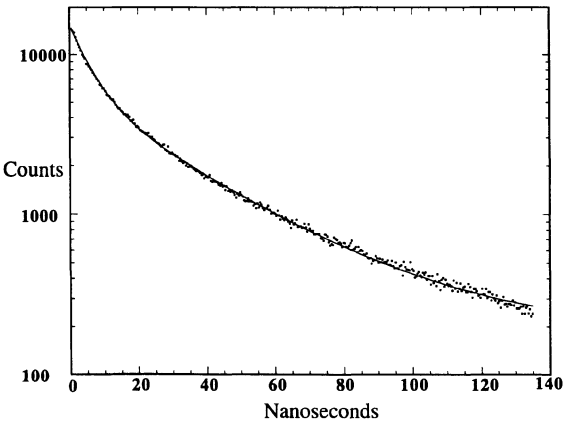

Figure 16. Typical fluorescence decay data for a crude oil. Because the decay is not linear on this log plot, a single exponential decay is inadequate to describe the data. The excellent fit (solid line) obtained using two exponential decays, validates the analysis procedure used here. This fitting procedure gives long and short lifetime components and populations.

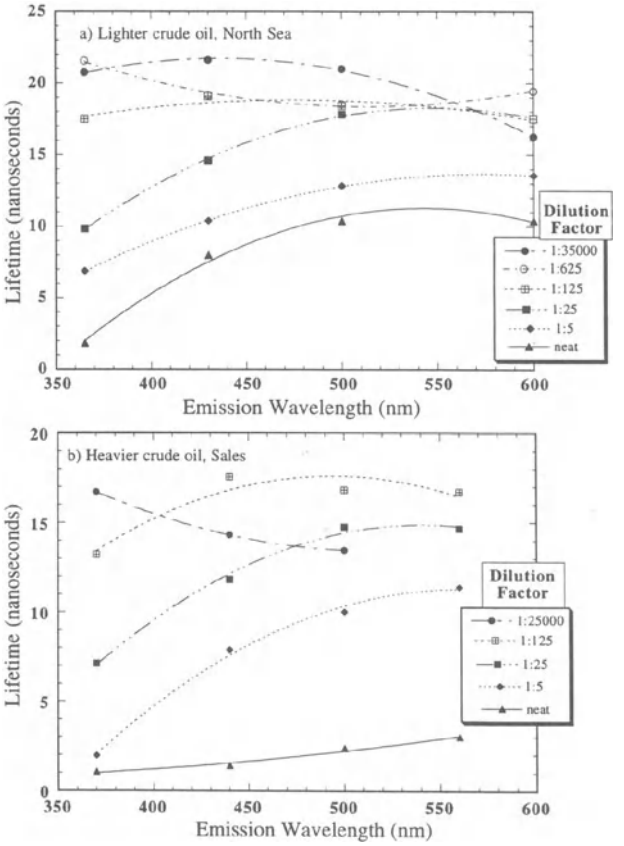

Figure 17. The long component fluorescence lifetimes for a) North Sea, a lighter crude oil and b) Sales, a heavier crude oil at different dilutions with 316 nm excitation and four emission wavelengths. Greater dilution yields less collisional decay, thus longer lifetimes. The heavier crude oil exhibits shorter lifetimes at given dilutions than the lighter oil due to larger inherent chromophore concentrations. For concentrated solutions, lifetimes are longer for longer emission reflecting the lower concentration of large, red-emitting chromophores than smaller, blue-emitting chromophores in crude oil.

nent decay does reflect the constituent lifetimes and populations of the original curve but, of course, some information is lost. All of the following analysis will be based on a two (or one) component fit. Generally, the population of the short lifetime component is much greater than that of the long lifetime component for all crude oils. For the lighter crude oils, the longer lifetime component does increase in population up to ~50%.[50]

Figure 17 shows the long-component fluorescence lifetimes for different concentrations of a lighter crude oil, North Sea (Figure 17a) and for a heavier crude oil, Sales, (Figure 17b). For the North Sea crude oil, the excitation wavelength is 316 nm, and emission wavelengths are 365 nm, 440 nm, 500 nm, and 600 nm; similar wavelengths were used for Sales crude oil. The shortest lifetimes are recorded for the neat crude oil and lifetimes grow as the concentration is reduced reflecting the decreasing importance of collisional decay.[50] The very dilute solution is minimally influenced by collisional effects so we treat these measured lifetimes, which are approximately 20 ns, as intrinsic. These data imply

Table 1. Selected fluorescence lifetime and population values for Sales crude oil

	370nm		440nm		500nm		560nm	
Dilution	τ	pop	τ	pop	τ	pop	τ	pop
Neat	1.05	1.	1.42	1.	2.38	0.5	3.03	0.56
					0.79	0.5	1.03	0.44
1:25000	16.71	0.15	14.3	0.14	13.48	0.14		
	2.76	0.85	2.9	0.86	2.9	0.86		

that energy transfer which accompanies an increase in concentration is not radiative. Radiative energy transfer does not provide an alternate decay mechanism for excited fluorophores and does not result in a decrease of fluorescence lifetimes. Table 1 lists some of the lifetime parameters obtained from fitting the Sales crude oil lifetime curves.[50]

For the lighter crude oil, dilution is seen to have a proportionally larger effect on lifetimes for short wavelength (365 nm) emission than for long wavelength (600 nm) emission particularly for concentrated solutions, where collisional effects are more important. The crude oils are much more concentrated in small chromophores than large chromophores; thus, due to their high concentration, the collisional decay rates are much higher and lifetimes shorter for the small, blue-emitting (large HO-LU gap) fluorophores than for the large, red-emitting (small HO-LU gap) fluorophores. The lifetimes of the neat solution of the heavier crude oil are quite short for all emission wavelengths unlike for the lighter crude oil, due to the higher concentration of fluorophores in the heavier crude oil. The lifetime data for the Sales sample (heavier crude oil) diluted by 5 is very similar to that of the neat North Sea oil, illustrating the systematic behavior of different crude oils.

Figure 18 shows the short lifetime component for Sales. Both the short and long lifetime components show the same dependence on concentration. The neat sample shows very short lifetimes; while a dilution by a factor of 5 still gives short lifetimes for short wavelength emission (blue emitters still too concentrated), but gives longer lifetimes with long wavelength emission. With further dilution, lifetimes generally increase. The lifetime data can be analyzed using the following expression.

$$\frac{1}{\tau_F} = k_F = k_{F0} + \left(k_{ET} + k_Q\right)[N] \tag{12}$$

where [N] represents the solution concentration of chromophores and fluorophores. Rearranging Eq. 12, one obtains

$$\frac{\tau_{F0}}{\tau_F} - 1 = \frac{k_Q + k_{ET}}{k_{F0}}[N] \tag{13}$$

We can determine if the data are consistent with a linear dependence of the quenching and energy transfer rates on concentration. By plotting $\tau_{F0}/\tau_F - 1$ vs concentration (Stern-Volmer plot), one directly obtains $(k_Q+k_{ET})/k_{Fo}$ as the slope.[31]

Figure 19 shows a Stern-Volmer plot of the long lifetime data for the 316 nm excitation, 365 nm emission for the North Sea crude oil. The linearity of the plot implies that indeed, the energy transfer and quenching mechanisms linearly depend on the concentration and are as indicated in Eq. 12. For the 316 nm excitation, 365 nm emission data both energy transfer and quenching reduce the fluorescence lifetime and are thus, not distinguishable.

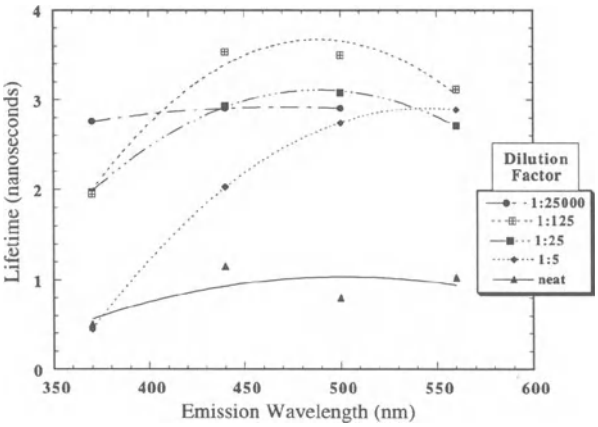

Figure 18. The short component fluorescence lifetimes for Sales crude oil show the same concentration dependence as the long component (Figure 17b) lifetimes. The neat sample shows short lifetimes at all emission wavelengths. Dilution by a factor of 5 yields very short lifetimes only for short wavelength emission reflecting the high concentration of blue emitters. Generally, greater dilution corresponds to greater lifetimes.

Figure 20 shows the Stern-Volmer analysis for the Sales lifetime data for each of the four emission wavelengths, 370 nm, 440 nm, 500 nm, and 560 nm. (Generally, the Stern-Volmer plots are more robust when large changes in lifetime are found; here, we attempt to obtain Stern-Volmer plots for the different emission wavelengths.) We make the assumption that population buildup is much faster than the decay. The assumption is accurate for short wavelength emission but only approximate for long wavelength emission. Approximately linear relations are found indicating that the collisional decay of excited state population linearly depends on concentration. The collisional decay rates per unit crude oil concentration normalized by k_{Fo}, the intrinsic fluorescence decay rate (slopes in Figure 20), are found to decrease with increasing emission wavelength. Assuming that collisions are equally effective for population decay for the blue emitting and red emitting fluorophores, the different decay rates in Figure 20 give relative populations of chromo-

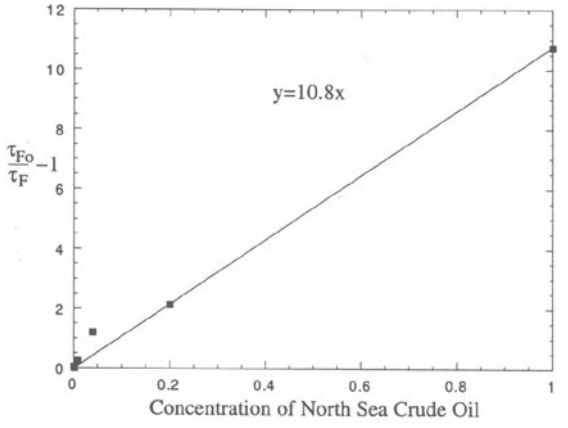

Figure 19. Stern-Volmer analysis of the long-component lifetime data, 316 nm excitation, 365 nm emission, for North Sea crude oil. The linearity of the plot implies that the collisional decay channels of energy transfer and quenching linearly depend on concentration. Some scatter in the data is obtained, in part, due to some nonuniqueness in fitting two lifetimes.

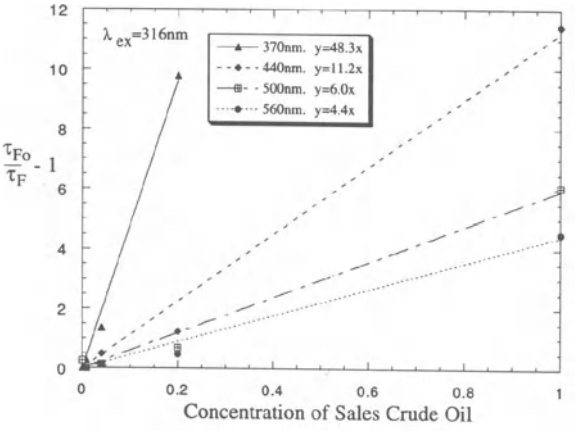

Figure 20. Stern-Volmer analysis of the lifetime data for Sales crude oil for 316 nm excitation and four different emission wavelengths. The larger slopes (collisional decay constants) for shorter wavelength emission reflect the larger concentration of blue emitting fluorophores in crude oils. The slope for the 370 nm emission data of Sales is 5 times larger than for the lighter crude oil (Figure 19) due to the larger fluorophore concentration. Some scatter in the data is obtained, in part, due to some nonuniqueness in fitting two lifetimes.

phores. Comparing Figures 19 and 20 for the 316 nm excitation, 370 nm emission, the factor of 5 larger slope for Sales vs North Sea simply reflects the factor of 5 greater concentration of chromophores in Sales.

Chromophore population ratios can be obtained from two independent measurements, optical absorption and fluorescence decay rates. In the electronic absorption edge, the value of electronic absorption at a given photon energy directly gives the relative population of chromophores with that energy HO-LU gap.[35] Likewise, in crude oils, the relative population of chromophores with a particular HO-LU gap is also directly related to the collisional decay rate of fluorescence emission at the corresponding wavelength.[50] Figure 21 shows the comparison of the absorption and lifetime estimates of the chromophore ratios. Perfect agreement for these two estimates would correspond to a straight line which passes through the origin. The agreement seen in Figure 21 is rather good corroborating that the optical absorption spectra of crude oils give the population distribution of chromophores.

One can generate order-of-magnitude estimates of the efficiencies of molecular encounters to yield energy transfer or quenching. Figure 17 shows that the intrinsic fluorescence decay constant is ~1/20 ns = 5×10^7/sec. To obtain a value of the collisional decay

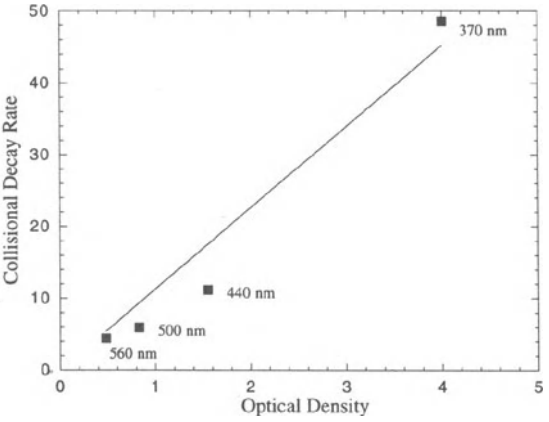

Figure 21. Comparison of the population ratios in Sales crude oil obtained by fluorescence decay rates and by optical absorption. The chromophore population is directly related to optical absorption and to collisional decay rates. Good agreement with the line y=ax is obtained with two very different methods to determine population ratios. Smaller HO-LU gap chromophores are much more abundant than large HO-LU gap chromophores in crude oils. (The cutoff wavelength for Sales is 999 nm, so the spectral region analyzed here is outside the Urbach tail; the increase in smaller chromophores is less than exponential)

constant per unit mole, we need an estimate of the concentration of chromophores in the crude oil which can collisionally de-excite 370 nm-emitting fluorophores. A rough estimate of the corresponding chromophore population follows: Sales crude oil has an absorption strength of approximately 2300 OD/cm at 370 nm. Assuming that the relevant aromatics have an average a value of absorption at 370 nm of 10^4 OD/cm, then we obtain a concentration of ~0.25 molar (roughly 2% aromatic by mole). Sales crude oil is about 5% asphaltene by weight, so this estimate is reasonable. This estimate does not include smaller aromatics such as benzene which have HO-LU gaps which are too large to be included. Using this rough value, we can approximate the value for the collisional decay constant $k_Q+k_E \sim 10^{10}$/molar/sec. This rate is approximately equal to the (diffusion-controlled) encounter rate in solutions.[31] Although these estimates are quite approximate, the implication is that encounters are very effective for energy transfer and quenching. This result is not surprising especially considering that there are roughly 10 collisions per encounter within the solvent cage. If the collisional decay constant were much smaller than the encounter rate, then the implication would be that only a few collisions between chromophores results in energy transfer or quenching.

5.3. Quantum Yields

Quantum yield studies of crude oils have been quite revealing, both of intrinsic molecular properties and of molecular dynamics. Quantum yields, number of photons emitted divided by number of photons absorbed, are sensitive to the intrinsic properties of molecules excited. Internal conversion, the conversion of electronic excitation energy to heat, is strongly affected by the HO-LU gap. In fact, as will be discussed, crude oils provide an excellent system to explore this dependence. Subtle structural features of aromatic molecules can result in dramatically different quantum yields. In spite of the variability of individual quantum yields, the large number of components of crude oils generate a well-behaved ensemble.

In addition to intrinsic molecular properties, quantum yields are strongly influenced by intermolecular interactions as indicated by Eq. 11. In crude oils, the quenching molecules are aromatics; the saturated molecular component behaves as a bath. The bath molecules may exert some influence on quantum yield as a sink for thermal energy, but do not interact with fluorophores with quasi-degenerate electronic states. On the other hand, other aromatic molecules can interact with excited fluorophores resonantly, provided the HO-LU gap of the aromatic is lower than the excitation energy. Quenching can result from the interaction of excited fluorophores with nonfluorescent and even with fluorescent chromophores.

Figure 22 shows the quantum yields for both neat and dilute solutions of various crude oils.[34] Light oils, being optically transmissive, have a short cut-off wavelength and heavy oils, being optically absorptive, have a long cut-off wavelength. The figure shows that, for all oils, neat and dilute, quantum yields increase with decreasing excitation wavelength. The trend of decreasing quantum yields with increasing excitation wavelength is known to extend into the NIR for crude oils.[33] This trend can be related to the ease of electronic excited states to relax all the way to the ground state via vibronic coupling and solvent collisions for fluorophores.[31] It is easier to thermalize electronic excitation energy if the excitation energy is not too large. Figure 22 also shows that the quantum yields for neat crude oils are much lower than for dilute crude oils due to intermolecular quenching among chromophores. Also, heavy oils, with their high chromophore concentration, suffer a much greater decrease in quantum yield in going from the dilute limit to neat solutions. This is in accord with the much shorter fluorescence lifetimes exhibited by neat heavy

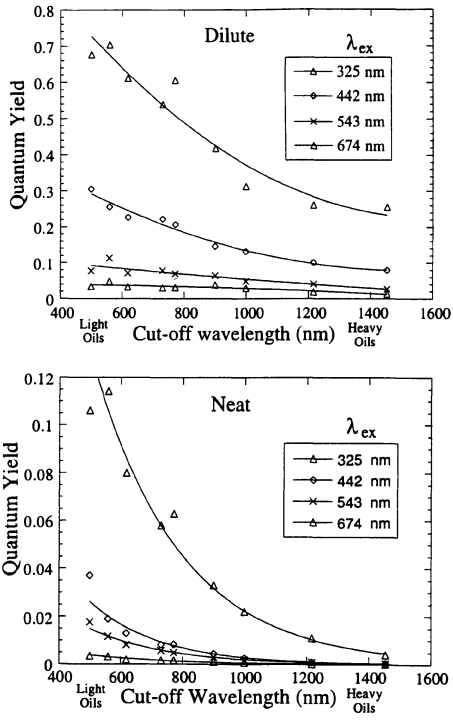

Figure 22. The absolute quantum yields for dilute (top) and neat (bottom) crude oils. The cut-off wavelength is an optical measure of the oil weight; heavy oils have a large cut-off wavelength. Quantum yields decrease greatly with increasing excitation wavelength due to greater internal conversion for small HO-LU gap molecules. Quenching from chromophore interactions causes neat crude oils to have much smaller quantum yields than dilute crude oils, especially for heavy oils. For the dilute case, the quantum yields of heavy oils are lower due to their greater fraction of small HO-LU gap chromophores, than for lighter crude oils.

crude oils than neat light crude oils due to rapid excited-state decay via intermolecular interactions of chromophores. The effects of excitation wavelength and of concentration will be examined in detail.

Figure 23 shows the large reduction of fluorescence quenching with dilution for a crude oil. Figure 24 shows the Stern-Volmer plot for two crude oils; if the simplistic model of Eqs. 7–11 apply, then the Stern-Volmer plot should yield a straight line.[50]

$$\frac{\Phi_o}{\Phi} - 1 = \frac{k_Q}{k_{Fo}}[Q] \tag{14}$$

where Φ and Φo mean the quantum yield with and without concentration quenching, respectively. These data are adequately fit using the Stern-Volmer equation implying accuracy for Eqs. 7–11. Furthermore, the slope, which gives the quenching rate as a function of crude oil concentration, is 5 times larger for Sales crude oil than North Sea crude oil due to the 5 times greater concentration of chromophores in Sales. This same factor of 5 was obtained by comparison of the Stern-Volmer plots of the fluorescence lifetimes of these two oils, shown in Figures 19 and 20. The source and detection wavelengths for the quantum yield and lifetime data are different preventing direct comparison of slopes; ratios can be compared. For a single crude oil, one can obtain the Stern-Volmer plots for a series of different excitation wavelengths. Figure 25 shows that for longer wavelength excitation, the collisional quenching rates are smaller.[33] Eq. 14 shows that the slope is proportional to concentration. The relevant concentration is not only of the crude oil, but of the quenchers in the crude oil. There are relatively few chromophores in crude oils which can quench molecules of small HO-LU gap; thus, red excitation shows a smaller slope in Fig. 25.

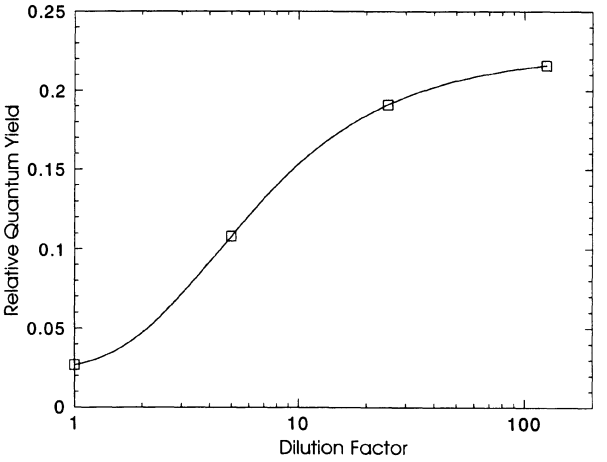

Figure 23. Relative quantum yield of Sales crude oil vs dilution. Substantial intermolecular fluorescence quenching is observed at high concentration. Energy transfer which also results from intermolecular interaction does not decrease the quantum yield.

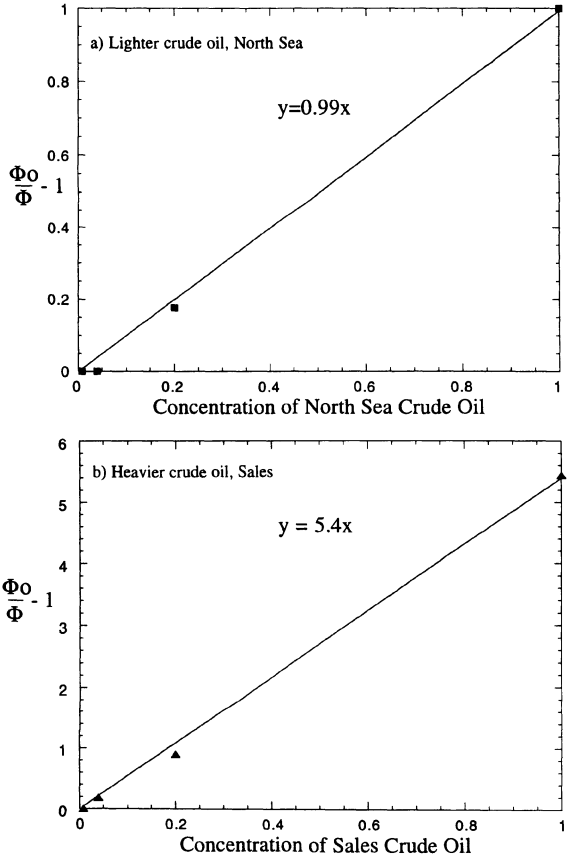

Figure 24. Stern-Volmer plot of the quantum yield data for a) North Sea (lighter) crude oil and b) Sales (heavier) crude oil showing that fluorescence quenching depends linearly on concentration. The quenching rate constant of Sales is 5 times larger than for North Sea in agreement with the lifetime decay rates for these two crude oils shown in Figures 19 and 20.

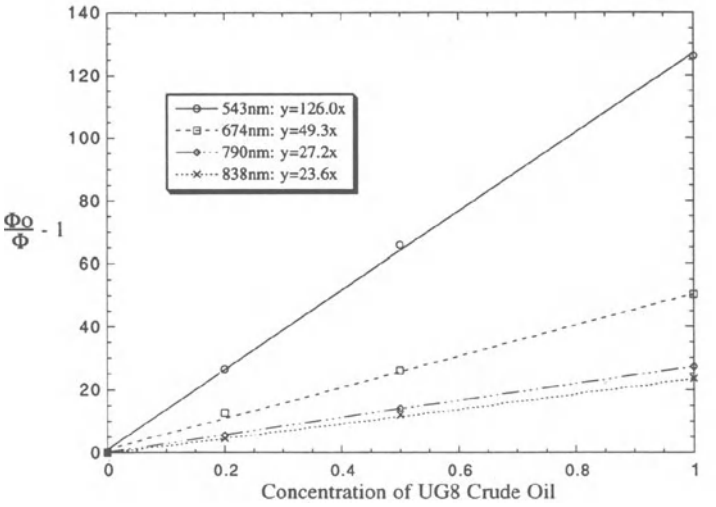

Figure 25. Stern-Volmer plot of the quantum yield data for UG8 crude oil showing that quenching is linearly dependent on concentration, thus simple models apply. High collisional quenching rates (larger slopes) are observed for shorter wavelength excitation due to the larger concentration of smaller, blue-absorbing chromophores in crude oils. This observation corroborates similar Stern-Volmer results for collisional rate constants determined by lifetime measurements (see Figure 20).

5.3.1. The Energy Gap Law. The plot of the quantum yield vs. excitation photon energy is shown in Figure 26 for Vixburg oil. The most plausible explanation for the decline in quantum yield with increasing wavelength is the exponential increase in the rate of internal conversion k_{ic} with decreasing HO-LU gap[51] as shown in Eq. 15.

$$k_{ic} = A \exp\left(-\frac{\Delta E}{\alpha}\right) \tag{15}$$

A is the frequency factor, ΔE is the HO-LU gap (and equals the photon energy) and α is an energy parameter. This equation accounts for the overlap integral of the ground vibrational state of the electronically excited state with the excited vibrational state of the

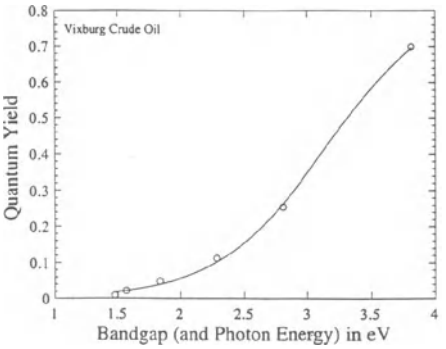

Figure 26. For crude oils, the dependence of quantum yield on HO-LU gap (or photon energy) is accurately reproduced with Eq. 16, using the Energy Gap Law. Smaller excitation energies yield larger rates of internal conversion. Fluorescence decay, which is largely independent of excitation wavelength, competes with internal conversion; thus, less fluorescence occurs with small HO-LU gaps.

ground electronic state. Figure 4 depicts this vibrational state overlap which largely governs the outcome of photoexcitation. The quantum yield dependence on photon energy is then given by

$$\frac{\phi}{\phi_o} = \frac{1}{1+\frac{A}{k_{Fo}}\exp\left(-\frac{\Delta E}{\alpha}\right)} \tag{16}$$

where ϕ and ϕ_o mean the quantum yield with and without internal conversion, respectively. k_{Fo} is the radiative decay rate for crude oils. Eq. 16 has been used to fit the quantum yield data presented in Figure 26. ϕ_o has been set equal to 0.85 instead of unity allowing for small but typical intersystem crossing for aromatic hydrocarbons.[31] Table 1 shows that k_{Fo} is about 10^9/sec for crude oils, thus, the two parameter fit gives $A \sim 10^{12}$ and $\alpha \sim 3500$ cm^{-1}. The frequency factor A has the correct magnitude for vibrationally induced processes. The energy parameter roughly equals the highest vibrational frequencies of the molecule. Essentially, the overlap of the respective ground and excited vibrational states decreases with increasing differences in the quanta of excitation where $\Delta E/\alpha$ roughly gives the mismatch of the number of quanta.[51] For λex = 350 nm, the number of quanta mismatch is about 9. Coupling through the highest energy vibrational modes reduces the quanta mismatch producing larger probabilities.[31]

The fit of Eq. 16 to the quantum yield data is quite good inspiring confidence in this analysis. Thus, the huge variation of quantum yield on excitation wavelength appears to be governed primarily by the systematics of rates of internal conversion. Furthermore, crude oils seem to represent a good system to confirm the validity of Eqs. 15 and 16. In spite of the expected wide applicability,[31] few systems, such as a group of selected pure compounds, properly demonstrate the energy gap law because idiosyncratic molecular properties tend to dominate. The very large number of contributing fluorophores in crude oils tends to average out individual molecular differences so that general trends can be observed, such as the energy dependence of internal conversion. Figure 27 plots, for many crude oils (including Vixburg crude oil of Figure 26), the relative dependence of the dilute-solution quantum yield on excitation wavelength.[34] All crude oils exhibit the same relative decline in quantum yield with increasing excitation wavelength, and are thus subjected to the governing principles of Eq. 15 and 16. Again, the systematic behavior of crude oils illustrates the strong correlation of their aromatic components.

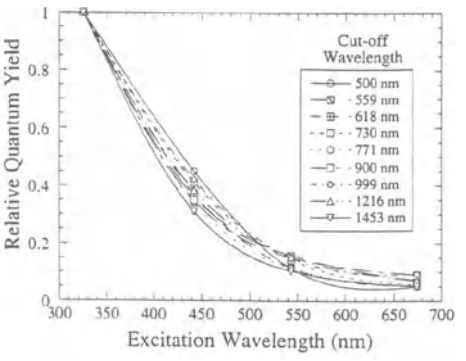

Figure 27. The dependence of the relative quantum yields on excitation wavelength for all crude oils is nearly the same. All crude oils exhibit the Energy Gap Law. This uniformity implies that the different crude oils have similar chromophores. The fraction of optical absorption due to large chromophores (which are less fluorescent) is greater for heavier crude oils and asphaltenes thereby reducing their quantum yields.

Figure 22 shows that dilute crude oils exhibit somewhat different absolute quantum yields. Different crude oils most likely have the same fluorophores for each spectral range measured. However, the crude oils do not possess the same ratios of these chromophores (in different total concentration). Otherwise, in the dilute limit the crude oils would be indistinguishable; yet their quantum yields differ. Heavy crude oils have a large fraction of optical absorption from large aromatics with their small quantum yields. Thus, the integrated quantum yield of dilute heavy crude oils is lower. For example, for 325 nm excitation, the quantum yield ratio for dilute solutions is ~2.5 for the lightest and heaviest crude oil shown in fig. 22. The implication is that for heavy crude oils, less than half of the absorption at 325 nm, is accounted for by large HO-LU gap molecules of large quantum yield. The other ~60% of the absorption in heavy crude oils is accounted for by small HO-LU gap molecules of small quantum yield. Correspondingly, the fluorescence spectra of dilute heavy crude oils show large red-shifts compared to corresponding spectra of light crude oils, as will be shown in the next section of this chapter.

Figure 28 plots the quantum yields at different excitation wavelengths for dilute solutions of an asphaltene, a resin, a crude oil without asphalt, and the whole oil. As expected, the quantum yields of the whole oil are bracketed by those of the oil constituents. The asphaltene quantum yield at 325 nm is even lower than that of the heaviest crude oil (25%) indicating that the asphaltene has the smallest proportion of small, blue-emitting chromophores. These smaller ring systems, which asphaltenes lack, have higher quantum yields than the larger ring systems. Thus, the asphaltenes are characterized by lower quantum yields, and heavy crude oils, with higher asphaltene fractions, also exhibit decreased fluorescence emission. For some crude oils, half of the optical absorption is due to their asphaltene fraction (depending on wavelength), this absorption will not produce much fluorescence emission.

The quantum yields of the resin and the crude oil without asphalt are similar in the spectral range investigated. The crude oil without asphalt is deficient of large aromatics consequently yielding large quantum yields. In addition, the resin also lacks large chromophores; it also has large quantum yields. The size of resin molecules is limited by the requirement of heptane solubility. For the longest wavelengths of excitation, the quantum yield of the whole crude oil is nearly equivalent to that of its asphaltene but much lower than the quantum yields of the resin and crude oil without asphalt. This is because the bulk of optical absorption of the oil for long wavelengths is due to the asphaltene fraction. For shorter wavelengths, the whole oil quantum yield approaches that of the resin and crude

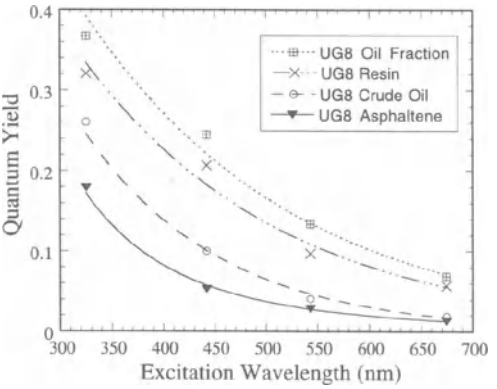

Figure 28. The quantum yields of UG8 samples: the asphaltene, resin, and oil fraction (crude oil without asphaltene and resin). The oil fraction and resin exhibit larger quantum yields throughout the spectral range due to their lack of large aromatic chromophores (which have small quantum yields). The quantum yield of the whole crude oil is similar to that of the asphaltene at long wavelength because here optical absorption of the crude oil is due its asphaltenes. At short wavelength the oil fraction and resins account for more optical absorption in the crude oil, so the quantum yield of the crude oil approaches those of the lighter fractions.

oil without asphalt fraction and is much higher than the quantum yield of the asphaltene. The optical absorption of the whole oil for the short wavelength range is largely due to the small chromophores. Because the asphaltene is deficient in small chromophores, the asphaltene contributes less to optical absorption in this spectral range.

5.4. Fluorescence Spectra

Energy transfer (Eq. 9) interactions of fluorophores produce large, measurable spectral effects in complex fluorophore mixtures such as crude oils. Energy transfer between dissimilar molecules always occurs from the molecule of larger HO-LU gap to the molecule of smaller HO-LU gap, where the excess energy is rapidly thermalized. Consequently, photoemission subsequent to energy transfer is characterized by a red-shift relative to the spectrum obtained from the initially excited molecule.

Figure 29 shows the fluorescence emission spectra of ten crude oils for many excitation wavelengths (300 nm, 350 nm, 400 nm, 470 nm, 543 nm, 674 nm, 790 nm, and 838 nm).[33] The left side of the figure shows spectra for neat crude oil solutions while the right side shows spectra for crude oils in the dilute limit. The crude oils in all figures are listed in order of cut-off wavelength (essentially lighter to heavier). The laser source peak is clearly seen in the four spectra obtained with longer wavelength excitation, due to scattered light from the sample. The fluorescence emission spectra show that there are a variety of fluorophores involved in the production of fluorescence from the crude oils. There is a large difference between the neat and dilute crude oil spectra for short wavelength excitations, thus collisional energy transfer is very important for high concentrations. Also, at short excitation wavelengths, there are significant variations in the spectra for different crude oils, particularly for the neat samples. Therefore, the particular distribution of fluorophores and their concentration strongly affect the fluorescence spectral profiles. The difference between spectra of neat and dilute crude oils decreases with increasing excitation wavelength. Also, the differences among spectra of different crude oils decrease with increasing excitation wavelength. Evidently, collisional energy transfer (with subsequent fluorescence emission) becomes less important for longer wavelength excitations even for very high concentrations associated with heavy crude oils. For long wavelength excitation, quenching, not energy transfer dominates the collisional processes due to the low quantum yields associated with small HO-LU gap chromophores.

Figure 30 confirms that energy transfer is a primary factor producing large spectral differences among crude oils for short wavelength excitation. The fluorescence spectra with 316 nm excitation of North Sea, a lighter crude oil and Sales, a heavier crude oil are plotted in Figure 30 as a function of oil concentration. With successive dilutions, the spectra of the crude oils show monotonically decreasing red-shifts. For higher chromophore concentrations, multiple energy transfer collisions cause greater red-shifts in fluorescence emission. The near equivalence of the spectra of neat North Sea crude oil and Sales crude oil dilute by a factor of 5 shows the concentration difference of these two crude oils. These two crude oils showed the same factor of 5 difference in concentration in analyses of fluorescence lifetimes (Figures 19, 20) and quenching (Figure 24). The convergence of results on the independent measurements of spectra, lifetimes and quantum yields produces strong validation of the underlying framework (Eqs. 7–11).

Figure 31 is a comparison of spectra for neat and dilute samples of a light oil (Brunei) and a heavy oil (Sales) at 300 nm, 470 nm, and 790 nm excitation wavelengths. Increasing the concentration of crude oils results in an increase in collisional energy transfer at 300 nm excitation as seen from the large red-shift for the neat samples of both the

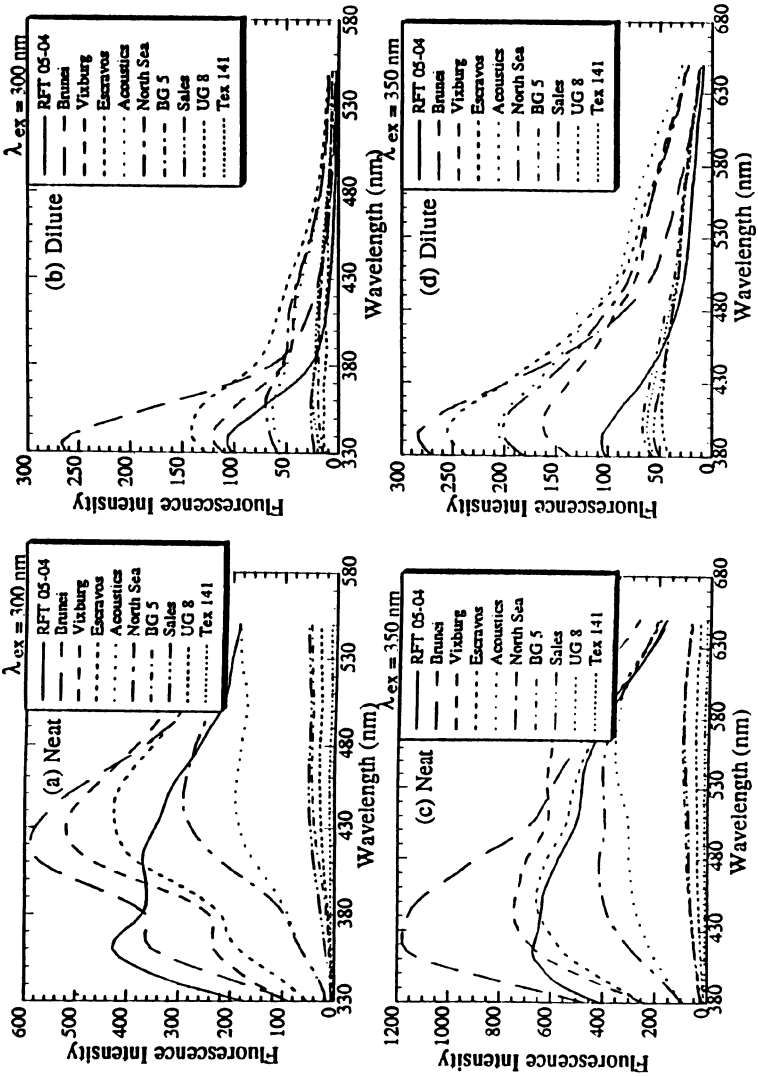

Figure 29a-p. Fluorescence emission spectra for ten crude oils (listed light to heavy) for neat and dilute samples for a series of excitation wavelengths from the ultraviolet to the near-infrared. Large collisional energy transfer produces differences between spectra for neat and dilute solutions with short wavelength excitation. Collisional energy transfer is nearly absent for long wavelength excitation where the spectra for neat and dilute solutions are nearly identical.

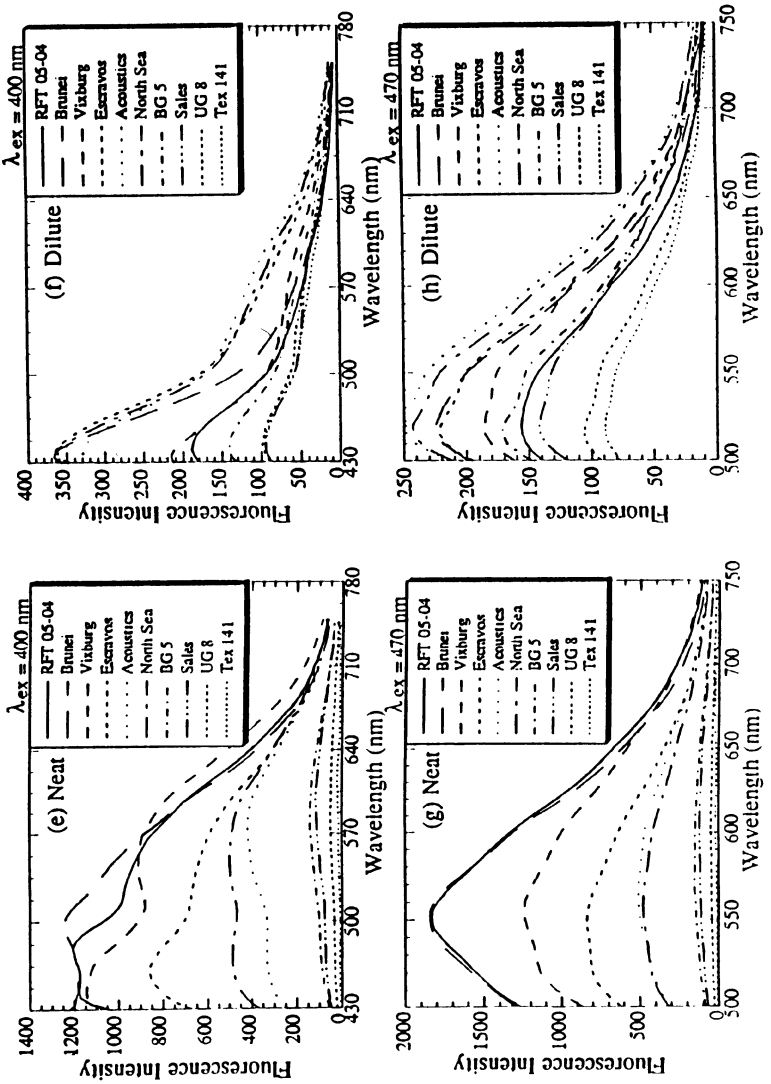

Figure 29. *(Continued)*

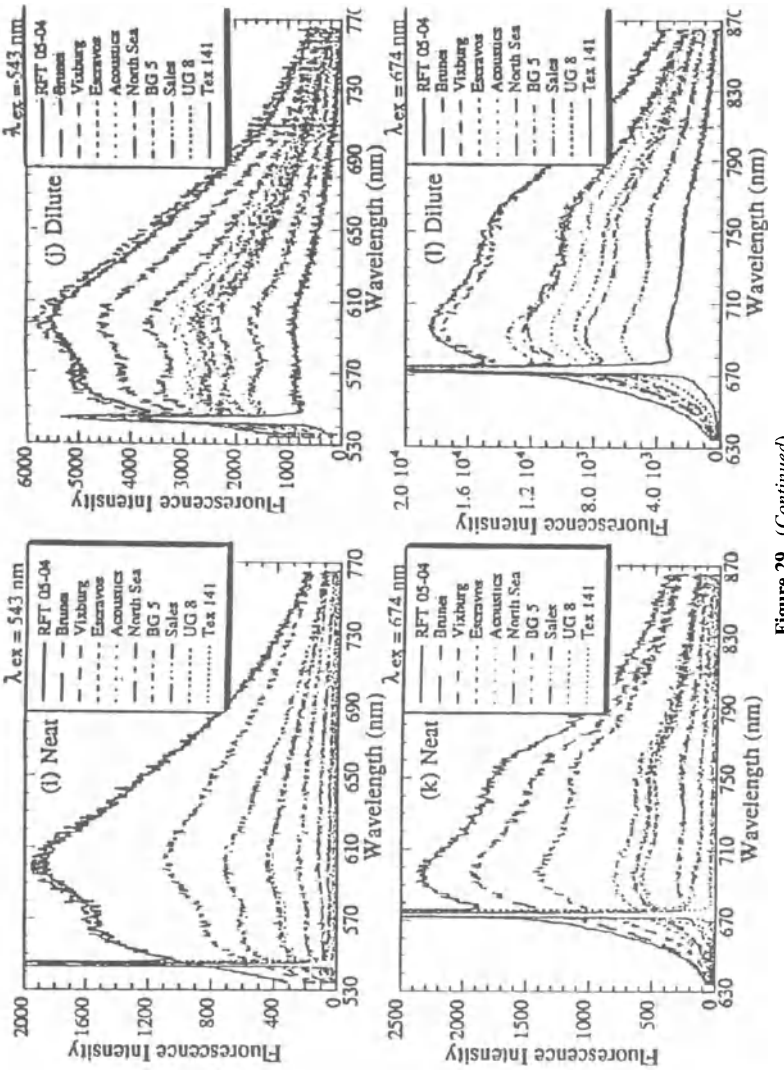

Figure 29. (*Continued*)

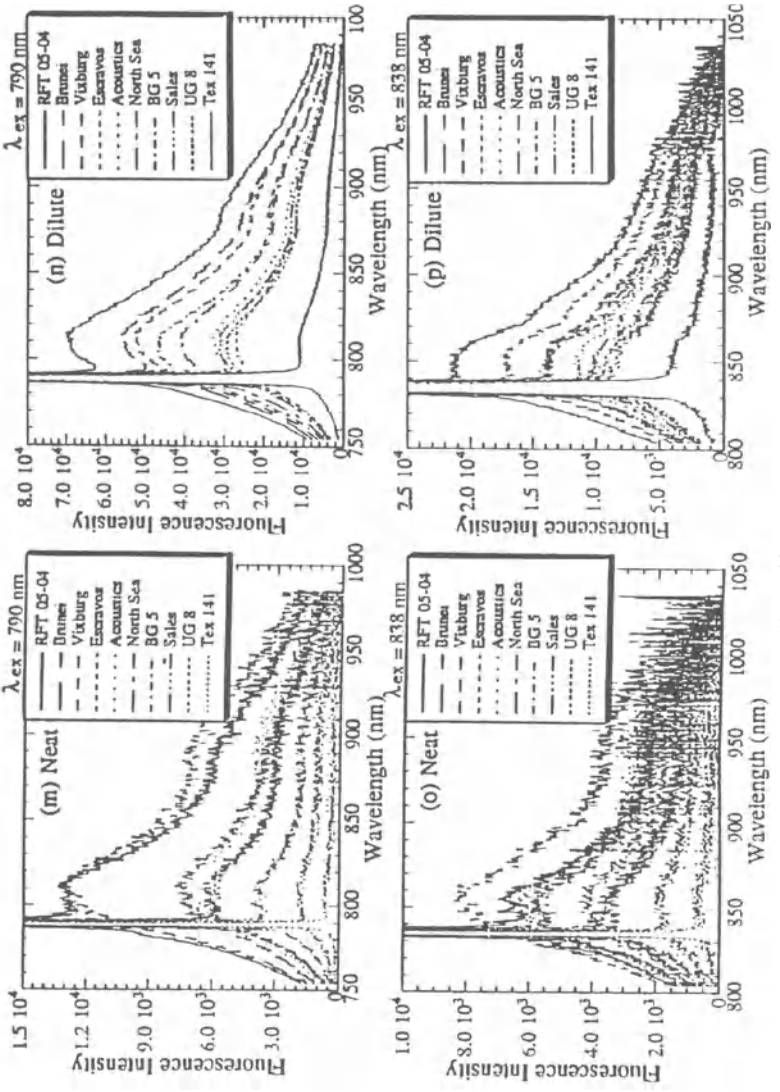

Figure 29. (*Continued*)

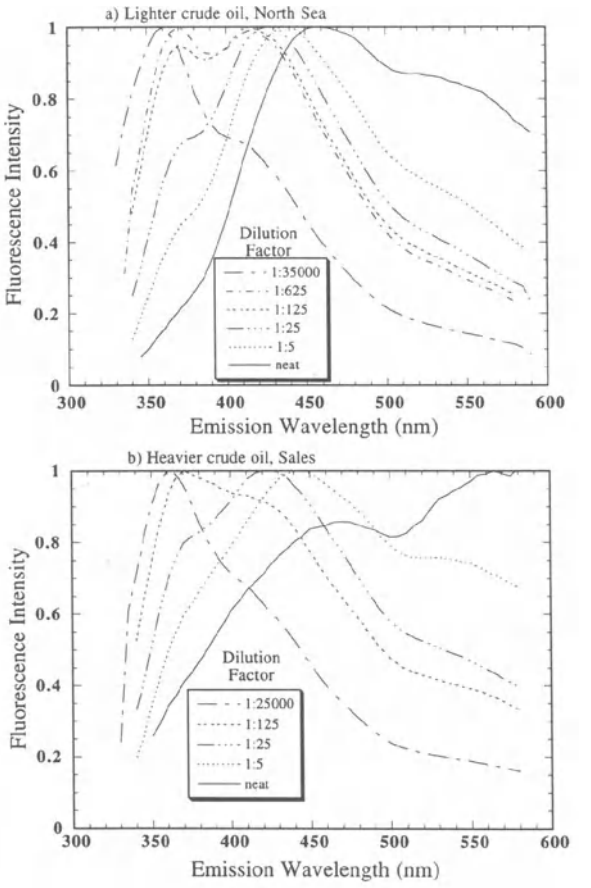

Figure 30. The emission spectra with 316 nm excitation for a) North Sea, a lighter crude oil and b) Sales, a heavier crude oil at different concentrations. A substantial red-shift with increasing concentration results from energy transfer.

light and heavy crude oils. The spectral red-shift in going from dilute to neat crude oils is evident for 470 nm excitation, but to a lesser extent. However for 790 nm excitation, there is no red-shift; the spectra of the neat and dilute solutions are nearly identical for each oil. Therefore, the collisional energy transfer effects are shown to decrease with increasing excitation wavelength. A quantitative analysis of energy transfer can be performed by using the spectral analysis as shown in Figure 32. The spectrum for the dilute crude oil is considered to be intrinsic, not influenced by energy transfer. The spectrum is normalized as shown in Figure 32 such that its maximum intensity at any wavelength equals but does not exceed that of the neat crude oil. The area under the normalized spectrum is compared to the area under the spectrum for the neat crude oil solution to determine the fractional change in the emission spectrum in going from the dilute to the neat limit, thus yielding the percent of energy transfer. The dotted spectrum in Fig. 31 illustrates this graphical determination of the fraction of energy transfer.

Figure 33 shows the fraction of energy transfer vs excitation wavelength for three crude oils ranging from light to heavy.[33] The fraction of energy transfer varies between ~1 to ~0 which is the maximum possible range of this parameter. The variation of energy transfer depends strongly and monotonically on the excitation wavelength. For short

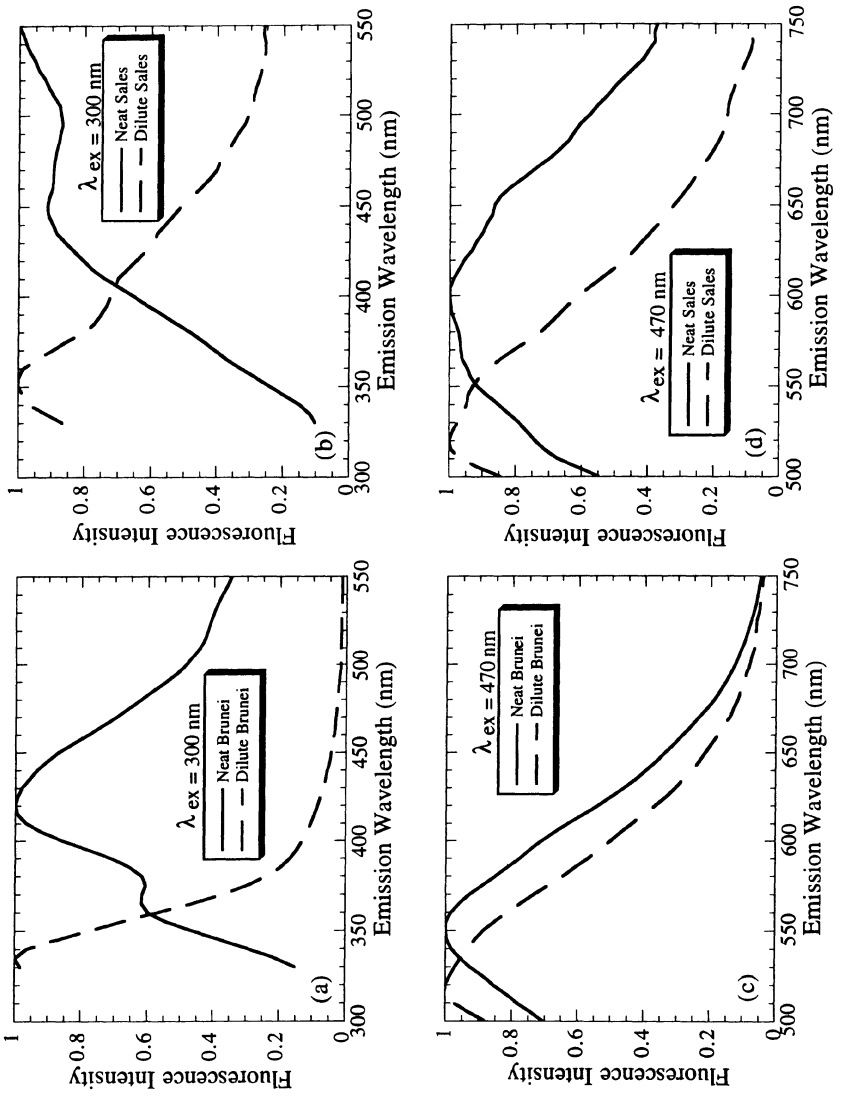
Fluorescence Intensity
Emission Wavelength (nm)
λ ex = 300 nm
Neat Brunei
Dilute Brunei
(a)
λ ex = 300 nm
Neat Sales
Dilute Sales
(b)
λ ex = 470 nm
Neat Brunei
Dilute Brunei
(c)
λex = 470 nm
Neat Sales
Dilute Sales
(d)

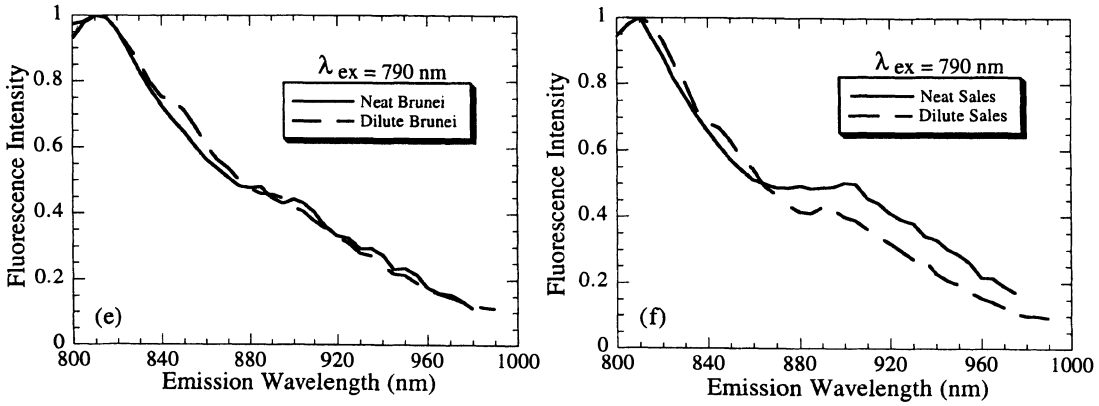

Figure 31. Fluorescence emission spectra for neat and dilute solutions of a light (Brunei) and a heavy (Sales) crude oil for 300 nm, 470 nm, and 790 nm excitation wavelengths. Collisional energy transfer produces large spectral differences between neat and dilute solutions for short excitation wavelengths. For 790 nm excitation, spectra for neat and dilute crude oils are the same; collisional energy transfer effects are absent.

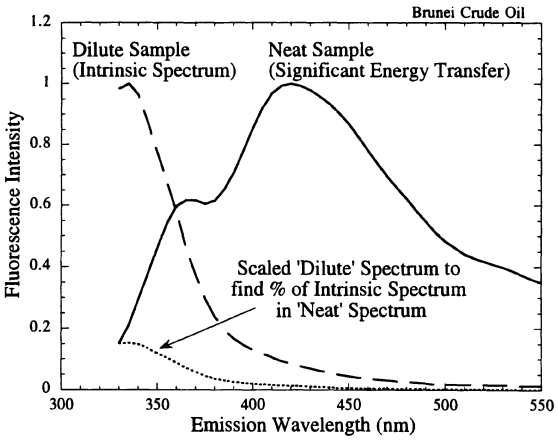

Figure 32. Energy transfer effects can be quantified with graphical analysis. The dilute sample exhibits no energy transfer so provides the intrinsic spectrum. The neat sample suffers from extensive red-shifts from energy transfer. The maximum fraction of the dilute sample fluorescence spectrum present in the neat sample spectrum is determined by normalizing the dilute sample spectrum to just 'fit in' the neat spectrum. The fractional area occupied by the dilute spectrum gives the intrinsic emission. This approximate procedure is sufficient because the extent of energy transfer varies tremendously.

wavelength excitation, nearly 90% of the fluorescence emission for neat crude oils results from collisional energy transfer. For longer wavelength excitations, virtually none of the fluorescence emission results from collisional energy transfer. This large dependence of energy transfer on excitation wavelength is almost independent of crude oil type. Yet, the different crude oils differ dramatically in their chromophore and fluorophore concentrations. With regard to energy transfer, all crude oils (except perhaps the very lightest) are in the high concentration limit. Therefore, the fraction of energy transfer is almost independent of the exact value of the large chromophore concentration. There is a small dependence of the collisional energy transfer on crude oil type. Heavier crude oils, with their much high chromophore concentration, show slightly more collisional energy transfer.

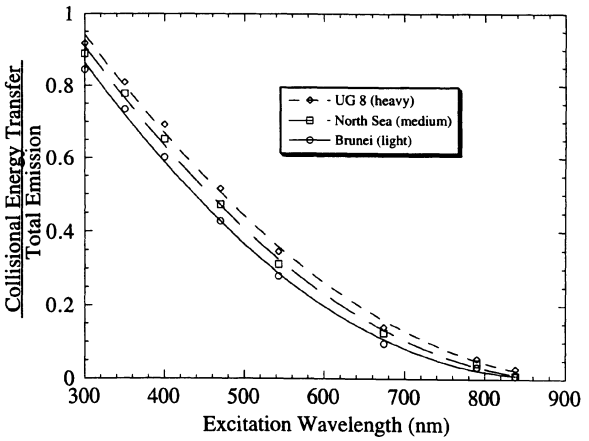

Figure 33. The ratio of energy transfer to total emission plotted vs excitation wavelength for three crude oils ranging from light to heavy exhibits several systematic trends. Collisional energy transfer varies from nearly 100% for the shortest wavelength excitation to nearly 0% for the longest wavelength excitation. All crude oils show nearly the same behavior. Thus, for crude oils, the fraction of collisional energy transfer is not a function of chromophore concentration; all crude oils are in the high concentration limit. The heavier crude oils exhibit slightly higher energy transfer due to higher chromophore concentrations.

Figure 34 plots both the energy transfer for the neat sample and the quantum yield for the dilute sample. The strong correlation shown in Figure 34 leads to the following explanation: as the concentration of a crude oil increases, more interactions occur among chromophores. With short wavelength excitation, small blue-absorbing and emitting chromophores are excited preferentially because of their larger number than red emitting chromophores. With intermolecular interaction, the excitation energy passes to the numerous slightly larger chromophores. Because their bandgap is large, their quantum yields are large so fluorescence results. With a sufficient number of interactions, almost all molecules which were initially excited will transfer their energy to chromophores with a somewhat smaller HO-LU gap producing red-shifted emission. For long wavelength excitation, only a small fraction of chromophores are fluorescent. If an excited fluorophore interacts with another large chromophore, it is most probably with a nonfluorescent chromophore. Thus, quenching is the end product of intermolecular interactions with these red-absorbing chromophores. The little fluorescence emission which results upon red excitation is from the few initially excited chromophores which have not been quenched. Figure 29 shows that as the excitation wavelength increases, the Stokes shift decreases and the relative magnitude of the hot bands (excitation from vibrationally excited states) increases. Even the small decrease in energy across the spectral range increasingly favors quenching over energy transfer in collisional processes for longer excitation wavelengths.

6. SMALL AROMATICS AND ASPHALTENES

6.1. No Short Wavelength Emission from Asphaltenes

The fluorescence emission spectra for short wavelength excitation (265 nm) are shown for two asphaltenes in Figure 35. In this figure, the asphaltene spectra are contrasted with the fluorescence emission spectrum of a light crude oil in which the spectral

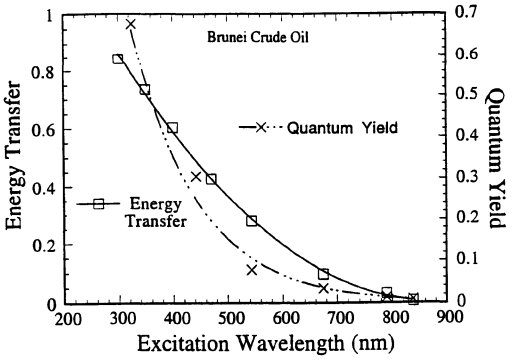

Figure 34. The fraction of fluorescence emission which results from energy transfer varies from ~100% to 0% with excitation wavelength. The cause of this large variation is the intrinsic (dilute solution) quantum yield of the chromophores involved in the intermolecular interactions. Energy transfer from chromophore interactions to a large HO-LU gap molecule is likely to result in emission due to their large quantum yields. Interactions involving small HO-LU gap chromophores produce only quenching due to tiny intrinsic quantum yields. Consequently, fluorescence spectra for neat crude oils are different for short wavelength excitation, depending on which fluorophores receive the excitation energy. With long wavelength excitation, intermolecular interaction produces only quenching, so all crude oil spectra are independent of concentration, and are the same.

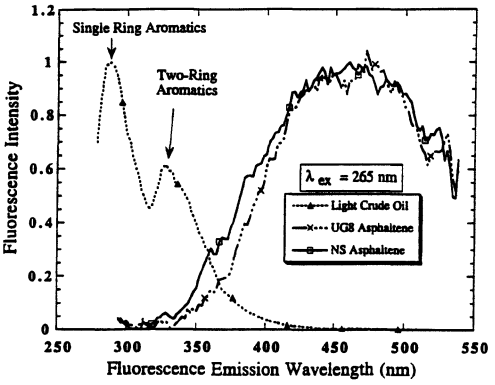

Figure 35. Fluorescence emission spectra of two asphaltenes and a light crude oil. For the crude oil, emission from 1 and 2 ring aromatics is identified. The asphaltenes lack significant spectral emission from these small aromatics. As will be shown intramolecular energy transfer is negligible; thus, asphaltenes lack small ring systems.

contribution from single ring aromatics and 2 fused-ring aromatics are observed as distinct emission maxima. The spectral range for emission from single aromatic rings is about 290 nm and from two ring aromatics is about 330 nm. The asphaltenes exhibit emission from large aromatic ring systems, with the emission maxima in the range of 450 nm to 500 nm but exhibit very little (yet finite) emission from 1 to 3 ring aromatic systems.[52]

Different spectral regions are correlated with the size of aromatic ring systems with varying degrees of confidence. Substituents, heteroatoms and different solvents can alter absorption and emission wavelengths for individual compounds. For multiple fused rings, structures with larger aspect ratio (kata-condensed) such as linear systems tend have absorption and emission shifted towards longer wavelengths than for structures with a small aspect ratio (peri-condensed). There is only a small variation in band locations for single rings systems, and larger variations for larger numbers of fused rings (e.g. 5 ring systems). Thus, the spectral range corresponding to small numbers of rings can be assigned with greater confidence.

Figure 36 shows the emission spectra for two asphaltenes for various excitation wavelengths. Figure 36a shows two spectra for NS asphaltene obtained with excitation at 265 nm and 290 nm. Both spectra in Figure 36a are quite similar and lack short wavelength emission. Figure 36b shows fluorescence emission spectra obtained for three excitation wavelengths (265 nm, 290 nm, and 340 nm) for UG8 asphaltene. Again, the emission spectra are fairly similar, all exhibiting a lack of short wavelength emission. This lack is not strongly affected by excitation wavelength, thus does not result from a peculiarity in the absorption spectra.

The correlation of the fluorescence emission spectra of asphaltenes with the population distribution of aromatic rings assumes that the fluorescence spectra are unaltered by inter- and intramolecular interactions. This chapter shows that fluorescence spectra can be significantly altered by electronic energy transfer between molecules. For instance, the fluorescence spectra of crude oils show significant red-shifts at high concentrations of crude oil solutions due to energy transfer. The red-shift occurs because, upon molecular collisions, electronic excitation energy is irreversibly transferred from molecules with larger electronic energy (thus short wavelength emission) to molecules with smaller electronic energy with concomitant thermalization of some of the excitation energy. The issue remains whether small aromatic moieties are present in asphaltenes, but do not fluoresce due to energy transfer. Here, we establish that the asphaltene solutions are not significantly influenced by inter- or intramolecular interactions by monitoring fluorescence spec-

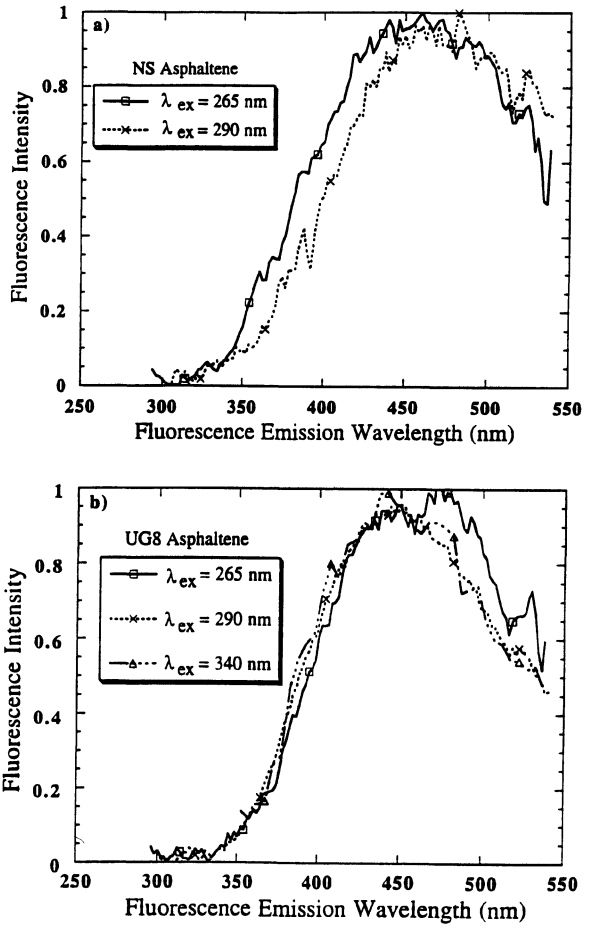

Figure 36. The fluorescence emission spectra of asphaltenes a) NS and b) UG8 are fairly insensitive to excitation wavelength indicating that the lack of emission from small aromatic rings is not caused by specifics of the asphaltene absorption spectrum.

tra and lifetime with increasing dilution. Intramolecular energy transfer effects are ruled out by our lifetime analyses of asphaltenes and de-asphaltened oils Thus, the correlation of fluorescence emission spectra with aromatic ring distributions can be made.

6.2. No Intramolecular Energy Transfer in Asphaltenes

In crude oils, molecular processes which give rise to electronic energy transfer, thus spectral shifts, also produce quenching. These processes provide other de-excitation pathways in addition to radiative decay. Thus, molecular energy transfer and collisional quenching necessarily result in a reduction of excited state lifetimes of electronically excited molecules. Eq. 17 gives the decay rate for a fluorescent molecule in solution.

$$k_F = k_{Fo} + k_Q[Q] + k_{ET}[Q'] + k_{Q^*} + k_{ET^*} \quad (17)$$

k_F is the measured fluorescence decay rate, k_{Fo} is the intrinsic fluorescence decay rate of the fluorophore (or of the initially-excited fluorophore moiety in a molecule containing

multiple fluorophore moieties). k_Q is the collisional decay rate with the quenchers of concentration [Q]. k_{ET} is the intermolecular energy transfer rate with fluorophores of concentration [Q']. k_{ET*} is the intramolecular energy transfer rate for the transfer of electronic excitation energy between two aromatic moieties within the same molecule, and k_{Q*} is the corresponding intramolecular quenching rate. Intermolecular effects can be eliminated by simple dilution as we have done here. The intramolecular processes of energy transfer and quenching are independent of concentration but dependent on molecular structure and molecular conformation. As collisional quenching and intermolecular energy transfer increase, for instance due to increased concentrations, the decay rate increases; thus, the measured fluorescence decay rate k_F increases. This decrease in lifetime can be monitored directly, as has been done for solutions of different crude oils of various concentrations.

The inextricable link between the spectral fluorescence red-shift induced by energy transfer and the reduction of excited state lifetimes (and reduction of fluorescence quantum yield) has been established for crude oils. Consequently, the extent of red-shift due to intra- and intermolecular energy transfer can be monitored by determining the extent of fluorescence lifetime reduction. Here we verify the concepts for asphaltenes and use lifetime measurements to determine the extent of spectral red-shift induced by energy transfer processes.

Figure 37a shows the fluorescence decay curves for dilute solutions of NS asphaltene and NS de-asphaltened crude oil (DAO) for excitation at 290 nm and emission at 330 nm.[52] In addition, the decay curve obtained for a concentrated solution of NS asphaltene (~10% by weight) is shown. This spectral range corresponds to excitation and emission of 2 ring aromatic moieties. The decay curve for the dilute asphaltene solution has relatively long lifetimes, as indicated in the figure; a few nanoseconds for the short component and a little over 12 ns for the long component. Typical fluorescence lifetimes of organic molecules are in the range of several to tens of nanoseconds. The fluorescence decay curves of crude oils also yield two fluorescence lifetimes, and the magnitudes are nearly the same as found for the asphaltenes. The fluorescence lifetimes of crude oils decrease considerably when energy transfer and quenching effects dominate. Figure 37a shows that a single, very small lifetime is obtained for the concentrated asphaltene solution, where quenching and energy transfer dominate excited state decay. The long lifetimes obtained for dilute asphaltene solutions indicate that energy transfer and quenching effects are not dominant for the 2 ring aromatics in asphaltenes.

The intrinsic fluorescence lifetimes for the asphaltene solutions are not known; however, a very good estimate for these values can be obtained from the dilute DAO solutions. Figure 37a shows that the dilute asphaltene and DAO solutions yield nearly the same decay curves for 2 ring aromatics. The low concentration of the solutions ensures that intermolecular effects are negligible. This was checked by observing no change in decay rates for increasing dilution. Furthermore, the DAO molecules in general do not contain two fluorescent moieties in one molecule, so do not suffer from appreciable intramolecular energy transfer. Yet, large energy transfer effects are observed for the concentrated asphaltene solution where a single, very small lifetime is measured. Thus, the similar decay curves for the asphaltene and the DAO indicate that the asphaltene also does not suffer from significant intramolecular energy transfer; the decay curve, and thus the asphaltene fluorescence spectrum are intrinsic.[52] The asphaltene lacks substantial emission from the 2 ring aromatics because they contain only a small population of these ring systems, not because of spectral perturbation from energy transfer.

The lack of significant intramolecular energy transfer does not necessarily mean that only one chromophore group resides in a single molecule. In fact, it is expected that those

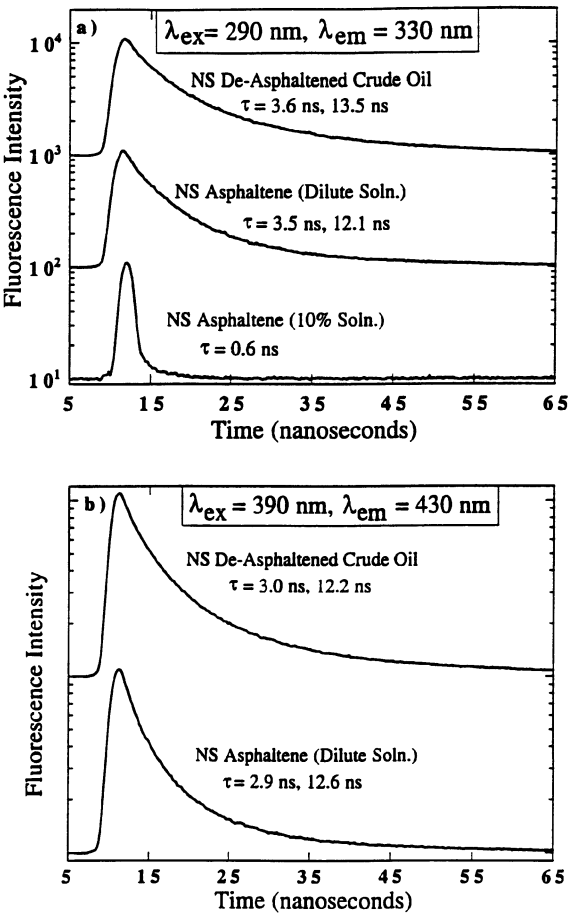

Figure 37. Fluorescence lifetime decay curves are shown for a) 2 ring aromatics and b) roughly 4 to 7 ring aromatics for NS asphaltene and NS de-asphaltened oil (DAO). Long fluorescence lifetimes are obtained for dilute asphaltenes; and these lifetimes are similar to those of the DAO. Thus, the dilute asphaltenes do not exhibit significant inter- or intramolecular energy transfer; the lifetimes, thus the fluorescence spectra are intrinsic. The concentrated asphaltene solution has a very short lifetime, here, for the 2 ring aromatics, due to rapid intermolecular energy transfer which also results in red-shifted spectra.

asphaltene molecules with a 1 or 2 ring aromatic group also have a second chromophore group elsewhere in the molecule; otherwise, the molecule would be soluble in heptane and would not be in the asphaltene fraction. The examination of various bichromophore molecules reveals that energy transfer or other intramolecular interactions become predominant only when the conformational geometry is optimal.[53] The emission spectra of a series of α,ω-di-3-pyrenyl alkanes (two pyrene groups connected by an alkane chain) show that if the chain length is too short or too long, then the emission is predominantly from the monomer. For chain lengths between 3 and 6 carbon atoms, there is substantial emission from both the monomer and the dipyrene excimer. Pyrene has an unusually long lifetime of ~500 ns, and alkyl chains are quite flexible so these molecules are optimal for observing intramolecular effects. For fluorophore groups with much shorter lifetimes, and more rigidly held, as would be expected for asphaltenes, the lack of intramolecular interactions between two chromophores can easily be understood. Nevertheless, if the small estimates of molecular weight for asphaltenes are correct (e.g. ~900), our results, that small aromatic rings are not generally present in asphaltenes, imply that many asphaltene molecules possess only one chromophore group.

Figure 37b shows fluorescence decay curves for dilute solutions of NS asphaltene and NS DAO for excitation at 390 nm and emission at 430 nm. This spectral range corresponds to fluorophores with very roughly 4 to 7 fused aromatic rings. Again, the asphaltenes exhibit relatively long lifetimes which are similar to the intrinsic fluorescence lifetimes found for crude oils. This implies that energy transfer effects are not very significant. Again, the asphaltene lifetimes are very similar to the DAO lifetimes, indicating that the measured asphaltene lifetimes are intrinsic. That is, $k_F \sim k_{Fo}$ in Eq. 17 because the other decay rates are very small. Figure 38 shows fluorescence decay curves for UG8 asphaltene and UG8 DAO illustrating that our observations are general. The lifetimes show that spectra of dilute asphaltenes are unaffected by inter- or intramolecular interactions for two-ring aromatics and for larger ring systems. Concentrated asphaltene solutions show large reductions of lifetimes due to intermolecular interactions.

Figure 39 shows the fluorescence decay curves for solutions of various concentrations of UG8 asphaltene. The excitation wavelength, 316 nm, and emission wavelength, 370 nm, correspond roughly to 3 and 4 ring aromatics. Energy transfer and quenching have an increasing impact on fluorescence lifetimes as the concentration increases. If the dilute asphaltene solutions exhibited some but not overwhelming intramolecular energy transfer, a moderate reduction in fluorescence lifetimes should be detectable, comparable to the measurable collisional effects for moderately concentrated solutions of asphaltenes. No significant intramolecular effects are detected in the decay curves; the fluorescence

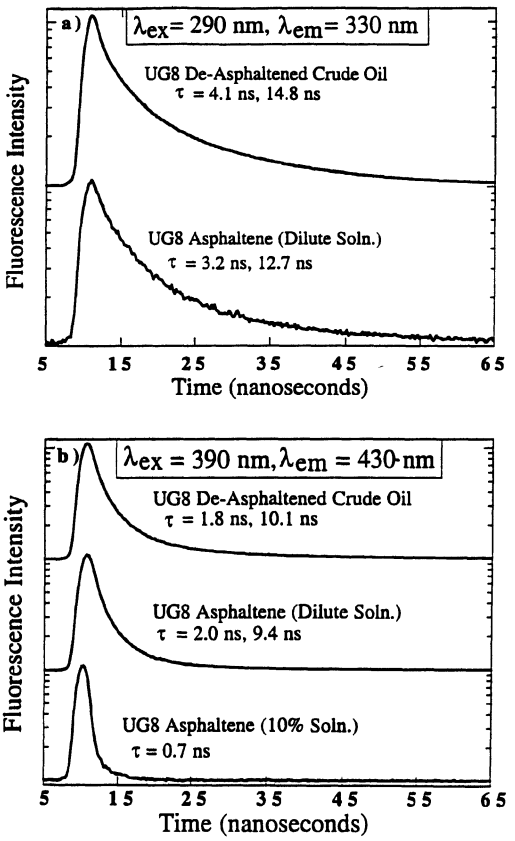

Figure 38. Fluorescence lifetime decay curves are shown for a) 2 ring aromatics and b) roughly 4 to 7 ring aromatics for UG8 asphaltene and UG8 de-asphaltened oil (DAO). Long fluorescence lifetimes are obtained for dilute asphaltenes, and these lifetimes are similar to those of the DAO. Thus, the dilute asphaltenes do not exhibit significant inter- or intramolecular energy transfer; the lifetimes, thus the fluorescence spectra are intrinsic. The concentrated asphaltene solution has a very short lifetime, here, for the larger aromatics, due to rapid intermolecular energy transfer which also results in red-shifted spectra.

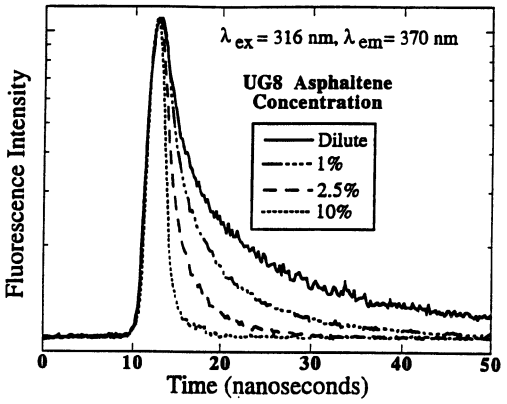

Figure 39. Fluorescence decay curves for UG8 asphaltene at different concentrations. Moderate degrees of intermolecular energy transfer are readily detected in fluorescence lifetimes. The nearly identical lifetimes for asphaltenes and DAO'S (Figures 37 and 38) indicate that no energy transfer takes place for dilute asphaltenes; the fluorescence emission spectra are intrinsic.

lifetimes and, thus, the fluorescence emission spectra of dilute asphaltene solutions are intrinsic. The fluorescence emission spectra can be used to ascertain population distributions of different sized aromatic rings.

6.3. Aromatic Ring Sizes of Asphaltenes

The examination of spectra from several asphaltenes reinforces the general conclusion that asphaltenes lack short wavelength emission. Figure 40 shows fluorescence emission spectra with 290 nm excitation from five asphaltenes. Some variability is observed in the asphaltene spectra implying differences in their aromatic ring populations. Nevertheless, the

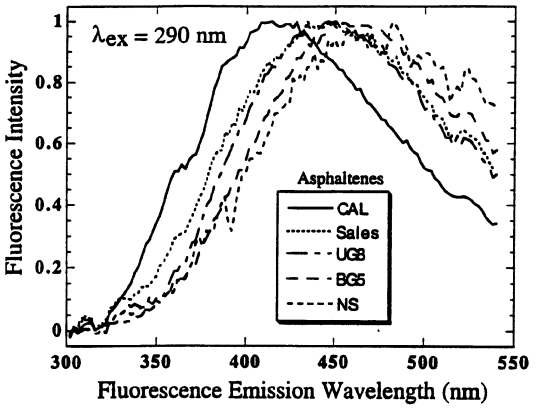

Figure 40. Fluorescence emission spectra for five asphaltenes; all asphaltenes lack emission from small aromatic molecules due to their low population in asphaltenes. The asphaltene with the greatest fraction of short wavelength emission (thus smallest aromatic rings) CAL, is known to be very polar with its large aliphatic sulfoxide content. Thus, for asphaltenes, higher polarity correlates with smaller aromatic rings.

unifying characteristic of the asphaltene spectra is the lack of emission in the short wavelength region. Because energy transfer effects are absent, the spectra are intrinsic. The much larger fluorescence emission of dilute asphaltene solutions at 400 nm than at 330 nm corresponds to a much larger population of large fused-ring systems than of 2 ring aromatics. By inference, the very small fluorescence emission of asphaltenes at 290 nm with 265 nm excitation indicates a very small population of single ring aromatics in asphaltenes as well. Bulk examination of these population ratios have not been achieved by any other method.

In a related system, coal pyrolysis tars, almost no fluorescence emission was observed below 300 nm with 260 nm excitation.[54] Using spectral analysis, intramolecular excimer formation was ruled out as a source for this lack of emission. However, the extent of intramolecular energy transfer was not determined. Perhaps the lack of short wavelength emission in these tars results from the lack of small aromatic ring systems.

For these asphaltenes, the asphaltene CAL exhibits anomalously large emission at shorter wavelengths indicating that this asphaltene has a larger fraction of smaller aromatic rings. Among these asphaltenes, CAL asphaltene has, by far, the highest content of sulfoxide,[27,55] which is a very polar chemical group. CAL is 2.6% sulfur by weight, of which 44% is sulfoxide; the sulfoxide fraction of the other asphaltenes is below 10%. Higher polarity of asphaltene molecules correlates with smaller molecular weight.[56] Our results show a similar inverse correlation between polarity and aromatic ring size. These inverse correlations follow from the definition of asphaltenes. In order for an organic molecule to be insoluble in heptane, it can have either high polarity or large molecular weight. Our results extend this concept; to be heptane insoluble, a molecule can be nonpolar but with a large aromatic ring system, or be polar with a smaller ring system. The sulfoxide sites are predominantly alkyl sulfoxides, not aromatic sulfoxides,[27] so molecular solubility is influenced by a combination of different functional sites.

Asphaltenes exhibit very little fluorescence emission in the spectral range at 290 nm corresponding to single ring aromatics and at 325 nm corresponding to 2 ring aromatics. This emission constitutes less than 1% of the total. In addition, asphaltenes show little emission in the spectral range at 370 nm corresponding roughly to 3 ring aromatics. We use these observations as a guide to indicate the relatively small populations of small aromatic ring systems in asphaltenes, compared to larger ring systems. However, it is difficult to determine precisely these population ratios due to the molecular complexity of asphaltenes and the unknown optical constants of the contributing structures. Destructive studies of asphaltenes have seen the presence of single ring aromatics.[57] However, the relative population of single ring aromatics to multiple ring systems was not determined. In fact, the fluorescence studies reported here also detect the presence of single ring aromatics. In addition, the fluorescence studies determine that the single ring systems are present in relatively low concentration.

The maximum fluorescence emission for asphaltenes occurs near 450 nm with significant fluorescence intensity out to 550 nm. It has been shown that many aromatic rings systems with 7 to 11 rings and without heteroatoms fluoresce with maxima in the 430 nm to 500 nm range.[58–60] The replacement of carbon with heteroatoms typically results in a red-shift of the fluorescence maximum if there is any spectral effect.[61] Thus, we estimate that the most predominant fused-ring systems present in asphaltenes are in the range of 4 to 10 rings. In addition, the Urbach tail results show an exponential decline of very large ring systems in asphaltenes. Estimates of the average size of asphaltene fused ring systems have varied widely from very small (1–4) to very big (>10).[62] We believe the methodology employed here is more direct, and thus more reliable. Scanning Tunneling Microscope results also obtain average ring sizes for asphaltenes in the range of 4 to 10 rings.[63]

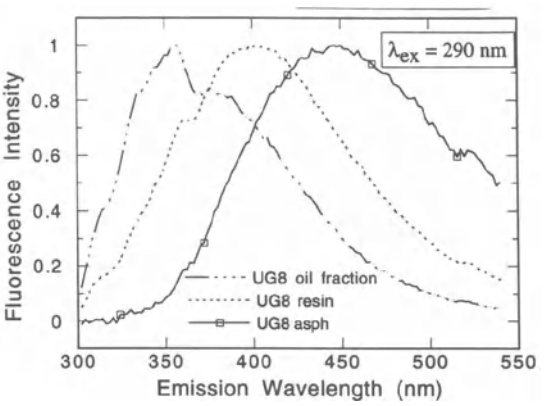

Figure 41. Fluorescence emission spectra for the asphaltene, resin, and oil fraction of UG8 crude oil, a heavy oil. The lighter fractions have greater emission at shorter wavelength (and less at longer wavelength) indicating smaller aromatics for the lighter fractions.

Figure 41 shows a comparison of asphaltene spectra with the spectra of the corresponding resin and crude oil without asphalt of UG8 crude oil. The UG8 asphaltene spectrum exhibits a maximum emission at ~450 nm and shows little emission in the 1 and 2 ring aromatic spectral region. The UG8 resin spectrum exhibits a maximum emission at ~400 nm and shows some emission in the spectral region corresponding to small rings. The crude oil without asphalt of this heavy oil exhibits a maximum emission at ~350 nm and exhibits considerable emission in the spectral range corresponding to small rings. Asphaltenes and resins correspond to defined crude oil fractions and do not vary grossly from different crude oils. On the other hand, the oil fraction of crude oils corresponds to all but the heaviest fraction for a given oil and thus, varies enormously when obtained from different crude oils. The crude oil UG8 is fairly heavy (asphaltene fraction is 9%), thus the UG8 crude oil without asphalt is somewhat heavy. The emission spectra of the asphaltenes, resins and maltenes show, in order, greater short wavelength emission, in accord with the expectation that the molecular size of the aromatic molecules decreases in the order asphaltenes > resins > crude oil without asphalt.

7. CONCLUSIONS

Optical measurements have been performed in the oil field for six decades to detect crude oil while drilling. In spite of this long history of optics with crude oils, only recently have studies exploited optical techniques, some new, some traditional, to expand greatly the understanding of crude oils and asphaltenes. The complexity of the components of individual crude oils and asphaltenes, along with the tremendous variation of crude oils (if not asphaltenes), inhibited scientific assault by these bulk measurement techniques. However, it turns out that one is not required to dismember chromatographically crude oils and asphaltenes into constituents to advance understanding. In fact, complex intermolecular dynamics can be studied only by maintaining the crude oil body whole. The large number of experimental parameters; wavelengths, quantum yields, lifetimes, spectra, concentrations, sample type, firmly constrain imagination with reality. Surprising systematics result, enforcing the vantage that crude oils and asphaltenes are of one rather well-behaved family.

REFERENCES

1. A.R. Smits, D.V. Fincher, K. Nishida, O.C. Mullins, R.J. Schroeder, T. Yamate, Society of Petroleum Engineers, Paper #26496 (1993); R. Badry, D. Fincher, O.C. Mullins, R.J. Schroeder, a. Smits, Oilfield Review, 6, 21 (1994).

2. P.L. DeLaune, SPWLA 33rd Annual Symposium (1992).
3. M.V. Reyes, SPE 25355, Asia Pacific Conference (1993).
4. N. Tsuzuki, K. Chaki, M. Yamamura, J. Jpn. Assoc. Pet. Tech., 56, 254 (1991).
5. V. Patel, E. Decoster, A. Douglas, R. Chambers, O.C. Mullins, X. Wu, M. Kane, P. Rabbito, T. Terabayashi, N. Itagaki, J. Singer, in Well Evaluation Conference, Venezuela 1997, Ed. J. Singer, Publisher, Schlumberger Surenco, CA (1997).
6. R.F. Rathbone, J.C. Hower, F.J. Derbyshire, Fuel, 72, 1177 (1993).
7. J.M. Shaver, L.B. McGown, Appl. Spec. 49, 813 (1995).
8. C.-Z. Li, F. Wu, H.-Y. Cai, R. Kandiyoti, Energy & Fuels, 8, 1039 (1994).
9. B.P. Tissot, D.H. Welte, "Petroleum Formation and Occurrence," 2nd ed. Springer-Verlag, Berlin (1984).
10. B. Durand, "Kerogen, Insoluble Organic Matter from Sedimentary Rocks," Technip, Paris (1980).
11. B. Pradier, C. Largeau, S. Derenne, L. Matinez, P. Bertrand, Org. Geochem. 16, 451 (1989); B. Pradier, P. Landais, A. Rochdi, A. Davis, Org. Geochem. 18, 241 (1992).
12. R.C. Burris in C.E. Barker, O.C. Kopp, (Eds.) Luminenescence Microscopy: Quantitative and Qualitative Aspects, SEPM (1991).
13. L.D. Stasiuk, L.R. Snowdon, Appl. Geochen. 12, 229 (1997).
14. J. Wang, X. Wu, O.C. Mullins, 51, 1890 (1997) Appl. Spectros.
15. J. Bezouska, J. Wang, O.C. Mullins, Accepted, Appl. Spectros.
16. J. Janata, M. Josowicz, D.M. DeVaney, Anal. Chem. 64, 207R (1994).
17. J. Lin, S.J. Hart, T.A. Taylor, J.E. Kenny, Proc. SPIE, Int. Soc. Opt. Eng. 2367, 70 (1994).
18. H.-G. Lohmannsroben, C. Kauffmann, Th. Roch, in G. Cecchi, T. Lamp, R. Reuter, K. Weber, (Eds.) Proc. Europto Series, SPIE 3107, 305 (1997).
19. M.U. Kumke, H.-G. Lohmannsroben, Th. Roch, J. Fluorescence, 5, 139 (1995).
20. S.D. Alaruri, M. Rasas, O.Alamedine,.S. Jubian, F. Al-Bahrani, M. Quinn, Opt. Eng. 34, 214 (1995).
21. G.V. Chilingarian, T.F. Yen, (Eds.) Bitumens, Asphalts and tar Sands, Elsevier Pub. Co. Amsterdam, (1978).
22. J.W. Bunger, N.C. Li, (Eds.), Chemistry of Asphaltenes, Amer. Chem. Soc., Wash D.C. (1981).
23. J.G. Speight, The Chemistry and Technology of Petroleum, Marcel Dekkker, Inc. New York (1980).
24. E.Y. Sheu, O.C. Mullins, (Eds.), Asphaltenes: Fundamentals and Applications, Plenum Press, New York (1996).
25. J.D. Payzant, D.D. McIntyre, T.W Mojelsky, M. Torres, D.S. Montgomery, O.P. Strausz, Org. Geochem., 14, 461 (1989).
26. T.F. Yen, J.M. Moldowan, (Eds.), Geochemical Biomarkers, Harwood Acad. Pub. Switzerlan, (1988).
27. O.C. Mullins, Ch 2 in Ref. 24.
28. M.A. Anisimov, I.K. Yudin, V. Nikitin, G. Nikolaenko, A. Chernoustan, H. Toulhoat, D. Frot, Y. Briolant, J. Phys. Chem., 99, 9576 (1995).
29. R. Siuniayev, in Physical Chemistry of Colloids and Interfaces in Oil Production, H. Toalhoat, J. Lecourtier (Eds.) Editions Technip., Paris (1992).
30. J.S. Buckley, G.J.Hirasaki, Y. Liu, S. Von Drasek, J.-X. Wang, B.S. Gill, Accepted, Petroleum Science Tech.
31. N.J. Turro, "Modern Molecular Photochemistry," Benjamin/Cummings Pub. Co., Menlo Park CA, (1978).
32. T.D. Downare, O.C. Mullins, X. Wu, Appl. Spectros., 48, 1483 (1994).
33. T.D. Downare, O.C. Mullins, Applied Spectros., 49, 754 (1995); T.D. Downare, O.C. Mullins, in SPIE Milestones Series Vol. MS 126, Laser Beam Diagnostics, R.N. Hindy, J.H. Hunt, Editors, SPIE Optical Engineering Press, Bellingham, WA, USA (1996).
34. C.Y. Ralston, X. Wu, O.C. Mullins, Appl. Spectros. 50, 1563 (1996).
35. O.C. Mullins, S. Mitra-Kirtley, Y. Zhu, Appl. Spectros. 46, 1405 (1992).
36. P.W. Atkins, Molecular Quantum Mechanics, Oxford University Press, Oxford, U.K. (1983).
37. J. Lakowicz, "Principles of Fluorescence Spectroscopy," Plenum Press, New York (1983).
38. W.R.A. Greenlay, B.R. Henry, J. Chem. Phys. 69, 82 (1978).
39. O.C. Mullins, Anal. Chem. 62, 508 (1990).
40. O.C. Mullins, Y. Zhu, Appl. Spectros., 46, 354 (1992).
41. T. Yokota, F. Scriven, D.S. Montgomery, O.P. Strausz, Fuel, 65, 1142 (1986).
42. F. Urbach, Phys. Rev. 92, 1324 (1953).
43. G.A.N. Connell, in Amorphous Semiconductors, M.H. Brodsky, (Ed.), Springer-Verlag, Berlin (1985).
44. G.D. Cody, T. Tiedje, B Abeles, B. Brooks, Y. Goldstein, Phys. Rev. Lett. 47, 1480 (1981).
45. N. Bacalis, E.N. Economou, M.H. Cohen, Phys. Rev. B, 37, 2714 (1988); S. John, M.Y. Chou, M.H. Cohen, C.M. Soukoulis, Phys. Rev. B, 37, 6963 (1988).
46. F. Wondrazek, A. Seilmeier, W. Kaiser, Chem. Phys. Lett. 104, 121 (1984).

47. S. Kinoshita, N. Nishi, A. Saitoh, T. Kushida, J. Phys. Soc. Jpn. 56, 4162 (1987).
48. Y. Zhu and O.C. Mullins, Energy and Fuels, 6, 545 (1992).
49. M.F. Quinn, S. Joubian, F. Al-Bahrani, S. Al-Aruri, O. Alameddine, Appl. Spectrosc. 42, 406 (1988).
50. X. Wang, O.C. Mullins, Appl. Spectros. 48, 977 (1994).
51. W. Siebrand, J. Chem. Phys., 46, 440 (1967).
52. C.Y. Ralston, S. Mitra-Kirtley, O. C. Mullins, Energy & Fuels, 10, 623 (1996).
53. F.C. De Schryver, N. Boens, J. Put, Advances in Photochem., 10, 359 (1977).
54. C.-Z. Li, F. Wu, H.-Y. Cai, R. Kandiyoti, Energy & Fuels, 8, 1039 (1994).
55. G.S. Waldo, O.C. Mullins, J.E. Penner-Hahn, S.P. Cramer, Fuel, 71, 53 (1992).
56. R.B. Long, Ch 2 in Ref. 22.
57. O.P Strauss, T.W. Mojelsky, E.M. Lown, Fuel, 71, 1355 (1992).
58. W.E. Acree, Jr., S.A. Tucker, J.C. Fetzer, "Polycyclic Aromatic Compounds," Vol. 2, 75 (1991).
59. W.E. Acree, Jr., S.A. Tucker, A.I. Zvaigzne, K.W. Street, Jr., J.C. Fetzer, H.-Fr. Grutzmacher, Appl. Spec. 44, 477 (1990).
60. S.A. Tucker, H. Darmodjo, W.E. Acree, Jr., J.C. Fetzer, M. Zander, Appl. Spec. 46, 1260 (1992).
61. I.B. Berlman, "Handbook of Fluorescence Spectra of Aromatic Compounds," Acedemic Press, New York (1971).
62. J.G. Speight, in "Polynuclear Aromatic Compounds," L.B. Ebert (Ed.) Amer. Chem. Soc. (1988).
63. G.W. Zajac, N.K. Sethi, J.T. Joseph, Scanning Micros. 8, 463 (1994).

Chapter III

MOLECULAR STRUCTURE AND INTERMOLECULAR INTERACTION OF ASPHALTENES BY FT-IR, NMR, EPR

R. Scotti* and L. Montanari

ENIRICERCHE S.P.A.
via Maritano 26, 20097
San Donato Milanese, Italy

1. INTRODUCTION

Asphaltenes are a problem in the production of heavier crude oils for their tendency to flocculate and precipitate during both oil production and oil refining.[1–3]

The need for a more efficient exploitation of heavy feedstocks has lead to an increased interest during the last years in elucidating the molecular structure of asphaltenes in order to understand their behaviour in thermal and catalytic processes.

By definition,[4] asphaltenes are a solubility class. They are the insoluble part of petroleum after addition of n-alkane solvents in a volume ratio at least 1(oil):40(solvent). They are dark brown to black friable solids with no definite melting point.

The molecular nature of petroleum asphaltenes have been the subject of many investigations.[5–18] Analytical and spectroscopic techniques usually give the mean characteristics of asphaltene fraction, which is composed of a distribution of highly differentiated and very complex aromatic molecules, surrounded and linked by aliphatic chains and heteroatoms. These molecules differ significantly in their chemical characteristics, as molecular weight, aromaticity, alkyl substitution, functional groups, heteroatoms and metal contents. Every technique is useful to give information about a particular aspect of the asphaltenes but it is necessary to integrate results from more than one technique in order to draw more general conclusions.

In the past the asphaltene fraction often was described in terms of a single, representative molecule composed with the mean contents of the elements and functional

* Present address: Università di Milano, Dipartimento di Scienza dei Materiali, via Emanueli, 15, 20126 Milano, Italy. Roberto.Scotti@mater.unimi.it

groups[15] derived from different techniques. This approach gave an idea of the structural complexity of asphaltenes but it could be misleading as it neglected the chemical differences between the molecules.

With regard to the analytical methods used to understand better the structure of native petroleum asphaltenes, Infrared Spectroscopy (IR) permits the identification and the determination of the relative abundances of some functional groups. IR has been used for 50 years to study coal and its derivatives as the knowledge of coal composition was essential in order to understand the chemistry of conversion processes[19–22] but already in 1956 Brandes[23] calculated the percentage of aromatic, naphthenic and paraffinic carbons in a series of gas oils. Later on petroleum compounds were investigated and considerable efforts have been made to analyze the structure of the nonvolatile fractions of petroleum, particularly the asphaltenes. For qualitative determinations, solutions, films, Nujol oil mulls and potassium bromide pellets can be used in conventional way. For absolute quantitative determinations, the extinction coefficients have to be properly calculated according to Beer's law, taking the precision and the accuracy of experimental parameters (e.g. cell thickness, light path, solvents and so on) into account but that sometimes cannot be done due to the signal overlapping.

Yen et al.[24,25] applied IR for the elucidation of the structure of petroleum resins and asphaltenes and proved that, using adequate compounds of known structure as references, the presence of many structural groups can be detected, their relative contributions estimated and their relative positions to one another determined. He also used the low temperature IR technique to study the alkylene nature and C-H out-of-phase ring bending vibrations of petroleum asphaltenes[26] and combining the results of X-Ray Diffraction (XRD), Nuclear Magnetic Resonance (NMR) and IR suggested that asphaltenes consist of a heavily substituted linked or katacondensed system.[27] Moreover ^{13}C-NMR and IR studies[28] showed that the aromatic ring system contains alicyclic and alkyl substituents. Yen also discussed the differences between petroleum- and coal-derived asphaltenes,[29] as other authors.[30,31]

The vibrational bands of oxygen containing functional groups are relatively strong and isolated and permit their identification. Carbonyl groups can be easily identified, however, the hydroxy- and amino-groups show characteristics which are not resolvable from each other.[32,33] Speight and Moschopedis studied the quinone-type oxygen in petroleum asphaltenes and resins[9] and the role played by the oxygen functions in hydrogen-bonding interactions which occur between them.[7] Hydrogen-bonding interactions were already studied by Petersen[34,35] in asphalts.

^{1}H-NMR has been extensively used to provide a detailed characterization of the various petroleum fractions. This technique, however, suffers from the disadvantages that the characteristic features of the carbon skeletons have to be calculated from the hydrogen distribution and approximations are required. More recently with the availability of ^{13}C-NMR spectroscopy it has been possible to obtain information directly about the average carbon skeletons of the molecules present in hydrocarbon mixtures. Average molecular parameters[5,8,10,12] as aromatic carbon fraction (f_a), average number of carbon per alkyl side chains (n) and average percent of substitution of aromatic carbon (A_s), were determined by combining the data from ^{1}H- and ^{13}C-NMR.

However, interpretation of the observed ^{13}C-NMR spectra is usually limited to the determination of the fraction of aromatic and aliphatic carbon. To interpret spectra of single compounds, it is usual to combine chemical shift data with the knowledge of resonance multiplicity. Thus singlet, doublet, triplet, and quartet multiplicities imply C, CH, CH_2 and CH_3 respectively. This assignment to carbon group type is achieved using other NMR methods as Distortionless Enhancement by Polarization Transfer (DEPT),[36,37] Gated

Spin Echo (GASPE)[38–41] and 2 D-NMR[42–43] which give further descriptions of the hydrocarbon skeleton of asphaltenes.

Moreover solid-state NMR[44] gives information about the chemical shielding anisotropy (CSA), which is not achievable in solution. The chemical shift of a nuclear spin depends upon the relative spatial orientation of the external magnetic field and the molecule to which the spin belongs. Due to this orientational dependence, chemical shielding is characterized by a second rank tensor (nine elements) but only the symmetric part of the shielding tensor (six elements) is measurable in an NMR experiment as the antisymmetric portion (three elements) produces only second-order effects in the external magnetic field. The shielding principal parameters (σ_{11}, σ_{22} and σ_{33}) can be obtained from the ^{13}C NMR spectral pattern of the powdered sample. This broad but highly characteristic band has break points which can be analyzed to obtain the tensor principal values of each chemically unique spin. This procedure has been used to evaluate the degree of condensation and of substitution of aromatic rings, not avaliable directly from NMR spectra in solution.

Fluorescence spectroscopy has been applied directly to crude oils or to asphaltene solutions and the absorption/emission behaviours of such a multicomponent system carefully studied.[45–50] In the oil industry fluorescence analysis is routinely used as an indicator of the presence of crude oil but this technique can be used also to explore structural information of asphaltene molecules as the condensation of aromatic rings from the differences in intensities and positions of the fluorescence bands.

Also destructive techniques, such as the use of oxidizing agents capable of selectively oxidizing aromatic carbons[17] and the experiments of flashpyrolysis coupled with GC-MS[9,51] were used to give more insights into the nature of aliphatic chains and of heteroatom speciation in asphaltenes. However this method concerns only a part of asphaltenes (oxidized or pyrolyzed ones) and several assumptions must be made to draw conclusions.

The tendency of the asphaltenes to aggregate is a well known characteristic usually studied in hydrocarbon solution. By means of Small-Angle Neutron Scattering (SANS),[52,53] the existence of aggregates in oil and their dimensions and shape as a function of the solvent were confirmed. Unfortunately this behaviour tends to preclude the correct determination of moleculer weight of asphaltenes.[54] In fact, the measurements by Vapour Pressure Osmometry (VPO)[11,55,56] are strongly affected by the temperature, the asphaltene concentration and the solvent polarity. In comparison to VPO, Gel Permeation Chromatography (GPC) has the advantage of giving the distribution of molecular weights rather than a single value of M_n but suffers from the lack of suitable standard compounds for calibration and the dependence on the dilution and temperature used during elution from the chromatographic column.[51] Also with greatest dilution compatible with the instrumental analytical sensitivity, it is not clear that the value of molecular weight is obtained for single unassociated molecules of asphaltenes. So the molecular weights can be better considered as relative values useful to compare different asphaltenes rather than absolute values.

Electron Paramagnetic Resonance (EPR) spectroscopy provides a convenient method for the investigation of paramagnetic species. EPR spectra of asphaltenes show the signals of two different paramagnetic centers: V(IV) in vanadyl group VO^{2+} and free radicals, which are the focus of interest in the present study.

VO^{2+} compounds have been deeply investigated[57–74] for many years in crude oils and their fractions (bitumens, asphaltenes) but also in kerogens and other carbonaceous materials. In crude oils vanadium and nickel organometallic compounds are present mainly as petroporphyrins but also as other porphyrin-like coordination spheres around the metal. The distribution of the different complexes depends on the origin of crude oils.

Unlike diamagnetic square planar Ni^{2+} the five coordinate square pyramidal vanadyl complexes are paramagnetic and their spectroscopic parameters (g-value, hyperfine coupling constant) are related to the ligand nature. Much effort has been directed toward the synthesis and the EPR characterization of vanadyl chelate models with different ligands: four nitrogen (4N), four sulfur (4S), four oxygen (4O) but also other possible combinations of these ligands.[59–61,63,64,72]

Other studies have been directed towards enhancing the nonporphyrin vanadyl signals by improving the separation procedures of the crude oil heavy fractions which contain vanadyl complexes.[59,70,73] As metals strongly affect hydrocracking and thermal cracking of heavy oils, the characteristics of vanadyl complexes were also followed before and after these processes.[77,78]

EPR studies on asphaltene free radicals, associated with unpaired π electrons stabilized by resonance in large aromatic ring system, are not numerous[75–84] even if the radical species and the problems involved in the analysis are similar to those found in coal and other carbonaceous materials.[85–102]

This work elucidates the molecular structures and the intermolecular interactions of seven asphaltenes from different origins by means of a large number of analytical and spectroscopic techniques. No technique used in this study is novel. The original aspect of the investigation is the attempt to integrate and interrelate all of the measurements. As already noted, asphaltenes are a complex system and only main characteristics can be obtained by different analysis methods. It is therefore particularly important to verify the consistency of the experimental data in order to understand if a parameter is really meaningful. So the same information has been obtained by independent techniques when possible and the results compared.

A two-steps approach is followed:[103,104]

1. The molecular features which differentiate the asphaltenes from the seven crude oils are obtained mainly by IR and NMR techniques. The internal consistency and the interdependence of the parameters are shown also comparing them with results obtained by other techniques (elemental analysis, fluorescence). Finally a relation between the molecular characteristics and the structural behaviours investigated by powder X-Ray Diffraction (XRD) was found.
2. Continuous wave EPR spectroscopy was utilized to study asphaltene free radicals, which behave as probes of the the molecular and structural characteristics of the asphaltenes, as the large molecules environment strongly influences the radical magnetic properties. The EPR parameters (g-value, line-width, line-shape), the dependence of EPR signal on temperature, the saturation behaviours, allowed the confirmation of some previous conclusions and improved the investigation of the intermolecular interactions between the asphaltenes molecules. Also the interaction of the polyaromatic molecules with oxygen was studied in order to verify the dependence of the magnetic properties on the gas surrounding the asphaltenes.

2. EXPERIMENTAL SECTION

Asphaltenes were isolated from crude oil Villafortuna (VI) and Gaggiano (GA); residues 350^+ °C Brent (BRE), Gela (GE) and Safaniya (SAFA); residues 550^+ °C Arabian Light (AL) and Belayim (BEL). Asphaltenes were precipitated with an excess of n-heptane (40:1),

sonicated for 20 minutes and then filtered. Asphaltenes were then purified by Soxhlet extraction with n-heptane for 8 hours and dried under vacuum at 100°C until constant weight.

Liquid state ^{1}H- and ^{13}C-NMR were carried out on a Bruker AMX-300 spectrometer operating at ^{1}H resonance frequency of 300 MHz and ^{13}C resonance frequency of 75.47 Mhz. ^{1}H-NMR spectra were obtained as $CDCl_3$ solution with a pulse width of 3.5 μs (30° flip angle), recycle delay of 2 s, data point of 8 K, tube diameter of 5 mm, spectral width of 18 ppm and at least 200 scans. ^{13}C-NMR spectra were obtained by applying an inverse gated decoupling technique to suppress NOE effect. Chromium acetyl-acetonate [$Cr(acac)_3$] (0.01 M in the final solution) was added to assure complete nuclear magnetic moment relaxation between pulses. These conditions are necessary to have quantitative ^{13}C-NMR signals. Operating conditions were: pulse width 2.7 μs (30° flip angle), data point 8 K, tube diameter 5 mm, solvent $CDCl_3$, spectral width 250 ppm, recycle delay 2 s, nearly 20,000 scans.

Solid state ^{13}C-NMR spectra were acquired on a Bruker CXP-300 operating at a ^{13}C resonance frequency of 75.47 MHz with pulse width of 2 μs (30° flip angle) and with the high power proton decoupler gated on during acquisition and off between pulses. A delay time of 4 s was applied between pulses. The spectral fitting was carried out by matching a properly phased experimental spectrum with the simulated one (TENSOR software, Bruker).

The GAted SPin Echo (GASPE) ^{13}C-NMR technique used was that proposed by Cookson and Smith[40–42] with the average scalar coupling constant J_{CH} of 125 Hz for aliphatic carbon. Spectra integration was carried out on C, CH_2 and $CH+CH_3$ sub-spectra. The GASPE and CSE (Conventional Spin Echo) sequences are shown in the following Scheme 1.

The ^{13}C part of the sequence is the simple spin echo procedure composed of a relaxation delay-90-τ-180-τ-data acquisition. This sequence gives the formation of an echo after the 2 τ period. All C resonances are shown in CSE spectrum. However, in the GASPE sequence ^{1}H irradiation is gated on, coincident with the 180° ^{13}C pulse. This causes a modulation of the intensity of the echo magnitude dependent on the scalar coupling constant J between C and corresponding H. This modulation can be used to identify resonance multiplicity. Generally eight GASPE and one CSE spectra are acquired to achieve the GASPE NMR editing. The GASPE(τ) acquired are: GASPE (1/4J), GASPE (1/2J), GASPE (3/4J), GASPE (1/J), GASPE (5/4J), GASPE (3/2J), GASPE (7/4J), GASPE (2/J).

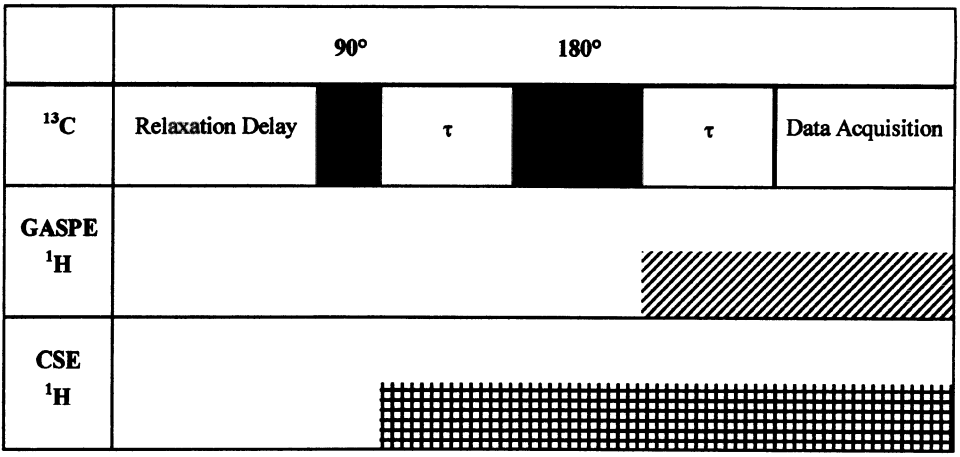

Scheme 1. ^{13}C Spin Echo pulse sequence. In combination with the upper ^{1}H decoupling yields a GASPE sequence while combined with the lower ^{1}H decoupling Yields a CSE sequence.

To obtain selected multiplet spectra the following summations were carried out:

- C = (1/2J) + (3/2J)
- CH_2 = [(CSE) + (2/J) + 2(1/J)] × 0.5 - C
- CH = 1.414 × [(1/4J)+(7/4J)–(3/4J)–(5/4J)] – [(CSE) + ((2/J) -2 (1/J)] × 0.5
- CH_3 = (CSE) + (2/J) – 2(1/J) – 1.414 × [(1/4J)+(7/4J)–(3/4J)–(5/4J)].

Fourier Transform IR (FT-IR) spectra have been recorded on a DIGILAB FTS-15E spectrometer in absorbance mode. Each spectrum resulted from the accumulation of 1000 scans with a spectral resolution of 4 cm^{-1} in the 4000–600 cm^{-1} spectral domain. Samples were prepared by mixing with spectroscopic grade KBr to obtain a 0.5 % (w/w) asphaltene/KBr mixture. Spectra were acquired relative to a pure KBr reference and analysis was focused on three regions of the spectrum: 2800–3200, 1500–1800 and 650–950 cm^{-1}. A deconvolution technique, using the Nelder-Head algorithm, was applied to evaluate the relative intensities of overlapped IR bands.

EPR spectra were recorded on a Varian E 112 spectrometer operating at 9.2 GHz microwave frequency and magnetic field modulation of 100 kHz. Asphaltene radical densities have been calculated by comparison with Varian Strong Pitch signal as standard with an error of ± 15%. DPPH (g = 2.0036) was used as the g marker and the microwave frequency was accurately read with a HP 5350 B frequency counter. The EPR resonant cavity was a Varian E-231 cavity with operation mode TE_{102}, equipped with a home-built temperature controller operating in a temperature range from -150 °C to 150 °C. Asphaltenes were introduced in 4 mm EPR tube and then evacuated for at least one hour under rotating pump (nearly 10^{-2} mbar) vacuum before measurement.

The GPC experiment were performed using a Waters 600 E pump for liquid chromatography equipped with a differential refractometer detector Waters 410. A set of six Waters μStyragel columns (300 mm × 7.8 mm I. D.) was used: 2 × 100 A, 2 × 500 A, 1 × 1000 A, 1 × 10000 A. The sample concentration was 0.1 %w/w, and the solvent flow rate was 1 ml/min. The calibration curve was obtained using 2 vanadyl-porphyrins (MW 543 and 679 daltons) and 2 fractions of a polycarbonate of bisphenol A (MW 3650 and 5230 daltons). The GPC data were acquired and processed with a NEC APC IV Power Mate1 personal computer and a Waters Maxima 825 software.

Fluorescence studies were carried out on a Perkin Elmer spectrofluorimeter (model LS-50B) equipped with a Xenon flash lamp. In addition to the excitation and emission spectra we obtained synchronous spectra both by scanning the range 300–700 nm with a fixed wavelength interval ($\Delta\lambda$ = 3 nm) (the usual Stokes shift between the 0–0 bands in the excitation and emission spectra in polycyclic aromatic compounds) and by scanning the same wavelength range with a constant energy difference ($\Delta\nu$ = -1400 cm^{-1}). Fluorescence spectra were recorded at room temperature at a concentration of 5 mg l^{-1} in perchloroethylene.

The XRD data were collected at ambient conditions using Philips equipment with monochromatic Cu Kα radiation (λ = 1.5418 Å), step-scan method, divergence slit of 1/4°. Typical scan: 2θ range = 2°-35°, step = 0.05°, time x step = 20". Data treatment was carried using the Siemens Diffrac AT package run on a IBM PC 330 p-75.

3. RESULTS AND DISCUSSION

The composition of the seven asphaltenes expressed as percent of carbon ($C_{\%}$), hydrogen ($H_{\%}$), nitrogen ($N_{\%}$) and sulphur ($S_{\%}$) from elemental analysis are tabulated in Table 1. The oxygen content ($O_{\%}$) is calculated by difference; therefore, caution is needed in the interpretation of any trend for the different asphaltenes.

Table 1. Elemental analysis and molecular weights

Asphaltene	C % w/w	H % w/w	N % w/w	S % w/w	O % w/w	H/C mol/mol	M_w
GE	79.7	6.9	1.1	10.8	1.5	1.04	3100
BEL	83.9	8.1	1.9	5.3	0.8	1.16	2170
SAFA	82.4	7.7	1.0	7.7	1.2	1.12	2870
AL	84.1	7.0	1.0	7.1	0.7	1.00	2301
BRE	86.9	7.4	1.1	2.1	2.6	1.02	2360
GA	88.5	7.1	1.0	2.7	0.7	0.96	2140
VI	90.3	6.1	1.0	1.9	0.8	0.81	1900

From top to bottom, the atomic H/C ratios, calculated from $H_{\%}$ and $C_{\%}$, and $S_{\%}$ decrease while $N_{\%}$ appear very similar for the seven asphaltenes.

Also GPC molecular weights (M_W) are reported. As previously observed, they can not be considered as absolute values but only used to compare the seven asphaltenes.

3.1. FTIR Spectroscopy

A typical FTIR spectrum of asphaltenes is shown in Figure 1. The different bands were assigned to:

3100–3640 cm^{-1}	O-H, N-H stretch;
3000–3100 cm^{-1}	aromatic C-H stretch;
2780–3000 cm^{-1}	aliphatic C-H stretch;
1640–1800 cm^{-1}	carbonyl C=O stretch;
1620–1590 cm^{-1}	aromatic C=C stretch;
915–852 cm^{-1}	aromatic C-H out-of-plane deformation (1 adj H);
760–730 cm^{-1}	aromatic C-H out-of-plane deformation (4 adj H).

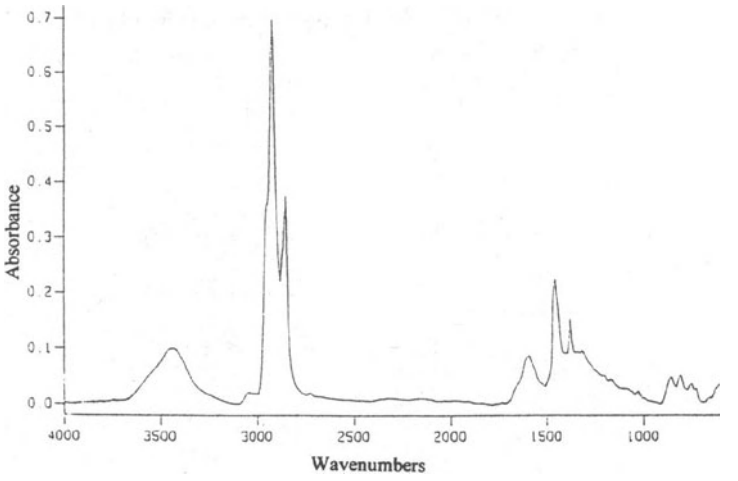

Figure 1. Typical FT-IR transmission spectrum of asphaltenes (GA).

Table 2. Molecular parameter from FT-IR

Asphaltene	R	n_{IR}	(C=O)	W
GE	3.34	6.0	0.44	1.56
BEL	3.21	4.9	0.34	1.63
SAFA	3.35	6.2	0.30	1.44
AL	3.81	5.1	0.29	2.18
BRE	3.07	2.8	0.19	1.43
GA	2.52	5.2	0.30	1.45
VI	2.59	3.8	0.18	2.26

In particular the bands at 2927 and 2957 cm^{-1} were attributed respectively to C-H stretch of CH_2 and CH_3 groups and permitted the calculation of the molar ratio of the two groups $R = n_{CH2}/n_{CH3}$. This ratio is a measure of the lenght of the side alkyl chains, the higher the ratio, the longer the side chain.

From spectra of 20 model compounds (normal and iso-alkanes and alkyl-aromatics) a linear correlation between the molar ratio R and the ratio between band intensities at 2927 cm^{-1} (I_{2927}) and 2957 cm^{-1} (I_{2957}) was found on the basis of the following relationship:

$$R = \frac{n_{CH2}}{n_{CH3}} = K\frac{I_{2927}}{I_{2957}} \quad (1)$$

where K= 1.243 is the slope of the plot R vs (I_{2927}/ I_{2957}) (linear correlation coefficient 0.996).The molar ratios R are reported in Table 2. They show a similar trend with the average number of carbon per alkyl side chain n obtained from NMR spectra as described in the next section.

Another important feature in the IR spectra of asphaltenes is the low intensity of signals in the region 3600–3000 cm^{-1}.This result indicates very low concentrations of OH and NH groups, which are often considered important for asphaltene aggregation via H bonds.[7]

Also, IR band intensities of carbonyl groups (1800–1640 cm^{-1}) are generally weak for the asphaltenes. The spectral zone 1800–1600 cm^{-1} was deconvoluted into three bands centered at 1700 cm^{-1} for ketones, aldehydes and carboxylic acids; 1650 cm^{-1} for highly conjugated carbonyls such as quinone-type structure and amides; 1600 cm^{-1} for aromatic C=C stretching. The normalized band intensities (intensity in arbitrary units / mg of sam-

Table 3. Normalized intensities of FT-IR bands in 1800–1600 cm^{-1} zone

Asphaltene	1700 cm^{-1}	1650 cm^{-1}	1600 cm^{-1}
GE	0.09	0.21	0.37
BEL	0.14	0.31	0.85
SAFA	0.13	0.13	0.60
AL	0.10	0.13	0.57
BRE	0.09	0.10	0.82
GA	0.24	0.10	0.81
VI	0.10	0.05	0.72

ple) are reported in Table 3. The 1735 cm^{-1} band of esters is too weak to be determined quantitatively and was not considered in deconvolution.

The intensity ratio

$$(C=O) = \frac{I_{1700} + I_{1650}}{I_{1700} + I_{1650} + I_{1600}} \quad (2)$$

was calculated. It is an empirical index of carbonyl abundances in the asphaltene molecules, with respect to aromatic moieties (Table 2). The parameter trend qualitatively agrees with a decrease of carbonyl content in more aromatic asphaltenes.

Another dimensionless molecular parameter can be obtained from the out-of-plane CH aromatic IR bands in the 930–700 cm^{-1} spectral range:

$$W = \frac{I_{915-852}}{I_{760-730}} \quad (3)$$

where $I_{915-852}$ is the intensity of aromatic C-H out of plane deformation with 1 adjacent H and $I_{760-730}$ the same with 4 adjacent H. The ratio W (Table 2) is related both to the degree of condensation and to the degree of substitution.[22] In this case the VI asphaltenes have higher W values as expected on the basis of their aromaticity as indicated by NMR results in the next section while the high W value of AL oil asphaltenes may indicate a greater degree of substitution.

3.2. NMR Spectroscopy

^{1}H and ^{13}C-NMR spectra of GA asphaltenes (as general example) are shown in Figure 2 where the main attributions of different spectral zones are emphasized. The choice of the different integration domains for ^{1}H-NMR spectra has been largely discussed in literature. Because of the overlap of signals, ^{1}H-NMR spectra have been divided into four regions:

-1.0–1.0 ppm	γ^{+} CH_3 (H_γ);
1.0–2.0 ppm	β^{+} CH_3, CH_2, CH (H_β);
2.0–4.0 ppm	α CH_3, CH_2, CH (H_α);
6.5–9.0 ppm	aromatic CH (H_{ar}).

The ^{13}C-NMR spectra have been divided into two different integration domains:

10–65 ppm	aliphatic C (C_{al});
100–170 ppm	aromatic C (C_{ar}).

The main molecular parameters from NMR spectra were calculated according to Dickinson's equations[10] and listed in Table 4.

They are the aromatic carbon fraction (f_a), the average number of carbons per alkyl side-chain (n) and the percent substitution of aromatic rings (A_s) for non bridging carbon atoms:

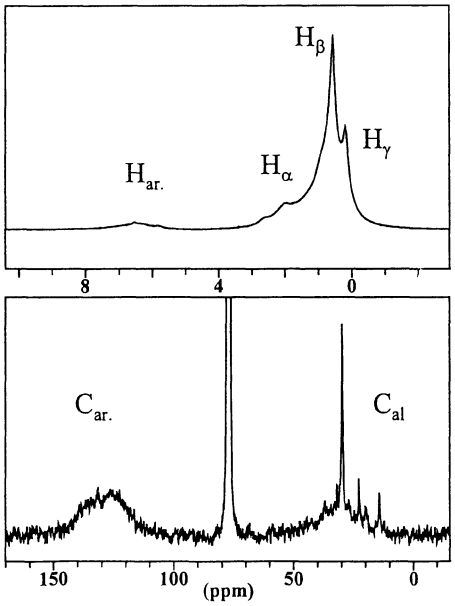

Figure 2. Typical ^{1}H (top) and ^{13}C-NMR (bottom) spectra of asphaltenes. Integration domains are indicated.

$$f_a = \frac{C_{ar}}{C_{ar} + C_{al}} \tag{4}$$

$$n = \frac{H_\alpha + H_\beta + H_\gamma}{H_\alpha} \tag{5}$$

$$A_S = \frac{100 \times C_{1S}}{C_1} = 100 \times \frac{C_{1S}}{C_{1S} + C_{1U}} \tag{6}$$

where C_{1S} is the percent substituted aromatic carbon

$$C_{1S} = \frac{C_\alpha \times C_{al}}{n} \tag{7}$$

Table 4. Average molecular parameter from NMR

Asphaltene	f_{ar}	n	A_s
GE	0.48	6.1	48
BEL	0.49	5.3	40
SAFA	0.51	6.5	49
AL	0.53	4.8	44
BRE	0.58	3.2	40
GA	0.60	4.6	35
VI	0.69	2.7	36

C_{1U} is the percent unsubstituted aromatic carbon

$$C_{1U} = 12 \times H_{ar} \times H_{\%} \tag{8}$$

and C_1 is the percent nonbridge aromatic carbon

$$C_1 = C_{1S} + C_{1U} \tag{9}$$

In the ^{13}C-NMR spectra of all investigated asphaltenes some prominent peaks are present due to long alkyl side-chains. The spectral assignment of these signals is the following:[105,106]

14.1 ppm	terminal methyl carbon of chain longer than C3;
close to 23 ppm	first methylene carbon ($-CH_2CH_3$) in long alkyl chains;
close to 32.7 ppm	second methylene carbon ($-CH_2CH_2CH_3$) in long alkyl groups;
close to 29.7 ppm	third or further methylene carbon in long alkyl groups ($-(CH_2)_n-CH_2CH_2CH_3$);
close to 20 ppm	internal methyl groups ($-CH(CH_3)CH_2-$) and methyl group α to an aromatic ring.

The relative molar fractions, evaluated from deconvolution of ^{13}C-NMR spectra, are included in Table 5. A common characteristic of the spectra is that the intensity of the peak at 32.7 ppm is considerably lower compared to the peaks at 14.1 and 23 ppm. Besides, the ratios between the latter peaks are nearly one except for the GE asphaltene.

These peculiarities are probably due to the presence of significant amount of cyclic aliphatic structure. The assignments of the prominent peaks is, in fact, strictly pertinent to the long aliphatic chains. With aliphatic cyclic structures which are generally substituted with branches, the α and β methylene groups show a large distribution of chemical shifts and they are not prominent peaks but they are part of the large peak centered at 29.7 ppm; the methyls (further than β position) resonate at the same position as for long chains (14 ppm). If there are a great amount of aliphatic cyclic structures (with short branches) they contribute to the peak of methyls at 14.1 ppm while they do not contribute to the prominent peak at 23 ppm: this seems the case of GE asphaltene.

Table 5. Relative molar abundance of ^{13}C-NMR peaks due to long alkyl side chains

Asphaltene	14.1 ppm	23 ppm	32.7 ppm	29.7 ppm	20 ppm
GE	0.20	0.13	0.07	0.46	0.14
BEL	0.12	0.09	0.03	0.55	0.21
SAFA	0.13	0.13	0.03	0.60	0.11
AL	0.11	0.10	0.05	0.47	0.26
BRE	0.12	0.12	0.05	0.43	0.28
GA	0.12	0.11	0.02	0.40	0.35
VI	0.12	0.12	0.05	0.32	0.39

Another important feature is that the molar fraction of C at 20 ppm increases for more aromatic asphaltenes (GA and VI) because of the increase of methyls in α to aromatic rings.

The molar ratios R from the IR (Table 2) show a similar trend with the parameters n from NMR spectra, but for a complete comparison between the two methods it is necessary to estimate the average molecular number of CH_3 in the alkyl side chains.

The interpretation of ^{13}C-NMR spectra for asphaltenes was limited to the division of spectral region into aromatic and aliphatic chemical shift ranges in order to obtain the fraction of aromatic carbon. To gain insight into CH_i (i=0,1,2,3) assignments and the relative abundances in the alkyl side-chains, spectral editing of carbon spectra was accomplished by using pulse methods that select carbons on the basis of the number of directly bonded protons.

Assignment of carbon types has been achieved using the Single Frequency Off-resonance Decoupling (SFORD) technique.[107] Asphaltenes, however, are complex mixtures yielding spectra that are largely congested. In this case the SFORD technique is of very limited value because of the great overlap of different C multiplets.

Another spectral editing technique that appeared to be more promising for asphaltenes was GASPE, because it was successfully used in quantitative determination of percentage abundances of different C group types for liquids derived from petroleum.[39]

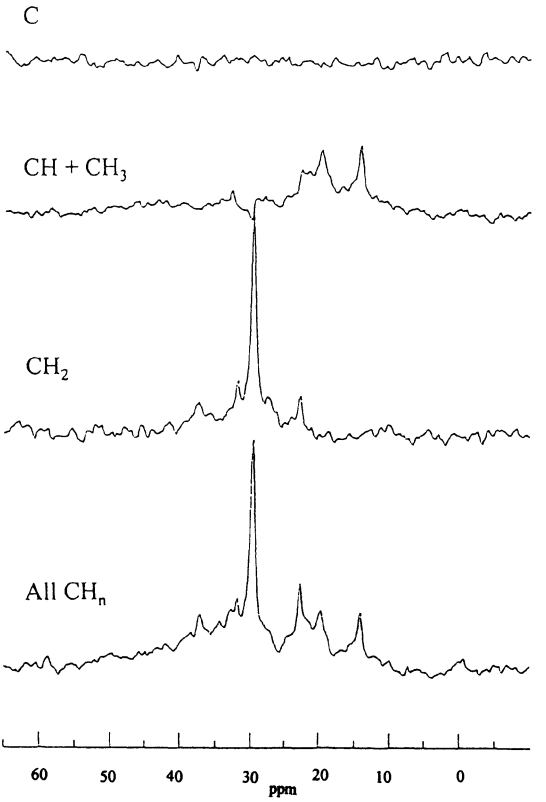

Figure 3. Conventional spin echo spectrum (bottom) and saturated CH_2, CH + CH_3 and C GASPE spectra for GA asphaltenes.

Some typical GASPE ^{13}C-NMR sub-spectra for the different CH_n multiplets of the asphaltenes are shown in Figure 3.

The $CH+CH_3$ sub-spectra are characterized by some prominent peaks in the 10–30 ppm region due to the different methyl groups, while a broad resonance (confirmed also in a DEPT 90° ^{13}C-NMR experiment in which only CH groups are displayed) in the 40–60 ppm range is due to the presence of different CH groups. To calculate the CH and CH_3 relative intensities we used a chemical shift cut-off at 30 ppm in the $CH+CH_3$ sub-spectra. None of the asphaltenes studied showed any aliphatic quaternary carbon signals. The relative molar fractions (f_{CHi}) of different CH_i groups (Table 6) are defined as:

$$f_{CHi} = \frac{n_{CHi}}{n_C + n_{CH} + n_{CH2} + n_{CH3}} = \frac{I_{CHi}}{I_C + I_{CH} + I_{CH2} + I_{CH3}} \quad (10)$$

where i = 0, 1, 2, 3; n_C, are the moles of aliphatic quaternary carbon C; n_{CH}, n_{CH2}, n_{CH3} are the moles of CH, CH_2, CH_3 groups and I_C, I_{CH}, I_{CH2}, I_{CH3} are their GASPE ^{13}C-NMR intensity.

It is interesting to observe that asphaltenes have different CH_3/CH molar ratios (hereafter referred to as Q): Q is nearly 1 for GE and BRE, while it is nearly 1.6 for SAFA, AL, BEL and is more than 3 for GA and VIL. Low Q values are probably due to the presence of cyclic aliphatic structure for which the presence of CH groups does not require two CH_3 end groups. High Q values are indicative of the relative abundance of CH_3 group probably due to a significant contribution of methyl group directly bond to aromatic carbons. Medium Q values may indicate an intermediate situation between the two described. These data provide evidence of a general trend for asphaltenes to have a major contribution of CH_3 groups in the alkyl side-chains according to their maturation.

From GASPE ^{13}C-NMR (f_{CH3}) and ^{1}H-NMR (n) data an average molecular methyl number ($\tilde{n}_{CH3}$) per side chain can be calculated:

$$\tilde{n}_{CH3} = f_{CH3} \times n \quad (11)$$

An average number of carbon per alkyl side-chain (n_{IR}) can be now evaluated:

$$n_{IR} = (R \times \tilde{n}_{CH3}) + \tilde{n}_{CH3} \quad (12)$$

where R was defined in equation (1). The assumption that the molar ratio R is equal to the ratio between the number of CH_2 and CH_3 groups in the average side chains was used in equation (12). In Table 2 n_{IR} values are reported and they are in good agreement with the n values obtained from NMR (Table 4).

Table 6. CH_i abundances from GASPE ^{13}C-NMR

Asphaltene	f_C	f_{CH}	f_{CH2}	f_{CH3}	Q
GE	–	0.20	0.57	0.23	1.15
BEL	–	0.13	0.65	0.22	1.69
SAFA	–	0.13	0.65	0.22	1.69
AL	–	0.14	0.64	0.22	1.57
BRE	–	0.21	0.58	0.21	1.00
GA	–	0.11	0.56	0.33	3.00
VI	–	0.11	0.50	0.39	3.54

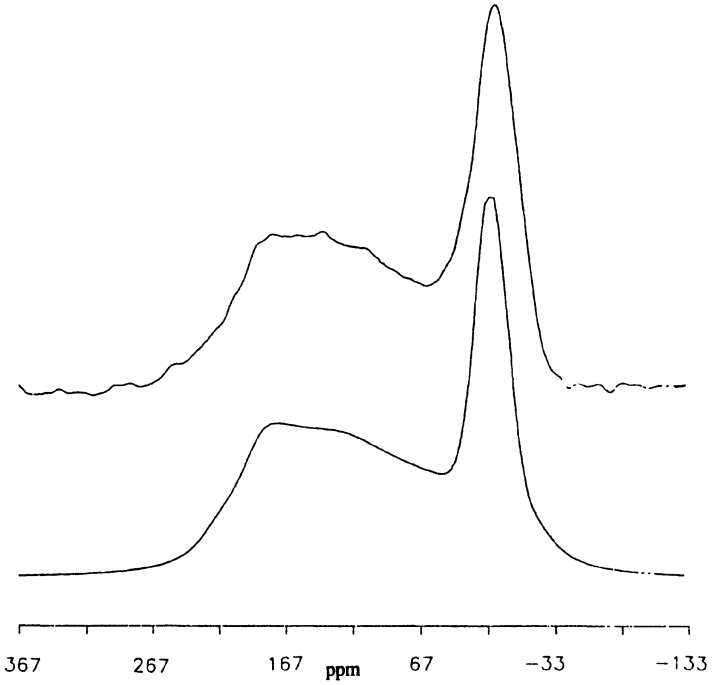

Figure 4. Experimental (top) and simulated (bottom) ^{13}C NMR static spectra of GA asphaltenes.

Greater insight into the type of condensation of the asphaltenes has been obtained by using solid state ^{13}C-NMR. Under static conditions, the ^{13}C-NMR spectra of asphaltenes (Figure 4 shows a typical example) have lineshapes which reflect the chemical shift anisotropy (CSA) of the different molecular carbons.[44] CSA is much greater for aromatic carbons than for aliphatic.

It is possible to extract the principal values of the CSA second rank tensor from NMR static spectra. For this purpose, the ^{13}C-NMR static spectra of asphaltenes have two main limitations:

- the aliphatic band covers the aromatic σ_{33} component preventing precise band fitting;
- the large linewidth prevents any precise quantification of the different carbon lineshapes and contributions.

A qualitative method to gain information about the different aromatic carbon abundances has been derived from the intensity ratio of the NMR band at 170 and 100 ppm (hereafter called F). The choice comes from the fact that inner and bridging aromatic carbons have an axially symmetric tensor with maximum intensity at nearly 160–190 ppm while protonated and substituted aromatic carbons have an orthorombic symmetric tensor with maximum intensity in the range 140–100 ppm. So higher F values correspond to larger sized polycondensed aromatic rings. In Figure 5 the F values are reported with some other model compounds.

Two main conclusions can be drawn: asphaltenes of different origin show similar average aromatic condensation with the exception of VI, which seems to be more condensed; the average number of polycondensed aromatic rings is estimated to be between 5 and 7.

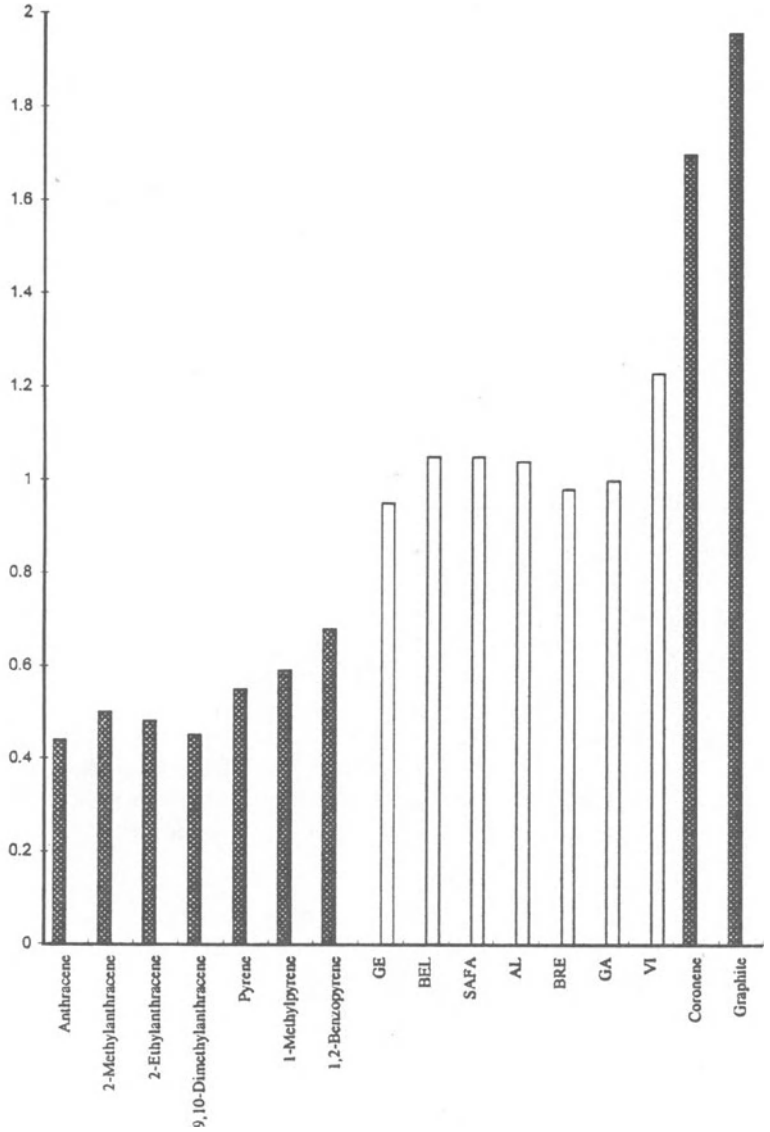

Figure 5. F values (intensity ratio of 170 and 100 ppm bands from solid state ^{13}C NMR) of the seven asphaltenes compared with some model compounds.

These results suggest that the aromatic clusters are linked in the average molecule by some heteroatom and aliphatic linkages, as proposed in literature.[16]

In order to have more insight into the nature of asphaltene aromatic cores the synchronous fluorescence methodology was applied to the VI and GE asphaltenes which represent the asphaltenes with the greater difference in aromatic contents (Table 4). It was suggested[108] that synchronous excitation technique offers several advantages in the analysis of polynuclear aromatic hydrocarbons (PAH), including narrowing of spectral bands,

enhancement in selectivity by spectral simplification, and a decrease of measurement time in multicomponent analysis. There are two ways to record synchronous spectra:

1. at fixed interval between excitation and emission ($\Delta\lambda$ = 3nm) in the case of PAH which is the usual Stokes shift between the 0–0 bands in the excitation and emission spectra);
2. at constant energy difference of one vibrational unit[93,109] which allow to register the fluorescence spectra of some PAH which do not exhibit strong 0–0 transitions.

The first correlation between the structure of a PAH compound and its fluorescence spectrum is reflected by the dependence of the energy of the 0–0 band with the ring size of the compound. The spectrum of cyclic compounds with a larger ring number occurs generally at a longer wavelength than for compounds with a smaller ring number. The synchronous technique can achieve some sort of spectral confinement and we can delimit the following interval of synchronous spectra: 260–300 nm: one ring, 300–330 nm: two rings, 340–400 nm: three rings (linear compounds have longer wavelength of not linear ones), 380–500 nm: four rings, 440–520 nm: five rings, 480–560 nm: six rings, 500–600 nm: seven rings.

Figure 6 shows the constant wavelength difference ($\Delta\lambda$=3nm) synchronous spectra of the GE and VI asphaltenes which show an envelope of signals between 300 and 600 nm confirming the complex nature of aromatic moieties in asphaltenes: the predominant peak for GE asphaltenes is at 458 nm while the component at wavelength over 500 nm is a shoulder; the same characteristics are shown for VI asphaltenes but the longer wavelengths components are at much higher concentration (almost the same intensity for the greater peak at 470 nm). The constant energy ($\Delta\nu$=-1400 cm^{-1}) spectra (Figure 7) are similar to the previous ones with the prevalent peak at 440 nm for GE asphaltenes and at 470 nm for VI ones. These values of synchronous wavelength found show that the medium size of aromatic clusters is of nearly 4–5 for GE and 5–7 for VI. These values are in a very good agreement with the size of aromatic clusters found with solid state ^{13}C-NMR as previously described.

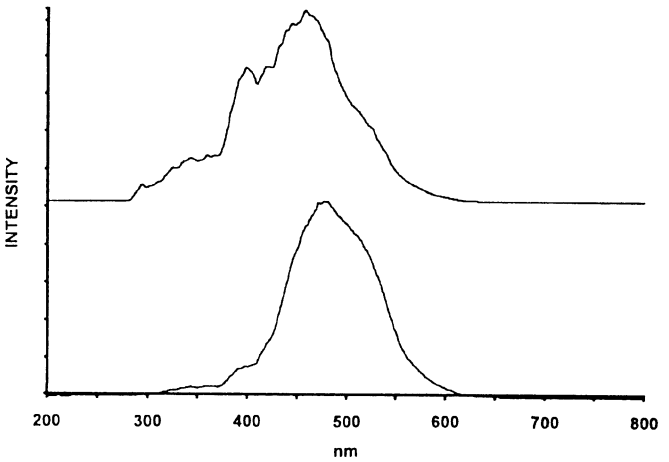

Figure 6. Constant wavelenght difference ($\Delta\lambda$=3nm) synchronous fluorescence spectra of GE (top) and VI (bottom) asphaltenes.

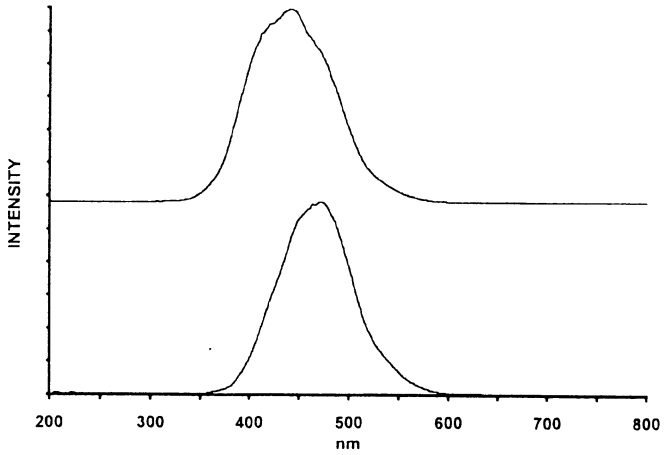

Figure 7. Constant energy difference (Δv=1400 cm^{-1}) synchronous fluorescence spectra of GE (top) and VI (bottom) asphaltenes.

The main molecular characteristics of the seven asphaltenes can be summed up as follows: when the carbon content increases, the aromaticity and the aromatic core size increase. On the other hand, the length of alkyl side chains, the heteroatom content and the molecular weight decrease. In other words, the smaller molecular weight asphaltenes are more aromatic, contain less heteroatoms (particularly S), and have shorter aliphatic side chains.

These behaviours are related to the structural characteristics. XRD spectra show a strong difference between VI and GE, the asphaltenes with maximum and minimum f_a (0.69 VI, 0.48 GE). Spectra of other asphaltenes are intermediate between GE and VI.

XRD spectra of asphaltenes show three characteristic peaks:

- a peak at 2θ about 25.2°, with an interlayer spacing (3.5 Å) close to the d_{002} (3.348 Å) of graphite, attributed to a graphite-like structure of condensed aromatic rings;
- a peak at 2θ of 18–19°, probably due to aliphatic and not condensed aromatic fraction;
- a third diffraction line, at low angles, with a spacing about 27–30 Å, attributed to a spatial order of the graphitic nuclei of the asphaltene aggregates. It is detectable for VI and generally for the more aromatic asphaltenes. Besides more intense the graphite line at 25.2°, more intense and defined is the low theta diffraction line.

This is a clear indication that asphaltene tendency to aggregate in solid state depends on the molecular characteristics. More aromatic asphaltenes with fewer and shorter aliphatic side chains have a greater tendency to aggregate in structures of stacked layers with a short range spatial order.

3.3. Electron Spin Resonance Spectroscopy

EPR spectra of asphaltenes show the signals of paramagnetic VO^{2+} cations in porphyrin or non porphyrin structures and of organic free radicals. The GA spectrum is reported in Fig. 8 as an illustrative example. V(IV) as vanadyl porphyrin, shows anisotropic

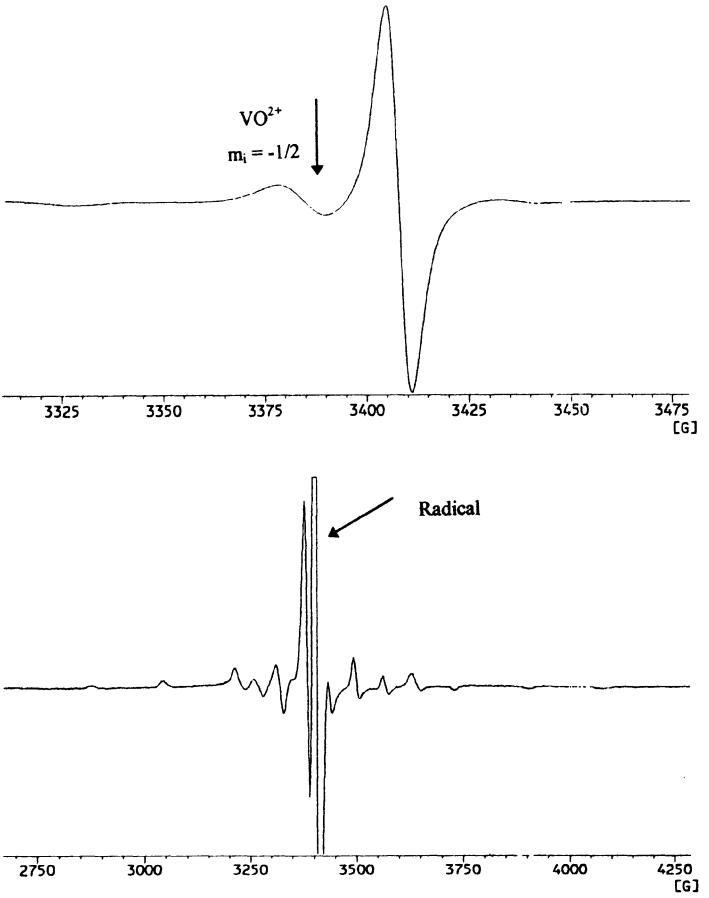

Figure 8. Typical EPR spectrum, recorded at 293 K, of a powdered sample of asphaltenes (GA). VO^{2+} porphyrin signal is shown in the bottom spectrum. Free radical signal and the m_i=-1/2 perpendicular hyperfine line of V are pointed out with a smaller scan range (top).

lines ($g_{||}$ = 1.965; $g_{\perp}$ = 1.985) with hyperfine structures ($A_{||}$ = 168.5 gauss; $A_{\perp}$ = 56.5 gauss) due to the tetragonal symmetry of the five coordinate square pyramidal vanadyl complex.

The radical signal is isotropic. Owing to the lack of hyperfine structure the only structural parameters are g-factors, lineshapes and linewidths.

3.3.1. Linewidth and Lineshape. Peak to peak separations of the EPR derivative peaks (ΔH_{pp}), full widths at half-height in EPR absorption peaks ($\Delta H_{1/2}$) and the lineshape ratio $R_s = \Delta H_{1/2} / \Delta H_{pp}$ are reported for all samples in argon, air or pure oxygen atmosphere (Table 7). There are small differences between the seven asphaltenes. Line shapes are intermediate between Gaussian, R_s = 1.18, and Lorentzian, R_s = 1.72, and only the oxygen partial pressure surrounding the samples slightly affects the linewidth. Unlike kerogenes,[110] linewidth does not decrease monotonically and R_s does not increase at higher aromaticity. Moreover linewidth broadening cannot be attributed unequivocally to unre-

Table 7. EPR parameters of asphaltenes in different atmospheres

		Argon				Air				Oxygen			
Asphaltene	g-value	ΔH_{pp}	$\Delta H_{1/2}$	R_s	N_s	ΔH_{pp}	$\Delta H_{1/2}$	R_s	N_s	ΔH_{pp}	$\Delta H_{1/2}$	R_s	N_s
GE	2.0034	5.78	8.05	1.39	1.1	5.78	8.05	1.39	1.4	5.80	8.04	1.39	1.7
BEL	2.0031	6.21	8.99	1.45	2.9	6.31	8.99	1.42	3.2	6.38	9.08	1.42	3.8
SAFA	2.0032	5.85	8.32	1.42	2.3	5.91	8.40	1.42	2.7	5.90	8.36	1.42	3.3
AL	2.0031	6.37	8.75	1.37	2.6	6.38	8.76	1.37	2.9	6.40	8.75	1.37	3.7
BRE	2.0029	6.09	8.88	1.46	4.2	6.07	8.78	1.45	5.3	6.12	8.89	1.45	7.5
GA	2.0029	5.23	7.38	1.41	2.8	5.12	7.31	1.43	3.1	5.25	7.38	1.41	3.5
VI	2.0028	6.31	9.26	1.47	6.3	6.27	9.26	1.48	7.9	6.35	9.50	1.50	9.9

solved hyperfine structure (in asphaltenes the hyperfine interaction is generally between the electron spin delocalized on aromatic π orbital and the nuclear magnetic moments of H attached to the aromatic C) of the EPR spectrum because no simple relation between molecular parameters as A_s or H/C ratio (Table 1) and ΔH_{pp} (Table 7) was found. This suggests that in asphaltenes the aromaticity and the different degree of substitution probably overlap their effect on the linewidth and the lineshape and that also the different number of spins could contribute to line width by dipolar interaction.

3.3.2. g-Value. The g-value is a parameter sensitive to the chemical environment of the unpaired electron although asphaltenes reflect the nature of a mixture of free radicals. These radicals are associated with delocalized π systems stabilized by resonance in polyaromatic centers.[75] The g-values of the seven asphaltenes range from 2.0028 to 2.0034. They are somewhat higher than those of the aromatic hydrocarbon radical ions and increase with the decreasing of f_a (Figure 9) and the related carbon content (Table 1). This indicates that atoms other than carbon and hydrogen are important in the electronic structures of the radicals as gleaned from the g-values dependence on the content of heteroatoms (Figure 9).

Requejo et al.[110] correlated this fact with the level of maturity of kerogens behind the assumption that immature kerogens have a higher content of oxygen, nitrogen and sulfur. In coal oxygen is believed to be the atom responsible of g-value shift (2.0029–2.0037) owing to formation of quinone or phenoxy radicals[86,94] which partially localize the radical wave function on the oxygen.

Yen[75] suggested a possible nature of asphaltenes radicals for comparison with literature pure model compounds. He showed that asphaltene g-values are closest to certain types of neutral radicals of carbon and nitrogen and are lower than those for the semiquinones.

As already noted by Petrakis,[86] however, comparisons between g-values of radicals in solid state with the isotropic g-values of pure compounds must be taken with caution. Although sulfur-containing radicals have g-values higher (about 2.0080)[111] than those found for the seven asphaltenes, the g-shift seems to strongly depend on the sulfur content (Fig. 9). Besides, the nitrogen content is nearly the same for all the asphaltenes, except BEL, in spite of different g-values and generally oxygen content is lower than in coal.

As a consequence, it is not possible to define the nature of radicals unequivocally but only to note the different level of heteroatoms in the delocalized π system. In a delocalized system, an unpaired electron spends its time on the different atoms; so the higher

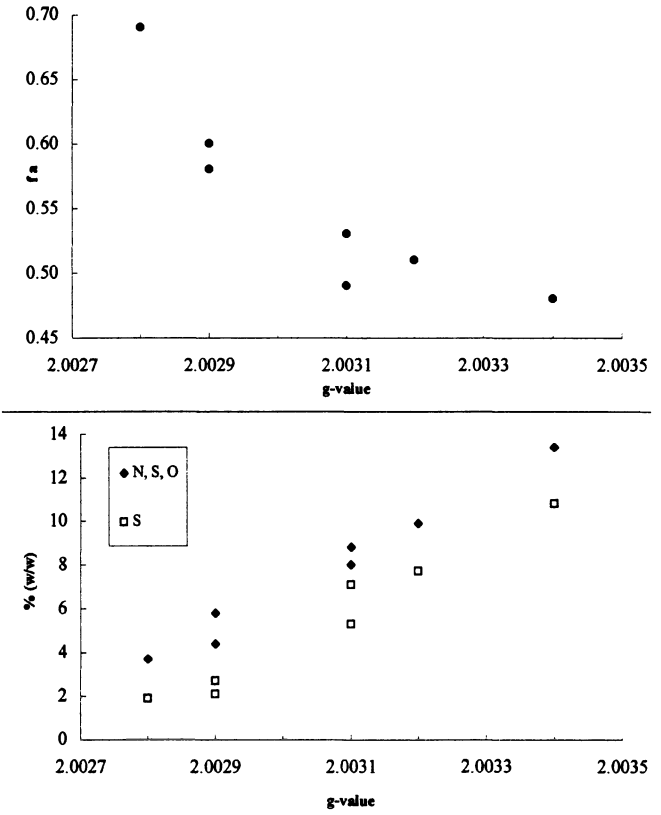

Figure 9. g-values of the asphaltenes radicals vs. aromatic carbon fraction f_a (top) and vs. weight percent of heteroatoms (bottom).

the amount of heteroatoms in the system, the higher the g-value. As g-values of the seven asphaltenes increase at increasing heteroatoms content (Figure 9), it means that many of them do not form functional groups in the aliphatic or naphthenic parts of asphaltenes molecules.

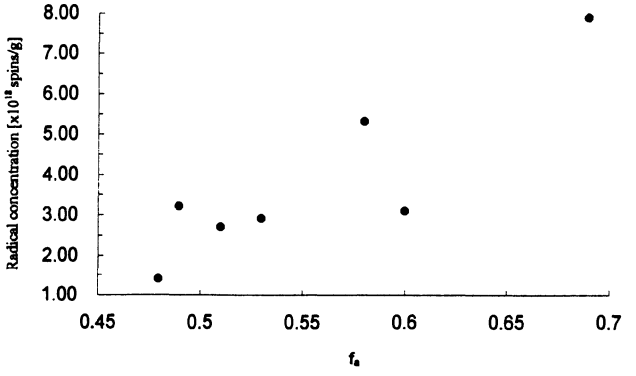

Figure 10. Radical content of the seven asphaltenes (expressed as spins/g) vs.aromatic C fraction f_a.

This result agrees with a previous XANES analysis[112] which showed that all of the asphaltene nitrogen is contained within aromatic rings and is pyrrolic or pyridinic and that also most sulphur is aromatic, expecially in thiophene groups.

3.3.3. Free Radical Concentration. The radical content of the seven asphaltenes, reported as spins/g of asphaltenes (N_r), shows an increasing trend with aromaticity f_a (Figure 10). This is particularly evident comparing the extremes of the series, the most aromatic VI and the least GE, but it is not strictly true for all samples (e.g. GA). A similar trend was found for other carbonaceus material such as coal[94] and kerogens[110] where it was related to the increase in the aromatic core of polynuclear aromatic moieties.

Considering the values of MW in Table 1, the fractional spin density per molecule can be calculated. The values (calculated from spectra recorded in air) range from 0.7 (GE) to 2.5 (VI) free radicals / 100 asphaltene molecules , similar to the values found by Strausz.[77]

3.3.4. Saturation. The saturation behaviour of the seven asphaltenes was studied by measuring the peak-to-peak amplitude on the first-derivative curves (I_{pp}) as a function of microwave power (P).

For homogeneously broadened lines the first derivative of the absorption lineshape function (Y') is given by:[113]

$$Y' = -\frac{2}{\pi}\frac{H_1 t_2^3 \gamma^2 (H - H_r)}{\left[1 + (H - H_r)^2 \gamma^2 t_2^2 + H_1^2 \gamma^2 t_1 t_2\right]^2} \tag{13}$$

where γ is the magnetogyric ratio, H is the variable external magnetic field, H_r is the resonant magnetic field, H_1 is the maximum amplitude of microwave magnetic field, t_1 is the spin-lattice relaxation time, t_2 is the spin-spin relaxation times. Then I_{pp} can be defined as:

$$I_{pp} = 2Y'_{max} \tag{14}$$

When the term $H_1^2\gamma^2\, t_1\, t_2 \ll 1$, it can be neglected and I_{pp} is proportional to the intensity of H_1 or equivalently to the square root of P. When $H_1^2\gamma^2\, t_1\, t_2 \gg 1$, I_{pp} decreases with increasing P (saturation). EPR spectra are usually recorded under the former condition and the applied microwave power should be small when relaxation times are long.

Homogeneous relaxation mechanism occurs when all free radical spins behave as a single spin system and have single values of t_1 and t_2. In other words the energy absorbed from the microwave field is distributed to all the spins and thermal equilibrium of the spin is maintained through resonance. In this case the EPR lineshape is lorentzian and the signal intensity linearly increases with the square root of P until the term $H_1^2\gamma^2\, t_1\, t_2$ can be neglected in (13).

Inhomogeneous relaxation mechanism occurs when each radical species has different relaxation behaviours which reflect different molecular structures and/or different interactions with the environment and gives rise to an independent narrow lorentzian EPR absorption. All these absorptions add up independently and yield a gaussian-shaped envelope. For inhomogeneously broadened lines I_{pp} increases monotonically to a limiting value with increasing P as the microwave energy is transferred only to those spins whose local fields satisfy the resonance condition.

The line shapes of the EPR asphaltene radical signals (see paragraph *3.3.2.*), are intermediate between gaussian and lorentzian and suggest that the relaxation mechanisms are not homogeneous, as expected for a complex system with a mixture of free radicals.

As the differences between the lineshapes of the seven asphaltenes are small, the saturation plots were calculated in order to get more information about the relaxation mechanisms, related to the radical structure, expecially with regard to the comparison between the seven asphaltenes.

Saturation measurements were made over the full range of P up to the maximum value of 200 mW. The plots I_{pp} vs $P^{1/2}$ were calculated after recording EPR spectra in argon, air, and pure oxygen. They strongly depend both on the nature of the asphaltenes and on the gas surrounding the sample as indicated by the comparison of the plots of the extremes of the series VI and GE (Figure 11) and of the values of microwave power (P_{max}) at which I_{pp} are maxima for the seven asphaltenes (Table 8). The increase of oxygen partial pressure gives rise to an increase of the inhomogeneous character of the saturation plots, but we can not exclude also a decrease in relaxation times. This leads to the conclusions that oxygen interacts with the asphaltene spins and that this interaction is stronger with the more aromatic asphaltenes. The nature of this interaction and its relation with the structural characteristics of the asphaltenes will be thoroughly discussed in the paragraph 3.3.5. The saturation plots were also calculated according to other two procedures in order to emphasize the differences between the I_{pp} vs $P^{1/2}$ plots and to point out better some characteristics of them.

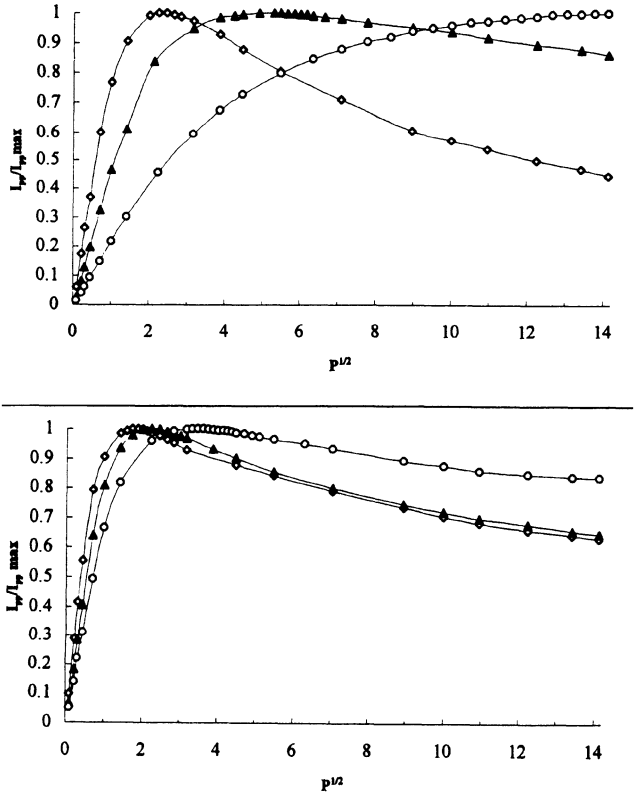

Figure 11. Plots of peak to peak amplitude I_{pp} vs. the square root of microwave power $P^{1/2}$ in argon (◊), air (▲) and oxygen (o) for VI (upper) and GE (lower) asphaltene radicals. I_{pp} values were normalised by defining I_{pp} max = 1 for each curves.

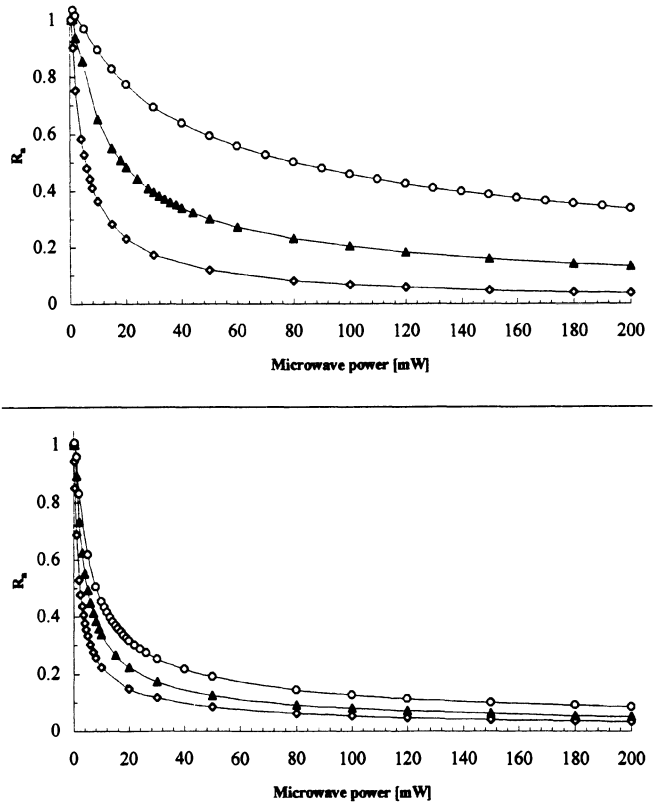

Figure 12. Plots of normalised amplitude R_n vs. microwave power P in argon (◊), air (▲) and oxygen (o) for VI (upper) and GE (lower) asphaltene radicals. R_n is defined by equation (15).

The first procedure was similar to that used by Blombergen, Purcell and Pound[104] and already applied to carbonaceous pitches by Singer et al.[95] In these plots the normalized EPR amplitude (R_n) is reported vs. P (Figure 12). R_n is given by:

$$R_n = \frac{(I_{pp}/P^{1/2})}{(I_{pp}/P_n^{1/2})} \tag{15}$$

where P_n is a power level in absence of saturation and I_{ppn} is the related peak to peak intensity.

This type of plot points out the effect of the saturation on the EPR intensity. In absence of saturation $R_n = 1$ and it is independent on power. When $R_n < 1$, the EPR line starts to saturate and I_{pp} is not proportional to the square root of P.

Plots in Figure 12 show that the saturation occurs for all samples also at very low microwave power when I_{pp} seems to increase linearly with $P^{1/2}$ (Figure 11). This means that also in this range of microwave power I_{pp} is not linearly proportional to the square root of P and therefore caution is needed in comparing the intensities of samples with different saturation behaviours.

Table 8.

	Argon		Air		Oxygen	
Asphaltene	$P_{1/2}$	P_{max}	$P_{1/2}$	P_{max}	$P_{1/2}$	P_{max}
GE	2.5	3-3.5	5.0	5	8.0	11-13
BEL	5.5	6-7	7.5	8-9	18.0	26
SAFA	3.5	4	5.0	5-6	14.0	16-17
AL	4.5	5	5.5	7	16.0	30-32
BRE	5.0	4-4.5	8.0	9-10	26.0	62-68
GA	4.5	5	7.5	7-8	22.0	48-52
VI	5.5	5-6	18.0	24-28	80.0	200

A significant parameter of these plots is $P_{1/2}$; it is the microwave power values at which R_n falls to one-half of its unsaturated value $P_{1/2}$ and the values for the seven asphaltenes are reported in Table 8 (the lower values of P, 0.1–0.2 mW, were chosen as P_n in calculating R_n). The meaning of $P_{1/2}$ is similar to P_{max} but its precision in order to compare the different plots is higher. For the same level of homogeneous/inhomogeneous character, the higher $P_{1/2}$ (or P_{max}), the lower relaxation times, especially t_1. In other words, a relaxation pathway more efficient occurs. The trends for both P_{max} and $P_{1/2}$ are similar; the values increase from GE to VI and strongly depend on the partial pressure of oxygen.

Singer et al.[95] used another particular type of saturation plot, first described by Portis,[105] as it is able to emphasize the differences between the plots at high microwave powers where the degree of saturation is high and to better differentiate between the homogeneous and inhomogeneous relaxation mechanisms.

The ordinate is the product

$$R_n \frac{\sqrt{P}}{\sqrt{P_{1/2}}} \tag{16}$$

and the abscissa the ratio

$$\frac{\sqrt{P}}{\sqrt{P_{1/2}}} \tag{17}$$

The experimental plots confirm that the oxygen interaction with the asphaltenes generally increases the inhomogeneous character of the relaxation even if it does not affect the lineshapes (Table 7). Besides large values of P_{max} and $P_{1/2}$ correlate with greater inhomogeneous character, as indicated by the comparison of VI and GE plots (Figure 13).

3.3.5. Dependence of EPR Intensity on Temperature and on Oxygen Partial Pressure. The oxygen has a great effect on enhancing the absorption intensity at 293 K of the asphaltene radicals as indicated by evaluating the spin concentration in argon, air or pure oxygen (Table 7). This effect is completely reversible and does not depend on the mode of addition of the gas but only on the partial pressure of it.

The m_i=-1/2 perpendicular hyperfine line of VO^{2+} signal (Figure 8) can be used as a reference standard to normalize the amount of asphaltene powder detected in the different atmosphere, as VO^{2+} lines remained unaffected by oxygen.[77]

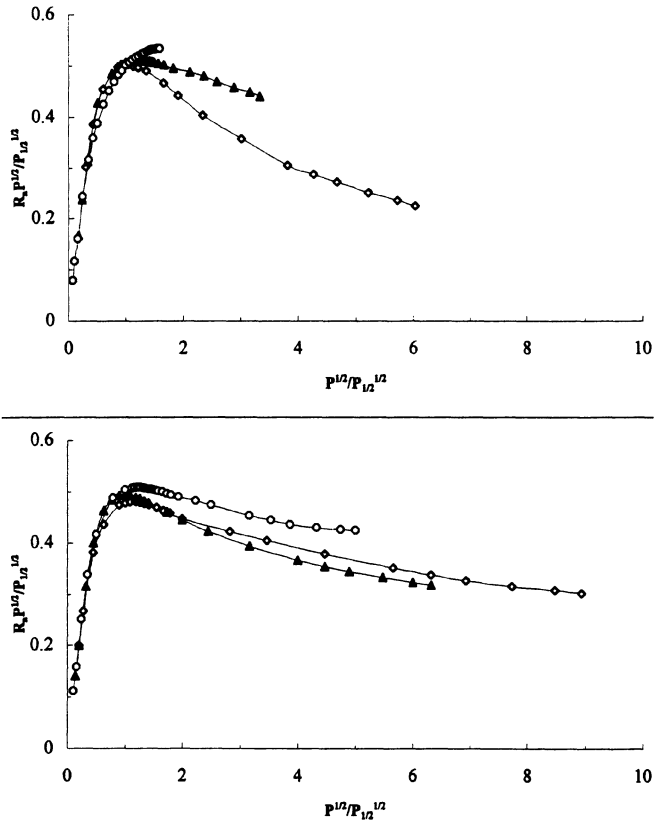

Figure 13. Portis plots in argon (◊), air (▲) and oxygen (o) for VI (upper) and GE (lower) asphaltene radicals. The ordinate and the abscissa are defined by equation (16) and (17).

The variation of EPR line-intensity with temperature was investigated in argon and pure oxygen. The results are reported for VI and GE (Figure 14).

In argon VI and GE radicals behave as paramagnetic molecules with S = ½ (doublet); there is a linear dependence of the reciprocal of EPR intensity on the absolute temperature (Figure 14) according to the Curie-Weiss law (the correlation coefficients are = 0.9989 for VI and = 0.9837 for GE):

$$I_d = \frac{C'}{T+\vartheta} \tag{18}$$

where I_d is the EPR intensity for doublets, C' is a constant, T is the absolute temperature and θ is an empirical constant expressed as a negative absolute temperature that corrects the temperature for non-zero intercept (θ = -34 for VI and θ = -207 for GE). Non-zero intercepts are common in solid paramagnetic materials, where intermolecular interactions cause the alignment of neighbouring magnetic moments and contribute to the value of the intercept.[116]

In oxygen the variation of the EPR intensity is dramatically different and does not follow the Curie-Weiss law (Figure 14). The increasing absorption with increasing the

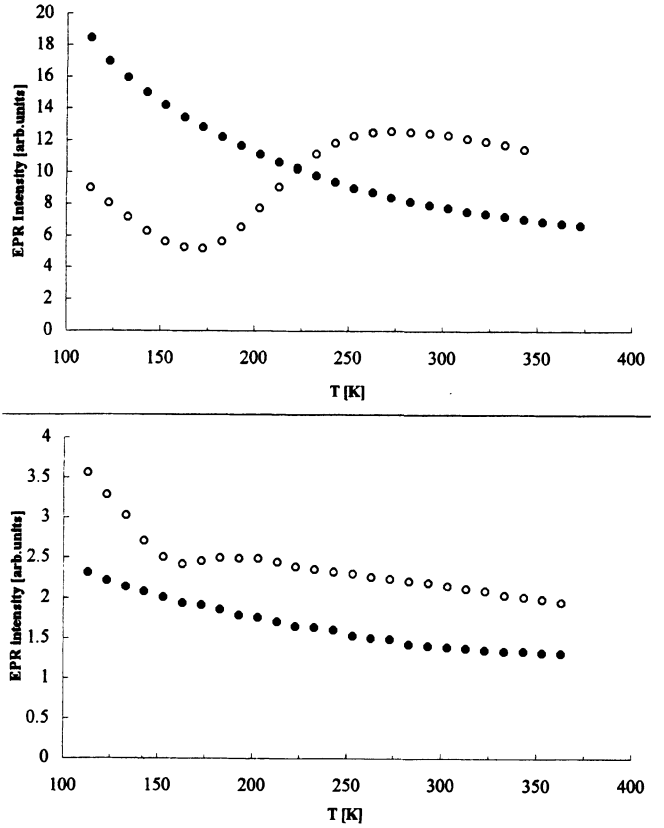

Figure 14. Variation of ESR line intensity with temperature in argon (•) and pure oxygen (o) for VI (upper) and GE (lower) asphaltene radicals.

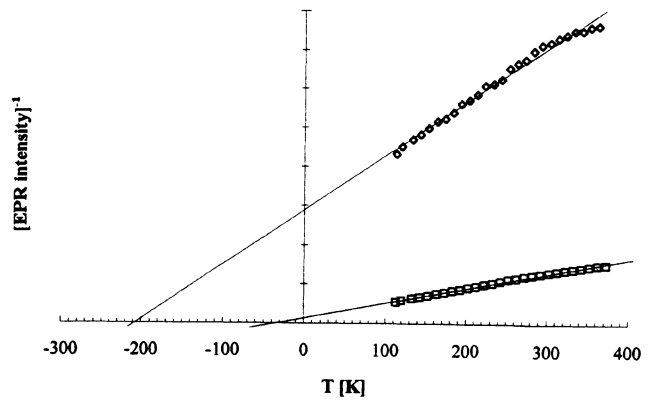

Figure 15. Linear dependence of the reciprocal of the ESR intensity on the absolute temperature for VI (□) and GE (◊) asphaltene radicals in argon. The intercepts between the calculated straight lines and the abscissa indicate the values of the empirical constants θ (θ=-207 for GE and θ=-34 for VI).

temperature is typical of a system with radical pairs where an appreciable interaction between unpaired electrons give rise to diamagnetic singlet ground levels and thermally accessible magnetic triplet.[117,118]

Assuming that the singlet-triplet states are present in addition to doublets according to Yen and Young,[76] the curves containing both temperature dependent processes have been simulate and the singlet-triplet separation energy J calculated.

The population of the triplet states (N_t) depends exponentially on the absolute temperature according to the Boltzmann factor:[118]

$$N_t \propto 3\exp(-\frac{J_{st}h}{kT}) \tag{19}$$

where J_{st} h is the singlet-triplet separation energy, h is the Planck constant and k is the Boltzmann constant. The relative population of the triplet states is:

$$\frac{N_t}{N_s+N_t} = \frac{3\exp\left(-\frac{J_{st}h}{kT}\right)}{1+3\exp\left(-\frac{J_{st}h}{kT}\right)} = \frac{3}{3+\exp\left(\frac{J_{st}h}{kT}\right)} \tag{20}$$

where N_s is the population of the singlet states. For a given population the EPR intensity depends on the reciprocal of the temperature (Curie law). So the intensity of the absorption of the triplet states I_t can be written as:

$$I_t = \frac{A}{T}\frac{1}{3+\exp\left(\frac{J_{st}h}{kT}\right)} \tag{21}$$

where A is a constant.

Assuming that singlet-triplet states are present in addition to doublets according to Yen and Young[76] the total EPR intensity I in oxygen is given by:

$$I = I_d + I_t = \frac{C''}{T} + \frac{A}{T}\frac{1}{3+\exp\left(\frac{J_{st}h}{kT}\right)} \tag{22}$$

where I_d is the intensity of the absorption of the doublet states and C" is a constant.

The curves I_{dt} vs T were simulated for VI and GE (Figure 16) according to relation (22) and the singlet-triplet state separations J_{st} were calculated with a least square method. The calculated values are: GE: A = 3,609; C"=142 ; J_{st} = 326 cm^{-1} and VI: A = 42,112; C"=151; J_{st} = 463 cm^{-1}.

In order to fit better the experimental trends, the doublet part of (22) was actually simulated according to Curie-Weiss law as in (18).

The calculated empirical constants are θ = -95 for VI and θ = -68 for GE).

The best fits qualitatively agree with the experimental points but the results are quite satisfactory only for GE. The assumption of a single value for the singlet-triplet separation in complex systems as asphaltenes is a strong approximation as it is strictly true for crys-

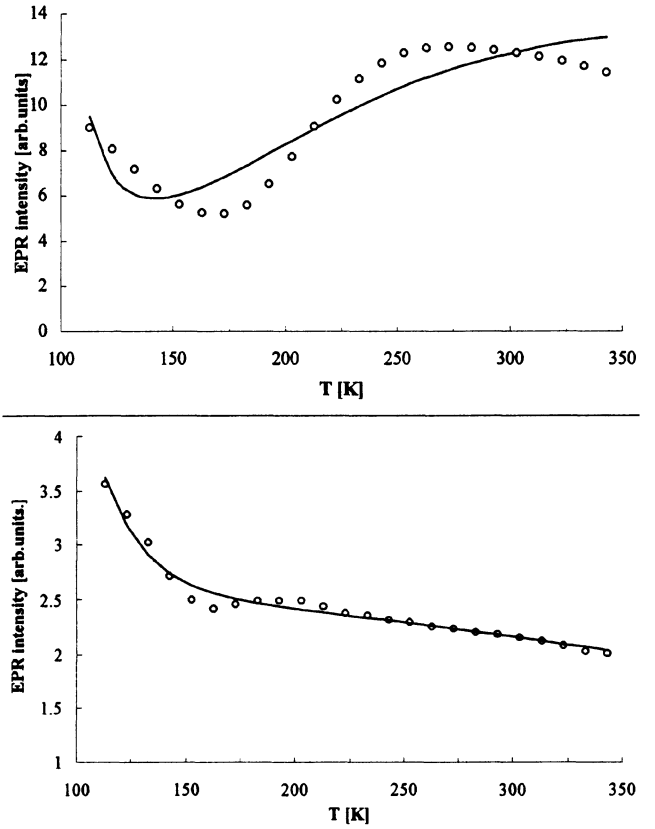

Figure 16. Simulation of the variation of ESR line intensity with temperature in pure oxygen for VI (upper) and GE (lower) asphaltene radicals according equation (22). (o) are the experimental points.

tals and pure compounds. In GE asphaltenes, radical pairs formation is much lower than in VI, and the trend I_{dt} vs T can be simulated like a single singlet-triplet states. The calculated J_{st} is very similar to the values calculated for other asphaltenes[77] and correspond quite well to a long-range interaction between free spins, according to the apparent absence of fine structure in EPR signal. In VI asphaltenes, the formation of radical pairs is very high as results from the trend of the EPR intensity. The superposition of singlet-triplet states with different separation energies precludes properly simulating the curve.

The dependence of EPR intensity on temperature and the saturation of the lines by increasing microwave power show a reversible interaction of the molecular oxygen with the asphaltenes. In oxygen EPR intensity does not follow the Curie law as it does in argon. This oxygen "effect" is completely reversible and it is stronger with more aromatic asphaltenes. The easy reversibility after evacuation of oxygen and the lineshape and the linewidth unaffected or only slightly affected by O_2 partial pressure exclude the formation of a permanent strong bond.

These results indicate a spin interaction with physically adsorbed oxygen, as already suggested for carbon and chars.[93] Such an interaction between aromatic molecules and molecular oxygen is known and has been theoretically studied[119] for smaller molecules

like benzene, which form a kind of complex oxygen-molecule bonded by a weak Van der Waals force. The formation of radical pairs occurs only after interaction with molecular oxygen. In addition to them also uncoupled radicals are present at the same time. Spin-spin interaction gives rise to diamagnetic singlet states and thermally accessible magnetic triplet states. This interaction superimposes its effects on the temperature dependence of EPR intensity to the noninteracting spins which behave as doublets and follow the Curie law. The apparent absence of fine structure of the triplet states is probably due to the inclusion of $0 \rightarrow 1$ and $-1 \rightarrow 0$ transitions in the line width because of a large distance between the free radical sites in the radical pairs,[78] confirmed by the values of the calculated singlet-triplet separation J_{st}. At lower temperatures the radical pairs are mainly in singlet states and the EPR line is due to doublets. At higher temperatures most of radical pairs are in thermally accessible triplet states.

Saturation plots depend on the relaxation times but cannot give unambiguous and separate information about t_1 and t_2 owing to the term in the denominator of equation (18) and to the intermediate behaviour between inhomogeneous and homogeneous broadening. Even if it is not possible to discuss the detailed ralaxation mechanism, the plots show that oxygen interaction strongly affects them. In spite of slight differences in the line widths (Table 7), the inhomogeneous character increases (Figure 13) with increasing oxygen partial pressure. The shift towards higher power values of P_{max} and $P_{1/2}$ does not preclude that also a more efficient relaxation pathway of the radical excited state with a variation in relaxation times occurs. In any case such an interaction is more important for more aromatic asphaltenes. The saturation plots in Ar show a slight difference that cannot depend on the atmosphere surrounding asphaltenes and have to be related to the nature of them. The differences cannot be explained as in carbonaceous pitchs with the increase of radical size and concentration, fewer protons and a greater electron delocalization.[95] These characteristics should result in strong exchange or dipolar interactions and a narrowed EPR line with Lorentian shape and homogeneous behaviour. However, these spectroscopic parameters vary slightly for the seven asphaltenes in Ar and generally in reverse order to that expected. Also in Ar, P_{max} and $P_{1/2}$ increase with aromaticity and the radical amount (Tables 7 and 8). We suggest that when no interaction with oxygen occurs, the saturation plots depend on a relaxation pathway that involves intermolecular interaction between aromatic layers as already seen in kerogens[110] and coal macerals.[86] The tendency to aggregate in graphite-like structure of stacked aromatic rings increases with aromaticity. In these structure there is an overlap between the π electronic states of adjacent molecules that could lead the radical to hopping from the host molecule to an adjacent one. This interaction is not due to an overlap of wave functions of adjacent radicals, as indicated by the absence of spectroscopic evidence of exchange processes. As already seen, only when oxygen adsorbs on asphaltenes surface there is a coupling of radicals. An indirect confirmation of intermolecular interactions comes from the following example. BRE asphaltenes coprecipitated together with long chain waxes. Their saturation plots (in air) after elimination of waxes has P_{max}= 9–10 and $P_{1/2}$ = 8.0, as reported in Table 8, higher than the values before the elimination P_{max}= 6 and $P_{1/2}$ = 4.5. As the aromaticity of asphaltenes molecules does not change after waxes elimination, the differences is more likely due to less ordered stacked structures in presence of waxes.

It was observed that oxygen has a great effect on enhancing the absorption intensity at 293 K (Table 7). The plots EPR vs. temperature (Figure 14) shows that the trends are actually much more complex and also depend on the nature of the asphaltenes. First of all different saturation behaviours make difficult the comparison of the EPR intensity of the same asphaltene radicals in different surrounding atmospheres owing to the inhomogeneous broadening and lower relaxation times in oxygen. Also at higher temperature the trip-

let states can explain the oxygen effect on enhancing the intensity as the intensity of the triplet is higher than that of the doublet.[120] According to these considerations the intensity of GE radical are higher in oxygen than in argon. The trend is different for VI radicals; the formation of radical pairs in oxygen is such that at lower temperatures, when the radical pairs are mainly in diamagnetic singlet states, the amount of residual doublets is lower than in argon at corresponding temperatures.

4. CONCLUSION

The molecular features which differentiate the asphaltenes from the seven crude oils have been investigated by a multidisciplinary and analytical characterization. The internal consistency and the interdependence of the parameters, mainly obtained by FT-IR and NMR techniques but compared with the experimental results by other techniques (elemental analysis, fluorescence), have been shown. A relation between the molecular characteristics and the structural behaviours investigated by powder X-Ray Diffraction (XRD) was also found.

The seven asphaltenes of different origin show a significant trend in molecular structure with increasing carbon content, which can be summed up as follows: more aromatic asphaltenes have shorter average length of aliphatic side chains, higher average aromatic core size and lower heteroatom content. These trends have interesting implications in the asphaltene tendency to aggregate. Particularly more aromatic asphaltenes have a more pronounced tendency to aggregate in graphite-like structures of condensed aromatic rings and also show a spatial order of the graphitic nuclei of the asphaltene aggregates with a spacing about 27–30 Å.

The average number of polycondensed aromatic cluster are less than eight for all asphaltenes. On the basis of this result, the average asphaltene molecule is better represented by isolated clusters of polycondensed groups consisting of between 5 and 7 rings jointed by aliphatic and heteroatom bridges.

The ^{13}C GASPE NMR technique gives clear evidence of the presence of CH groups in the asphaltene aliphatic chains, which are not easily observed with conventional NMR because of the broadness of their absorbance. The presence of condensed aliphatic cyclic structures is inferred from the abundance of CH groups compared to the CH_3. The aliphatic cyclic structures are more present in more aliphatic asphaltene, while they tend to disappear in more aromatic ones.

Continuous wave EPR spectroscopy was utilized to study asphaltene free radicals, which behave as probes of the the molecular and structural characteristics of the asphaltenes, as the large molecules environment strongly influences the radical magnetic properties.

Magnetic properties of unpaired electrons of asphaltenes radicals are sensitive to the chemical environment and to the aggregated structure of the asphaltenes themselves.

The g-values of the EPR signals of petroleum asphaltenes show that heteroatoms play an important role in the electronic structures of the radicals even if it is not possible to define the nature of radicals unequivocally but only to note the different level of heteroatoms in the delocalized π system.

The evolution of EPR intensities with the microwave power and with temperature turn out to be dependent on molecular nature of asphaltenes and on the presence of an oxygen atmosphere. In particular in a nonparamagnetic gas the electron spin relaxation mechanism seems to be caused by an exchange mechanism between adjacent molecules. Moreover oxygen molecules appear to interact in a stronger way with more aromatic asphaltenes and this interactions causes the appearance of singlet-triplet states in place of

the original doublet states. The dependence of EPR intensities in argon gas on temperature follows the Curie law and confirms that even at high spin densities the free radicals don't produce coupled state (triplet-singlet states).

The hyphothesis assumed to explain the EPR relaxation mechanism agreed with the higher ring number condensation found in aromatic asphaltenes.

LIST OF SYMBOLS

A	constant in relation (17);
$A_{\|\|}$	hyperfine coupling parallel to a symmetry axis;
$A_{\perp}$	hyperfine coupling perpendicular to a symmetry axis;
A_s	average percent of substitution of aromatic carbon;
C'	constant in Curie-Weiss law, relation (13);
C''	constant in relation (17);
$C_{\%}$	percent of C (w/w%);
C_{al}	^{13}C-NMR intensity of aliphatic carbon;
C_{ar}	^{13}C-NMR intensity of aromatic carbon;
C_l	percent of nonbridge aromatic carbon;
C_{lS}	percent of substituted aromatic carbon;
C_{lU}	percent of unsubstituted aromatic carbon;
(C=O)	empirical index of carbonyl abundances from FTIR;
f_a	aromatic carbon fraction;
f_{CHn}	relative molar fractions of different CH_i groups (i = 0, 1, 2, 3);
F	intensity ratio of 170 and 100 ppm bands from solid state NMR;
$g_{\|\|}$	g component for H parallel to axis of symmetry;
$g_{\perp}$	g component for H perpendicular to axis of symmetry;
h	Planck constant;
H	variable external magnetic field;
$H_{\%}$	percent of H (w/w%);
H_l	maximum amplitude of microwave magnetic field;
H_r	resonant magnetic field;
H_{α}	^{1}H-NMR intensity of H in α CH_3, CH_2, CH;
H_{β}	^{1}H-NMR intensity of H in β^+ CH_3, CH_2, CH;
H_{γ}	^{1}H-NMR intensity of H in γ^+ CH_3;
H_{ar}	^{1}H-NMR intensity of aromatic H;
H/C	atomic ratio of C and H;
I_C	GASPE ^{13}C-NMR intensity of aliphatic quaternary carbon C;
I_{CH}	GASPE ^{13}C-NMR intensity of CH groups;
I_{CH2}	GASPE ^{13}C-NMR intensity of CH_2 groups;
I_{CH3}	GASPE ^{13}C-NMR intensity of CH_3 groups;
I_d	EPR intensity for doublets;
I_{pp}	peak-to-peak amplitude on the first-derivative curves;
I_{ppn}	peak to peak amplitude related to P level in insaturated regime;
I_{xxxx}	intensity of a particular IR band (xxxx is the value in cm^{-1});
J	scalar coupling constant between C and corresponding H;
J_{st}	singlet-triplet separation energy (cm^{-1});
k	Boltzmann constant;
K	angular coefficient in relation (1);

m_i quantum number for the z component of the nuclear spin angular momentum;
n average number of carbon per alkyl side chains from NMR;
n_C moles of aliphatic quaternary carbon C;
n_{CH}, moles of CH;
n_{CH2} moles of CH_2;
n_{CH3} moles of CH_3;
$\tilde{n}_{CH3}$ average methyl number per side chain;
n_{IR} average number of carbon per alkyl side-chain from FTIR;
$N_{\%}$ percent of N (w/w%);
N_r radical content (spins/g) from EPR;
N_s population of the singlet states;
N_t population of the triplet states;
$O_{\%}$ percent of O (w/w%);
P microwave power;
$P_{1/2}$ P value at which R_n falls to one-half of its unsaturated value;
P_{max} value of P at which I_{pp} is maximum in a I_{pp} vs $P^{1/2}$ plot;
P_n power level in the insaturated regime;
Q molar ratio of CH_3 and CH groups from GASPE ^{13}C-NMR;
R molar ratio of CH_2 and CH_3 groups from FTIR;
R_n normalized EPR amplitude according relation (20);
R_s EPR lineshape ratio;
S spin quantum number;
$S_{\%}$ percent of S (w/w%);
t_1 spin-lattice relaxation time;
t_2 spin-spin relaxation time;
T absolute temperature;
Y' first derivative of EPR absorption lineshape function;
W ratio of aromatic C-H with 1 an 4 adjacent H from FTIR;
γ magnetogyric ratio;
$\Delta H_{1/2}$ full width at half-height in EPR absorption peak;
ΔH_{pp} peak to peak widths of EPR derivative peak;
θ empirical constant in Curie-Weiss law, relation (13);
λ wavelength;
ν frequency;
σ chemical shielding principal component;
τ delay time.

ACKNOWLEDGMENTS

The authors are grateful to ENI group for financial support and to Dr. Marco Clericuzio, Dr. Gastone Del Piero, Dr. Philippe Iwanski, Mr. Walter Stringo for their scientific and technical contributions.

REFERENCES

1. Dickakian, G., Seay, S., Oil Gas J., 85, 47 (1988).
2. Sheu, E.Y., Detar, M.M., Storm, D.A., De Canio, S.J., Fuel, 71, 299 (1992).

3. Cornahan, N.F., Quintero, L., Pfund, D.M., Fulton, J.L., Smith, R.D., Capel, M., Leontaritis, K., Langmuir, 9, 2035 (1993).
4. "Annual Book of ASTM Standards", American Society for Testing and Materials, Philadelpia, Part 24, Standard No. D-2006 (1978).
5. Knight, S.A., Chem Ind., 11, 1920 (1967).
6. Koots, J.A., Speight, J.G., Fuel, 54, 179 (1975).
7. Moschopedis, S.E., Speight, J.G., Fuel, 55, 187 (1976).
8. Dereppe, J.M., Moreax, C., Castex, H., Fuel, 57, 435 (1978).
9. Moschopedis, S.E., Speight, J.G., ACS Div.Pet.Chem. Preprints, 24, 910 (1979).
10. Dickinson, E.M., Fuel, 59, 290 (1980).
11. Speight, J.G., ACS Div.Pet.Chem. Preprints, 26, 825 (1981).
12. Gillet, S., Rubini, P., Delpuech, J.J., Escalier, J.C., Velentin, P., Fuel, 60, 226 (1981).
13. Long, R.B., Speight, J.G., Rev.de l'Institut Francaise du Petrole, 44, 205 (1989).
14. Speight, J.G., ACS Div.Pet.Chem. Preprints, 34, 321 (1989).
15. Speight, J.G., "4th Intl. Conf. on the Stability and Handling of Liquid Fuels", US Dept. Energy, 169, (1992).
16. Strausz, O.P., Mojelsky, T.W., Lown, E.M., Fuel, 71, 1355 (1992).
17. Mojelsky, T.W., Ignasiak, T.M., Frakman,Z., McIntyre, D.D., Lown, E.M., Montgomery, D.S., Strausz, O.P., Energy Fuels, 5, 83 (1992).
18. Mitra-Kirtley, S., Mullins, O.C., van Elp, J., George, S.J., Chen, J., Cramer, S.P. J.Am.Chem.Soc., 115, 252 (1993).
19. Speight, J.G., Appl.Spectr.Reviews, 5, 211 (1971).
20. Wang, J.H., Griffiths, P.R., Fuel, 64, 229 (1985).
21. Sobkowiak, M., Reisser, E., Given, P., Painter, P., Fuel, 63, 1245 (1984).
22. Benkhedda, Z., Landais, P., Kister, J., Dereppe, J.M., Monthioux, M., Energy Fuels, 6, 166 (1992).
23. Brandes, G., Brennstaff.Chem., 37, 263 (1956).
24. Yen, T.F., Erdman, J.C., ACS Div.Pet.Chem. Preprints, 7, 5 (1962).
25. Yen, T.F., Wu W.H., Chilingar, G.V., Energy Sources, 7, 203 (1984).
26. Yen, T.F., Nature Phy.Sci., 233, 36 (1971).
27. Yen, T.F., Wen, C.S., Kwan, J.T., Chow, E., in "Oil sand and oil shale", Strausz, O.P., Lown, E.M., (Eds.),p.309, Verlag Chemie International, Berlin (1978).
28. Bunger, J.W., Li, N.C., (Eds.), "Chemistry of asphaltenes", Amer.Chem.Soc., Washington D.C. (1981).
29. Yen, T.F., ACS Div.Pet.Chem. Preprints, 24, 901 (1979).
30. Friedel, R.A., Schulz, J.L., Sharkey, A.G., Fuel, 47, 403 (1968).
31. Williams, R.B., Chamberlain, N.F.,6th World Petrol. Congr. Frankfurt, paper 17, section V, (1963).
32. Chilingarian, G.V., Yen, T.F., (Eds.), "Bitumens, asphalts and tar sands", Elsevier Pub. Co. Amsterdam (1978).
33. Tissot, B.P., Welte, D.H., "Petroleum formation and occurrence", Springer Verlag, Berlin (1984).
34. Petersen, J.C., Fuel, 46, 295 (1967).
35. Barbour, R.V., Petersen, J.C., 46, 273 (1967).
36. Barron, P.F., Bendall, M.R., Armstrong, M.J., Atkins, A.R., Fuel, 63, 1276 (1984).
37. Dereppe, J.M., Moreaux,C., Fuel, 64, 85 (1974).
38. Snape, C.E., Marsh, M.K., ACS Div.Pet.Chem. Preprints, 30, 20 (1985).
39. Snape, C.E., Ladner, W.R., Petrakis, L., Gates, B.C., Fuel Proc. Techn., 8, 155 (1984).
40. Cookson, D.J., Smith, B.E., Fuel, 62, 34 (1983).
41. Cookson, D.J., Smith, B.E., Anal.Chem., 57, 864 (1985).
42. Cookson, D.J., Smith, B.E., Fuel, 66, 11 (1987).
43. Snape, C.E., Ray, G.J., Price, C.D., Fuel, 65, 877 (1986).
44. Sethi, N.K., Pugmire, R.J., Facelli, J.C., Grant, D.M., Anal. Chem., 60, 1574 (1988).
45. Ebherardt J.E., Nguyen T.H., Read R., Org. Geochem., 2, 145 (1992).
46. Zhu Y., Mullins O.C., Energy Fuels, 6, 545 (1992).
47. Mullins O.C., Zhu Y., Appl.Spectr., 46, 354 (1992).
48. Mullins O.C., Mitra-Kirtley S., Appl.Spectr., 46, 1405 (1992).
49. Wang, X., Mullins, O.C., Appl. Spectr., 48, 977 (1994).
50. Mullins, O.C., Wang, X., ACS Div.Pet.Chem.Preprints, 39, 457 (1994).
51. Payzant, J.D., Lown, E.M., Strausz, O.P., Energy Fuels, 5, 445 (1991).
52. Overfield, R.E., Sheu, E.Y., Sinha, S.K.,Liang, K.S., Fuel Sci.&Techn.Int.,7, 611 (1989).
53. Ravey, J.C., Decouret, G., Espinat, D., Fuel, 67, 1560 (1988).

54. Speight, J.G., Wernick, D.L., Gould, K.A., Overfield, R.E., Rao, B.M.L., Savage, D.W., Rev.de l'Institut Francaise du Petrole,40, 51(1985).
55. Al-Jarrah, M.M., Al-Dujaili, A.N., ., Fuel Sci.&Techn.Int., 7, 69 (1989).
56. Chung, K.E., Anderson, L.L., Wiser, W.H., Fuel, 58, 847 (1978).
57. Tynan E.C., Yen T.F., Fuel, 48, 191 (1969).
58. Yen, T.F., Boucher, L.J., Dickie, J.P., Tynan, E.C., Vaughan, G.B., J.Inst.Petroleum, 55, 87 (1969).
59. Boucher, L.J., Tynan, E.C., Yen, T.F., Inorg.Chem, 7, 731 (1968).
60. Boucher, L.J., Tynan, E.C., Yen, T.F., Inorg.Chem, 7, 2665 (1968).
61. Boucher, L.J., Tynan, E.C., Yen, T.F., Inorg.Chem, 8, 689 (1969).
62. Tynan, E.C., Yen, T.F., J.Magn.Reson., 3, 327 (1970).
63. Dickson F.E., Petrakis L., Anal. Chem.,46, 1129 (1974).
64. Malhotra V.M., Buckmaster M.A., Fuel, 64, 335 (1985).
65. Reynolds, J.G., Liquid Fuels Technol., 3, 73 (1985).
66. Graham, W.R.M., ACS Div.Pet.Chem.Preprints, 31, 608 (1986).
67. Asaoka, S.,Nakata,S.I.,Shuoto, J.,Takeuchi,C.,ACS Div.Pet.Chem.Preprints,31,597(1986).
68. Khulbe, K.C., Chan, B.W., Manoogran, A., Patmore, D.J., Fuel, 65, 1594 (1986).
69. Atherton, N.M., Fairhurst, S.A., Hawson, G.J., Magn.Res.Chem., 25, 829 (1987).
70. Reynolds J.G., Gallegos E.J., Fish R.H., Komlenic J.J.. Energy Fuels, 1, 36 (1987).
71. Malhotra, V.M., Buckmaster, M.A., ACS Div.Pet.Chem.Preprints, 34, 185 (1989).
72. Hwang, J.S., Al-Tuabi, M.O.H., El-Sayed, L., Energy Fuels, 8, 793 (1994).
73. Nali M., Corana F., Scilingo A., Scotti R.: Fuel Sci. Tech. Int., 12, 593 (1994).
74. Graham, W.R.M., in "Electronic Magnetic Resonance of the Solid State", Weil J.A. (Ed.), The Canadian Society for Chemistry, Ottawa, Canada (1987).
75. Yen T.F., Erdman J.G., Saraceno A.J., Anal.Chem., 34, 694 (1962).
76. Yen T.F., Young D.K., Carbon 111, 33 (1973).
77. Niizuma S., Steele C.T., Gunning H.E., Strausz O.P., Fuel, 56, 249 (1977).
78. Yen, T.F., ACS Div.Pet.Chem.Preprints, 24, 901 (1979).
79. Wright,B.V., Kalkwarf,D.R., Smith,R.D., Hardy,D.R., Hazlett,R.N., Fuel, 64, 591 (1985).
80. Malhotra, V.M., Buckmaster, M.A., Org.Geochem., 8, 235 (1985).
81. De Sousa J.J.F., Vugman, N.V., Costa Neto, C., Bull.Magn.Reson., 9, 96 (1987).
82. Senglet, N., Faure, D., des Courieres, T., Bernasconi, C., Guilard, R., Fuel, 69, 203 (1990).
83. Niizuma, S., Iwaizumi, M., Strausz, O.P., AOSTRA J.Res., 7, 217 (1991).
84. Khulbe, K.C., Mann, R.S., Lu, B.C.Y., Lamarche G., Lamarche, A.M., Fuel Process Technol., 32, 133 (1993).
85. Retcofsky, H.L., Thompson, G.P., Raymond, R., Friedel, R.A., Fuel, 54, 126 (1975).
86. Petrakis L., Grandy D.W., Anal.Chem., 50, 303 (1978).
87. Kwan, C.L., Yen, T.F., Anal.Chem., 51, 1225 (1979).
88. Dack, S.W., Hobday, M.D., Smith, T.D., Pilbrow, J.R., Fuel, 62, 1510 (1983).
89. Dack, S.W., Hobday, M.D., Smith, T.D., Pilbrow, J.R., Fuel, 63, 39 (1984).
90. Dack, S.W., Hobday, M.D., Smith, T.D., Pilbrow, J.R., Fuel, 64, 219 (1985).
91. Dack, S.W., Hobday, M.D., Smith, T.D., Pilbrow, J.R., Fuel, 62, 222 (1985).
92. Singer, L.S., Lewis, I.C., Carbon, 22, 487 (1984).
93. Gutsze A., Orzeszko S.: Adv.Coll.Int.Sci., 23, 215 (1985).
94. Silbernagel B.G., Gebhard L.A., Dyrcacz G.R., Bloomquist A.A., Fuel, 65, 558 (1986).
95. Singer L.S., Lewis I.C., Doetschman D.C., in "Electron Magnetic Resonance of the Solid State"Weil, J.A. (Ed.), The Canadian Society for Chemistry, Ottawa, Canada (1987).
96. Thomann, H., Silbernagle, B.G., Jin, H., Gebhard, L.A., Tindall, P., Dyrkacz, G.R., Energy Fuels, 2, 333 (1988).
97. Silbernagle, B.G., Bernardo, M., Thomann, H., Fuel, 72, 1219 (1993).
98. Azami, K., Yokono, T., Sanada, Y., Uemura, S., Carbon, 27, 177 (1989).
99. Bakr, N.J., Akiyama, M., Sanada, Y., Org.Geochem., 15, 595 (1990).
100. Retcofsky, H.L., Stark, J.M., Friedel, R.A., Anal.Chem., 40, 1699 (1968).
101. Austen, D.E.G., Ingram, D.J.E., Tapley, J.G., Trans.Faraday Soc., 54, 400 (1958).
102. Robson, D., Assabgny, F.Y.T., Ingram, D.J.E., Nature, 221, 51 (1969).
103. Calemma, V., Iwansky, P., Nali, M., Scotti, R., Montanari, L., Energy Fuels, 9, 225 (1995).
104. Montanari, L., Clericuzio, M., Del Piero, G., Scotti, R., Appl.Magn.Res., 14, 81 (1998).
105. Gupta, P.L., Dogra, P.V., Kuchhal, R.K., Kunimar, P., Fuel, 65, 515 (1986).
106. Rafenomanantsoa, A., Nicole, D., Rubini, P., Lauer, J.-C., Energy Fuels, 8, 618 (1994).
107. Ernst, R.R., J.Chem.Phys., 45, 3485 (1966).

108. Vo Dinh T., Anal. Chem., 50, 396 (1978).
109. Kershaw J.R., Fuel, 74, 1104 (1995).
110. Requejo, A.G., Gray, N.R., Freund, M., Thomann, M., Melchior, M.T., Gebhard, L.A., Bernardo, M., Pietroski, C.F., Msu, C.S., Energy Fuels, 6, 203 (1992).
111. Bielski B.H.J., Gebicki J. M., "Atlas of Electron Spin Resonance Spectra", p. 606–613, Academic Press, New York, N.Y. (1967).
112. Mullins,O.C., in "Asphaltenes: fundamentals and applications", Sheu, E.Y., Mullins, O.C., (Eds.), Chap. 2, p.53, Plenum Press, New York (1995).
113. Wertz J.E., Bolton J.R., "Electron Spin Resonance", p.456, Chapman and Hall, NewYork-London (1986).
114. Blombergen N., Purcell E.M., Pound R.V., Phys.Rev., 73, 679 (1948).
115. Portis A.M., Phys. Rev., 91, 1071 (1953).
116. Drago R., "Physical methods in chemistry", chap. 11, p. 416, W.B.Saunders Company, Philadelphia-London-Toronto (1977).
117. Bijl D., Kainer H., Rose-Innes A.C., J.Chem.Phys., 30, 765 (1959).
118. Wertz J.E., Bolton J.R., "Electron Spin Resonance", p.249, Chapman and Hall, NewYork-London (1986).
119. Granucci G., Persico M., Chem.Phys.Lett., 205, 331 (1993).
120. Poole, C.P., "Electron Spin Resonance (A comprehensive treatise on experimental techniques)" 2nd edition, p. 412, Wiley Interscience Publication-John Wiley & Sons, New York (1983).

Chapter IV

SELF-ASSOCIATION OF ASPHALTENES

Structure and Molecular Packing

Eric Y. Sheu

Fuels and Lubricants Technology Department
Texaco Inc.
P.O. Box 509
Beacon, New York 12508

1. INTRODUCTION

Asphaltene represents the most refractory fraction of petroleum liquids. It is defined by the solubility in alkyl solvents, such as pentane or heptane [1,2]. For example, heptane asphaltene is defined as the fraction in the petroleum liquid that is insoluble in heptane but soluble in toluene.

The importance of asphaltene in the petroleum industry is through its negative impact on various petroleum operations, such as exploration, production, transportation, and refining [3–11]. In exploration, asphaltene may alter the flow phase of the reservoir; in production, it may plug the wellbore; in transportation, it may precipitate, and eventually clot up the pipeline; in refining, it hinders the refining yield. These are well known phenomena experienced during many years of operations and/or processes.

Many of the problems described above are related to a fundamental characteristic of asphaltene—the strong self-association propensity [1,2,8–11]. Apparently, the solubility defined asphaltene fraction has certain physical characteristics that lead to its insolubility in heptane (or pentane). These characteristics may also lead to their self-association, flocculation, sedimentation, and precipitation in an organic environment or along the operation/process streams. The importance of the self-association of asphaltene can be easily understood in practical applications where flocculation and precipitation of asphaltene are costly stumbling blocks. Mansoori [5,6] has been working on the subject of "arterial blockage", both experimentally and theoretically. Many valuable results have been produced by his group, giving us a good understanding on asphaltene or asphaltene/wax blockage phenomena. Much of his work is related to the fundamental characteristics of asphaltenes, since the self-association of asphaltene is the early stage of arterial blockage.

In order to avoid or resolve the problems caused by asphaltene, or even make use of its characteristics, one needs to have a good understanding of these phenomena at the molecular level. In this chapter the characteristics of asphaltene will be discussed. The starting point is naturally the self-association phenomena, a readily observable experimental phenomenon resulted from combination of its many molecular properties [12–16]. Since the self-association of asphaltenes may differ from the conventional micellization process of surfactants, asphaltene aggregates will be used in this chapter instead of asphaltene micelles.

From statistical mechanical theory point of view, information about each fundamental property (generally represented by a parameter) that is involved in the self-association process should be reflected in the aggregate structure, size, polydispersity, and growth characteristics. These properties can thus be identified and characterized through examination of the aggregate size, shape, polydispersity, as well as their responses to chemical, electrical and/or mechanical perturbation. Having this concept in mind, one can design a logical approach to uncover the self-association process by studying the static and dynamic structure of the aggregates under various physical conditions.

Many research reports have shown that the asphaltene aggregates are on the colloidal length scale [17–31], far smaller than the length scale of many classical experimental probes. Thus, the techniques used should have probes comparable to the colloidal length scale, in order to accurately determine the structure and other statistical mechanical parameters of the asphaltene aggregates. There are many direct and indirect spectroscopic methods available, among them the small angle neutron scattering (SANS) and small angle X-ray scattering (SAXS) are the most suitable techniques from the length scale and resolution point of view. Both techniques are readily available, superb in resolution, and the statistical mechanical theories for data analysis are mature. More importantly, both techniques can be applied for *in situ* measurements which open up the possibility for kinetic study.

In addition to the structural studies, other characteristics of asphaltene should be investigated in order to map out a complete picture. These include its (1) surface properties (2) interfacial properties (3) short range bulk properties and (3) long range bulk properties. All these properties are closely tied with petroleum processing. For example, the relevant petroleum operations/processes to asphaltene surface and interfacial properties are caustic wash, residue wash, tar-sand separation, oil recovery, oil emulsification and de-emulsification, etc. The short range bulk properties are related to the inter-asphaltene short range interactions which result in self-association, flocculation, sedimentation, and precipitation processes. The long range bulk properties are important for oil-in-water emulsion and can regulate the emulsion stability.

The surface and interfacial properties were discussed in an earlier book chapter [11] and in many articles [32–43]. They will not be discussed here. In this chapter the focus will be on the bulk properties. Four major subjects will be discussed. The first part will be devoted to the colloidal structure of asphaltene aggregates, including their size, shape and polydispersity using SANS. In this study, short range interactions are involved while the long range interactions are less important. A brief description of the schemes for unambiguous analyses of the scattering data will be given. The second part makes use of hydrochloric acid (HCl) as a polar probe to "measure" the molecular packing of the asphaltene aggregates (through forming asphaltene/HCl/toluene water-in-oil asphaltene emulsions). This process involves both long and short range interactions, along with the interfacial characteristics. This study sets a base for the molecular dynamic simulation study to be presented in the last part. The third part is a phase separation study, measuring the kinetics

along the phase separation path. It is essential for many petroleum processes, such as production and transportation. The last part is a molecular dynamic simulation study for asphaltene self-association in toluene. This simulation makes use of all analytical data obtained from the previous experiments to identify the impact from each thermodynamic parameters on the self-association process. A scenario, based on the results from these four studies, is proposed for asphaltene self-association, flocculation and sedimentation processes.

2. REVIEW

Asphaltene self-associates has been reported long ago [7,17–23,25–29]. For many decades, this self-association phenomenon was investigated through rheological experiments [7,17,25–29,44–46]. Since rheological experiments represents a macroscopic experimental method, it should be good for the macroscopic length scale only. This is equivalent to saying that the conclusion drawn from the rheological experiments should be reconciled or validated, at least from a more rigorous scientific point of view.

Dwiggin performed the first solid X-ray experiment exposing the molecular inside of asphaltene in solid state [47, 48]. He concluded that asphaltene does exhibit cluster-like structure. Since the experiments were performed in the solid phase the self-association of asphaltene in petroleum liquids is still obscure. More concrete evidence was later obtained through surface tension measurements [39–43] and micro-calorimetric study [49]. These experiments, together with the fractal structural studies, provide direct evidence of asphaltene self-association and their fractal growth in organic solvents. These experiments more or less confirm the prediction of the asphaltene structure on various length scale proposed by Yen [20]. While these experiments confirm Yen's structural model, a more fundamental question arises—what are the relevant thermodynamic or statistical mechanical parameters? This has been the most difficult question to answer. It not only requires many techniques to synergistically reveal all characteristics of such a complex system but also needs sophisticated modeling work to map out accurate scenarios.

In fact, the reported studies on the aggregate structures, which carry most of the thermodynamic and statistical mechanical information, differ from study to study. For example, the shape of the asphaltene aggregates in organic solvents has been reported as sphere [24,31], disks [50,51], and cylinders [52], while high polydispersity of the aggregates appears to be a general consensus. With the shape being in contradiction, an accurate statistical mechanical picture of the aggregation mechanism can hardly be established. Since all shapes reported are based on scattering methods and analyzed using presumed structural models, it is extremely difficult to judge the merit of one analysis scheme and/or model from another. In order to surmount this hurdle, constructing a model-independent analysis scheme is desperately needed, not only for mitigating the confusion but for revealing the true aggregation mechanism of asphaltene. In this chapter, a model-independent method will be introduced and applied to analyze the SANS data. The complimentary results on the shape of the aggregates will be compared with the model dependent methods. Hopefully, this non-biased approach will bring better structural information about asphaltene and lead to development of practical technology for better petroleum operations.

In the last part of this chapter, computer simulations are presented to accurately map out the aggregation process and the structure of the aggregates. Several computer simulations were reported before [53,54] to described the structures. The purposes of these mo-

lecular dynamics simulation experiments are multi-fold. They can provide a clear aggregation path and the resulting aggregate structures. In addition, the relevant molecular parameters, such as molecular structural distribution, effect of the electrostatic interactions etc., can be incorporated to examine their influence. However, the simulations require rigorous analytical data as input to make the results accurate and convincing. In other words, the computer experiments still largely rely on the experimental data which may or may not be accurate. Therefore, the conclusions drawn from the computer simulations may still be in jeopardy for a system as complex as asphaltene.

3. MATERIALS AND EXPERIMENTS

3.1. Materials

Two series of asphaltene samples were used for the experiments presented in this chapter. They are derived (using heptane) from the Ratawi vacuum resid and the Arabia Medium Heavy vacuum resid respectively. The extraction process is standard. A weight (resid) to volume (heptane) ratio of 1 to 40 were mixed under nitrogen for over 8 hours at room temperature. The insoluble fraction (asphaltene) was extracted by filtration and dried under nitrogen. Prior to each experiment the asphaltene solutions were prepared by re-dissolving asphaltene in the proper organic solvents. All solvents used are HPLC grades. For small angle neutron scattering (SANS) the solvents used were deuterated to enhance the scattering contrasts between aggregates and the solvents.

3.2. Small Angle Neutron Scattering Measurement

SANS experiments were performed at two national laboratories, Argonne National Laboratory (ANL) and National Institute of Standards and Technology (NIST). At ANL, the asphaltene/toluene two-component systems were measured at room temperature. The neutrons at ANL are generated from a spallation source. The time-of-flight mechanism was used for the SANS spectrometer. By this method, the range of the wave length, λ, used spans ~ 0.5 to 14 Å. The configuration of the spectrometer was adjusted, together with the λ range, to cover a spatial resolution, Q (= $4\pi/\lambda \sin(\theta/2)$, θ is the scattering angle), from 0.008 to 0.35 $Å^{-1}$.

SANS experiments performed at the National Institute of Standards and Technology (NIST) were for asphaltene/toluene/HCl emulsions. They were performed on the specific spectrometer, NG-7 small angle neutron spectrometer. At NIST, the neutron beam was generated from a 25 MW heavy water reactor. A velocity chopper was used to select a mono-energetic neutron group for SANS study, as oppose to the time-of flight used in ANL. The λ was selected at 10 Å and the Q range was adjusted to span 0.004 to 0.25 $Å^{-1}$.

3.3. Conductivity Measurement

Conductivity measurements were performed using a Hewlett Packard Low Frequency Analyzer (model HP4192A) as well as a simple hand-held static conductivity meter (VWR Scientific Model 2052). The conductivity cell for the HP4192A analyzer is a Rosemont glass immersion cell with cell constant equal to 1. The cell consists of four anodized platinum plates to prevent double layer effect near the plates. The sample cell is a regular beaker containing 50 ml of sample. The distance between the cell and the beaker

wall was kept at 2 cm or wider to maintain the homogeneity of the local electric field. Low speed stirring was applied during measurements to maintain the sample isotropy. In the frequency range of 5 Hz to 100 kHz, the conductivity remains independent of the frequency. We thus fixed the frequency at 100 kHz. The conductivity was measured as a function of asphaltene concentration and as a function of the added pH=1.0 HCl volume. All measurements were performed at T = 25 °C.

3.4. Viscosity Measurement

The viscosity measurements were performed using a Brookfield low shear rate viscometer with a 0–1000 centipoise working range and a 0.1% accuracy of the full scale. The cell was a cuvette cell, immersed in a temperature bath. The open end of the cuvette cell was capped to prevent solvent evaporation. Ratawi or Arabia Medium Heavy (AMH) asphaltene/toluene solution was first prepared with known asphaltene concentration. At time zero, known amount of heptane was added to initiate the phase separation. The viscosity was measured continuously as the phase separation process proceeds. The measurement was terminated when sedimentation occurs at the bottom of the cuvette cell and the viscosity starts to decrease drastically. A viscosity versus time curve was constructed for each separation process. Temperature was kept at 25 °C through out the experiment.

4. THEORY

4.1. Small Angle Neutron Scattering Technique

Small angle neutron scattering (SANS) is a powerful tool for characterization of the suspension structure in the colloidal length scale. Asphaltene aggregates certainly fall into this category. SANS detects the momentum transfer (or scattering angle and phase shift) of the incident neutrons after interacting with the suspended particles. The wavelength of the neutrons used in SANS can be selected from ~ 1 to 30 Å, which is comparable to or smaller than the suspended particles. Thus, the momentum transfer resulting from the neutron-particle interactions will carry combined information of particle size, shape and inter-particle interactions. SANS measurement gives the scattering intensity as a function of the scattering angle (equivalent to the momentum transfer) which carries particle (in this case the asphaltene aggregates) structure and their interaction parameters. However, one needs to extract these parameters through a proper data analysis. A typical model analysis depends on structures, polydispersity and interactions between particles. Ambiguity may arise when simultaneously extracting these parameters. Thus, caution should be taken whenever models are used for analyzing SANS data. Under certain conditions, a model independent analysis scheme may be used for limited analysis of the data, such as surface to volume ratio which helps identify the particle shapes. Combining the model independent with the model dependent analyses is a more reliable approach and the results are usually unambiguous. In the following fundamental structural analysis schemes will be described (4.1.1.). In addition, a model independent method for shape analysis will be presented (4.1.2.).

4.1.1. Model Dependent Structural Analysis. The scattering intensity distribution function of a SANS measurement, I(Q), represents the distribution of the scattered neutron at a subtended angle θ. Q is the momentum transfer which depends on scattering angle θ

and wave length by $Q=4\pi/\lambda \sin(\theta/2)$. For detailed derivation of the following equations, the readers can refer chapter I of Ref. [11].

For an isotropic monodisperse suspension system I(Q) can be expressed in terms of the structural and interaction parameters as [55–57]

$$I(Q) = N_p(\Delta\rho)^2 V_p P(Q) S(Q) \tag{1}$$

where N_p is the number density of the particles (in this case the asphaltene aggregates), $\Delta\rho$ is the scattering contrast between the aggregates and the solvent, and V_p is the particle volume, P(Q) is the particle structure factor governed by particle shape and size. S(Q) is the inter-particle structure factor, governed by inter-particle interactions. Because the samples studied here are organic and dilute, the long range interactions can be neglected and S(Q) can be taken as unity. However, polydispersity should be taken into account in Eq. (1). I(Q) in this case becomes

$$I(Q) = < N_p > (\Delta\rho)^2 < V_p >< P(Q) > \tag{2}$$

where

$$< P(Q) >= \frac{\int V_p^2 P(Q) dV_p}{\int V_p^2 dV_p} \tag{3}$$

In the model dependent analysis, a particle shape and a size distribution function are presumed to fit the experimental I(Q) using Eq.(2). The adjustable structural parameters account for particle size, shape, and size distribution function, are extracted through data fitting. In many cases, there are too many adjustable parameters used for fitting. This can yield ambiguous or physically meaningless results, due to multiple conversions. In order to avoid such ambiguity and be able to justify the presumed structures and their distribution functions, a self-consistent check is often needed. In the following such a self-consistent check method is described.

This self-consistent check method is based on an assumption—the function of the size distribution does not change with increasing asphaltene concentration. Under this assumption, $\Delta\rho$ will be independent of the concentration. With this assumption one can presume a structural model and a size distribution function to fit the data. In the course of data fitting, one can lump $<N_p>$, $\Delta\rho$, and $<V_p>$ into a pre-factor, A. After fitting, $\Delta\rho$ ($=A/<N_p><V_p>$) can be calculated using the extracted structural parameters and the presumed distribution function (see the result section for details). If $\Delta\rho$ varies with asphaltene concentration, then the presumed distribution is not correct [56], otherwise, it may be an appropriate model. One can repeat this process for different structures and size distribution functions until consistent results are obtained.

4.1.2. Model-Independent Analysis Scheme. As expressed in the previous section, I(Q) is a function of the structural function P(Q) which requires a model in order to proceed with the analysis. If a model independent analysis is to be used, it can only be applied at the integrated level of P(Q). This means that some detailed structural information will be lost. As a result, the model-independent analysis cannot provide as rich informa-

tion as the model-dependent analysis, as far as the analysis of P(Q) is concerned. In fact, the most reliable parameter that can be obtained from a model independent analysis is the surface to volume ratio (S/V) of the asphaltene aggregates. It can help identify the shape of the aggregates via comparing with the model-dependent analyses. Mathematically, it sets a sufficient condition to reject certain shapes presumed in the model dependent analysis. However it cannot adequately and rigorously determine the shape of the aggregates.

The starting point of the S/V analysis is the scattering function of an arbitrary object at position $\vec{r}_i$ (see Figure 1). Taking the nuclei's scattering cross section distribution within the object as $\rho(\vec{r}_i)$, then the intra-particle scattering function can be expressed,

$$F(\vec{Q}) = \int_V dV\rho(_i r)e^{i\vec{Q}\cdot\vec{r}_i} \tag{4}$$

The scattering intensity distribution function I(Q) is the total integration of the complex conjugate of the intra-scattering function $F(\vec{Q})$

$$I(\vec{Q}) = F(\vec{Q})F(\vec{Q})^* = \int_{V_i} dV_i \int_{V_j} dV_j \rho(\vec{r}_i)\rho(\vec{r}_j)e^{-i\vec{Q}(\vec{r}_j-\vec{r}_i)} \tag{5}$$

If one replaces the scattering cross section correlation between ith and jth nuclei with their scattering contrast $\Delta\rho_{ij}$, and assumes the system is isotropic, then the ensemble average of the phase factor $e^{-i\vec{Q}(\vec{r}_j-\vec{r}_i)}$ becomes sinQr/Qr where r is the distance between two nuclei [58]. If one further assumes that the contrast is only realized between the nuclei that form the particle and those form the solvent, then one can replace the contrast with the mean fluctuation of the scattering length density between the particle and the solvent. With these restricted conditions, the I(Q) becomes

$$I(Q) = V\int_0^\infty 4\pi r^2 dr\gamma(r)\frac{\sin Qr}{Qr} \tag{6}$$

where V is the particle volume and $\gamma(r) = <\rho(\vec{r}_i)\rho(\vec{r}_j)>$ is the so called Debye correlation function, representing the average of the product of two scattering fluctuations at position $\vec{r}_i$. Taking the auto-correlation, i.e., r=0, then

$$V\gamma(r=0) = V(\Delta\rho)^2 = \frac{1}{2\pi^2}\int_0^\infty Q^2 dQI(Q) \tag{7}$$

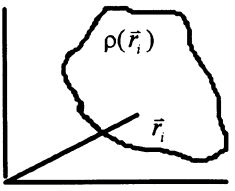

Figure 1.

Eq.(7) is the mean fluctuation of the scattering length density, in which the integral $\int_0^\infty Q^2 dQI(Q)$ is the "invariant", ξ, related to the total surface to volume ration (S/V). Porod [57] made use of this invariant and related it to the total scattering surface S at the large Q limit by

$$\lim_{Q\to Q_{max}} I(Q) = (\Delta\rho)^2 \frac{2\pi}{Q^4} S \tag{8}$$

Using Eq. (7) and Eq. (8) one can easily derive S/V for a homogeneous particle as

$$\frac{S}{V} = \pi \frac{\lim_{Q\to\infty} I(Q)Q^4}{\xi} \tag{9}$$

As one can see for Eq. (7) and Eq. (9) the structural model of the aggregates is not involved, and S/V can be obtained directly from the experimental data I(Q) at the large Q limit.

In the case of asphaltene, the aggregates are not homogeneous, thus, the problem becomes very complex if one were to detail all the scattering sites within the aggregates. One way to deal with such complication is to approximate the inhomogeneity with a perturbed homogeneous approach.

In an inhomogeneous particle the argument of using the auto-correlation is not enough, since there exists contrast between ith and jth nuclei within an aggregate. Thus, Eq. (5) should be fully manipulated to account for all contrasts within the particle. An approximate method is to express the scattering function at the asymptotic Q. In this Q regime one can still regard the small Q range to have constant scattering length density without contradicting the S/V expression in Eq. (8). With this perturbation approach I(Q) can be modified as

$$I(Q) \underset{Q\to\infty}{\approx} \iiint_{i=j} dV\rho(\bar{r}_i)\rho(\bar{r}_j) + \frac{2\pi(\Delta\rho)^2}{Q^4} S = C_0 + C_4 S \tag{10}$$

The first term is the contribution from the inhomogeneity within a particle. It is a constant, representing the non-zero slope, C_0, in the Porod's plot ($I(Q)Q^4$ versus Q^4). The new Porod's plot according to Eq.(10) should oscillate about the straight line $C_0 Q^4 + C_4$.

In order to reconstruct the S/V for a inhomoheneous system, a new invariant ξ* is defined as

$$\xi^* = \xi + \frac{C_4}{Q_{max}} \tag{11}$$

The approximate surface to volume ratio can be written as

$$\left(\frac{S}{V}\right)^* = \frac{\pi^2 C_4}{\xi^*} \tag{12}$$

Eq. (12) is the equation used for evaluation of the surface to volume ratio of the asphaltene aggregate. In this analysis, only the measured I(Q) is needed. No structure modeling will be involved. Once S/V is determined, one can compare with the S/V obtained from the model fitting. For example, when one presumes a spherical model to fit the data, the surface to volume ratio will be 3/<R> (<R>=average radius). For cylindrical particles and flat particles it will be 2/<R> and 2/t (t = thickness of the flat particle) respectively. Upon each fitting, one can compute S/V using the extracted structural parameters and compare with the S/V obtained from Eq.(12).

4.2. Conductivity and Its Indication

4.2.1. Molecular Packing of Asphaltene Aggregates. The molecular packing of the asphaltene aggregates should in principle differ from a surfactant system, in part due to the inhomogeneity of the asphaltene molecular structures. How do asphaltene molecules pack in an organic solvent to form aggregates and what is the fundamental structural difference between the surface and the core of the aggregates? These are two main questions yet to be answered. Although colloidal structures are understood to some certain extend, the fundamental packing mechanism of asphaltene molecules in an aggregate is still unknown.

In this section an indirect method is applied to address this problem. This method "measure" the packing using an electrolyte probe—aqueous HCl with pH=1.0. The HCl molecules mix with asphaltene/toluene solution to form water-in-oil emulsions. The HCl molecules incorporated with the asphaltene aggregates act as a structural probe. When small quantity of HCl are incorporated with this asphaltene solution, HCl will prefer to enter the core of the asphaltene aggregate to avoid the direct contact with the highly hydrophobic toluene solvent. When HCl molecules are incorporated within the aggregates, they will reside at the polar sites of the aggregates. These polar sites form the basic packing scheme of the aggregates.

Experimentally, one can characterize the packing scheme by measuring the system conductivity and its dependence on HCl concentration. This is because the conductivity of the HCl carrying asphaltene aggregates will vary in a manner reflecting the distribution of the electrolytes residing in the aggregates. However, this argument will fail if the attached HCl molecules alters the structures. Therefore, one should verify this method by checking if the HCl containing aggregates redistribute upon increasing asphaltene concentration. In addition, one needs to construct a phenomenological model to relate the conductivity with the molecular packing mechanism. The model can be expressed explicitly as a function of the HCl concentration. With the model, one simply measures the conductivity as a function of HCl volume fraction at a given asphaltene concentration and analyze the data using the phenomenological model.

In the following a simple equation will be derived to relate the conductivity data with the intra-aggregate structure. The starting point is a simple system containing two identical spherical particles of charge Z and -Z. The chemical potentials of the two particles at the thermal equilibrium can be expressed as

$$2\mu_0 = \mu_z + \mu_{-z} \tag{13}$$

where μ_0 is the chemical potential of a neutral particle. The chemical potentials of the charged and the uncharged particles can be expressed

$$\mu_o = \mu_o^o + k_B T \ln X_o \tag{14}$$

$$\mu_Z = \mu_Z^o + k_B T \ln X_Z \tag{15}$$

$$\mu_{-Z} = \mu_{-Z}^o + k_B T \ln X_{-Z} \tag{16}$$

where X_i is the mole fraction of the ith specy. From Eq. (13) to (16) one obtains

$$X_Z = X_{-Z} = X_o \exp\left[\frac{-Z^2 e^2}{2k_B T \varepsilon_o \varepsilon_r}\right] \tag{17}$$

where e is the electron charge and ε_0 is the permittivity of vacuum. When an electric field E is applied, the current passing through the solution can be written as,

$$I = Ze X_Z V_Z \tag{18}$$

where V_Z is the velocity of the particle with charge Z. The velocity can be expressed by Stoke's equation as,

$$V_z = \frac{F_z}{6\pi\eta r_h} \; ; \; F_z = ZeE \tag{19}$$

where η is the solvent viscosity. From Eq. (17) – (19), the conductivity σ can be obtained,

$$\sigma = \frac{I}{E} = \frac{z^2 e^2 X_Z}{6\pi\eta r_h} \tag{20}$$

Eq. (20) shows that the static conductivity of a solution depends on the charges of the suspended particles, their mole fractions, solvent viscosity and the hydrodynamic radius of the particle. Among these parameters, the particle charges and the mole fractions are primary parameters and can be controlled experimentally. The hydrodynamic radius of the particles, r_h, is a derived parameter from the Stoke-Einstein equation. One thus should measure σ as a function of one of the primary parameters and relate the conductivity behavior to the intra-structure of the asphaltene aggregate using some presumed packing models. The parameter we chose is the HCl volume fraction.

In order to establish a relation between σ (the measurable quantity) and the intra-structure a presumed packing condition is needed. Based on this packing condition one can derive its corresponding mathematical expression for σ using the primary parameters which one can vary experimentally. With the formula and the presumed packing conditions, one can analyze the experimental data to validate the presumed packing conditions. This process provides a sufficient condition to prove the presumed packing condition from a mathematical point of view. It is not an adequate condition, unless all packing conditions are evaluated and experimentally tested against all controllable primary parameters. Unfortunately, only one experimental parameter, the HCl concentration, can be used to validate the presumed packing conditions in this case. Thus, the packing scheme so obtained should only be taken as a suggestion.

Two monomer packing schemes are presumed here for asphaltene aggregates. In both schemes the asphaltene aggregates are assumed to have a polar core. The first one is similar to a surfactant based microemulsion droplet (water-in-oil droplet) where the polar ends of the asphaltenes (the polynuclear aromatic rings) point inward. When HCl is added, these asphaltenes accommodate the HCl molecules in their polar cores to form a water droplet coated with the asphaltene molecules (act as surfactants) and suspended in the toluene bulk phase. The droplet responds to the increasing HCl volume fraction with a three-dimensional expansion.

The second packing scheme has asphaltene molecules inter-locked within the aggregates. Because of the wide structural distribution of the monomers, we assume there exists cavities within the aggregates. When HCl is added, the HCl molecules reside in these cavities. Since the asphaltene monomers are inter-locked, the droplet sizes do not expand upon increasing HCl. Once the cavity space is filled with HCl, the system can no longer take extra HCl. At this point, either percolation or phase separation will occur when more HCl is added. For these two packing conditions, the solution conductivity behaves differently as a function of the uptake volume of HCl solution, which provides the basis for verification.

If the packing is like a water-in-oil emulsion, then, the only parameter independent of the HCl content is the effective asphaltene head area. It is the area of the polar end of the molecules facing inward [59]. Taking this area as a_H then $a_H N_{Asp}$ (N_{Asp} is the number of asphaltene monomers per unit volume) is the total surface area of the polar core per unit volume of the sample. Assuming the droplets are spherical, then the total volume fraction of the disperse phase is

$$\phi = \frac{4}{3}\pi r^3 N_D \tag{21}$$

and the total surface area S is

$$S = a_H N_{Asp} = 4\pi r^2 N_D \tag{22}$$

or

$$r^2 = \frac{a_H N_{Asp}}{4\pi N_D} \tag{23}$$

where N_D is the number of droplets per unit volume of the solution. Since the total charges of an aggregate is proportional to the added HCl volume (i.e., $Ze \sim \phi_w/N_D$), one can substitute Eq. (17) – (19) and Ze into Eq. (20) to get

$$\sigma = (\phi_w + \phi_{Asp})\phi_w^2 \frac{2}{\eta a_H^2 N_{Asp}^2} \tag{24}$$

or

$$\frac{\sigma}{\phi_w^2} = K(\phi_w + \phi_{Asp}) \tag{25}$$

where K is a proportional constant containing a_H, N_{Asp} and η. These three parameters were kept constant in our study. Eq. (25) can be used to examine if the packing is similar to a water-in-oil emulsion. This can be done by plotting σ/ϕ_w^2 as a function of ϕ ($=\phi_w + \phi_{asp}$). If a linear relation is not shown, this model is incorrect, otherwise, it may apply.

On the other hand, if the asphaltene molecules are inter-locked within the micelles, the movement of the molecules within an aggregate would be rather difficult. No re-distribution of the droplets is expected to occur when HCl is added. In other word, the sizes of the droplets (r_h in Eq. (20)) would remain constant. In this case, the conductivity will depend only on the number of charges (or the volume) of the added HCl solution, or

$$\sigma \propto \phi_w^2 \tag{26}$$

This packing condition can be checked by plotting σ as a function of ϕ_w^2.

4.2.2. Percolation Mechanism. As the added aqueous phase saturates the polar sites and the cavities, either the asphaltene aggregates percolate to accommodate more aqueous phase or phase separation will occur. If percolation occurs, one can adopt the theory developed by Grest et al. to identify and characterize it [60]. They derived a set of simple equations to describe the percolation of a water-in-oil emulsion/microemulsion that contains water droplets,

$$\begin{aligned} \sigma &\propto (\phi_c - \phi)^{\mu} \quad for\ \phi > \phi_c \\ \sigma &\propto (\phi - \phi_c)^{-s} \quad for\ \phi < \phi_c \end{aligned} \tag{27}$$

where μ and s are percolation exponents and are considered universal for many water-in-oil microemulsions. In the case of asphaltene/HCl/toluene it is expected to differ from this theory. Details are discussed in the discussion section.

4.3. Viscosity and the Kinetics of Asphaltene Phase Separation

The intent of using low shear viscosity measurements for a phase separation study is to derive a simple viscosity equation that can be used for detecting the kinetic process of asphaltene phase separation. This is similar to the measurement of the size evolution of the laser ring to track the spinnodal decomposition process. In petroleum phase separation involving asphaltene, the first stage is the flocculation, and followed by sedimentation and precipitation. The flocculation stage is the most important stage giving a warning sign of the resulting sedimentation. It is also the stage where the dispersion phase remains in the solution and an analytical formulation can be derived without involving the dynamic change of dispersion concentration.

The viscosity equations to be derived here will be for the flocculation stage only. The initial condition is a homogeneous asphaltene solution with asphaltene concentration above the aggregation onset concentration (there exists asphaltene aggregates). The system at this stage is stable and in the equilibrium state with asphaltene aggregates suspended in the bulk phase. When the precipitation process is initiated, either by lowering the pressure or by introducing heptane into the asphaltene/toluene solution, the flocs start to form and eventually lead to precipitation.

Assuming the flocs are monodisperse and taking d as the average diameter of an elemental asphaltene aggregate, by which the flocs are formed, the flocs radius of gyration $R_g(t)$ at time t can be expressed as [61–64]

$$R_g(t) \sim N(t)^{\frac{1}{f}} d \tag{28}$$

where f is the fractal dimension of the floc, and N(t) is the number of the elemental aggregates in a flocculate. With the formation of the fractal flocs, the volume fraction of the disperse phase is modified from

$$\phi = N(t)\frac{\pi}{6} d^3 \rho(t) \tag{29}$$

to

$$\phi_{eff} \sim N(t)\frac{4\pi}{3} R_g^3 \rho(t) \tag{30}$$

where $\rho(t)$ is number density of the particles. Let ν be the density of the elemental aggregates, the total weight of the disperse phase will be

$$W = N(t)\frac{\pi}{6} d^3 \rho(t)\nu \tag{31}$$

and the effective volume fraction of the disperse phase will be

$$\phi_{eff} = k(8W/\nu)N(t)^{\frac{3}{f}-1} \tag{32}$$

Where k is a proportional constant. Now, taking the simplest form for the relative viscosity η_r, the Einstein equation, one arrives at

$$\eta_r = 1 + 2.5\phi_{eff}(t) = 1 + 20k\frac{W}{\nu} N(t)^{\frac{3}{f}-1} \tag{33}$$

or

$$\ell n\left\{\frac{[\eta_r(t)-1]\nu}{20kW}\right\} = \left(\frac{3}{f}-1\right)\ell n[N(t)] \tag{34}$$

If we further assume the flocculation process is diffusion limited in the concentration regime studied here [65–66] and the process is governed by the Smoluchowski equation, then N(t) ~ t, and Eq. (34) becomes

$$\ell n\left\{\frac{[\eta_r(t)-1]\nu}{20kW}\right\} = \left(\frac{3}{f}-1\right)\ell n[t] \tag{35}$$

Eq. (35) is the equation to be used. It provides the fractal dimension when one analyzes the viscosity as a function of time according to Eq. (35).

One should note that the Einstein equation is for hard spheres at dilute concentration only. By adopting the Einstein equation we assume the fractal flocs are hydrodynamically spherical and the entrapped solvent molecules are static with respect to the asphaltene molecules that form the flocs.

A similar equation can be derived for a polydisperse system (the fractal flocculates). The average number of micelles in each flocculate, <N(t)>, in this case can be expressed as

$$< N(t) >= \frac{\int N(t) H\{N(t)\} dN(t)}{\int H\{N(t)\} dN(t)} \tag{36}$$

where H(x) is the size distribution of the flocculates. By taking the Stauffer's argument, H(x) can be obtained as [67]

$$H[N(t)] = \frac{< N(t) >^{\tau-2} N(t)^{\tau}}{\Gamma(2-\tau, \frac{1}{< N(t) >})} \exp\left[-\frac{N(t)}{< N(t) >}\right] \tag{37}$$

Using <N(t)> and H[N(t)]one can go through similar exercise to get

$$\phi_{eff}(t) = \frac{Kd^3 < N(t) >^{\tau-2}}{\Gamma\left(2-\tau, \frac{1}{< N(t) >}\right)} < N(t) >^{-\tau+\frac{3}{f}+1} \Gamma\left(-\tau+\frac{3}{f}+1, \frac{N(t)}{< N(t) >}\right) \tag{38}$$

where $\Gamma(x,y)$ is the incomplete Gamma function. Eq.(11) can then be incorporated into the Einstein viscosity equation to get η_r. Since the distribution function of the flocs are not available, the monodisperse model is used in this chapter.

4.4. Molecular Dynamic Simulation—The Computation Scheme

As mentioned earlier, the energies involved in the asphaltene self-association process are the central parameters yet to be determined, in order to understand the asphaltene self-association mechanism. Molecular dynamic simulation provides a good opportunity for this purpose. However, before setting up the simulation conditions, the approach should be logically designed based on the molecular thermodynamic nature of the system.

From the thermodynamics point of view, the conventional aggregation or micellization processes are largely driven by the hydrophilicity-hydrophobicity imbalance. Other energies, such as packing, double layer interactions, etc., often play minor roles only. The self-association of asphaltenes appear to be different. This is because asphaltenes are defined based on the solubility which results in a class of materials potentially having very different molecular structures among themselves. Their only similarity may be that most of the molecules consist of certain degrees of polynuclear aromaticity. These can are revealed in elemental analysis, H/C ratio or in NMR studies. It is thus very difficult to distinguish a hydrophilic portion from a hydrophobic portion for a given asphaltene molecule. Additionally, asphaltenes only self-associate in the organic media with low per-

mittivities. This is equivalent to saying that the hydrophilicity-hydrophobicity imbalance will not be the governing factor, and that the interactions between asphaltene molecules are short ranged. In the past decade, experiments, theories and even computer simulations have been reported on this issue. Good progress has been made, however, the fundamental understanding of the self-association mechanism is still lacking. The main factor is the limited understanding of the physical and chemical characterization of the aggregates and the kinetic process of the aggregation.

The difficulty in any simulation is always the same—to accurately mimic the real systems. For the simulation appropriate initial conditions must be set up. This requires in-depth knowledge of the system. In the case presented here, the Ratawi vacuum residue (VR) derived asphaltene was chosen because it has been well studied in our laboratory. Data regarding its elemental analysis, chemical properties, and physical properties are readily available for us, allowing construction of a more accurate molecular structures, distribution and the initial configuration of the simulation.

The simulation consists of 64 asphaltene molecules ranging in size from 3 rings to 11 rings structures. The ring distribution was based on the Gaussian distribution with the peak at the 7 ring structure [68]. Two systems were modeled. One at a concentration of 0.015 wt % (below the aggregation onset concentration) and the other above it at 5 wt %. The size of the cell was chosen to represent the system at the desired densities (concentrations). With the above concentrations, the corresponding cell dimensions are 743.0 Å and 108.8 Å, respectively. The molecular dynamic (MD) simulation was performed using CERIUS2 [69]. The molecules were placed randomly in the cell using the amorphous cell module in the Cerius2 package to define the initial configuration. This was followed by energy minimization. During the energy minimization process, the Dreiding force field was used to account for both inter- and intra-molecular interactions except the electrostatic ones [70]. A dielectric continuum of 3.5 was used to model the solvent. The Dreiding Force field was not used to compute the electrostatic interactions because it calculates the monopole-monopole interactions only. One can still use the Dreiding Force field for computing electrostatic interactions, provided the monopole-monopole interactions calculated can represent a good estimate of the intra-molecular dipole moments. We tested several computation packages on this issue. We used charge equilibration, MOPAC6 [71], and CHARMM [72] to compute the electrostatic interactions for simple molecules and evaluate the dipole moments estimated. The results were compared with the experimental values; single ring and double ring molecules were the test cases. MOPAC6 was found to be far superior to the other two packages as far as dipole moment representation is concerned. We thus calculated the electrostatic charges using MOPAC6. The MD simulation was lasted for 250 pico-seconds (ps) where the system energy starts stabilize.

5. RESULTS

5.1. Structure of Asphaltene Aggregates

5.1.1. Model Analysis. Several presumed structural models and their size distribution functions were tested for many sets of SANS data. From the fittings quality, monodisperse cylindrical structure and the spherical structure with a Schultz size distribution are two good candidates to describe the Ratawi aggregate structure in toluene (see Figure 2). In order to differentiate these two models, the self-consistent check process described in the experimental section was used. In this process the contrast of the aggregates should re-

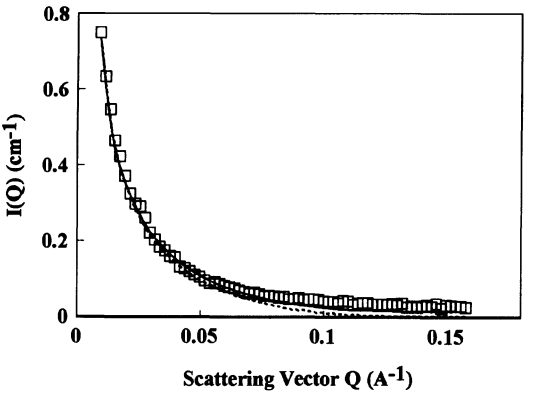

Figure 2. SANS data fitting using spherical Schultz model (solid line) and the monodisperse cylindrical model (dash line).

main unchanged upon increasing asphaltene concentration. The contrasts for spherical particle with Schultz size distribution function and for the monodisperse cylindrical particle are derived in the following.

The Schultz distribution function is similar to the Gaussian distribution, but with a right skewness. The explicit form of the Schultz distribution is

$$f(R)=\left[\frac{z+1}{<R>}\right]^{z+1}\frac{R^{z}e^{-\frac{(z+1)R}{<R>}}}{\Gamma_{z}(z+1)} \tag{39}$$

where Γ_z (x) is the gamma function, <R> and z is a polydispersity parameter, relating to the polydispersity as

$$\frac{\sqrt{<R^2>-<R>^2}}{<R>}=\frac{1}{\sqrt{z+1}} \tag{40}$$

The contrast term in Eq. (2), $\Delta\rho$, can be derived in terms of the extracted structural parameters from the mono-cylindrical model and from the spherical model with the Schultz size distribution function. For a monodisperse cylindrical particle of cross sectional radius R and length L, N_p can be written as [24,56]

$$N_p=\frac{CK}{\pi R^2 L} \tag{41}$$

where C is the concentration and K a proportional constant relating concentration to particle volume fraction. Using Eq.(41) $\Delta\rho$ can be expressed in terms of C, A, R, and L as

$$\Delta\rho=\frac{A}{C\bullet R^2\bullet L} \tag{42}$$

where A is the pre-factor used to fit the experimental data (I(Q)=A<P(Q) with A being the adjustable parameter in the fitting). For a spherical particle with the Schultz size distribu-

Table 1. Δρ values as function of concentration and temperature

Asphaltene concentration*	Temperature = 25 °C		Temperature = 35 °C		Temperature = 43 °C	
	Δρ (S.S)	Δρ (M.C)	Δρ (S.S)	Δρ (M.C)	Δρ (S.S)	Δρ (M.C)
0.5	5.50	1.52	5.14	1.37	5.17	3.48
1.0	5.40	1.26	5.03	1.46	5.12	2.89
2.0	5.54	1.64	5.27	1.92	5.26	2.00
3.0	5.63	1.64	5.33	1.96	5.42	1.98
5.0	5.45	1.69	5.30	2.22	5.33	2.14

*(wt %)

tion, Δρ can be derived by incorporating the Schultz distribution, Eq. (39) into Eq. (2) to get [24,56]

$$\Delta\rho = \frac{A \bullet \left[\dfrac{z+1}{<R>}\right]^3}{C \bullet (z+6)(z+5)(z+4)} \tag{43}$$

Table 1 gives Δρ values as a function of asphaltene concentration. The Δρ values for the Spherical Schultz (S.S) model remain nearly constant while it varies with asphaltene concentration in the mono-cylindrical model (M.C). We thus conclude that the spherical model with the Schultz distribution in size is more suitable than the monodisperse cylindrical model for describing asphaltene aggregates.

5.1.2. Surface to Volume Ratio Analysis. Figure 3 shows I(Q) from two spectrometers, one from NIST and the other from ANL. The Q of NIST reaches a much smaller range and is able to exhibit the clustering structure discussed in Yen's model [20]. The sudden up-turn of I(Q) at small Q makes the modeling work difficult. Thus, one should use the model independent model to evaluate S/V and determine the shape before making model dependent analysis.

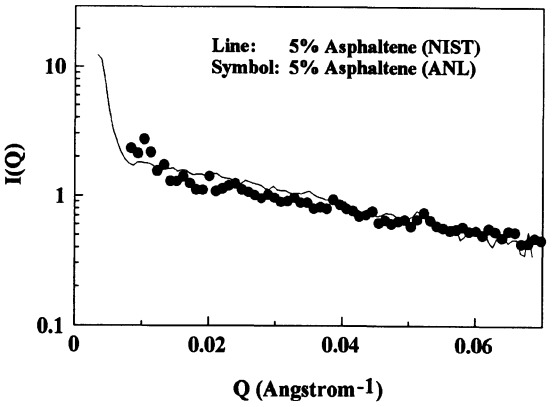

Figure 3. I(Q) from two spectrometers.

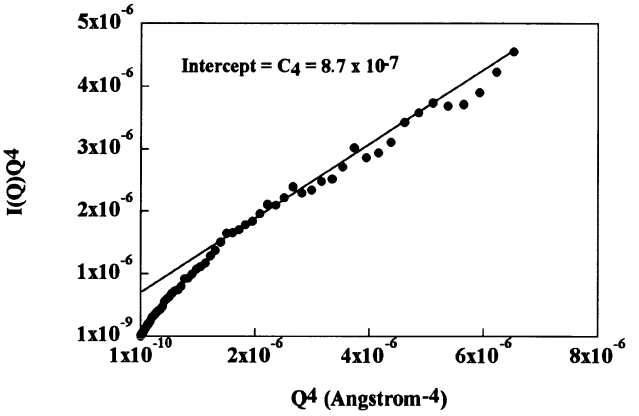

Figure 4. Porod plot of the asphaltene in toluene.

Figure 4 shows the Porod's plot using Eq. (10–12) where C_0 and C_4, and thus S/V of the asphaltene aggregates can be obtained unambiguously. Figure 5 compares the S/V so obtained and those from the model dependent fitting. Obviously, a spherical model is more convincing than the other two structures. One may argue that the slight deviation of the data may justify slight oblate structure. However, the data are closer to a spherical geometry than to either a cylindrical or a flat particle.

5.2. Conductivity Study

5.2.1. Molecular Packing of the Asphaltene Aggregates. Figure 6 shows the conductivity as a function of asphaltene concentration in toluene. The volume fraction of the aqueous phase, ϕ_w, is kept at 0.18. The conductivity is proportional to asphaltene concentration in a fairly linear fashion. This indicates that Ze and r_h in Eq.(20) remain constant while X_Z linearly increases with asphaltene concentration. It also suggests that the asphaltene aggregates do not grow with increasing concentration. Instead, more similar size

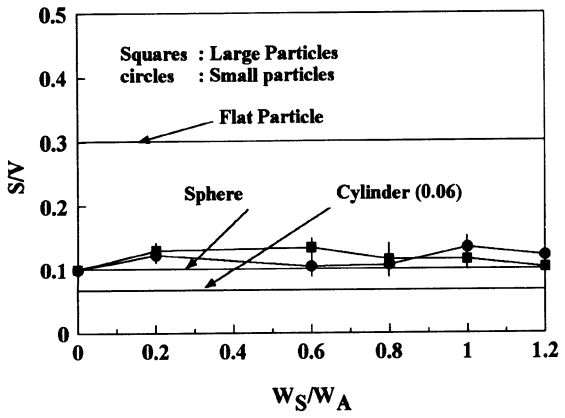

Figure 5. S/V from model independent method (solid circles and squares) and from model dependent methods. W_s and W_s are weight ration between the added SDS surfactant and asphaltene respectively.

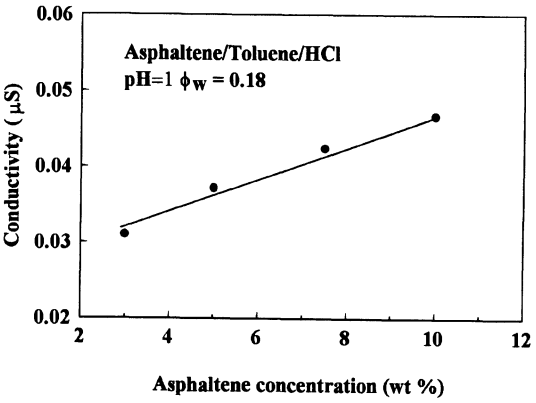

Figure 6. Conductivity of asphaltene /toluene/HCl solutions as a function of asphaltene concentration with water volume fraction ϕ_w kept at 0.18.

micelles are formed. This justify the method of using HCl as a probe for investigation of the molecular packing. It also justifies Eq. (25) and (26).

To validate the presumed packing schemes, we first examine the microemulsion droplet model. Figure 7 shows the analysis using Eq. (25). The curve is obviously not linear. This suggests that asphaltene aggregates do not swell in three dimensions like a water-in-oil microemulsion droplet. Thus, this model is not appropriate.

As we plotted the data according to Eq.(26) (see Figure 8) linearity appeared. At 1 wt % asphaltene concentration, this linear behavior persists for ϕ_w up to about 0.06. Figures 9 to 12 show the same plots for asphaltene wt % of 3, 5, 7.5, and 10. These data were collected using the simple hand-held conductivity meter. Even with such a simple conductivity meter, the curves are still fairly linear. This evidence favors the non-growing model with the monomers inter-locked in the aggregates. It also suggests that monomers are packed irregularly and there are substantial cavity spaces within the aggregates. A possible scenario for HCl uptake is as follows. HCl molecules exhibit stronger affinity for the polar core of the asphaltene aggregates at certain sites than the solvated solvent. When HCl is added, some solvent molecules in the cavities are forced to replaced by aqueous HCl near

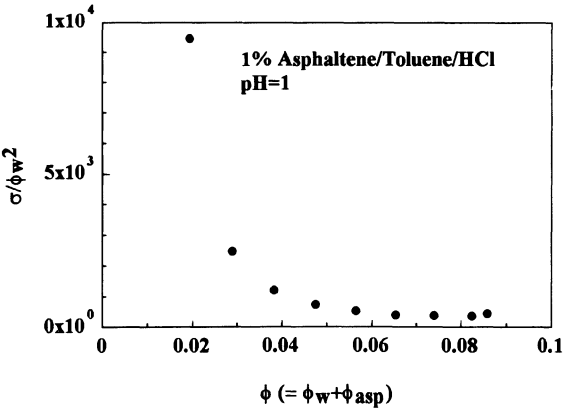

Figure 7. σ/ϕ_w^2 as a function of ϕ_w plotted according to Eq. (25).

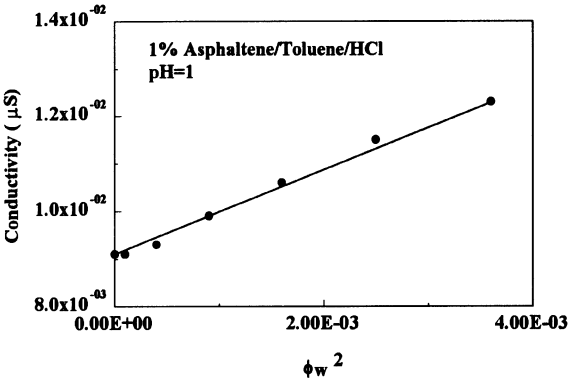

Figure 8. σ as a function of ϕ_w^2 plotted according to Eq.(26).

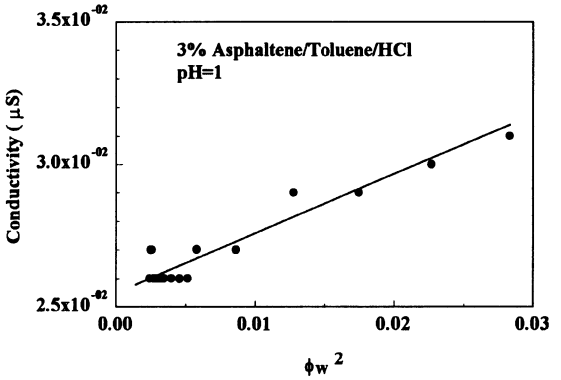

Figure 9. Same plot as Figure 8 for 3 wt % asphaltene.

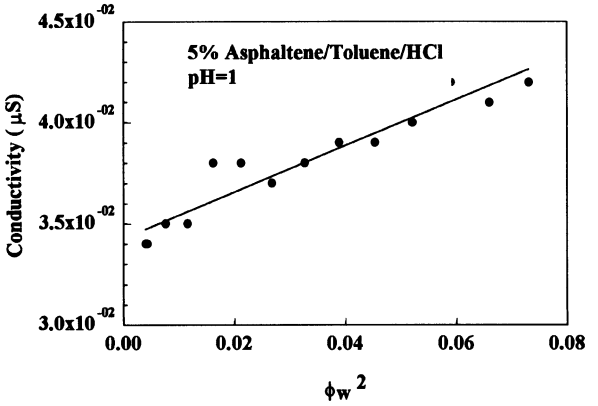

Figure 10. Same plot as Figure 8 for 5 wt % asphaltene.

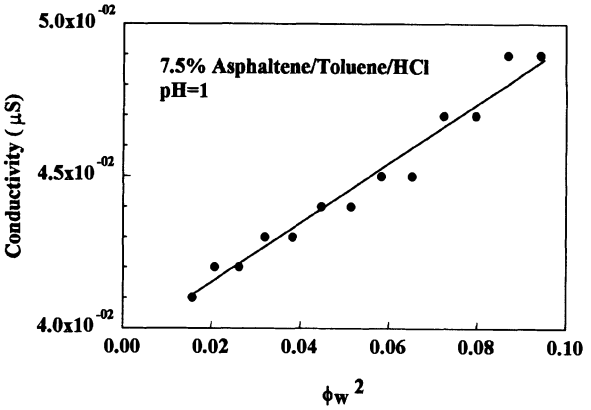

Figure 11. Same plot as Figure 8 for 7.5 wt % asphaltene.

the polar sites. Due to the packing constraint (the monomers are more or less interlocked), the energy required to unfold an aggregate is too high. As a result, the aggregates do not swell or re-distribute upon HCl addition. Instead, they continue to accommodate HCl via repelling the solvent molecules out of the aggregates.

5.2.2. Percolation Mechanism of the Asphaltene Aggregates. When the cavities are filled with HCl, the Ratawi asphaltene aggregates percolate to accommodate more HCl before the phase separation occurs. This is evident in Figure 13 which shows the conductivity plot of the 1 wt % asphaltene solution for ϕ_w up to ~ 30%. Its demonstrate a series of phenomena upon increasing HCl. The curve shows a ϕ_w^2 behavior at low ϕ_w regime (Figure 9). As ϕ_w goes beyond 0.06, the conductivity starts to increase rapidly suggesting an onset of percolation. The solution phase separates at $\phi_w \sim 0.12$.

Figure 14 shows the analysis according to the Grest et al. theory (Eq.(27)). Linear behavior shows for both $\phi > \phi_c$ and $\phi < \phi_c$. The percolation concentration determined was at $\phi_w = 0.08$. The exponents obtained were $\mu=0.5$ and $s= 0.24$, considerably lower than the

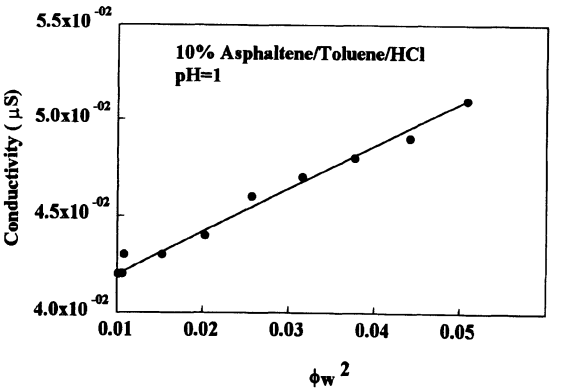

Figure 12. Same plot as Figure 8 for 10 wt % asphaltene.

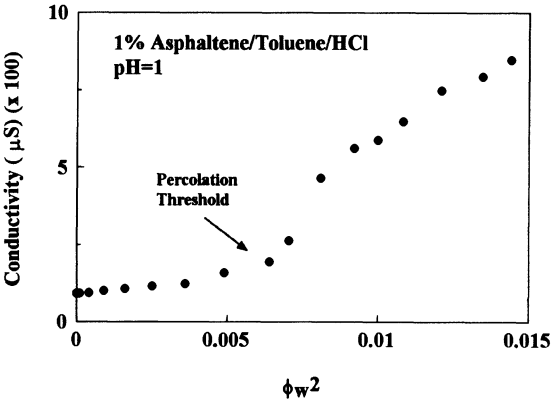

Figure 13. Conductivity of asphaltene /toluene/HCl solution as a function of water content. Percolation can be identified at ϕ_w ~ 0.08.

water-in-oil microemulsions (μ = 2 ± 0.2 and s=1.2 ± 0.2) [73–78]. This point will be discussed in the discussion section.

5.3. Viscosity and Fractal Dimension of the Asphaltene Aggregates

Figure 15 shows the viscosity evolution as a function of time for 2.1 wt % Ratawi asphaltene in a 75/25 toluene/heptane mixed solvent. The toluene asphaltene solution was prepared first and added heptane at time zero when the viscosity measurement starts. At beginning the viscosity dropped for a little while, then remained constant for approximately 1.5 hours before starting to increase which is an indication of flocculation. The detailed mechanism of the viscosity drop and the following "induction" period is not known. The flocculation process follows the trend described in Eq. (35) closely. When it goes beyond 400 minutes the viscosity started to decrease rapidly. This is likely due to the sedimentation where asphaltene dropped out of the solution. The volume fraction of the disperse phase starts to decrease, thus lowered the viscosity.

Figure 16 shows the analysis according to Eq. (35). The fractal dimension so obtained is 1.8 which is a reasonable number. The time range selected for this analysis was from 150 minutes to 350 minute where we assumed only the flocculation process was occurring. Of course flocculation and sedimentation may occur simultaneously. Coupling of

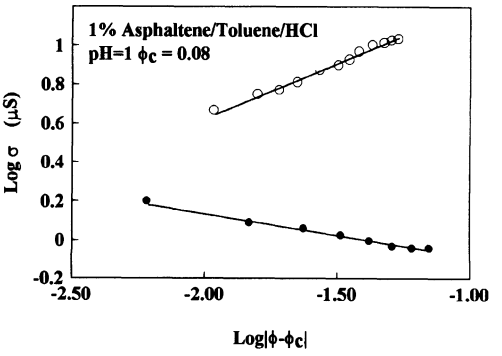

Figure 14. Plot for the asphaltene/toluene/HCl conductivity according to the Grest et al. theory.

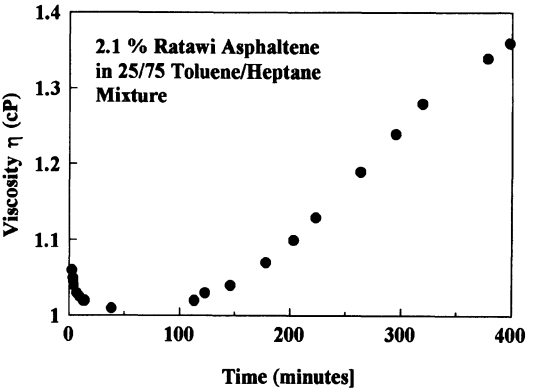

Figure 15. Viscosity as a function of time from 2.1 wt % of Ratawi asphaltene in 75/25 toluene /heptane mixed solvent.

these two processes to describe their effect on the viscosity is very complex. A separation publication will be devoted to this subject.

A similar phenomenon was observed for AMH asphaltene at 2.3 we % (see Figure 17). The fractal dimension is lower (1.53), indicative of a faster precipitation kinetic process. The fractal dimension obtained (1.53) agrees with that obtained from a small angle neutron scattering analysis [79]. This justifies the analysis derived here.

Figure 18 shows the results from the AMH at 5%, the effect of sedimentation sets in at ~ 400 minutes. A even lower fractal dimension (1.49) was obtained as expected, since the precipitation kinetic process is expected to be faster for higher asphaltene concentration.

Figure 19 shows the reversibility study of the 2.3 wt % AMH sample. The precipitated sample from Figure 17 was sealed at 25 °C for 15 hours, then sheared with vortex mixer for 1 minute. The viscosity measurement was then performed. The viscosity appeared to reach plateau much faster (see Fig. 15 and 19), however, the fractal dimension is higher. This means that the flocculates are better packed and are more stable against flocculation. It may be a kinetic effect—the flocs continue to adjust their packing and arrive at a higher packing density.

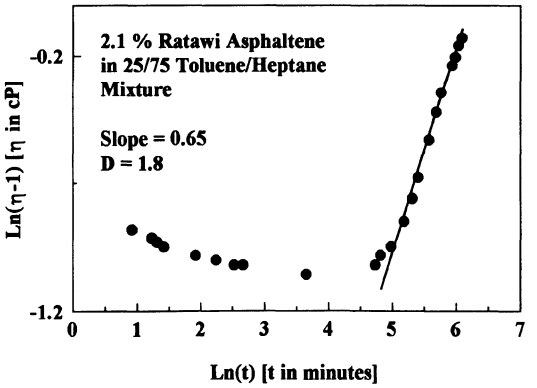

Figure 16. Analysis of Figure 15 according to Eq. (35). A fractal dimension of 1.8 was obtained.

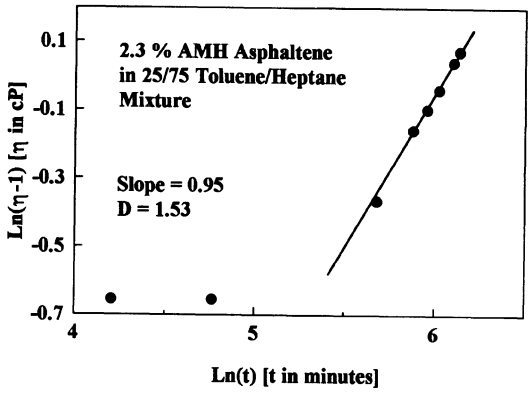

Figure 17. Same plot as Figure 16 for 2.3 wt % of AMH asphaltene.

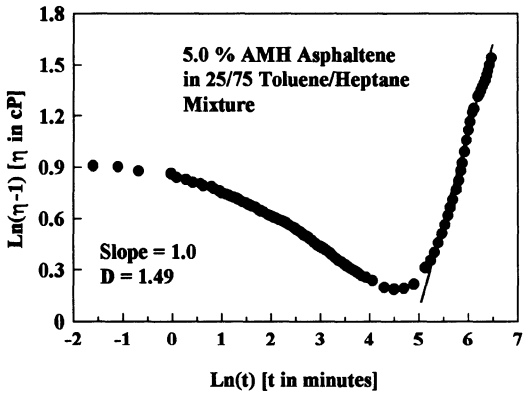

Figure 18. Same plot as Figure 16 for 5 wt % AMH asphaltene in 75/25 toluene/heptane mixed solvent.

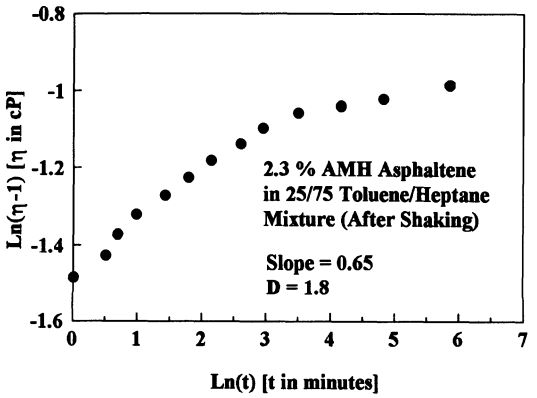

Figure 19. Shaking of the Figure 15 sample reveals similar flocculation process but with higher fractal dimension.

5.4. Molecular Dynamic Simulation

Figure 20 and 21 show the simulation results for the 0.015 wt % and 5 wt % respectively. As one can see, the 0.015 wt % does not show significant self-association. Dimers do exist, but no large aggregates are observed. On the other hand, the 5 wt % system shows aggregates of various sizes. F (see Figure 21) is a small aggregate while B, C, D and E are large ones of different shapes. Their common feature is the short range stacking phenomenon. The maximum stack observed contains approximately 7 asphaltene molecules. This is comparable to the model proposed by Yen [20] derived from the X-ray work on asphaltene solids. In solution, the stacking appears to be similar. However, the stacks are loose and somewhat irregular (see D in Figure 21). Aggregate B is a good example. It consists of many short range stacks linked loosely together. As a result the aggregates do not show well defined cylindrical shape. It appears more like a sphere. This is also true for aggregate A, C and E. Aggregate D is more like a cylinder although the stacking direction changes after 7th molecules. We also found a monomer in this simulation (unmarked molecule in Figure 21) which may or may not be significant. In order to evaluate the importance of the dipole-dipole interaction, we used the charges obtained from charge equilibration method to compute the electrostatic contribution, which underestimates the dipole moments for simple molecules. The result shows a collapse of the molecules into a single huge aggregate. Since the experimental data from SANS and SAXS [11,30,31,50,51] have

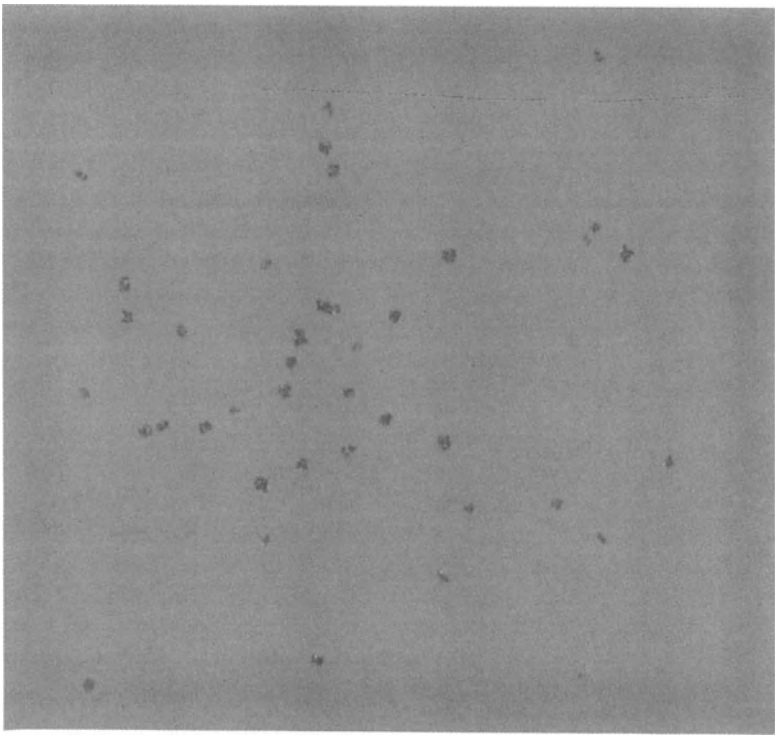

Figure 20. Molecular dynamics simulation for 0.015 wt % Ratawi asphaltene in toluene. No significant aggregates were observed, as the concentration is below CMC.

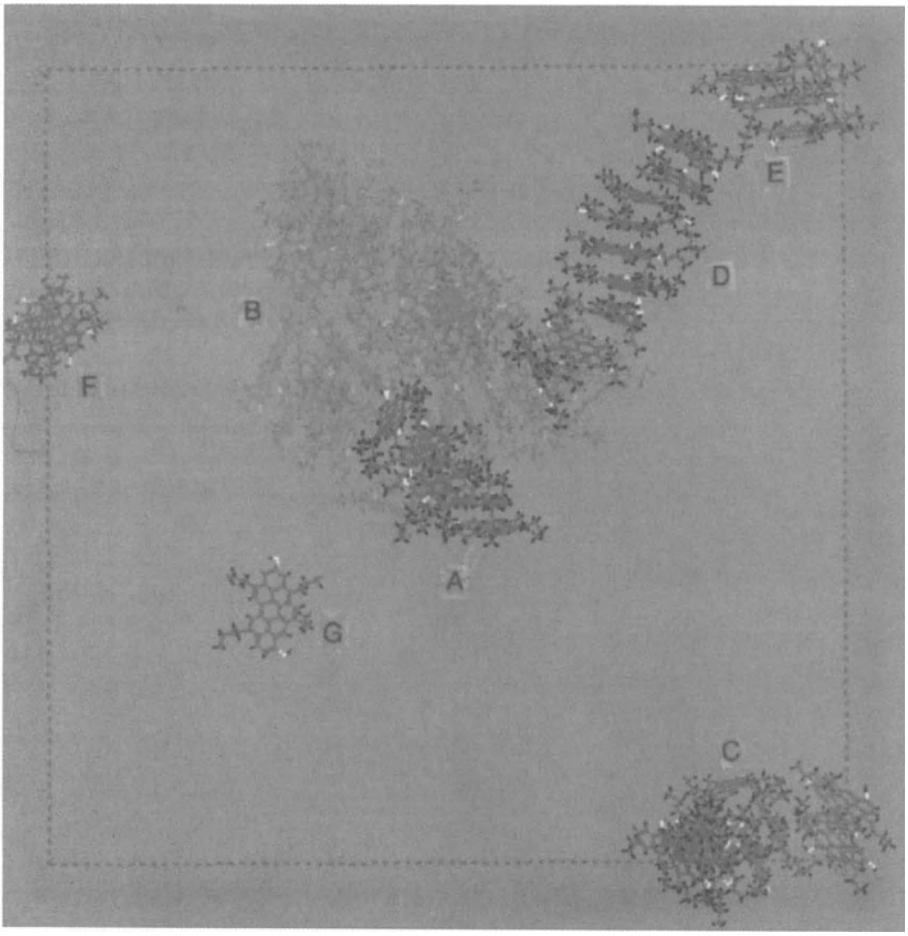

Figure 21. Same study as Figure 20 for 5 wt % asphaltene. Aggregates form via stacking. Due to molecular shape distribution, the maximum stacks observed was 7 and the stacks are loose, resulting in spherical-like aggregates rather than cylindrical. A - F are aggregates of various sizes and G is an unassociated monomer.

indicated that the average size of the aggregates is approximately 30–100 Å, the occurrence of a collapse single aggregate phase is highly unlikely. This suggests, at least indirectly, that dipole-dipole interaction must play an important role in controlling the self-association process.

6. DISCUSSION AND FUTURE PERSPECTIVE

6.1. Percolation and Molecular Packing

The result obtained from Grest et al. [60] analysis (see Fig. 14) confirms the difference of the percolation process of asphaltene/HCl/toluene system from a surfactant based microemulsion system [73–78]. The critical exponents obtained for the asphaltene/tolu-

ene/HCl system is roughly 4–5 times smaller. The molecular mechanism behind the percolation process is worth a lengthy discussion.

Percolation is usually recognized from the sudden increase of a physical parameter (conductivity in this case) as a function of an experimentally controllable parameter (ϕ_w in this case). Many water-in-oil microemulsions exhibit this phenomenon. Asphaltene/toluene/HCl system may be classified as a water-in-oil microemulsion, although its packing scheme differs as we have shown in the conductivity study. The conductivity data show a percolation-like phenomenon (see Fig. 13). This is further confirmed by the analysis using the Grest et al. [60] theory via its linearity below and above the percolation threshold. As for the much smaller s and μ obtained, one can be argued as follows.

The conductivity near the percolation threshold solely depends on the hopping rate of the charges between percolated aggregates. In asphaltene/HCl/toluene complexes, HCl molecules reside near the polar sites in the core. In other word, they are caged near the polar sites. This restricts their movement within the aggregates, unlike the charges in a water-in-oil microemulsion droplet where charge carriers can move freely within the water pool. Due to this caging effect, the charges hopping between two aggregates involve more steps. Before a charge carrier hops from one aggregate to the other it may have hopped several steps among the polar sites within the resident aggregate. This lowers the rate of conductivity increase at the percolation transition. On the other hand, the inter-droplet hopping of a surfactant based microemulsion involves only one step. The charges can move freely within the droplet. The only hurdle to hop over in order to reach the other droplet is to cross the surfactant layer.

If one assumes each hopping of a charge carrier in an asphaltene aggregate follows the same critical behavior described in the Grest et al. [60] theory, (i.e., $\mu \sim 2.0$ and $S \sim 1.2$) then the 4 - 5 time smaller of μ and s means that it requires approximately 4 to 5 hops to reach the other aggregate. This estimate may be approximate, but at least gives a crude sketch of the structure of an asphaltene aggregate and their polar site density. Certainly, more studies are needed to understand the relevance between the values of μ and s and the number of monomers per asphaltene which has been suggested to be ~ 5 to 10 from the computer simulation result presented in this work.

6.2. Computer Simulation and Its Implications

The asphaltene self-association, although related to the dipole moment as shown in the computer simulation, is a rather peculiar process. If one takes the self-association as a phase separation, is it a process similar to a spinodal decomposition, a micellization process, or a nucleation process? From the data shown here and evidence presented from other studies, no concrete conclusion can be made. Here we like to propose a scenario which theorists can use as the basis to perform further study.

In the work of Wang et al. [80] dealing with the effect of the dipole moment on the nucleation process, the authors concluded the that dipole moment should vanish in order for the nucleation process to go on. Assuming asphaltene system to be isotropic at the dilute concentration regime (i.e., below the aggregation onset concentration) and start to aggregate according to a nucleation process when the concentration exceeds the aggregation threshold. In the initial stage of the aggregation, the molecules containing polynuclear aromatics may stack together as one can see from the simulation. As the stacking goes on, it becomes less and less regular. This can be realized from that fact that the molecular structures are inhomogeneous. Although the stacking becomes less and less regular, a net dipole moment may be resulted from the stacking. This net dipole moments can arise from

the structural arrangement of the atoms in the molecules and/or the heteroatoms (Nitrogen, sulfur, nickel, vanadium etc.) which are commonly found in asphaltenes. When the net dipole moments of the stacks become non-zero, the nucleation process is suppressed and the growth of the aggregates slowed down, and eventually stopped. This may be why the phase separation (or aggregation process) occurs but is terminated at a microscopic length scale. Because it is terminated at the colloidal length scale, it appears to be similar to a micellization process, even though the energies involved are completely different.

While the continuous growth of the aggregates is slowed down by the reduction of the net dipole moment, the second stage of aggregation starts where the elemental aggregates cluster into larger fractal objects. During this second stage, the packing energy and the fractal kinetics set in. The clustering process eventually stops when the fractal growth process equilibrates with the thermodynamic process, or when the fractal space saturates the 3-D space in the case of high concentration. Because of the influence from the thermodynamic equilibrium there exists an equivalent activation energy during the fractal growth process. As a result, the fractal geometry of the cluster shows a reaction limited process as indicated in a earlier SANS study [77].

6.3. Future Perspectives

The above description about the asphaltene aggregation mechanism is only a proposed scenario. It should be validated or discarded based on more experimental and computer simulation evidence. To understand the asphaltene aggregation processes and its relevance to phase separation, one should include (1) characterization of the kinetic process of the self-association and the follow-up clustering processes. The clustering process occurs at rather low concentration as indicated in the SANS study in Fig. 3. Techniques available for this study may be pulsed X-ray scattering, freeze-fracture transmission electron microscopy with digitization capability, and possibly viscosity or dynamic light scattering. (2) *in situ* measurement of the dipole moment effect on slowing down of the aggregation process. ESR may provide such an opportunity. More sophisticated computer simulation experiment and with larger number of molecules for better presentation of the real system (the polydispersity is an important parameter and should be well represented in a simulation study) may be able to provide similar information as well. The work of Galtsev et al. [81] using electron-nuclear double resonance spectroscopy gives some insight of the stacks but was not able to map out a concrete association mechanism. Nevertheless, this technique may be a convincing one for providing accurate information. Similarly, the scanning tunneling microscopy is simple and accurate. However, the sample pretreatment is needed to insure good experimental data [82]. (3) the phase separation process as a function of pressure, temperature and solvent quality, as presented in the viscosity section in this chapter. The recent work by Anisimov et al. [83] using dynamic light scattering allows one to detail the microscopic world of the phase separation. It is an excellent probe for sedimentation studies of ultra dilute systems. However, this work did not look into the separation mechanism in detail, thus was not able to characterize the fundamental mechanism of the phase separation path.

ACKNOWLEDGEMENT

The author would like to thank Charles Glinka of National Institute of Standards and Technology (NIST) and P. Thyagarajan of the Intense Pulsed Neutron Source (IPNS) of

Argonne National Laboratory (ANL) for their technical assistance on SANS experiments. The author also acknowledge the support of NIST, US department of Commerce and IPNS, for providing the SANS facilities used in this experiment. The IPNS is operated under the auspices of the US department of Energy, BES-Materials Science, under Contract W-31–109-Eng-38, to whom thanks are extended for the use of their facilities.

REFERENCES

1. J. G. Speight, *The chemistry and Technology of Petroleum*. Marcel Dekker, New York, (1980).
2. J. G. Speight, *Fuel Science and Technology Handbook*. Marcel Dekker, New York 1193 pp (1990).
3. T.F. Yen, "The role of asphaltene in heavy crude and tar sands." In: R.F. Meyer and C.T. Steele (Editors), *The Future of Heavy Crude and Tar Sands*, McGral-Hill, New York, pp 174–179 (1980).
4. R. S. Sanders, R. S. Chow and J. H. Masliyah, J. Coll. Int. Sci., 174, 230 (1995).
5. J. Escobedo and G. A. Mansoori, SPE 23696, paper presented at the Second Latin American Petroleum Engineering Conference, II LAPEC of the SPE held in Caracas, Venezuela, March 8–11 (1992).
6. G. A. Mansoori, T. S. Jiang, and S. Kawanaka, *Arabian J. Sci. & Eng.*, 13, 17 (1988).
7. J. H. Pfeiffer, *The Properties of Asphaltic Bitumen*. Elsevier, Amsterdam, 285 pp. (1950).
8. J.W. Bunger and N.C. Li, *Chemistry of Asphaltenes*. Advances in Chemistry Series 195. American Chemical Society, Washington D.C. (1981).
9. T.F. Yen and G.V. Chilingarian (editor) *Asphaltenes and Asphaltes, 1*, Elservier, Amsterdam (1994).
10. M.K. Sharma and T.F. Yen (editors) *Asphaltene Particles in Fossil Fuel Exploration, Recovery, Refining, and Production Processes*, Plenum Press, New York (1994).
11. E. Y. Sheu and D. A. Storm, "Colloidal Properties of Asphaltenes in Organic Solvents" In *Asphaltenes - Fundamentals and Applications*, edited by E. Y. Sheu and O. C. Mullins, Plenum Press, New York (1995).
12. Marusk H. P., and Rao, B. M. L., *Fuel Sci. & Tech. Int., 5*(2) 119 (1987).
13. B. Shiffert, J. Kuczinski, and E. J. Papirer, *J. Coll. Int. Sci.*, 135, 107 (1990).
14. Eric Y. Sheu and D. A. Storm, *Energy & Fuel*, 8, 552 (1994).
15. B. Tissor, *Rev. Inst. Fr. Pet.*, 36(4), 429 (1981)
16. B. Tissot, D. H. Welte, Petroleum Formation and Occurrence; 2nd Ed., Spring Verlag, Berlin, pp 538 (1984).
17. F. J. Nellensteyn, Oxfor Univ. Press, London, 4, 2760 (1938).
18. J. P. Dickie and T. F. Yen, *Analy. Chem.*, 39,(14)1847 (1967).
19. S. S. Pollack, and T. F. Yen, *Analytical Chemistry*, 42(6) 23 (1970).
20. T. F. Yen, *Am. Chem. Soc., Div. Petrol. Chem. Preprint, 17(1)*: 102–104 (1972).
21. I. A. Eldib, H. N. Dunning and R. J. Bolen, *J. Chemical & Eng. Data*, 5(4) 550, 1960.
22. B. R. Ray, P. A. Witherspoon and R. E. Grim, J. Phys. Chem., 61, 1296 (1957).
23. T.F. Yen, *Energy Source*, 1(4): 447–463 (1974).
24. E.Y. Sheu, K.S. Liang, S.K. Sinha, and R.E. Overfield, *J. Coll. Int. Sci., 153*, 399 (1992).
25. F.J. Nellensteyn, *Chem. Weekblad, 28*, 313 (1931).
26. F. J. Nellensteyn and N. M. Roodenburg, *Chem.-Zeiyung, 545*, 819 (1930).
27. C. Mack, *Phys. Chem., 36*, 2901 (1932).
28. J. P. Pfeiffer and R. N. J. Saal, *J. Phys. Chem., 44*, 139 (1940).
29. H. Eiler, *Kolloid-Z Z. Polym.*, 97, 313 (1941).
30. E.Y. Sheu, D.A. Storm and M.M. De Tar, *J. Non-crystal. Sloids, 131–133*, 347 (1991).
31. Xu, Yingnian; Koga, Yoshikata; Strausz, Otto P., Fuel, 74(7), 960–4 (1995).
32. L. Schramm, R. G. Smith, and J. A. Stone, *Colloids and Surfaces*, 11, 247 (1984).
33. S. Acevedo, M. A. Ranaudo, G. Escobar, L. Gutierrez and P. Ortega, *Fuel*, 74(4) 595 (1995).
34. E.M. Trujillo, *Soc. Petro. Eng. AIME*, 645, Aug. (1983).
35. Y. Xu, *Energy & Fuel*, 9, 148 (1995).
36. K. C. Khulbe, G. H. Neale, and V. Hornof, *Fuel Proc. Tech.*, 19, 61 (1988).
37. H. A. Nasr-El-Din and K. C. Taylor, *Colloid and Surfaces*, A: 75, 169 (1993).
38. G. Gonzalez and A. Middea, Golloids and Surfaces, 33, 217 (1988).
39. O. V. Rogacheva, R. N. Rimaev, V. Z. Gubaidullin, and D. K. Khakimov, *Kolloidnyi Zhurnal*, 42(3) 586 (1980).
40. E. Y. Sheu, M. M. De Tar, D. A. Storm, and S. J. DeCanio, *Fuel*, 71, 299 (1992).

41. E.Y. Sheu, M.M. De Tar and D.A. Storm, "Surface Activity and Dynamics of Asphaltenes." In: M.K. Sharma and T.F. Yen (editors) *Asphaltene Particles in Fossil Fuel Exploration, Recovery, Refining, and Production Processes*, 115 pp Plenum Press, New York (1994).
42. S.E. Taylor, *Fuel, 71*, 1338 (1992).
43. E.Y. Sheu and D.A. Storm, *Fuel, 73,* 1368 (1994).
44. K. C. Kyriacou, R. E. Baltus and P. Rahimi, *Fuel,* 67, 109 (1988).
45. R. E. Baltus, K. C. Kyriacou, V. V. Sivaramakrishna, and P. Rahimi, *AICheE Symposium Series*, No. 266, Vol. 84, 50 (1988).
46. D. A. Storm and E. Y. Sheu, *Energy & Fuel*, 9, 168 (1995).
47. C. W. Dwiggins Jr., J. Phys. Chem. 69, 3500, (1965).
48. C. W. Dwiggins Jr., J. Appl. Cryst. 11, 615, (1978).
49. S. I. Anderson and K. S. Birdi, *J. Coll. Int. Sci., 142*, 497 (1991).
50. P. Herzog, D. Tchoubar, and D. Espinat, *Fuel, 67,* 245 (1988).
51. J. C. Ravey, G. Ducouret, and D. Espinat, *Fuel, 67*, 1560 (1988).
52. Thiyagarajan, P.; Hunt, Jerry E.; Winans, Randall E.; Anderson, Ken B.; Miller, Jeffrey T., Energy & Fuels, 9(5), 829–33 (1995).
53. I. Kowalewski, M. Vandenbroucke, A. Y. Huc, M. J. Taylor, and J. L. Faulon, *Energy & Fuel*, 10, 97–107 (1996).
54. J. Murgich, J. Rodriguez, and Y. Aray, *Energy & Fuel*, 10, 68–76 (1996).
55. L. A. Feigin and D. I. Svergun, *Structure Analysis By Small Angle X-ray and Neutron Scattering,* Plenum Press, New York (1987).
56. E. Y. Sheu, *Phys. Rev. A., 45,* 2428 (1992).
57. G. Porod, "General Theory", in O. Glatter and O. Kratky edited *Small Angle X-ray Scattering*, Academic Press, New York (1982).
58. P. Debye, *Ann. Physik*, 46, 809 (1915).
59. M. Borkovec, *J. Chem. Phys.*, 91(19) 6268 (1989).
60. G. S. Grest, I.Webman, S. A. Safran and A. L. R. Bug, *Phys. Rev. A* 33, 2842 (1986).
61. H. E. Stanley and N. Ostrowsky eds, *On Growth and Form,* Martinus Nijhoff Publisher, New York (1986).
62. D. P. Landau and F. Family, Eds., *Kinetics of Aggregation and Gelation,* North Holland, Amsterdam, (1984).
63. R. Pynn and A. Skeltorp, Eds. *Scaling Phenomena in Disordered System,* Plenum New York (1986).
64. J. Feder, *Fractal*, Plenum, New York (1988).
65. T. Jøssang, J. Feder, and E. Rosenqvist, *J. Chem. Phys.* 120, 1–30, 1984.
66. J. Feder, T. Jøssang,, and E. Rosenqvist, *Phys. Rev. Lett.* 53, 1403, 1984.
67. D. Stauffer, in *On Growth and Form,* edited by H. E. Stanley and N. Ostrowsky, Martinus Nijhoff Publisher, New York (1986).
68. C. Y. Ralston, S. Mitra-Kirtley and O. C. Mullins, *Energy & Fuels*, 10, 623 (1996).
69. Cerius2 is marketed by BIOSYM/Molecular Simulations Inc., 9685 Scarnton Road, San Diego, California, USA.
70. Mayo, S. L.; Olafson, B. D.; Goddard III, W. A. *J. Phys. Chem.* 1990, 94, 8897.
71. MOPAC6 is a semi empirical package available from Quantum Chemistry Program Exchange (QCPE), Indiana University.
72. CHARMm (Brooks, B. R.; Bruccoleri, R. E; Olafson, B. D.; States, D. J.; Swaminathan, S.; Karplus, M., *J. Comput. Chem.*, 1983, 4, 187).
73. J. Peyerelasse and C. Boned, *Phys. Rev. A* 41, 938 (1990).
74. M. Lagure, *J. Phys. Lett.*, 40, L331 (1979).
75. M. I. Clarkson, *Phys. Rev. A.* 37, 2079 (1988).
76. S. K. Mehta et al., *Phys. Rev. E.*, 50, 4759 (1994).
77. J. P. Straley, *Phys. Rev. B* 15, 5733 (1977).
78. I. Webman et al., *Phys. Rev. B* 16, 2593 (1977).
79. Y. C. Liu, E. Y. Sheu, S. H. Chen, and D. A. Storm, *Fuel,* 74, 1352 (1995).
80. Kusaka, I.; Wang, Z.-G.; Seinfeld, J. H., J. Chem. Phys., 103(20), 8993–9009, (1995).
81. V. E. Galtsev, I. M. Ametov and O. Y. Grinberg, *Fuel*, 74(5) 670 (1995).
82. B. A. Watson and M. A. Barteau, *Ind. Eng. Chem. Res.*, 33, 2358 (1994).
83. M. A. Anisimov, I. K. Yudin, V. Nikitin, G. Nikolaenko, A. Chernoutsan, H. Touhoat, D. Frot, and Y. Briolant, *J. Phys. Chem.*, 99, 9577 (1995).

Chapter V

COLLOIDAL STRUCTURAL EVOLUTION FROM STABLE TO FLOCCULATED STATE OF ASPHALTENE SOLUTIONS AND HEAVY CRUDES

D. Espinat, E. Rosenberg, M. Scarsella,* L. Barre, D. Fenistein, and D. Broseta

Institut Français du Pétrole
1-4 Avenue de Bois Préau, 92852
Rueil Malmaison, Cedex, France

1. INTRODUCTION

The petroleum industry is often concerned with the production, transportation and refining of heavy crude oils rich in asphaltenes. A successful addressing of the many difficulties encountered in these processes relies on a precise understanding of the chemical properties and colloidal behavior of asphaltenes under various thermodynamic and flow conditions. Whereas asphaltenes are generally considered to be the major factor responsible for these difficulties, the influence of the other constituents of oil, such as resins, must not be overlooked.

Asphaltenes and resins, the heaviest components of the oil, may flocculate during the reservoir exploitation as a result of a change in the thermodynamic (pressure, temperature, composition) or flow conditions.[1] Flocculation may thus appear during secondary oil recovery, when water or gas (such as for instance carbon dioxide or light hydrocarbons) are injected in the reservoir, inducing pore plugging and permeability reduction.[2,3] The reservoir wettability and therefore the oil flow properties may be altered by asphaltene flocculation and/or adsorption onto the pore surfaces.[4–6] Near the well bore shearing is an additional factor that may lead to formation damage. Asphaltene flocculation and deposition also induce severe damages by fouling and plugging production and surface handling

* Present address: Università degli Studi di Roma « La Sapienza », Dipartimento di Ingegneria Chimica, dei Materiali delle Materie Prime e Metallurgia, Via Eudossiana, 18, 00184, Roma, Italia.

facilities (e.g., downhole submersible pumps, tubing, flowlines, etc.). In order to remedy these problems, various methods have been proposed, based for instance on physical removal or on solvent soaks with aromatic solvents blended in some cases with dispersants.[7] The objective of the current research is to find additives that prevent or delay asphaltene deposition.[8–13] These asphaltene deposition inhibitors are supposed to act similarly to resins by having a peptizing capability. The separation of crude oil from water is another important topic and the role of components such as asphaltenes, porphyrins and waxes for stabilizing emulsions has been highlighted.[14,15] For instance, the "chocolate mousse" created by accidental sea pollution is a stable water-in-oil emulsion. This stability has been explained by the formation at the oil/water interface of a highly condensed film, rich in asphaltenes and in other high molecular weight species.[16–18]

Concerning the refining process, the decrease of the consumption of fuel oil and the increase in the demand of gasoline and middle distillates necessitate the conversion of atmospheric or vacuum residues.[19,20] It becomes necessary for the refiner to upgrade heavier crude oils of lesser quality, in particular with high sulfur content.[21] The refining of these complex feedstocks requires the conversion of heavy fractions. Several processes exist, based either on thermal cracking (visbreaking or coking) that give lighter products, or on catalytic cracking without hydrogen (fluid-bed catalytic cracking) or with hydrogen (hydrocracking) that allow the conversion of vacuum distillates. In thermal processes, instability of the visbroken products may appear giving rise to phase separation, sludge formation, viscosity increase, due the modification of the proportion of acidic and basic asphaltenes, the conversion of an important part of the resins and the solubility modification of some heavy asphaltene molecules which are converted into more aromatic entities. In catalytic processes, acid catalysts can be deactivated because of coke formation or metal deposition, strongly depending on the asphaltene concentration. Consequently, a deasphalting pretreatment is proposed in order to reduce the asphaltene concentration in the feedstocks.[19] Whereas our knowledge has considerably improved in the last two decades, some parameters of these refinery processes are still unknown or uncontrolled. For example, there are instances in which feedstocks with very similar composition convert in a different way or can induce a different aging of the catalysts. Further progress in this field will stem from experimental investigations on processes occurring within a short span of time and under severe conditions (high temperatures and pressures, presence of hydrogen).

Bitumen is another topic where basic research on asphaltenes and their molecular environment is an important issue.[22–24] Residues coming from atmospheric or vacuum distillation, visbreaking and thermal cracking are commonly used to produce bitumens.[25] The characteristics of bitumen as a binder depend on various properties, such as for instance adhesion or rheological behavior. These properties are strongly influenced by the chemical composition of the bitumen and the macroscopic organization of asphaltenes.[26] The rheological (sol- or gel-like) behavior can be tailored to the industrial needs by the addition of polymers (e.g., olefins, SBS, EVA). A large amount of work has been carried out to characterize the rheological properties of various types of bitumens and several methodologies have been developed in this sense.[27] Little is known, however, on the relationship between these rheological properties and the macroscopic organization of asphaltenes, resins and added polymers within the bitumen matrix. Another important topic is the aging of bitumen, which is also likely to be related to the evolution with time of asphaltene content and macroscopic organization.

A better understanding of the properties of asphaltenes and their interactions with the other constituents of oils or residues (such as resins) is highly desirable as it may help

in explaining the difficulties encountered and then proposing new solutions. A brief survey of the work published in this domain is presented in next section.

2. OVERVIEW OF OUR KNOWLEDGE

Asphaltenes are operationally defined as the components of crude oil or residues that are insoluble in light hydrocarbons such as *n*-pentane or *n*-heptane. They correspond to the heaviest and most polar among the constituents of oil and residues.[28,29] The fraction soluble in the light hydrocarbon, referred to as the maltenes, contains a large variety of compounds that may in turn be separated (usually by liquid chromatography) into three classes of compounds: the saturates, the aromatics and the resins (SAR fractionation). The proportion of the different fractions (SAR) and asphaltenes varies strongly from one crude to another one. Numerous investigations have been carried out concerning the *chemistry of asphaltenes.* These complex molecules have been abundantly studied using many analytical and spectroscopic methods after their isolation from the crude oil or from different types of heavy fractions coming from refining processes. The elemental analysis shows a predominant amount of carbon (≈80 % w/w) and hydrogen (≈8 % w/w), together with heteroatoms such as sulfur, oxygen, nitrogen, nickel and vanadium, the proportion of which may vary considerably for asphaltene fractions having different sources. The proportion of metals (nickel and vanadium) does not generally exceed a few hundreds of ppm. Carbon 13 magnetic resonance[30,31] provides information on the different types of carbon molecules (e.g., aromatic or paraffinic), which is useful for aromaticity determination. Similarly, different types of hydrogen[32] can be observed by proton magnetic resonance. One thus distinguishes aromatic, naphthenic, methylenic, α-substituted next to aromatics and terminal methyl hydrogens. The pyrolysis approach provides data on the length and quantity of aliphatic chains. Another method based on the oxidation catalysed with ruthenium[33,34] has been used to identify the different structural units of asphaltenes. It has been observed that the extent of aromatic condensation is low and that highly pericyclic aromatic structures are present in very small amounts, whereas the aliphatic/naphtenic domains have a large extent. Following carbon–hydrogen structure determination many works have been carried out to investigate the location of heteroatoms and their role in influencing the polarity, the acid-base character and thus the definition of the solubility properties of the asphaltene species. Various methods coupled to fractionation or chemical reactions such as pyrolysis have been carried out. Infrared spectroscopy has provided important information concerning the chemical functions present in asphaltenes or in other petroleum products. Carboxylic, phenolic, ketonic, ester functions have been identified.[35–37] The presence of hydrogen bonds has been demonstrated by infrared spectroscopic. Mass and EXAFS/XANES spectroscopies have shown that the major part of nitrogen is located in heterocyclic species (e.g., pyrrole, carbazole or pyridine),[37–40] whereas the easy elimination of oxygen during pyrolysis experiments supports the view that oxygen is not totally included in cyclic molecules. On the contrary, sulfur is included in thiophene-like structures such as benzothiophenes, dibenzothiophenes or even more condensed molecules.[40–42] Other types of sulfides have been observed by Yen.[43] Ignasiak *et al.*[44–45] has proposed a polymer-like structure in which sulfur participates to the link of basic elements in more or less extended configurations.

The metal environment has also been an important topic for the scientific and industrial community. It seems that most of the nickel or vanadium atoms are included in porphyrins. The application of separation techniques such as size exclusion chromatography

or reversed-phase chromatography with specific detection methods, electron paramagnetic resonance and EXAFS/XANES[46] spectroscopy has been successful for separating vanadium porphyrin and non-porphyrin compounds.[47–49] It must be underlined that, in view of the low metal concentration in asphaltene fractions, only a small part of the molecules contains metal atoms such as vanadium or nickel.

All techniques previously mentioned have been able to deduce simple structural parameters, which may be used for deriving a tentative average asphaltene (Figure 1) or resin molecule.[34–50] To this purpose the use is made of more or less complex softwares[51,52] allowing a multidimensional approach, such as those developed for the representation of kerogen chemical structure.[53] The difficulty of these investigations is how to link several blocks of the molecule (e.g. polynuclear aromatic or naphtenic rings) or the particular functionalities detected by characterization methods. The average structure obtained can be mistaken. Nevertheless, such work has had the merit to generate molecular models helpful to understand the chemical evolution of these macro-cyclic molecules during various processes. The average structure of asphaltene molecules can be simply described with condensed polynuclear aromatic rings connected to alkyl side-chains.

While a large amount of work has been dedicated to asphaltenes, resins have been the subject of much less attention. These entities, like asphaltene molecules, contain polyaromatic and naphtenic rings but the naphthenic character is more pronounced. NMR spectroscopy[54–55] has shown that resins are in average smaller than asphaltenes and possess much longer aliphatic side-chains. It must be recalled that asphaltenes and resins are two contiguous classes of components separated from a continuum of molecules according to their solubilities in a low molecular weight alkane solvent. Therefore the size and chemical composition of some asphaltene molecules can be very close to those of some resins.

The industrial applications of conversion processes in which temperature plays an important role has emphasized the need for research on the behaviour of asphaltenes as a function of temperature. Several investigations[36,56,57] have been concerned with the evolution of asphaltenic material with the heating temperature. Heating up to 350°C, small quantities of methane or ethane are detected. This production increases and hydrogen sulfide begins to appear for heating temperatures ranging from 350°C to 410°C. For temperatures reaching 410°C, the conversion strongly increases, giving rise to lighter products such as n-alkanes with up to 36 carbon atoms and olefins. Coke formation is also detected as a result of aromatic condensation and asphaltene dehydrogenation. It has been suggested that this thermal conversion can be interpreted as a depolymerization of the asphaltene molecules due to the break of sulfur or carbon bonds, leading to smaller units such as resins. Heating to still higher temperatures produces the elimination of the functionalities and a strong reorganization of the chemical structure towards a graphitic arrangement. During hydrotreating processes, such as hydrodesulfurization or hydrodemetallation, thermal secondary cracking is suggested in competition with catalytic activity.[58]

In addition to investigations on the chemistry of asphaltenes, another complementary approach concerning the *colloidal structure* of asphaltenes has been undertaken. Within this approach, asphaltenes in solution or in their natural medium are considered as a system exhibiting heterogeneities. The extent of these heterogeneities varies from the nanometer to the micron, corresponding respectively to the elementary asphaltene molecules and to the huge aggregates generated by the flocculation process.

Early works have been concerned with asphaltenes in the solid state. As demonstrated by electron microscopy, the size of the elementary asphaltene entities varies between 2 and 10 nanometers.[59–62] Wide angle X-ray scattering has allowed to gain an

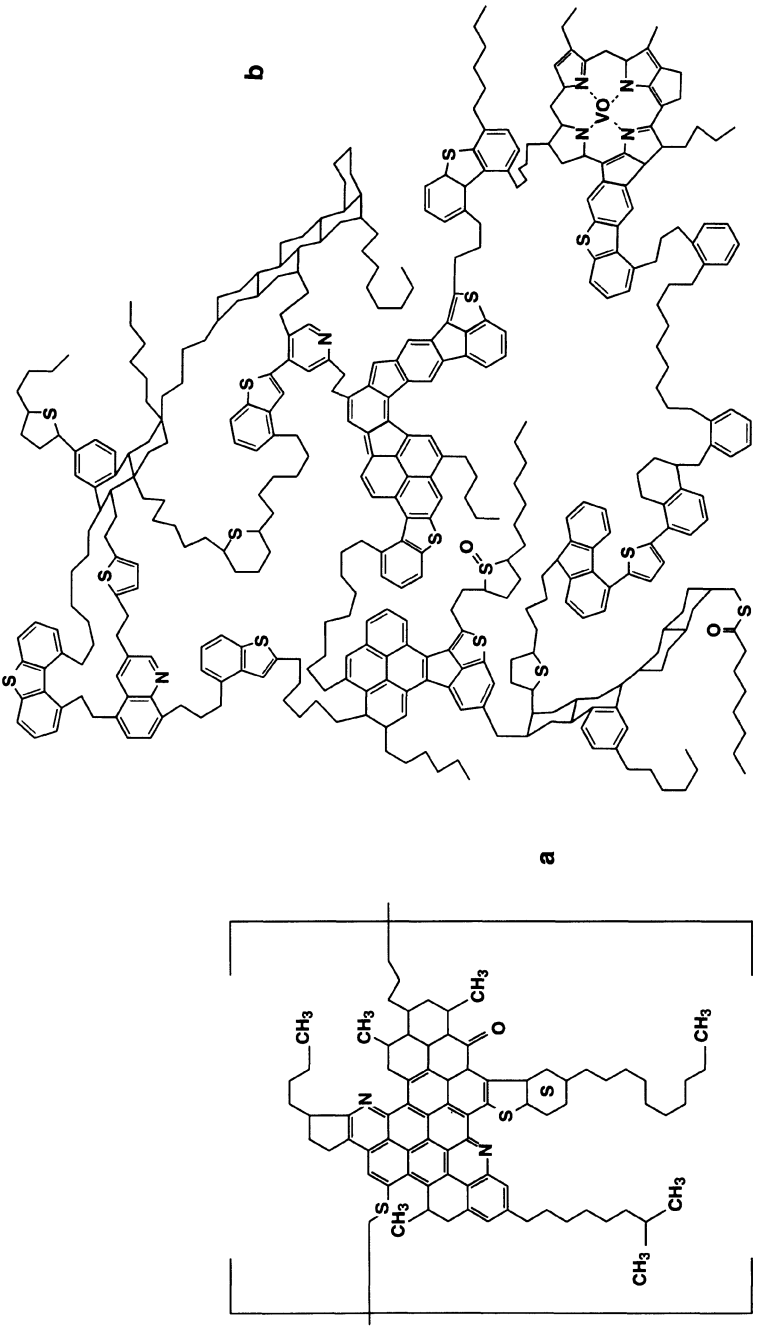

Figure 1. Illustration of average structure for two different asphaltenes - (a) Venezuelan crude oil[29] (b) Athabasca asphaltene.[34]

insight into the asphaltene macrostructure.[63–65] This technique has been used to obtain the interlamellar distance (i.e., the distance between two aromatic layers), the aromatic layer diameter, the height of the unit cell and the number of lamellae contributing to the stacking of aromatic rings, and finally the distance between two neighboring aliphatic chains (Figure 2a). On the basis of these investigations, Yen *et al.*[63] proposed in the early 60's a model providing an extended view of the asphaltene macrostructure (Figure 2b) that distinguished four different entities: the elementary molecule, the particle, the micelle and the aggregate. The structure of the molecule is similar to the one presented in Figure 1a and consists schematically of an aromatic region connected to aliphatic chains. The particle, called the crystallite, is formed by the stacking of several planar aromatic parts of the molecules, probably by π–π association or hydrogen bonds (Figure 2b). Particles can fur-

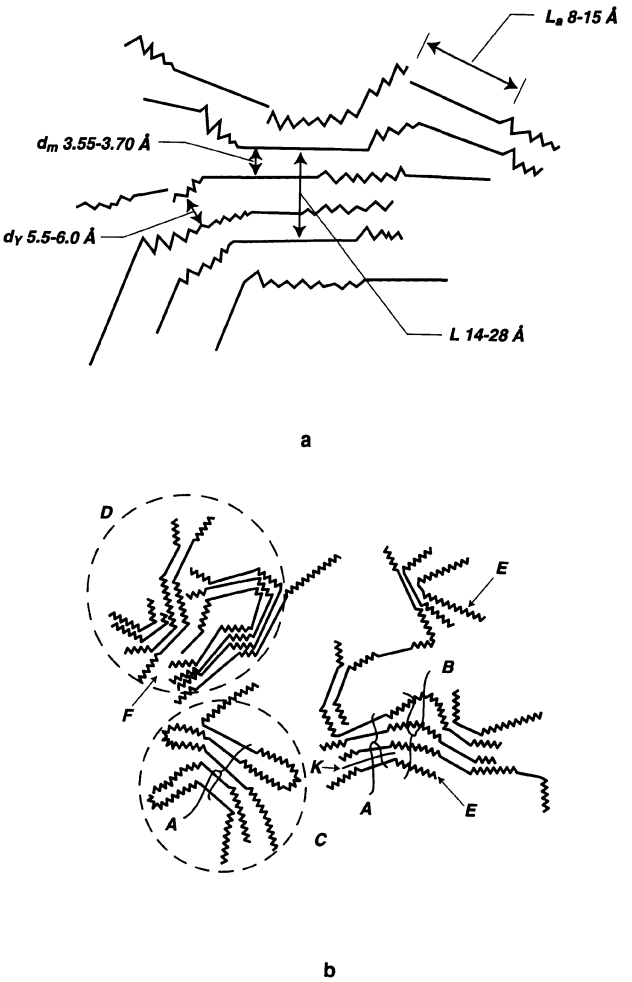

Figure 2. Structure of asphaltenes[63] - (a) cross-sectional view where L_a is the diameter of an aromatic sheet, d_m and d_γ are respectively the spacing between aromatic sheets or aliphatic side-chains, L is the extension of the aromatic cluster, (b) macroscopic structure of asphaltenes.

Table 1. Average molecular weights of asphaltenes from several crudes by various techniques[70]

Technique	Molecular weight
Ultracentrifugation[59,71]	300000
Osmotic pressure[75]	80000
Ultrafiltration[77]	80000–140000
Boiling point elevation[78]	2500–4000
Freezing point depression[75,76]	600–6000
Vapor pressure osmometry[79,80]	1000–8000
Viscosity[81,82]	900–50000
Light scattering[83,84,85]	1000–4000

ther associate into micelles, and micelles can form large aggregates. These different entities may be linked by different kinds of interaction. Resins can also interact with asphaltenes. Molecular weights in the range of 1000–4000 have been proposed for sheets, 4000–10000 for particles and 40000–40000000 for micelles. Nevertheless, this model suffers from severe limitations. It has been deduced from investigations on asphaltene (solid) powder and it is not firmly proved that this model holds in solution. The influence of hydrogen bonds is not taken into account and the extension of the aromatic layers is likely to be overestimated. Various studies have in fact concluded to lower average ring numbers.[66–69]

Many techniques have been applied to the characterization of the colloidal structure of asphaltenes and resins in solution. One of the major difficulties for interpreting the data stems from the strong polydispersity of asphaltenes in solution, which manifests itself in the wide range of molecular weights observed experimentally when using different measurement methods (cf. Table 1, collected by Speight *et al.*[70]). These methods are in fact sensitive to different molecular averages of the solute. The techniques that measure colligative properties (such as boiling point elevation, freezing point depression, vapor pressure and osmotic pressure) determine the number average molecular weights of the solute, whereas film balance, ultracentrifuge, viscosity or scattering measurements are related to averages that give more importance to high molecular weights.[22,59,71–73] In addition, the interpretation of the data is rendered difficult by association effects that occur even in very dilute solutions. These effects (and therefore the apparent molecular weight) have been shown to depend on asphaltene concentration, solvent and temperature.

Ultrafiltration experiments have been carried out with membranes with pore diameters in the range of 5 to 35 nanometers, confirming the occurrence of large colloidal aggregates in asphaltene solutions.[77] In a subsequent study, Briant and Hotier,[78] carrying out a series of filtration experiments, were able to retain more than 80% of their (dissolved) asphaltenes on filters with an average pore diameter of 25 nanometers, while this quantity dropped to around 30% for filters with pore diameters in the range of 50 nanometers.

Viscosimetric measurements have been carried out for asphaltenes both in solution and in their natural medium.[78,82,83,86,87] It is recalled here that the viscosity behavior is a decisive point for many industrial applications and that the presence of asphaltenes is responsible for the high viscosities encountered in residues or heavy crude oils. The viscosity of dilute solutions and residues relative to the solvent (i.e., pure solvent or maltenes) is observed to increase linearly with asphaltene (low) volume fraction, the observed slope or intrinsic viscosity being in the range of 6–8, which is much larger than the expected Einstein's value (=2.5) hard spheres. These important values have been interpreted

in different ways. Reerink[82] interpreted his data using a model of flat ellipsoids, while Sheu and coworkers proposed a model of solvated spheres.[86] For concentrated solutions or residues various models have put forward to interpret the strongly nonlinear viscosity increase with concentration, together with a non-Arrhenius dependence of the viscosity with temperature.[86]

The small angle scattering techniques, allowing the measurement of molecular weights and radii of gyration of dispersed colloids, have been widely utilized in the past three decades, starting with the pionering work by Dwiggins.[88–90] Using a Bonse-Hart type of X-ray diffractometer, Dwiggins detected in natural crude oils small asphaltic colloids, having radii of gyration between 2 and 4 nanometers as well as, in some instances, very large aggregates of several hundreds of nanometers. Kim and Long[91] did also observe the presence of small particles with sizes in the range of 2 to 4 nanometers for asphaltenes both in solution and in its natural solvent (deasphalted oil). More recently, several groups[86,92–105] have utilized small angle X-ray and neutron scattering methods, sometimes coupled with other techniques, not only for determining the molecular weights and radii of gyration of asphaltic colloids, but also with the purpose of gaining an insight into the polydispersity, geometrical shape and internal structure of these colloids. Various shape models have been employed to account for the scattering data, including models of disks,[92,93,102] spheres[86,96,100] and rods[97,101] with some amount of an appropriately chosen polydispersity. Very recently, models of asphaltic particles possessing a fractal-like internal structure have been proposed.[105,106] The structural evolution of these colloids has been followed by small angle scattering techniques as a function of temperature,[96,97,104] pressure[102] or solvent composition.[104] Increasing the temperature leads to a molecular weight lowering (or disaggregation), whereas a pressure increase (at constant temperature) promotes aggregation when the solvent is near-critical. Fractions obtained by size exclusion chromatography have been also characterized by small angle neutron scattering.[92] The addition of n-heptane induces an increase of the molecular weight.[95] It now appears that X-ray or neutron scattering techniques are well developed and can be used for the characterization and comparison of various asphaltenes extracted from crude oils or other heavy fractions produced by various treatments. It has been in particular shown that asphaltenes aggregates after visbreaking operation are bigger than those obtained after hydrotreatment.[92,99] It is worth mentioning here that light scattering measurements are limited to extremely dilute solutions (volume fractions below 0.5 or 0.1 %) as asphaltenes are strongly absorbent and fluorescent in the visible domain.[107] To overcome these difficulties measurements have been carried out using a long wavelength laser source (1024 nm) for which the absorption is low.[85]

We have previously insisted on the large polydispersity of asphaltenes. One way to simplify the treatments of the data obtained with various techniques is to make a fractionation. Several approaches have been carried out using selective fractionation with different solvents, ultracentrifugation[72] or preparative liquid or gel-permeation chromatographies. Speight[108] has summarized the methods that can be used for separation, most of these being utilized for the fractionation of the deasphalted oil. Nevertheless, some methods are recommended for asphaltene fractionation as a function of their chemistry: acidic, basic and neutral fractions can be obtained and for neutral fractions it is possible to distinguish aromatic and non aromatic entities. The gel or size exclusion chromatography (GPC or SEC), which has been more extensively applied,[109,110] separates particles according to their hydrodynamic volumes by eluting them through a porous column: large particles cannot enter small pores and are eluted first, whereas small particles travel a more tortuous path through the pores and are eluted last. The practical difficulties

encountered with this technique relate to the detection of the eluted fractions and to the residual adsorption of asphaltenes onto the gel filling the column (in practice this adsorption is limited by the addition of pyridine[111] or lithium salts[112] to the solutions). The interpretation of GPC results is not straightforward as the calibration curves established for narrow polymer (e.g., polystyrenes) cannot be utilized with molecules that differ not only in size but also in chemical content. A satisfactory way to calibrate the column is to use fractions obtained by GPC and measure their molecular weight by other techniques, such as vapor pressure osmometry,[113,114] ultracentrifuge,[110] scattering measurements[92,112] or osmometry.[109] All these measurements have shown that the polydispersity of asphaltenes is very large. The real problem is the preparation of sufficiently narrow asphaltenes fractions for calibration. Acevedo *et al.*[115] have used both dialysis and chromatography in order to improve this fractionation. Chemical analysis of the different GPC fractions reveal that the largest asphaltene molecules exhibit a more pronounced poly-aromatic character[45,113,116] and are more concentrated in sulfur and metals.[116]

One of the major conclusions of investigations on the asphaltene colloidal state is that asphaltene molecules self-associate in solution to give rise to more or less extended aggregates. On the basis of surface tension and calorimetric measurements, micellar-like structures have been proposed[86,117–120] for the 'basic' asphaltene aggregates, these aggregates being in turn capable of association into structures of larger scales. The critical micelle concentration (below which asphaltenes are fully dissociated) lies in the range of 0.1%, meaning that in practice asphaltenes are under a micellar form even in dilute suspensions. In presence of resins, asphaltenes might form smaller micellar-like structures, more stable against flocculation. An unsolved question concerns the forces involved in the micellization mechanism. These forces include van der Waals as well as π–π interactions between aromatic nuclei, dipolar[121] and charge-transfer[122] interactions and hydrogen bonds. H-bonding has been identified even in very dilute asphaltene solutions.[123] The addition of resins to asphaltene solutions has the effect of enhancing H-bonding as a result of specific resin-asphaltene interactions or of asphaltene dissociation.[35] The blocking of the H-bonding sites of asphaltenes by methylation or silylation has in fact been shown to lead to asphaltenes of smaller molecular weight.[123–125]

Flocculation is another important issue as it has many detrimental consequences on oil exploitation and production. The growth of large aggregates under changes in thermodynamic (e.g., composition or pressure) conditions has in fact dramatic macroscopic effects such as large viscosity increases and deposition of sediments. From a practical point of view it is of interest to predict the conditions of incipient flocculation that delineate regions of colloidal stability from regions of precipitation. Although there exist experimental evidences of kinetic and irreversible effects, several thermodynamic models have been proposed to predict flocculation in these systems.[126] On the experimental side, most studies have been concerned with the flocculation of asphaltenes induced by the addition (at ambient pressure and temperature) of a solvent (e.g., a low molecular weight alkane) to the solution or to crude oil, whereas in practice (e.g., in the reservoir) this phenomenon often occurs under a variation of pressure (at usually high pressures and temperatures). The experimental methods employed include optical microscopy,[107] viscosimetry,[78,107,127] filtration,[78] light transmission or scattering[128] as well as more sophisticated techniques such as quasi-elastic[129] radiation scattering and conductivity measurements.[130] Atomic force microscopy[131] has also been utilized to observe aggregates deposited onto mica surfaces. It is important to point out here that asphaltenes do not precipitate at once: the most aromatic and heteroatom-rich asphaltenes precipitate first and give rise (when redissolved in a good solvent) to the largest aggregates.[132]

From these studies of flocculating (or near-flocculating) asphaltene suspensions, it appears[133,134] that the static and dynamic properties of such systems have some analogies with those predicted by the classical models of colloidal aggregation, such as percolation or the so-called diffusion-limited and reaction-limited colloid aggregation (DLCA and RLCA).[135–137] Scattering experiments indicate in fact that large asphaltene aggregates possess a very open (solvated), self-similar (fractal-like) internal structure.[105–107] In addition the kinetic variation of flocculating aggregates may be interpreted within the framework of these models.[129] No clear-cut picture has emerged yet and some more experimental work is needed to measure other characteristic parameters such as the aggregate size distribution. The conditions under which the different mechanisms of aggregation (DLCA, RLCA or percolation) prevail have not been clearly identified either.

Geochemical investigations on the structure of kerogen might shed some light on the colloidal structure of asphaltenes.[138–140] There are in fact evidences that kerogen, the organic matter trapped in sedimentary rocks, is a precursor of petroleum constituents, among which asphaltenes are the closest to kerogen in chemical composition. These constituents are formed by a complex process of thermal maturation and migration from the source rock to the reservoir rock. These evidences stem from an analysis of the byproducts of pyrolysis experiments, which are supposed to mimic the thermal maturation process over a reasonable time scale.[141] The macrostructure of kerogen that emerges from these and other studies[142] consists of a more or less crosslinked macromolecular network (cf. Figure 3).[142,143] Asphaltenes might therefore also consist of similar cross-linked entities. According to Altgelt and Boduszynski[144] such crosslinking considerably reduces the entropy of mixing in a solvent and therefore is responsible for the poor solubility of asphaltenes in many solvents (as is the case for polymers in a solvent).[145]

While the description of the asphaltene macrostructure in simple solvents has been an important challenge in the last thirty years, the morphology of asphaltenes in their natural medium is less well understood. Two structural models for crude oils have been proposed. Figure 4 illustrates Pfeiffer and Saal's[22] peptization model, in which asphaltenes form the center of some micellar entities surrounded and stabilized by resins and then by the other constituents of oil. These authors suggested that a nearly continuous transition exists from the most polar entities (asphaltenes) at the center of the micelles to the less polar (aliphatic) entities forming the surrounding medium. Whenever a shortage of resins occurs, attraction forces are created giving rise to association between micelles (Figure 4-b) and ultimately to an extended gel-type structure (Figure 4-c). Yen's[146] model depicts the asphaltenes in their natural medium as gathered in oil-external or reversed micelles (Figure 5), the center of the micelle being composed of polar groups associated by hydrogen bonding or charge transfer interactions.[147] Oil-external micelles can revert to oil-internal ones depending of the surrounding medium properties. Aggregation of several micelles can form supermicelles and further aggregation can give rise to giant supermicelles or liquid crystal structures. Today, one of the present challenges for the research is to extend to real asphaltene-rich systems (e.g., crude oils and residues) the techniques and models that have been used with some success to analyse asphaltenes in pure or simple solvents. Unfortunately, only a few techniques can be used for investigating crude oils or heavy fractions, among which X-ray small-angle appear to be very promising.[87,95] Other techniques like atomic force microscopy or scanning electron or fluorescence microscopies have provided important insights into the macroscopic organization of real material such as asphalts.[148] In this latter study, the authors have identified in some asphalts beehive-like network structures with more or less spherical pores of around 6 μm in diameter.

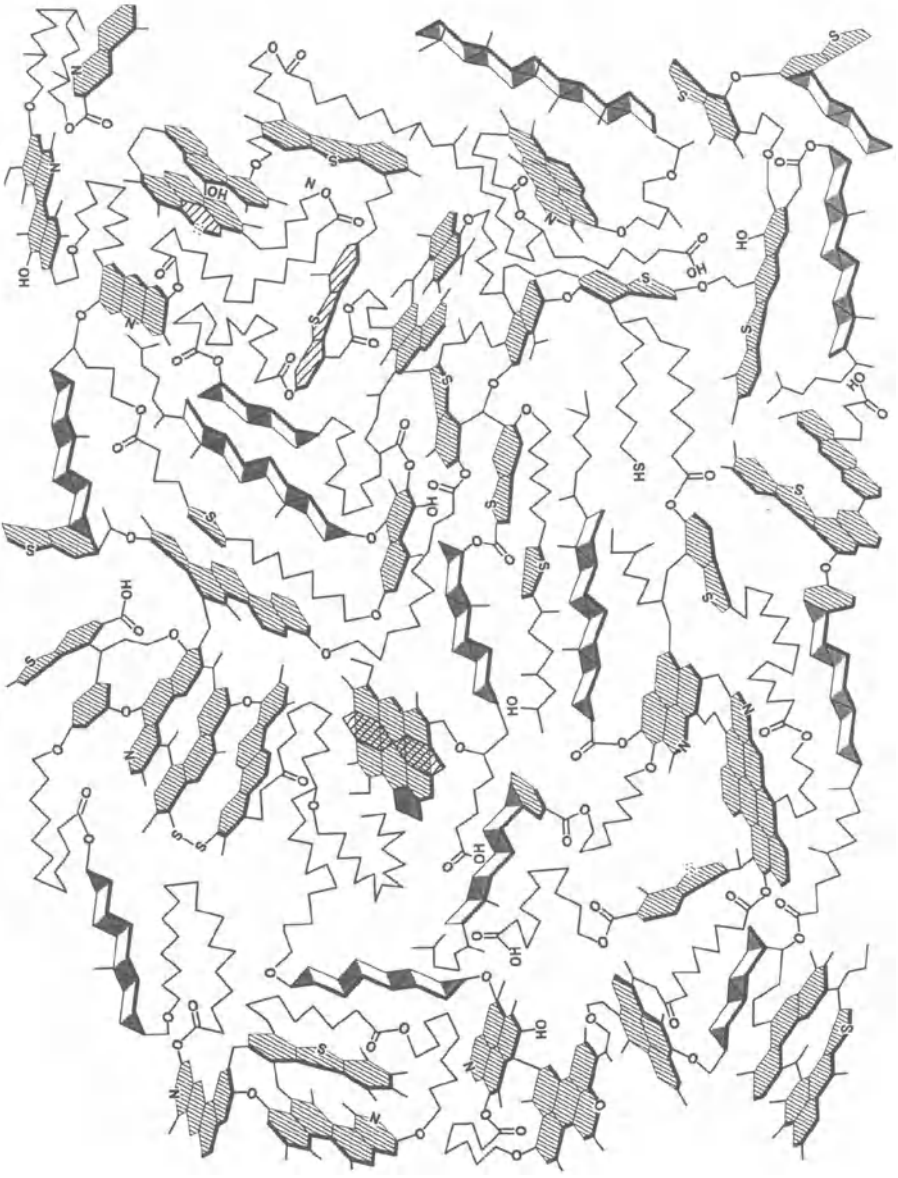

Figure 3. Kerogen structure (ref. 143).

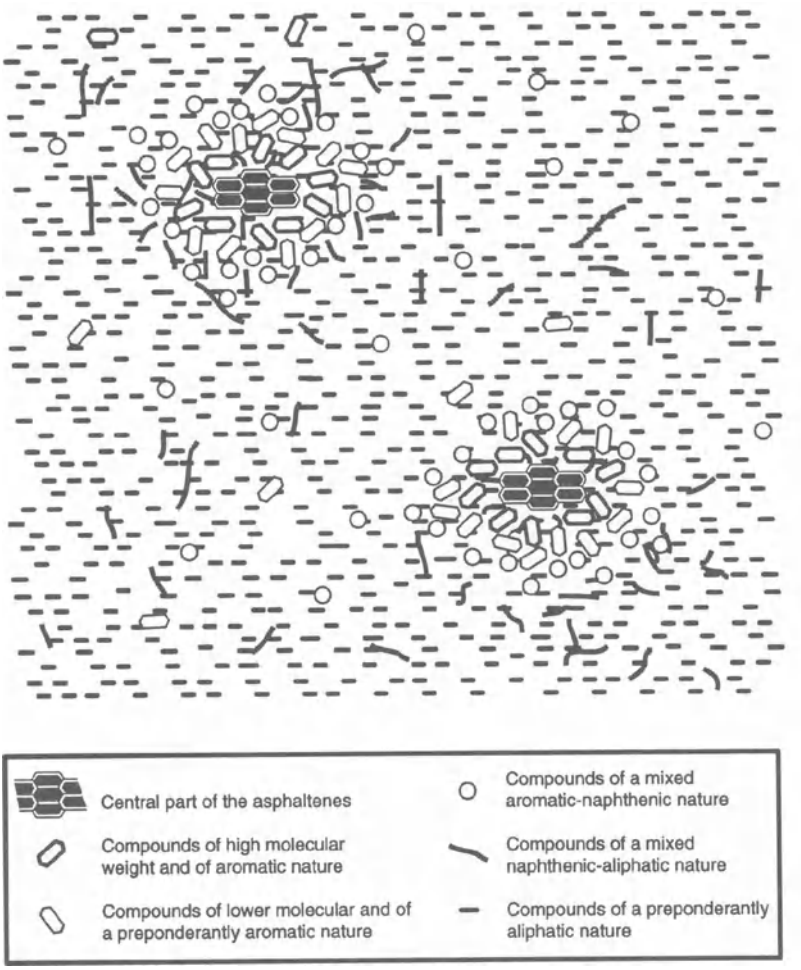

Figure 4. Asphaltene molecules in their natural environment.[22] (a) peptized asphaltene micelles.

Rheological measurements are also of a great interest for improving our understanding of real systems properties.[86,87,149–152] Crude oils or heavy fractions can exhibit newtonian or non-newtonian behavior. Vacuum residues may exhibit a yield value which is characteristic of a three-dimensional organization.[87] This macrostructure is very dependent on the temperature as the yield stress increases progressively disappears when the temperature increases. Storm and Sheu[151] have measured the viscosities of a vacuum residue (Ratawi) diluted with various quantities of the corresponding maltene fraction, from which they inferred the intrinsic viscosity of the asphaltenes. They found values close to those obtained for asphaltenes in a solvent. The viscoelastic properties of heavy oils and bitumens have also been investigated as a function of temperature or composition.[150] In particular, the addition of polymers such as olefins, SBS to bitumen has the effect of altering its rheological properties towards a more elastic behavior.[25] Viscosimetric measurements carried out on residues under the temperature and pressure conditions of refinery processes are very scarce.[152]

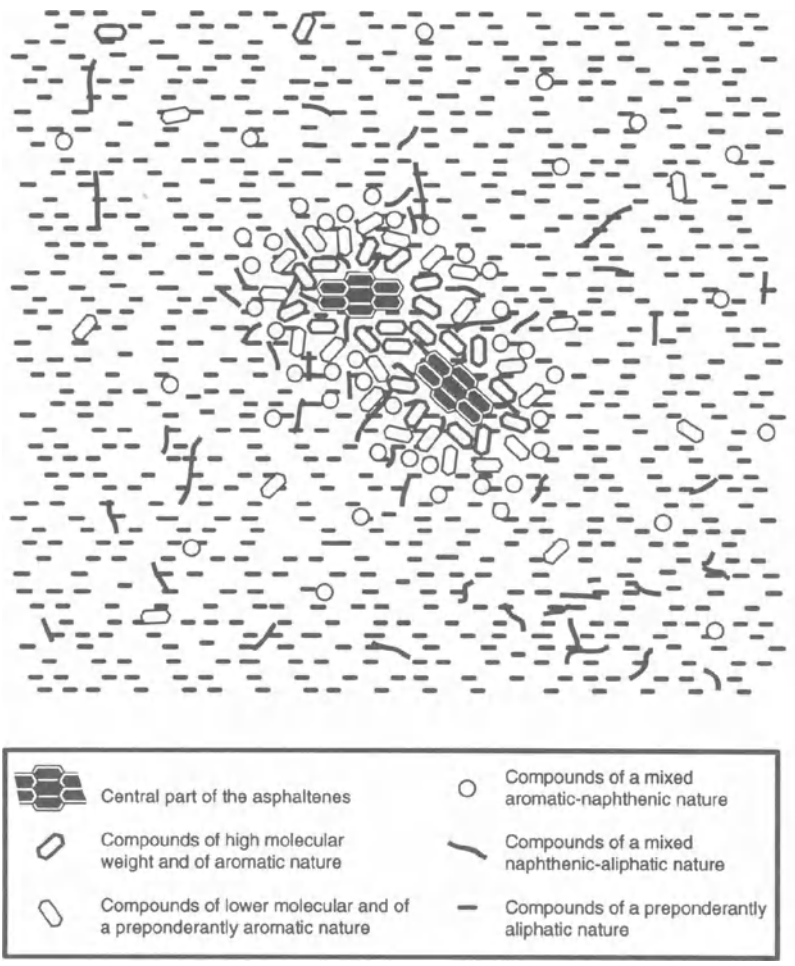

Figure 4b. Aggregated asphaltene micelles.

Research on the properties of asphaltenes and other heavy fractions (such as resins) has thus been focused on the two following topics: the chemical characterization and the colloidal state. A quite good description of the average local order and chemistry of these heavy compounds exists. Some progress can still be performed to develop new analytical techniques or improve existing methods. Such progress could thus help in better quantifying the various types of sulfur or nitrogen atoms present in asphaltenes and resins and determining more precisely the aromatic and naphtenic ring sizes as well as the aliphatic chain lengths and how these entities are linked together. The detailed knowledge of chemical composition is not, however, sufficient to explain the irregular macroscopic behavior frequently observed in various industrial applications. Chemical characterization is crucial for the understanding of catalytic reactions, but as mentioned previously, heavy fractions of similar chemical composition may exhibit very different catalytic behavior. Likewise, it has been observed that crude oils having quite similar compositions may or may not pro-

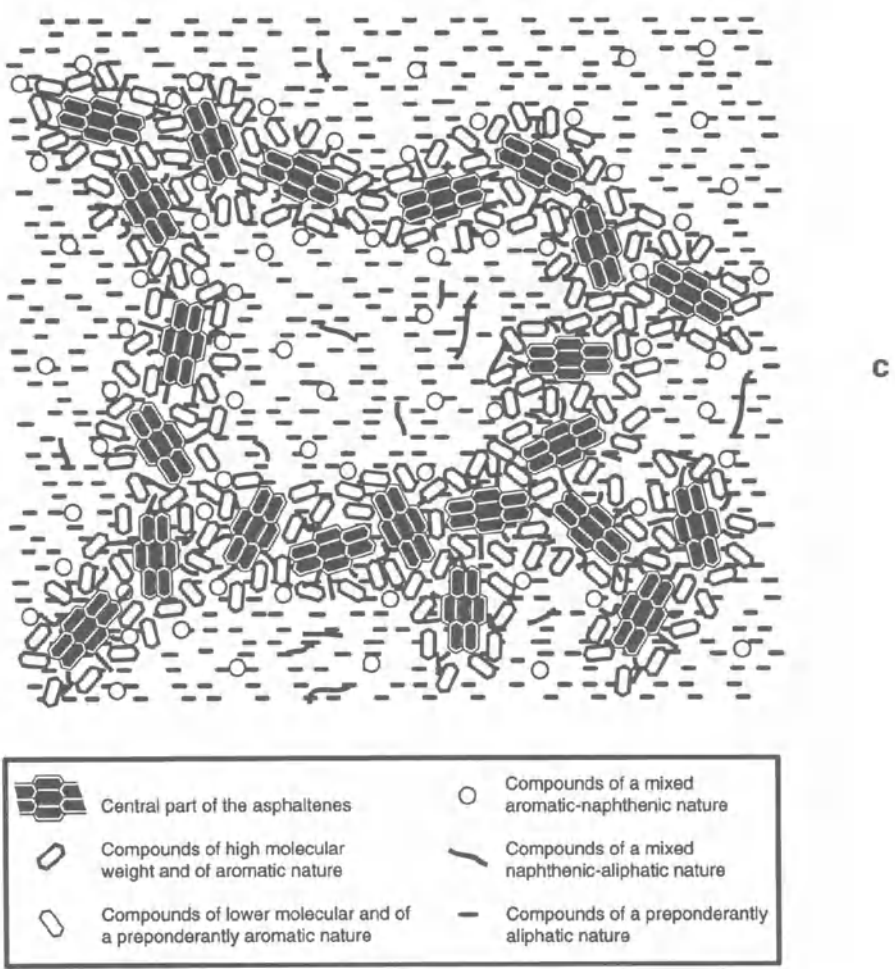

Figure 4c. Gel structure due to micelles aggregation.

duce deposits in the reservoir or in surface facilities. Some crude oils may thus show dramatic instabilities although they contain a small quantity of asphaltenes.

These observations have motivated an important research effort whose purpose is to understand the colloidal behavior of these complex materials. We present below the work recently carried out at the French Institute of Petroleum by using three different but complementary techniques of colloidal characterization: small-angle scattering, cryo-scanning electron microscopy and viscosimetry. These techniques are presented in next Section (3), together with the preparation and analysis of the various asphaltenes and resins used. Section 4 presents the results obtained on: asphaltene solutions (4.1), near-flocculating solutions, with the addition of a flocculant (n-heptane), resins solutions (4.2) and finally natural systems (4.4), including vacuum or atmospheric residues as well as crude oils. The physical picture that emerges from these data is briefly summarized and discussed in the last Section (5).

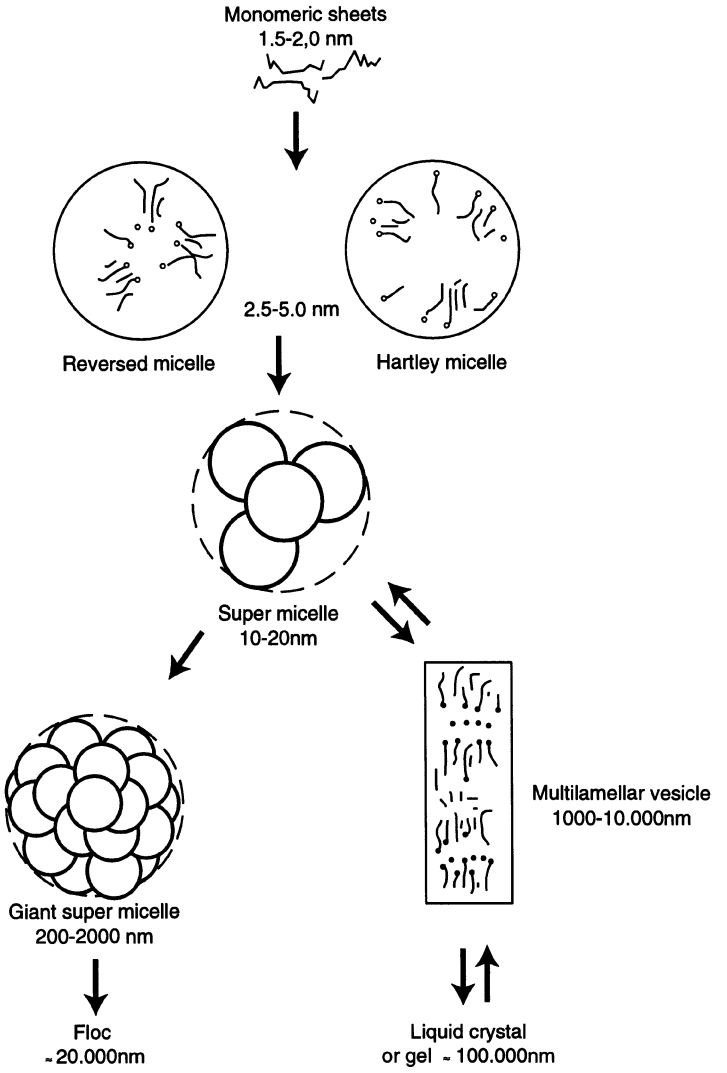

Figure 5. Aggregation of asphaltene micelles (circles indicate polar functional groups).[146]

3. EXPERIMENTAL

3.1. Methods

3.1.1. Small Angle Scattering Techniques.[153,154] The measurement of the scattering of a radiation (X-ray, neutron or light) at small angles is a powerful tool for probing the colloidal structure from nanometric to submicronic scales. In the case of asphaltenes the use of conventional light scattering is limited to extremely dilute solutions (concentrations below 0.1%) as these compounds are strongly absorbent and fluorescent in the visible do-

main. We will therefore focus our presentation on the small-angle X-ray and neutron scattering (SAXS and SANS) techniques. Both techniques have been extensively used in recent years for examining the colloidal structure of asphaltenes both in solution and in their natural medium (such as in a real oil or a residue).

3.1.1.1. *Principle.* The quantity that is measured in a SAXS or SANS experiment is the intensity I(Q) scattered over a range of scattering vectors Q, whose modulus is defined as

$$Q = \frac{4\pi}{\lambda}\sin\theta \tag{1}$$

where λ is the wavelength of the incident radiation and θ the (small) angle of observation. In order to perform our experiments, we have used two X-ray arrangements: a Huxley-Holmes type camera for SAXS and a Double Crystal Camera[155] specially designed for scattering measurements at ultra-small angles (USAXS). The Q-range accessible with these two instruments is very extended from 6.10^{-4} to 0.5 $Å^{-1}$. A special setup has been developed in order to perform experiments at high temperatures up to 500K.

SANS measurements have been performed using two different spectrometers (PAXE and PACE) at the Leon Brillouin Laboratory (LLB - CE Saclay - France). We have adopted appropriate conditions in order to obtain scattering curves in the largest possible Q-range ($3.5.10^{-3} - 1.6.\ 10^{-2}$ $Å^{-1}$).

The measured intensity I(Q) probes the correlations between asphaltene regions over a scale of order 1/Q. Small-angle scattering experiments reveal therefore the spatial structure of asphaltenes over length scales between a few and several tens (or hundreds in the case of USAXS) of nanometers. The scattering spectra I(Q) of asphaltene solutions are usually interpreted within the two-component (i.e., the asphaltenes and the solvent or surrounding medium) approximation:

$$I(Q) = nV^2 (\rho_A - \rho_S)^2 F(Q)S(Q) = \phi V(\rho_A - \rho_S)^2 F(Q)S(Q) \tag{2}$$

In these Eqs. n is the number per unit volume of particules with volume V (V is proportional to the molecular weight M of the particles), ϕ=nV the particle volume fraction, ρ_A and ρ_S are the scattering length densities of asphaltene and solvent or surrounding medium. F(Q) is the particle form factor (i.e., the scattering that would be obtained from a single isolated particle, with the following normalization F(Q=0)=1) and S(Q) the structure factor that accounts for interparticle correlations. The form and structure factors depend strongly on the underlying physical model employed for representing asphaltene colloids. We present and discuss below various colloidal models, together with their corresponding form and structure factors.

3.1.1.2. The Scattering Contrast. As appears in Eq. 2, a sufficient contrast between the scattering length densities ρ_A and ρ_S must exist in order to obtain measurable intensities. They are calculated according to the following formula:

$$\rho = \frac{\Sigma_i b_i}{v} \tag{3}$$

Table 2. X-ray and neutron scattering lengths (b) for different elements

Elements	b -X-ray scattering (10^{-12} cm)	b - Neutron scattering (10^{-12} cm)
H	0.282	−0.374
D	0.282	0.667
^{12}C	1.69	0.665
^{14}N	1.97	0.94
O	2.26	0.58
S	4.51	0.28

where v is a volume of scattering material and b_i the scattering length of the atom i present in the volume v. The scattering length (Σb_i) is calculated by averaging the scattering lengths of each atomic constituent over the composition of asphaltenes (as determined from the elemental analysis) and solvent or surrounding medium. In real materials (crude oils or residues) the elemental analysis of the maltenes is also required. To obtain the scattering length, the determination of volumetric masses of both components is also necessary. We have compared in Table 2 the X-ray and neutron scattering lengths for different elements. For X-ray radiation, the scattering length of an atom is proportional to the number of electrons since $b=b_0 z$ ($b_0=0.282.10^{-12}$ cm) where z is the atomic number.[156] For neutron scattering, the radiation interacts with the atoms' nuclei and b depends on the nature of the nuclei (cf. for instance in Table 2 the important variation of b for hydrogen and deuterium).

Consequently with X-rays the scattering length density is proportional to the electronic density. Asphaltenes, being the heaviest and most polar among the constituents of oil, exhibit a 'natural' contrast with other organic compounds, thus allowing SAXS measurements to be carried out not only on asphaltene solutions but also on real oils or residues. With neutrons, the use of deuterated solvents is required in practice to obtain a sufficient contrast. For real materials the presence of different isotopes (e.g., deuterium and hydrogen) induces a significant Q-independent incoherent scattering that masks the elastic contribution (Eq. 2). In practice, the use of SANS is limited to asphaltene and resins in deuterated solvents.

3.1.1.3. Form and Structure Factors for Various Colloidal Models. Particles are assumed to be homogeneous with some characteristic shape (e.g., spherical, cylindrical, discoidal, etc..), whose geometrical parameters (e.g., the sphere radii) obey a certain size distribution. This distribution, which reflects the more or less strong polydispersity found experimentally is usually strongly skewed towards small particles. A log-normal distribution is very often considered (but other types of distributions can be considered, cf. below Eq. 20). Within this approach the particles are assumed to be uncorrelated (i.e., S(q)=1) which, strictly speaking, is valid for *dilute* solutions. A generalization of Eq. 2 to polydisperse systems is used

$$I(Q) = (\rho_A - \rho_S)^2 \sum_k n_k V_k^2 F_k(Q) \tag{4}$$

in which n_k is the number density of particles with volume V_k (proportional to their molecular weight M_k) and form factor $F_k(Q)$. We list here the form factors for simple geometries:

1) spheres of radius R and volume V

$$F(Q) = V\left(3\frac{\sin(QR) - QR\cos(QR)}{(QR)^3}\right)^2 = V\Phi^2(QR) \tag{5}$$

2) cylinders of axial length 2H, cross-sectional radius R and volume V

$$F(Q) = V\int_0^{\frac{\Pi}{2}} \frac{\sin^2(QH\cos\alpha)4J_1^2(QR\sin\alpha)}{(QH\cos\alpha)^2(QR\sin\alpha)^2}\sin\alpha d\alpha \tag{6}$$

where J_1 is the first order Bessel function and the parameter α is the angle between the scattering vector Q and the cylinder axis.

This complex expression (6) can be simplified in some limiting cases:

- rods of length 2H, radius R (2H>> R) and volume V, in the Q-range defined as followed:

$$QR \leq 1 \text{ and } QH >> 1 \qquad F(Q) = V\frac{\pi}{(2QH)}.\exp\left(-\frac{(QR)^2}{4}\right) \tag{7}$$

- flat cylinders of radius R, thickness 2H (R>>2H), and volume V, in the following Q-range:

$$QH \leq 1 \text{ and } QR >> 1 \qquad F(Q) = V\frac{2}{(QR)^2}\exp\left(-\frac{(QH)^2}{3}\right) \tag{8}$$

3) ellipsoids of axes lengths (2a,2a,2xa) and volume V:

$$F(Q) = V\int_0^{\frac{\Pi}{2}} \Phi^2(Q.a.\sqrt{\cos^2(\alpha) + x^2\sin^2(\alpha)}).\cos(\alpha).d\alpha \tag{9}$$

where Φ is the function defined in expression 5 and α the angle between the scattering vector Q and the ellipsoid.

In practice, the geometrical and polydispersity parameters are fitted to the experimental data. This procedure is cumbersome for non-spherical geometries as the number of parameters to be fitted is important.

In the low Q region (i.e., for sizes larger than the particle sizes), referred to as the Guinier regime, an expansion of $F_k(Q)$ in Eq. 4 leads to a simple, model-independent (therefore also applying to aggregating or polymer-like particles, see below) expression for the scattered intensity:

$$I(Q) = \phi(\rho_A - \rho_S)^2 V_w.\left(1 - Q^2R_{gz}^2/3\right) = I_{Q\to 0}\left(1 - Q^2R_{gz}^2/3\right) \tag{10}$$

In this expression $\phi = \Sigma n_k V_k$ is again the particle volume fraction, V_w and R_{gz}^2 are certain averages of the volumes and radii of gyration of the particles (see below Eqs. 11 and 12). It is convenient here to introduce the molecular weights $M_k = V_k d_A N_{Av}$, (d_A being the asphaltene volumetric mass and N_{Av} Avogadro's number) and $M_w = V_w d_A N_{Av}$. The average M_w is the weight average molecular weight, which is defined as:

$$M_w = \frac{\sum_k n_k . M_k^2}{\sum_k n_k . M_k} = V_w d_A N_{Av} \tag{11}$$

From Eq. (10) this quantity is deduced from the forward scattering $I_{Q\to 0}$:

$$M_w = V_w d_A N_{Av} = \frac{d_A N_{Av}}{(\rho_A - \rho_B)^2} \frac{I_{Q\to 0}}{\phi} \tag{12}$$

R_{gz}^2 is the z-average square radius of gyration:

$$R_{gz}^2 = \sum_k n_k . M_k^2 . R_{gk}^2 / \sum_k n_k . M_k^2 \tag{13}$$

Alternative forms of Eq. (10) are sometimes utilized (these forms are equivalent in the Guinier regime where $qR_{gz}<1$), such as Guinier's law:

$$I(Q) = I_{Q\to 0} \exp\left(-\frac{Q^2 R_g^2}{3}\right) \tag{14}$$

and Zimm's expression:

$$I(Q) = \frac{I_{Q\to O}}{\left(1+\frac{Q^2 R_{gz}^2}{3}\right)} \tag{15}$$

In practice, the logarithm of the measured intensities are plotted as a function of Q^2 (Guinier) or the inverse intensities as a function of Q^2 (Zimm). The linear regime (if any) is then identified and the averaged radius of gyration and molecular weight (or volume) of the particles are extracted from a least-squares fit.

At this point we have not taken interactions and correlations between particles into account, considering in fact very dilute solutions. These correlations manifest themselves in the structure factor. For dilute solutions, it may be shown that, to leading order in ϕ and Q:

$$\frac{K\phi}{I(Q)} = \frac{1}{M_w}\left[1+\frac{Q^2 R_{gz}^2}{3}\right] + 2A_2\phi \tag{16}$$

where $K = (\rho_A - \rho_S)^2 d_A / N_{Av}$ and A_2 is a certain average of the second virial coefficient that describes particle-particle interactions ($A_2<0$ for attractive interactions, $A_2>0$ for repulsive interactions). Then, small-angle scattering measurements on solutions with several different particle dilutions will provide a determination of M_w, R_{gz} and the second virial coefficient A_2. In practice $K\phi/I(Q)$ is plotted as a function of $Q^2+A\phi$ (A being an appropriate constant) and R_{gz} and A_2 are extracted from the two limiting straight lines (one corre-

sponding to $\phi \rightarrow 0$, the other one to $Q \rightarrow 0$). These two straight lines have the same intercept, equal to $1/M_w$. This representation is called a Zimm plot.

Other types of colloidal materials possess some internal structure because they are made up of repeat units (with some average composition) joined by either loose or covalent binding. Loose binding may occur because these units find themselves in the minimum of their interaction potential. The particles then resemble aggregates whose properties depend on the formation process and the nature of the interaction potential. Typical aggregates are those grown (from initially isolated units) by the so-called diffusion- and reaction-limited colloidal (or cluster) aggregation (DLCA and RLCA) processes. The first growth process (DLCA), which occurs in systems with a strongly attractive interaction potential, is governed by Brownian diffusion: each time a structural unit or cluster meets (by diffusion) another structural unit or cluster these two entities join and form a larger aggregate.[135,136] The second (much slower) growth process (RLCA) occurs in systems in which the interparticle interaction potential displays an energy barrier that needs to be overcome for the entities to join. These two kinds of aggregates represent in fact two limiting situations and have some very distinctive static and dynamic properties. Another type of frequently encountered colloidal material is made up of covalently linked subunits and consists typically of polymer-like structures (with possibly some degree of branching).

In both types of colloids the repeat units are of molecular size and therefore the form factor $F(Q) \approx 1$ for the Q range spanned in SANS and SAXS experiments. The intensity scattered is proportional to the structure factor S(Q) of these aggregates or polymer-like structures.

We first consider *dilute* systems. In the (Guinier) low Q regime ($QR_{gz} < 1$) the previous expressions (Eqs. 10 and 14) for the scattered intensity hold. We focus here on the intermediate range of scattering vectors ($QR_{gz} > 1$ but $Qa < 1$, a being a typical size for these repeat units), where the behavior of I(Q) yields an information on the internal structure of the scattering object. The intensity scattered by aggregates or polymer-like structures usually behaves over this intermediate range of scattering vectors as a power law:

$$I(Q) \approx Q^{-D} \tag{17}$$

where D is the fractal dimension characterizing the internal structure of the scattering objects.[157] The fractal dimension D is the exponent that relates the mass to the dimension of the object: let M(r) be the mass included in a sphere of radius r (originating at the center of mass of the fractal object), then D is defined as $M(r) \approx r^D$, where r varies from the size a of the repeat unit to the object's overall radius R. The maximum value of D is 3 (corresponding to dense, homogeneous objects). The density of a fractal object is not constant but decreases with increasing dimension r:

$$d \approx \frac{M(r)}{r^3} \approx r^{D-3} \tag{18}$$

Fractal dimensions of typical aggregates range from $D \approx 1.7$ (DLCA) to 2.1 (RLCA).[135,136] The fractal dimension of linear polymer chains range from 1.7 (swollen chains, i.e. chains in a good solvent) to 2 (gaussian chains, i.e. chains in a theta-solvent), while branched polymer chains near a connectivity (sol-gel) transition have a fractal dimension equal to 2 (in a good solvent).[137]

In the case of polydisperse fractal objects, the observed scattering exponent in the intermediate regime (see Eq. 17) also reflects the polydispersity of these objects. In fact, an expression similar to Eq. (4) must be used:

$$I(Q) = (\rho_A - \rho_S)^2 \sum_k n_k V_k^2 S_k(Q) = K \int n(M) M^2 S_M(Q) dM \tag{19}$$

in which K is a constant and the structure factors of fractal objects with mass M, $S_M(Q)$, behaves as Q^{-D} in the intermediate scattering regime. For many aggregating or polymer-like structures the distribution of objects n(M) (i.e., the number of fractal objects with mass M) exhibits the following scaling behavior

$$n(M) = \overline{M}^{-2} f\left[M / \overline{M}\right], \tag{20}$$

where $\overline{M}$ is an average or typical mass and f(x) is the scaling function that describes the shape of the cluster mass distribution. The mass $\overline{M}$ increases with time for DLCA or RLCA aggregates, whereas it diverges to infinity for systems approaching a percolation (sol-gel) transition. The scaling function f decays very rapidly (faster than any power law) for x>1 (i.e., for M> $\overline{M}$) and behaves for x<1 as a power law $f(x) \approx x^{-\tau}$, where τ is (like the fractal dimension) an exponent characteristic of the structure, e.g., τ=0 (DLCA), 1.5 (RLCA) or 2.2 for systems close to a connectivity (sol-gel) transition. Then, injecting Eq. (20) into Eq. (19) leads again to a power law behavior for the scattered intensity:

$$I(Q) \approx Q^{-d} \tag{21}$$

where the apparent fractal exponent $d=D(3-\tau)$ if $\tau>2$ and $d=D$ if $\tau<2$.[158,159]

Several *ad-hoc* expressions have been worked out for the scattering function of *dilute* polydisperse fractal objects over the whole range of scattering vectors (from the Guinier to the intermediate regime) and the reader is referred to references[105,160] for more details.

To lowest order in ϕ the scattering intensity of (dilute) fractal entities is described by Zimm's expression (Eq. 15). As the volume fraction increases these fractal entities start to overlap. When these objects are large enough there exists a concentration regime (referred to as semidilute) where these objects are strongly interpenetrated but nevertheless the volume fraction remains low. The overlap concentration $\phi^* \approx M / R_g^3$ (for which the overall concentration equals the concentration inside the fractal objects) delineates the dilute and semidilute regimes. In the semidilute regime the scattering intensity has the same structure than in the dilute regime (cf. Eq. 15):

$$I(Q) = \frac{I_{Q \to 0}}{1 + Q^2 \xi^2} \tag{22}$$

the length ξ corresponding to the correlation length (of concentration inhomogeneitites). This length may be viewed as the size of uncorrelated entities or blobs below which the fractal correlations still hold. This length tends to $R_g / \sqrt{3}$ in the dilute regime ($\phi<\phi^*$) and decreases with increasing concentration. Well in the semidilute regime ($\phi>\phi^*$) ξ decreases according to a power law in ϕ (with an exponent that depends on the fractal dimension D).

It may be shown[161] that $I_{Q\to 0}$ is proportional to the volume fraction ϕ and to the mass of these correlated entities (or 'blobs') M_b:

$$I_{Q\to 0} \approx \phi M_b \approx \phi \xi^D \qquad (Q>1/\xi) \tag{23}$$

$I_{Q\to 0}$ crosses over to the dilute expression (Eq. 12) for low ϕ. In the intermediate regime ($Q>1/\xi$), the scattering intensity should still behave as Eq. (17).

3.1.2. Cryo-Scanning Electron Microscopy.[162–164] Scanning electron microscopy is a fundamental technique for the description of a sample texture. However, the very low vacuum pressure (10^{-5} torr) imposed by the use of an electron beam limits its standard application to solid samples. In liquid containing samples like gels or suspensions, the direct removal of the liquid would inevitably lead to changes in the native structure. An alternative possibility for preparing such samples is to solidify the liquid by freezing it and maintain the sample at low temperature during the observation. Such low temperature methods have been first developed by biologists for the study of living cells. Since then, cryo preparation equipments have become commercially available and the use of low temperature methods has become general for the study of liquid containing samples. A summary of rapid freezing methods is provided (reference 163).

An Oxford-Hexland cryotrans CT1500 system interfaced to a JEOL JSM6300F scanning electron microscope was used for our experiments.

The studied suspension is introduced into a drilled copper stub (1mm diameter cavity), covered with a thin copper plate (in contact with the liquid) and, finally, rapidly frozen by plunging into sub-cooled nitrogen at a temperature of about 63K. The stub is then transferred into a cryo-preparation vacuum chamber, which is a cold stage maintained at 108K. The copper plate is then removed in vacuum in order to cleave and expose a fresh fracture plane of the sample. The cleaved sample is then transferred into the cold stage of the microscope which is maintained at 83K. A heater in the stage enables the temperature to be raised to any preset value from 83K to 323K. The sublimation process is controlled by the SEM image observation. For the vacuum of the microscope chamber, the appropriate sublimation temperature of toluene is about 158K. Our observations have been made at this temperature, and the sublimation process was followed as a function of time. The porous texture of the sample corresponding to an etching depth of several micrometers was typically revealed after about 40 minutes. If necessary, the sublimation process was stopped and the sample coated with gold in order to improve the image quality. Observations have been performed at low voltage and in secondary electron mode.

3.1.3. Viscosimetry. Viscosimetric measurements have provided one of the earliest evidences of the colloidal nature of asphaltene in solutions or in their natural medium.[165] From the increase in viscosity induced by the presence of asphaltenes in the medium, some information can be extracted concerning the properties of these colloids. We focus here on the region of linear viscosity increase that is observed for high asphaltene dilutions (asphaltene volume fractions ϕ below 2–3%). The slope of the linear portion of the relative viscosity as a function of the volume fraction ϕ is by definition the intrinsic viscosity $[\eta]$ of the dissolved colloids:

$$\eta_r = \frac{\text{Solution viscosity}}{\text{Solvent viscosity}} = 1 + [\eta]\phi \tag{24}$$

Equivalently, $[\eta]$ is the limiting value for $\phi=0$ of the reduced specific viscosities:

$$[\eta] = \lim_{\phi \to 0} \frac{(\eta_r - 1)}{\phi} \tag{25}$$

The intrinsic viscosity $[\eta]$ is related to the colloidal hydrodynamic volume. For hard spheres $[\eta]$ is equal to Einstein's value, 2.5. Viscosimetric measurements carried out on asphaltenes in a solvent or in their natural medium[82,86,87,151] yield intrinsic viscosity values in the range of 6–8 or above, indicating that the hydrodynamic volume of an asphaltene particule is much higher than that of the hard sphere with an equivalent quantity of asphaltene material.

Various interpretations have been proposed for these significant intrinsic viscosities and hydrodynamic volumes. Reerink,[82] assuming that asphaltene particules are compact objects elongated and ellipsoidal in shape, inferred the ratio of the major axis to minor axis for such ellipsoids. Sheu and coworkers,[86] assuming that these particules are solvated spheres occupying an effective volume fraction ϕ_{eff}, inferred the values of ϕ_{eff}/ϕ, i.e., the ratios of the hydrodynamic volume V_{eff} of the particule (containing asphaltene and the solvent trapped inside the particle) to the volume V occupied by asphaltene material only:

$$\frac{\phi_{eff}}{\phi} = \frac{V_{eff}}{V} = \frac{[\eta]}{2.5} \tag{26}$$

The volume of asphaltene material in the particle is proportional to its molecular weight: $M=d_A V N_{av}$, while for particles of radius R the effective volume V_{eff} is proportional to R^3. Thus, within this model of solvated spheres, the intrinsic viscosity should be equal to:

$$[\eta] = 2.5 \frac{4\pi R^3/3}{V} = \psi \frac{R^3}{M} \tag{27}$$

and should therefore measure the effective volume occupied per unit mass of the particle (ψ is a constant in Eq. 27). It is worth mentioning that Eq. 27 has been verified experimentally for other colloidal systems, e.g. for polymers in solution, where it is referred to as the Flory-Fox[166] equation.

3.2. Sample Preparation

Asphaltenes were prepared according to the AFNOR T60–115 method from various crude oils and residues. The corresponding maltenes (i.e., the fraction soluble in n-heptane) were separated in turn (SAR fractionation) by elution in a column filled with silica and alumina with the following solvents: n-heptane, a toluene/n-heptane (1/3, 2/3) mixture, then a toluene, 1–2 dichloroethane and methanol (1/3,1/3,1/3) mixture.

The elemental analysis of these various asphaltenes and the resins from a Safaniya vacuum residue (VR) have also been determined, leading to the chemical compositions gathered in Table 3. The asphaltenes and resin contents of some crude oils and the corresponding atmospheric and vacuum residues are listed in Table 4.

Table 3. Chemical composition of (i) asphaltenes extracted from different crude oils or vacuum residues, (ii) Safaniya vacuum residue resins. The amount of asphaltenes in these crude oils is given

Products - Asphaltene contents (% w/w)	Asphaltene chemical composition
A – 0.6	$C_{7.27}H_{8.0}N_{0.055}O_{0.2}S_{0.023}$
B – 14	$C_{6.79}H_{8.02}N_{0.13}O_{0.1}S_{0.215}$
D – 4	$C_{7.35}H_{8.57}N_{0.112}O_{0.08}S_{0.011}$
M – 1	$C_{7.36}H_{7.9}N_{0.095}O_{0.13}S_{0.008}$
R – 24	$C_{6.73}H_{6.88}N_{0.005}O_{0.06}S_{0.357}$
V – 9	$C_{6.68}H_{7.69}N_{0.005}O_{0.08}S_{0.337}$
W – 4	$C_{6.825}H_{6.5}N_{0.093}O_{0.11}S_{0.159}$
Safaniya crude oil – 1.5	$C_{6.96}H_{7.2}N_{0.078}O_{0.07}S_{0.228}$
Safaniya vacuum residue – 15	$C_{6.87}H_{7.49}N_{0.072}O_{0.08}S_{0.236}$
Safaniya vacuum residue resins	$C_{6.86}H_{9.6}N_{0.05}O_{0.081}S_{0.187}$

4. COLLOIDAL MACROSTRUCTURE

4.1. Asphaltene Solutions

4.1.1. Investigations by Scattering Techniques. Our first approach has been to characterize by X-ray or neutron scattering techniques asphaltenes in a simplified environment, consisting of a good solvent.[92–95] The small-angle scattering spectra of asphaltene solutions display some very generic features, an example of which is given in Figure 6. This figure depicts the X-ray scattering spectrum of a solution with 5.45% (w/w) asphaltenes of a Safaniya vacuum residue (VR) in toluene. This spectrum was obtained by using a combination of SAXS and USAXS cameras that allowed us to explore a very large range of scattering vectors (Q from 5 10^{-4} $Å^{-1}$ to 2 10^{-1} $Å^{-1}$). Two regions (delineated by the scattering vector Q_1 in Figure 6) can be distinguished in the spectra of asphaltene solutions: i) a region at low and intermediate scattering angles where the scattered intensity is characterized by a quasi-plateau at low Q followed by a strong decrease at higher Q and ii) a region at very low scattering angles where the scattered intensity rises sharply with decreasing Q. The latter region, usually accessible with USAXS instruments, indicates the presence of large-scale (>50–100 nanometers) heterogeneities in the solution, which we further discuss at the end of this Section. In the following we focus on region (i), accessi-

Table 4. Resin and asphaltene contents (% w/w) for R and B crude oils, Safaniya vacuum residue (VR), B atmospheric residue, W atmospheric and vacuum residues. R/A is the ratio resins to asphaltenes

	Resin concentration (% w/w)	Asphaltene concentration (% w/w)	R/A
Safaniya vacuum residue (VR)	25	15	1.66
R crude oil	21	22	0.95
B crude oil	27	14	1.9
B atmospheric residue	30	15	2
W atmospheric residue (AR)	22	6	3.66
W vacuum residue (VR)	28	22	1.27

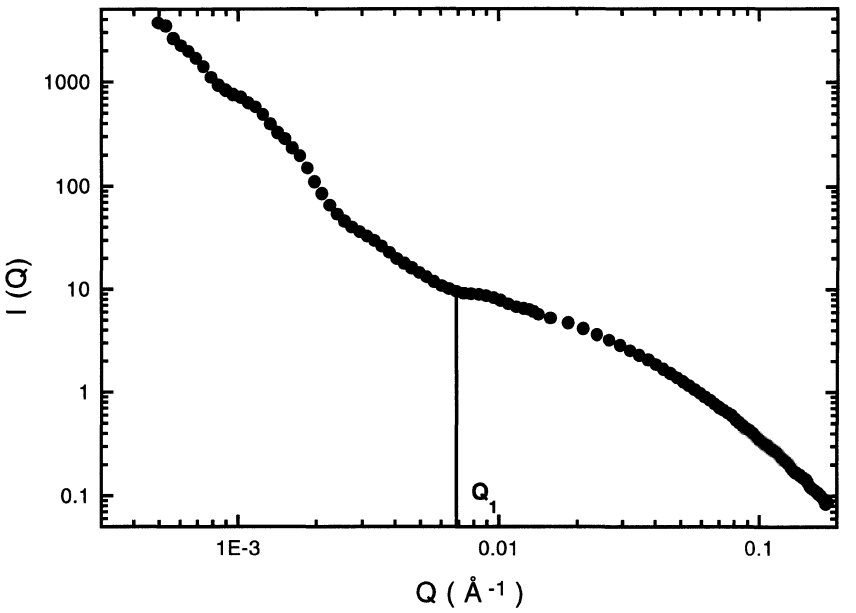

Figure 6. X-ray scattering of Safaniya vacuum residue asphaltenes in solution in toluene (5.45 % w/w).

ble with most X-ray and neutron spectrometers, which reflects heterogeneities of restricted extension (a few tens of nanometers) corresponding to the single asphaltenic particles or aggregates. After explaining the procedures used for interpreting the scattering spectra in terms of size, molecular weight, shape and internal structure for these entities, we present and discuss experimental scattering data for asphaltenes in various solvent, temperature and concentration conditions. We also compare SAXS and SANS data obtained on identical samples.

4.1.1.1. Treatment of Scattering Data.[104,154] As a *first step* in the treatment of the spectrum some simple characteristic regions and laws are identified, such as typically: i) in the low Q region, a Guinier or Zimm behavior, from which the molecular weight and radius of gyration of the asphaltene entities are extracted and ii) for intermediate and large Q a scaling dependence of the type $I(Q) \approx Q^{-D}$ (cf. Section 3.1.1). Then a structural model for the asphaltene entities consistent with the behavior for intermediate and large Q (ii) is chosen. It is worth mentioning here that different structural models may give rise to similar spectra: for instance the value $D \approx 2$, which is very often observed experimentally, is consistent with models of homogeneous disk-like particles (cf. Eq. 8) or with aggregates having an internal structure characterized by a fractal dimension ≈ 2 (cf. Eq. 17). In a *second step*, the complete expressions for the form or structure factors are used (e.g. Eqs. 5, 6, or 9 for dilute spheres, cylinders or ellipsoïds) and the corresponding parameters (i.e., the radius for spheres, the cross-sectional radius and axial length for cylinders, etc.) are adjusted so that the calculated spectrum fit the experimental data. In order to account for the data it is often necessary to introduce some additional parameters characterizing the polydispersity of the asphaltene entities (e.g., the standard deviation and the average value for log-normal size distributions, the exponent τ and $\overline{M}$ for distributions of the type represented by Eq. 20).

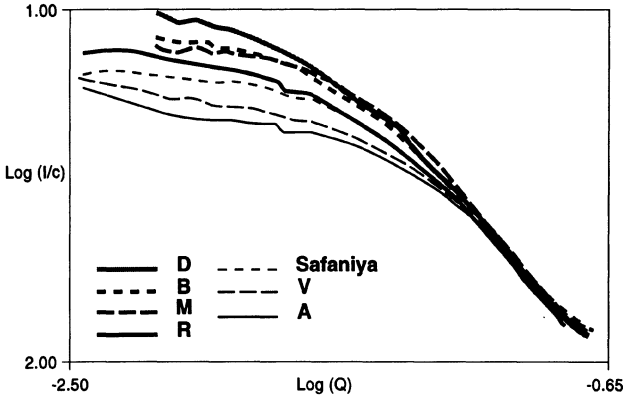

Figure 7. SANS scattering curves for various asphaltenes extracted from different crude oils, D, B, M, R, Safaniya crude oil,V,A. The scattering intensity is corrected by the asphaltene concentration (c) in deuterated toluene.

This type of treatment has been extensively applied in the literature.[86,87,92,93,95,104] We have demonstrated[95] that, using realistic size distributions, different models (spheres, disks or ellipsoids) are able to fit the experimental data. In our opinion the results of such treatments should be taken with caution. However, as already emphasized, the information extracted from the low Q behavior, i.e., the weight-average volume V_w or molecular-weight M_w (see Eq. 12) and the z-average radius of gyration (see Eq. 13), is more robust and model-independent as it does not depend in particular on whether the asphaltene entities are assumed to be homogeneous particules or have some internal structure.

As an example the data in Figure 7 corresponding to dilute solutions of asphaltenes of various origins in toluene have been treated by a least-squares fitting procedure with a model of spheres having a log-normal distribution for the radii (characterized by an average radius and a standard deviation). Results of this treatment are gathered in Table 5. The fitted size distributions for asphaltenes R, W, B, D are plotted in Figure 8. It appears that the distribution is skewed towards small particles, but yet the largest particles are numer-

Table 5. Size parameters deduced from curve fitting procedure (sphere model) for various asphaltenes in solution in toluene (see Table 3) (R_0 is the average radius of the log-normal distribution, σ the standard deviation,[95] <V> is the volume average)

Asphaltenes	R_0 (A)	σ	<V> (A^3)
A	6.3	0.6	130000
B	9.6	0.62	700000
D	11	0.64	1200000
M	18	0.48	550000
R	4.6	0.72	480000
Safaniya crude oil	12	0.54	370000
V	5.7	0.63	180000
W	8	0.57	170000
Safaniya vacuum residue	8.5	0.6	340000

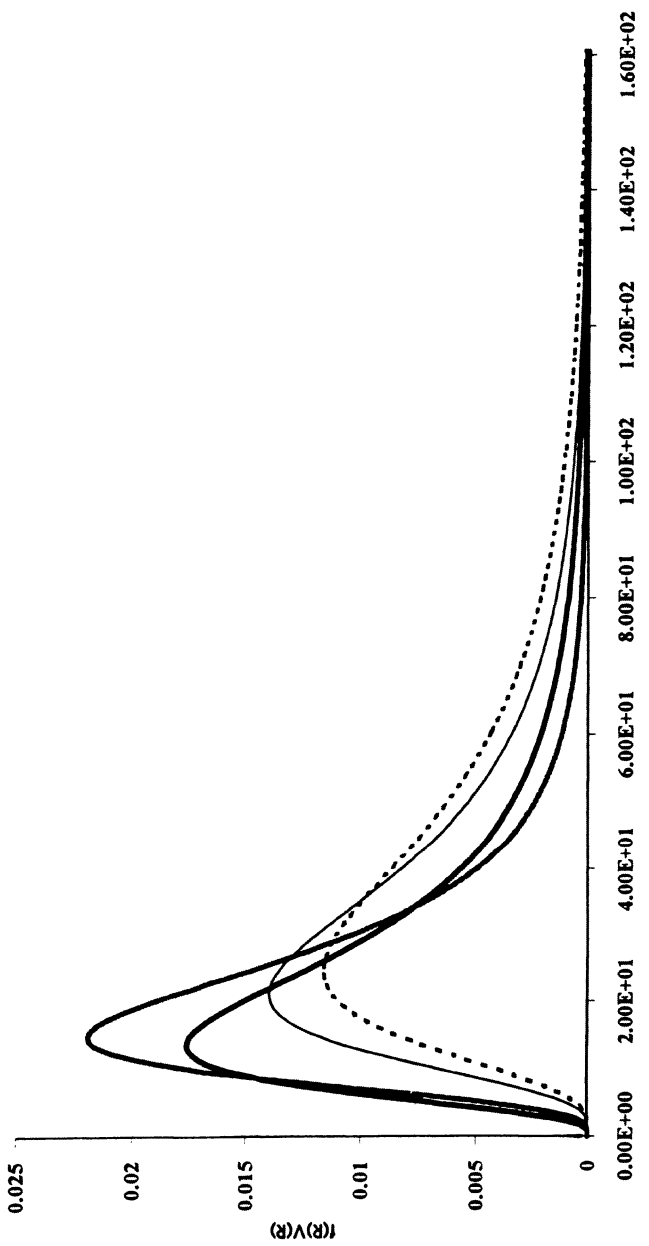

Figure 8. Volume size polydispersity calculated by curve fitting procedure (spherical particles) for various asphaltenes in solution in toluene - (see Table 3) W ($\overline{}$), R (—), B(—),

ous enough to have a strong influence on the scattering signal. The primary information that can be (at first glance) extracted from Figure 7 is a classification of the different asphaltenes according to the position of the quasi-plateau $I_{Q\to 0}$, i.e. according to their volume or molecular weight (cf. Eq. 12).

It is worth mentioning that powerful tools such as molecular simulation softwares could in principle be utilized to calculate more complex models of asphaltene entities[167] and their scattering spectra. To our knowledge, such an approach has not been attempted yet.

4.1.1.2. Concentration Effects. Figure 9a shows a SANS Zimm plot carried out for solutions in toluene of asphaltenes from Safaniya vacuum residue. The concentration range was in the range 0.1–4.7 % w/w. Two domains can be observed; the first one concerns the highest concentrations (2.5–4.7 % w/w) where the second virial coefficient is near zero and the second one concerns very low concentration values (Figure 9b). We succeeded in performing experiments at very low asphaltene concentration (0.025 % w/w). We have deduced by extrapolation at Q=0 and C=0, the weight average molecular weight (Mw = 61700 g.mole^{-1}), at C=0 the radius of gyration (Rg = 48.3 Å), and finally for Q=0 the second virial coefficient (A_2 = -2.33. 10^{-4} cm^3.mole.g^{-2}). This coefficient is very low and slightly negative, which can be an indication either that asphaltenes are not solubilized in a very good solvent or that the average molecular weight is concentration dependent. We have plotted on Figure 10 the variations of the mean-square radius of gyration and the extrapolated intensity at Q=0 as a function of the asphaltene concentration. These values has been calculated from SAXS and SANS experiments. Up to 5% w/w, the scattered intensity is proportional to the concentration and the radius of gyration remains constant. Above 5% w/w asphaltene concentration, we do not observe a linear evolution of the intensity and the radius of gyration decreases. We are no longer in the approximation of a dilute regime. For low concentrations, asphaltenes aggregates are independent and the scattering intensity is then proportional to the concentration of these asphaltene clusters and depends on the form factors of each aggregate type (see formula 4). As the concentration raises, aggregates are progressively in contact and the scattering intensity is no longer sensitive to the average size of the particles but depends on a characteristic length much smaller than the average size (see Section 3.1.1—formula 22). Cabane[168] has discussed and illustrated this behavior (Figure 11) which can explain the decrease of the apparent radius of gyration (Figure 10). This concept is in good agreement with the molecular description of the asphaltene molecules as illustrated on Figure 1. Several more or less extended asphaltene macromolecules, showing a similar polymer-like structure, with covalent bonds between aromatic and aliphatic basic entities, can be in interaction via π–π associations or hydrogen bonds. The size of these macromolecules shows a large polydispersity. As concentration increases, they can come into contact and may be interpenetrated.

4.1.1.3. Comparison between SAXS and SANS Data. We have compared small angle neutron and X-ray scattering data (Figure 12) of Safaniya Vacuum Residue asphaltenes. The intensity is corrected by the concentration and the contrast term which was calculated according to the chemical composition (see section 2). The two curves are very similar at small Q values ($Q \approx 10^{-2}$ Å^{-1}), and SAXS intensity becomes higher for Q greater than 5. 10^{-2} Å^{-1}. This behavior can be explained by contrast term variations. We know that asphaltenes are mainly composed of aromatic and aliphatic blocs; if we compare the electronic densities for X-rays or the coherent scattering length density for neutrons (Fig-

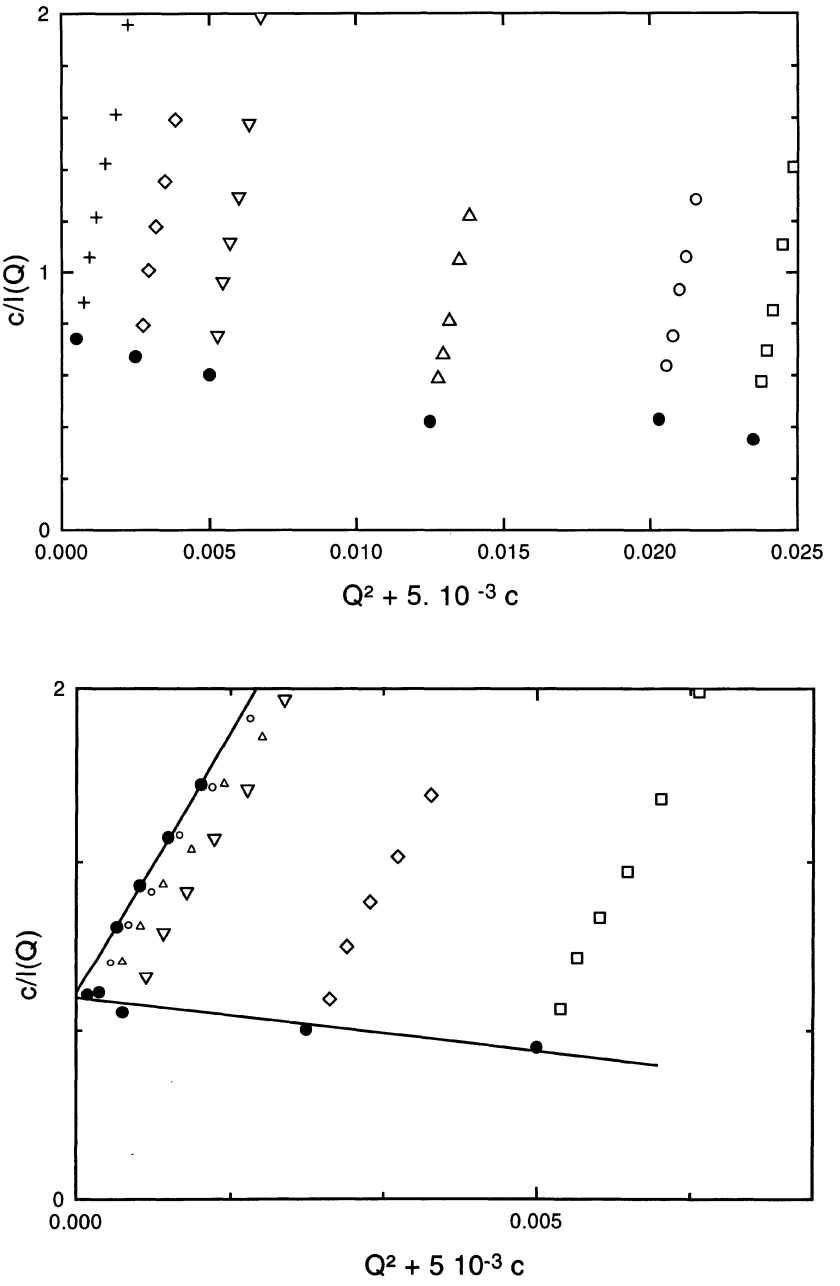

Figure 9. Zimm-plot for small angle neutron scattering curves of Safaniya Vacuum Residue asphaltenes in toluene - Asphaltene concentrations (c: %w/w) [a] (crosses: 0.1, diamonds: 0.5, down triangles: 1, up triangles: 2.5, open circles: 4, squares: 4.7) - [b] (open circles: 0.025, up triangles: 0.05, down triangles: 0.1, diamonds: 0.5, squares: 1) - Full circles correspond to extrapolations for Q=0 or c=0.

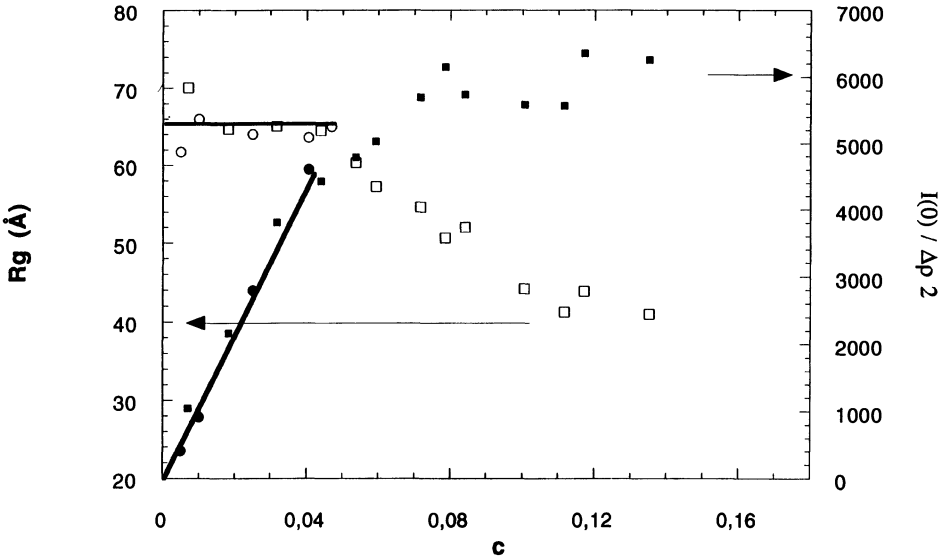

Figure 10. Mean-square radius of gyration (R_g) (○○○: SANS experiments, □□□: SAXS data) and scattered intensity extrapolated at Q=0 (I(0)) (■■■: SAXS, ●●●: SANS) as a function of the concentration of Safaniya Vacuum Residue asphaltenes in solution in toluene ($\Delta\rho^2$, contrast term).

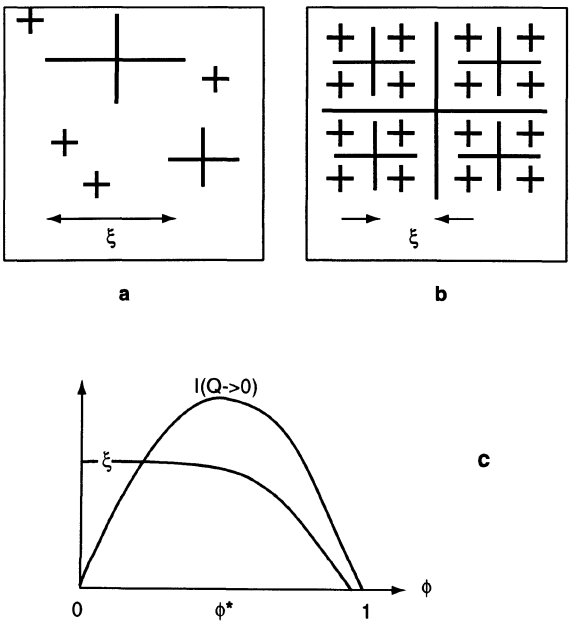

Figure 11. Characteristic length ξ for density fluctuations for diluted system (a), and concentrated one (b). (c) Evolution of ξ and the scattered intensity at Q=0 as a function of the concentration.[168]

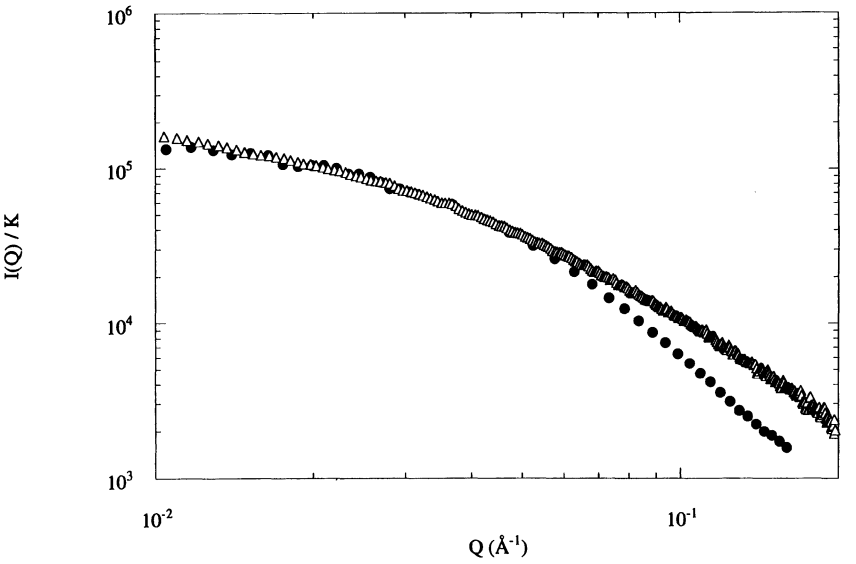

Figure 12. Comparison of SAXS and SANS curves of Safaniya VR asphaltenes in toluene. The scattering intensity is divided by the asphaltene concentration and the contrast term ($K=c.\ \Delta\rho^2$).

ure 13), we can observe that X-ray or neutron contrasts are not identical for the different blocs. We have calculated the ρ term (formula 3), for hydrogenated and deuterated toluene, Safaniya VR asphaltenes, aromatic and aliphatic regions. According to NMR characterization, we have considered simple molecules, perylene (five benzene rings) and pentadecane ($C_{15}H_{32}$) for chemical representation of respectively aromatic and aliphatic regions. One can notice for SANS, that the contrast term ($\Delta\rho^2$) is much higher for aliphatic entities than for aromatic ones in deuterated toluene. On the contrary, X-rays are predominantly sensitive to the aromatic species of asphaltenes. Consequently, at large Q-values, each technique will "see" different regions (aromatic or paraffinic) of the asphaltene molecules and the scattered intensity will be different. At small Q-values, both techniques will be sensitive to the aggregation of (i) aromatic entities for X-rays and (ii) paraffinic parts for neutron, but large asphaltene aggregate size is defined by both types of entities, aromatic and paraffinic. In consequence, each technique will give the same scattering, which means same aggregate size. We can compare this behavior, with any gray circle you can draw on your computer screen; if you look at this picture far from your screen (small Q), you will see the gray circle, but if you have good eyes close to the screen you will see black and white dots (large Q).

4.1.1.4. Solvent and Temperature Effects. We have investigated the effect of solvents and temperature on the molecular weight of asphaltenes by small angle neutron scattering (Figure 14). We have confirmed that the average molecular weight is strongly dependent on the nature of the solvent.[74] Good correlation has been found between this molecular weight and the dipolar moment of the solvent molecules (Figure 15). The average molecular weight is much larger in benzene than in pyridine. An increase of the temperature is followed by a decrease of the size of the asphaltene particle. We can notice that for sufficiently high temperature, the molecular weight of asphaltenes as a function of the

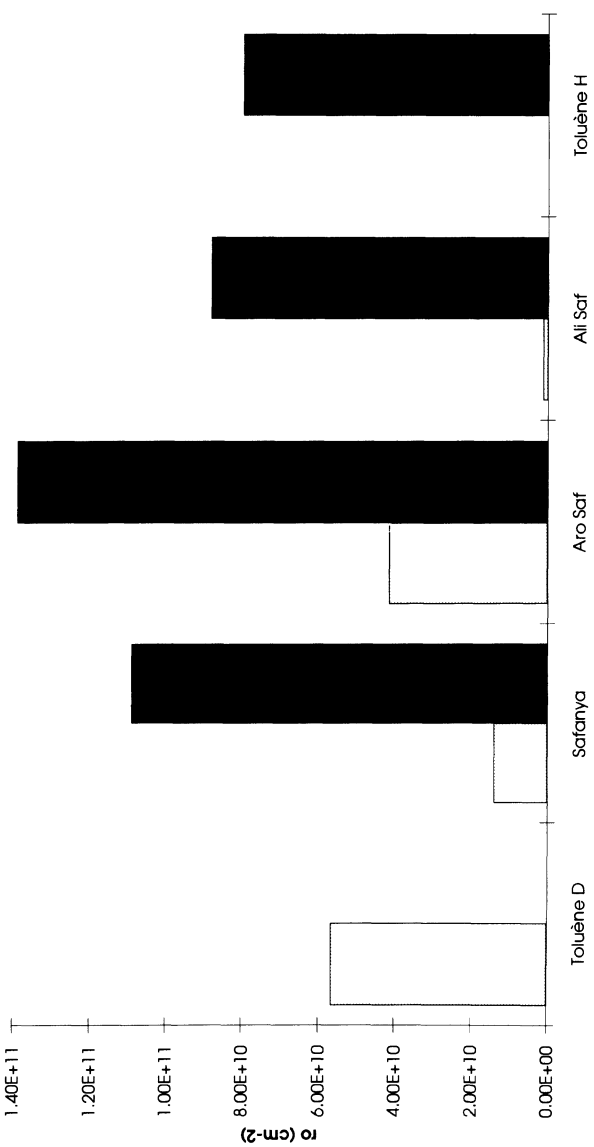

Figure 13. Comparison of contrast term between SAXS (solid bars) and SANS (outline) methods for Safaniya VR asphaltenes - ρ is the electronic density for X-rays and the coherent scattering length density for neutrons: it has been calculated according the asphaltene composition (see Table 3), perylene for aromatic regions of the molecule, pentadecane ($C_{15}H_{32}$) for aliphatic ones.

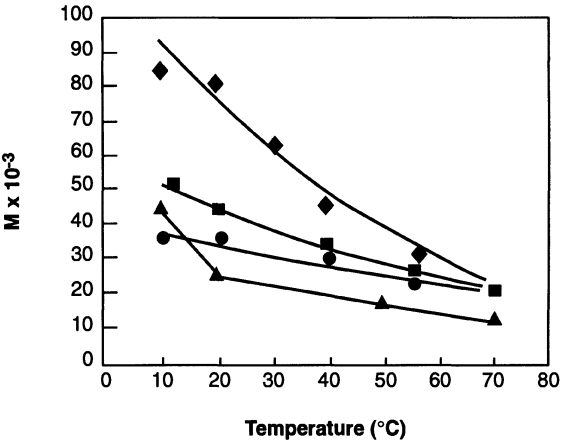

Figure 14. Average molecular weight evolution of Safaniya vacuum residue asphaltenes in solution in different solvents and as a function of temperature (SANS experiments). ■ ortho-xylene, ◆ benzene, ● tetrahydrofuran, ▲ pyridine.

solvent seems to reach an unique value, suggesting a dissociation to the molecule. We can suggest that for higher temperatures, de-aggregation will take place giving rise to elementary asphaltene molecules. The asphaltene behavior in various solvents, as a function of temperature increase or concentration decrease is good proof of the self-association of these entities.

4.1.1.5. Upturn of I(Q) at Very Low Q. An upturn of the X-ray scattered intensities at very low Q ($Q<3–4\ 10^{-3}$ Å^{-1}) is usually observed for asphaltenes, both in solution (see Figures 6 and 16) and in their natural medium (cf. next Section). This indicates the pres-

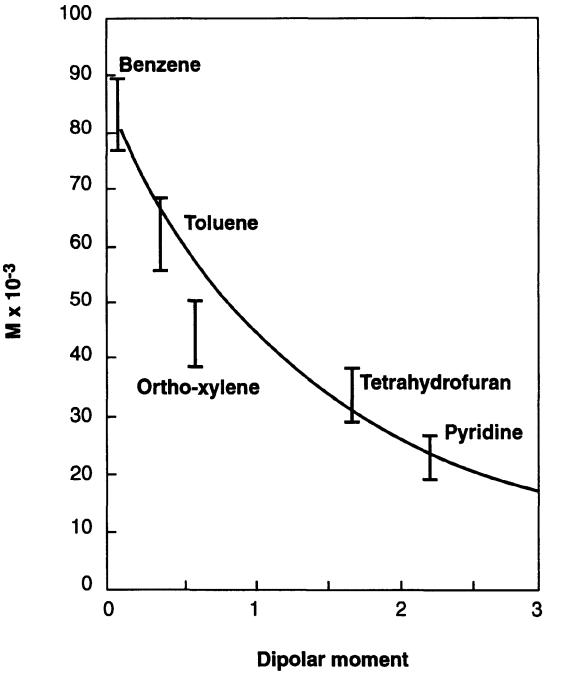

Figure 15. Average molecular weight of Safaniya vacuum residue asphaltenes in solution in different solvents and as a function of dipolar moment of the solvent (SANS experiments).

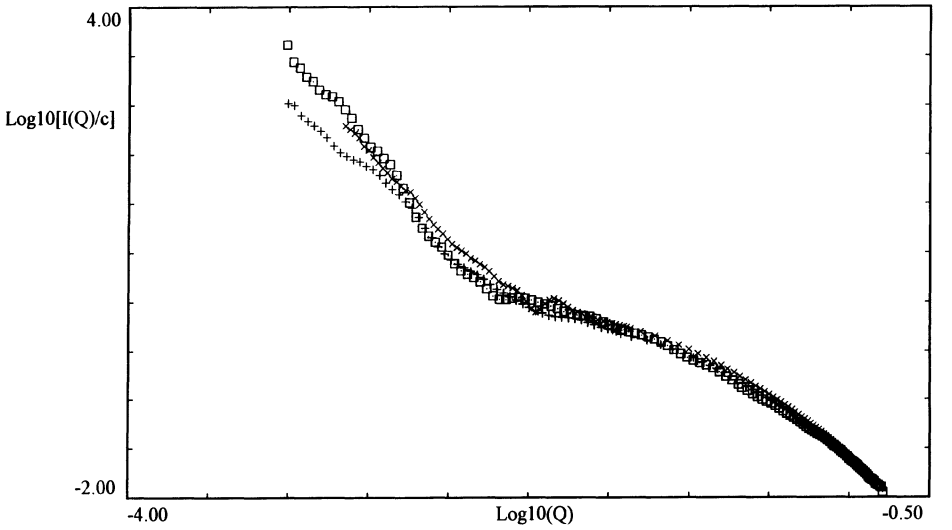

Figure 16. Small angle X-ray scattering of various asphaltenes in solution in toluene. (□) D, (x) R, (+) Safaniya vacuum residue (see Table 3).

ence of large-scale (>2π/Q) heterogeneities in the medium. The steep increase of I(Q) with decreasing Q (the apparent exponent d such that $I(Q) \approx Q^{-d}$ lies in the range of 2.5–3) indicates that these heterogeneities are quite dense. We have verified that this intense scattering at very low Q exists for asphaltenes of various origins (Figure 16) and is roughly proportional to the concentration, at least for concentrations in the range from 2 to 10 % w/w (Figure 17).

This behavior is reminiscent of what is sometimes observed in polymer solutions, where it is referred to as the 'Picot-Benoit' effect.[169] Its physical origin is unclear: it might be

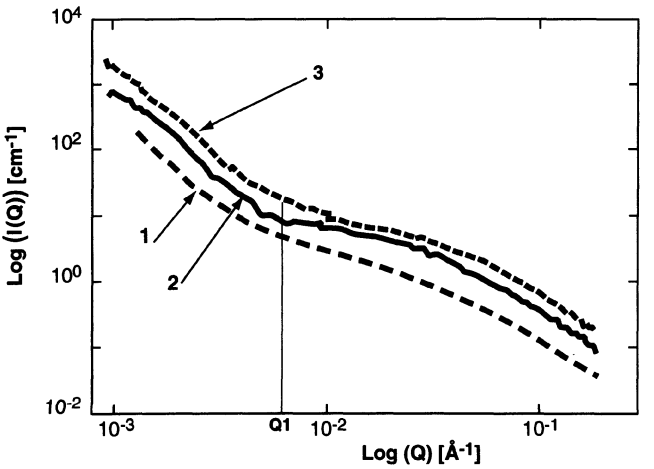

Figure 17. Small angle X-ray scattering of Safaniya vacuum residue asphaltenes in solution in toluene for three different asphaltene concentrations: (1) 2 % w/w; (2) 6 % w/w; (3) 10 % w/w.

due to the presence of some micro-gels. This effect can be removed by ultracentrifugation or filtration, which seems to be also the case with asphaltene solutions (see next paragraph). This upturn at very low Q is also often observed in gels and several theories have been proposed to explain these inhomogeneities in the network structure (they are reviewed in ref. [169]). A plausible hypothesis is that asphaltene solutions contains some pieces or remainings of the original kerogen three-dimensional network. To further understand the nature of these heterogeneities, the acquisition of scattering data 1) on more dilute asphaltene solutions (i.e., for concentrations below 1%) and 2) at still lower Q would be highly desirable.

Two types of models have been proposed for SAXS data interpretation (Figure 18):

1) in the first situation (Figure 18-a), small asphaltene molecules form complex aggregates; various types of interaction between these molecules can be suggested, according to the literature, as van der Waals forces and/or hydrogen bonding. Asphaltenes molecules are micelles, whose size can vary; their contribution to SAXS intensity is observed at large Q values (Q>Q1). The spatial distribution of these aggregates can give rise to asphaltene concentration or density fluctuations. Thus, extended regions, rich in aggregates, exhibit an asphaltene concentration (C2) higher than the average concentration of the solution. Consequently, in other regions, the concentration is much lower (C1). These density fluctuations can justify the increase of the scattered intensity.
2) in the second situation (Figure 18-b), polydispersed asphaltenes molecules or micelles, which sizes are rather small, coexist with more or less dense big aggregates with produce a strong scattering contribution at very small Q.

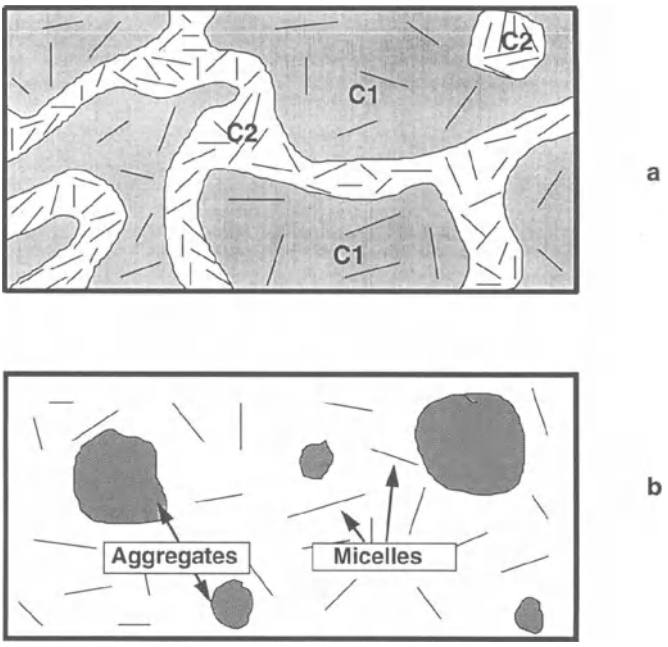

Figure 18. Aggregation models for asphaltene solution in good solvent. (a) the concentration (density) fluctuations, C1 and C2 are respectively the concentration of dark and bright zones, (b) mixed system of huge aggregates and asphaltenes micelles (dark lines represent asphaltene micelles).

We have tried to distinguish between these two different situations (Figure 18 a or b) by using additional techniques. Ultracentrifuge was used at high angular velocity. We have mentioned in the introduction that this method was already applied to the asphaltene molecular weight determination.[59,71,72] A 9 % w/w Safaniya VR asphaltene solution in toluene was submitted to high velocity centrifuge (4200 rd. s^{-1}) during ten hours. We have verified that the sedimentation of asphaltene species is a long time process. After ten hours treatment, we have recovered at the bottom of the centrifuge cell a dark, viscous deposit. The supernatant solution was still dark, like the initial suspension. The upper part of this supernatant was collected, the asphaltene concentration being close to 2% w/w. The bottom was also collected; its asphaltene concentration has been found close to 50 % w/w. Supernatant and bottom fractions were either concentrated by toluene evaporation for the first one, or diluted in toluene for the second fraction and scattering data has been collected (Figure 19). The important result of SAXS data is the absence of the scattered intensity at small Q-values (Q<Q1) for the supernatant fraction. Thus, it is possible to isolate asphaltene molecules which will not have tendency to form large dense aggregates or density fluctuations. The chemical composition analysis of both fractions has shown that the bottom fraction is more aromatic and has an higher oxygen content than the supernatant one.

"What is the evolution of these large heterogeneities as temperature increases?" We have tried to answer to this question by USAXS experiments. We should suggest that temperature increase will homogenize the asphaltene solution by dispersion of the aggregates forming dense regions. Figure 20 shows a comparison of SAXS data of 6% w/w Safaniya VR asphaltenes in toluene at 293K and 353K. Scattering at large Q-values is strongly modified by temperature increase due to the lowering of the average molecular weight of

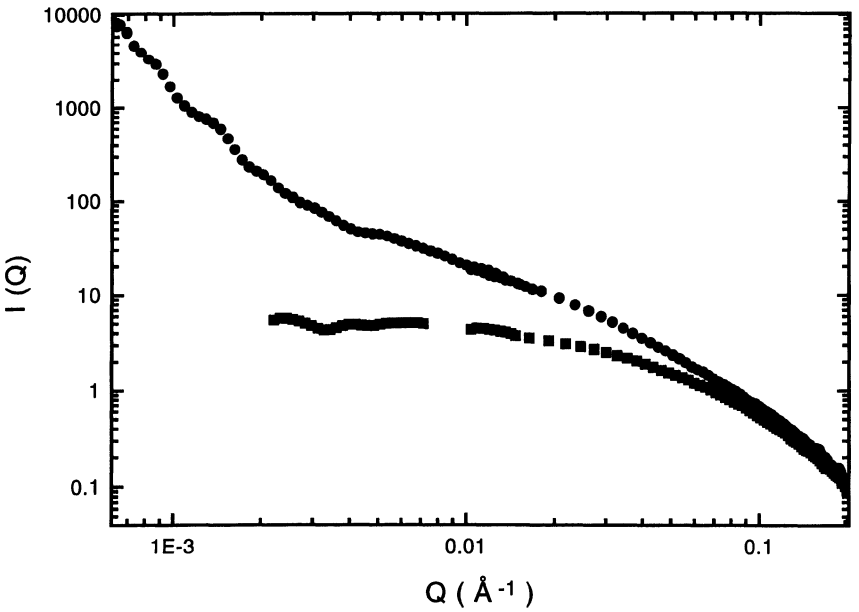

Figure 19. X-ray scattering of supernatant and bottom fractions (Safaniya VR asphaltenes) obtained by ultracentrifuge. (■) supernatant, (●) bottom.

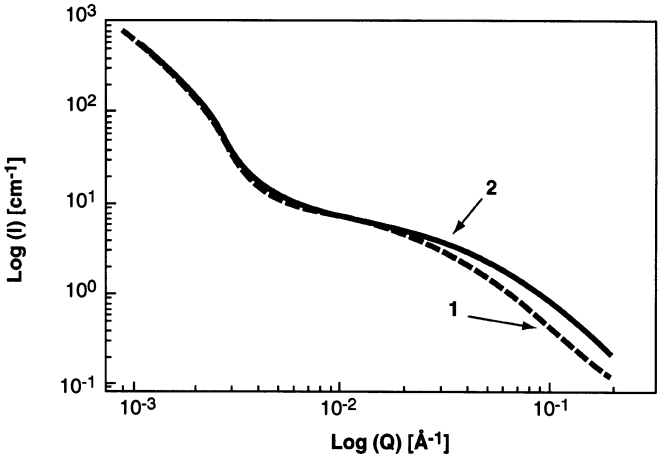

Figure 20. Small angle X-ray scattering of Safaniya VR asphaltenes in toluene (6% w/w) for two temperatures. (1) 293K, (2) 353K.

asphaltenes (see Figure 14). Small Q intensity has not changed during temperature modification. The density fluctuations appear to be stable as temperature increases. We can propose two different explanations to this strange behavior:

1) 353K is not a sufficiently high temperature to modify interactions responsible for the fluctuations. However, we have seen that temperature increase is followed by decrease of the average molecular weight (measured at large Q). In consequence, we should conclude that different types of interactions might exist between asphaltene species.
2) dense and more or less extended regions having a gel-like structure are present. They can be compared to micro-gels which have been observed in polymers solution and are eliminated by filtration. We have made previously the hypothesis that micro-gels might be responsible for an intense scattering in the small Q-range, sometimes called Picot-Benoit effect.[169] "How can we describe these particular macrostructures?" Looking at the hypothetical asphaltene molecule presented in Figure 1, we see that aromatic or naphtenic blocs are linked by aliphatic chains. We can suggest larger macromolecules, exhibiting size polydispersity and probably more crosslinked. This macromolecule and kerogen (see Figure 3) can exhibit similar structural characteristics. The strain existing in the bridges connecting aromatic sheets could reduce swelling of the structure. Size lowering of the large macromolecules imposes carbon-carbon break and thermal cracking at temperatures, close to 573K, much higher than 353K. The fraction of total mass of asphaltenes in solution involved in these extended macrostructures still remains unknown.

In order to gain insight into the morphology of these large scale heterogeneities, we have performed cryoscanning electron microscopy experiments (Cryo-SEM).[95]

4.1.2. Cryo-SEM Investigation of Asphaltene Solution in Toluene. A 2% and 4% w/w Safaniya vacuum residue asphaltene solutions in toluene have been observed with a scan-

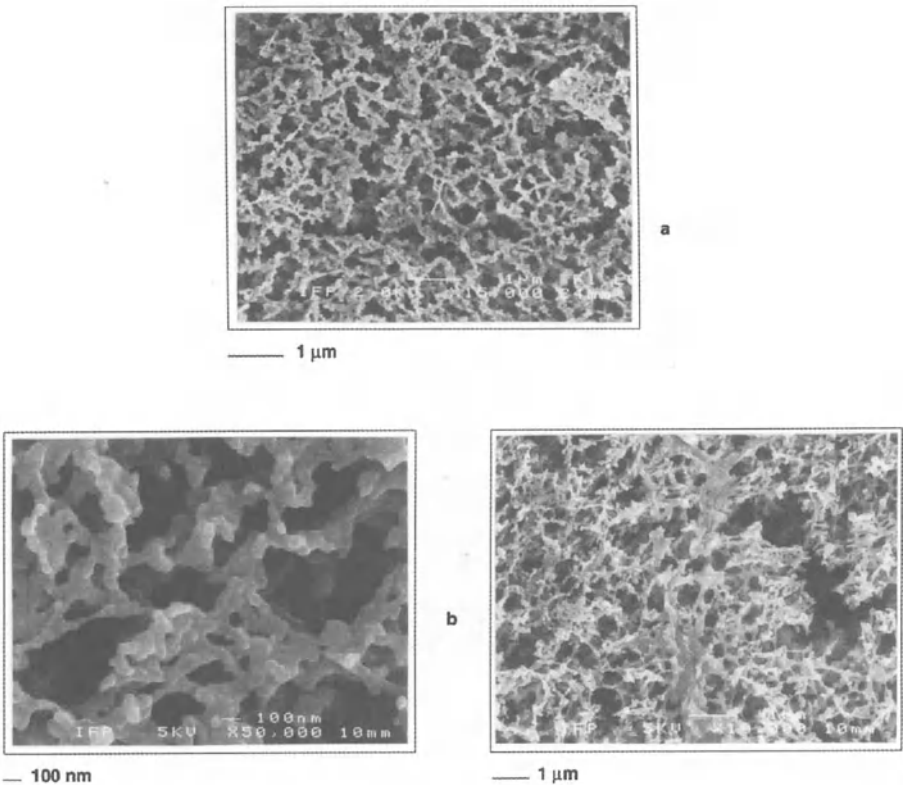

Figure 21. Cryo-SEM images of Safaniya vacuum residue asphaltenes in solution in toluene. (a) 2% w/w asphaltene concentration, (b) 4 % w/w at higher magnification.

ning electron microscope at different magnifications (Figure 21 a-b). The sample preparation and the observation mode have been presented in the experimental section. The image exhibits an heterogeneous material where bright regions form a complex network where pores of very different sizes are observed. After quenching of the asphaltene solution and transfer into the microscope, the sample temperature is progressively increased up to 63K under high vacuum (10^{-6} torr). According to the colligative properties of the solution, if asphaltene concentration differs from one region to another one, the sublimation temperature will be affected. The same experiment, for pure toluene has been performed and the image obtained has not exhibited a heteregeneous system. We have concluded that the asphaltene concentration is not homogeneous in the solution. We can propose that for low-concentrated asphaltene regions, the toluene is sublimated for lower temperature, giving rise to dark pores (see Figure 21). For more concentrated regions, it will be necessary to reach higher temperatures, which is not the case in Figure 21. Toluene is not yet sublimated. If there were no variation of the asphaltene concentration, the toluene sublimation will occur for one defined temperature and it would be impossible to reveal the macrostructure seen in Figure 21.

4.2. Flocculation Process by N-Heptane Addition to Asphaltene Solutions

The asphaltene flocculation process has been investigated by adding various quantities of n-heptane to asphaltene solutions in toluene. Both viscosimetry and scattering techniques have been applied in order to get a better description of the suspension structure evolution.

The viscosities of Safaniya VR asphaltenes[170] were obtained in toluene and in toluene/heptane mixture (55/45 % w/w) for asphaltene volume fractions (ϕ) between 1 and 10 % (Figure 22). The viscosity vs. asphaltene volume fraction curves shows two different domains: (i) in the first one, corresponding to volume fraction below 3 %, the viscosity increases linearly, (ii) in the second one ($\phi > 3\%$) a strong increase of the viscosity is measured. This increase of the viscosity is more pronounced when n-heptane is added (Figure 22). The intrinsic viscosity of the asphaltene molecules can be calculated from viscosimetric measurements at low volume fractions (see formula 25 and Figure 22). We have plotted intrinsic viscosity vs. n-heptane concentration (Figure 23). As flocculant concentration increases, we first observe a decrease of the intrinsic viscosity, up to 15 %, and then a strong increase up to 45% which corresponds to the flocculation threshold (see introduction). These results are in good agreement with previous works.[78]

Scattering curves (SANS) display on Figure 24 a strong increase of the intensity ($Q \approx 3.\ 10^{-3}\ A^{-1}$) indicating that asphaltene molecules grow in size and in molecular weight, except for heptane fractions between 0 and 15 %. Molecular weights as a function of the radii of gyration (see formula 14) are plotted in a double-logarithmic representation for Safaniya VR asphaltenes (Figure 25). The points seem to line up on straight lines of slope

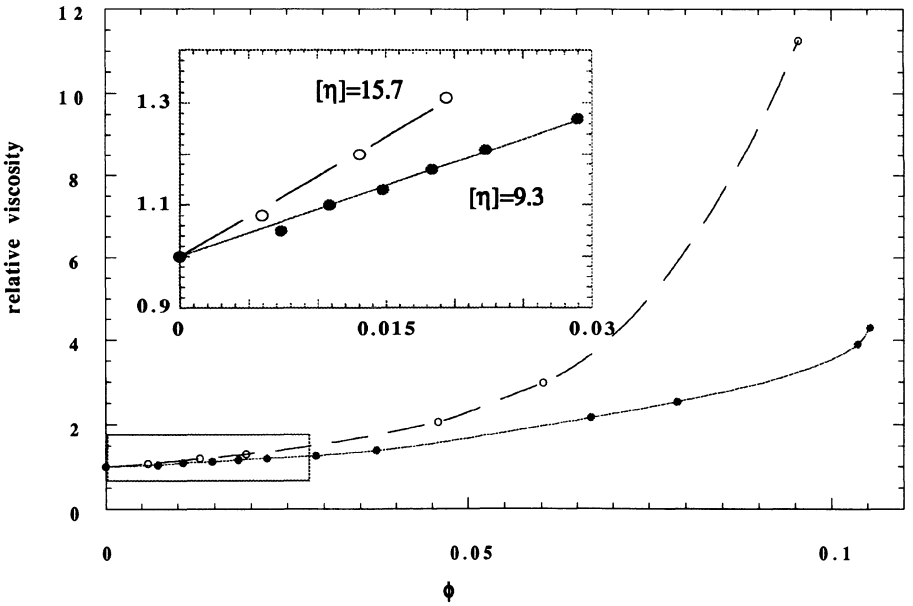

Figure 22. Relative viscosity and intrinsic viscosity of Safaniya VR asphaltenes in solution in pure toluene (●) and a mixture toluene/heptane (55/45 %w/w) (o) as a function of asphaltene concentration (ϕ).

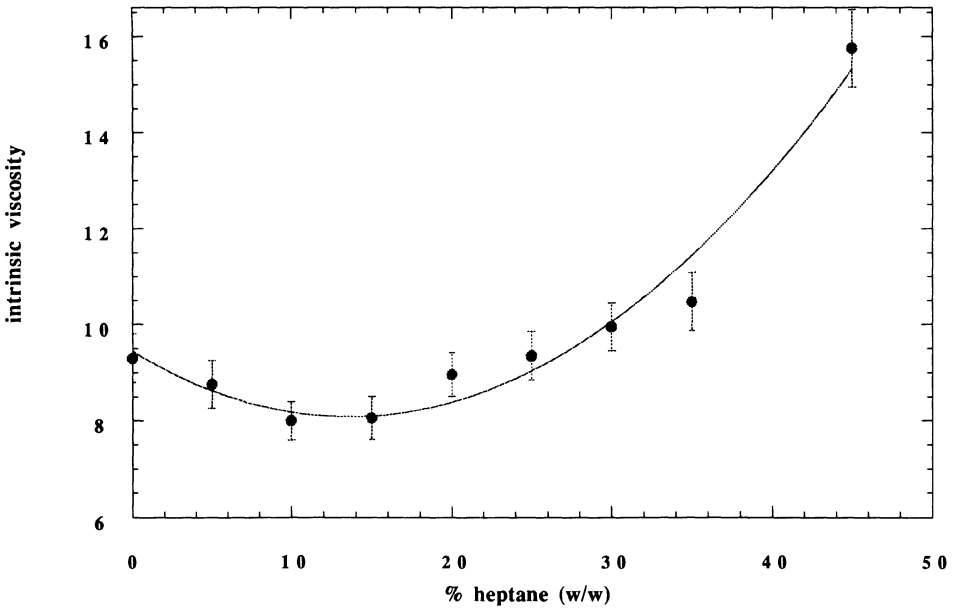

Figure 23. Intrinsic viscosity of Safaniya VR asphaltenes in solution in mixtures toluene/heptane, as a function of n-heptane weight concentration.

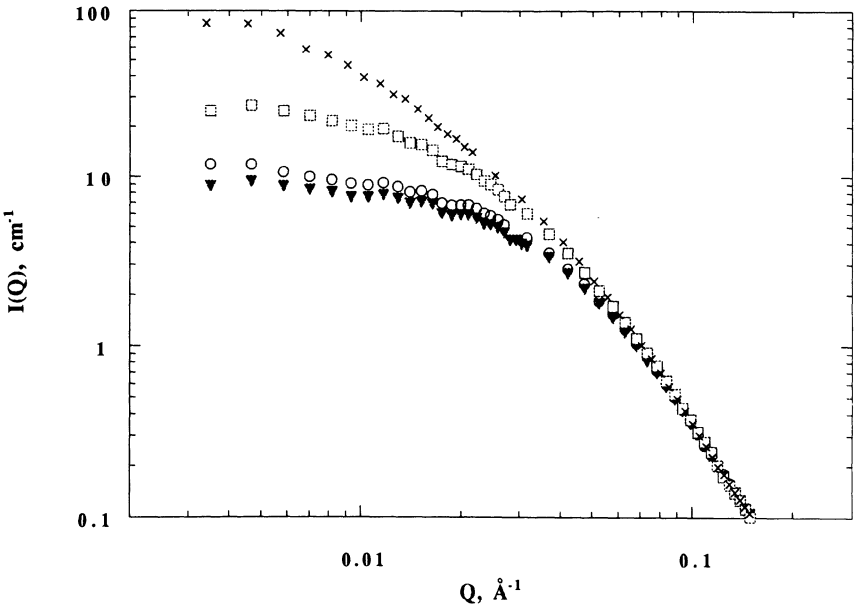

Figure 24. SANS data for 2% w/w Safaniya VR asphaltene for different mixtures of toluene/heptane, (▼) 100/0, (○) 85/15, (❑) 65/35, (x) 55/45.

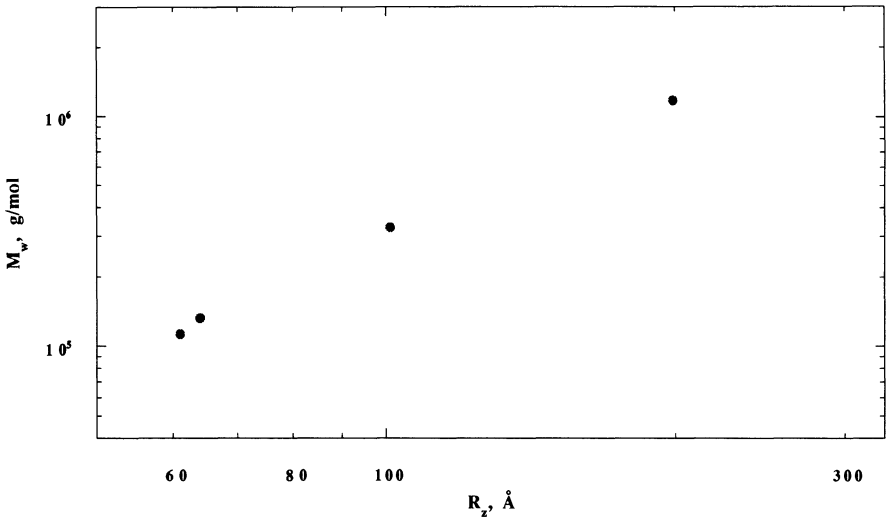

Figure 25. Molecular weight vs. radius of gyration for Safaniya VR asphaltenes.

2.05 ($M_W \approx R_z^{2.05}$). We have compared the viscosimetric and neutron scattering data. As explained in the experimental section dedicated to viscosimetric measurements, the intrinsic viscosities of solvated objects must be proportional to their volume per unit of mass, or to the volume occupied by the asphaltene aggregate (R_z^3) relative to the volume of asphaltene material inside this aggregate (M_W or I(Q=0)). Comparison between intrinsic viscosity and the ratio (R_z^3/M_W) is shown on Figure 26 as a function of n-heptane concentration. We can see that these quantities, [η] and (R_z^3/M_W), exhibit parallel variations.

The n-heptane addition effect on the density fluctuations has been followed by SAXS experiments (Figure 27). Except a small increase of the intensity for small Q (Q<Q1), as n-heptane content raises, the Q dependence of the intensity is not strongly changed ($I(Q) \approx Q^{-2.7}$). For higher heptane concentration (50% w/w), the asphaltene solution being flocculated, the scattered intensity shows a huge increase. The exponent of the power-law dependence of the intensity is close to 4 ($I(Q) \approx Q^{-3.7}$). This observation reveals the presence of large and dense asphaltene particles in the solution. Larger aggregates may exist, but their contribution to the scattering intensity will be predominant at smaller Q-values, not accessible with the Bonse-Hart camera used for our experiments.

4.2.1. Cryo-SEM Flocculation Study. Cryo-SEM technique was applied to follow the aggregation process when n-heptane is added. We have first observed n-heptane (35% w/w) low concentrated asphaltene suspension (Figure 28). We must point out that this suspension did not exhibit any huge aggregates detected by the naked eyes. We can distinguish two different morphologies: (i) the first one reproduces the network structure which has been previously observed without flocculant addition; thin bright filaments, corresponding to asphaltene highly concentrated regions are still present, (ii) the second one does not show anymore the network morphology, but denser, more homogeneous aggregates are formed, whose size is close to one micrometer. They indicate the onset of the flocculation and probably have their origin in the aggregation of some asphaltene mole-

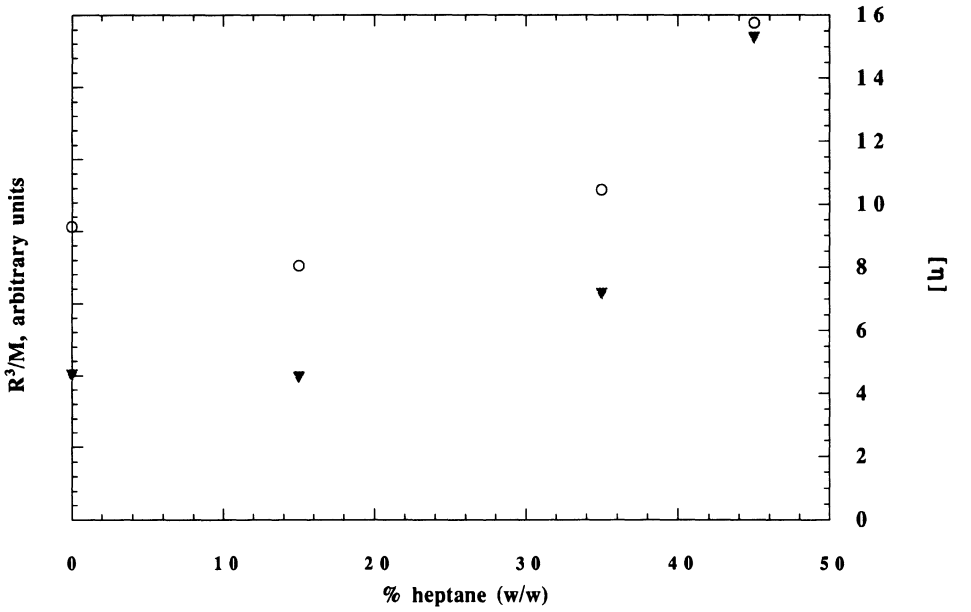

Figure 26. Intrinsic viscosity (○) and ratio (R_z^3/M_w) (▼) as a function of n-heptane weight fraction (asphaltenes Safaniya VR in suspension in toluene/heptane).

cules which are very sensitive to the presence of heptane. This behavior has been confirmed by filtration experiments of asphaltene solutions in toluene with increasing amount of n-heptane.[132] The first insoluble fraction recovered with the lowest amount of flocculant contains asphaltenes of higher molecular weight, higher aromaticity and more pronounced polar character.

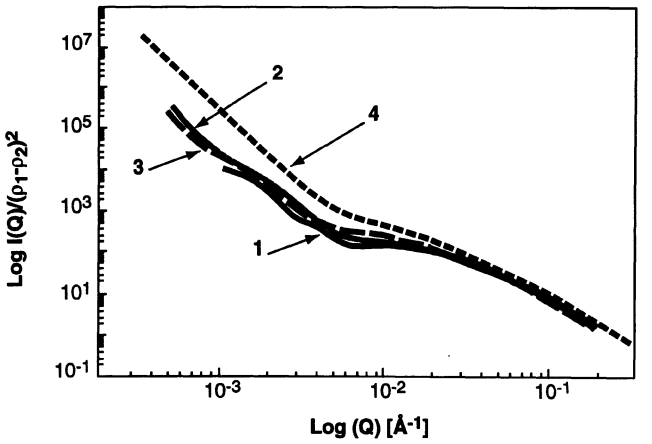

Figure 27. SAXS data for 2% w/w Safaniya VR asphaltene for different mixtures of toluene/heptane. (1) 100/0, (2) 80/20, (3) 65/35, (4) 50/50.

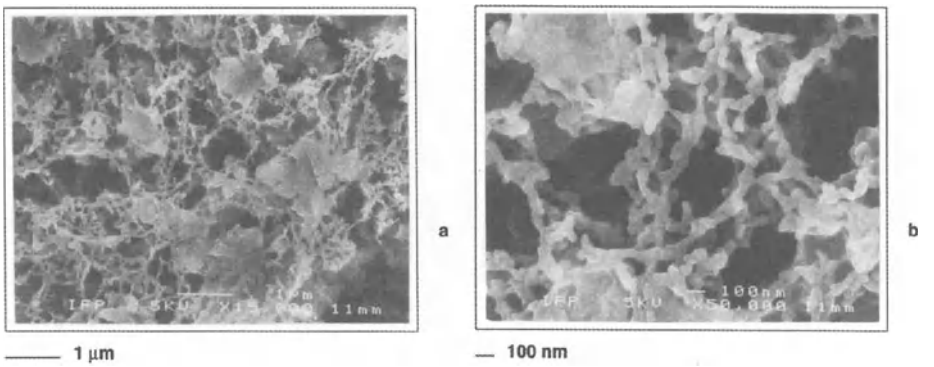

Figure 28. Cryo-SEM pictures of 2% w/w Safaniya vacuum residue asphaltene suspension in toluene with n-heptane (35% w/w) - (a) low magnification, (b) high magnification.

Another Safaniya VR asphaltene suspension (2% w/w) containing 65% w/w n-heptane in toluene has been observed in cryo-microscopy. Figure 29 displays two characteristic pictures for different magnifications. Large fractal aggregates are easily observed. A part of the solution has been deposited on a carbon grid used for transmission electron microscopy analysis and then quenched as explained in the experimental section. We can see on picture 29, the well defined holes of the carbon of the grid. The network morphology has quite disappeared giving rise to denser and isolated aggregates. They exhibit a large polydispersity, the size of some of them can reach several micrometers. High magnification image depicts the fractal structure formed by aggregation of small clusters whose size is near 0.1 µm. Finally, we have performed cryo-microscopy analysis with the same asphaltene in solution in a heptane/toluene (80/20) mixture, well above the flocculation threshold. Huge aggregates could be easily visualized by the naked eyes. We have collected one of them, and further deposited on the carbon grid (Figure 30). Fractal aggregates are still present; the inside asphaltene concentration is much higher that the average concentration. Fig. 30-b shows that the basic cluster of the fractal aggregate is larger than 0.1 µm and has grown in comparison with that in a 65 % w/w heptane solution.

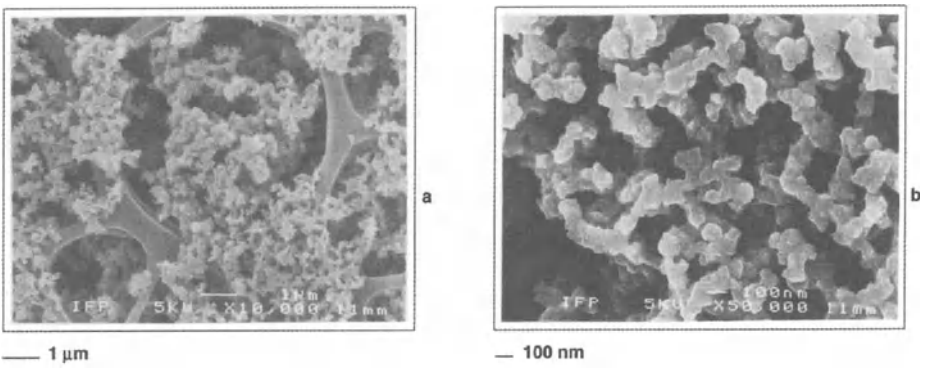

Figure 29. Cryo-SEM pictures of 2% w/w Safaniya vacuum residue asphaltene suspension in toluene with n-heptane (65% w/w). (a) low magnification, (b) high magnification.

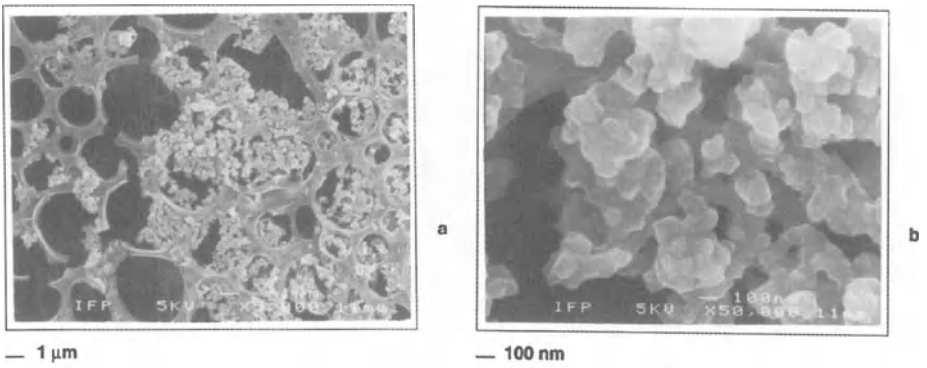

Figure 30. Cryo-SEM pictures of 2% w/w Safaniya vacuum residue asphaltene suspension in toluene with n-heptane (80% w/w). (a) low magnification, (b) high magnification.

4.3. Resin Solutions

Figure 31 displays a comparison of small angle X-ray scattering data for asphaltenes and resins Safaniya vacuum residue. We can observe similarities for both spectra:

1. at very low Q-values, an important increase is also detected for the resin suspension indicating the presence of large density fluctuations. We can remark that the transition between small and large Q-values, Q1, is larger for resins than for asphaltenes. We can suggest that the minimum fluctuation size is smaller for resins than for asphaltene suspensions.
2. at low and intermediate Q, the pseudo-plateau corresponds to an intensity much smaller than for asphaltene solution, corresponding to a smaller weight average molecular weight (M_w = 3500). The Q-dependence of the scattered intensity is

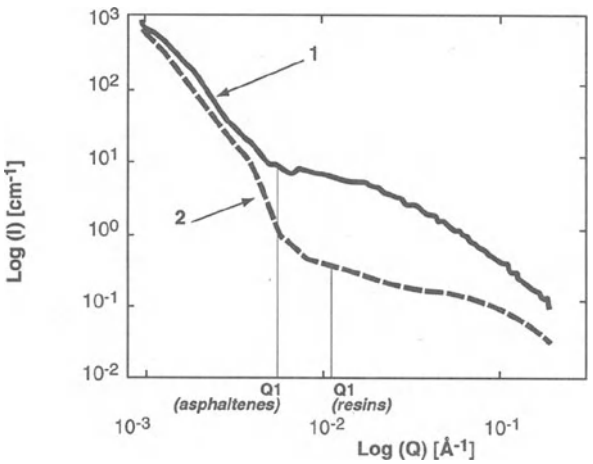

Figure 31. Comparison of SAXS data for asphaltenes and resins in toluene. (1) 6% w/w asphaltenes in toluene, (2) 6% w/w resins in toluene.

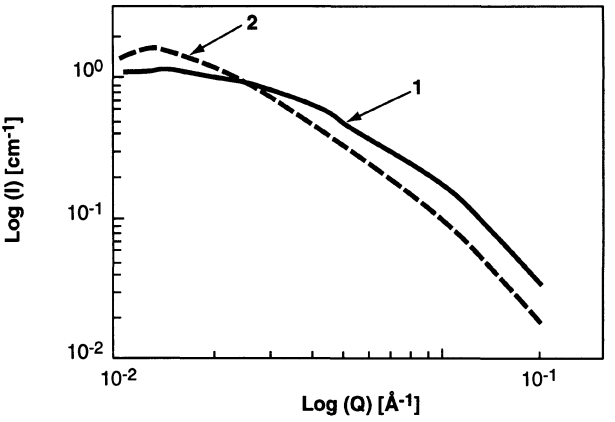

Figure 32. Comparison of SAXS data for a mixture Safaniya VR asphaltenes (2% w/w) and resins (4% w/w) in toluene (1), and for a 2% w/w Safaniya VR asphaltenes in solution in toluene (2).

different from that observed for asphaltenes; we have measured a more diffuse scattering indicating the presence of small entities. It seems that resins and asphaltenes have a similar behavior. We have verified that, as is the case for asphaltene molecules, an increase of the temperature is followed by a decrease of the average molecular weight (M_w = 2500 at 350K).

Many works of the literature have shown that resins are the best solvent of asphaltenes.[128] We have applied scattering methods in order to investigate the good solvent effect of resin addition on the solubilization of asphaltene molecules. On Figure 32 are plotted large-Q X-ray scattering intensity for a pure asphaltene solution and a mixture of asphaltenes plus resins in toluene. The scattering intensity measured for higher Q when resins are added to asphaltene solution exhibits a significant increase. This behavior is easily understandable because of the presence in suspension of small entities (resins) whose contribution is higher at large scattering vectors. On the contrary, we can observe a scattering decrease at small Q values ($Q<2.10^{-2}$ A^{-1}) characteristic of solution macrostructure modification. In order to clarify this behavior, we have compared the scattering curve of the mixture of asphaltenes plus resins with the sum of the intensities measured for pure asphaltenes and for pure resins (Figure 33). The curve measured for the sum is larger than

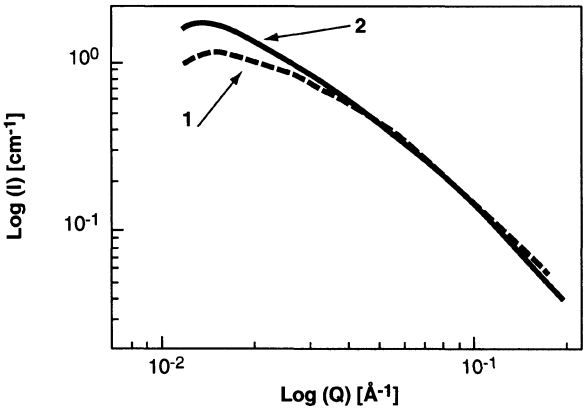

Figure 33. X-ray scattering curves for a mixture of Safaniya vacuum residue asphaltenes and resins: (1) 2% w/w asphaltene + 4 % w/w resins in toluene, (2) the sum of scattering intensity for pure asphaltenes (2% w/w) and pure resins (4% w/w) in toluene.

the intensity of the mixture asphaltenes plus resins, which can be interpreted by a decrease of the asphaltene average molecular weight. These experiments are in favor of the good solvent properties of resins.

4.4. Macrostructure Investigation of Natural Systems

The characterization of asphaltene macrostructure in solution or their flocculation is still an important issue for better understanding of the involved mechanisms, but we need, for industrial purpose, more information about the structure of asphaltenes in their natural environment. Small angle X-ray scattering has been applied in this aim. We will summarize in this section some results obtained concerning several systems such as crude oils, atmospheric or vacuum residues and maltenes.

4.4.1. Small Angle X-Ray Scattering of Crude Oils, Vacuum Residue, and Maltenes. Figure 34 shows the X-ray scattering curves of pure Safaniya vacuum residue and its maltenes at room temperature. We can easily distinguish two different domains:

1. $Q>10^{-2}$ A^{-1}: the curves after a pseudo-plateau, exhibits a pronounced decrease of the intensity as Q increases. This behavior corresponds to the scattering of small dense regions. It is difficult to quantify the contribution to the contrast term (see formulae 2 and 3) of each type of molecules which are present in the residue. According to the SAXS theory, we can assert that these regions have a high electron density and are probably related to more or less aggregated aromatic parts of the asphaltenes. It clearly appears that the average size of these regions are smaller in maltenes than in vacuum residue.
2. $Q<10^{-2}$ A^{-1}: for Safaniya vacuum residue, an intense scattering ($I(Q)\approx Q^{-2.2}$) is measured indicating the presence of large density fluctuations, similarly to asphaltene suspensions. No experimental points are plotted in these small-Q regions for Safaniya vacuum residue maltenes, because no intense scattering has

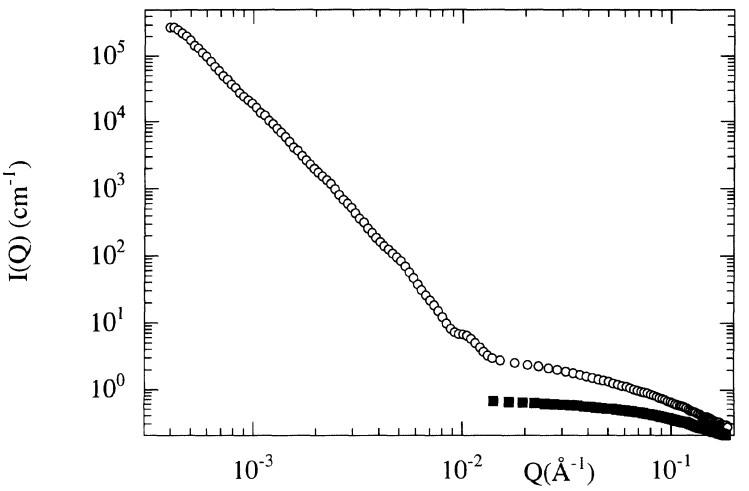

Figure 34. Small angle scattering of pure Safaniya vacuum residue (○) and its maltenes (■).

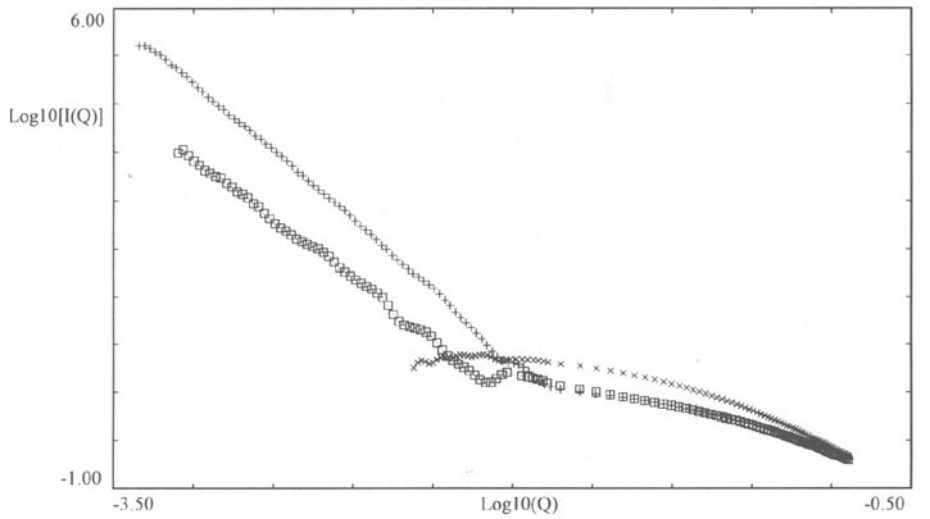

Figure 35. Small angle X-ray data for three natural systems: (XXX) R crude oil, (+++) Safaniya vacuum residue and B crude oil (❑❑❑).

been measured. This observation suggests that the presence of asphaltenes is responsible for these large fluctuations. We can suggest a heterogeneous distribution of aromatic regions in the material giving rise to large dense domains.

We have compared the X-ray scattering of several pure systems (Figure 35). Scattering curves obtained for two crude oils B and R are compared to the Safaniya VR scattering. Important variations can be detected. The scattering at large Q is identical for crude B and Safaniya VR, whereas crude oil R exhibits much intense scattering and consequently heterogeneities of larger scale. At small Q values an intense scattering is measured for crude B, but we can notice that the Q-dependence is not identical to the one observed for Safaniya VR. No increase of the intensity at small Q is measured for crude oil R: no large heterogeneities are present. The asphaltene concentration being very high for this crude (see Table 4), we can suggest a volume homogeneous distribution of the asphaltenes. We can propose an illustration of this behavior by two figures (Figure 36 a-b) which have been published by van Garderen et al.[171] These authors have simulated the aggregation processes considering various models. For Figure 36-a, we can imagine that each elementary symbol represents the aromatic regions of the asphaltene micelles whose size is close to several nanometers. At much larger scale, inside the square of the figure, whose size is close to a fraction of micrometer, the spatial distribution of the symbols or asphaltenes is homogeneous. Different situations are depicted in Figure 36-b; the spatial distribution is not yet homogeneous. If symbols are representative of asphaltene species and are drawn alone in Figure 36, we can suggest that other fractions constituting the crude oil or residue, such as resins, aromatics and saturated fractions, will fill spaces existing in between asphaltenes.

Diluted Safaniya VR in toluene has been analyzed by SAXS (Figure 37). The shape of the curves has not been strongly modified in comparison with those measured for asphaltene solutions. Even if the maltene fraction is present, the intense small-Q scattering

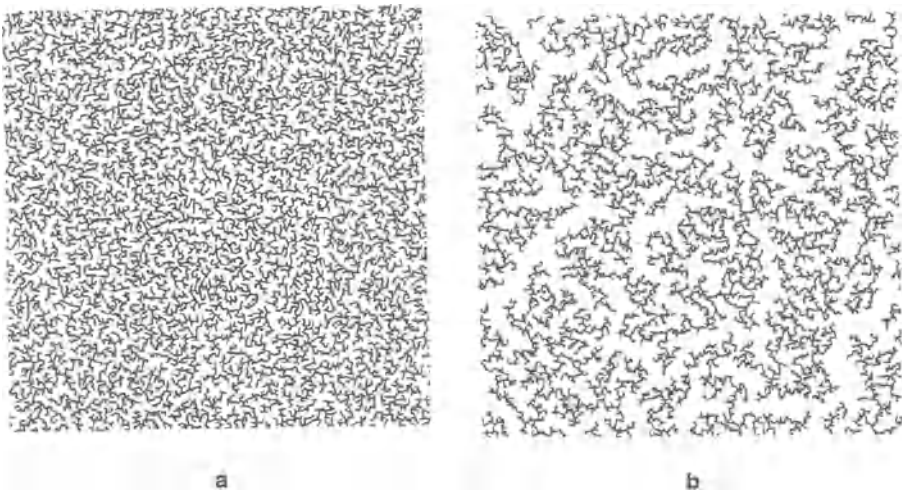

Figure 36. Examples of simulated aggregates:[171] (a) filled space, (b) large heterogeneities.

is still present. The heterogeneities macrostructure is therefore not modified by the presence of maltenes.

4.4.2. SAXS Investigation of Distillation Products, Atmospheric, and Vacuum Residues. Figure 38 shows SAXS curves of B crude oil and the corresponding atmospheric residue. We find the same scattering behavior for both samples. Two domains, defined by Q-values greater or lower than 10^{-2} A^{-1}, are easily distinguished. High Q-values data show a decrease of the scattering after atmospheric distillation. The asphaltene concentration being very similar for both samples, the decrease of the intensity can be attributed either to the presence of smaller elementary dense asphaltenic regions, or to a variation of the contrast term between asphaltene and maltenes. During atmospheric distil-

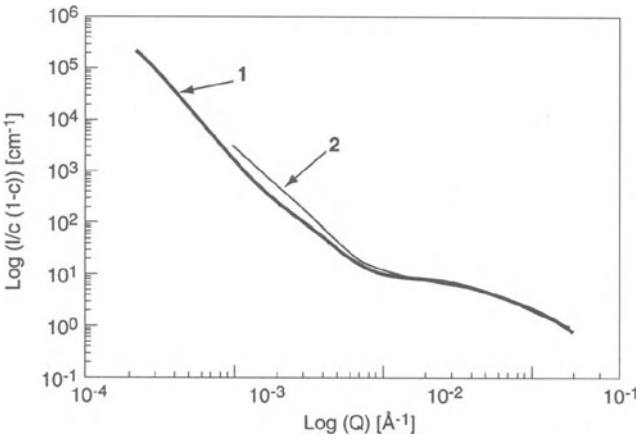

Figure 37. SAXS data of diluted Safaniya vacuum residue in toluene: (1) 10% w/w, (2) 34 % w/w.

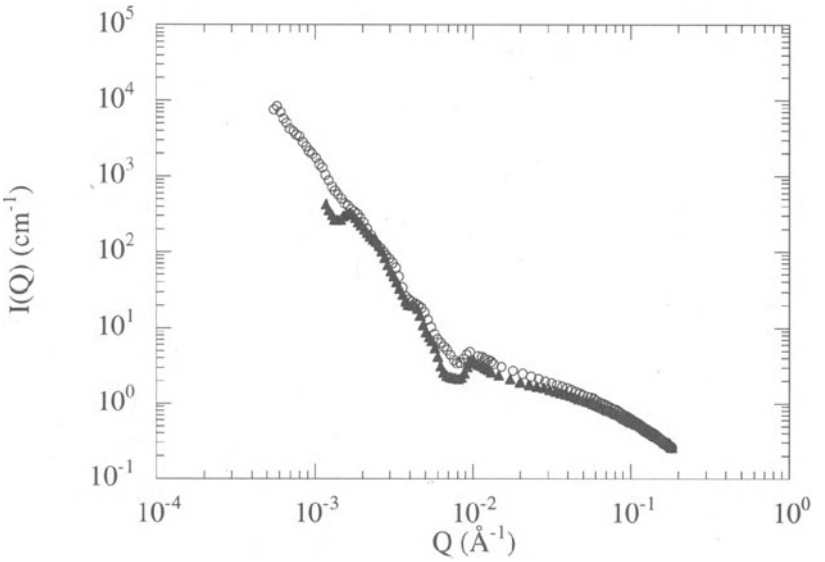

Figure 38. Small angle X-ray scattering of B crude oil (○○○) and corresponding atmospheric residue (▲▲▲).

lation, asphaltenes are not modified and many light fractions of the crude oil are eliminated. Consequently, the surrounding medium of asphaltenes becomes denser giving rise to a decreasing of the contrast term. The range of low Q exhibits similar evolution of the intensity for crude and atmospheric residue. Much more important differences between scattering data of W atmospheric and vacuum residue are displayed in Figure 39. The asphaltene concentration has been strongly raised by vacuum distillation, from 6% w/w for atmospheric product to 22 % w/w for vacuum residue (see Table 4). The asphaltenes to resins ratio has been also modified after vacuum distillation (see Table 4). Maltenes prepared from atmospheric residue exhibit a very low scattering in the extended Q-range investigated. If W atmospheric residue scattering vs Q shows a classical behavior, it is not the case for the corresponding vacuum residue. Two domains can be clearly separated:

1. $Q>4.10^{-3}$ A^{-1}: the scattering intensity follows a power-law dependence vs. Q ($I(Q) \approx Q^{-1.88}$), which can be compared to fractal dimension of aggregates obtained by diffusion-limited cluster-cluster mechanism (D_f = 1.8). We can describe the macrostructure of this residue as small dense, probably aromatic, particles forming fractal-like aggregates whose sizes can exceed several hundreds nanometers.
2. $Q<4.10^{-3}$ A^{-1}: another power-law is found ($I(Q) \approx Q^{-3.1}$), characteristic of large fluctuations. We can suggest, as illustrated in Figure 36-b, that the previous huge fractal aggregates do not fill the space giving rise to less dense, i. e. poorly concentrated asphaltene regions.

An investigation of the rheological behavior of this material has not been yet realized, but we have observed very different aspects for W vacuum residue and for R crude oil which have quite the same asphaltene concentration. The first one seems to have gel-like elastic properties and the second one flows more easily and does not clearly exhibit viscoelasticity. Explanation of this behavior is not straightforward; we can suggest differ-

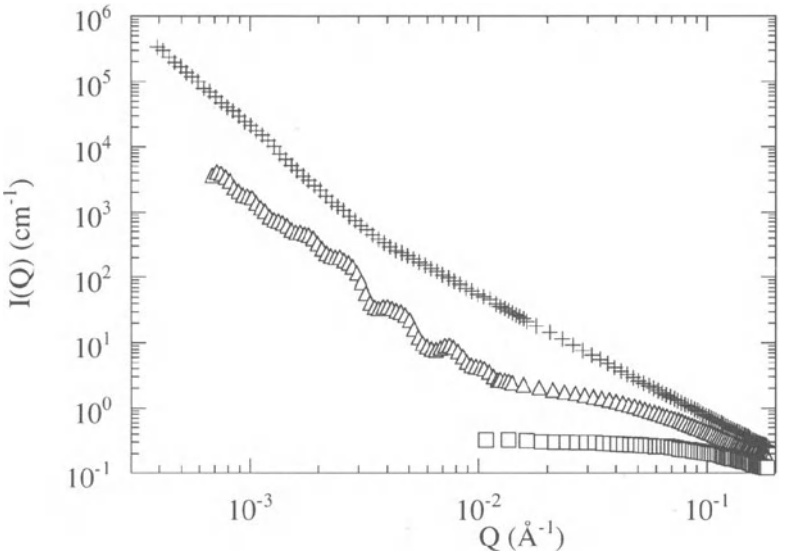

Figure 39. SAXS curves of real products: (+++) W vacuum residue, (ΔΔΔ) W atmospheric residue and (❑❑❑) W maltenes.

ent types of interaction between asphaltenes, stronger in the case of W vacuum residue than for R crude oil. Maltenes can have special properties which are going to influence asphaltene interactions. If we look at the asphaltene composition (see Table 3), we can remark that W crude oil asphaltenes have a more pronounced aromatic character than asphaltenes extracted from R crude. These observations confirm that there is not a simple correlation between the asphaltene concentration and the rheological properties of crude oils.

We have plotted in Figure 40 X-ray scattering curves of maltenes from W atmospheric and vacuum residues. They do not show important differences, except at small Q (10^{-2} A^{-1}), where intense scattering is observed for maltenes extracted from vacuum residue. This behavior can be related to the densification of maltenes after vacuum residue, due to light fractions elimination, responsible to aggregation of basic molecules. A radius of gyration of 1 nm has been estimated for maltenes from the atmospheric residue.

4.4.3. SAXS Investigation of the Effect of Temperature on Safaniya Vacuum Residue. The macrostructure evolution of natural products as a function of temperature is an important issue, not only because many of these heavy fractions are heated at high temperature during industrial processes, but also because structural information can be extracted out from the evolution of SAXS data. We know that crude oils or residues are rich in paraffins which form huge crystals at room temperature. They can of course have an important influence on the scattering curve. It is absolutely necessary to verify whether the heterogeneities observed at small or large scales, at low temperature, remain at higher temperatures.

We have investigated the thermal evolution of Safaniya VR up to 573 K. Figure 41 shows the X-ray scattered signal from room temperature to 423 K and 473 K. The inten-

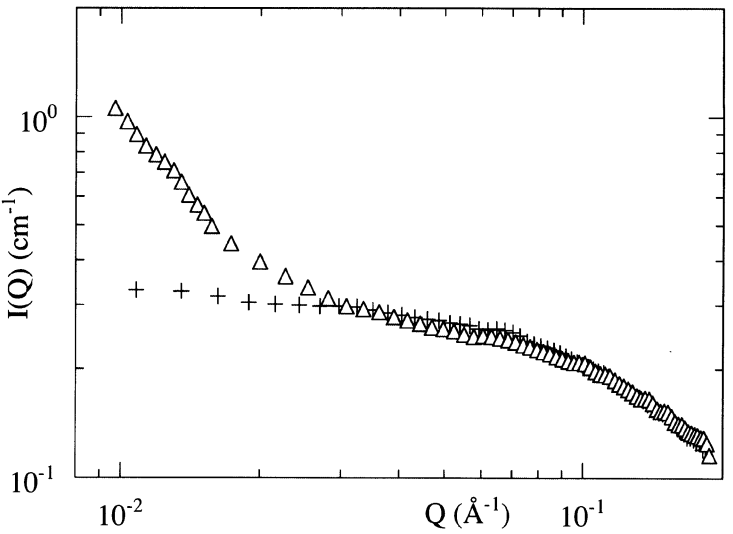

Figure 40. X-ray scattering of W maltenes: (ΔΔΔ) extracted from vacuum residue and (+++) from atmospheric residue.

sity at very small Q, close to 5.10^{-4} A^{-1}, has decreased, but for higher Q, no important evolution of the curve is depicted. This observation confirms the good temperature stability of large heterogeneities. It is obvious that such fluctuations at 473 K cannot be caused by paraffinic crystals in the material. We can think of strongly aggregated domains, due to van der Waals forces or crosslinking, as was previously discussed concerning asphaltene suspensions in toluene. We have explored higher temperatures (573 K), and Figure 42 displays the corresponding scattering data. In this temperature range, we can suspect the beginning of thermal cracking. Two different results have been obtained out for two separate

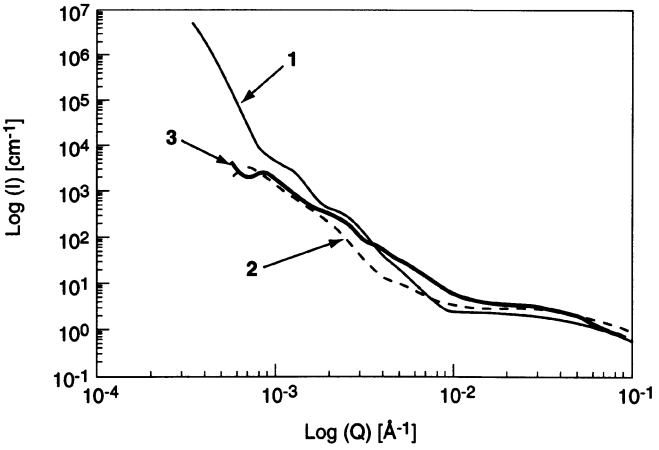

Figure 41. SAXS of Safaniya vacuum residue at 293K (1), 423K (2) and 473K (3).

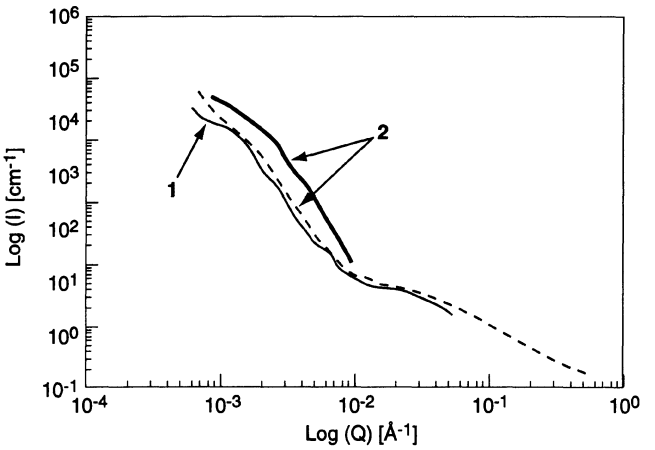

Figure 42. Small angle X-ray scattering of Safaniya VR at 473K (1) compared with two different SAXS curves obtained at 573K (2).

samples of apparently similar composition. The first experiment has provided identical scattering data to those obtained at 473 K. The SAXS data given by the second experiment are slightly different and show an important increase of the intensity ($Q<10^{-2}$ A^{-1}). We confirm the heterogeneities stability for highest temperatures. An interpretation of the second experiment can be proposed considering the onset of thermal cracking. We can suggest that the cracking begins locally, producing less dense regions due to liquid-like structure of light hydrocarbons. The consequence of these domains on the scattering curve will be an enhanced scattering at low Q if the size of these domains is large enough.

5. CONCLUSION

We have presented a series of results concerning the colloidal state of asphaltenes or resins in solution or in their natural medium obtained by the use of the following complementary techniques: small angle scattering, viscosimetry and cryo-scanning electron microscopy. All these experiments have confirmed the complex colloidal structure of asphaltenes even in good solvents. Asphaltenes have a propensity to form aggregates, the size of which strongly varies with the composition of the surrounding medium and temperature. These colloidal systems exhibit extended fluctuations and are very heterogeneous. These main features still remain to be understood. We have recalled the various types of interactions (van der Waals, hydrogen bonds, etc.) which can explain molecular aggregations, but some additional work is required in order to improve our knowledge of the driving forces behind such association processes. We can suggest interaction energy calculation between asphaltene molecules which can be made using molecular simulations of representative molecules, taking into account the influence of the solvent. We have highlighted several experimental evidences indicating that asphaltene aggregates exhibit some polymer or fractal-like behavior. We have proposed the concepts of effective and real volumes for asphaltene aggregates. The first one is larger than the real volume occupied by asphaltene material but can vary as a function of the solvent quality, similarly to polymer swelling. We can consider that up to an asphaltene concentration close to several weight

percents, depending of the solvent quality and the size of the aggregates, we are in the dilute regime and the scattering is sensitive to isolated asphaltene aggregates. Above this concentration, analog to the polymer overlap threshold ϕ^*, asphaltene aggregates interpenetrate and overlap each other.

The origin of large scale fluctuations is still mysterious; we have suggested two different images, one corresponding to special molecular interactions between asphaltene species, the other to large aggregates coexisting with smaller asphaltene molecules. These huge aggregates may be remainings of the kerogen structure, and resemble microgels well known in polymer science. Ultracentrifuge experiments have demonstrated the possible fractionation of two types of molecules, some of them giving rise to large fluctuations. These first investigations must be pursued in a more systematic way, requiring asphaltene fractionations in solution or for low-viscous real material. We can suggest filtration experiments where larger aggregates, or crosslinked complex macromolecules will be retained on the filter. Centrifuge or ultracentrifuge could be performed producing several fractions, which could be further investigated by scattering methods or viscosimetry and analytical techniques for precise chemical composition determination. We have seen the influence of temperature which contributes to a decrease of the average molecular weight, but have little influence on the large scale heterogeneities. This point should require further investigations. In particular, it should be interesting to realize experiments in the USAXS domain at much higher temperature in order to explore if heterogeneities tend or not to disappear. We can expect a pronounced decrease of the asphaltene or resin molecular weight, corresponding to the dissociation of the aggregates into elementary molecules. This approach will necessitate carrying out experiments under high pressures, especially for investigations in solvents with low boiling temperatures at atmospheric pressure.

Another important issue is the characterization of asphaltenes in real systems. We have shown that small angle X-ray scattering technique can be successfully applied. Nevertheless, additional experiments should be performed in order to really understand which information can be carried out from SAXS diagrams. We have suggested that scattering originates from aromatic regions. Artificial crude oils made by the same maltene fractions but containing various amounts of asphaltenes can help us for improved scattering treatments. Viscosimetry and rheology methods can also provide interesting new information. Fractionations, as for asphaltene solutions, can be used for a better understanding of the large scale fluctuations observed in natural products.

These different suggestions can open new research area; they probably need laborious sample preparations, but are necessary for giving a better insight into the colloidal behavior of asphaltenes, resins or natural systems.

ACKNOWLEDGMENTS

The authors are grateful to "Laboratoire Leon Brillouin", CEN - SACLAY (France), and particularly to J. P. Cotton and J. Teixeira for making available to us SANS spectrometer. We would like to thank Th. Zemb and J. Lambart for USAXS experiments and their useful comments. We have also benefited from interesting discussions with J. N. Roux (Laboratoire Central des Ponts et Chaussées -Paris) and R. Ober from the Collège de France. We also would like to thank P. Courtin, from Paris VI University who realized the ultracentifuge separations.

REFERENCES

1. J. Briant, Revue de l'Institut Français du Pétrole, 1, (1963).
2. M. R. Islam, "Role of asphaltenes on oil recovery and mathematical modeling of asphaltene properties," Asphaltenes and Asphalts 1, 249 (1994).
3. A. Danesh, D. Krinis, G. D. Henderson and J. M. Peden, Chem. Eng. Res. Des. 66, 339 (1988).
4. L. Minssieux, SPE Paper 37250 presented at the SPE International Symposium on Oilfield Chemistry in Houston (Texas), 401 (1997).
5. A. T. Turta, J. Najman, A. K. Singhal, S. Leggitt and D. Fischer, SPE Paper 37287 presented at the SPE International Symposium on Oilfield Chemistry in Houston (Texas), 703 (1997).
6. J. S. Buckley , Y. Liu, X. Xie and N. R. Morrow, SPE/DOE 35366 presented at EOR Symposium in Tulsa, 22 (1996).
7. W. K. Stephenson, "Producing Asphaltene Crude Oils: Problems and Solutions," Petroleum Engineer, 24 (1990).
8. Chia-Lu Chang and H. S. Fogler, Langmuir 10, 1749 (1994).
9. Chia-Lu Chang and H. S. Fogler, Langmuir 10, 1758 (1994).
10. P. Groffe, J. L. Volle and A. Ziada, SPE 30128, SPE Europe Formation Damage Conference, The Hague, (1995).
11. M. N. Bouts, R. J. Wiersma, H. M. Huijs and A. J. Samuel, SPE Paper 28991 presented at the SPE International Symposium on Oilfield Chemistry in San Antonio (Texas), 481 (1995).
12. M. B. Manek, SPE Paper 28972 presented at the SPE International Symposium on Oilfield Chemistry in San Antonio (Texas), 269 (1995).
13. S. J. Allenson and A. Marjorie, SPE Paper 37286 presented at the SPE International Symposium on Oilfield Chemistry in Houston (Texas), 699 (1997).
14. E. Papirer, C. Bourgeois, B. Siffert and H. Balard, Fuel 61, 732 (1982).
15. R. C. Little, Fuel 53, 246 (1974).
16. C. M. Blair, Chem. Ind. (London), 538 (1960).
17. S. A. Berridge, M. T. Thew and A. G. Loriston-Clarke, J. Inst. Petrol. 54, 333 (1968).
18. G. D. M. Mackay, A. Y. McLean, O. J. Betancourt and B. D. Johnson, J. Inst. Petrol. 59, 164 (1973).
19. A. Billon, F. Morel, M. E. Morrison and J. P. Peries, Revue de l'Institut Français du Pétrole 49(5), 495 (1994).
20. F. Morel, S. Kressmann, V. Harlé and S. Kasztelan, "Hydrotreatment and hydrocracking of oil fractions," edited by G.F. Froment, B. Delmon and P. Grange, Elsevier Science, 1 (1997).
21. J. G. Speight, "Asphaltene Characterization and Use in Understanding Processes" Symposium on the Role of Asphaltenes in Petroleum Exploration, Production and Refining, 207th National Meeting, ACS, San Diego, 200 (1994).
22. J. P. Pfeiffer and R. N. Saal, Journal of Physical Chemistry 44, 139 (1940).
23. D. A. Anderson, D. W. Christensen and H. Bahia, Journal of Association of Asphalt Paving Technologists 60, 437 (1991).
24. T. F. Yen, American Chemical Society, Division Fuel Chemistry 15(1), 93 (1971).
25. C. Giavarini, in "Asphaltene and Asphalts" Developments in Petroleum Science 1, Edited by T. F. Yen and G.V. Chilingarian , Elsevier Science, Amsterdam, 381 (1994).
26. T. F. Yen, Asphaltenic Materials, Encyclopedia of Polymer Science and Engineering 1–10, Wiley and Sons, New York, (1988).
27. E. J. Dickinson and H. P. Witt, Trans. Soc. Rheol. 18, 591 (1974).
28. J.G. Speight, "The chemistry and technology of petroleum" Second Edition, Marcel Dekker, Inc. (1991).
29. J.W. Bunger, N. C. Li, "Chemistry of asphaltenes" Advances in Chemistry Series 195, American Chemical Society (1981).
30. E. M. Dickinson, Fuel 59, 290 (1980).
31. M. Bouquet and A. Bailleul, Fuel 65, 1240 (1986).
32. J. K. Brown , W. R. Ladner and N. Sheppard, Fuel 39, 79 (1960).
33. T. W. Mojelsky, T. M. Ignasiak, Z. Frakman, D. D. McIntyre, E. M. Lown, D. S. Montgomery and O. P. Strausz, Energy and Fuels 6, 83 (1992).
34. O. P. Strausz, T. W. Mojelsky and E. M. Mown, Fuel 71, 1355 (1992).
35. S.E. Moschopedis and J.G. Speight, Fuel 55, 187 (1976).
36. R. G. S. Ritchie, R. S. Roche and W. Steedmann, Fuel 58, 523 (1979).
37. J. G. Speight and S. E. Moschopedis, Preprints Div. Petrol. Chem., Am. Chem. Soc., 26(4), 907 (1981).
38. J. G. Speight and S. E. Moschopedis, Preprints Div. Petrol. Chem., Am. Chem. Soc., 24(4), 1007 (1979).

39. R. J. Clerc and M. J. O'Neal, Anal. Chem. 33, 380 (1961).
40. O. C. Mullins Asphaltenes - Fundamentals and Applications, Edited by E. Y. and O. C. Mullins Plenum Press 53 (1995).
41. J.G. Speight and R. J. Pancirov, Liquid Fuels Technol. 2, 287 (1984).
42. K. D. Rose and M. A. Francisco, J. Am. Chem. Soc. 110, 637 (1988).
43. T. F. Yen, Energy Sources 1, 447 (1974).
44. T. Ignasiak and O. P. Strausz, Fuel 57, 617 (1978).
45. T. Ignasiak, A. V. Kemp-Jones and O. P. Strausz, J. Org. Chem. 42, 312 (1977).
46. J. Goulon, A. Retournard, P. Friant, C. Goulon-Ginet, C. Berthe, J.F. Muller, J. L. Poncet, R. Guilard, J. C. Escalier and B. Neff, J. Chem. Soc. Dalton Trans. 1095 (1984).
47. W. R. Biggs, J. C. Fetzer, R. J. Brown and J. G. Reynolds Liquid Fuels Technology 3(4), 397 (1985).
48. W. R. Biggs, J. C. Fetzer, R. J. Brown and J. G. Reynolds Liquid Fuels Technology 3(4), 423 (1985).
49. R. H. Fish, J. J. Komlenic and Brian K. Wines, Anal. Chem. 56, 2452 (1984).
50. J.W. Bunger, Norman C. Li, " Chemistry of asphaltenes " Advances in Chemistry Series 195, American Chemical Society (1981) voir figure 1.
51. H. H. Kiet, S. L. Malhotra, L. P. Blanchard, "Structure parameter analysis of asphalt fractions by a modified mathematical approach" Analytical Chemistry 50, 1212 (1978).
52. M. Oka, H. C. Chang, G. R. Gaualas, Fuel 56, 3 (1977).
53. I. Kowalewski, M. Vandenbroucke, A. Y. Huc, M. J. Taylor and J. L. Faulon, Energy and Fuels 10, 97 (1996).
54. A. Koots and J. G. Speight, Fuel 54, 179 (1975).
55. T. Suzuki, M. Itoh, Y. Takegami and Y. Watanabe, Fuel 61, 402 (1982).
56. J. G. Erdman and J. P. Dickie, Preprints ACS Div. Petr. Chem. 9,69 (1964).
57. J. G. Speight, Fuel 49, 134 (1970).
58. Y. Miki, S. Yamadaya, M. Oba and Y. Sugimoto, J. of Catal. 83, 371 (1983).
59. R. S. Winniford, J. Inst. Petrol. 49(475), 215 (1963).
60. P. J. Dickie and T. F. Yen, A.C.S., Div. Petrol. Chem. Preprints 12 B117, 2 (1966).
61. P. J. Dickie and T. F. Yen, Anal. Chem.39, 1848 (1967).
62. H. Reerink, A.C.S. Preprints Div. Petrol. Chem. 16 D18, 1 (1971).
63. T. F. Yen, J. G. Erdman and S.S. Pollack, Anal. Chem. 33(11), 1587 (1961).
64. J. G. Speight, Proc. Nat. Sci. Found. Symp. Fund. Org. Chem. Coal, Knoxville TN, 125 (1975).
65. M. A. Sadeghi, G. V. Chilingarian and T. F. Yen, Energy Sources 8(2/3), 99 (1966).
66. R. G. S. Ritchie, R. S. Roche and W. Steedman, Fuel 58, 523 (1979).
67. R. C. Schucker and C. F. Keweshan, A.C.S. Div. Fuel, Chem. 25(3), 155 (1980).
68. J. G. Speight and R. J. Pancivarov, A.C.S. Div. Fuel, Chem. 28(5), 1319 (1983).
69. S. El-Mohamed, M. A. Archard, F. Hardouin and G. Gasparoux, Fuel 65, 1501 (1986).
70. J. G. Speight, D. L. Wernick, K. A. Gould, R. E. Overfield, B. M. L. Rao and D. W. Savage, Revue de l'Institut Français du Pétrole 40(1), 51 (1985).
71. B. R. Ray, P. A. Witherspoon and R. E. Gorin, J. Phys. Chem. 61, 1296 (1957).
72. H. Reerink and J. Lijzenga, J. Inst. Petrol. 59, 211 (1973).
73. J. M. Swanson, Journal of Physical Chemistry 46, 141 (1942).
74. S. E. Moschopedis, J. F. Fryer and J. G. Speight, Fuel 55, 227 (1976).
75. J. W. Labout, in Properties of Asphaltic Bitumen, Edited by J. P. Pfeiffer, Elsevier, New York, 35 (1950).
76. J. G. Speight and S. E. Moschopedis, Fuel 56, 344 (1977).
77. H. J. Neumann, Erdol und Kohle, 865 (1965).
78. J. Briant and G. Hotier, Revue de l'Institut Français du Pétrole 38(1), 83 (1983).
79. R. L. Griffin, W. C. Simpson and T. K. Miles, Am. Chem. Soc. Div. Petrol. Chem. 133rd Meeting, San Francisco, (1958).
80. K. H. Altgelt, Preprints A. C. S., Div. Petrol. Chem. 13(3), 37 (1968).
81. J. A. Koots and J. G. Speight, Fuel 54, 179 (1975).
82. H. Reerink, Ind. Eng. Chem. Prod. Res. Develop. 12(1), 83 (1973).
83. K. H. Altgelt and O. L. Harle, Ind. Eng. Chem. Prod. Res. Develop. 14(4), 240 (1975).
84. I. L. Markhasim, O. D. Svirskaya and L. N. Strads, Kolloid. Z. 31, 299 (1969).
85. P. G. Gottis and J. R. Lalanne, Fuel 68, 804 (1989).
86. E. Y. Sheu and D. A. Storm, "Colloidal properties of asphaltenes in organic solvents," in Asphaltenes - Fundamentals and Applications, Edited by E. Y. Sheu and O. C. Mullins, Plenum Press, 1 (1995).
87. Ch. Bardon, L. Barre, D. Espinat, V. Guille, Min Hui Li, J. Lambard, J. C. Ravey, E. Rosenberg and T. Zemb, Fuel Science and Technology Int'l 14(1–2), 203 (1996).
88. C. W. Dwiggins Jr, J. Appl. Cryst. 11, 615 (1978).

89. C. W. Dwiggins Jr, The Journal of Physical Chemistry 69(10), 3500 (1965).
90. C. W. Dwiggins Jr, J. Appl. Cryst. 13, 572 (1980).
91. H. Kim and R. B. Long, Ind. Eng. Chem. Fundam. 18, 60 (1979).
92. J. C. Ravey, G. Ducouret and D. Espinat, Fuel 67, 1560 (1988).
93. P. Herzog, D. Tchoubar and D. Espinat, Fuel (67), 245 (1988).
94. D. Espinat, J. C. Ravey, V. Guille, J. Lambart, T. Zemb and J. P. Cotton, Journal de Physique IV 3, 181 (1993).
95. L. Barre, D. Espinat, E. Rosenberg and M. Scarsella, Revue de l'Institut Français du Pétrole 52(2), 161 (1997).
96. E. Y. Sheu, K. S. Liang, S. K. Sinha and R. E. Overfield, Journal of Colloid and Interface Science 153(2), 399 (1992).
97. R. E. Overfield, E. Y. Sheu, S. K. Sinha and K. S. Liang, Fuel Sci. Tech. Int. 7(5–6), 611 (1989).
98. D. A. Storm, E. Y. Sheu and M. M. DeTar, Fuel 72(7), 977 (1993).
99. N. Senglet, C. Williams, D. Faure, T. Des Courieres and R. Guilard, Fuel 69, 72 (1990).
100. Y. Xu, Y. Koga and O.P. Strausz, Fuel 74(7), 960 (1995).
101. P. Thiyagarajan, J. E. Hunt, R. E. Winans, K. Anderson and J. T. Miller, Energy and Fuels 9, 829 (1995) (a verifier).
102. N. F. Carnahan, L. Quintero, D. M. Pfund, J. L. Fulton, R. D. Smith, M. Capel and K. Leontaritis, Langmuir 9, 2035 (1993).
103. M. Y. Lin, E. B. Sirota and H. Gang, A. C. S. National Meeting, Symposium on Asphaltene and Heavy Oils, (1997).
104. D. Espinat, Revue de l'Institut Français du Pétrole 46(6), 773 (1991).
105. Y. C. Liu, E. Y. Sheu, S. H. Chen and D. A. Storm, Fuel 74, 1352 (1995).
106. H. Rassamdana and M. Sahimi, AIChE Journal 42(12), 3318 (1996).
107. S. El Mohamed, F. Hardouin and H. Gasparoux, Journal de Chimie Physique 85(1), 135 (1988).
108. J.G. Speight, "Fractionation" Chapter 9 in "The chemistry and technology of petroleum" Second Edition, Marcel Dekker, Inc., 309 (1991).
109. B. Brulé, J. Liq. Chromatogr. 2, 165 (1979).
110. H. Reerink and J. Lijzenga, Anal. Chem. 47(13), 2160 (1975).
111. D. H. Buchanan, L. C. Warfel, S. Baley and D. Lucas, Energy and Fuels 2, 32 (1988).
112. G. Ducouret, PhD Thesis, Paris VI University (1987).
113. K. H. Altgelt and E. Hirsch, Separation Science 5, 855 (1970).
114. T. M. Ignasiak, M. Kotlyar, N. Samman, D.S. Montgomery and O.P Strausz, Fuel 62, 363 (1983).
115. S. Acevedo, G. Escobar, L. B. Gutierrez and J. D'Aquino, Fuel 71, 1077 (1992).
116. G. Hall and S. P. Herron, A. C. S. Div. Petrol. Chem. 9–14 (1979).
117. S. I. Andersen and J. G. Speight, Fuel 72(9), 1343 (1993).
118. S. I. Andersen and K. S. Birdi, Journal of Colloid and Interface Science 142(2), 497 (1991).
119. D. A. Storm, R. J. Barresi and E. Y. Sheu, "Evidence for the Micellization of Asphaltenic Molecules in Vacuum Residue," Symposium on Petroleum Chemistry and Processing, presented before the Division of Petroleum Chemistry, Inc. 210th National Meeting, A.C.S. Chicago, 776 (1995).
120. E. Y. Sheu, M. M. DeTar, D. A. Storm and S. J. DeCanio, Fuel 71, 299 (1992).
121. H. P. Maruska and B. M. L. Rao, Fuel Sci. Tech. Int. 5(2), 119 (1987).
122. E. Y. Sheu, M. M. De Tar and D. A. Storm, Fuel 73(1), 45 (1994).
123. T. Ignasiak, O.P. Strausz and D. S. Montgomery, Fuel 56, 359 (1977).
124. T. Ignasiak, Kemp-Jones, A.V. and Strausz, O.P. ACS Div. Fuel Chem. Prepr. 22 (3), 126 (1977).
125. K.A. Gould, Fuel 58, 550 (1979).
126. R. Cimino, S. Correra, A.D. Bianco and T.P. Lockhart, "Solubility and Phase Behavior of Asphaltenes in Hydrocarbon Media" in Asphaltenes—Fundamentals and Applications, Edited by E. Y. Sheu and O. C. Mullins, Plenum Press, 1 (1995).
127. J. Escobedo and G.A. Mansoori, SPE Production & Facilities, 115 (1995).
128. G. Hotier and M. Robin, Revue de l'Institut Français du Pétrole 38(1), 101 (1983).
129. M. A. Anisimov, I. K. Yudin, V. Nikitin, G. Nikolaenko, A. Chernoustan, H. Toulhoat, D. Frot and Y. Briolant, J. Phys. Chem. 99, 9576 (1995).
130. P. Fotland, H. Anfindsen and F.H. Fadnes, Fluid Phase Equilibria 82, 157 (1993).
131. H. Toulhoat, C. Prayer and G. Rouquet, Colloids and Surfaces A: Physicochemical and Engineering Aspects 91, 267 (1994).
132. V. Szewczyk, F. Behar, E. Behar and M. Scarsella, Revue de l'Institut Français du Pétrole 51(4), 575 (1996).
133. A. S. Janardhan and G. A. Mansoori, Journal of Petroleum Science and Engineering 9, 17 (1993).

134. B. Dabir, M. Nematy, A. R. Mehrabi, H. Rassamdana and M. Sahimi, Fuel 75(14), 1633 (1996).
135. M. Adam and D. Lairez, "Sol-gel Transition" *in* The Physical Properties of Polymeric Gels, Edited by J.P. Cohen Addad, John Wiley and Sons, 87 (1996).
136. P. Meakin, "Simulation of Aggregation Processes" *in* The fractal Approach to Heterogeneous Chemistry, Edited by D. Avnir, John Wiley and Sons, 131 (1989).
137. M.Y. Lin, H.M. Lindsay, D.A. Weitz, R.C. Ball, R. Klein and P. Meakin, *in* Fractals in the Natural Sciences, M. Fleischmann, D.J. Tildesley and R .C. Ball Eds., Princeton Paperbacks, pp. 71–87 (1989).
138. B. P. Tissot and D. H. Welte, "Petroleum formation and occurrence", Springer-Verlag (1984).
139. M. L. Bordenave, "Applied Petroleum Geochemistry," Editions TECHNIP, (1992).
140. B. P. Tissot, "Characterization of heavy crude oils and petroleum residues", International Symposium - Lyon 25–27 juin 1984, Edition TECHNIP, 3–18.
141. F. Behar and R. Pelet, Journal of Analytical and Applied Pyrolysis 8, 173 (1985).
142. D. Vitorovic, "Structure elucidation of kerogen by chemical methods", in Kerogen, Edited by B. Durand, Editions TECHNIP, 301 (1980).
143. F. Behar and M. Vandenbroucke, Org. Geochem. 11, 15 (1987).
144. K. H. Altgelt and M. M. Boduszynski, "Composition and Analysis of Heavy Petroleum fractions", Marcel Dekker Inc., 463 (1994).
145. P. J. Flory, "Principles of Polymer Chemistry", Cornell University Press, Ithaca, New York, (1953).
146. T. F. Yen, in "Encyclopedia of Polymer Science and Engineering", Edited by M. Grayson and J. I. Krochwitz, Wiley, Second Edition, 1 (1988).
147. H. Lian, J.-R. Lin and T. F. Yen, Fuel 73(3), 423 (1994).
148. L. Loeber, O. Sutton, J. Morel, J. M. Valleton and G. Muller, Journal of Microscopy 182(1), 32 (1996).
149. R. N. J. Saal and J. W. A. Labout, J. Phys. Chem. 44, 149 (1940).
150. J. M. Dealy, The Canadian Journal of Chemical Engineering 57, 677 (1977).
151. D. A. Storm and E. Y. Sheu, Fuel 72, 233 (1993).
152. A. Cohen, G. Di Bernardo and D. Decroocq, Revue de l'Institut Français du Pétrole 43(2), 281 (1988).
153. A. Guinier and G. Fournet, "Small Angle Scattering of X-rays", Wiley New York, (1955).
154. D. Espinat, Revue de l'Institut Français du Pétrole 45(6), 775 (1990).
155. J. Lambard and Th. Zemb, J. Appl. Cryst. 24, 555 (1991).
156. J. P. Cotton, "Introduction to scattering experiments", in Neutron, X-Ray and Light Scattering: Introduction to an Investigate Tool for Colloidal and Polymeric Systems, edited by P. Lindner and Th. Zemb, Elsevier Science Publishers, 3 (1991).
157. J. Teixeira, J. Appl. Cryst. 21, 781 (1988).
158. J. E. Martin, J. Appl. Cryst. 19, 25 (1986).
159. T. Nicolai, D. Durand and J.C. Gimel, Phys. Rev. B 50, 16357 (1994).
160. S. H. Chen, J. Rouch and P. Tartaglia, Croat. Chem. Acta 65, 533 (1992).
161. J. Bastide and S.J. Candau, *in* Physical properties of Polymeric gels, Ed. J.P. Cohen Addad, Wiley, 159 (1996).
162. A. W. Robards and U. B. Sleytr, *Low temperature methods in biological electron microscopy* , Elsevier, (1985).
163. L. Loeber, « *Etude de la structure des cakes d'argile formés sur les parois des puis au cours du forag* » , PhD Thesis - University of Paris VI , (1992).
164. O. Fassi, « *Caractérisation à l'échelle du pore de la mouillabilité des roches réservoirs* » , PhD Thesis - University of Paris VI , (1992).
165. O. Mack, J. Phys. Chem. 36, 2901 (1932).
166. P.J. Flory and T.G. Fox, J. Am. Chem. Soc. 73, 1951 (1951).
167. J. Murgich, J. Rodriguez M. and Yosslen Aray, Energy and Fuels, 10, 68 (1996).
168. B. Cabane, "Growth: a brief guide for the use of scattering techniques", in Neutron, X-ray and Light Scattering: Introduction to an Investigate Tool for Colloidal and Polymeric Systems, Edited by P. Lindner and Th. Zemb, Elsevier Science Publishers, 247 (1991).
169. J. Bastide and S.J. Candau *in* The Physical Properties of Polymeric Gels, Edited by J.P. Cohen Addad, John Wiley and Sons, 87 (1996).
170. D. Fenistein, L. Barre, D. Broseta, D. Espinat, A. Livet and M. Scarsella, accepted to Langmuir
171. H. F. van Garderen, W. H. Dokter, T. P. M. Beelen, R. A. Van Santen, E. Pantos, M. A. J. Michels and P. A. J. Hilbers, J. Chem. Phys., 102(1), 480 (1995).

Chapter VI

MOLECULAR AND COLLOIDAL STRUCTURE OF COAL ASPHALTENES AND OTHER HEAVY SOLVENT SOLUBLE COMPONENTS

Masashi Iino and Toshimasa Takanohashi

Institute for Chemical Reaction Science
Tohoku University
Katahira 2-1-1, Aoba-Ku
Sendai 980-77, Japan

1. INTRODUCTION

Coal is a complex organic substance in which aromatic and heteroaromatic rings with hydroxyl and alkyl groups are connected through the bonds such as methylene and ether, and naphthene rings. Coal has a wide range of chemical compositions and properties, and ASTM classification widely used defines anthracite, low, medium, and high-volatile bituminous coal, subbituminous coal, and lignite, according to their heating value, volatile matter and fixed carbon content. The carbon % of coal, expressed as dry and mineral matter free basis, is in the range of about 65–95 % and increases with coal rank, i.e., from lignite to anthracite, with the accompanying decrease of oxygen and hydrogen %. Coal also generally includes a small percentage of minerals that can be removed by acid washing.

Coal contains or produces heavier components than petroleum. A heavier component than asphaltene, i.e., preasphaltene, defined as benzene (or toluene) insoluble/pyridine (or tetrahydrofuran) soluble component. Recently, a heavier component than preasphaltene can be obtained using a powerful solvent, carbon disufide – *N*-methyl-2-pyrrolidinone mixed solvent. So, coal chemists can offer the information about association behaviors of these heavy components, which seem not to exist in petroleum. The chemical structures of asphaltenes from coal and petroleum seem to be different in aromaticity, functional group such as OH groups, and probably molecular weight and shape, resulting in different colloidal structures and formation dynamics in solution. It is our impression that research on chemical structures on coal and coal-derived substances is active and much progressed, but behaviors and structures of the solution state such as colloidal structures and viscosity

are not well understood, compared to those for petroleum, probably because heavy components from coal are little commercially used as themselves.

Related to this review, solution properties and chemical structure of coal asphaltenes, and noncovalent bonding in coal were reviewed by Steedman[1] in 1985, and Stenberg et al.[2] in 1982, respectively.

2. MOLECULAR STRUCTURE

2.1. Preparation of Coal-Derived Asphaltenes and Other Heavy Solvent Soluble Components

Coal-derived asphaltenes and other heavy solvent soluble components are obtained from solvent extraction, various solubilization reactions, carbonization (tar), and liquefaction, of coal. Solubilization reactions used are pyrolysis, covalent bond breaking by various reagents, and chemical modification of coal such as alkylation, silylation, and hydrogenation. Usually coal-derived components are separated by solvent fractionation into oil, asphaltene, and preasphaltene. Oil is a soluble fraction in *n*-alkane, usually *n*-pentane or *n*-hexane. Asphaltene is a fraction soluble in benzene or toluene and insoluble in *n*-alkane, while preasphaltene is soluble in pyridine or tetrahydrofuran (THF) and insoluble in benzene or toluene. Preasphaltene is a heavier component than asphaltene and oil, since pyridine and THF are a better solvent for coal molecules than benzene. Kinetic study on coal liquefaction usually assumes the reaction steps of coal → preasphaltene → asphaltene → oil.

Solvent extractions of coal usually give low extraction yields. The extraction yields for exhaustive Soxhlet extractions with pyridine, one of the best solvent for coal extraction, are a few % to about 40 % for coals of a wide range of rank. The dependency of the pyridine extraction yields on carbon % of coals shows maximum at around 85–88 carbon %. By using quinoline as an extraction solvent at 300 °C the yield of 50 % was obtained from bituminous coals,[3] and the authors concluded that the extract obtained is indigenous in the coal, not the products from some solubilization reactions, though at 300 °C the breaking of weak covalent bonds in coal is possible to occur. Recently Iino et al.[4] have found that 1:1 (volume ratio) carbon disulfide – *N*-methyl-2-pyrrolidinone mixed solvent gives more than 50 wt% of extraction yields for several bituminous coals at room temperature. Solvent fractionation of the extracts obtained gave a heavier component than preasphaltenes, i.e., pyridine insoluble/the mixed solvent soluble fraction.

Generally cleavage of covalent bonds connecting two aromatic clusters (aromatic ring systems including hydroaromatic structure) has been considered to be necessary to obtain a large amount of solvent soluble substances. This is based on, so called "two phase structure model", i.e., coals consist of covalently bound cross-linked networks which are not soluble in any solvent and a small amount of low-molecular weight constituents trapped in the networks. This model derives from (1) coals show elastic and swelling behaviors; (2) NMR studies of coals differentiate mobile and immobile constituents; (3) extraction yields of coals are usually very low. Recently the "associated structure model" in which coal consists of giant aggregate of solvent soluble molecules, has been proposed, based on extraction yields higher than 50 % which were obtained without any solubilization reactions for some bituminous coals.[5,6] The authors think that for several bituminous coals the associated structure model is more probable. Even if the associated structure model is correct, cleavage of covalent bonds connecting two aromatic clusters is needed to

get low molecular weight substances such as asphaltenes. There are many methods to solubilize coal. The chemical structures and properties of coal-derived substances obtained depend on both a kind of coal and a reaction used.[7] If methylene or ether bonds which connect aromatic clusters are selectively cleaved, the structure of aromatic systems can be preserved. However, even if a simple reagent is used, the reactions occurred are often very complex with many side reactions.

A mild depolymerization of coals by phenol has been carried out using acid as a catalyst.[8–10] The use of *p*-toluenesulphonic acid as a catalyst was found effective for pyridine solubilization of coals of different rank.[9] Olah et al.[11] found that HF-BF_3-H_2 system was effective for depolymerization of coal under mild conditions, resulting in an increase in the extractability of coal in pyridine and cyclohexane. Reductive alkylation has been also used to undergo bond cleavage in coals in liquid ammonia and in THF.[12–15] By reductive alkylation extensive cleavage of carbon–heteroatoms (O, S, N) bonds occurs, compared to little cleavage of carbon–carbon bonds. Oxidation generally destroys the aromatic rings in coals as well as causing cleavage of methylene and ether bond.

Asphaltenes and other components are also obtained from coal tar and coal liquefaction products. Coal liquefactions are carried out at 400 – 550 °C using hydrogen and/or hydrogen-donating solvent, and catalyst, in laboratories or plants of various scale.

The solvent fractionation of coal-derived substances is not so simple, since the order of the solvents used, i.e., pyridine → benzene → hexane or the reverse order, and fractionation conditions such as temperature and time surprisingly change the yields of each component. The removal of the solvent used from coal-derived substances, especially pyridine, is another problem. Drying *in vacuo* at 80 – 120 °C is often insufficient to remove a solvent retained strongly in them. Washing with special solvents such as supercritical carbon dioxide is reported to be effective for pyridine removal.[16–19] It is not rare that the recovered components after solvent stripping from a solution are found to become not completely soluble in the solvent used, probably due to the change in their association state.[20,21] It is concluded that the composition of oil, asphaltene and preasphaltenes obtained depends upon the association state among these molecules and so upon the separation method used.

Snape and Bartle[22,23] proposed the factors that differentiate oil, asphaltene, and preasphaltenes, by examining their structures and molecular weights. These are molecular weight, M_n, acidic OH%, and size of aromatic rings (the ratio of internal (bridgehead) aromatic carbon to total carbon, C_{int}/C). Acidic OH% and C_{int}/C are related to the solubility decrease by association due to hydrogen bonding and π–π interactions between aromatic rings, respectively. As the values of these parameters increase, the solubility decreases. Figure 1 shows a three dimensional description by the three parameters and shows that the volume within boundary corresponds to oil, and the volume outside the boundary, to asphaltenes and heavier components.[23] Ouchi[24] proposed a simpler criterion which uses aromaticity (f_a) and molecular weight for the differentiation of oil, asphaltenes and preasphaltenes of petroleum and coal-derived materials.

2.2. Structural Parameter and Model

Brown–Ladner structural parameters[25] based on elementary analysis and ^{1}H-NMR spectra have been widely used for the average structural description of coal-derived substances. They are f_a, σ, and H_{ars}/C_{ars} in Eq. (1–3). f_a is the aromaticity, defined as the atomic ratio of aromatic carbon to that of total carbon. σ is the degree of substitution on the aromatic rings (the ratio of substituents to H). H_{ars}/C_{ars} is the degree of condensation of

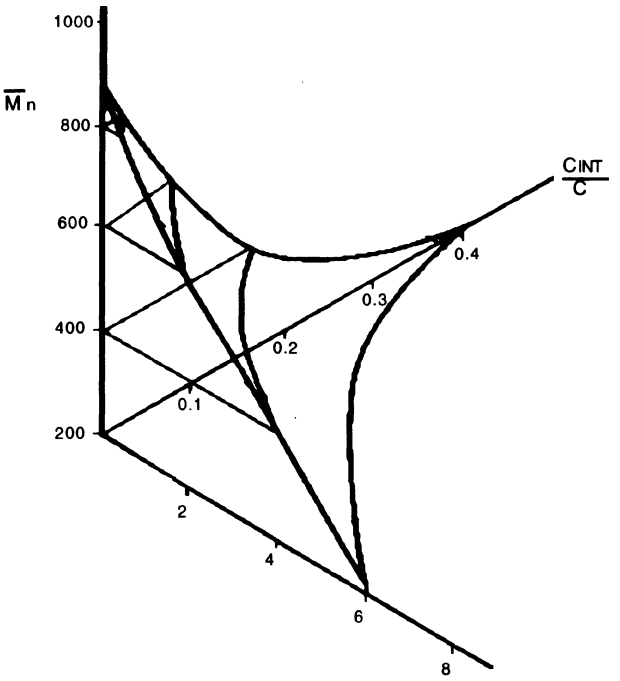

Figure 1. Differentiation between oil and asphaltene on three-dimensional plot of *M*n versus % acidic OH versus C_{int}/C.[23] Volume within boundary corresponds to oil.

aromatic rings, i.e., the aromatic hydrogen to carbon ratio of the hypothetical unsubstituted aromatic rings, from which the size of aromatic rings can be approximately estimated.

$$f_a = \frac{C/H - H_\alpha^*/x - H_0^*/y}{C/H} \tag{1}$$

$$\sigma = \frac{H_\alpha^*/x + O/H}{H_\alpha^*/x + O/H + H_{ar}^*} \tag{2}$$

$$H_{ars}/C_{ars} = \frac{H_\alpha^*/x + O/H + H_{ar}^*}{C/H - H_\alpha^*/x - H_0^*/y} \tag{3}$$

where C/H and O/H are atomic ratios and $H_\alpha^*=H_\alpha/H$, $H_0^*=H_0/H$, and $H_{ar}^*=H_{ar}/H$. H_α/H, H_0/H, and H_{ar}/H are the fractions of hydrogen on α-carbon atoms, on other non-aromatic carbon atoms, and on aromatic carbon atoms, respectively. Deriving the equations above, nitrogen and sulfur are neglected, and all oxygen is assumed to be phenolic oxygen.

In Table 1 the structural parameters reported for various coal extracts were summarized, including the results by modified Brown-Ladner equations (Retcofsky and Friedel,[26] Kanda et al.[27]) and by recent solid state ^{13}C-NMR (Fletcher et al.[28]). Table 1 shows that the

Table 1. Structural parameters reported for various coal extract components

Coal	Carbon %	Conditions: Solvent	Temp. (°C)	Time (h)	Yield (%)	Structural parameters: f_a [a]	H_{ars}/C_{ars} [b] $((f_a'-f_a^B)/f_a')^{i,28}$	σ [c] $((f_a^N-f_a^B)/(f_a'-f_a^B))^{j,28}$	Literature
Loy Yang	65.5	Toluene	320	1	16.2	0.30	1.00	0.72	Redlich[39]
Beulah-Zap	71.6	Pyridine	115	120-168	3.1	0.48	0.79[i]	0.53[j]	Fletcher[28]
Wyodak	73.6	Pyridine	115	120-168	6.2	0.53	0.77[i]	0.54[j]	Fletcher[28]
Illinois #6	76.9	Pyridine	115	120-168	27.9	0.68	0.75[i]	0.49[j]	Fletcher[28]
Taiheiyo	77.9	Quinoline	350	4	46.1	0.71	0.88	0.43	Iwata[3]
Blind Canyon	79.4	Pyridine	115	120-168	32.1	0.57	0.74[i]	0.50[j]	Fletcher[28]
Akabira	81.2	Quinoline	350	1	94.0	0.79	0.81	0.48	Iwata[3]
Lewiston	82.0	Pyridine	115	120-168	14.7	0.73	0.75[i]	0.44[j]	Fletcher[28]
Lower Kittanning	82.3	Acetone[d]	25	0.75	6.7	0.70	0.81	0.47	Iino[30]
		Pyridine[d]	25	3	29.5	0.77	0.76	0.53	Iino[30]
		CS_2-DMA[e]	25	3	10.0	0.85	0.79	0.36	Iino[30]
Pittsburgh #8	82.6	CS_2[f]	25	16	4.0	0.61	0.71	0.40	Retcofsky[26]
		Pyridine	115	120-168	26.5	0.69	0.75[i]	0.46[j]	Fletcher[28]
Pittsburgh	82.7	Pyridine	25	16	–	0.72	0.66	0.41	Iino[30]
Markham Main	83.1[g]	Toluene	350[h]	–	17.0	0.77	–	0.45	Bartle[31]
Bayswater	83.6	Quinoline	350	4	70.0	0.82	0.78	0.41	Iwata[3]
Miike	83.9	Quinoline	350	4	96.7	0.75	0.75	0.46	Iwata[3]
		Acetone[d]	25	0.75	9.4	0.65	0.80	0.52	Iino[30]
		Pyridine[d]	25	3	21.6	0.69	0.80	0.63	Iino[30]
Daiyon	84.0	Quinoline	350	4	81.6	0.77	0.76	0.48	Iwata[3]
Upper Freeport	86.2	Acetone[d]	25	0.75	7.4	0.74	0.69	0.39	Iino[30]
		Pyridine[d]	25	3	22.0	0.78	0.72	0.48	Iino[30]
		CS_2-DMA[e]	25	3	30.0	0.79	0.71	0.51	Iino[30]
		Pyridine	115	120-168	14.9	0.74	0.76[i]	0.41[j]	Fletcher[28]
Zao Zhuang	86.9	Acetone[d]	25	0.75	7.4	0.68	0.68	0.47	Iino[30]
		Pyridine[d]	25	3	26.9	0.74	0.66	0.59	Iino[30]
		CS_2-DMA[e]	25	3	28.7	0.82	0.69	0.40	Iino[30]
Indian Ridge	87.4	Quinoline	350	4	63.0	0.84	0.65	0.35	Iwata[3]
Goonyella	87.9	Quinoline	350	4	93.2	0.83	0.68	0.42	Iwata[3]
Shin-Yubari	88.1	Quinoline	350	4	97.4	0.80	0.66	0.43	Iwata[3]
		Acetone[d]	25	0.75	6.1	0.65	0.80	0.49	Iino[30]
		Pyridine[d]	25	3	33.0	0.70	0.63	0.65	Iino[30]
		CS_2-DMA[e]	25	3	17.7	0.76	0.71	0.44	Iino[30]
Balmer	89.4	Quinoline	380	4	52.1	0.86	0.64	0.35	Iwata[3]
Pocahontas #3	89.7	Pyridine	115	120-168	0.5	0.74	0.68[i]	0.40[j]	Fletcher[28]
Beatrice	91.5	Quinoline	370	4	42.0	0.89	0.64	0.29	Iwata[3]

[a]Atomic ratio of aromatic carbon to that of total carbon. [b]Aromatic hydrogen to carbon ratio of the hypothetical unsubstituted aromatic rings. [c]Degree of substitution of the aromatic rings. [d]Acetone soluble (AS) and acetone insoluble / pyridine soluble (PS) fractions, respectively obtained from fractionation of the carbon disulfide – *N*-methyl-2-pyrrolidinone mixed solvent extract. [e]Pyridine insoluble / carbon disulfide – *N,N*-dimethylacetoamide (DMA) mixed solvent soluble fraction (PI') obtained from fractionation of the carbon disulfide – *N*-methyl-2-pyrrolidinone mixed solvent extract. [f]CS_2 soluble fraction obtained from fractionation of the pyridine extract. [g]Carbon % of extract. [h]Supercritical extraction under 10 Mpa pressure. [i]The parameter corresponding to H_{ars}/C_{ars}, f_a'=Aromatic carbon %. f_a^B=Aromatic bridgehead carbon %. [j]The parameter corresponding to σ, f_a^N=nonprotonated aromatic carbon %.

extraction yields are dependent upon a kind of solvent and extraction conditions used. When acetone or CS_2 was used as an extraction solvent, the yields were less than 10 %. While, when a better solvent such as pyridine and quinoline was used, higher yields were obtained, although the yields depend on coal rank. Coals with carbon % of 85–88 % generally gave the highest extraction yields. Quinoline extraction at 350–380 °C gave yields

higher than 90 wt%, probably due to some covalent bond cleavages at such high temperatures. Table 1 shows that aromaticity (f_a) ranges widely from 0.48 for Beulah-Zap lignite to 0.89 for Beatrice low-volatile bituminous coal, i.e., f_a increases with increasing coal rank, indicating that aromatization reaction proceeds by coalification process. Degree of condensation of aromatic rings (H_{ars}/C_{ars}) is 0.74–0.88 for the extracts of low-rank coals (carbon % < 80 %) corresponding to 1–3 rings, and 0.63–0.81 for those of higher-rank coals (80 % < carbon % < 91 %) to 2–4 rings. Degree of substitution of the aromatic rings (σ) is 0.29–0.65, regardless of coal rank.

Retcofsky and Friedel[26] investigated the structure of extracts of a bituminous coal (82.7 carbon %). The carbon disulfide soluble portion, which is about 4 % of the original coal, was obtained by extracting the coal with pyridine at room temperature, followed by the extraction of the pyridine extract with carbon disulfide. By considering the result that 41 per cent of the oxygen in the coal used was phenolic,[29] H_{ar} was calculated by Eq. (4)

$$H_{ar} / H = H_{ar+O} / H - 0.41O / H \tag{4}$$

where H_{ar+O}/H is the fraction of aromatic and phenolic hydrogen. Kanda et al.[27] modified the Brown–Ladner equations, in which the number of aromatic peripheral hydrogen atoms is corrected for heterocyclic O, N, S atoms, and oxygen atoms were separated into phenoxyl and heterocyclic oxygens. Iwata et al.[3] obtained the quinoline extracts from various ranks of coals at 350–380 °C. The quinoline extracts were further extracted with pyridine at room temperature and the extraction yield attained a maximum of 85 %. The structural parameters calculated from both quinoline extracts and pyridine extracts showed a good agreement.

Iino et al. found[4,5] that a 1:1 carbon disulfide – *N*-methyl-2-pyrrolidinone mixed solvent gave high extraction yields, more than 50 wt%, for several bituminous coals at room temperature. No significant bond cleavage has been observed to occur during the extraction. The extracts obtained, i.e., the mixed solvent soluble fractions, were further fractionated with acetone and pyridine into acetone soluble (AS) fraction, acetone insoluble/pyridine soluble (PS) fraction, and pyridine insoluble (PI) fraction which is a heavier fraction than preasphaltenes, as shown in Figure 2.[4] The structure parameters of each fraction, which were re-calculated values of those in reference 30 using modified Brown-Ladner equations,[27] are shown in Table 1. For the bituminous coals the aromaticity, f_a, generally increased as the fraction became heavier, i.e., AS < PS < PI', while H_{ars}/C_{ars} is similar among three fractions. PI' is carbon disulfide – *N*,*N*-dimethylacetoamide mixed solvent soluble fraction of PI.[30]

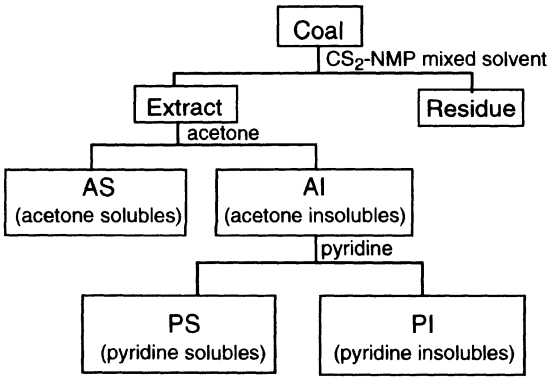

Figure 2. Fractionation procedure of the extract obtained from carbon disulfide – *N*-methyl-2-pyrrolidinone (CS_2–NMP) mixed solvent extraction.[4]

Fletcher et al.[28] have carried out Soxhlet extraction of eight Argonne coals using pyridine purged with argon and followed by a novel washing procedure to remove pyridine, and compared structural parameters of the extracts and residues, which are obtained by using solid state ^{13}C -NMR. They estimated 12 informative structure parameters from their careful and detailed NMR analysis, but in Table 1 only 3 parameters corresponding to Brown-Ladner's parameters are shown. They estimated that the number of aromatic carbons per cluster of the extracts shown in Table 1 is 10 –17, smaller than that of the corresponding residues. Bartle et al.[31] carried out supercritical toluene extraction of coal at 350 °C. From the structural analysis of the extract fractions, using ^{1}H-NMR, ^{13}C-NMR, gas chromatography and mass spectroscopy, model structures for asphaltene (petroleum ether-insoluble/benzene soluble fraction) were suggested. The aromatic ring size is 1–2 rings, and all aromatic clusters are connected directly (biphenyl-type) or by methylene carbon or ether oxygen, resulting in a rather rigid structure.

Many results on structural parameters and structure models of solvent solubles obtained from dissolution reaction of coals have been reported. Makabe and Ouchi studied[32–34] the average structure of asphaltenes and preasphaltenes from mild hydrogenation, i.e., a treatment using NaOH-alcohol system at 300 °C and 350 °C. The NaOH–alcohol treatment was found to make the coals nearly completely soluble in pyridine. These coal products are expected to keep their original aromatic cluster structure, since the treatment was performed under mild conditions. The coals of low coal rank, i.e., Taiheiyo (77.3 carbon %) and Akabira (81.2 carbon %) coals, have tetralin-type rings, while a higher rank coal, Shin-Yubari coal has a 4 ring aromatic nucleus and nearly two naphthenic rings are attached to it. Mild hydrogenation products of Yubari coal studied by Ouchi et al.[35,36] also have 3–4 aromatic ring. The SRC products (solvent refined coal, 94% soluble in quinoline) from a bituminous coal were analyzed by Curie point pyrolyzer and ^{13}C-NMR, and aromatic ring structures in an Akabira bituminous coal were determined as shown in Figure 3.[37]

Charlesworth[38] carried out structural analysis of asphaltenes from hydrogenation of Loy Yang coal at 350, 425, and 500 °C, using ^{13}C-NMR, ^{1}H-NMR, IR and UV spectroscopy. The results indicate that aromaticity, f_a, increase as the hydrogenation temperature

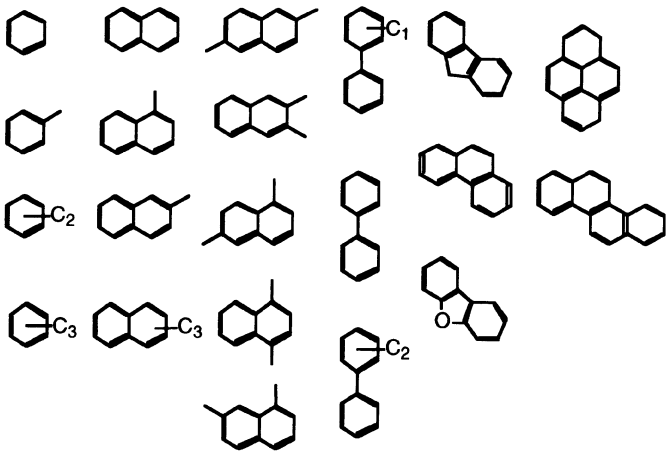

Figure 3. Aromatic ring structures estimated for a Japanese bituminous coal.[37]

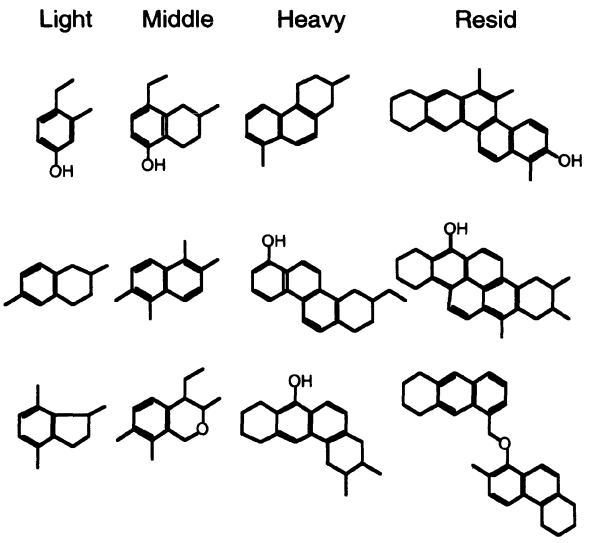

Figure 4. Model structures for the fractions separated by distillation of heavy liquefaction liquid.[40]

rises and most of the saturated carbon atoms are naphthenic carbons, and there are very few side chains or methylene bridges. Chemical structure of asphaltenes from Loy Yang coal (65.5 carbon %) from heat treatment have also been also investigated by Redlich et al.[39] The asphaltenes obtained at 320 °C were suggested to be obtained from physical extraction without any dissolution reactions and their structural parameters are also shown in Table 1 . The liquefaction of a bituminous coal (79.3 carbon %) was carried out at 500 °C by Anderson et al.[40] The products obtained were 10 % gases, 5 % light oil (b.p. < 250 °C), 55 % heavy liquid, 15 % char, and 15 % water. The heavy liquids were further separated by distillation into light, middle, heavy fractions, and resid. The structures of each fractions estimated from the structural parameters based on the modified Brown–Ladner equation,[27] are shown in Figure 4. The structures are considerably different among the fractions, from light fraction to resid, though they are obtained from the same coal. This may be attributed to the high hydrogenation temperature of 500 °C. Increasing the severity of the treatment seems not only to break linkages between aromatic clusters, but also to break hydroaromatic rings, resulting in reduction of size and number of rings. Snape and Ladner[41] studied chemical structures of asphaltenes from three coal liquefaction processes, namely solvent refined coal (SRC), hydrogen-donor solvent liquefaction (HDS), and supercritical gas extraction (SCG). The degree of substitution of the aromatic rings for the asphaltenes from liquefactions tends to be low compared to the extracts described above.

Shinn constructed[42] the structure model of Illinois No.6 coal (79.4 carbon %) using the detailed information on its chemical structures and liquefaction products. Figure 5 shows the model structures for the liquids obtained from the short-contact time i.e., mild liquefaction of low H_2 consumption, which are used to construct a structure model of the coal itself.[42] These model molecules seem to correspond to preasphaltenes, i.e., high molecular weight materials containing many polar functional groups, since in this mild liquefaction only reactive bridges are broken, and many functional groups are preserved. The model structures for the liquids from severe liquefaction with increased temperature and residence time are shown in Figure 6.[42] In general, the products are shifted towards lighter fractions, i.e., low-molecular weight

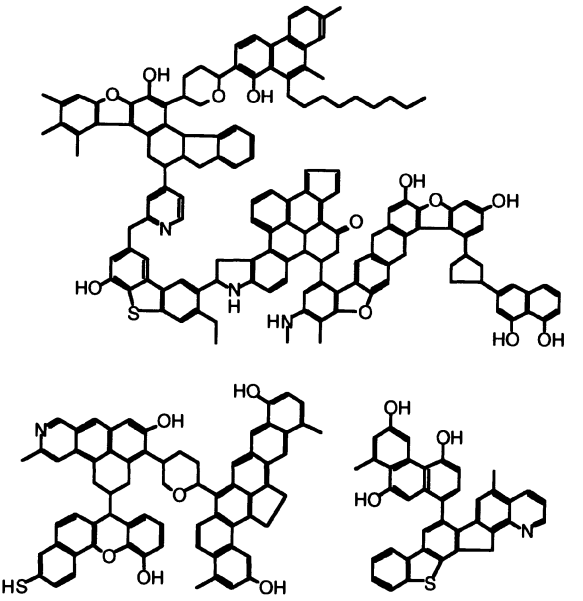

Figure 5. Model structures for the products of mild liquefaction of a bituminous coal.[42]

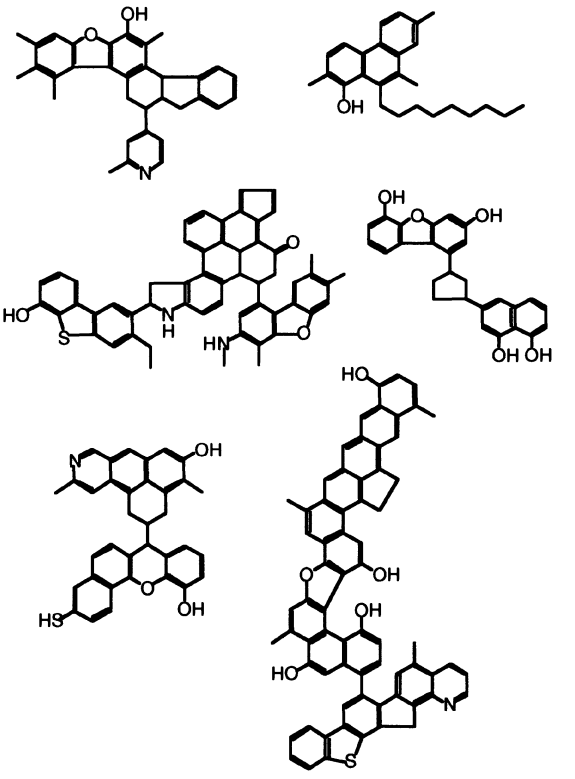

Figure 6. Model structures for the products of severe liquefaction of a bituminous coal.[42]

and less functional groups, suggesting the occurrence of further depolymerizations as well as removal of functional groups. Figure 6 shows that some condensation reactions increasing the size of aromatic rings also occur in severe liquefaction.

Nakamura et al.[43] estimated model structures for the fractions obtained from the extraction at room temperature. A bituminous coal (86.9 carbon %) was extracted with carbon disulfide – *N*-methyl-2-pyrrolidinone mixed solvent and the extract (63% yield, daf) was further fractionated into pyridine–insoluble (PI), pyridine soluble/benzene insoluble fraction (PS, preasphaltene),benzene soluble/hexane insoluble (BS, asphaltene), and hexane soluble (HS, oil). BS, PS, and PI fractions were further hydrogenated under mild condition using Adkins catalyst, according to the method by Katoh and Ouchi.[44,45] The hexane soluble oils thus obtained from BS, PS and PI by the hydrogenation, together with the original HS were analyzed by using mass spectrometry and high pressure liquid chroma-

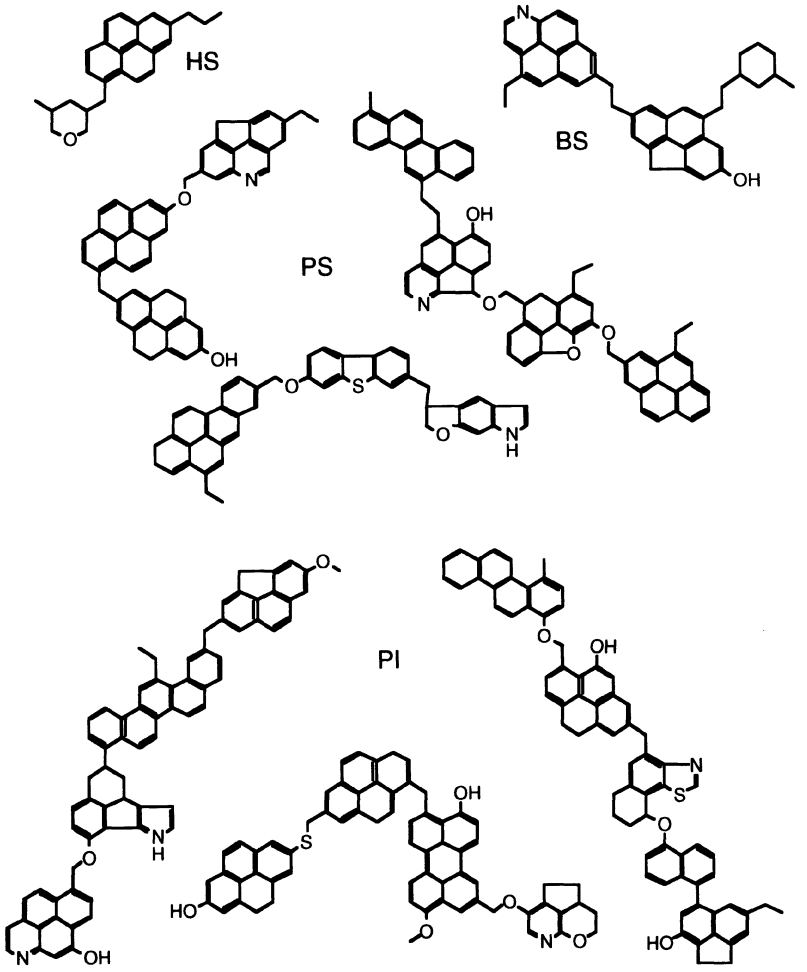

Figure 7. Model structures for HS, BS, PS, and PI fractions from the room temperature extraction of a bituminous coal.[43]

tography (HPLC) using a column packing which can separate substances according to ring size. Aromatic compounds with 3–4 ring size were the main products, independent of the heaviness of fractions, although aromaticity, f_a, and heteroatom content increased as the fraction became heavier. The model structures estimated for HS, BS, PS and PI molecules are shown in Figure 7.[43] The difference among the fractions are mainly molecular weight, the quantity of functional groups, and aromaticity.

2.3. Structural Difference between Asphaltenes from Coal and Petroleum

It is difficult to generalize the similarity and difference between the structures of asphaltenes from coal and petroleum, since the structures obtained depend upon source materials used and methods and conditions to get asphaltenes, especially for coals. Yen[46] has investigated the differences between coal-derived and petroleum asphaltenes. The detailed structure analysis for the asphaltenes from a Laquinillas crude petroleum in Venezuela and from liquefaction of high volatile bituminous coal in West Kentucky in USA by the Synthoil process, respectively, suggests that (1) the aromaticity of the petroleum-derived asphaltenes is lower than that of coal-derived asphaltenes; (2) the aromatic ring sizes of the petroleum-derived asphaltenes are larger than those of coal-derived asphaltenes; (3) the aliphatic substituents of the petroleum-derived asphaltenes are longer that those of the coal-derived asphaltenes; (4) the molecular weight of petroleum-derived asphaltenes is around 10 times higher than that of coal-derived asphaltenes; (5) petroleum-derived asphaltenes are less polar than coal-derived asphaltenes.

Snape and Bartle[22] obtained various structure parameters of preasphaltenes, asphaltenes and oils obtained from solvent extraction of a UK bituminous coal and a US lignite, a Turkish crude oil, an athabasca tar sand, and a Turkish asphaltite, respectively, as shown in Table 2. Table 2 shows that the petroleum asphaltenes have higher molecular weight and contain less oxygen, acidic OH and basic nitrogen than the bituminous coal-derived asphaltenes. The size of the aromatic nuclei in the petroleum asphaltenes is 3–6 rings, and 2–3 rings for the coal-derived oil, asphaltene, and preasphaltene. Mullins et al.[47] compared

Table 2. Analytical data for benzene insolubles (BI), asphaltenes (As), and *n*-pentane solubles (*n*-Ps) of petroleum and coal-derived extracts[22]

	Petroleum samples						Coal-derived substances solvent extracts				
	Crude oil		Bitumens								
	Turkish crude oil		Athabasca		Turkish asphaltite		UK coal			US lignite	
	As	*n*-Ps	As	*n*-Ps	As	*n*-Ps	BI	As	*n*-Ps	As	*n*-Ps
C%	81.9	82.5	78.9	82.3	83.3	84.0	77.8	80.0	85.2	75.0	82.5
H%	7.9	11.0	8.4	10.8	7.2	8.9	5.4	6.3	9.2	10.1	12.2
O%	ND	ND	4.1	2.8	1.4	0.6	12.4	10.1	4.2	13.8	5.2
N%	0.6	0.2	1.1	0.4	1.1	0.2	2.4	ND	ND	0.3	0.2
S%	9.7	4.4	7.5	3.7	7.0	7.0	0.9	ND	ND	0.7	0.8
H/C	1.18	1.59	1.27	1.56	1.03	1.19	0.83	0.94	1.29	1.60	1.76
M_n	2000	430	1750	470	1610	390	1500	590	370	910	510
Acid OH%	0.8	0.1	1.4	0.6	0.5	ND	8.2	6.3	2.2	4.7	3.1
Basic N%	ND	ND	0.2	0.1	ND	ND	ND	ND	ND	ND	ND
f_a	0.54	0.22	0.43	0.24	0.59	0.47	0.79	0.72	0.51	< 0.2	< 0.2

BI, Benzene insolbules; As, Asphaltene (*n*-pentane insoluble/benzene solubles), *n*-Ps, *n*-Pentane solubles; ND, Not determined.

molecular structure of nitrogen in coal with that of asphaltenes by using XANES spectroscopy and reported that coals and petroleum asphaltenes are similar with regard to their high concentrations of pyrroles and pyridine among nitrogen functional groups.

Generally, the aromatics of lignites have 1–2 rings and about one naphthenic ring with aliphatic chains and oxygen-containing functional groups such as hydroxyl and carboxyl groups. As coal-rank increases, i.e., coalification proceeds, both the number and size of aromatic rings increase, while oxygen-containing functional groups decrease. Bituminous coals with 85–87% carbon have 3–4 aromatic ring size. Molecular weights of coal-derived asphaltenes are lower than those of petroleum-derived asphaltenes. The reason may be that molecular weights of coal-derived asphaltenes, which have lower solubility by hydrogen bonding and polarity due to oxygen-containing functional groups, must be low to be benzene soluble. While, long aliphatic chains of petroleum asphaltenes increase solubility in benzene by disrupting molecular association.

3. COLLOIDAL STRUCTURE

3.1. Interactions Responsible for Colloidal Structure Formation

Hydrogen bonds and $\pi - \pi$ interactions are considered mainly responsible for associative behaviors of coal-derived asphaltenes and other components, though charge transfer and ionic interactions also may contribute. Stenberg et al. reviewed[48] these interactions in coal and their effects on coal extractability, and viscosity and molecular weight measurements of coal-derived liquids. Sternberg et al.[48] separated asphaltenes obtained from the liquefaction products of Kentucky high volatile bituminous coal into acidic/neutral and basic components by dry HCl gas and measured their ^{1}H-NMR spectra. The broad peak at 5.35 ppm due to hydroxyl groups in the spectrum of the acidic component shifts toward lower ppm and broadens when the basic component is added to the acidic component, indicating the formation of hydrogen bonds between them. They have also found that 50 % of the acidic/neutral component of the asphaltene, which is now free of asphaltene bases, is soluble in hexane, i.e., converted to oil fraction, due to the breaking of the hydrogen bonds between asphaltene acids and bases. Acidity and basicity of acidic/neutral and basic components are attributed to acidic phenolic OH and pyrrole NH, and basic nitrogen in pyridine rings and ether oxygen, respectively. The results above do not imply that asphaltenes consists of acidic and basic components in a 1:1 ratio. The concentrated carbon disufide solution of an acid/neutral component of asphaltene shows a broad IR band at 3250 cm^{-1} which is attributed to intermolecular hydrogen bonds between molecules of the acid/neutral component.[49] Near-IR and ^{1}H-NMR studies of hydrogen bonding between the hydroxyl group of *o*-phenylphenol (OPP) with asphaltenes and their acidic and basic components show that the IR band of the free OH group of OPP at 1.44 μm (6944 cm^{-1}) is reduced rectilinearly when the basic component is added to its CS_2 solution, while no acidic component caused a decrease in the 1.44 μm absorbance, indicating the hydrogen bonding of the basic component with the OH of OPP.[50] OPP was selected because their self-association is sterically hindered.[51] Interactions of model compounds, i.e., OPP and pyridine, with asphaltene acid and base fractions were also studied using NMR.[51] Molar enthalpy of the interaction of pentane soluble oil with asphaltene (A) and its acidic/neutral (AA) and basic (BA) components is in the order BA > A > AA, and correlates well with the ^{1}H-NMR downfield chemical shift of the OH signal of OPP as a function of added asphaltene (A, AA, BA) concentration in carbon disufide solvent.[52] Molar enthalpy of the interaction of

quinoline with A, AA, BA, silylated A, and oil were also measured.[53] As described later, silylation and acetylation of OH group of coal-derived substances increase their solubilities, which confirms that intermolecular hydrogen bonding plays a key role in solubility of coal-derived substances.[54–56] Larsen and Baskar[57] offered the evidence for the breaking of hydrogen bonds in coal by polar solvents such as pyridine. Miura et al.[58] developed the method of quantitative estimation of various hydrogen bonds in raw and heat-treated coals by FTIR and DSC analysis.

Hirsch[59] carried out detailed X-ray scattering measurements of coals of various ranks. From the results obtained the models for stacking structures of aromatic rings in coals were proposed, as shown in Figure 8, which shows the change of stacking structures with coal rank, and stacking order increases with coal rank. Recent research by X-ray diffraction[60] indicates that aliphatic moieties attached to the aromatic rings in bituminous coals cause distortions in the stacking structures. X-ray diffraction study on the structure of coal derived asphaltenes were carried out by Schwager and Yen,[61] using the same method they used for petroleum asphaltenes, and obtained the following results. Condensed aromatic sheets (clusters) are suggested to be stacked on top of each other with the sheets parallel, and with aliphatic chains or naphthenic rings protruding from the edges. The asphaltene obtained by Synthoil liquefaction process indicates that the average interlayer distance ranges from 3.57 to 3.76 Å; the average interchain distance is between 4.81 to 5.35 Å; and the average diameter of the aromatic clusters perpendicular to the plane of

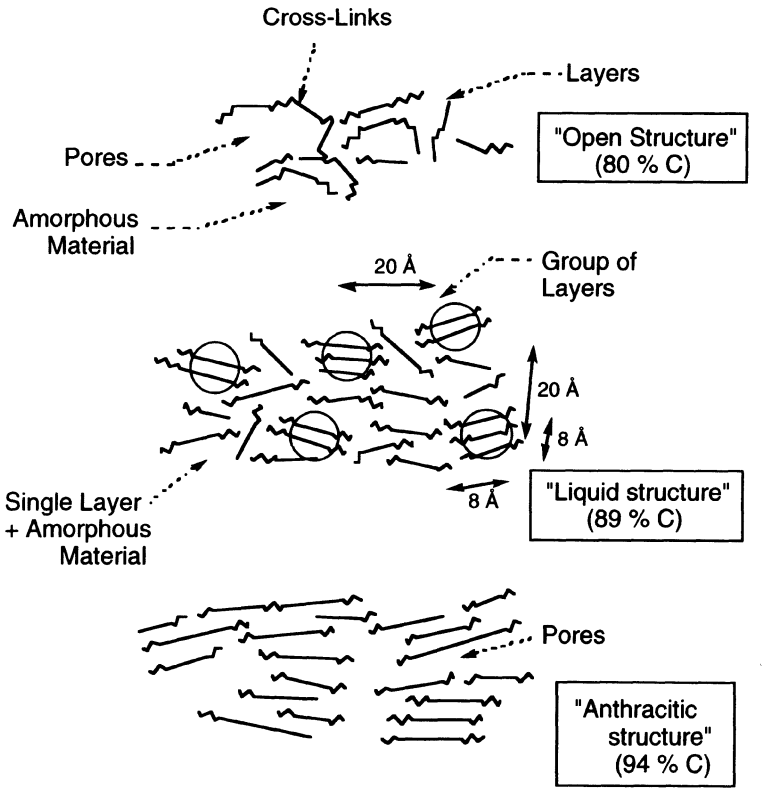

Figure 8. Changes of stacking order with coal rank.[59]

the sheets ranges between 9.4 to 12.2 Å. The average effective number of aromatic sheets associated in a stacked cluster is 4. It should be noted that graphite-like parallel stacking of aromatic rings is not always favored especially for small aromatic compounds, compared to other orientations such as perpendicular orientation between rings.[62] Base-catalyzed C-alkylation at carbons such as benzylic methylene carbons in coal for a low-volatile bituminous coal with high aromatic carbon content (f_a = 0.85) increases the extraction yield in pyridine, depending on the size of the alkyl group introduced. The larger alkyl groups disrupt the stacking of aromatic rings and make the coal more soluble.[63]

The contribution of charge transfer (electron donor – acceptor) interaction to associated structure of coal-derived substances is not well understood, because of the difficulty of its separation from other interactions. π–π interactions between aromatic rings described above are considered to include van der Waals, charge transfer, and other interactions. Schwager et al.[61] suggested the formation of charge transfer complexes of asphaltenes with electron acceptors such as I_2 and tetracyanoethylene (TCNE), though the evidences offered seem not so clear. Liu et al.[64] also found that the addition of a small amount of TCNE increases the extraction yields of several coals and the solubilities of coal extracts, probably due to the formation of charge transfer complexes between TCNE and coal molecules. While, Nishioka et al.[65] reported that charge transfer interactions are relatively strong forces in high-volatile bituminous coals. Duber and Mikosz[66] identified the triplet state due to charge transfer interactions or organic biradicals in bituminous coals by ESR measurements, though Retcofsky et al.[67] showed no existence of the triplet states in coals.

Boiling point reflects intermolecular forces. White and Schmidt[68] have found that the mid-boiling point (about 450–800 K) of distillates from H-Coal and Wilsonville liquefaction products is a linear function of their average molar volume and average molar polarizability, which are directly related to van der Waals interaction. White and Schmid wrote that the results obtained support, but not prove, the conclusion that van der Waals forces are the dominant intermolecular forces, determining their boiling points. While, for low boiling range of SRC-II liquefaction distillates, which contain substantial amounts of phenolic substances, the boiling points do not show the linearity with molar volume and polarizability. This suggests that the contribution of hydrogen bonding to the total intermolecular forces increases as the boiling point of the distillates decreases, as the concentration of hydrogen bonding species increases.

3.2. True Solution or Suspension?

When we treat a solution of coal-derived substances, we are often asked, "Is this a true solution or a suspension?" Hombach wrote in his paper[69] as follows. There are some fine particles in coal solutions which are really not dissolved. These particles are able to pass through a common filter, therefore they are not as easily detected as an insoluble residue. As the use of the term "colloid" leads to so many misunderstandings, the author (Hombach) suggests the term, "suspension" when the substance is not truly dissolved and the term "solution" when the substance is in a molecular dispersion. The difference is, in terms of physical chemistry, the contrast between the effect of surface energy in the first case and the effect of solvation enthalpy in the latter. As the surface energy increases rapidly with decreasing particle size, the size of particles reaches a lower limit to be in suspension, below which aggregation and precipitation of the particles occur. Hombach showed from scanning electron microscope (SEM) studies that for coal-derived substances

about 0.15 μm of particle size is a lower limit. Although a practicable experimental method must be found for determining whether we are dealing with a solution or a suspension, a solution of coal-derived substance is considered to be a true solution after the filtration by 0.15 μm membrane filter. Larsen and Lee[70] recommended the following procedure for differentiating a coal-derived suspension from a true solution: (1) filtration through a 0.2–0.5 μm filter; (2) centrifugation of the solution at over 100 000 g; (3) re-dissolution of a solid obtained by evaporation of a solvent. Of course, it is a quite different case if insoluble substances form by air oxidation or other chemical reactions.

3.3. Colloidal Structures

3.3.1. Solubilities. The solubilities of coal-derived substances increase by silylation by hexamethyldisilazane , i.e., OH $OSiC(CH_3)_3$ or acetylation of OH groups.[52, 54, 71] The results for silylation of a bituminous coal ("untreated coal" in Table 3), and pyridine extracts of the raw and heat treated coal are shown, together with their hydroxyl oxygen content in Table 3.[71] Table 3 shows that 58 % of preasphaltene was converted to a lighter fraction, i.e., asphaltene, by silylation. These results can be attributed to loss of intermolecular hydrogen bonds among coal molecules. Similarly, the pyridine extraction yields of a high-rank bituminous coal (89.6 carbon %) increase from 5% to 90 % by C-octylation at carbons such as benzylic methylene carbons, probably due to the disruption of the π–π stacking of aromatic rings by the introduction of the large octyl group.[63]

As described in Section 2, the heavier extract fraction than preasphaltene, i.e., pyridine insoluble fraction, PI, is obtained by the extraction with 1:1 carbon disulfide – *N*-methyl-2-pyrrolidinone mixed solvent and further fractionation with pyridine, as shown Figure 2.[4] Sanokawa et al.[72] have found that 30–50 % of PI became insoluble in the mixed solvent, but the solubilities recovered by the re- addition of the separated extract fractions (AS and PS in Figure 2) or the addition of the compounds which have strong interaction with coal molecules, to PI.[5,64,72] Especially, tetracyanoethylene (TCNE) and tetracyanoquinodimethane (TCNQ) were found to be very effective. All the solubility experiments above were done using 0.2 μ membrane filter, suggesting that there is no supended particles, described in Section II-B. The results for TCNE addition are shown in Table 4.[5] Table 4 shows that the addition of only 10 mg (2.5 wt%) of TCNE to 0.4 g of PI increased the solubility of PI from two coals in the CS_2 – NMP mixed solvent from 59.6 and 68.4 % to 97.6 and 98.7 %, respectively. Moreover, 14.2 and 31.9 % of the mixed solvent soluble fractions (MS) of PI became pyridine solubles, as shown in the footnote of Table 4. Solubility used here is the fraction of 0.4 g of PI dissolved in 50 ml of the carbon disulfide – *N*-methyl-2-pyrrolidinone mixed solvent at room temperature under ultrasonic irradiaion

Table 3. Effect of silylation on solubility of coal and coal extracts in benzene[71]

	Untreated coal		Pyridine extract[a] of untreated coal		Pyridine extract[a] of tetralin treated coal	
	Before silyl.	After silyl.	Before silyl.	After silyl.	Before silyl.	After silyl.
Benzene insol./pyridine sol. fraction(wt%)	19	10	100	42	67	40
Benzene sol. fraction (wt%)	0	9	0	58	33	60
Hydroxyl oxygen[b]		5.7		5		3.4

[a] 19% and 97% of extraction yields, respectively. [b]Hydroxyl content (wt%) of trimethylsilylated benzene soluble product by silicon analysis.

Table 4. Solubility increase of pyridine insoluble extract fraction (PI) by the addition of tetracyanoethylene (TCNE)[5]

	MI[b]	MS[b]
PI[a] (from Zao Zhuang coal), 0.4g	40.4	59.6
PI 0.4g + TCNE 0.01g	2.4	97.6[b]
PI[a] (from Upper Freeport coal), 0.4g	31.6	68.4
PI 0.4g + TCNE 0.01g	1.3	98.7[c]

[a] Pyridine insoluble fraction of the carbon disulfide – *N*-methyl-2-pyrrolidinone mixed solvent extract. [b]MI and MS are the mixed solvent insoluble and soluble fractions, respectively. [c]These MS include 14.2% (based on MS) and 31.9% of pyridine soluble fractions, respectively.

for 30 min. The studies on IR spectra of the extract fractions and reversibility of the effect of TCNE addition suggest that the solubility increase is caused by the breaking of noncovalent bonds in associated structures of coal molecules by TCNE, which interacts and form new associates with coal molecules which are soluble in the mixed solvent.[5] As the forces for the associate formation charge transfer interaction must be considered first, but the situation here seems more complex, because other strong electron acceptors such as dichlorodicyano-*p*-benzoquinone (DDQ) and *p*-chloranil were not effective for increasing solubility.[64] The extraction yields with the CS_2 – NMP mixed solvent for several bituminous coals also greatly increased by the addition of a small amount of TCNE.[64,73]

3.3.2. Molecular Weight. Molecular weight can be determined from physical properties of a molecularly dispersed solution. It is very difficult to determine a true molecular weight of coal-derived substances, since they tend to associate even at high dilution, and possibly contain fine insoluble substances, i.e., a suspension. Schwager et al.[74] have found that the molecular weights extrapolated at infinite dilution for asphaltenes from five liquefaction processes and their O-silylation derivatives in vapor pressure osmometry (VPO) measurements are almost identical in benzene and THF, respectively. This implies that coal-derived asphaltenes approach complete dissociation as their concentrations approach infinite dilution in both benzene and THF. Molecular weights of 5 asphaltenes obtained are in the range of 380–560 amu. From the comparison of the slope of the molecular weights vs. concentration curve which is considered as a measure of association, hydrogen bonding is suggested to be responsible for association of coal-derived asphaltenes.[75] Hombach[69,75] indicated that usual osmometric methods including VPO is not recommended for molecular weight determinations for complex coal-derived substances, since the van't Hoff equation used for osmotic pressure is not applicable for the substances with polydispersed molecular weights and inhomogeneous chemical structures such as coal asphaltenes. Collins et al.[76] also suggested that there is no accurate method for the molecular weight determinations of coal-derived substances, since coal solutions cannot be viewed as a solution of a series of polymer homologues which is a necessary condition for use of osmotic or light-scattering methods.[76] Hombach[75] has reported that a fraction obtained by ultrafiltration (0.2 and 0.035 μm pore filter) in pyridine solution of pyridine extract from a solubilized bituminous coal have very high molecular weights, i.e., 1.59×10^6 using a low-angle laser light-scattering method. Larsen et al.[77]showed that for relatively low molecular weight coal-derived substances mass spectrometry is available, and molecular weights determined by ^{252}Cf plasma desorption mass spectrometry are in good agreement with those obtained by field ionization mass spectrometry and gel permeation chromatography. As-

phaltenes from distillation residues of liquefaction products of various coals have 260–330 of number-average molecular weight by ^{252}Cf plasma desorption mass spectrometry.[77]

Lee et al.[78] used VPO as a means for determination of the degree of association of coal-derived substances. From the relation between molecular weight and concentration of coal-derived substances in solution, the dissociation constants of dimer, trimer, and higher multimers, and their distribution change with concentration were determined.

3.3.3. Viscosity. Viscosity of coal-derived substances in solution and bulk is related to their associated structures, and in coal liquefaction processes it is important to control high viscosity of coal–solvent mixtures. Bockrath et al.[79] measured the viscosities of preasphaltene, asphaltene (and its acid/neutral and basic components), and oil (pentane soluble) of coal-derived liquids from liquefaction. Figure 9 shows the viscosity of the mixtures of various compositions of acid/neutral and basic asphaltenes for fixed total asphaltene fraction (30 % asphaltene in oil). Figure 9 shows that the viscosity of the mixtures in the oil (upper curve) is greater than would be expected on the basis of a simple additive relationship (lower curve), suggesting that hydrogen bonding between acid/neutral with basic asphaltenes increases viscosity. The preasphaltenes, on a weight basis, have approximately twice the effect on viscosity as do the asphaltenes, probably due to their larger molecular weight and functionality in comparison to the asphaltenes.[79] Bockrath et al.[80] also have showed that intermolecular association involving hydrogen bonding is a prime factor for the viscosity increase which occurred with increased asphaltene concentration in a reference solvent. Similarly the importance of hydrogen bonds largely involving phenolic OH in the viscosity increase was suggested.[50] Arganinski and Jones[81,82] also suggest that the influence on the viscosity of coal-derived preasphaltenes and model compounds in THF was the order hydrogen bonding > molecular weight >> degree of aromatic condensation (charge transfer interaction).

3.3.4. Surface Tension. Surface tension is used for analyzing colloidal properties such as micelles formation. Hayasaka et al.[83] measured the surface tension of *N*-methyl-2-

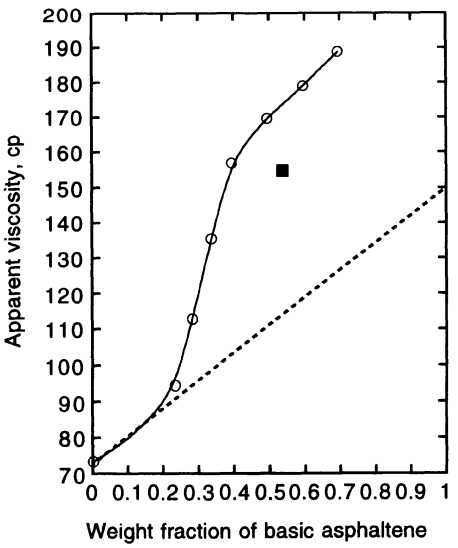

Figure 9. Visosity (upper curve) of the mixtures of various compositions of the acidic/neutral and basic components of asphaltene in pentane soluble oil at 60 as a function of base content.[79] Total asphaltene concentration is fixed as 30 % in the oil. The lower curve is calculated assuming a simple additive relationship from the viscosity of each componenet in the oil.

pyrrolidinone (NMP) solution of acetone soluble (AS) and acetone insoluble/pyridine soluble (PS) fractions of the carbon disulfide – *N*-methyl-2-pyrrolidinone mixed solvent extract of a bituminous coal by the Wilhelmy method. The surface tensions of the solutions freshly prepared by the dilution of the concentrated solution with NMP changed with time, and it took several hours to attain an equilibrium state of lower surface tension. This suggests that the rate of the re-construction to a new association state are very slow. The equilibrium surface tensions of NMP solution of AS decreases with AS concentration and a discontinuity point at some concentration (0.1–0.3 g/dL for two different As's) are observed, where the slope in the surface tension - ln *c* plots changes, suggesting that at this concentration association state abruptly changes, such as the formation of micelles. The discontinuities observed in this study are not so distinct as the case reported for pyridine solution of a petroleum asphaltene by Sheu et al.[84,85] The discontinuity concentration for the petroleum asphaltene was also found to be about 0.03 g/dL, one order lower than those for the coal extracts, reflecting the difference of micelle structures probably due the difference between chemical structure, molecular weight and shape of both constituents. For PS from the same coal as AS, on the other hand, discontinuity was not observed. Further study is needed to clarify this.

3.3.5. X-Ray Analysis. Ho and Briggs[86] used small angle X-ray scattering measurements to determine the size and shape of micelles (associates) from asphaltene and preasphaltene in a solvent such as pyridine and THF. The fraction of asphaltene or preasphaltene forming micelles in solution depends on their concentration and molecular size, π–π and/or hydrogen bonding properties of the solvent and on the agitation. A stepwise association state of micelles proposed is shown in Figure 10.[86] The majority of the micelles are spherical with a diameter of 22–38 Å, and the larger micelles in the 80–100 Å range and greater than 220 Å are also present. Floc structures with dimensions in excess

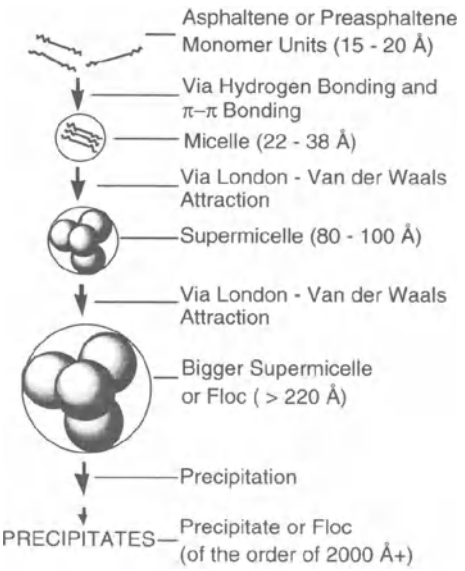

Figure 10. Proposed association mechanism of asphaltenes and preasphaltenes in solution.[86]

Table 5. Fractal dimention, d, and particle radius, R_0, for untreated and O-methylated pyridine extracts in solutions[89]

Coal	C %[a]	Treatment	Fractal dimention d	Ro (Å)
Illinois No. 6	78	untreated	ND	72±6
		O-methylated	1.70±0.04	72±6
Wyodak-Anderson	75	untreated	1.79±0.01	81±6
		O-methylated	2.46±0.01	91±6
Beulah-Zap	73	untreated	2.13±0.03	85±6
		O-methylated	2.29±0.04	85±6

[a] Maf. ND, not determined.

of 1000 Å form when asphaltene – solvent systems are allowed to stand for extended periods, which are destroyed by mechanical shear as in ultrasonic agitation. Upon extended standing the floc structure returns. Schwager et al.[87] showed from X-ray diffraction analysis of asphaltenes (not in solution) that the average stacking height of the aromatic clusters, L_c, ranges between 10.6–13.6 Å, corresponding to the average number of aromatic sheets of 3.9 – 4.8. The average layer diameter of the sheets is 8.0–10.3 Å. The application of small-angle X-ray scattering techniques to the study of oxidized aged coal liquefaction products indicates that the rapidly increasing viscosity is well correlated with the appearance of larger colloidal scattering centers, with average radii of gyration in the region of 50 Å.[88]

3.3.6. Small-Angle Neutron Scattering. Although small-angle neutron scattering (SANS) studies on the size distribution and shape of petroleum asphaltene associates in solution have been actively carried out, only a few SANS studies on coal-derived substances were reported so far. Cody, Thiyagarajan et al.[89,90] measured SANS of deuteropyridine solutions of pyridine extracts and their O-methylated derivatives from three coals shown in Table 5.[89] Laser desorption mass spectrometry of the extracts, untreated and methylated, indicates a predominance of relatively low mass materials, with molecular weight of the order 300 and a mass envelope which tails off around a thousand daltons.[89] Table 5 shows the fractal dimension, d, and particles radii, R_0, in their pyridine solution. Table 5 indicates that the solution structure of the extracts exists as small particles, with radii about 80 Å, and the values of d (<3) indicate that the small particles further form a randomly assembled, loosely extended aggregates, as shown in Figure 11. Considering the molecular weights and radii for the particles, the elemental particles are themselves aggregates of the extract molecules. ξ in Figure 11, the radius of the loose aggregates could not be estimated due to the lower limit of Q. O-methylation is expected to decrease aggregation and/or make aggregates more loose, since hydrogen-bonding interac-

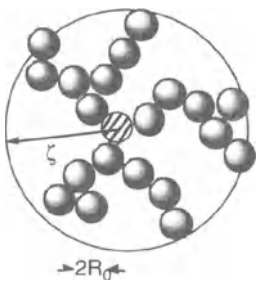

Figure 11. A simple depiction of a pyridine solution of pyridine extract.[89] The double-headed arrow highlights the smallest scattering length in the system, the diameter ($2R_0$) of the smallest particle. The circle depicts the radial limit of the aggregates, with a radius ζ.

tions are considered to constitute the dominant associative interparticle interaction. However, Table 5 suggests that the change in the solution state due to O-methylation is slight, and it induces more densed packing of aggregates for the two coals, in which *d* increases by O-methylation. The effect of hydrogen bonding on the solution structure is, then, considered to be manifested predominantly in the topology of the extended aggregated structures i.e., in the magnitude of *d*. SANS data on the carbon disulfide – *N*-methyl-2-pyrrolidinone mixed solvent extracts in solution by Cody, Thiyagarajan et al.[91] are interesting. The solution of pyridine insoluble/the mixed solvent soluble component, PI (Figure 2) in the mixed solvent contains no large aggregates, but the solution of pyridine extract from the same coal, which may be a lighter component than PI, contains large aggregates, though a light component seems less aggregative due to low content of functional groups.

There seems to be still disagreement regarding the shape of aggregates of petroleum asphaltenes in solution. SANS is undoubtedly a powerful tool to reveal complex colloidal structures of asphaltenes and other heavy components of petroleum and coal, with the combination of other chemical and physical methods. But we have to wait for some time until clear pictures about their size and shape are obtained.

3.3.7. Computer Simulation. Computer-aided molecular design (CAMD) has been utilized in the designs of the drugs and new functional materials. Recently, it has been applied to coal.[92–95] Energetically stable three dimensional structure (conformation) of the extract fractions of coal was constructed by computer simulation.[95] The structure in the energy-minimum state for three model molecules (Figure 12-b) of acetone-insoluble/pyri-

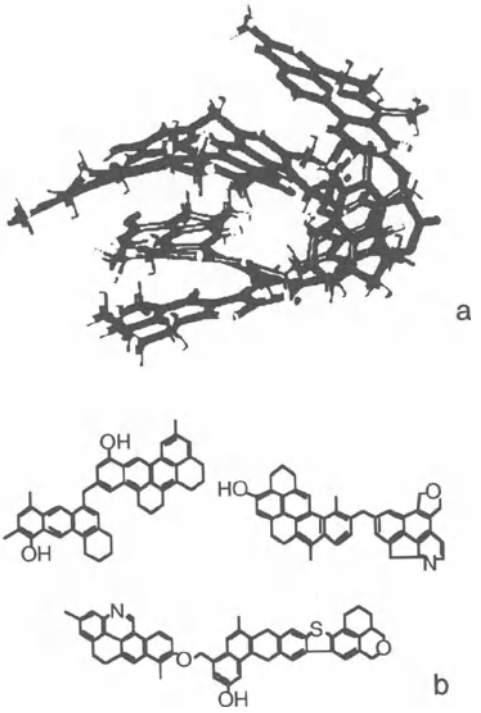

Figure 12. An associated structure (a) simulated for three molecules (b) of PS (acetone insoluble/pyridine soluble fraction) of a bituminous coal.[95]

dine soluble fraction, PS, obtained from the carbon disulfide – *N*-methyl-2-pyrrolidinone mixed solvent extraction of a bituminous coal is shown in Figure 12-a.[95] The most stable structure for the PS fraction was estimated to be an associated structure and the π–π interactions between aromatic ring systems play a major role to form the association. For a detailed discussion on association behaviors of coal-derived substances in solution a lot of reliable data on their structures and thermodynamics such as a phase diagram in solution are needed.

4. CONCLUSION

The chemical structures of asphaltenes from coal are different from petroleum asphaltenes in their higher content of aromatic rings and functional groups such as OH groups, and lower molecular weight. Coal also has heavier components than asphaltenes, i.e., preasphaltenes and further heavier ones, which cannot be usually obtained from petroleum. The structures of these components are not well understood, as compared to those of asphaltenes and oils. Comparison of colloidal structures and formation dynamics of coal-derived asphaltenes (and heavier components than asphaltenes) in solution with those of petroleum-derived asphaltenes may be fruitful for a clear understanding of these complex, but challenging targets. However research on these issues has not yet been extensively carried out for coal derivatives, compared to those for petroleum, probably because heavy components from coal are little commercially used as themselves. More researches on the issues above and also those on thermodynamics of extreme complex, multi-component mixtures such as asphaltenes in solution, which include a phase diagram and a gel - sol transitions, is highly needed, together with more precise chemical structure elucidations of coal and coal derivatives.

REFERENCES

1. W. Steedman, Fuel Process. Technol., 10, 209 (1985).
2. V.I. Stenberg, R.J. Richard, J. Baltisberger, K.M. Patal, K. Raman, N.F. Woolsey,in "Coal Science," M.L. Gorbaty, J.W. Larsen, I. Wender (Ed.) Academic Press, New York, Vol.2,125 (1982).
3. K. Iwata, H. Itoh, K. Ouchi, Fuel Process. Technol., 3, 25 (1980) .
4. M. Iino, T. Takanohashi, H. Ohsuga, K. Toda, Fuel, 67, 1639 (1988).
5. M. Iino, H. Liu, N. Hosaka, H. Kurose, T. Takanohashi, Prepr. Pap.-Am. Chem. Soc., Div. Fuel Chem., 42(1),248 (1997).
6. M. Nishioka, Fuel, 72, 1719 (1993).
7. B.C. Bockrath, R.P. Noceti, Fuel Process. Technol., 2, 143 (1979).
8. L.A. Heredy, M.B. Neuwarth, Fuel, 41, 221 (1962).
9. K. Ouchi, K. Imuta, Y. Yamashita, Fuel, 44, 205 (1965).
10. L.J. Darlage, J.P. Weidner, S.S. Block, Fuel, 53, 54 (1974).
11. G.A. Olah, M.R. Bruce, E.H. Edelson, A. Husain, Fuel, 63, 1130 (1984).
12. H.W. Sternberg, C.L.D. Donne, P. Pantages, E.C. Moroni, R.E. Markby, Fuel, 50, 432 (1971) .
13. H.W. Sternberg, C.L.D. Donne, Fuel, 53, 172 (1974).
14. N. Cyr, M. Gawlak, D. Carson, B. Ignasiak, Fuel, 62, 412 (1983).
15. B. Ignasiak, D. Carson, M. Gawlak, Fuel, 58, 833 (1979).
16. C.J. Collins, E.W. Hagaman, R.M. Jones, V.F. Raaen, Fuel, 60, 359 (1981).
17. T.G. Squires, C.G. Venier, J.D. Hunt, J.C. Shei, B.F. Smith, Fuel, 61, 1170 (1982) .
18. R.R. Chambers Jr., D. Mckamey, Fuel, 63, 868 (1984).
19. N.E. Cooke, R.P. Gaikwad, Fuel, 63, 1468 (1984) .
20. F.K. Schwager, B.M. Thamers, Anal. Chem., 49, 2363 (1978).

21. A. Marzec, D. Bodzek, T. Krzyzanowska, in "Organic Chemistry of Coal," ACS Symposium Series 71, J.W. Larsen (Ed.), Am. Chem. Soc., 71 (1978).
22. C.E. Snape, K.D. Bartle, Fuel, 63, 883 (1984).
23. C.E. Snape, K.D. Bartle, Fuel, 64, 427 (1985).
24. K. Ouchi, Fuel, 64, 427 (1985).
25. J.R. Brown, W.R. Ladner, Fuel, 39, 87 (1960).
26. H.L. Retcofsky, R.A. Friedel, Fuel, 47, 487 (1968).
27. M. Kanda, M. Kooriki, Y. Sanada, Fuel, 57, 676 (1978).
28. T.H. Fletcher, S. Bai, R.J. Pugmire, M.S. Solum, S. Wood, D.M. Grant, Energy & Fuels, 7, 734 (1993).
29. S. Friedman, M.L. Kaufman, W.A. Steiner, I. Wender, Fuel, 40, 33 (1961).
30. M. Iino, T. Takanohashi, S. Obara, H. Tsueta, Y. Sanokawa, Fuel, 68, 1588 (1989).
31. K.D. Bartle, T.G. Martin, D.F. Williams, Fuel, 54, 226 (1975).
32. M. Makabe, K. Ouchi, Fuel, 58, 43 (1979).
33. M. Makabe, K. Ouchi, Fuel Process. Technol., 2, 131 (1979).
34. K. Ouchi, K. Suzuki, T. Katoh, H. Itoh, Fuel, 64, 133 (1985).
35. T. Sakabe, K. Inoue, K. Ouchi, H. Honda, J. Fuel Soc. Jpn., 32, 610 (1953).
36. K. Iwata, F. Mondragon, H. Itoh, K. Ouchi, Fuel, 63, 1528 (1984).
37. M. Nomura, K. Matsubayashi, T. Ida, S. Murata, Fuel Process. Technol., 31, 169 (1992).
38. J.M. Charlesworth, Fuel, 59, 865 (1980).
39. P. Redlich, W.R. Jackson, F.P. Larkins, Fuel, 64, 1383 (1985).
40. L.L. Anderson, K.E. Chung, R.J. Pugmire, J. Shabtai, in "New Approaches in Coal Chemistry." ACS Symposium Series 169, B.D. Blaustein, B.C. Bockrath, S. Friedman (Eds.), Am. Chem. Soc., 2231981 (1978).
41. C.E. Snape, W.R. Ladner, Fuel Process. Technol., 8, 155 (1984).
42. J.H. Shinn, Fuel, 63, 1187 (1984).
43. K. Nakamura, T. Takanohashi, M. Iino, H. Kumagai, M. Sato, S. Yokoyama, Y. Sanada, Energy & Fuels, 9, 1003 (1995).
44. T. Katoh, K. Ouchi, Fuel, 64, 1260 (1985).
45. T. Katoh, K. Ouchi, Fuel, 66, 58 (1987).
46. T.F. Yen, Amer. Chem. Soc., Div. Pet. Chem., Prep., 24, 901 (1979).
47. O.C. Mullins, S. Mitra-Kirtley, J.V. Elp, S.P. Cramer, Applied Spectroscopy, 47, 1268 (1993).
48. H.W. Sternberg, R. Raymond, F.K. Schweigehardt, Science, 188, 49 (1975).
49. F.R. Brown, S. Friedman, L.E. Makovsky, F.K. Schweighardt, Appl. Spectrosc., 31, 241 (1977).
50. S.R. Taylor, N.C. Li, Fuel, 57, 117 (1978).
51. F.K. Schweighardt, R.A. Friedel, H.L. Retcofsky, Appl. Spectrosc., 30, 291 (1976).
52. K.C. Tewari, N. Kan, D.M. Susco, N.C. Li, Anal. Chem., 51, 182 (1979).
53. K.C. Tewari, J. Wang, N.C. Li, H.J.C. Yeh, Fuel, 58, 371 (1979).
54. K.M. Patel,V.I. Stenberg, R.J. Baltisberger, N.F. Woolsey, K.J. Klabunde, Fuel, 59, 449 (1980).
55. K.A. Gould, Fuel, 58, 550 (1979).
56. C.E. Snape, K.D. Bartle, Fuel, 58, 898 (1979).
57. J.W. Larsen, A.J. Baskar, Energy & Fuel, 1, 230 (1987).
58. K. Miura, K. Mae, F. Morozumi, Prepr. Pap.-Am. Chem. Soc., Div. Fuel Chem., 42(1),209 (1997).
59. P.B. Hirsch, Proc. Roy. Soc., A226, 143 (1954).
60. D.L. Wertz, M. Bissell, Energy & Fuels, 8, 613 (1994).
61. I. Schwager, T.F. Yen, Fuel, 58, 219 (1979).
62. E.M.Y. Quinga, J.W. Larsen, Energy & Fuels, 1, 300 (1987).
63. M. Miyake, L.M. Stock, Energy & Fuel, 2, 815 (1988).
64. H. Liu, T. Ishizuka, T. Takanohashi, M. Iino, Energy & Fuels, 7, 1108 (1993).
65. M. Nishioka, L.A. Gebhard, B.G. Silbernagel, Fuel, 70, 341 (1991).
66. S. Duber, J. mikosz, Fuel, 72, 267 (1993).
67. H.L. Retcofsky, M.R. Hough, M.M. Maguire, R.B. Clarkson, Am. Chem. Soc. Adv. Chem. Ser.,192, 37 (1981).
68. C.M. White, C.E. Schmidt, Fuel, 66, 1030 (1987).
69. H.-P. Hombach, Fuel, 61, 215 (1982).
70. J. W. Larsen, D. Lee, Fuel, 62, 918 (1983).
71. D. Seyferth, D.P. Duncan, H.W. Sternberg, Fuel, 58, 74 (1979).
72. Y. Sanokawa, T. Takanohashi, M. Iino, Fuel, 69, 1577 (1990).
73. T. Ishizuka, T. Takanohashi, O. Ito, M. Iino, Fuel, 72, 579 (1993).
74. I. Schwager, W.C. Lee, T.F. Yen, Anal. Chem.,49, 2363 (1977).
75. H.-P. Hombach, Fuel, 60, 663 (1981).

76. C.J. Collins, R. Triolo, M.H. Lietzke, Fuel, 63, 1202 (1984).
77. J.W. Larsen, A.R. Lapucha, P.C. Wernett, W.A. Anderson, Energy & Fuel, 8, 258 (1994).
78. W.C. Lee, I. Schwager, T.F. Yen, Prepr. Pap.-Am. Chem. Soc., Div. Fuel Chem., 23(2), 37 (1978).
79. B.C. Bockrath, R.B. Lacount, R.P. Noceti, Fuel Process. Technol., 1, 217 (1978).
80. B.C. Bockrath, R.B. Lacount, R.P. Noceti, Fuel, 59, 621 (1980).
81. M.B. Jones, J.K. Argasinski, Prepr. Pap.-Am. Chem. Soc., Div. Fuel Chem., 30(4), 250 (1985).
82. J.K. Argasinski, M.B. Jones, Prepr. Pap.-Am. Chem. Soc., Div. Fuel Chem., 32(1), 604 (1987).
83. K. Hayasaka, T. Takanohashi, M. Iino, Energy & Fuels, 10, 262 (1996).
84. E.Y. Sheu, M.M. De Tar, D.A. Storm, Fuel, 67, 1639 (1988).
85. E.Y. Sheu, D.A. Storm, Fuel, 73, 1368 (1994).
86. B. Ho, D. Brigs, Colloids Surf., 4, 285 (1982).
87. I. Schwager, P.A. Farmanlan, J.T. Kwan, V.A. Weinberg, T.F. Yen, Anal. Chem., 55, 42 (1983).
88. M. Kalliat, P.W. Schmidt, D.H. Finseth, Fuel, 63, 1178 (1984).
89. G.D. Cody, P. Thiyagarajan, R.E. Botto, J.E. Hunt, R.E. Winans, Energy & Fuels, 8, 1370 (1994).
90. P. Thiyagarajan, G.D. Cody, J.E. Hunt, R.E. Winans, Prepr. Pap.-Am. Chem. Soc., Div. Fuel Chem., 40(3),397 (1995).
91. G.D. Cody, M. Obeng, P. Thiyagarajan, Energy & Fuels, 11, 495 (1997).
92. G.A. Carlson, Energy & Fuels, 6, 771 (1992).
93. J.L. Faulon, K.A. P.G. Hatcher, G.A. Carlson, K.A. Wenzel, Fuel Process. Technol., 34, 277 (1993).
94. M. Nomura, K. Matsubayashi, T. Ida, S. Murata, Fuel Process. Technol., 31, 169 (1992).
95. T. Takanohashi, M. Iino, K. Nakamura, Energy & Fuels, 8, 395 (1994).

Chapter VII

CHARACTERIZATION AND PHASE BEHAVIOR OF ASPHALTENIC CRUDE OILS

Kevin A. Ferworn[1] and William Y. Svrcek[2*]

[1]PENCOR Process Technologies, Inc.
8826 Interchange Drive
Houston, Texas 77054
[2]University of Calgary
Chemical and Petroleum Engineering
Calgary, Alberta, Canada T2N 1N4

1. INTRODUCTION

The development of thermodynamic and kinetic models describing asphaltene precipitation and deposition from both pressurized (live) and atmospheric (dead) crude oils has been hampered by a lack of detailed characterization and phase behavior data. Specifically, standard laboratory analyses that are suitable for vapor–liquid equilibria (VLE) modeling are usually insufficient for representing complex molecular structures such as asphaltene micelles.

Asphaltene molecules (or micelles) are a specific solubility class of petroleum and are most commonly found in heavy oils or bitumens; that is, asphaltenes are defined as the n-pentane or n-heptane insoluble fraction of an oil.[1] This operational definition is a consequence of the extremely complex structure of asphaltenes which include highly aromatic cores, long chain aliphatic groups, heteroatoms (nitrogen, sulfur and oxygen) as well as trace quantities of heavy metals (vanadium and nickel). Therefore, it is virtually impossible to describe any asphaltene purely by its chemical structure.

Asphaltene molecules are believed to be surrounded by resins that act as peptizing agents which maintain the asphaltenes in a colloidal dispersion (as opposed to a solution) within the crude oil.[2] The resins are typically composed of a highly polar end group, which often contain heteroatoms such as oxygen, sulfur and nitrogen, as well as long, non-polar paraffinic groups.[3] The resins are attracted to the asphaltene micelles through their

* Formerly with DBR Fluid Properties, Inc.

end group. This attraction is a result of both hydrogen bonding through the heteroatoms and dipole-dipole interactions arising from the high polarities of the resin and asphaltene.[4] The paraffinic component of the resin molecule acts as a tail making the transition to the relatively non-polar bulk of the oil where individual molecules also exist in true solution.

Numerous experimental investigations have been undertaken to study the general nature and specific parameters that affect asphaltene deposition. However, most of the reported data are restricted to measurements at ambient pressure conditions on stock tank oils. Consequently, they do not provide adequate information for petroleum production processing. Asphaltene precipitation (for example, in well tubings, flowlines and/or process equipment), normally occurs at elevated temperature and pressure conditions. It has been established that the effect of composition and, in turn, of pressure on asphaltene deposition is stronger than the effect of temperature. However, there still exists some disagreement in the literature regarding the effect of temperature on asphaltene precipitation. In general, the parameters and properties that are reported to affect asphaltene deposition and/or flocculation include:

- Composition
- Pressure
- Asphaltene and resin concentrations in the reservoir fluid
- Electrokinetic effects induced by streaming potential generation during reservoir fluid flow
- Temperature
- Water-cut

With respect to pressure, asphaltene precipitation is expected to begin at pressures in excess of saturation. This finding is mainly based on field observations in well tubings which indicate that asphaltene deposition occurs below the depth at which the bubble point pressure is expected. This phenomenon was largely ascribed to the different compressibilities of the lighter ends and the heavier components of live crude oil. As a matter of fact, the relative volume fraction of the lighter ends within the crude would increase as the pressure of the single-phase reservoir fluid approaches its bubble point. Such an effect is similar to adding a light hydrocarbon (precipitant) to a crude causing asphaltene depeptization. Below the bubble point, the low molecular weight hydrocarbons vaporize from the liquid as a gas phase causing an increase in the density of the liquid phase (i.e., a change in the liquid composition). Recognizing that increased light ends can cause asphaltene precipitation, the vaporization of light ends can result in an increased asphaltene solubility in the crude oil.

The ratio of resins to asphaltenes is often more important than the absolute asphaltene content. In fact, severe asphaltene precipitation can often be encountered in reservoirs with very low total asphaltene contents. Conversely, there have been reports of high asphaltene content oils that show no appreciable deposition. For example, the Mata-Acema crudes (in Venezuela) with asphaltene contents of 0.4 to 9.8 wt % have asphaltene deposition problems, whereas, the Boscan crude with 17.2 wt % asphaltene content does not have asphaltene deposition problems.[5] As a general rule, oils containing 1:1 or greater weight ratio of resins to n-pentane asphaltenes are less subject to asphaltene deposition.[3]

The available laboratory and field data indicate that asphaltenes separated from crude oils consist of various molecules with molecular weights ranging from below 1000 to hundreds of thousands.[6,7,8] Such an extensive range of asphaltene size distribution suggests that asphaltenes may be partly dissolved and partly suspended/peptized in the crude

oil. While the first scenario is a relatively well understood reversible thermodynamic process, the latter is a more complex, irreversible colloidal mechanism.

Based on the previous discussion, the structure, characteristics and phase behavior of asphaltenes and asphaltenic oils are very complex. As a consequence, alternative analytical techniques (e.g., Gel Permeation Chromatography, Field Desorption Mass Spectroscopy) have been utilized to characterize both the molecular size and structure of asphaltenes and other heavy molecules. Further, the phase behavior of both live and dead asphaltenic crudes has been measured. As such, the experimental program was undertaken with the goal of providing comprehensive compositional and phase behavior data for predictive precipitation models.

2. EXPERIMENTAL EQUIPMENT AND PROCEDURES

2.1. Asphaltene and Crude Oil Characterization

As mentioned previously, standard compositional analysis to C_7+, C_{30}+ or even C_{90}+ are usually insufficient for mathematically representing the large, aromatic structures attributed to asphaltene molecules. As a consequence, more detailed compositional methods have been developed to represent these heavy molecules both in terms of molecular size and structure.

2.1.1. Gel Permeation Chromatography. Gel Permeation Chromatography (also referred to as Size Exclusion Chromatography) is a liquid column chromatographic technique which sorts molecules according to molecular size and shape.[9] The sample solution is introduced into the column, which is filled with a highly cross-linked, porous packing, and is then carried through the separation zone by a mobile effluent. The size classification takes place by repeated exchange of the solute molecules between the bulk solvent of the mobile phase and the stagnant liquid phase within the pore space of the packing. The pore size range of the packing determines the molecular size separation characteristics of the column. The distributed sample exiting the chromatographic column is identified with a refractive index (RI) or ultra violet (UV) detector that presents the concentration response against retention time or volume.

Figure 1 provides a schematic of the GPC apparatus used for the measurement of petroleum molecular weight distributions. The main component of the system was a Hewlett-Packard, HP 1090A, high performance liquid chromatograph (HPLC). The operation of the chromatograph and injection system was controlled by a personal computer which also directed data acquisition.

Petroleum samples were dissolved in tetrahydrafuran to prepare 1 wt% solutions for injection to the HPLC. Tetrahydrafuran (THF) was also used as the carrier solvent in this application at a constant flow rate of 0.1 mL/min. Injection volumes to the apparatus were made in 15 μL increments and the system temperature was maintained at 30°C. Molecular separation occured through two GPC columns charged with PLgel, a highly cross-linked spherical polystyrene / divinylbenzene matrix. Columns of 100Å and 1000Å pore sizes allowed for the separation of compounds with molecular weights ranging from 10–40,000 g/mole. Each column was 30 cm in length with an inside diameter of 7.55 mm.

As the reference sample was eluted from the separation columns, a refractive index detector measured its concentration; this response was plotted against elution time to produce a distribution profile. In order to convert these elution profiles to molecular weight dis-

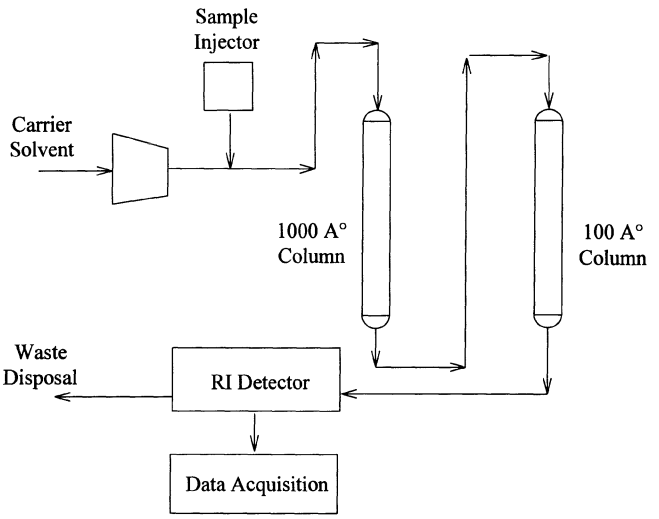

Figure 1. Gel Permeation Chromatography (GPC) experimental schematic with separation columns in series and a Refractive Index Detector.

tributions, the raw data was usually transformed by a calibration curve developed from the elution times of standard polystyrene compounds through the GPC. However, a number of researchers have discussed the problem of converting elution profiles to distributions for molecules with structures not similar to the standards.[10,11] Specifically, GPC separates molecules based on their molecular characteristics (which include molecular size, shape, polarity, charge, etc.) as opposed to their molecular weight. As a consequence, molecules of varying structure (but the same molecular weight) may elute at different times.

In response to this concern, new calibration techniques that consider the structure of the reference and sample molecules have been introduced. However, these methods require extensive analytical data including proton nuclear magnetic resonance (^{1}H NMR) and elemental analysis measurements.[11] For this reason, a simpler analytical technique was used to correct the calibration curve; this was accomplished by replacing the polystyrene standards with actual hydrocarbon molecular groups.[12] An advantage of GPC is the ability to separate and collect specific fractions of the sample during measurement.[10] As a result, oil fractions were gathered at different elution times and then analyzed for their weight average molecular weight by Vapor Pressure Osmometry (VPO). These results were then used to develop a new calibration curve for the GPC apparatus. In short, the new calibration curve yielded more representative molecular weight distributions than those obtained by conversion from polystyrene standards.[12]

While the resolution of crude oils into molecular weight distributions represented a marked improvement over simple lumped components in thermodynamic model predictions, different physical properties may be exhibited by compounds of similar molecular weights (for example, a paraffinic and highly aromatic molecule of the same molecular weight will have very different densities, melting temperatures, etc.).[1] Similarly, a narrow boiling fraction of petroleum may contain molecules of widely ranging molecule weights due to their structural differences. Therefore, it is important to classify the whole crude distribution into sub-fractions based on molecular structure. In this work the selected separation scheme was a S.A.R.A. representation (Saturates, Aromatics, Resin and Asphalte-

nes). This scheme was selected as it separates the asphaltene fraction and provides a quantitative estimate of the crude resin (or polars) concentration. Additionally, the saturates fraction is useful as a tie to more common C_{30}+ GC analyses that are usually completed on pressurized samples before they are flashed to atmospheric conditions.

Two methods were used in the separation of atmospheric oils into their S.A.R.A. constituents. 1) a High Performance Liquid Chromatographic (HPLC) method utilizing the GPC experimental system and 2) a Liquid– Solid Chromatographic (LSC) method based on the principles of gel-clay adsoption.

The HPLC method consisted of three main steps.[13,14] A sample of crude oil was dissolved in known volume of normal pentane. The mixture was then shaken for at least 8 hours at which time the asphaltenes were filtered from the precipitant/oil mixture. Finally, the pentane solubles (deasphalted oil containing saturates, aromatics and resins; often called maltenes) were processed through the HPLC.

The key to the separation of the saturate, aromatic, and resin fractions of the crude oil by HPLC was the type of column chosen to complete the fractionation. A column packed with an alkyl amine modified silica gel was utilized as it offered unique selectivity for the paraffinic (saturate) and aromatic hydrocarbons in crude oil. It is important to note that the experimental apparatus for HPLC separations was the same as that for GPC measurements except for the energy analysis column and a column switching valve for backflushing. The HPLC apparatus is shown in Figure 2.

As the pentane solubles were introduced to the HLPC column, the fractions were adsorbed onto the column packing. The characteristics of each hydrocarbon group dictated their retention time within the packing and the net result was that the saturate fraction eluted first and was sampled by a refractive index (RI) detector. The aromatics eluted next and an ultraviolet absorbance (UV) detector measured their composition. Finally, the column was backflushed and the resins (or polars) were sampled and measured by the UV detector. To conclude the analysis, the fractions were collected and weighed providing an overall mass balance.

A second method (liquid–solid chromatography, LSC) was also utilized for the preparation of S.A.R.A. fractions that were later analyzed using Field Desorption Mass Spectroscopy. The LSC procedure is common to petroleum laboratories and is standardized for use throughout the industry.[15] A small sample of crude oil was dissolved in a

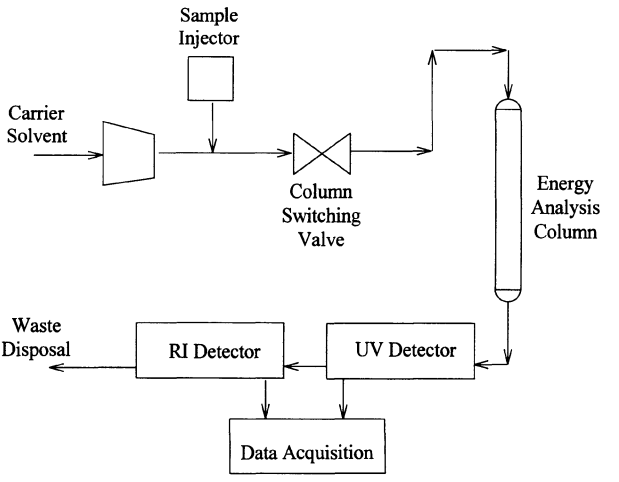

Figure 2. High Performance Liquid Chromatography (HPLC) experimental schematic. The system is similar to the GPC apparatus but contains an Energy Analysis separation column, Refractive Index and Ultra Violet detectors and a switching valve for backflushing the system.

volume of benzene equal to the sample weight in grams. When fully dissolved, n-pentane was introduced in a measured volume for each mL of benzene previously added.[16] This mixture was stoppered, shaken for a short period and then left to stand for at least two hours. The solids were filtered and washed with hot pentane until the washings were colorless; this filter residue represented the asphaltene fraction of the original crude.

The filtrate from this process was transferred to a chromatographic column charged with glass wool and Attapulgus clay (or Fuller's Earth). After recycling the mixture through the column for at least two hours, the resin fraction of the crude was absorbed onto the clay while the saturate and aromatic fractions were drained into a kettle. The resins were desorbed from the clay by refluxing methyl ethyl ketone for a period of one hour. After evaporating the ketone solvent, the remaining fraction represented the resin component of the crude.

The saturate/aromatic mixture was then fed to a second chromatographic column charged with alumina over a base of silica gel. The solution was followed into the column by n-pentane and then benzene. The pentane effluent was collected and then evaporated to dryness to yield the saturate fraction. Similarly, the benzene effluent was treated to produce the aromatic fraction.

This LSC procedure was used to prepare S.A.R.A. fractions for analysis by Field Desorption Mass Spectroscopy.

2.1.2. Field Desorption Mass Spectroscopy. Field Desorption Mass Spectroscopy (FDMS) has shown promise for the molecular characterization of heavy hydrocarbon molecules.[15] Specifically FDMS was selected for heavy component analysis as it can ionize molecules without initial vaporization; this permits the analysis of non-volatile components (i.e., asphaltenes).

In FDMS molecules are adsorbed on an emitter which is typically a 10 μm tungsten wire covered with carbon microneedles (the role of the emitter is chiefly to produce a high electric field focused on the tip of its microneedles due to their very small radii of curvature). An electric current is applied to the emitter (with a potential gradient approaching 10^8 volts/cm). Under the influence of these fields a valence electron tunnels from the molecule to the anode to produce an ion radical. With accurate control of the emitter current the molecular ion is released from the anode with minimum fragmentation producing a mass spectra for even the heaviest organic molecules.

A Micromass Autospec Mass Spectrometer was utilized for characterizing heavy hydrocarbon samples (the Autospec is a high resolution, magnetic sector instrument). In a typical trial, approximately 10 μg of sample was coated onto the emitter. It should be noted that consistent loading of sample onto the emitter was crucial to the operation of the spectrometer and required a significant amount of experience.[17] Additionally, the small sample size resulted in short run times which reduced the time available for tuning the spectrometer on a sample before taking the spectrum. In order to minimize the limitations of the small single charge, multiple samples were often run and then integrated.

2.2. Asphaltene and Crude Oil Phase Behavior

Asphaltene and crude oil phase behavior measurements are categorized depending on whether the procedures utilize live or dead oil samples. Specifically, the measurement of asphaltene particle size distributions was completed on atmospheric samples while the asphaltene precipitation onset tests were performed on live, pressurized fluids.

2.2.1. Asphaltene Particle Size Distributions. The measurement of the kinetics of asphaltene precipitation was performed with a Brinkmann 2010 laser particle analyzer. This apparatus is a direct particle size analyzer; that is, no calibration is required. The analyzer is driven by a personal computer that executes operational software and controls data collection. The basic concepts involved in the operation of the analyzer are as follows.

A fine, low-energy red beam is emitted by a Helium/Neon laser and focused through a series of objectives to a rotating wedge prism. The prism spins the laser beam into a circular, optically defined path and is focused thereafter to a spot smaller than one micron inside the measuring cell. The beam diverges after the cell onto a photodiode, registering optical power. As the scanning radius of the circular path is defined and the rate of rotation of the prism is precisely monitored, the peripheral velocity of the beam is easily determined. The basis of measurement is to monitor the optical power impinging on the photodiode against time. As the beam strikes the first interface of a light-scattering or light-absorbing particle, a discreet, sharp decay of the signal occurs and a lower level is maintained during the transition period. At the second interface, the signal recovers upward to the initial value, producing a time-based square pulse. The length of this pulse multiplied by the angular velocity of the beam provides the diameter of the measured particle.

As in many experimental applications involving crude oils, the opacity of a petroleum or petroleum-precipitant mixture is key to determining alterations in the system conditions. For example, researchers[18,19] have discussed the difficulty in visually determining the onset of asphaltene agglomeration and have therefore, utilized experimental techniques including small angle neutron and x-ray scattering. In this work, a microflow cell was employed to overcome laser absorption by the dark fluid.[20,21] The sampling region in this cell was approximately 1 mm thick allowing for the laser beam to pass through even relatively dark oil mixtures while still scanning and measuring the sample.

A schematic of the experimental apparatus for the measurement of asphaltene agglomerate particle size distributions is given in Figure 3. Initially, the fluid reservoir was charged with a given volume of n-alkane precipitant. An injection of the required volume (or mass) of asphaltic crude oil was made to the reservoir and upon first contact, asphaltenes began to agglomerate and precipitate. The reservoir was sealed (to prevent external oxygen from access to the mixture) and the fluids were stirred throughout the experiment to ensure that the asphaltenes were well suspended. Finally, a vortex breaker was also installed to destroy the vortex created by the magnetic stir bar; the main objective in this technique was to keep the asphaltene agglomerates suspended in the crude oil-precipitant mixture.

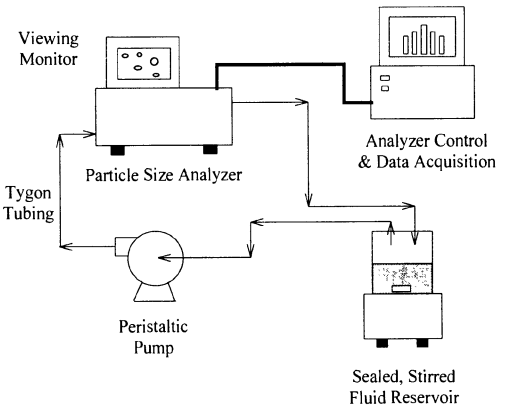

Figure 3. Laser Particle Analysis schematic including fluid reservoir, circulation pump, particle size analyzer and viewing monitor.

Initial experiments were completed at 22°C and atmospheric pressure although the development of a new thermodynamic cell allowed for the measurement of asphaltene agglomeration kinetics at elevated temperatures and pressures.[22]

2.2.2. Asphaltene Precipitation Onset Measurements. The experimental system utilized for the measurement of live oil asphaltene precipitation onset conditions is shown schematically in Figure 4. The solids detection system (SDS) is based on the transmittance of a low intensity laser light through fiber optic transmission probes mounted across a visual phase behavior cell. The main body of the cell consisted of a Pyrex glass cylinder 20.3 cm long with an internal diameter of 3.2 cm. This translates to an effective working volume of approximately 130 cm^3. The cylinder was housed inside a steel shell with vertical tempered glass plates to permit visual observation of the internal Pyrex tube. The volume, and hence pressure of the fluids under investigation, were controlled by a variable volume displacement pump. The same displacement fluid was connected to the outer steel shell to maintain a balanced differential pressure on the Pyrex cylinder. Equilibration of the fluid under investigation was achieved by means of a specially designed, magnetically coupled, impeller mixer. The entire PVT cell was mounted inside a temperature controlled, forced air circulation oven. The cell temperature was measured with a platinum RTD and displayed on a digital indicator with an accuracy of 0.2°F while pressure was monitored with a calibrated digital Heise pressure gauge. The maximum operating pressure and temperature for the SDS are 15,000 psi and 360°F, respectively.

The laser utilized in the SDS operates in the near IR spectrum and provides good sensitivity for the measurement of crude oil phase behavior. The laser has an power rating of 10^{-3} W and will register approximately 10^{-6} W on the power meter (which is sensitive to readings of 10^{-12} W) through a medium grade oil.

The entire system is controlled by a software package that accomplishes two significant objectives. First, a computerized pump is controlled to adjust the system pressure at a defined rate. Second, the software (in real time) records and presents the system temperature, pressure, solvent volume, time and most importantly, the transmitted power level of the detector.

Initially, the visual PVT cell was completely cleaned and evacuated with the temperature of the air-bath set to the desired value. Subsequently, 50–70 cm^3 of crude oil was isobarically charged to the cell (at a pressure in excess of the solid formation pressure at that temperature) from the storage cylinder using a displacement pump. At this point, the SDS components were mounted across the full length PVT cell windows and a reference scan of the light transmittance through the oil was performed. The pressure of the cell was then lowered isothermally at a programmable rate while the cell contents were mixed continuously. The experiment was stopped soon after a drop in the power of transmitted light is observed, which corresponds to the onset formation of a solid phase. This process was repeated at different temperatures to generate a complete phase behavior envelope (i.e., a PT diagram). To test for the reversibility of the solid precipitation, the pressure of the test fluid was increased and the corresponding power was measured. If the measured power increased and returned to its value prior to the solid precipitation, the precipitation was deemed reversible. Alternatively, if the transmitted power did not increase, the deposition was termed irreversible.

The SDS was also used to identify the onset of solids formation from a given crude oil due to isobaric solvent or diluent injection. The procedure involved charging a known amount of oil sample to the pre-cleaned and evacuated PVT cell (note, the system dead space prior to sample charging was less than 0.5 cm^3). Thereafter, the transmitted power

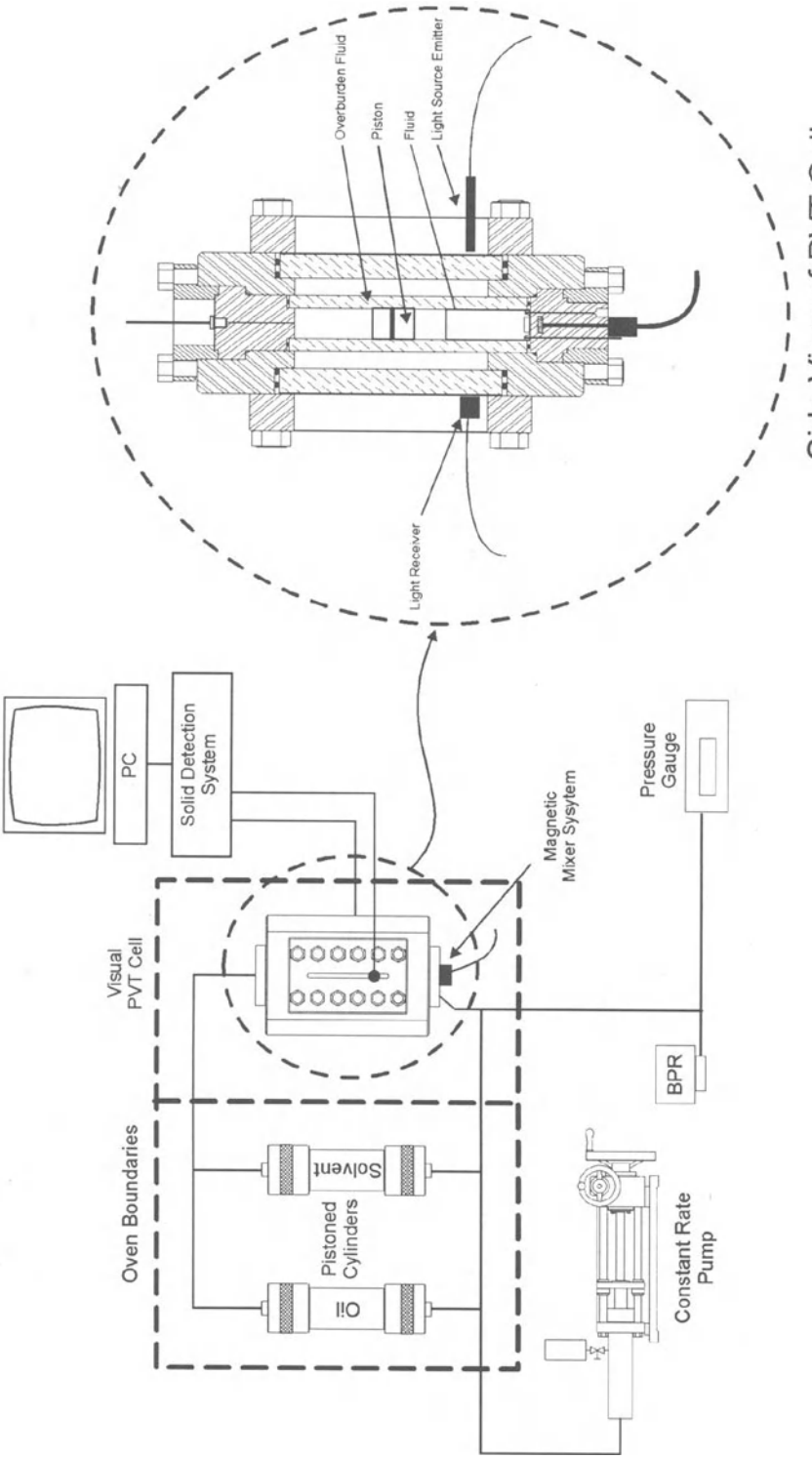

Figure 4. Schematic of the Solids Detection System (SDS) with an exploded view of the visual PVT cell. The cell and storage cylinders are maintained in a temperature controlled air-bath. Diagram courtesy DB Robinson Research Ltd.

was measured and recorded continuously (in real time) while the solvent/diluent was injected and agitated at a programmable rate.

3. RESULTS AND DISCUSSION

One atmospheric crude oil and three live oil samples were utilized in the characterization and phase behavior measurements. The atmospheric oil sample was a bitumen from Cold Lake, Alberta, Canada (note, bitumens are defined as fluids with boiling points > 950°F and viscosities > 10,000 cP). Cold Lake bitumen has average molecular weight of 575 g/mole and an n-pentane asphaltene content of approximately 18% by weight. The three live oil samples were bottomhole, black oil samples taken from the Gulf of Mexico with standard condition gas-oil ratios (GORs) between 1000 and 1500 scf/STB. Importantly, the live fluids were maintained in a single-phase condition well above their saturation pressures prior to the initiation of the phase behavior experiments.

3.1. Asphaltene and Crude Oil Characterization

3.1.1. Gel Permeation Chromatography. Figure 5 shows the continuous molecular weight distributions for the S.A.R.A. fractions of Cold Lake crude oil as separated by the HPLC method. While the areas under each curve represent the relative concentration of that fraction in the original oil, it was also possible to determine the weight average molecular weight of that structural group. From Figure 5, the concentrations of the saturate, aromatic, polar and asphaltene fractions were 33.1%, 24.8%, 24.7% and 17.4% by weight, respectively while the weight average molecular weights were 341, 368, 852, and 1975 g/mole. It should be noted that the asphaltene molecular weight distribution shown in Figure 5 was obtained from the subtraction of a Cold Lake pentane deasphalted oil from the original virgin sample and not from an asphaltene solution run through the GPC. This was important, as the problems of asphaltene association or agglomeration in terms of experimental measurements have been previously discussed.

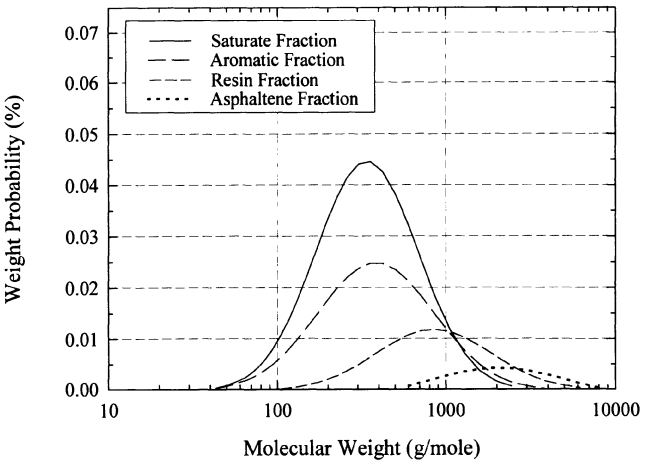

Figure 5. Molecular Weight Distributions of S.A.R.A. fractions separated from Cold Lake bitumen by the HPLC method. Distributions were measured by Gel Permeation Chromatography.

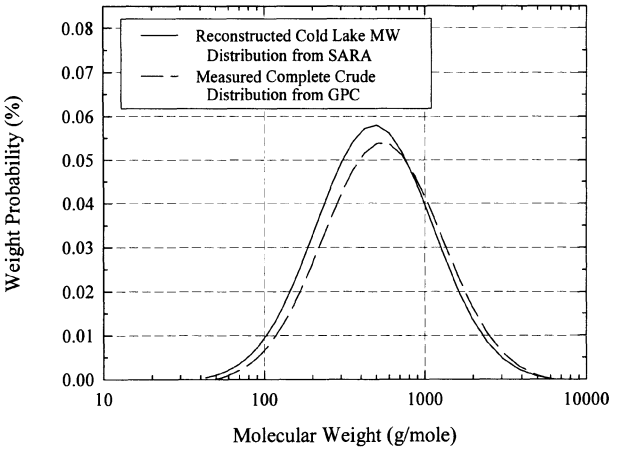

Figure 6. Measured and mathematically reconstructed Molecular Weight Distributions of Cold Lake bitumen. Distributions were measured by Gel Permeation Chromatography.

The continuous molecular weight distributions from Figure 5 were integrated to reconstruct the original Cold Lake crude oil (Figure 6). The solid line was the sum of the four separate fractions (which include the original, subtracted asphaltene distribution) while the dashed line represented the initial molecular weight distribution measured separately.

The agreement between the two techniques was strong although it should be noted that the right sides of the two curves must coincide, as this was where the asphaltene fraction was taken for the S.A.R.A. analysis.

Each of the S.A.R.A. fraction distributions from Figure 5 were fitted with log-normal distribution functions which are ideal for the entry of compositional data into predictive deposition models. For example, thermodynamic and kinetic model calculations[12] can be completed using a continuous thermodynamic approach or by creating pseudocomponents based on a gaussian quadrature technique.[23,24,25] In this manner, a representation of the molecular size and structure of the whole oil and its S.A.R.A. fractions was available for input to the model.

3.1.2. Field Desorption Mass Spectroscopy. Like the GPC characterization, FDMS was used to characterize Cold Lake bitumen and its S.A.R.A. sub-fractions. Note, a table is provided later in this section comparing the LSC separation to that previously obtained using the HPLC technique.

Figure 7 is plot of the Cold Lake saturates separated by the LSC procedure and analyzed using FDMS. From this diagram, the saturates display a fairly narrow distribution up to a molecular weight of approximately 750 g/mole after which it tails off with very small concentrations to approximately 2000 g/mole). It should also be noted that the saturate light ends were not well represented with this method. As a result, standard C30+ analyses (which extend to a molecular weight of approximately 450 g/mole) were tied against this data to provide a complete molecular representation of the crude fraction.

Like the GPC data, the molecular weight distribution of the saturates fraction (as well as the whole oil, aromatics and polars) were fitted with log-normal distributions. A

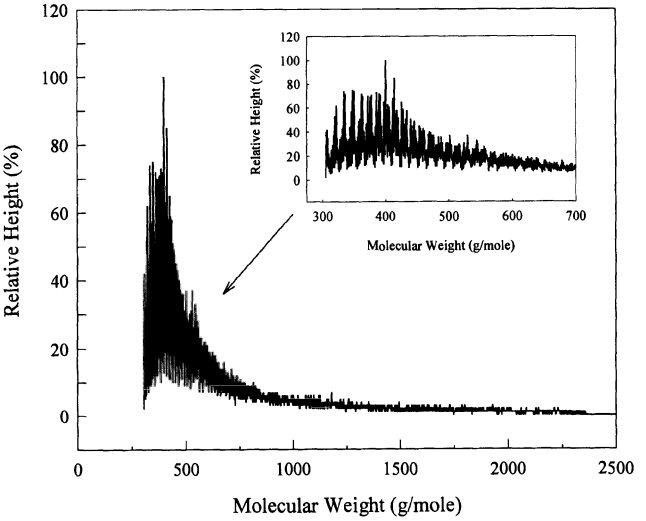

Figure 7. Molecular weight distribution of Cold Lake saturates separated by the LSC method. Distribution measured by field desorption mass spectroscopy.

separate plot of each of the S.A.R.A. fractions is provided in Figure 8. Note, in a similar manner as employed for the GPC data, the FDMS asphaltene distribution was obtained by subtracting the saturate, aromatic and polar traces from the whole oil. However, recent advances have suggested that disassociated asphaltene distributions will be measured in the future. Specifically, the FDMS appears to be an appropriate tool for making these meas-

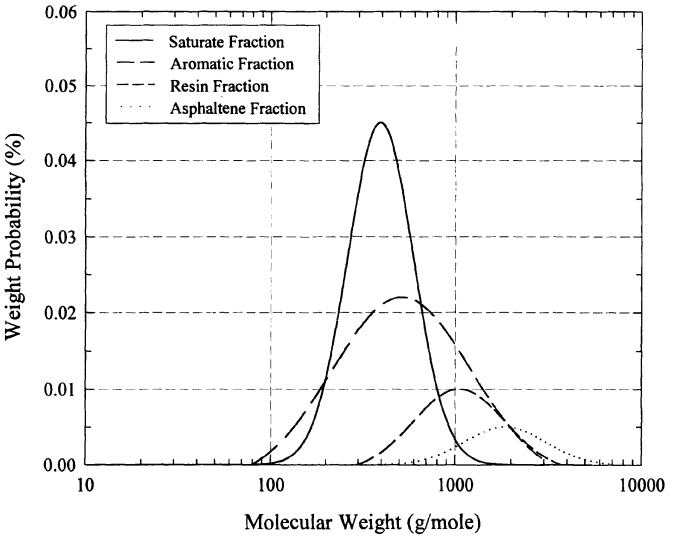

Figure 8. Molecular weight distributions of S.A.R.A. fractions separated from Cold Lake bitumen by the LSC method. Distributions measured by field desorption mass spectroscopy.

Table 1. Weight average molecular weights of Cold Lake S.A.R.A. fractions measured by GPC and FDMS

Cold Lake bitumen fraction	HPLC fraction concentration (wt%)	LSC fraction concentration (wt%)	GPC weight average molecular weight (g/mole)	FDMS weight average molecular weight (g/mole)
Saturates	33.1	32.8	341	355
Aromatics	24.8	23.4	368	472
Polars	24.7	25.3	852	1010
Asphaltenes	17.4	17.4	1975	1920

urements but will require a properly prepared sample of asphaltene dissolved in a solvent that has the necessary properties for adsorption onto the emitter.

Comparing the FDMS and GPC data provided in Figure 5 and Figure 8, there is certainly a qualitative similarity in the magnitude and location of the distributions. In order to evaluate the quantitative differences between the methods, Table 1 and Figure 9 were prepared. Table 1 compares the fraction concentrations and weight average molecular weights.

Based on the data in Table 1, there is good consistency between the HPLC and LSC separation methods for generating the S.A.R.A. fractions from the Cold Lake bitumen. These values validate and support the use of the HPLC method for two reasons, as the results were comparable with the standard LSC technique. First, the HPLC method was simpler to execute, requires less experimental time and reduced the possibility of losses. Second, the weight average molecular weights measured by GPC and FDMS were quite comparable with the largest differences occurring for the aromatic and polar fractions.

A graphical representation of the GPC and FDMS reconstructed molecular weight distributions is provided in Figure 9.

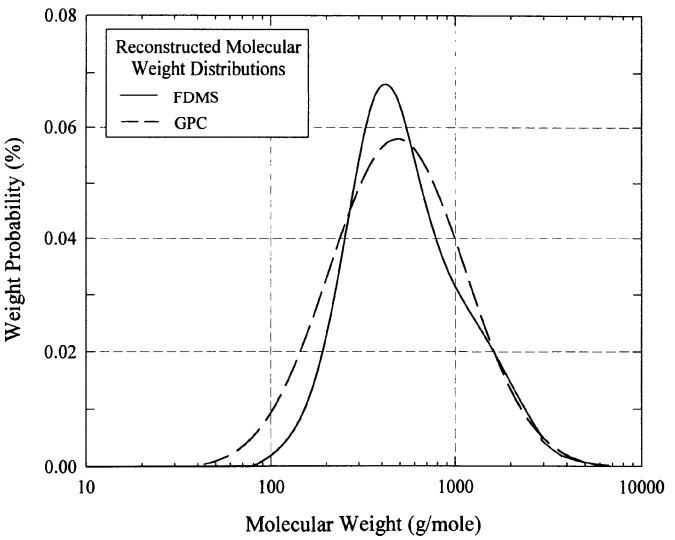

Figure 9. Reconstructed molecular weight distributions of Cold Lake bitumen measured by gel permeation chromatography and field desorption mass spectroscopy.

As for the tabular data, there is good consistency between the overall integrated distributions from the GPC and FDMS characterizations of the Cold Lake bitumen sample. In general, the FDMS distribution appears to be slightly narrower which results in a higher maximum weight probability percent after the traces are normalized. The similarity between the distributions also supports the use of the alternative calibration method used to convert the GPC elution profiles to MW distributions using actual oil sample molecular weights measured by Vapor Pressure Osmometry.

3.2. Asphaltene and Crude Oil Phase Behavior

3.2.1. Dead Oil Particle Size Distributions. An example of an asphaltene agglomerate particle size distribution is provided in Figure 10 for Cold Lake asphaltenes precipitated by 5 mL volumes of n-pentane per gram of bitumen at atmospheric conditions. Like the GPC and FDMS characterization data, the particle size analysis was well represented by a log-normal distribution function which is also shown on the plot (the mean particle size of this distribution is approximately 210 μm). In general, the regression coefficients for the particle size analyzer data were slightly less exact than those obtained from the GPC apparatus.[12]

It has been stated that an adjustment in both the diluent-oil ratio and in the type of diluent used will affect the characteristics of the precipitated asphaltenes. To evaluate that hypothesis, asphaltene particle size distributions were measured for various combinations of diluents and diluent-oil ratios with Cold Lake bitumen.

Figure 11 shows the variation in the mean particle size of Cold Lake asphaltenes deposited by various normal paraffin diluents at a constant dilution ratio of 20:1 (that is, 20 mL of diluent per gram of bitumen). The data in Figure 11 indicates that the larger paraffinic molecules precipitate asphaltenes of a decreased overall average particle size. This finding was consistent with expectations as the smaller paraffin molecules shift the equilibrium in the bulk oil to a greater extent than the larger molecules which were more comparable to those structures already in existence in crude oils.

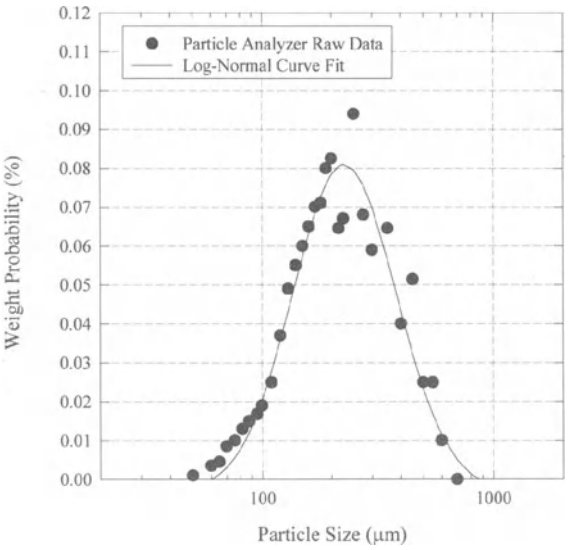

Figure 10. Measured and mathematically fitted particle size distribution of asphaltene agglomerates from Cold Lake bitumen diluted with 5 volumes of n-Pentane per gram of bitumen.

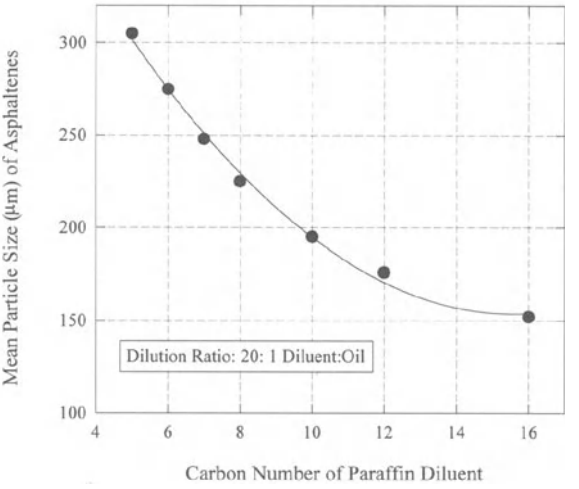

Figure 11. Mean particle size of asphaltenes vs. carbon number of paraffin diluent used to initiate precipitation. An increase in the carbon number of a paraffinic diluent resulted in a smaller mean particle size of precipitated asphaltenes.

For comparison, the effect of increasing dilution ratio on the characteristics of n-heptane precipitated asphaltene agglomerates is shown in Figure 12. The important features of this figure are twofold: first, there was a critical dilution ratio at which the precipitation of asphaltenes begins. Second, beyond a dilution ratio of approximately 40:1, no measurable increase in the average particle size was evident.

It is interesting to note that the particle size data follows similar behavior to the total amounts of asphaltenes precipitated in bench scale experiments. That is, a mathematical relationship appeared to exist between the mean particle size of the agglomerated asphaltenes and the total quantity (wt%) of asphaltenes precipitated from the Cold Lake bitumen. In other words, the use of weak diluents produced fewer asphaltene agglomerates of a smaller average size.[12]

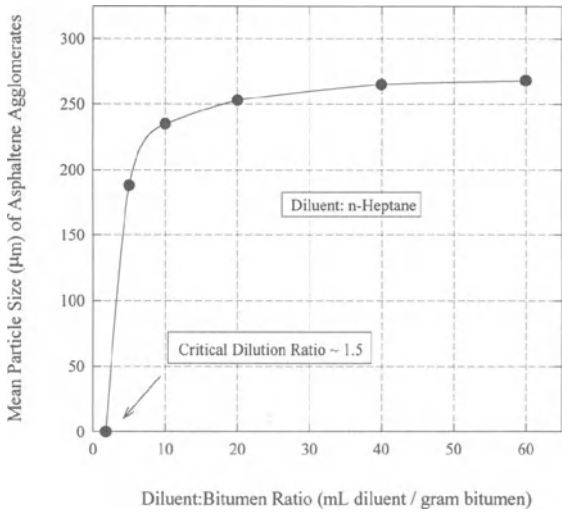

Figure 12. Mean particle size of Cold Lake asphaltene agglomerates vs. the diluent: bitumen ratio of n-heptane to oil. An increase in the carbon number of a paraffinic diluent resulted in a larger mean particle size of the precipitated asphaltenes to a maximum limit at a dilution ratio of approximately 40:1.

These findings were consistent with earlier published material for pressurized oils diluted with normal paraffins ranging from Ethane through Decane.[26] In that study an increase in the carbon number of the paraffin diluent also produced smaller asphaltene particles in lower quantities.

3.2.2. Asphaltene Precipitation Onset Phase Behavior. The live oil asphaltenic crude oil phase behavior measurements were completed on the three Gulf of Mexico samples in the solids detection system described earlier. Figure 13 represents transmittance data through live oil #1 which was initially maintained at a constant pressure of 9000 psi. The experiment was started by isothermally reducing pressure at a predefined rate while continuously agitating the cell contents. The transmitted power through the cell began to rise as pressure was decreased due to continuous reductions in the overall fluid density (note, this behavior has also been observed in paraffin wax precipitation studies where the optical transmittance decreased during cooling trials as the overall fluid density began to increase). The trend continued uninterrupted until the bubble point pressure was reached at approximately 5300 psi. At this point the rapid decrease in transmitted power was due to the presence of gas bubbles refracting the laser beam through the cell. Note, after a period of time, vapor-liquid equilibrium was reached and the transmittance through the liquid phase stabilized in the vicinity of the saturation pressure.

To conclude the experiment, the system pressure was returned to the starting condition of 9000 psi at which time the initial transmitted power (3.2 μW) was reestablished. As expected, without the presence of asphaltene precipitation, the experimental path was fully reversible.

Figure 14 contains the transmittance data for the second Gulf of Mexico fluid. In this experiment the reservoir pressure was again isothermally reduced (from 13,000 psi) with the corresponding increase in transmitted power. It is interesting to note that the rise of this single-phase data is less pronounced than for the first live oil. As the second oil was

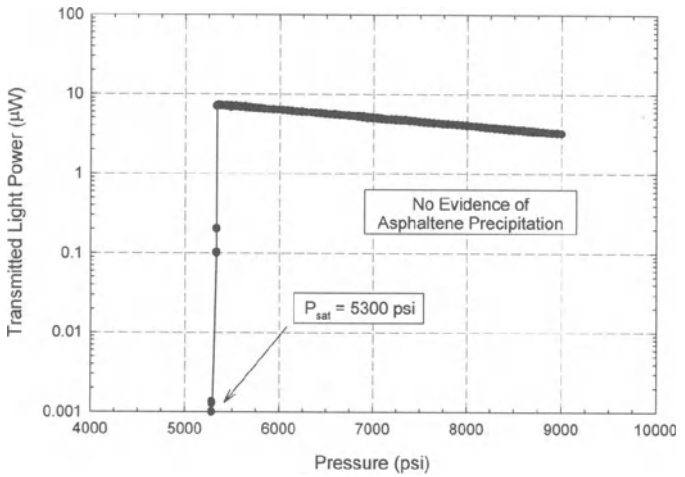

Figure 13. Transmitted laser power vs. operating pressure for a live oil without asphaltene precipitation due to pressure drop. The continuous increase in transmitted power was due to the decrease in the single-phase fluid density with decreasing pressure. The continuous increase indicated that asphaltene agglomerates did not form to a critical size which interrupted the laser through the PVT cell. The sharp decrease in transmittance was indicative of the fluid bubble point pressure.

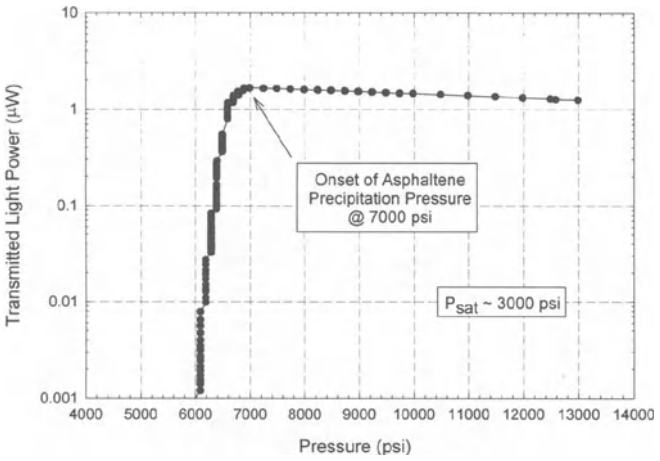

Figure 14. Transmitted laser power vs. operating pressure for a live oil with asphaltene precipitation due to pressure drop. The drop in the transmitted power was due to the presence of asphaltene agglomerates which scattered and absorbed the transmitted laser beam.

slightly heavier than the first, this finding was consistent with the theory that the transmittance (or change in transmittance) is related to the compressibility or density of the fluid. In any event, the rise in the optical transmittance continued until a pressure of approximately 7000 psia where the signal power decreased by almost three orders of magnitude due to the formation and growth of asphaltene agglomerates (note, reference testing has shown that asphaltenes agglomerates must grow to a size of approximately 10 μm before transmitted power reductions are noticeable). Perhaps the most interesting observation for this second Gulf of Mexico sample is that its bubble point pressure was previously established at 3000 psi. Therefore, asphaltene precipitation was noticeable some 4000 psi above saturation.

To conclude the experiment, the system pressure was returned to the initial condition of 13,000 psi. Interestingly, the transmitted power reached a value of 0.3 μW after approximately 12 hours of constant agitation with the magnetic mixer followed by an additional 12 hour stabilization period. Therefore, a significant portion of the precipitated asphaltenes re-dissolved into the oil indicating a fairly high degree of reversibility for this fluid.

The final phase behavior diagram represents transmitted power data gathered on a third Gulf of Mexico live oil during a differential liberation experiment (note, this fluid showed evidence of asphaltene precipitation due to pressure drop above the saturation pressure in a previously conducted precipitation onset trial). A differential liberation is a standard PVT analysis test in which the live oil is flashed in a step-wise manner below the saturation pressure (at reservoir temperature) with the produced vapor removed and analyzed at each step.

Figure 15 contains transmittance data collected at each of the differential liberation pressure steps. Not surprisingly, the data shows decreasing transmittance with decreasing pressure as the residual oil becomes heavier with the continued vaporization of light ends. However, unlike a number of reference samples that did not show evidence of asphaltene precipitation, the decrease in transmittance was not continuous. That is, at a pressure of

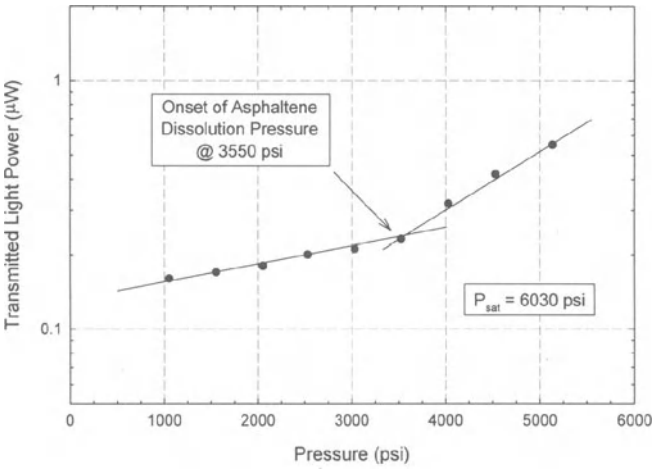

Figure 15. Asphaltene precipitation lower phase boundary obtained during a differential liberation (PVT) test. The break in the transmitted optical power data was likely indicative of asphaltene re-dissolution into the increasingly heavier oil as light ends were continually liberated and removed from the system.

3550 psi the continuous decrease in the optical power was interrupted. Without additional evidence, it appeared likely that the precipitated asphaltenes were beginning to return to solution at this point due to the increasing "heaviness" or solvating power of the residual oil.

The differential liberation test represents a type of pseudo-lower phase boundary measurement for the asphaltene precipitation envelope. A true lower boundary would exist if the overall system composition had remained constant; that is, if produced vapors had not been removed from the system. Therefore, an additional trial was conducted where the gas phase was allowed to remain in the system. This procedure also yielded a slight break in the transmitted power data but was less obvious than that shown in Figure 15. As a result, more tests are needed to determine its validity.

The type of data generated in Figures 13, 14, and 15 may be used to generated vapor-liquid-solid phase behavior envelopes. Although much of the work to date has been of a proprietary nature, it may be stated that for a sample set of approximately 6 live oils, the precipitation onset and dissolution boundaries have varied marginally with changes in temperature. Perhaps this finding begins to validate the earlier statement that asphaltene precipitation is a process that is most sensitive to pressure and composition and to a lesser extent, temperature.

4. CONCLUSIONS

In order to improve the predictive capabilities of thermodynamic and kinetic models describing asphaltene precipitation, detailed analytical characterization data and phase behavior of live and dead crude oils have been measured. Gel Permeation Chromatography and Field Desorption Mass Spectroscopy have been used to generate continuous molecular weight distributions of an oil and its S.A.R.A. fractions. Comparisons showed good consistency between the techniques although the Mass Spectroscopy method was preferred, as it

was simpler to execute, required less experimental time and reduced the possibility of losses. In either case, the heavy molecular structures in the oil were represented with continuous distribution functions that were ideal for input into the mathematical models.

The phase behavior of asphaltenic oil samples has been measured using particle size analysis on atmospheric oils and a solids detection system on live oils. For atmospheric oils, the data showed a relationship between the asphaltene agglomerate particle size distribution and the total quantity of asphaltenes precipitated. For live oils, the solids detection system was shown to have the ability to measure asphaltene precipitation onset pressures at conditions above the saturation pressure. Also, the system was used to observe at least partial reversibility of asphaltene precipitation upon repressurization for specific fluids. An estimation of the asphaltene precipitation re-dissolution (or lower) phase boundary was obtained during differential liberation PVT tests. Finally, initial measurements suggested that asphaltene precipitation is less sensitive to alterations in temperature than pressure and compositional variations.

ACKNOWLEDGMENTS

The Alberta Research Council, under the supervision of Mr. Marvin Rawluk, executed the FDMS measurements. The Pharmaceutical Production Research Facility in Calgary, Alberta, provided the GPC experimental system. The asphaltene phase behavior data was collected at DB Robinson Research Ltd., in Edmonton, Alberta, by Mr. Mark Kennedy, Mr. Craig Borman and Mr. David Murray, under the direction of Dr. Ahmed Hammani.

REFERENCES

1. Speight, J.G. "The Chemistry and Technology of Petroleum". Second Edition, Marcel Dekkar Inc., New York, 1991.
2. Pfeiffer, J.P. and Saal, R.N.J. Presented at the Sixteenth Colloid Symposium, Stanford University, California, July 6–8, 1939, p. 139.
3. Koots, J.A. and Speight, J.C. Fuel, 54, 1975, p. 179.
4. Chang, C-L. and Fogler, H.S. Langmuir, 10, 1994, p. 1749.
5. Leontaritis, K.J. and Mansoori, G.A. Journal of Petroleum Science and Engineering, 1, 1988, p. 229.
6. Speight, J.G., Wernick, D.L., Gould, K.A., Overfield, R.E., Rao, B.M.L. and Savage, D.W. Revue De L'Institut Francais Du Petrol, 40, 1985, p. 51.
7. Storm, D.A., DeCanio, S.J., DeTar, M.M and Nero, V.P. Fuel, 69, 1990, p. 735.
8. Moschopedis, S.E., Fryer, J.F. and Speight, J.G. Fuel, 55, 1976, p. 227.
9. Yau, W.W., Kirkland, J.J. and Bly, D.D. "Modern Size-Exclusion Chromatography: Practice of Gel Permeation and Gel Filtration Chromatography". John Wiley & Sons, New York, 1979.
10. Champagne, P.J., Monolakis, E. and Ternan, M. Fuel, 64, 1985, p. 423.
11. Rodgers, P.A., Creagh, A.L., Prange, M.M. and Prausnitz, J.M. Ind. & Eng. Chemistry Research, 26, 1987, p. 2312.
12. Ferworn, K.A. "Modeling of Asphaltene Precipitation". Ph.D. Thesis, 1995, University of Calgary, Calgary, Canada.
13. Dark, W.A. Journal of Liquid Chromatography, 5(9), 1982, p. 1645.
14. Leontaritis, K.J. and Mansoori, G.A. Journal of Petroleum Science and Engineering, 2, 1989, p.1.
15. American Society for Testing and Material., Standard Method D-2007. "Clay-Gel Adsorption Chromatography Method for Hydrocarbon Group Analysis".
16. Speight, J.G. and Moschopedis, S.C. "On the Molecular Nature of Petroleum Asphaltenes". Chemistry of Asphaltenes, J.W. Bunger and N.C. Li (Editors), American Chemical Society, Washington, D.C., 1981, p. 1.
17. Altgelt, K.H. and Boduszynski, M.M. Marcel Dekkar Inc., New York, 1994.

18. Yen, T.F. "Present Status of the Structure of Petroleum Heavy Ends and its Significance to Various Technical Applications". American Chemical Society, Division of Petroleum Chemistry, Preprints, 17(4), 1972, p. 102.
19. Overfield, R.E., Sheu, E.Y., Sinha, S.K. and Liang, K.S. Fuel Science and Technology International, 7(5–6), 1989, p. 611.
20. Ferworn, K.A., Svrcek, W.Y. and Mehrotra, A.K. Industrial and Engineering Chemistry Research, 32, 1993a, p. 955.
21. Ferworn, K.A., Mehrotra, A.K. and Svrcek, W.Y. Canadian Journal of Chemical Engineering, 71, 1993b, p. 699.
22. Nielsen, B.B., Svrcek, W.Y., and Mehrotra, A.K. Industrial and Engineering Chemistry Research, 33, 1994, p. 1324.
23. Cotterman, R.L., Bender, R., and Prausnitz, J.M. Industrial and Engineering Chemistry Process Design and Development, 24, 1985a, p. 194.
24. Du, P.C. and Mansoori, G.A. Fluid Phase Equilibria, 30, 1986, p. 57.
25. Huang, S.H. and Radosz, M. Fluid Phase Equilibria, 66, 1991, p. 23.
26. Nighswander, J.A., Kalra, H., and Majeed, A. Proc. AIChE Spring National Conf., March 1993.

Chapter VIII

CONDUCTIVITY OF ASPHALTENES

Per Fotland and Hilde Anfindsen

Norsk Hydro E&P Research Centre
5020 Bergen, Norway

1. INTRODUCTION

Asphaltenes have been studied extensively over the past 50–60 years.[1–2] A number of experimental techniques have been employed. The simplest and most widely used technique is the measurement of the solubilities of isolated asphaltenes in various organic liquids, both aromatic solvents and flocculants like pentane.[3–4] These studies yield valuable information with regard to the solubility parameters of asphaltenes. Advanced scattering techniques like neutron (SANS) and x-ray (SAXS) scattering have been used in order to elucidate the size and shape of asphaltene particles in solution.[5–7] The focus of the different studies has varied depending on the area of application. Information with regard to the structure of asphaltenes is required in areas like crude oil production, paving asphalts, refinery processes, etc.[8–12] This chapter will focus on the area of oil production.

Precipitation of asphaltenes in crude oil production can be detrimental to the economy of an oil field. In particular offshore fields with sub-sea completions are costly to clean regularly, if asphaltene deposits downhole become a problem. Even small amounts of precipitated material per volume of crude might, in a short time, lead to large deposits in the tubing of a well. The volume rate of these wells might be 3000–4000 Sm^3 (Standard cubic meter, i.e. the standard state is 1 bar and 15°C) and interventions in sub sea wells leads to lost production and costly operations, in the order of 1–2 million dollars per intervention (not counting lost production of 8–12 days). It is therefore vital to have information on the phase behavior of the asphaltene fraction at both reservoir and production conditions.

The need for information on the asphaltene phase diagram of crude oil, necessitates the use of good downhole samples and reliable measurement techniques. This has lead to the development of the so called monophasic downhole samples. The sampling tool utilised is designed to keep the pressure on the sample at, or above the reservoir pressure at all times. This is necessary in order to keep the asphaltenes in solution, because once they have precipitated there is no guarantee that they will resolubilize if the pressure and temperature of the sample is restored. Once the sample arrives at the laboratory, the pressure

is kept at reservoir pressure and the temperature is restored to reservoir temperature. It is common practice to equilibrate the samples for about one week, prior to measurements.

There are a number of different measurement techniques used in order to determine the onset of asphaltene flocculation. Among these are; gravimetry, different optical techniques, interfacial tension[13–15] and electrical conductivity. However, there still exists some uncertainty as to which method is the most reliable. Ideally measurements with several different techniques should be performed on the same crude but as indicated above good samples are expensive and therefore hard to obtain.

According to Conway,[16] non-aqueous solvents can be classified in two different classes, namely as protic and aprotic. The protic solvent molecules have functional groups which contains labile protons. The most typical example of these molecules are carboxylic acids (-COOH), but also alcohols and nitrogen containing groups might be protic solvents. Reservoir crude belongs to the other group, i.e. the aprotic solvents. The hydrogen atoms are predominantly bound to carbon in stable covalent bondings. At normal conditions, hydrogen in C-H bonding is not available for exchange.

The polar fraction of crude oil is known to contain heteroatoms; nitrogen, sulfur and oxygen in addition to metals like vanadium, nickel and iron. A number of different structures have been determined for asphaltene molecules and labile protons can be found in many of these. Resins, although a lighter fraction, also contains heteroatoms and should therefore be expected to contain labile protons.

So, a typical crude oil is a mixture of protic and aprotic solvents. For most crudes the aprotic fraction dominates, but in the case of heavy oils this might not be true. The protic fraction of the crude has the potential of becoming ionized and also being stabilized by other protic molecules or by permanent or induced dipoles. It is therefore likely that the asphaltene and resin fraction of any crude oil contains a certain fraction of ions. Some of these ions can exist as free ions and other in associated states.

The fraction of polar molecules in crude oil is not enough to bring the dielectric constant any higher than 2–4, the oil must consequently be regarded as a low permittivity solvent. By interpretation of the dielectric constant one should keep in mind that symmetrical molecules might have quadropoles. For instance, dioxane is completely soluble in both water and oil. By looking at the dielectric constant one should expect dioxane to be soluble in oil, but not in water. By symmetry the dipolar moment is zero, but knowledge of the structure 'explains' the solubility in water. The same argument could apply to crude oil. Even though the dielectric constant is low the fraction of quadropoles and similar electrical structures might act as solvent molecules for ions. Both molecules with a high dipolar moment and those with zero moment can be responsible for solvating ions in hydrocarbons. Gemant[17] points out that; "It is possible that the distribution of these molecules in the solution is not uniform but rather dielectrically enriched in the vicinity of ions where the electric field is high".

The saturation solubility is exponentially related to the standard free energy of bringing the particular molecule from the solid state to the solvated ionic state. Thus any changes in the solvent that brings about small changes in the standard free energy might result in a significant change of solubility. It is well documented that the asphaltene solubility of a reservoir crude may change drastically upon decreasing the pressure. A decrease in pressure leads to expansion of the components with highest compressibility, thus the volumetric concentration of asphaltenes decreases. The overall result of this expansion is that the oil becomes more aprotic.

This chapter will focus on the electrical conductivity of crude oil as a technique for determination of both the onset of asphaltene flocculation and the implication for the structure of asphaltenes. In contrast to the large number of asphaltene articles published,

very few are concerned with the measurement of electrical conductivity. Application of electrical conductivity in science is mainly linked to salts, acids and bases in aqueous media. The electrical conductivity of asphaltenes and crude oil has been much less studied.

2. A SUMMARY OF LITERATURE ON ASPHALTENES AND ELECTRICAL CONDUCTIVITY

Below is a short summary of some of the contributions in the literature to the conductivity of asphaltenes. The articles previously written by the present authors[18–20] will be reviewed in the next section with additional data.

2.1. Brief Review of Conductivity Articles

In 1974 *S. Penzes and J.G. Speight*[21] performed conductivity studies on fractions of Athabasca bitumen in benzene, pyridine and nitrobenzene. The Athabasca asphaltenes were dissolved by stirring for four hours before measurements were performed. The temperature was varied in the range of 20–50°C by heating at a rate of 0.3°C/min.

Their results show that the conductivity increases both as a function of concentration and temperature. They also show that the conductivity increases when the dielectric constant of the solvent increases. In fact, this increase can be correlated with a corresponding decrease in molecular weight. So, the authors report strong evidence that " the asphaltene portion of an oil does indeed have the ability to participate in charge transfer systems."

Another study on the electrical nature of asphaltene deposition is provided by *P. Lichaa and L. Herrere*[22] in 1975. The asphaltene fractions employed were taken from both crude oil and solid deposits from the tubing. Two sets of electrical experiments were performed. The first experiment measured the degree of electro-deposition, by subjecting an asphaltene solution to a high DC electric field. The reported field strength was of the order 250 kV/m. The asphaltene solutions were subjected to this field for three days. Upon inspection, only the negative electrode contained any deposition and it was identified that it consisted mainly of asphaltenes. One additional point of interest is the fact that the Boscan crude contains natural inhibitors for asphaltene deposition. No deposition was found when the diluents were fractions of the Boscan crude. It should also be noted that by reversing the polarity of the electrodes the deposited material remigrated to the negative electrode.

The second experiment consisted of microscopically observing the movement of asphaltene particles under the influence of a DC field. The field strength was lower but of the same order of magnitude as in the first experiment. The movement of the particles is reported to be rectilinear and circular. After a given period of time the particles were seen to deposit on the negative electrode.

Both experiments indicate that the asphaltene particles have a net positive charge. They also conclude "that electrical effects play an important role in the asphaltene deposition problem."

In the next article of *P.M. Lichaa*[23] he extends the usage of the previously described electro-deposition experiment. The asphaltenes were isolated from 7 different crudes and the observations confirm those of his first study. By using electromicrography the size of the particles was determined. The sizes were found to vary in the range of 10 - 5000 Å and the aggregates were therefore classified as colloids. Furthermore, the article describes measurements of the zeta potential and electric charge of the asphaltenes and the results agree with the previous findings.

The two articles by Lichaa points out a number of interesting topics relating to asphaltene problems but only the electrical part has been reviewed in this report.

In 1978, Kendall[24] measured the conductivity of medium heavy crude oil as a function of temperature. His measurements showed that the resistivity increases exponentially with the inverse temperature. In a log-lin plot the resistivity turns out to be linearly proportional to the inverse temperature. As the conductance and resistance are inversely proportional, his study indicates that the conductivity increase exponentially with increasing temperature. Kendall uses the theory of semi-conductors to explain his finding, but also remarks that the observed results could be due to contamination of brine or other colloidally dispersed matter.

In 1985 Maruska et. al.[25] published an extensive study on the electrical transport processes in heavy hydrocarbon fluids. The material they studied was called Catalytic Cracking Bottoms (CCB) and was taken from the bottom stream of a distillation tower. Their results included measurements of both AC and DC conductivity. In the AC mode both conductivity and the dielectric response were recorded. The CCB was diluted in n-paraffins, cyclo-paraffins, white mineral oils and aromatics.

The conductivity as a function of wt% solvent shows an initial increase. As more solvent is added the conductivity values level off and proceed through a relatively broad maximum. After the maximum the conductivities decrease and approaches that of pure solvent. Although not noted in the paper, it is of interest to see that the curves for the aromatics (i.e. toluene, xylene, mesitylene and tetraline) all preserve their curvature throughout the scan, while those for the simple paraffins (nC5-nC9) change curvature at different weight fractions of added solvent. The point of change in curvature coincides with the onset of precipitation of asphaltenes and this will be dealt with in a later paragraph. A long term stability test of the DC conductivity was also performed. This test used a field strength of 1000 kV/m for 3 months. The recorded conductivities showed no time dependence and no electrode reactions or coatings were observed.

Maruska et al. explains the conductivity in terms of pi-electron charge transfer between polynuclear aromatic hydrocarbons. They specifically mention that the CCB contains mainly naphtalene, phenanthrene, chrysene, perylene, pyrene, benzanthracene and benzopyrene. Whenever planar overlap of these and like molecules takes place within the liquid, then charge transfer is possible. The difference in the conductivity curves of the n-alkanes and the aromatics is explained by the fact that aromatics will enhance charge transfer while aliphatic molecules will hinder the transfer of charges.

Another article addressing the topic of heavy oil distillation residues was published by Siffert et al. in 1989.[26] The object of the paper was to investigate the presence of surface charge on heavy oil residues in organic media. The authors measured the zeta-potential of several different residues from Boscan and Safaniya crudes. The following solvents were used; acetic acid, methanol, acetone, formamide and ethylenediamine. The results are discussed in terms of the solvents donor number and acceptor number, which relates to the ability of the liquid to donate electrons in a reaction between donor and acceptor molecules. In their conclusion they state that the stability of residues and asphaltenes in various solvents relies upon the surface charge of the particles. Furthermore, the charge of the particles stems from the charge transfer of the surrounding liquid and not from classical ion-counterion mechanisms. The authors continue to conclude that in oils the surface charge is very small "since the disperison medium is formed essentially by saturated hydrocarbons having a very low charge transfer capacity."

An investigation of "asphaltenes in polar solvents" was published in 1991 by Sheu et al.[27] The purpose of the paper is to verify that asphaltene molecules self-associate. The

asphaltene fractions were extracted from Ratawi crude by heptane precipitation. The asphaltenes were dissolved in toluene and frequency scans of the conductivity, at different temperatures, were recorded. The conductivity data show a strong temperature dependence at low frequencies and virtually no temperature dependence at high frequencies.

The same authors published a paper on the dielectric properties of asphaltene solutions in 1994[28]. Again the source of asphaltenes was a distillation residue. The purified asphaltenes were dissolved in toluene and conductivity was measured as a function of temperature. The results of this study were almost identical to their first study. This supports the view that charges move freely on a short time scale (high frequency), i.e. within an asphaltene aggregate. The low conductivity at low frequencies, indicates that the charge transfer between aggregates is restricted.

An article published in 1995 by MacMillan et al.[29] focused on the topic of "evaluating asphaltene precipitation based on laboratory measurements and modelling." The conductivity measurements contained in this paper were solely for the purpose of detecting the onset of asphaltene precipitation. Furthermore, they used optical fluoresence and visual observations to verify the flocculation onset. By titrating the crude with a flocculant (n-alkane) they observed that the conductivity initially increases due to increased mobility of the ions. However, they do not comment on the fact that their conductivity values increase at the point of precipitation. In a remark about the method they claim that the conductance values contain a high background contribution from the equipment. This may account for the somewhat surprising behavior of the conductivity at and after the onset.

2.2. Overall Conclusions

As is evident from the above list, all of the contributors are working with purified asphaltenes. The isolation procedure most commonly used is by precipitation with an n-alkane (nC7). The asphaltenes are then redissolved or dispersed in various solvents. The objective of the studies is mainly focused on downstream applications or solely to investigate the structural properties of the asphaltenes. Very little is mentioned about the applicability of the results with regard to the reservoir oil. In the literature, in general, there still seem to be a dispute whether the asphaltene precipitation is reversible or not.

It seems that all of the above mentioned papers conclude that asphaltenes are colloids and possess a net charge. The mechanism by which they gain this net charge is somewhat unclear but the electronic properties of the surrounding medium might be of importance. The conductivity of the asphaltenes is also seen to increase as a function of increasing temperature. Some of this effect can be attributed to a decrease in viscosity, but in some systems an excessive increase is observed and this is explained by an activation like charge transfer.

An increase in asphaltene concentration also leads to increasing conductivty values. None of the above papers have tried to calculate the molar conductivity. This property is commonly used for interpretation of conductivity data in terms of interactions between conducting entities. However, asphaltenes are not pure components and as such the molar concentration can only be approximated, so this source of error should be kept in mind upon interpreting such data.

By increasing the dielectric constant of the solvent media, the conductivity is seen to increase. This agrees well with the theory of ions, but can also be correlated to electron donor properties of the solvent. In non polar media the asphaltene conductivity is very low, indicating either restricted charge transfer between the asphaltenes or heavily aggregation to ion pairs and higher aggregates. This is also refelected by the fact that asphaltenes are insoluble in n-alkanes.

Conclusions with regard to net charge are difficult as two different studies show conflicting results. Strong evidence is presented to show that the particles have positive net charge due to electro-deposition, while equally strong evidence finds no electro-deposition. It is somewhat unclear from the studies whether measurements are performed on dispersions or on solutions. This might affect the results of electro-deposition measurements. It should however be remarked that a number of studies show that the asphaltenes have a defined zeta-potential and therefore possess net charge.

Overall, there is plenty of evidence for the existence of a net charge on asphaltenes. It would therefore be worthwhile to investigate and utilize this property of the asphaltenes. The next chapter will review some of the existing data published by the present authors and include new data.

3. CONDUCTIVITY MEASUREMENTS; EXPERIMENTAL CONSIDERATIONS

3.1. Experimental Set-Up

As previously mentioned, the measurement of electrical conductivity of crude oils and asphaltene fractions has two purposes; a) to detect the onset of flocculation and b) to study the structure of asphaltenes in solution. For both cases a cell with a large electrode area and small spacing between electrodes are required. The present description of experimental set-up relates to the one used by the authors.

A coaxial cylindrical cell geometry was chosen. Two different cells were built, i.e. one for high pressure and temperature applications and one for studies at atmospheric pressure. Both cells have an internal spacing between electrodes of approximately 1.5 mm. The cell constant of the 1 bar cell is 0.0029 cm^{-1}, while the cell constant of the high pressure cell has not been determined because only relative values of the conductance are required. The conductance values of oil as measured by the high pressure cell is in the range of 0.2–2 μS. The cells have ports for inlet and outlet of fluid and are connected to a mixing chamber with a stirrer and to a high pressure pump, used for circulating the fluid in a closed loop.

The cell is connected to a HP4192A measurement bridge. If frequency scans are needed this can be achieved by controlling the conductance meter by a PC. Further details of the set-up can be found in references.[18–20]

3.2. Measurements

The metering bridge was used in an AC parallel mode. This means that the actual circuit is defined as a parallel resistance (R) - capacitance (C) circuit. In addition there is a software option for fitting the experimental spectrum to almost any equivalent circuit in order to check for unwanted contributions to the conductivity.[30] This option was used to determine the exact value of the DC conductivity. This value is only needed if the results are being compared to models of electrical conductivity in non-polar solvents. By utilizing this software, the resistance and inductive elements of the wiring are taken into account. Both these values should be kept at a minimum because they may influence the resonance peak significantly. Otherwise, readings at 1kHz were regarded as sufficient.

The applied voltage was 1 volt which results in a field strength of approximately 700 V/m. This is negligible with respect to the field strength surrounding the ions, which

is of the order 10^8 V/m.[16] So, any interference of the applied field with the conducting species was neglected. It should also be noted that the Wien effect of increased conductivity with increasing field strength is only significant at 10^6 V/m and higher.[31] The Debye-Falkenhagen[31] effect of increased conductivity with increasing frequency will not interfere with the calculations of the DC conductivity, as it occurs at high frequencies.

During the operation of the experimental set-up described above certain precautions need to be taken, 1) make sure that resonance effects are minimized, 2) keep the wiring fixed and follow closely the recommendation as set out in the manual of the instrument and 3) keep the set-up isolated above ground. If point 1 is overlooked one can get too high conductivity values and the results might be jammed with artifacts relating to the set-up. Regarding point 2, if the wiring is not fixed the capacitance of the total circuit might vary during measurements and this could lead to changing values of the resonance frequency which again influences the conductivity (note that even an empty cell will give conductivity values depending on the measurement frequency employed). The last point (3) is particularly difficult to satisfy but never the less, very important. If, at any point, the circuit is grounded or partially grounded the values could switch between different levels or fluctuate to the extent that readings become impossible.

3.3. Material and Fluids

The purified asphaltenes were obtained from core samples of a North Sea reservoir. The solid material was isolated by extraction using the Soxthec principle. The solvents were used as received. Further details can be found in reference.[20] The following solvents were used; benzene, tetrahydrofurane, pyridine, trichloroethane and dichloromethane.

3.4. Estimation of Molar Conductivities

The molecular weight was measured by freezing point depression in benzene in the range of 800–1400 g/mol. For calculations of molar concentrations the molecular weight was set equal to 1000 g/mol. Furthermore, it was assumed that only 10% of the asphaltenes were contributing to the conductivity as potential ions. Both of these assumptions are uncertain and this must be kept in mind while interpreting the conductivity data. Molecular weights of asphaltenes may vary a lot according to measurement procedure and solvents.[32–33]

3.5. Conductivity Model

The measurements of molar conductivity were matched to the Fuoss model[34,35] of conductivity in low permittivity media. The model of Fuoss is based on the formation of ion pairs and triple ions as chemical entities. Petrucci[36] has shown that the existence of both ion pairs and triple ions can be deduced from a purely physical point of view. That is, there is no need to invoke equilibrium constants in order to account for the formation of the ionic aggregates.

The point of this investigation is not to test the various conductivity models, but to look for indications that conform with the notion that some fraction of the asphaltenes might behave as ions in low polar media. In the present interpetration we have used the Fuoss model. Briefly, the theory accounts for ion pairs and triple ions in the form;[34]

$$A^+ + B^- = (A^+B^-) \qquad K_a = a_{AB}/(a_A a_B) \qquad \text{ion pairs from free ions} \tag{1}$$

$$(AB) + (AB) = ABA^+ + B^- \qquad \text{triple ions from ion pairs} \tag{2}$$

K_a is the equilibrium constant and a denotes activity. The formation of ion pairs is favoured by increasing concentration and/or decreasing the dielectric constant of the solvent. The ion pairs act as dipoles and are therefore electrically neutral and will cause the molar conductivity to decrease. In contrast the ion pairs which form triply associated ions will cause the conductivity to increase.

The existence of ion pairs can be tested by fitting the conductivity data to the model proposed by Fuoss. The equation has the following form:

$$\Lambda = \alpha(\Lambda_0 - S(\alpha c)^{0.5} + E\alpha c \ln(\alpha c) + I_1 \alpha c + I_2(\alpha c)^{1.5}) \quad (3)$$

The Λ is the molar conductivity, Λ_o is the molar conductivity at infinite dilution and c is the concentration of ions. The fraction of free ions is denoted by α and is determined by an iterative procedure involving the equilibrium constant of the ion pair formation, the Debye Huckel mean ionic activity constant and the radii of the conducting species. For simplicity the radii was set equal to 50 Å, the exact value of the radius was not critical for the fitting procedure. The constants S, E, I_1, and I_2 are calculated from knowledge of the dielectric constant, viscosity and the temperature. The only unknowns which are varied in order to obtain a fit, are the equilibrium constant of equation 1 and Λ_o. The best fit was obtained by a minimization procedure.

In order to check for the presence of triply associated ions, Fuoss has shown that the data can be plotted according to the following simple equation;

$$\Lambda c^{0.5} = Ac + B \quad (4)$$

Where A and B are regarded as unknown constants. Thus a linear relationship between the product $\Lambda c^{0.5}$ versus c would be an indication of triple ions.

4. RESULTS AND DISCUSSSION

4.1. Conductivity of Purified Asphaltenes in Organic Solvents

Figures 1 and 2 show the DC conductivity of asphaltenes in benzene and tetrahydrofuran respectively. In the same figures are the application of equation 4 shown. Both curves show an initial decrease of molar conductivity. The benzene case seems to approach a minimum. At approximately 0.0025 M there appears to be a break in the curve. A linear curve in the concentration range of 0.001 to 0.0025 M indicates the presence of triple ions.

The tetrahydrofuran measurements have the same initial appearance but a well defined minimum is observed at 0.00025 M and at approximately 0.001M there appears to be a break in the curve. Again the application of equation 4 shows a linear region indicating the presence of triple ions.

Equation 3 cannot be used in these two cases due to potential triple ion formation. Furthermore, equation 3 cannot predict a minimum in the molar conductivity as a function of concentration.

The conductivity of asphaltenes in 30% pyridine in benzene, and in pure pyridine, is shown in Figures 3 and 4, respectively. The conductivity shows a monotonic decrease as a function of concentration for both curves. According to the Fuoss theory this behavior is related to the formation of ion pairs. The solid lines of the figures show the best fit to

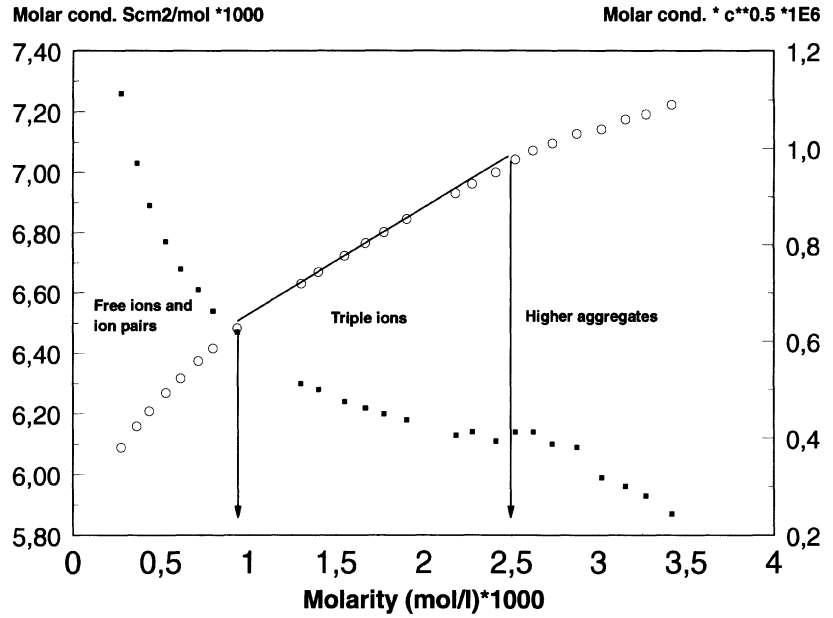

Figure 1. The molar conductivity (black squares) and the conductivity times the square root of the molarity (open circles) as a function of the molarity of asphaltenes in benzene. The straight line indicated between the two arrows is evidence of the existence of triple ions. Temperature is 20°C.

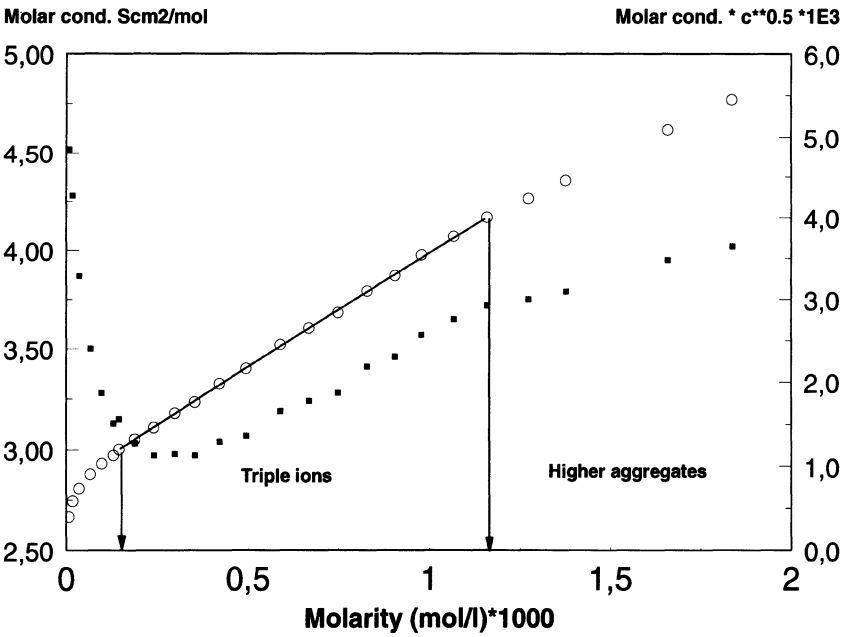

Figure 2. The same as figure 1, but the solvent is tetrahydrofuran. Temperature is 20°C.

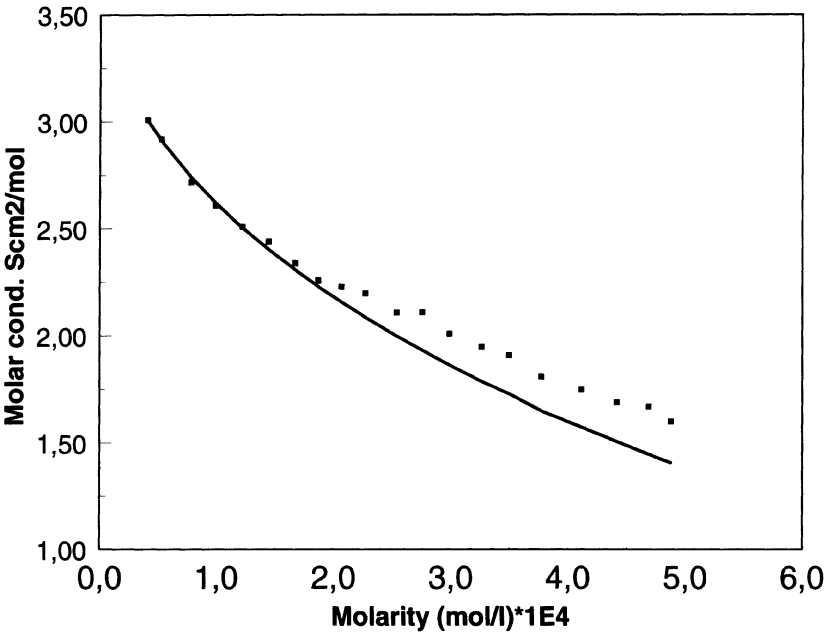

Figure 3. The conductivity of asphaltenes in a mixture of 30% pyridine in benzene. The solid line represents a fit to equation 3. Temperature is 20°C.

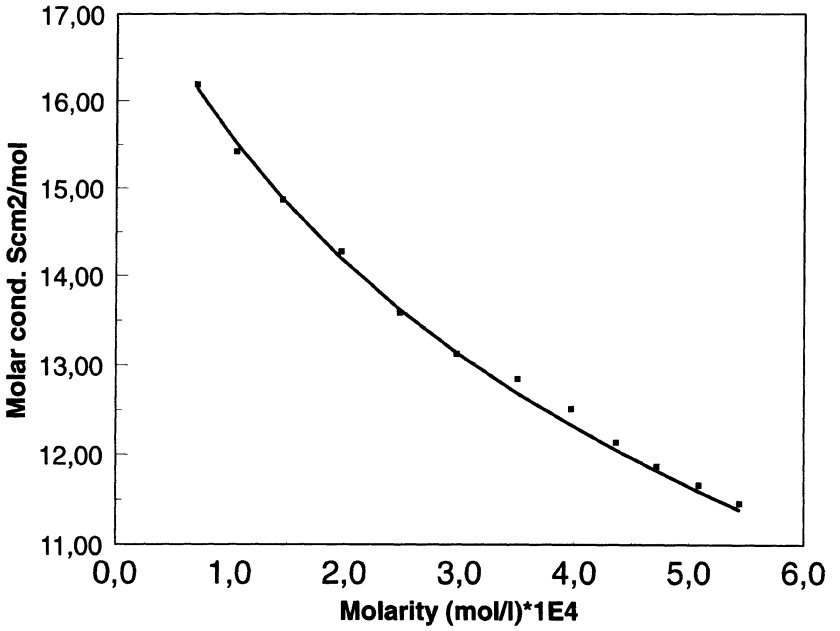

Figure 4. The molar conductivity of asphaltenes in pyridine. The solid line represents a fit to equation 3. Temperature is 20°C.

Table 1. The table lists the dielectic constant, molar conductivity at infinite dilution (Λ_0) and the ion pairing constant according to equation 1

Solvent	Dielectric constant	Λ_0 Scm^2/mol	Ion pairing constant
Pyridine	12.75	17.80	1.6E6
80% THF in benzene	5.89	4.70	6.2E8
10% benzene in Tri.	5.76	1.10	8.7E6
30% Pyr. in benzene	4.55	0.37	2.3E5

THF is tetrahydrofuran, Tri denotes trichloroethane and pyr. denotes pyridine.
The conductivity of the pure solvents was in all cases found to negligible

equation 3. The fit indicates that it is physically plausible that asphaltenes can exist as ions and ion pairs.

Table 1 shows a listing of the various experiments that has been performed with the molar conductivity at infinite dilution, the dielectric constant of the mixture and ion pairing constant. In some experiments no fit to equation 3 could be made. Table 1 also shows that the molar conductivity at infinite dilution increase as a function of increasing dielectric constant.

No definite conclusions can be made concerning the ion pairing constant except that the large values indicates a strong tendency of the ions to form ion pairs. This is to be expected due to the low dielectric constants. Pyridine which has the highest dielectric constant has also the lowest ion pairing constant.

4.2. Conductivity as an Indicator for Asphaltene Precipitation

As the conductivity seems to be related to the state of the asphaltenes in solution, it is also reasonable to assume that the conductivity will be sensitive to precipitation of asphaltenes. When asphaltenes precipitate, the fraction of ions is reduced and this should lead to a decrease in conductivity.

In Figures 5 to 7 are the titration experiments shown. All figures relate to the same crude, which was a typical black oil with an asphaltene content (C5) of 0.6 wt%. Figure 5 shows the crude diluted with xylene. Xylene is regarded as being a good solvent for asphaltenes and, as such, is not expected to induce asphaltene precipitation. The squares in Figure 5 represent the conductance of the solution. The curve has the same appearance as the one measured by Maruska et al. Initially the conductivity increases due to increased ion mobility or a reduced activation energy for charge transfer. Xylene itself has negligible conductivity and a dilution of the asphaltenes in the crude must therefore lead to a decreasing conductivity. At the maximum, the effect of dilution cancels the effect of increased mobility . After the maximum, the dilution effect is dominant and the conductivity values approaches that of pure xylene.

The connected circles of Figure 5 show the weight normalized conductivity (wnc). This value is obtained by dividing the conductivity with the weight fraction of oil at the given point. The resulting parameter, wnc, bears resemblance to the molar conductivity. The weight fraction of oil is proportional to the weight fraction of asphaltenes and if we assume that the molecular weight is constant, then the wnc is proportional to the molar conductivity. In Figure 5 the curve is seen to increase monotonically as a function of dilution. This is in good accordance with the measurements presented in the previous section. The classical interpretation is that in the absence of ionic interactions the conductivity is

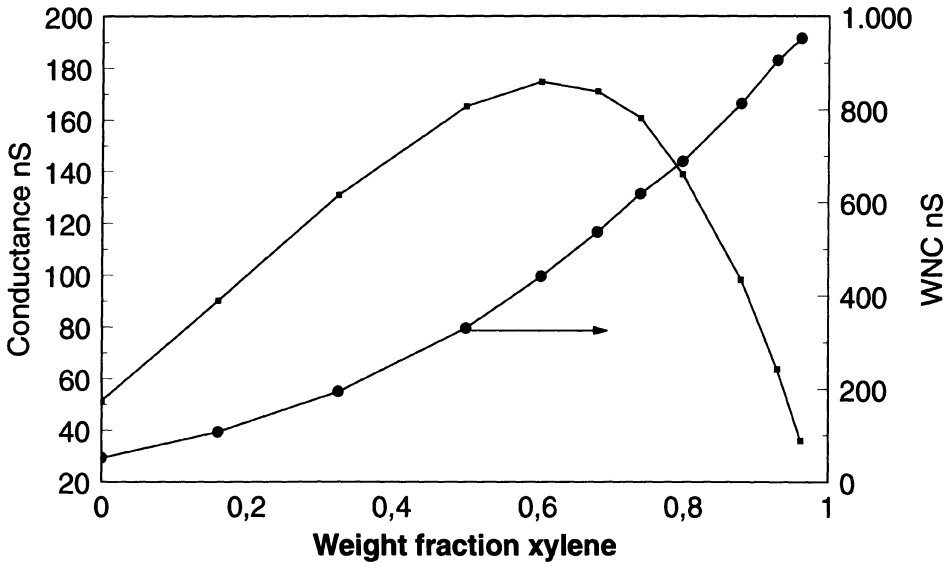

Figure 5. The conductivity (squares) and weight fraction normalized conductivity (circles) of crude oil as a function of weight fraction xylene. Temperature is 20°C.

at a maximum, i.e. the molar conductivity at infinite dilution. Adding ions to the solution increases the overall conductivity but decreases the conductivity per molecule i.e. the wnc.

The smoothness of the curve indicates that no major structural changes or phase changes take place.

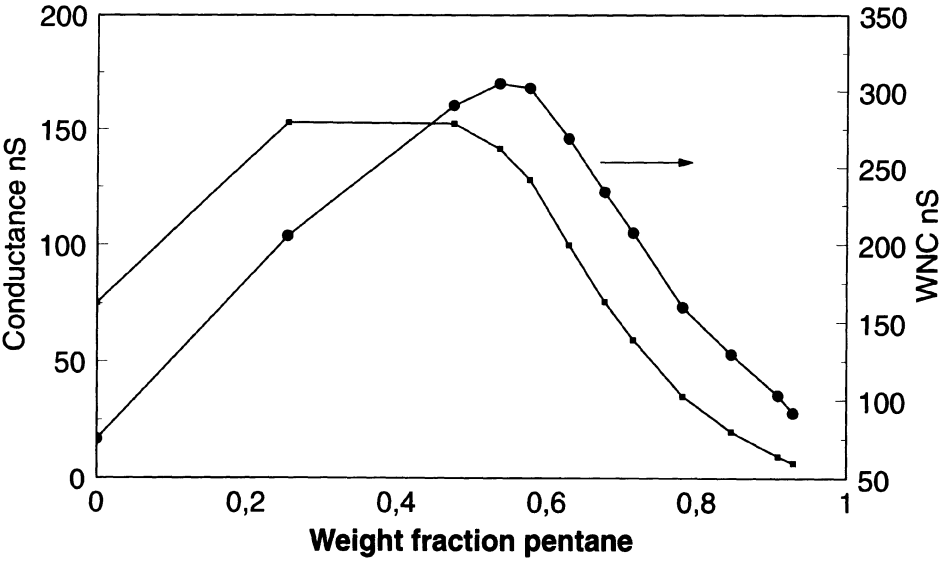

Figure 6. The conductivity (squares) and weight fraction normalized conductivity (circles) as a function of weight fraction pentane. Temperature is 20°C.

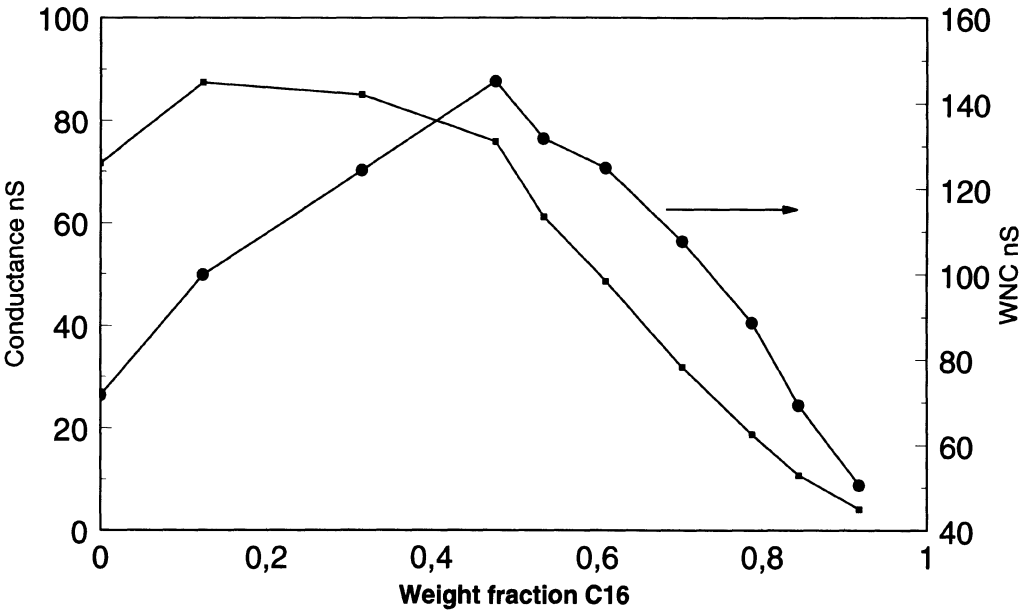

Figure 7. The same as figures 5 and 6 but using hexadecane as flocculant. Circles relates to the wnc and squares to the conductivity. Temperature is 20°C.

Figures 6 and 7 show the same as Figure 5 but the curves display precipitation. For the conductivity curves the same initial behavior is seen, but at a given point the curves changes curvature from convex to concave. The connected circles is the wnc, and now a clear maximum is evident. This maximum coincides with the change of curvature in the conductivity curve (squares) and marks the precipitation of asphaltenes.

Apparently the maximum in the wnc does not conform with the theory of ions. The reason for this apparent discrepancy, is the fact that when we weight normalize by the fraction of oil or equivalently, asphaltenes, we do not account for the precipitated asphaltenes. Therefore, the weight fraction of asphaltenes used for normalization is too large and the wnc values are too low.

The dilution has been repeated for a number of different crudes ranging in asphaltene content from 0.1 wt% to 20 wt% and the same conductivity profiles are seen for all of them. We have also studied the effect of different n-alkanes on the onset (C2-C16). A summary of these results is shown in Figure 8. The weight and mole fraction of the solvent at onset are displayed as function of the n-alkane density.

The form of the onset curve of Figure 8 is somewhat surprising. One would expect the onset to increase linearly as a function of density or alkane carbon number. However, for this crude there seem to be a maximum around decane. In fact nC15-nC16 induces asphaltene precipitation at lower mole fractions than n-C2. Measurement of precipitated weights shows the regular behavior i.e. the weigths precipitated decrease monotonically upon increasing the molecular weight of the flocculant.

It seems that n-C16 precipitates a selective portion of the asphaltenes at low mole fractions. More studies are needed in order to derive firm conclusions regarding this effect. The same effect has been observed on other crudes, so the effect is not unique to the above mentioned crude.

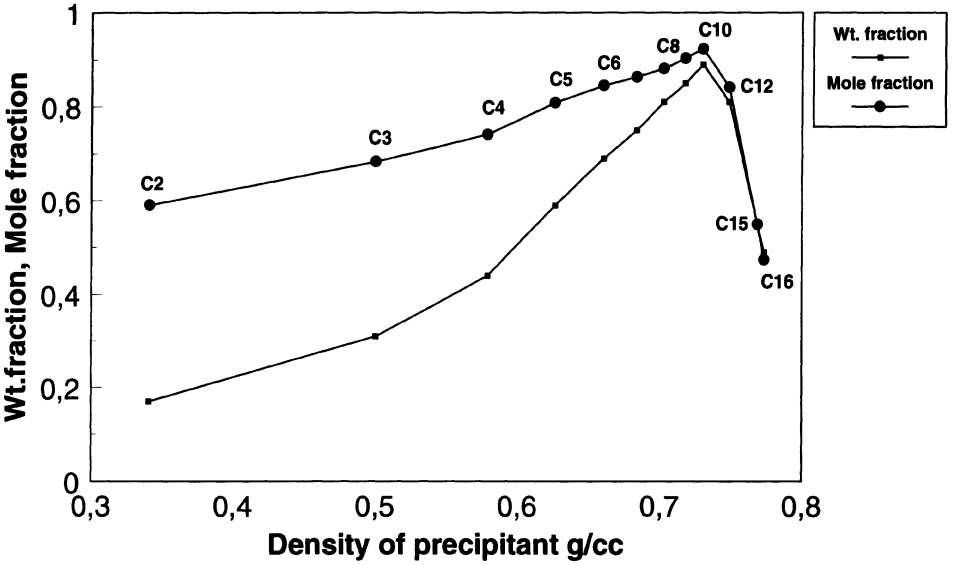

Figure 8. The onset of asphaltene precipitation as a function of density of the precipitant used. The n-alkane is indicated in the curve. Note that the measurements using ethane, propane and butane were conducted at 150 bar and the rest at atmospheric pressure. Temperature is 20°C.

The previous results indicate that conductivity also may be used for diagnostic purposes on reservoir crudes. In Figure 9 is shown a pressure depletion on a reservoir sample which was sampled by a monophasic sampler. These sampling tools allows one to withdraw a sample of the crude at bottomhole conditions and maintain the bottomhole pressure. The sample is transferred to storage bottle at reservoir pressure and at a temperature well above the wax precipitation point. At the lab, the sample is restored to reservoir conditions for approximately one week. A subsample is then transferred at reservoir pressure and temperature to the measurement cell.

Figure 9 should be read from the highest pressure to the lowest. Initially the conductivity is seen to decrease and reach a minimum at reservoir pressure. It then increases towards a sharp maximum which indicates the precipitation of asphaltenes. As pressure is further reduced the conductivity falls in a linear manner.

The recovery process of the field, which corresponds to the crude in Figure 9, is water-alternating-gas injection (WAG). As the crude is undersaturated a large amount of the injected gas will dissolve in the reservoir oil and thereby increase its volume and saturation pressure. This process might also lead to an increased asphaltene precipitation pressure. A study of the conductivity using injection gas was therefore conducted. The result can be seen in Figure 10. Both the conductivity and wnc is shown. As before, there is an initial increase in conductivity but before the dilution effect starts to dominate, the asphaltenes precipitate. This is visualized by the maximum in the wnc. So, in conclusion the gas injection process will spontaneously induce asphaltene precipitation at reservoir conditions. The composition at which the onset occurs is approximately 25 mole% injection gas. For this particular crude, at 25 mole% injection gas, the bubble point is still well below the reservoir pressure. This implies that the asphaltene precipitation pressure increases parallel to or more steeply than the saturation pressure. By the conductivity

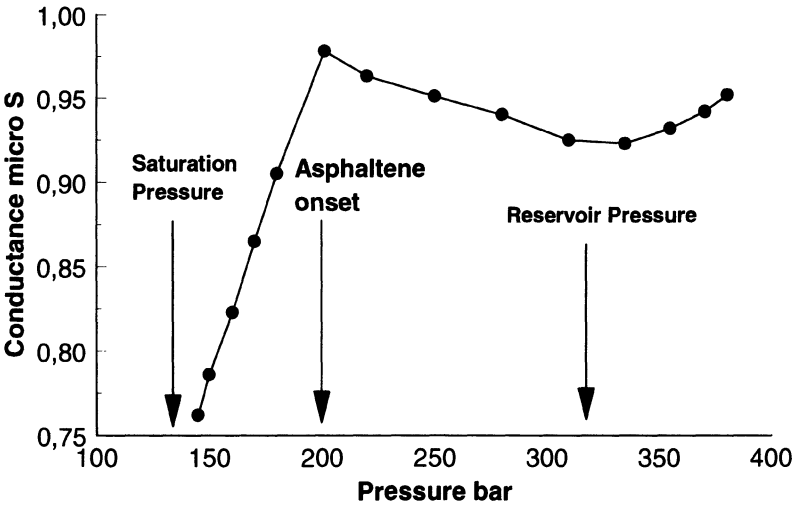

Figure 9. The conductivity of a reservoir oil sampled by a monophasic sampler. The temperature was 92°C. Asphaltene onset is seen at 200 bar which is approximately 70 bar above the saturation pressure and 120 bar below the reservoir pressure.

technique the phase diagram in terms of asphaltene precipitation pressure versus composition can easily be determined.

4.3. Probing the Reversibility of Asphaltene Precipitation by Conductivity

As is seen in the previous sections, the conductivity behavior of crude oil and asphaltenes has a reasonably good qualitative description. It would therefore be of interest to

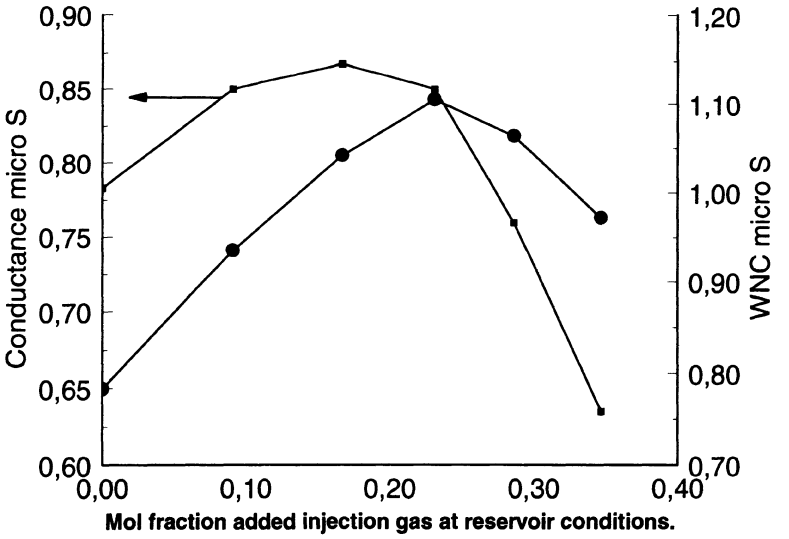

Figure 10. Dilution of a reservoir oil with injection gas at reservoir conditions of 320 bar and 92°C. The onset is seen at approximately 25 mole% injection gas.

probe the reversibility of asphaltene precipitation by pressure cycling a crude with known precipitation pressure. True reservoir samples are expensive and difficult to obtain, a model system has therefore been designed.

A crude sample from a gas cap reservoir was pressurized with ethane in order to determine the precipitation pressure at a given amount of ethane. Once this pressure was determined, a new sample was charged to the cell, the pressure raised well above the known precipitation pressure and the given amount of ethane was added. At this composition the crude will precipitate asphaltenes by pressure depletion at the previously determined pressure.

Figure 11 shows the result of the above described procedure. All curves relate to the same sample, but as indicated, the pressure was cycled with different equilibrium times at the high pressure condition.

Figure 12 shows the same experiment conducted with propane as gas component. Both figures show a decrease in precipitation pressure from the first to the second pressure depletion. This indicates either that some irreversible process has taken place or that the kinetics for resolubilizing the asphaltenes are slow. It should be noted that both stirring and circulation of the fluid was performed throughout the equilibration time.

In particular the ethane case of Figure 11 shows an effect which might be interpreted as two precipitation pressures. The first occurs at approximately 450 bar, where a well defined maximum is seen. The slope of the decrease after the maximum then decreases and then at 150 bar a sudden increase in the slope is again observed. This second 'precipitation pressure' agrees well with the pressure cycles taken at 72 and 240 hours equilibration time.

The same effect is seen for the propane case, although not equally pronounced as for the ethane case. Figure 13 shows the resulting precipitation pressure from Figures 11 and 12 plotted as a function of equilibrium time in the high pressure state.

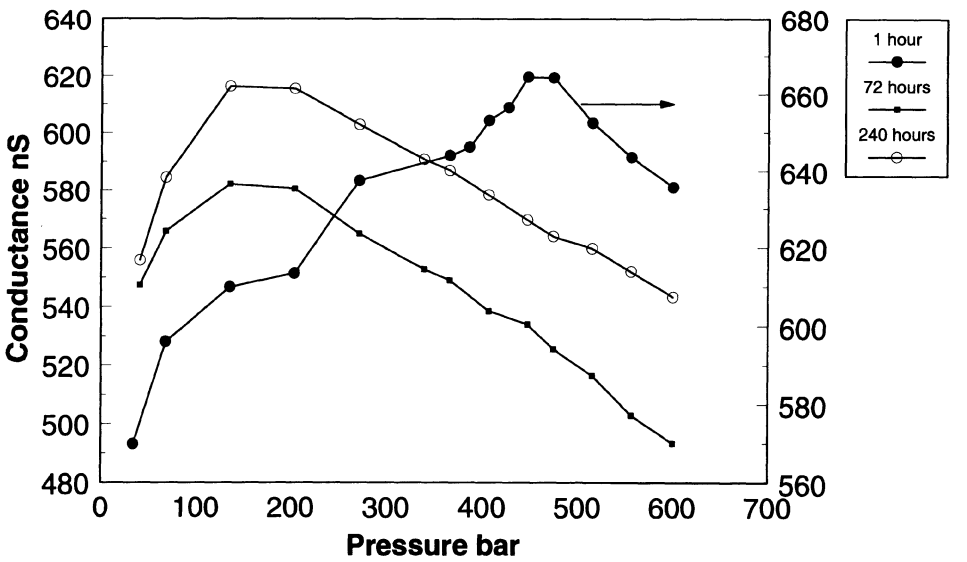

Figure 11. Measurements of conductivity as a function of pressure. The three curves represents different equilibria as shown by the legend. The first pressure depletion (taken at 1 hour after gas addition at 600 bar) clearly shows the highest precipitation pressure. Temperature is 20°C.

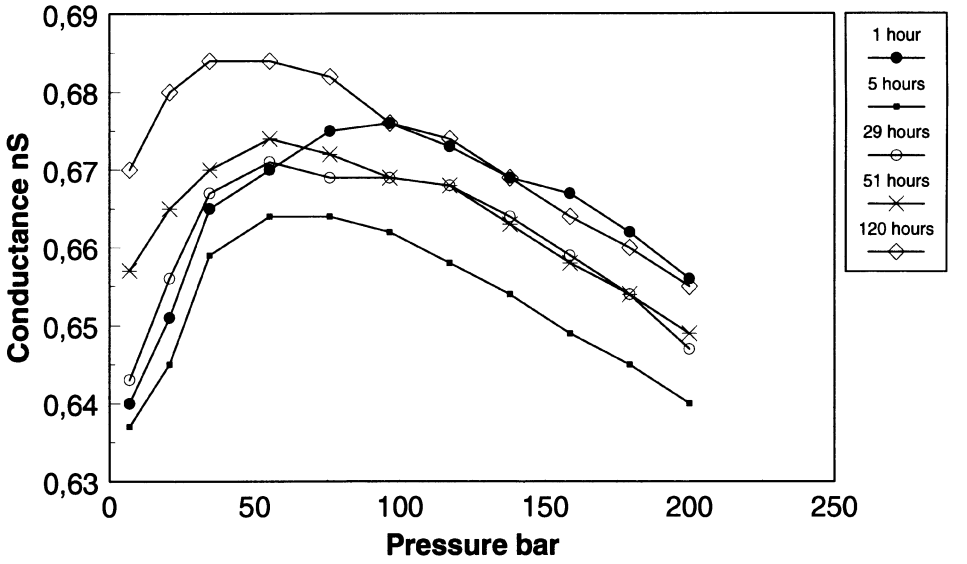

Figure 12. The same experiments as in figure 11, but propane was used as gas component. Temperature is 20°C.

The onset curve for ethane falls rapidly from 450 to 175 bar, while the onset pressures for propane decrease in a more slow fashion. Since reversibility is being probed, the two sets of measurements should have been performed at equal equilibrium times. Therefore, conclusions with regard to comparison is hard to reach. As remarked above it seems however certain that the onset pressure is sensitive to the pressure history of the sample.

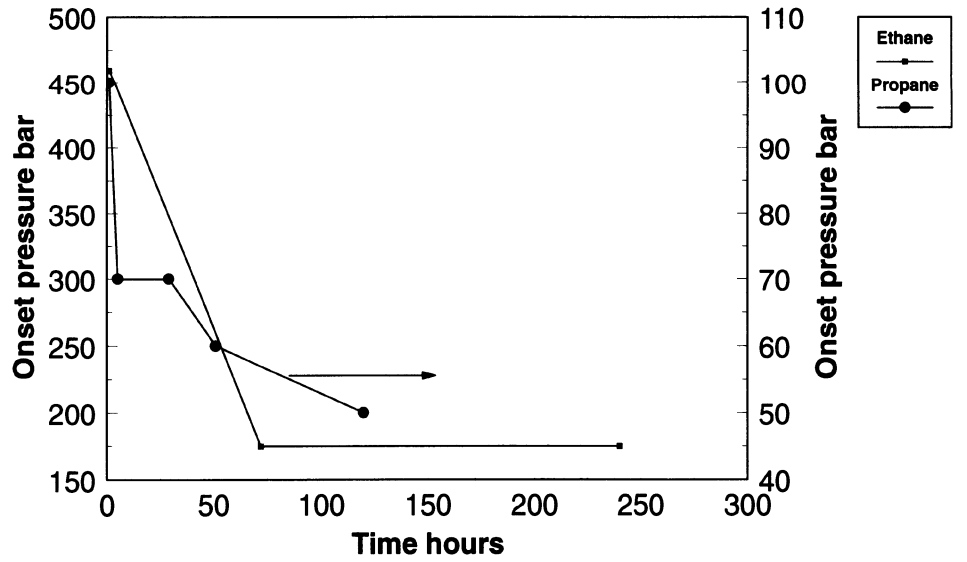

Figure 13. The asphaltene precipitation pressure as function of equilibration time. Temperature is 20°C.

These results imply that downhole sampling should be carried out with monophasic samplers. The effect of not controlling the pressure could be to ignore a potential asphaltene precipitation. This is shown in the next set of experiments which were performed using three different samples from the same region of a North Sea oil field. The reservoir pressure is approximately 450 bar and the temperature is 114°C. The reservoir oil is volatile with low asphaltene content (0.1wt%). The first sample was a conventional bottomhole sample which during storage was kept in a two phase state, i.e. the pressure is below the bubble point.

The second and third samples were monophasic samples. However, the pressure was not maintained at reservoir pressure for either of the samples. For one sample the pressure was lowered to approximately 360 bar and the other to 420 bar. The effect of the pressure history on the conductivity profiles is evident as seen in Figure 14. The observed conductivity of the conventional bottomhole sample is virtually constant. The conductivity increase as pressure decreases can possibly be attributed to a decreasing viscosity. In contrast, the conductivity of the 360 bar monophasic sample is decreasing as pressure is decreased. At 380 bar there is a slight anomaly in the curve indicating some structural changes taking place. The 420 bar sample also shows an initial decrease in conductivity as pressure is depleted, but at around 400 bar a shallow minimum appears and a peak is observed at 385 bar. The conductivity below 385 bar falls toward the bubble point at 330 bar.

The 420 bar sample of Figure 14 bears some resemblance to the curve shown in Figure 9. Both curves show a decrease towards a minimum and then a maximum indicating the dropout of asphaltenes. It is interesting to note that the initial decrease occurs when pressure is reduced for the second time. The sample in Figure 9 was sampled at 320 bar but prior to measurements the pressure was raised to 380 bar, and then reduced again. The

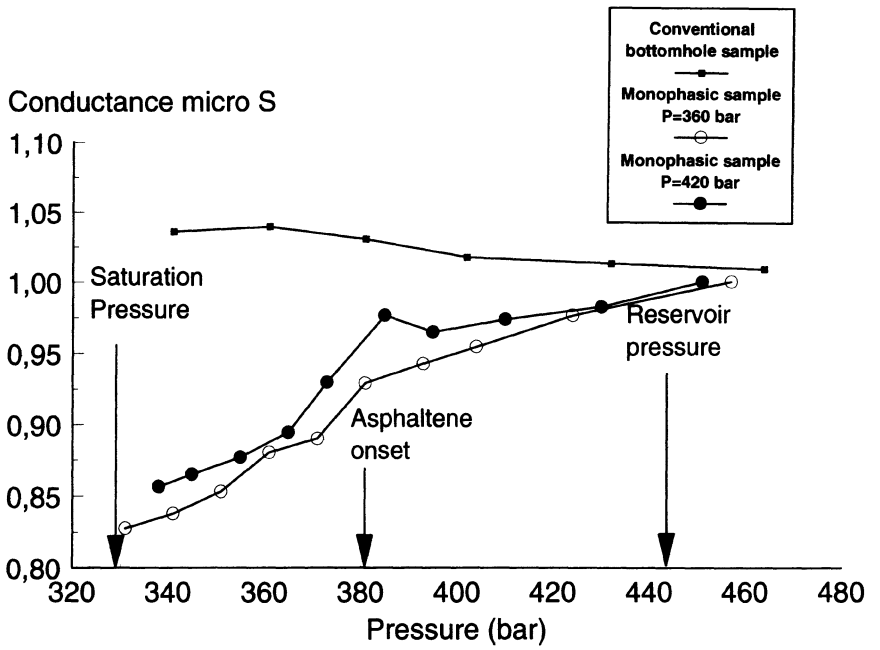

Figure 14. The conductivity of three different live crude samples is shown as a function of pressure. The temperature is 114°C.

minimum occurs approximately at the reservoir pressure. If the pressure of the 420 bar case of Figure 14 had previously been lowered to approximately 400 bar, then these two observations would possibly be in agreement.

With regard to conductivity and within the time frame of the above experiments, the precipitation of asphaltenes seems to be irreversible. In particular the pressure history is important. Once the crude has been pressure depleted, the asphaltenes precipitation pressure changes. Trying to establish the original state of the asphaltenes was not possible, i.e. the precipitation pressure did not increase as a function of equilibrium time at high pressure conditions. Qualitatively, similar irreversible behavior has been seen for live reservoir crudes. The results show that only monophasic samples can give a good determination of the asphaltene precipitation pressure.

From the above experiments it is likely that structural changes takes place as a function of pressure. The original state of the asphaltenes may be as monomeric units or small micelles. As pressure decreases the asphaltenic units starts to flocculate at a given pressure. As the pressure is further reduced more flocs are formed. Upon increasing the pressure again, the asphaltene fraction responsible for the high pressure flocculation point does not redissolve to their initial state. However, they might become colloidally suspended, but give no or very small contribution to the conductivity. The second flocculation point repeats itself by pressure cycling and so, this process must be considered reversible. We are therefore facing two different types of flocculation, i.e. one reversible and one irreversible. The irreversible fraction is responsible for the high pressure flocculation point. To complicate the matter even more, it is likely that different crudes will have different behavior with regard to reversibility.

5. CONCLUSIONS

By performing measurements of the conductivity of asphaltenes dissolved in various organic solvents the ionic properties of the asphaltenes can be deduced. Crude oil contains a variety of structures which have the potential of becoming ionized and can be responsible for the solvatization of ions.

The presence of aggregates and/or molecules with a net charge in crude oil, have been demonstrated in a number of independent experimental works.

Asphaltenes dissolved in organic solvents show the characteristics of ions in low permittivity media. Indications of ions, ion pairs and higher aggregates have been detected.

The precipitation of asphaltenes is reflected in the electrical conductivity of the oil. The flocculation onset can be probed both by pressure depletion on monophasic reservoir oil samples and by changing the composition at constant pressure as in a gas injection process.

Conductivity measurements indicates the possibility of a reversible and an irreversible precipitation pressure. Cycling through the flocculation pressure a number of times shows a hysteresis effect. The first pressure depletion seems to give the highest flocculation onset.

Pressure history of the resevoir oil is important for evaluation of experimental data regarding precipitation pressure.

REFERENCES

1. F.J. Nellensteyn, World Petr. Congr. Porcs., 2, 616, (1933).
2. J. Ph. Pfeiffer, R.N.J. Saal, J. Phys. Chem., 44, 139, (1940).

3. E.Y.Sheu, O.C. Mullins ed.,Plenum Press,NY, 'Asphaltenes: Fundamentals and Applications' 'Solubility and Phase Behaviour of Asphaltenes in Hydrocarbon Media' (1995).
4. T. F. Yen, T.F. Yen, (Ed.), "Asphaltenes and Asphalts, 1." Developments in Petroleum Science, 40A, Elsevier Science B.V., 1994.
5. J.C.Ravey, G.Ducouret, D.Espinat, Fuel, 67,Nov. (1988).
6. D.Espinat, J.C.Ravey, SPE 25187 (1993).
7. D.Espinat, J.C.Ravey, V.Guille, J.Lambard, T.Zemb, J.P.Cotton, Journal De Physique IV, 3,181 (1993).
8. J.G.Speight, 'Molecular Models for Petroleum Asphaltenes and Implications for Processing 'Eastern Oil Shale Symposium Nov.13–15 (1991).
9. J.G.Speight, 'Latest Thoughts on The Molecular Nature of Petroleum Asphaltenes' Am.Chem.Soc. Dallas meeting, April 9–14 (1989).
10. T.F.Yen, Energy Sources, 1,4,447 (1974).
11. O.P.Strauz, T.W.Mojelsky, E.M.Lown, 'The Molecular Structure of Asphaltene: An Unfolding Story' Eastern Oil Shale Symposium Nov.13–15, (1991).
12. T.F.Yen, 'Present Status of The Structure of Petroleum Heavy Ends and its Significans to Various Technical Applications' Am.Chem.Soc. New York meeting, August 27-September 1 (1972).
13. N.E. Burke, R.E. Hobbs, S.F. Kashou, J. Petr. Tech. November, 1440, (1990).
14. B.J. Fuhr, L. Cathrea, K.H. Coates, A.I. Majeed, Fuel, 70, 1293, (1991).
15. L.T. Vuong, "Asphaltene Deposition and its Role in Enhanced Oil Recovery Miscible Gas Flooding Processes." M.Sc. Thesis, Dept. of Chem. Eng. University of Ill. at Chicago.
16. B.E. Conway, "Ionic Hydration in Chemistry and Biophysics." Studies in Physical and Theoretical Chemistry 12, Elsevier Scientific Publsihing Company, (1981).
17. A. Gemant, "Ions in Hydrocarbons." Interscience Publishers, (1962).
18. P. Fotland, H. Anfindsen, F.H. Fadnes, Fluid Phase Equilibria, 82, 157, (1993).
19. P. Fotland, Fuel Science and Tech. Int'l. 14 (1&2) 313, (1996).
20. P. Fotland, H. Anfindsen, Fuel Science and Tech. Int'l., 14 (1&2), 101, (1996).
21. S.Penzes, J.G.Speight, Fuel, 53, 192 (1974).
22. P.M.Lichaa, L.Herrere, SPE 5304, (1975).
23. P.M.Lichaa, Oil Sands, 609 (1977).
24. E.J.M.Kendall, The Journal of Canadian Petroleum Technology, July-Sep. 37 (1978).
25. H.P.Maruska, E.O.Forster, J.H.Enard, IEEE Transactions on Electrical Insulation, EI-20, 6 (1985).
26. B.Siffert, J.Kuczinski, E.Papirer, Journal of Colloid and Interface Science, 135, 1, 107 (1990).
27. E.Y.Sheu, M.M.De Tar, D.A.Storm, Fuel, 73,1, 45 (1994).
28. E.Y.Sheu, D.A.Storm, M.M.De Tar, Journal of Non-Crystalline Solids 131–133, 341 (1991).
29. D.J. MacMillan, J.E. Tackett Jr., M.A. Jessee, T.G. Monger-McClure, SPE 28990, (1995).
30. Boukamp, The computer program and user manual is available from Prof. Boukamp at the University of Twente, Netherland.
31. S. Glasstone, "Textbook of Physical Chemistry." D. Van Nostrand Company, Second ed. (1946).
32. J.G.Speight, ' Solvent Effects in The Molecular Weights of Petroleum Asphaltenes' Am.Chem.Soc. New York Meeting, Aug. 23–28, (1981).
33. J.G.Speight, D.L.Wernick, K.A.Gould, R.E.Overfield, B.M.L.Rao, D.W.Savage Revue De L'institut Francais Du Petrole, 40,1, 51 (1985).
34. R.M. Fuoss, F. Accascina, "Electrolytic Conductivity." Interscience Publishers Inc. (1959).
35. L.P. Safonova, A.M. Kolker, Russian Chemical Reviews, 61 (9), 959, (1992).
36. S. Petrucci, E.M. Eyring, J. Phys. Chem. 95, 1731, (1991).

Chapter IX

A NEW SUSPENSION VISCOSITY MODEL AND ITS APPLICATION TO ASPHALTENE ASSOCIATION THERMODYNAMICS AND STRUCTURES

Moon-Sun Lin, J. M. Chaffin, R. R. Davison, C. J. Glover,* and J. A. Bullin

Center for Asphalt and Materials Chemistry
Department of Chemical Engineering
Texas A&M University
College Station, Texas 77843

1. INTRODUCTION

Asphalt cement has been used over a century for roadway construction in United States. Historically, one of the most extensively studied physical properties has been the viscosity of the asphalt binder, in particular, how the viscosity of the asphalt binder changes during a pavement's lifetime. Many attempts have been made to relate the viscosity of the binder to its chemical composition and molecular structure. One complicating factor to understanding the exact relationship between viscosity and chemical composition arises from the extremely complex chemical composition (an asphalt may contain thousands of individual components). Another complicating factor arises from the ever changing chemical composition of the binder throughout the pavement's lifetime as a result of low temperature oxidation. As a result, most attempts to correlate a binder's viscosity to the binder's chemical composition have been in terms of only a few pseudo-components. The components found to have the greatest influence on the viscosity are referred to collectively as the asphaltenes.

Many researchers (Sheu et al., 1991a, Storm et al., 1993; Reerink and Lijzenga, 1973; Rao and Serrano, 1986) have shown that the viscosities of asphalts and heavy petroleum residua are greatly influenced by the colloidal structure of asphaltenes present in those materials. Asphaltenes are very complex organic macromolecules which are defined

* To whom correspondence should be sent.

as the insolubles in a selected paraffin solvent such as n-pentane, n-hexane, or n-heptane. Dickie and Yen (1967) showed, using X-ray diffraction, that asphaltenes appear as unit sheets composed of a highly condensed polynuclear aromatic ring system with extended alkyl sidechains attached to the ring structure. They also showed that asphaltenes form clusters and micelles through strong aromatic π-π association. The presence and the structure of clusters of asphaltene molecules has also been studied using various scattering techniques such as small-angle X-ray scattering (SAXS) (Pollack, 1970; Dwiggins, 1965; Senglet et al., 1990; Kim and Long, 1979) and small-angle neutron scattering (SANS) (Ravey et al., 1988; Overfield et al., 1989; Sheu et al., 1991b).

There are many conflicting hypotheses on the structure of asphaltene aggregate particles. Ravey et al. (1988) separated asphaltenes into several fractions with narrower molecular distributions and showed that asphaltenes appear to be polydispersed disc-like particles in several solvents using SANS techniques. They also showed that the extent of polydispersity of asphaltenes does not change the conclusion that the shape of asphaltene aggregates should be disc-like. On the other hand, Sheu et al. (1991a) concluded that Ratawi asphaltene particles are spherical and the distribution of asphaltene particle size follows the Schultz distribution (Zimm, 1948). However, in general, asphalts are composed of two phases, an associated phase which is composed of asphaltene aggregates, and a dispersed phase which is composed of maltenes, a mixture of aromatics and saturates.

The presence of asphaltene association has a very profound influence on the viscosity of asphaltic materials. Lin et al. (1995a) have shown that both the original asphaltenes and those asphaltenes produced by oxidation form associating particles and result in an increase in asphalt viscosity in a similar manner. They used a modified two-parameter Pal-Rhodes (1989) model to describe the relationship between asphalt viscosity and asphaltene content for seven asphalts. The Pal-Rhodes model (Pal and Rhodes, 1989) was originally used to describe the viscosity/concentration relationship of emulsions and is given as:

$$\eta_r = \frac{\eta}{\eta_0} = (1 - K\phi)^{-2.5} \tag{1}$$

where η and η_0 are the viscosity of the emulsion and the viscosity of the solvent, respectively. η_r represents relative viscosity and ϕ is the volume fraction of particles. K is the solvation constant which accounts for the effects of association. The exponent -2.5 is the result of assuming the association is spherical in shape. Despite the simplicity of the Pal-Rhodes model, Sheu et al. (1989) have successfully used Equation (1) to describe the viscosity of asphaltene solutions as functions of asphaltene concentration up to 25% in several organic solvents. They also used many other viscosity models to describe the asphaltene solution viscosity as functions of asphaltene concentration. From all the models used, they concluded that asphaltene particles are spherical and solvated by the solvents used. Lin et al. (1995a) used a modified two-parameter version of Equation (1) by letting the exponent of -2.5 to be a free parameter, v, to account for non-sphericity of the asphaltene particles. They showed that this modified Pal-Rhodes model can successfully describe the asphalt viscosity as functions of asphaltene content for a very wide range of asphaltene contents up to 60% by weight. Many researchers (Eilers, 1948; Reerink and Lijzenga, 1973; Heukelom and Wijga, 1971; Sheu et al., 1991a; Storm and Sheu, 1993) have attempted to describe the viscosity/asphaltene relationship using existing or newly-developed models. A realistic viscosity model for relating asphalt viscosity to asphaltene con-

tent has to account for both the effect of the shape of asphaltene particles and the effect of asphaltene molecular association. However, the common difficulties in applying models to the asphalt viscosity/asphaltene relationship is that the viscosity/asphaltene relationship of asphalts is highly dependent on asphalt composition, especially maltene composition (Lin et al., 1995b) and that the model parameters obtained by regression can not adequately describe the severity of asphaltene association and the solvation power of maltenes. In the present work, a suspension viscosity model is developed to account for the effect of particle size distribution, the effect of particle shape, and the effect of molecular association. This model is applied to describe asphalt viscosity as a function of asphaltene content and is capable of extracting several asphaltene aggregate structural parameters from viscosity and asphaltene content measurements.

2. EXISTING VISCOSITY MODELS FOR NON-ASSOCIATING SUSPENSIONS

2.1. Monodispersed, Non-Associating Suspensions

The first model to describe the increase in viscosity due to the presence of solid particles was developed by Einstein (1906). In Einstein's treatment, particles were assumed to be perfectly spherical, monodispersed, and non-interacting. The model relates the viscosity of the solution to the volume fraction of solid particles.

$$\eta = \eta_0(1 + 2.5\phi) \tag{2}$$

Again, similar to Equation (1), the coefficient of 2.5 assumes that the shape of suspension particles is spherical. Equation (2) is usually only valid for particle concentrations up to 2–10% by volume, dependent on the system. Equation (2) does not adequately describe the viscosity of the suspension at higher particle concentrations because the particles begin to interact hydrodynamically (Frankel and Acrivos, 1967). Models for more concentrated suspensions have been developed using the viscosity mean-field theory. The Mean-field theory states that the differential increase in suspension viscosity as a result of adding a small amount of particles to a concentrated suspension can be described using the differentiated form of Equation (2) with η_0 replaced by η.

$$d\eta = 2.5\eta d\phi \tag{3a}$$

or

$$\frac{d\eta}{\eta} = 2.5 d\phi \tag{3b}$$

where $d\eta$ is the increment of viscosity on the addition of a small amount of particle volume fraction $d\phi$. Equations (3a) and (3b) assume that the small amount of particles is added into a new solvent environment having a viscosity equal to the suspension viscosity η. The viscosity of the suspension as a function of volume fraction can be obtained by integrating Equation (3b) to obtain Equations (4a) and (4b).

$$\ln\left(\frac{\eta}{\eta_0}\right) = \int_{\eta_0}^{\eta} \frac{d\eta}{\eta} = \int_0^{\phi} 2.5 d\phi = 2.5\phi \tag{4a}$$

or

$$\eta = \eta_0 e^{2.5\phi} \tag{4b}$$

Equation (4b) has a higher applicable concentration limit than Equation (2) but still only describes the suspension viscosity up to moderate particle concentration. Generally, It has been observed that the solution viscosity increases more than exponentially at high particle concentration. The sharp increase in viscosity is caused by the limited free space available for the solvent to flow at high concentration. In fact, when the particle concentration reaches its maximum value, ϕ_{MAX}, the suspension viscosity will increase to infinity due to the entire loss of free space. Mooney (1951) introduced a crowding factor, $(1-\phi/\phi_{MAX})^2$, to account for the loss of free space as concentration increases. Mooney replaced $d\phi$ with $d\phi/(1-\phi/\phi_{MAX})^2$ in Equations (3a) and (3b) and integrated to obtain Equation (5),

$$\eta = \eta_0 \exp(a)\left(\frac{2.5\phi}{1-\frac{\phi}{\phi_{MAX}}}\right) \tag{5}$$

The crowding factor represents the fact that the available free volume fraction for particles is $(1-\phi/\phi_{MAX})$ at particle volume fraction ϕ. Kreiger and Dougherty (1959) replaced $d\phi$ with $d\phi/(1-\phi/\phi_{MAX})$ in Equation (3b) to obtain Equation (6), which is known as Kreiger-Dougherty equation.

$$\eta = \eta_0\left(1-\frac{\phi}{\phi_{MAX}}\right)^{-2.5\phi_{MAX}} \tag{6}$$

Rutgers (1962a, 1962b) published two extensive reviews of the viscosity/concentration models. He identified 96 equations from the literature that described the viscosity/concentration relationships of suspensions. Comparing experimental data with those equations, he concluded that those 96 equations can be reduced to five useful ones. Sudduth (1993a) found that the derivative forms of those five useful equations can generalized as Equation (7).

$$\frac{d\eta}{\eta} = \frac{\nu d\phi}{\left(1-\frac{\phi}{\phi_{MAX}}\right)^{\sigma}} \tag{7}$$

where σ is the "particle interaction coefficient", which is an indicator of the magnitude of the particle interaction in the suspension, and ν is the particle shape factor and is equal to 2.5 for perfectly spherical particles. Equations (4b), (5), (6) can be obtained by integrating Equation (7) using σ equal to 0, 2, and 1, respectively. The generalized Equation (7) shows that the maximum particle packing volume fraction (ϕ_{MAX}) is a very important parameter in describing the viscosity/concentration function. It is well known that ϕ_{MAX} is a function of particle size distribution because smaller particles can fit in the empty space entrapped between larger

particles. Therefore, it is generally assumed that Equation (7) is applicable to polydispersed suspension systems with ϕ_{MAX} a function of the particle size distribution.

2.2. Effect of Particle Size Distribution

A number of researchers (Furnas, 1931; Farris, 1968; Dabak and Yucel, 1987; McGeary, 1961; Ouchiyama, 1984; Lee, 1970; and Sudduth, 1993b; Sudduth, 1993c) studied the effects of particle size distribution on ϕ_{MAX}. McGeary (1961) studied the maximum packing fraction as a function of particle size distribution by packing metal spheres in a glass container. He found that ϕ_{MAX} for monodispersed particles is 0.625 and is independent of particle size. For binary mixtures of particles, ϕ_{MAX} was found to be a function of the ratio of the diameter of larger particle to that of smaller particle, R. Furthermore, ϕ_{MAX} reaches a maximum value of 0.84 when R approaches infinity. The maximum values of ϕ_{MAX} for ternary and quaternary particle mixtures were found to be 0.9 and 0.951, respectively, and increases with the width of the particle size distribution. In fact, the maximum value of ϕ_{MAX} for any arbitrary particle size distribution can be calculated using a simple packing scheme (Sudduth, 1993b). Sudduth (1993b) defined the ϕ_{MAX} for a mixture of N different particle sizes having a given particle size distribution as ϕ^N_{MAX} and the maximum value of ϕ_{MAX} for mixtures of N different particle sizes as ϕ^N_{ULT}, respectively. Note that there is only one value of ϕ^N_{ULT} for any mixtures of N particle sizes. For monodispersed suspensions, ϕ^1_{ULT} is equal to ϕ^1_{MAX} or Equation (8),

$$\phi^I_{ULT} = \phi^I_{MAX} \tag{8}$$

For mixtures of two different particle sizes, ϕ^2_{ULT} occurs when the smaller particles can entirely fit in the empty space between larger particles and would be given as (Sudduth, 1993b)

$$\begin{aligned}\phi^2_{ULT} &= \phi^1_{ULT} + \left(1-\phi^1_{ULT}\right)\phi^1_{MAX} \\ &= \phi^1_{MAX} + \left(1-\phi^1_{MAX}\right)\phi^1_{MAX}\end{aligned} \tag{9}$$

Similarly, for mixtures of N different particle sizes, a recursive relation yield

$$\begin{aligned}\phi^N_{ULT} &= \phi^{N-1}_{ULT} + \left(1-\phi^{N-1}_{ULT}\right)\phi^1_{MAX} \\ \phi^1_{ULT} &= \phi^1_{MAX}\end{aligned} \tag{10}$$

The solution to Equation (10) can be easily obtained and is given by Sudduth (1993b) as follows:

$$\begin{aligned}\phi^N_{ULT} &= \phi^I_{MAX}\sum_{k=1}^{N}\left(1-\phi^I_{MAX}\right)^{k-1} \\ &= 1-\left(1-\phi^1_{MAX}\right)^N\end{aligned} \tag{11}$$

With a ϕ^1_{MAX} of 0.625 (McGeary, 1961), ϕ^2_{MAX}, ϕ^3_{MAX} and ϕ^4_{MAX} can be calculated using Equation (11) to be 0.86, 0.95, and 0.98, respectively. However, ϕ^N_{ULT} occurs only for

some optimal particle size distribution but provides an upper limit for ϕ^N_{MAX}. In general, ϕ^N_{MAX} is a "functional", a function of functions, which can be written as follows:

$$\phi^N_{MAX} = \phi^N_{MAX}(P(D)) \tag{12}$$

where P(D) is the particle size distribution function and D is the particle diameter. Sudduth (1993b) used a semi-empirical equation given in Equation (13), which is an extension of the binary system, based on McGeary's data (1961), for polydispersed suspension:

$$\phi^N_{MAX} = \phi^N_{ULT} - (\phi^N_{ULT} - \phi^I_{MAX}) e^{0.268\left(1-\left(\frac{\overline{D}_5}{\overline{D}_1}\right)\right)} \tag{13}$$

$\overline{D}_1$ and $\overline{D}_5$, which represent the average particle diameter with the first and fifth order, are given in Equations (14) and (15):

$$\overline{D}_1 = \int D P(D) \mathrm{d}D \tag{14}$$

$$\overline{D}_5 = \frac{\int D^5 P(D) \mathrm{d}D}{\int D^4 P(D) \mathrm{d}D} \tag{15}$$

Although Equation (13) is an empirical best fit of a binary system, it generally gives a fairly good prediction of ϕ^N_{MAX}. Ouchiyama (1984) gave a theoretical derivation of $\phi^N_{MAX}(P(D))$ using a simplified statistical model. However, the resulting expression of $\phi^N_{MAX}(P(D))$ is quite complicated and does not generally give a better prediction of ϕ^N_{MAX} than Equation (13).

3. DEVELOPMENT OF A NEW VISCOSITY MODEL FOR ASSOCIATING SUSPENSIONS

Molecular association, especially for strongly interacting molecules such as asphaltenes, has a profound influence on the rheology of the suspension solution. Formation of particle aggregates gives rise to an increase in the "effective volume" of the particles due to entrapment of empty space within the aggregates as shown in Figure 1. A simple approach to account for this increase in effective particle volume is scaling the dry particle volume fraction by a solvation constant, K. By substituting $K\phi$ for ϕ in Equation (7) and integrating, a suspension model that accounts for particle size distribution and molecular association can be generalized as given in Equation (16).

$$\ln\left(\frac{\eta}{\eta_0}\right) = \begin{cases} \dfrac{\nu\phi^N_{MAX}}{1-\sigma}\left[1-\left(1-\dfrac{K\phi}{\phi^N_{MAX}}\right)^{1-\sigma}\right] & \text{if } \sigma \neq 1 \\ -\nu\phi^N_{MAX}\ln\left(1-\dfrac{K\phi}{\phi^N_{MAX}}\right) & \text{if } \sigma = 1 \end{cases} \tag{16}$$

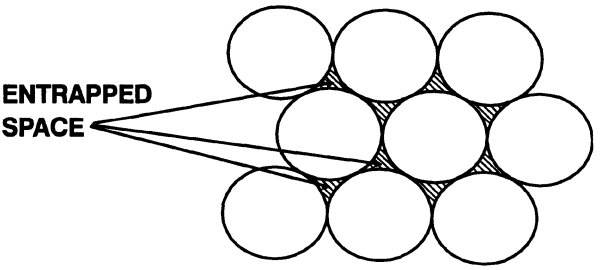

Figure 1. Representation of space entrapment of particle association.

For the simplified case with ϕ_{MAX} and σ equal to 1 and ν equal to 2.5, Equation (1), the Pal-Rhodes model (1989), is obtained. Despite the simplicity of Equation (1), Sheu et al. (1991a) showed that this equation can adequately describe the viscosity/concentration function for complex systems such as asphaltene/toluene solutions at asphaltene concentrations up to 25% by weight.

Molecular association is usually induced by two processes, thermodynamic equilibrium and shear induced-association. An increase in the collision rate of suspended particles can be caused by applying a high shear rate which gives rise to the temporary formation of aggregates. This process is further complicated by the shear thinning behavior of typical non-newtonian fluids. Fortunately, at low shear rates, shear induced association is negligible. At a low shear rate, the rheological behavior of interacting suspensions is greatly influenced by the thermodynamic equilibrium of the association processes. A simplified molecular association process can be formulated as follows:

$$\begin{aligned} A_1 + A_1 &\overset{K_{e2}}{\rightleftharpoons} A_2 \\ A_2 + A_1 &\overset{K_{e3}}{\rightleftharpoons} A_3 \\ &\vdots \\ A_{N-1} + A_1 &\overset{K_{eN}}{\rightleftharpoons} A_N \end{aligned} \tag{17}$$

where A_N represents the aggregate with N molecules or monomers and K_{eN} represents the equilibrium constant for the formation of A_N. To simplify Equation (17), all of the equilibrium constants can be assumed to be approximately the same.

$$K_{e2} = K_{e3} = \ldots = K_{eN} = \ldots = K_e \tag{18}$$

In reality, asphaltenes are not pure compounds but complex mixtures. Each different molecule in asphaltenes may have a different association constant. If one assumes that the K_{eN} are all different, a relationship relating K_{eN} to the number of particles in an aggregate has to be established. However, this distribution of association constants is very difficult to model and, therefore, is neglected. The validation of the assumption that all K_e values are

the same can be justified only by the ability of the model to predict data. Based on Equation (18), the concentration of aggregates of all sizes can be written as:

$$\begin{aligned}
[A_2] &= K_e[A_1]^2 \\
[A_3] &= K_e[A_2][A_1] = K_e^2[A_1]^3 \\
[A_4] &= K_e[A_3][A_1] = K_e^3[A_1]^4 \\
&\vdots \\
[A_N] &= K_e[A_{N-1}][A_1] = K_e^{N-1}[A_1]^N \\
&\vdots
\end{aligned} \tag{19}$$

The total concentration of particles, c_P in mol/L, is defined as:

$$\begin{aligned}
c_P &= \sum_{N=1}^{\infty} N[A_N] \\
&= [A_1]\left\{1 + 2K_e[A_1] + 3(K_e[A_1])^2 + \ldots + N(K_e[A_1])^{N-1} + \ldots\right\} \\
&= \frac{[A_1]}{\left(1 - K_e[A_1]\right)^2}
\end{aligned} \tag{20}$$

Furthermore, the total concentration of aggregates of all sizes, [A], can be expressed as:

$$[A] = \sum_{N=1}^{\infty}[A_N] = \frac{[A_1]}{1 - K_e[A_1]} \tag{21}$$

Combining Equations (20) and (21), the distribution function of N-molecule aggregates can be obtained.

$$P(N) = \frac{[A_N]}{[A]} = (1 - K_e[A_1])(K_e[A_1])^{N-1} \tag{22}$$

The average number of molecules per aggregate then becomes

$$\begin{aligned}
\overline{N} &= \sum_{N=1}^{\infty} N P(N) = \left(1 - K_e[A_1]\right)\sum_{N=1}^{\infty} N\left(K_e[A_1]\right)^{N-1} \\
&= \frac{1}{1 - K_e[A_1]}
\end{aligned} \tag{23}$$

To evaluate the size of the N-molecule aggregate, the knowledge of the structure of molecular association is needed. In nature, compact and spherically symmetric aggregates are the most frequently encountered and the most (structurally) stable. Experimental (Oono, 1978; Mercer et al., 1979) and theoretical (Mandelbrot, 1982) studies indicate that the radius of gyration (R_G) of spherical aggregates (i.e., the average distance from a particle to the center of gravity) increases with the diameter of the single particle and with the square root of the number of particles per aggregate, i.e.,

$$(R_G)_N \sim N^{\frac{1}{2}} D_0 \tag{24}$$

As viscosity is a bulk property, it can tell us nothing about the shape of the asphaltene molecule, so for simplicity the molecules will be assumed to be spherical. However, for the associated particle, studies (Grimson and Barker, 1987) show that, in general, Equation (24) should be replaced by Equation (25),

$$(R_G)_N \sim N^{\frac{1}{f_D}} D_0 = \left(\frac{C}{2}\right) N^{\frac{1}{f_D}} D_0 \tag{25}$$

where C is a constant and f_D represents the fractal dimension of the aggregation structure with $f_D \leq 3$. When f_D is equal to 3, the particle volume fraction of aggregate approaches ϕ^1_{MAX} as N approaches infinity. On the other hand, when f_D is less than 3, the molecular volume fraction of aggregate decreases continuously with increasing N, and finally approaches zero for a very large N. With the aid of Equation (25), the volume of an N-particle aggregate is given as:

$$V_N^{agg} = \frac{4\pi}{3}(R_G)_N^3 = \frac{4\pi}{3}\left(\frac{C}{2}\right)^3 N^{\left(\frac{3}{f_D}\right)} D_0^3 \tag{26}$$

where C is independent of D_0 but may be a function of f_D. The solvation constant K_N for N-particle aggregates is then given in Equation (27),

$$K_N = \frac{V_N^{agg}}{NV_0} = \frac{\frac{4\pi}{3}\left(\frac{C}{2}\right)^3 N^{\left(\frac{3}{f_D}\right)} D_0^3}{N\frac{4\pi}{3}\left(\frac{D_0}{2}\right)^3} = C^3 N^{\left(\frac{3-f_D}{f_D}\right)} \tag{27}$$

where V_0 is the volume of a single molecule, which is assumed to be a sphere. The total solvation constant K in Equation (16) is the sum of all the contributions from every aggregate.

$$K = \sum_{N=1}^{\infty} K_N P(N) = C^3 (1 - K_e[A_1]) \sum_{N=1}^{\infty} N^{\left(\frac{3-f_D}{f_D}\right)} (K_e[A_1])^{N-1} \tag{28}$$

In Equation (28), $[A_1]$ is not an easily measured quantity and is usually unknown. In contrast, the total particle concentration, c_P, can easily be converted to total particle weight or volume fraction. Fortunately, $[A_1]$ can be related to c_p by solving Equation (20) to give

$$[A_1]=\frac{1}{K_e}+\frac{1-\sqrt{1+4K_e c_P}}{2K_e^2 c_P} \tag{29}$$

However, c_p is still not a convenient quantity to work with and needs to be converted to a quantity that can be measured directly such as volume fraction or weight fraction. c_P can be converted to total particle volume, ϕ, as shown in Equation (30) in which the individual molecules are assumed to be spherical.

$$\begin{aligned}\phi &= 6.023\times10^{23} c_P\left(\frac{\text{mole}}{\text{L}}\right)\times\frac{4\pi}{3}\left(\frac{D_0(\text{m})}{2}\right)^3\times\left(\frac{1000\text{L}}{\text{m}^3}\right)\times\left(\frac{1}{0.625}\right)\\ &= 5.0458\times10^{26} c_P D_0^3\end{aligned} \tag{30}$$

where 0.625 is the maximum packing volume fraction for solid spheres of uniform size (McGeary, 1961). By combining Equations (28), (29), and (30), the solvation constant, K, can be expressed as a function of ϕ:

$$K= C^3\left(\frac{-1+\sqrt{1+2\kappa_1\phi}}{\kappa_1\phi}\right)\sum_{N=1}^{\infty} N^{\left(\frac{3-f_D}{f_D}\right)}\left(1+\frac{1-\sqrt{1+2\kappa_1\phi}}{\kappa_1\phi}\right)^{N-1}$$

$$\text{where}\quad \kappa_1=\left(\frac{3.9637\times10^{-27}K_e}{D_0^3}\right) \tag{31}$$

$\phi^N{}_{MAX}$ in Equation (16) is also dependent on particle size distribution, P(D), which is given in Equation (22). By substituting Equation (22) into Equations (14) and (15), expressions for $\overline{D}_1$ and $\overline{D}_5$ can be obtained

$$\overline{D}_1 = C D_0\left(\frac{-1+\sqrt{1+2\kappa_1\phi}}{\kappa_1\phi}\right)\sum_{N=1}^{\infty} N^{\left(\frac{1}{f_D}\right)}\left(1+\frac{1-\sqrt{1+2\kappa_1\phi}}{\kappa_1\phi}\right)^{N-1} \tag{32}$$

$$\overline{D}_5=\frac{CD_0\sum_{N=1}^{\infty} N^{\left(\frac{5}{f_D}\right)}\left(1+\frac{1-\sqrt{1+2\kappa_1\phi}}{\kappa_1\phi}\right)^{N-1}}{\sum_{N=1}^{\infty} N^{\left(\frac{4}{f_D}\right)}\left(1+\frac{1-\sqrt{1+2\kappa_1\phi}}{\kappa_1\phi}\right)^{N-1}} \tag{33}$$

By combining Equations (13), (32), and (33), $\phi^N{}_{MAX}$ can be evaluated.

4. EXPERIMENTS

4.1. Methodology

To study the effects of the maltene phase composition on the viscosity/asphaltene relationship, several experiments were designed to systematically control both asphaltene and saturate content in asphaltic materials. Three core asphalts from the Strategic Highway Research Program (SHRP) (AAA-1, AAF-1, and AAG-1) representing a wide variety of crude sources were examined in this study. Each asphalt was fractionated into asphaltenes, aromatics, and saturates. Blends of asphaltenes/aromatics/saturates in varied ratios were produced using fractions from the same asphalt, and these blends were then aged in a pressurized oxygen vessel (POV). The increase in asphalt viscosity and asphaltene content due to oxidation was measured using dynamic mechanical analysis (DMA) and solvent precipitation using n-hexane, respectively.

4.2. Separation of Asphalts into Asphaltenes, Aromatics, and Saturates

The asphalts were separated into asphaltenes, aromatics, and saturates through a combination of the "Giant Corbett" procedure described by Peterson et al. (1994) and the procedure outlined in ASTM D4124. Following asphaltene precipitation from a 20:1 (vol/wt) n-hexane solution, the "Giant Corbett" procedure was used to perform an initial separation of aromatics and paraffin material. The paraffin fraction from each separation still contained residual low molecular weight naphthene aromatics and was therefore further fractionated into saturates and light naphthene aromatics using the procedure in ASTM D4124 (1994). The purity of the saturate fractions was monitored by measuring the UV absorbance at 254 nm at the exit of an NH_2-activated High Performance Liquid Chromatography (HPLC) column. The light naphthene aromatics were blended with the aromatics from the initial "Giant Corbett" separation. This mixture of aromatic materials is referred to as the aromatic fraction throughout the rest of this study. The solvent was removed from the aromatic and saturate fractions using a rotary evaporation apparatus and the recovered fractions were analyzed by gel permeation chromatography (GPC) to confirm that complete solvent removal had been achieved (Burr et al., 1990).

4.3. Blend Preparation

Because of the miscibility of the components, saturate/aromatics blends were produced by simple mixing. Blends containing asphaltenes were obtained by dissolving and mixing the components in toluene and then recovering the resulting asphaltic material. This was the best way to maximize homogeneity of the blend. Solvent recovery was performed at relatively low temperatures to eliminate potential solvent aging (Burr et al., 1994). Complete solvent removal was confirmed by GPC (Burr et al., 1990). The approximate composition in terms of weight percent asphaltene and weight percent saturates for all blends produced are tabulated in Table 1.

4.4. Oxidative Aging

Several 1.5 g ± 0.05 g samples of each blend were aged in the POV under atmospheric air pressure. The blends which were initially asphaltene free were aged at 87.8, 93.3, and 98.8°C for up to four weeks and the blends which originally contained asphalte-

Table 1. Corbett-type composition of blends for three asphalts studied

	% Asphaltenes		
% Saturates	0	7	15
0	SHRP AAA-1	SHRP AAA-1	SHRP AAA-1
	SHRP AAF-1		SHRP AAF-1
	SHRP AAG-1	SHRP AAG-1	SHRP AAG-1
7	SHRP AAA-1	SHRP AAA-1	SHRP AAA-1
	SHRP AAF-1		SHRP AAF-1
	SHRP AAG-1	SHRP AAG-1	SHRP AAG-1
15	SHRP AAA-1	SHRP AAA-1	SHRP AAA-1
	SHRP AAF-1		SHRP AAF-1
	SHRP AAG-1	SHRP AAG-1	SHRP AAG-1

nes were aged only at 98.8°C for three weeks. Note that the blends which are initially asphaltene free will form asphaltenes upon aging.

4.5. Viscosity Measurement of Aged and Unaged Materials

The rheological properties of interest were the zero frequency limiting dynamic shear viscosities (η^*_0) measured at temperatures of 0, 10, 25, 40, 60, and 90°C with a Carri-Med CSL 500 Control Stress Rheometer with a 500 μm gap. At 60 and 90°C, a 2.5 cm composite parallel plate geometry was used. At the lower temperatures, a 1.5 cm stainless steel parallel plate geometry was used. For temperatures at which the viscosity was independent of frequency, the viscosity at a frequency of 0.1 rad/sec was used to approximate η^*_0. At temperatures at which η^*_0 of the material cannot be approximated by the 0.1 rad/sec viscosity, η^*_0 was determined by constructing a master curve according to the time-temperature superposition principle as described by Ferry (1980).

4.6. Asphaltene Content Determination

Asphaltene contents in weight percentage (%*AS*) of the aged blends was measured directly by precipitation in n-hexane as described by Pearson et al. (1986). Approximately 0.2 grams of aged material was weighed into a scintillation vial, 20 mL of n-hexane was added, and the solution was sonicated until the asphalt sample was completely dispersed. After overnight equilibration, the asphaltenes were separated by filtering the solutions through pre-weighed PTFE (polytetrafluoroethylene) membrane 0.45 μm syringe filters. Following filtration, the filters were dried in an oven at 140°C for one hour and post-weighed 2 hours after removal from the oven.

4.7. Asphaltene Molecular Weight Determination

The molecular weight distribution of asphalts was determined using a GPC technique with a WATERS HPLC system consisting of a WATERS 600E controller/solvent delivery system, a WATERS 700 Satellite Autosampler, a WATERS 410 Differential Refractometer and a WATERS 486 tunable UV spectrometer. To achieve good separation, three columns having pore sizes of 1000, 500, and 50 Å were connected in series to ac-

commodate the wide range of molecular sizes commonly found in asphalts. The columns with 500, and 1000 Å pore size were 7.8×305 mm containing 7μm particles of styrenedivinylbenzene co-polymer packing, obtained from WATERS. The column with a pore size 50 Å was 7.5x600 mm with 5μm particles and was obtained from Polymer Laboratories LTD. A flow rate of 1.0 mL/min, a column temperature of 40°C, and a 100 μL injection volume were used for the samples. 0.2±0.05 gram of asphaltene sample was dissolved in 10 mL THF and filtered using a 0.45μm PTFE syringe filter before injection. Chromatograms were recorded using a PC through an A/D interface. The number average molecular weight (M_n) then was calculated from the molecular weight distribution based on a calibration using polystyrene standards at a concentration of 0.025 g/mL.

5. APPLICATION OF THE DEVELOPED MODEL TO VISCOSITY/ASPHALTENE RELATIONSHIP

5.1. Approximation of Solvation Constant, K

One problem with using Equation (31) to describe the viscosity as a function of particle concentration is the slow convergence of the infinite series summation when κ_1 is larger than 10^5. For rapid evaluation, an approximation to the infinite series summation needs to be established in order to complete the parameter estimation with a practical amount of computation time. The summation in Equation (31) can be generalized as given in Equation (34).

$$S(\alpha,\beta)=\sum_{N=1}^{\infty} N^{\alpha}\beta^{N-1} \tag{34}$$

This summation is a function of two parameters, α and β. In general, the summation $S(\alpha,\beta)$ cannot be evaluated analytically unless α is an integer. The difficulty is that $S(\alpha,\beta)$ increases rapidly to infinity as β approaches unity, and an accurate numerical evaluation of $S(\alpha,\beta)$ requires as many as 10,000 terms when β is equal to 0.995. Unfortunately, in the case of the viscosity/asphaltene relationship under investigation, the value of β often lies between 0.995 and 1.0, so that an accurate evaluation of $S(\alpha,\beta)$ is practically impossible using term by term summation.

By taking the partial derivative of Equation (34) with respect to β, Equation (35) is obtained.

$$\begin{aligned}\frac{\partial S(\alpha,\beta)}{\partial\beta} &= \sum_{N=1}^{\infty} N^{\alpha}(N-1)\beta^{N-2} \\ &= \frac{1}{\beta}\left(\sum_{N=1}^{\infty} N^{\alpha+1}\beta^{N-1} - \sum_{N=1}^{\infty} N^{\alpha}\beta^{N-1}\right) \\ &= \frac{1}{\beta}\left(S(\alpha+1,\beta)-S(\alpha,\beta)\right)\end{aligned} \tag{35}$$

Equation (35) can be rewritten as Equation (36)

$$S(\alpha+1,\beta)=S(\alpha,\beta)+\beta\frac{\partial S(\alpha,\beta)}{\partial\beta} \tag{36}$$

When α is equal to zero,

$$S(0,\beta)=\sum_{N=1}^{\infty}\beta^{N-1}=\frac{1}{1-\beta} \tag{37}$$

Combining Equations (36) and (37), $S(\alpha,\beta)$ can be evaluated analytically as long as α is an integer. $S(\alpha,\beta)$ for α from 1 to 4 are given below:

$$S(1,\beta)=\frac{1}{(1-\beta)^2}$$

$$S(2,\beta)=\frac{1+\beta}{(1-\beta)^3}$$

$$S(3,\beta)=\frac{1+4\beta+\beta^2}{(1-\beta)^4}$$

$$S(4,\beta)=\frac{1+11\beta+11\beta^2+\beta^3}{(1-\beta)^5}$$

Hence, the solution of $S(\alpha,\beta)$ for an integer α has the general form,

$$S(\alpha,\beta)=\frac{P(\alpha,\beta)}{(1-\beta)^{\alpha+1}} \tag{38}$$

Equation (38) should also be valid for an non-integer α but the exact form of $P(\alpha,\beta)$ cannot be solved analytically. Fortunately, in the present study, the physically meaningful values of α lie between 0 and 2, and $P(\alpha,\beta)$ can be approximated by Newton forward interpolation with three known functions, $P(0,\beta)$, $P(1,\beta)$, $P(2,\beta)$,

$$P(\alpha,\beta)=1+\alpha\Delta P(0,\beta)+\frac{\alpha(\alpha-1)}{2!}\Delta^2P(0,\beta)+\frac{\alpha(\alpha-1)(\alpha-2)}{3!}\Delta^3P(0,\beta)+\cdots\cdots$$

$$\approx 1+\alpha\Delta P(0,\beta)+\frac{\alpha(\alpha-1)}{2!}\Delta^2P(0,\beta)$$

$$\approx 1+\alpha(1-1)+\frac{\alpha(\alpha-1)}{2!}\{[(1+\beta)-1]-(1-1)\}$$

$$\approx 1+\frac{\alpha(\alpha-1)}{2!}\beta$$

or

$$P(\alpha,\beta) \approx 1+\frac{\alpha(\alpha-1)}{2}\beta\,,\ 0\le\alpha\le 2 \tag{39}$$

Substituting Equation (39) into Equation (38), the approximation for $S(\alpha,\beta)$ is given in Equation (40),

$$S(\alpha,\beta) \approx \frac{1+\dfrac{\alpha(\alpha-1)\beta}{2}}{(1-\beta)^{\alpha+1}} \tag{40}$$

Equation (40) gives errors less than 5% for entire range of β, regardless how close β is to 1.0, for $0\le\alpha\le 2$. With the aid of Equation (40), the required computation time for parameter optimization is reduced significantly. By employing Equation (40), the infinite series summation in Equation (31) can be approximated as given in Equation (41):

$$\sum_{N=1}^{\infty} N^{\left(\frac{3-f_D}{f_D}\right)}\left(1+\frac{1-\sqrt{1+2\kappa_1\phi}}{\kappa_1\phi}\right)^{N-1} \sim \frac{1.0+\dfrac{\left(\dfrac{3-f_D}{f_D}\right)\left(\left(\dfrac{3-f_D}{f_D}\right)-1.0\right)\left(1+\dfrac{1-\sqrt{1+2\kappa_1\phi}}{\kappa_1\phi}\right)}{2}}{\left(\dfrac{\sqrt{1+2\kappa_1\phi}-1}{\kappa_1\phi}\right)^{1+\left(\frac{3-f_D}{f_D}\right)}} \tag{41}$$

5.2. Additional Assumptions for Parameter Reduction

The suspension model developed in the present work can be applied to describe the $\eta_r/\%AS$ relationship of asphalt as a function of saturate content and temperature for SHRP AAA-1, SHRP AAF-1, and SHRP AAG-1. For a given asphaltene/maltene pair, Equation (16) requires 6 parameters, ν, ϕ^1_{MAX}, σ, κ_1, C, f_D, which is very impractical. Several assumptions that must be made to reduce the number of parameters are listed below:

1. $\eta_r/\%AS$ relationships are assumed to be of the "Pal-Rhodes type" so that the particle interaction coefficient, σ, is assumed to be 1.
2. the particle size distribution is assumed to be very wide, which means ϕ^N_{MAX} approaches unity.
3. the shape factor, ν, the packing geometry constant, C, and the fractal dimension f_D, are assumed to be the same for blends from the same crude source due to the similarity among each fraction.

Assumptions (1) and (2) eliminate two constants from the Sudduth equation, Equation (7), leaving only the shape factor to be determined. This effectively eliminates parameter in-

teractions in this equation. Without the assumptions outlined above, each individual saturates/aromatics blend would require six parameters to fully describe its $\eta_r/\%AS$ behavior using Equation (16) at each viscosity measurement temperature. With the assumptions outlined above, the first saturates/aromatics blend using the fractions from a given asphalt requires only four parameters, ν, C, f_D, and κ_1. Each additional blend using the fractions from the same asphalt requires only one additional parameter, κ_1.

For example, three saturates/aromatics blends were produced using SHRP AAA-1 materials. These three blends were then aged in the POV to give $\eta_r/\%AS$ relationships for each blend. The viscosities for several of the samples were measured at six different temperatures, resulting in 18 $\eta_r/\%AS$ relationships. Without the assumptions above, 108 parameters would be needed to utilize Equation (16). The two-parameter Pal-Rhodes model would require 36 parameters. With the assumptions outlined above, only 21 parameters are necessary. Unfortunately, a slight difficulty involved is that all 18 $\eta_r/\%AS$ curves must be fit simultaneously to determine the optimal values for ν, C, f_D, and the κ_1s.

6. RESULTS AND DISCUSSION

The optimal model parameters for blends made of the fractions from the same asphalt were determined simultaneously by fitting $\eta_r/\%AS$ data using Equation (16), Equation (31), and Equation (41) with the assumptions described above. The $\eta_r/\%AS$ curves were assumed to be functions of both temperature and saturate content for blends from a given asphalt. For example, for blends from SHRP AAA-1, the blend containing no saturates will have a different $\eta_r/\%AS$ curve from the blend containing 7% saturates and the blend containing 15% saturates. This is because the solvent power of the maltene is expected to be decreased in the presence of saturates. In addition, the $\eta_r/\%AS$ curve ($\%AS$ usually ranges from 0% to 40%) for a given saturate content was constructed by connecting 3 sections of the $\eta_r/\%AS$ curve obtained by oxidatively aging blends containing 0% original asphaltenes (which results in $\%AS$ from 0% to 15%), 7% original asphaltenes (which results in $\%AS$ from 7% to 25%), and 15% original asphaltenes (which results in $\%AS$ from 15% to 40%). Therefore, the optimal parameters obtained for $\eta_r/\%AS$ for a given saturate content is an "average" of the original and aging-produced asphaltenes. However, the differences in the $\eta_r/\%AS$ relationships for the original and aging-produced asphaltenes were not significant for the materials investigated in the present study (Lin et al., 1995a).

Figures 2, 3, and 4 show that the model developed in the present study is capable of describing the $\eta_r/\%AS$ data quite well for blends from SHRP AAA-1 containing 0%, 7%, and 15% saturate contents, respectively. Good agreements are obtained for SHRP AAG-1 and SHRP AAF-1 as shown in Figures 5 through 10. In general, Figures 2, 3, and 4 show, as expected, that the effect of asphaltenes on the increase in viscosity is much more pronounced at low temperature than at high temperature. This trend is undoubtedly due to the reduction of maltene solvent power as a result of the decrease in temperature (Lin et al., 1996).

The equilibrium constant for asphaltene association, K_c, for each curve can be converted directly from the fitting parameter, κ_1, according to Equation (31) if the volume of a single asphaltene molecule in the dry state is known. With the assumption of sphericity, the volume of an asphaltene molecule in the dry state can be estimated from its density, ρ (g/mL) which is usually close to unity, and its molecular weight which can only be approximated using the number average molecular weight, M_n from GPC. The average dry volume of an asphaltene molecule can be estimated using Equation (42).

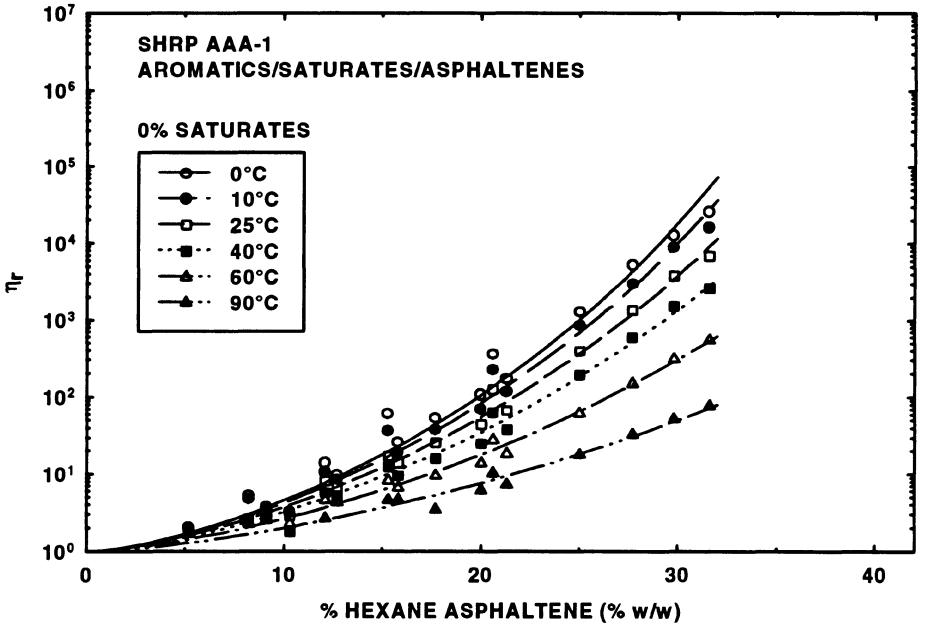

Figure 2. The effect of temperature on the $\eta_r/\%AS$ of SHRP AAA-1 containing 0% saturates.

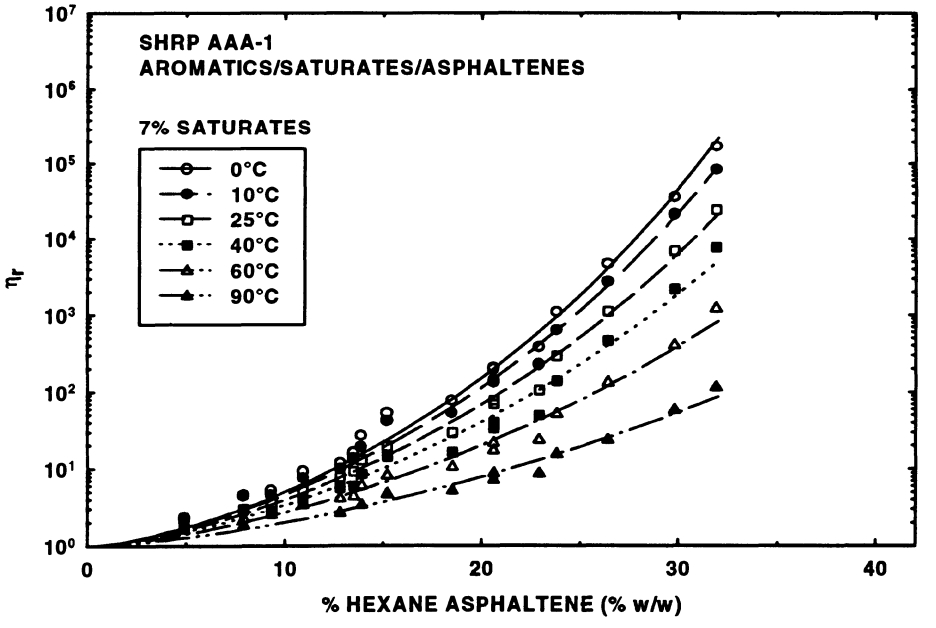

Figure 3. The effect of temperature on the $\eta_r/\%AS$ of SHRP AAA-1 containing 7% saturates.

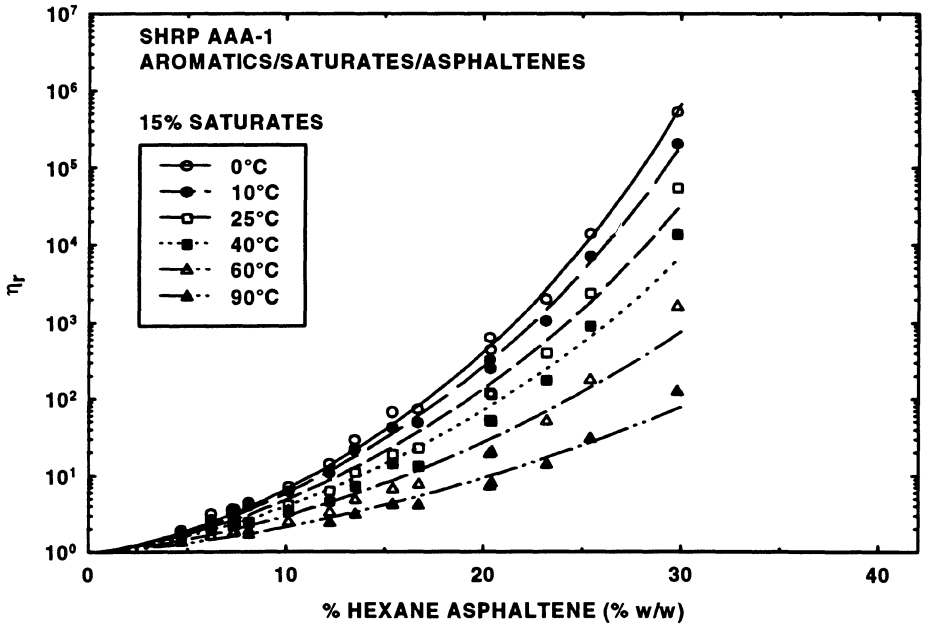

Figure 4. The effect of temperature on the $\eta_r/\%AS$ of SHRP AAA-1 containing 15% saturates.

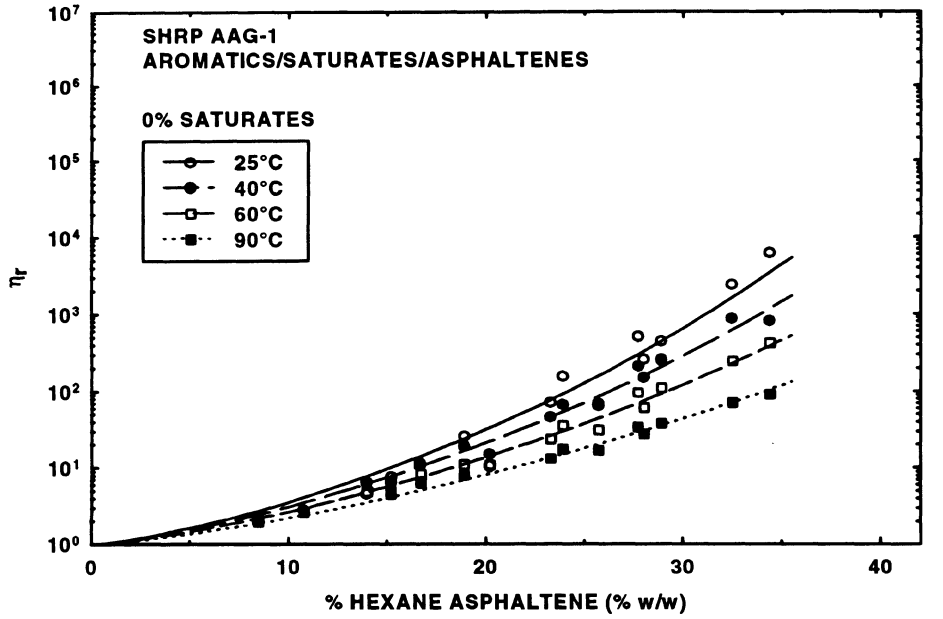

Figure 5. The effect of temperature on the $\eta_r/\%AS$ of SHRP AAG-1 containing 0% saturates.

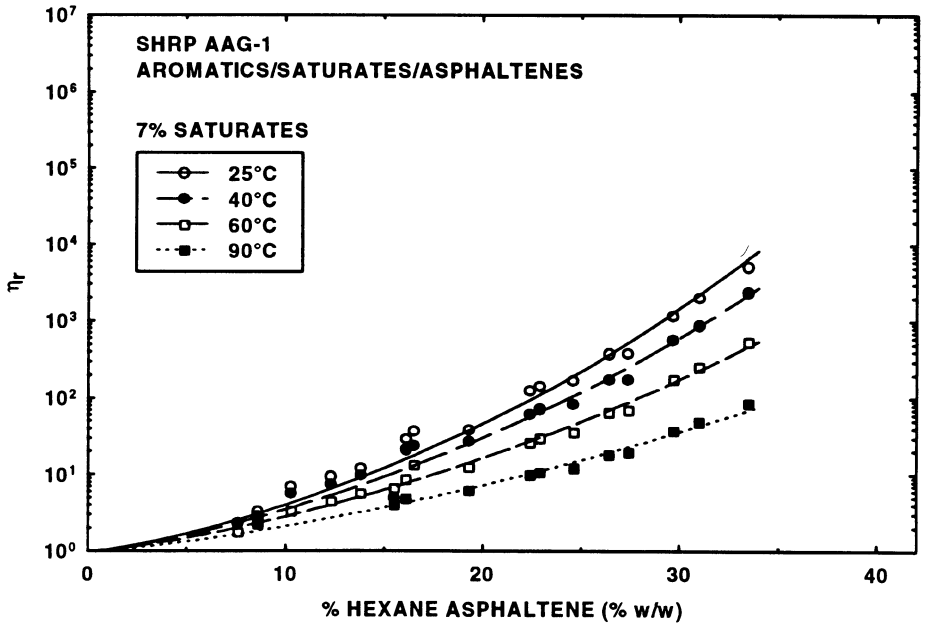

Figure 6. The effect of temperature on the $\eta_r/\%AS$ of SHRP AAG-1 containing 7% saturates.

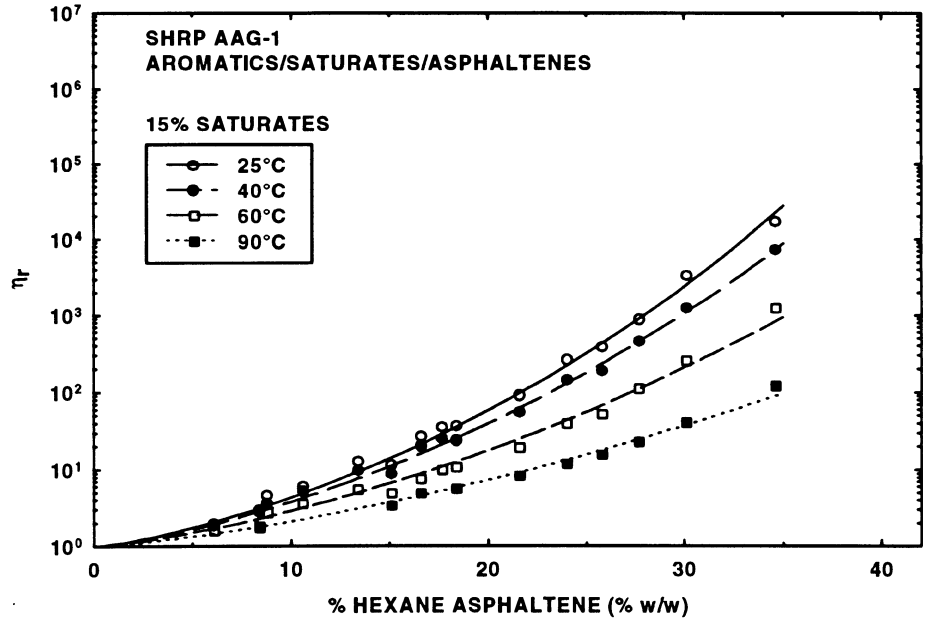

Figure 7. The effect of temperature on the $\eta_r/\%AS$ of SHRP AAG-1 containing 15% saturates.

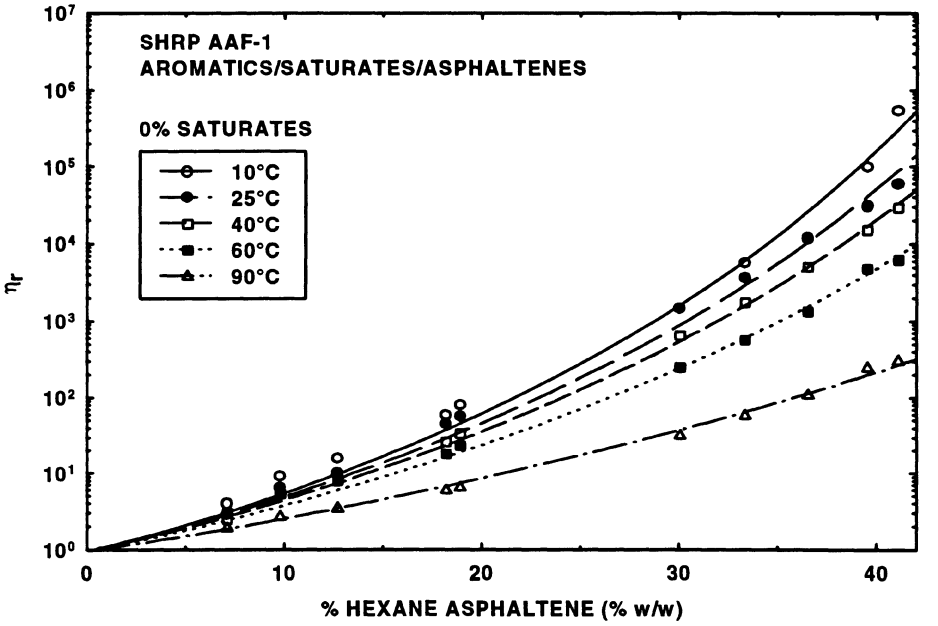

Figure 8. The effect of temperature on the $\eta_r/\%AS$ of SHRP AAF-1 containing 0% saturates.

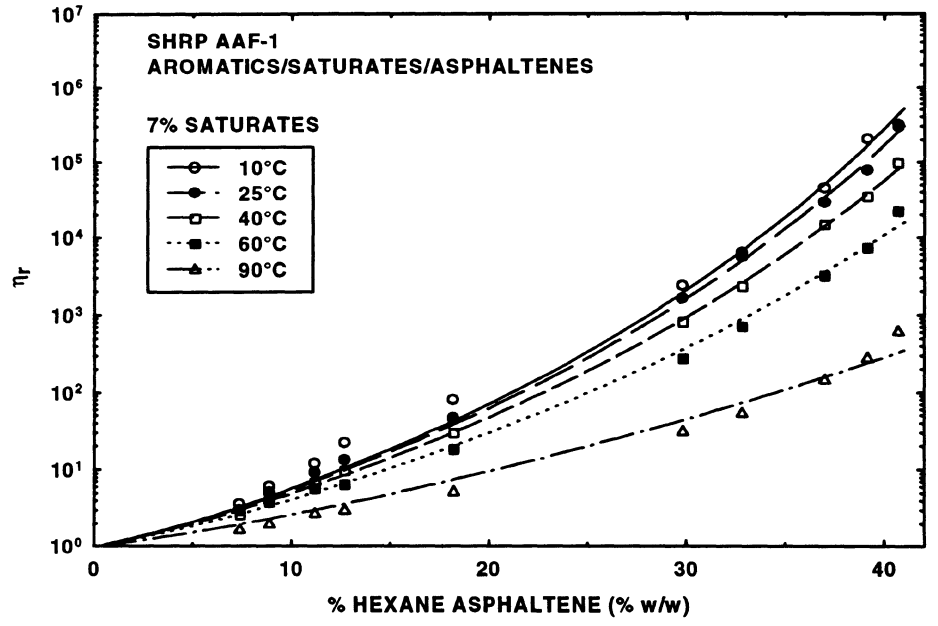

Figure 9. The effect of temperature on the $\eta_r/\%AS$ of SHRP AAF-1 containing 7% saturates.

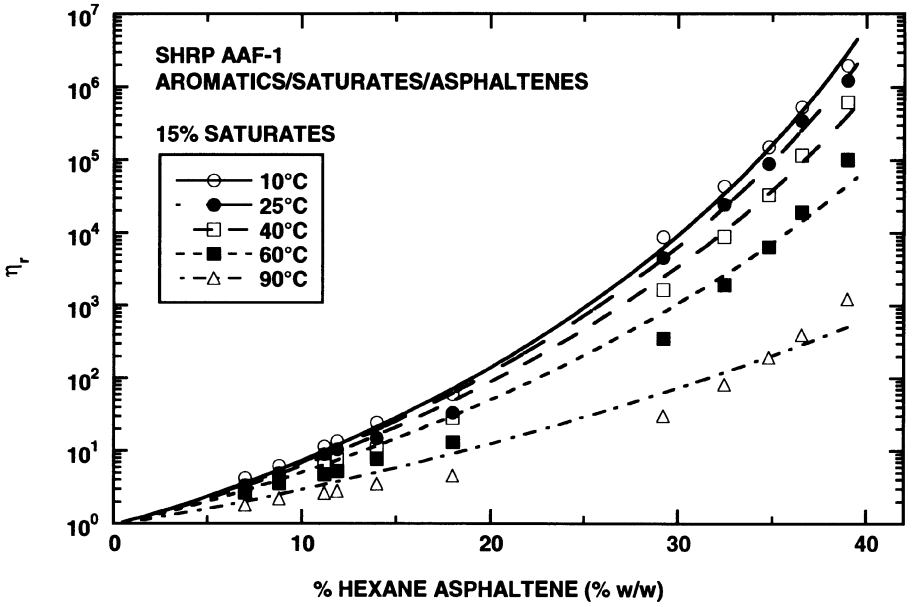

Figure 10. The effect of temperature on the $\eta_r/\%AS$ of SHRP AAF-1 containing 15% saturates.

$$D_0^3 = \left(\frac{3\times 2^3}{4\pi}\right)\times \frac{0.625\times M_n\left(\frac{g}{mol}\right)\left(\frac{1\,mol}{6.023\times 10^{23}}\right)}{\rho\left(\frac{g}{mL}\right)\left(\frac{10^6\,mL}{m^3}\right)} = \frac{1.9819\times 10^{-30} M_n}{\rho}(m^3) \tag{42}$$

The constant 0.625 is the maximum packing volume fraction for solid spheres (McGeary, 1961). For SHRP AAA-1, the number average molecular weight obtained from GPC is 1338, the density is approximated as 1 (g/mL), and the dry volume of an asphaltene molecule thus is estimated to be 1.388×10^{-27} (m^3). By substituting the optimized value of κ_1 and the estimated D_0^3 into Equation (31), the equilibrium constant K_e can be calculated at each temperature.

With knowledge of the equilibrium constant K_e for asphaltene association, the standard Gibb's free energy of formation for asphaltene association is given by Equation (43).

$$\Delta G^0 = -RT\ln K_a = -RT\ln(K_e K_\gamma) \sim -RT\ln K_e \tag{43}$$

K_a and K_γ are the equilibrium constants in terms of activity and the activity coefficient, respectively. Here, K_γ is assumed to be approximately unity. From thermodynamic relations, the standard heat and entropy of formation can be obtained from Equations (44) and (45), respectively.

$$\Delta H^0 = \frac{\partial\left(\frac{-\Delta G^0}{T}\right)}{\partial\left(\frac{1}{T}\right)} \tag{44}$$

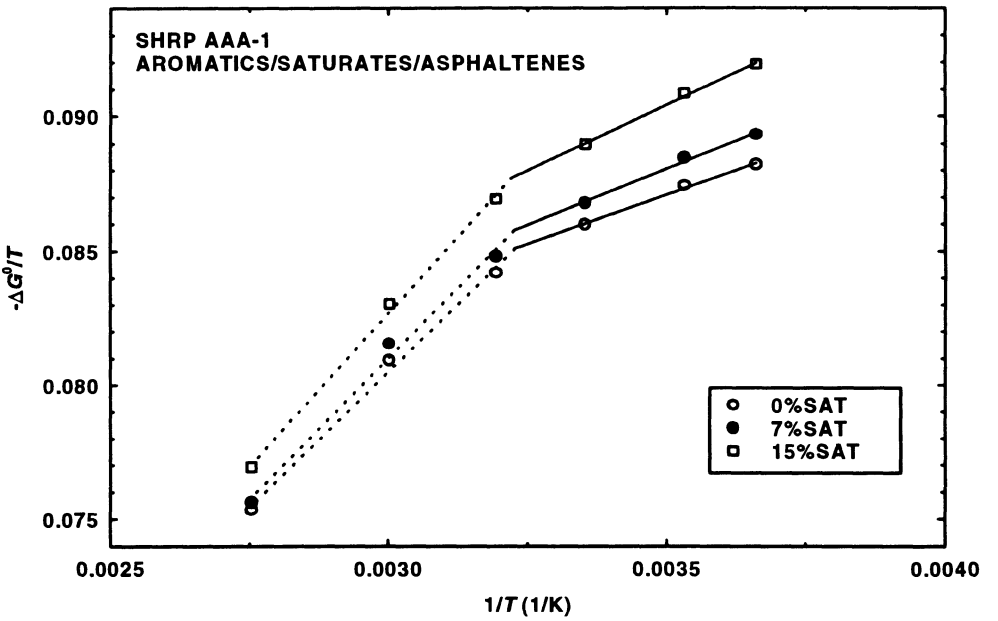

Figure 11. The effect of temperature and saturates on $(-\Delta G^0/T)/(1/T)$ relationship of SHRP AAA-1 blends.

$$\Delta S^0 = \frac{\Delta H^0 - \Delta G^0}{T} \tag{45}$$

Figure 11 shows that the quantity $(-\Delta G^0/T)$ increases as $1/T$ increase for blends from SHRP AAA-1. Figure 11 also illustrates that, for a given temperature, $(-\Delta G^0/T)$ increases with saturate content. A larger value of $(-\Delta G^0/T)$, or more negative ΔG^0, indicates a stronger association, or less dispersion, of asphaltenes. The developed suspension model correctly describes the observed phenomena that the presence of saturates and the decrease in temperature both reduce the solvent power of the maltene and, therefore, aggravate asphaltene association. Figures 12 and 13 show similar behavior for SHRP AAG-1 and SHRP AAF-1. Figures 11, 12, and 13 also indicate that $-\Delta H^0$ increases as temperature increases.

Table 2 lists the calculated ΔG^0, ΔH^0, ν, C, and f_D for SHRP AAA-1 at the temperatures studied. The data in Table 2 show that ΔG^0 is only slightly dependent on temperature and that ΔG^0 decreases as saturate content increases. This decrease in ΔG^0 with saturate content again shows that the presence of saturates in the maltene favors aggregation. The ΔG^0, ΔH^0, ν, C, and f_d for SHRP AAG-1 and SHRP AAF-1 are listed in Tables 3 and 4, respectively. The ΔG^0 values obtained for SHRP AAA-1, SHRP AAF-1, and SHRP AAG-1 range from -22 to -33 kJ/mol and The ΔH^0 values obtained range from -17.0 to -26.2 kJ/mol at 298.15 K. Petersen (1971) showed that the standard Gibb's free energy of formation, ΔG^0, for the self-association of 2-quinolone dimer and mixed dimers of 2-quinolone with benzoic, cyclohexanecarboxylic, and 4-cyclohexylbutanoic acids in carbon tetrachloride (CCl_4) at 295.15 K are -25.56, -26.6, -24.8, and -24.18 kJ/mol, respectively, which are very close to the values obtained in this study. However, he showed that the hydrogen-

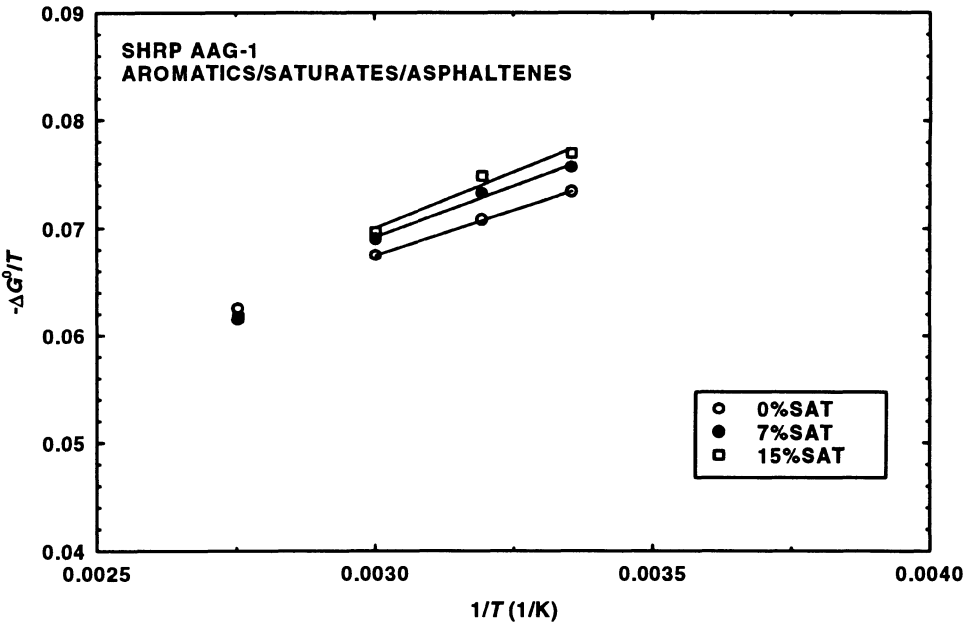

Figure 12. The effect of temperature and saturates on $(-\Delta G^0/T)/(1/T)$ relationship of SHRP AAG-1 blends.

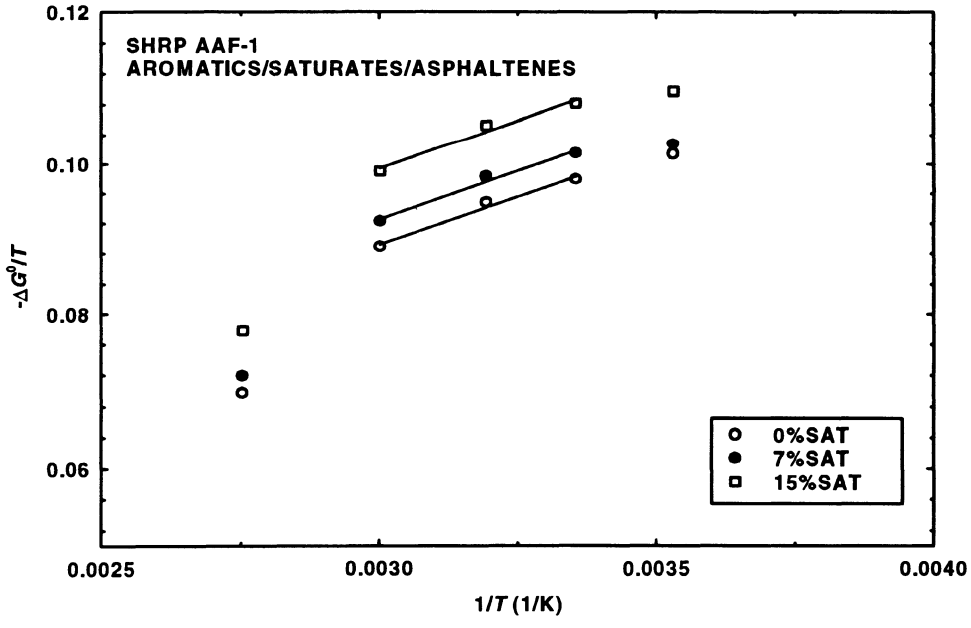

Figure 13. The effect of temperature and saturates on $(-\Delta G^0/T)/(1/T)$ relationship of SHRP AAF-1 blends.

Table 2. The estimated ΔG^0, ΔH^0, ν, C, and f_D for SHRP AAA-1

	ΔG^0 (kJ/mole)[1]			ΔH^0 (kJ/mole)*					
T (K)	0% sat	7% sat	15% sat	0% sat	7% sat	15% sat	ν [1]	C [1]	f_D [1]
–	–	–	–	–	–	–	17.0 ± 0.4	0.255 ± 0.007	1.51 ± 0.01
273.15	−24.1 ± 0.4	−24.4 ± 0.4	−25.1 ± 0.4	−7.3	−8.4	−9.7	–	–	–
283.15	−24.8 ± 0.4	−25.0 ± 0.4	−25.7 ± 0.4	−7.3	−8.4	−9.7	–	–	–
298.15	−25.6 ± 0.4	−25.9 ± 0.4	−26.5 ± 0.4	−7.3	−8.4	−9.7	–	–	–
313.15	−26.4 ± 0.4	−26.6 ± 0.4	−27.2 ± 0.4	−20.2	−21.0	−22.8	–	–	–
331.15	−26.8 ± 0.4	−27.0 ± 0.4	−27.5 ± 0.4	−20.2	−21.0	−22.8	–	–	–
363.15	−27.4 ± 0.5	−27.5 ± 0.5	−27.9 ± 0.5	−20.2	−21.0	−22.8	–	–	–

*ΔH^0 is estimated within linear range with no error estimation due to insufficient data. [1]Errors are estimated for 95% confidence interval (Milton and Arnold, 1990).

Table 3. The estimated ΔG^0, ΔH^0, ν, C, and f_D for SHRP AAG-1

	ΔG^0 (kJ/mole)[1]			ΔH^0 (kJ/mole)*					
T (K)	0% sat	7% sat	15% sat	0% sat	7% sat	15% sat	ν[1]	C[1]	f_D[1]
–	–	–	–	–	–	–	17.4 ± 0.8	0.405 ± 0.013	1.74 ± 0.02
298.15	−21.9 ± 0.7	−22.6 ± 0.7	−22.9 ± 0.7	−17.0	−19.1	−20.9	–	–	–
313.15	−22.2 ± 0.7	−22.9 ± 0.7	−23.4 ± 0.7	−17.0	−19.1	−20.9	–	–	–
331.15	−22.5 ± 0.7	−23.0 ± 0.7	−23.2 ± 0.7	−17.0	−19.1	−20.9	–	–	–
363.15	−22.7 ± 0.8	-22.3 ± 0.8	−22.4 ± 0.8	–	–	–	–	–	–

*ΔH^0 is estimated whithin linear range with no error estimation due to insufficient data.
[1]Errors are estimated for 95% confidence interval (Milton, 1990).

Table 4. The estimated ΔG^0, ΔH^0, ν, C, and f_D for SHRP AAF-1

	ΔG^0 (kJ/mole)[1]			ΔH^0 (kJ/mole)*					
T (K)	0% sat	7% sat	15% sat	0% sat	7% sat	15% sat	ν[1]	C[1]	f_D[1]
–	–	–	–	–	–	–	13.1 ± 0.1	0.666 ± 0.002	2.23 ± 0.00
283.15	−28.7 ± 0.1	−29.1 ± 0.1	−31.1 ± 0.1	–	–	–	–	–	–
298.15	−29.2 ± 0.1	−30.2 ± 0.1	−32.3 ± 0.1	−25.8	−26.2	−26.1	–	–	–
313.15	−29.7 ± 0.1	−30.8 ± 0.1	−33.0 ± 0.1	−25.8	−26.2	−26.1	–	–	–
331.15	−29.6 ± 0.2	−30.7 ± 0.2	−33.0 ± 0.2	−25.8	−26.2	−26.1	–	–	–
363.15	−25.3 ± 0.2	−26.1 ± 0.2	−28.2 ± 0.2	–	–	–	–	–	–

*ΔH^0 is estimated whithin linear range with no error estimation due to insufficient data.

[1]Errors are estimated for 95% confidence interval (Milton, 1990).

bonding strength (heat of formation, ΔH^0) for the same dimer and mixed dimers in CCl_4 at 295.15 K are -36.39, -51.08, -43.13, and -43.54 kJ/mol, respectively, which is much higher than the estimated values obtained in this study. The higher bonding energy for association of model compounds in his study is somewhat expected because 2-quinolone is very polar in comparison of typical asphaltene molecules. However, the Gibb's free energy of formation is related to the difference in the solubility parameters between solute and solvent. The solubility parameter of 2-quinolone is over 14.0 Hildebrands which is much higher than that of typical asphaltenes. On the other hand, the solubility parameter of CCl_4, which is 8.6 Hildebrands, is also much higher than that of typical maltenes. Thus, the difference in the solubility parameters between 2-quinolone and CCl_4 and the difference in the solubility parameters between asphaltenes and maltenes should be close in magnitude. Petersen (1971) also reasoned that the association of those species in his study would be expected to be similar to asphalts.

Critical micellization concentration (CMC) is one of the most important phenomena for typical association processes. Many researchers (Sheu et al., 1991b; Andersen and Birdi, 1991) measured the CMC of asphaltenes in various solvents. Sheu et al. (1991b) measured the CMC of Ratawi asphaltenes in pyridine and nitrobenzene by measuring the surface tension of those asphaltene solutions. They found the values of CMC of Ratawi asphaltenes at 25°C to be 0.02 wt% in pyridine and 0.05 wt% in nitrobenzene, respectively. Interestingly, despite the high solvent power of pyridine and nitrobenzene as indicated by their solubility parameters, the CMC of asphaltenes in these two solvents is quite low. Andersen and Birdi (1991) determined the CMC of asphaltenes in several polar solvents and the mixtures of solvents using calorimetry. They showed that, generally, the CMC of asphaltene solutions is dependent on the solubility parameter of the solvent used and the CMC decreases as the solubility parameter of the solvent increases. Therefore, it is reasonable to expect that the CMC for asphaltene/maltene systems should be much lower than the CMC of asphaltenes in either pyridine and nitrobenzene in that the solvent power of maltenes is obviously much lower than that of pyridine or nitrobenzene (Lian et al., 1994). In the present study, the CMC of asphaltene/maltene systems can be estimated from ΔG^0. The relation between ΔG^0 and the CMC is given in Equation (46) (Hunter, 1986).

$$\Delta G^0 = -RT\ln K_e \approx RT\ln(\text{CMC}) \tag{46}$$

Where CMC is in mol/L. Rearranging Equation (46), the CMC is given in terms of K_e as follow:

$$\text{CMC} \approx \frac{1}{K_e} \tag{47}$$

The estimated values of CMC for the asphaltenes/maltenes studied at 25°C are tabulated in Table 5. As shown in Table 5, the estimated values of CMC for SHRP AAA-1, AAG-1, and AAF-1 are much lower than the CMC measured by Sheu et al. (1991b) due to the low maltene solvent power. Figures 14, 15, and 16 show that the asphaltene monomer concentration for SHRP AAA-1, SHRP AAG-1, and SHRP AAF-1 increases rapidly with the addition of asphaltenes to the maltenes and then quickly reaches a nearly constant concentration, which is the CMC. Additionally, as shown in Table 5 and Figures 14, 15, and 16, for a given asphaltene/maltene pair, the CMC decreases as the saturate content of maltene increases. This is explained by the reduction in the maltene solvent power as a re-

Table 5. Estimated CMC for asphaltene/maltene systems studied

	CMC (g/L)		
Asphaltene/Maltene	0% SAT	7% SAT	15% SAT
SHRP AAA-1	0.043	0.039	0.030
SHRP AAG-1	0.113	0.086	0.074
SHRP AAF-1	0.007	0.005	0.002

[1]CMC is estimated using Equation (47).

sult of the presence of saturates in maltenes. Figure 17 shows the effect of solvents on the CMC of asphaltenes. In Figure 17, the data for pure solvents are reported by Andersen and Birdi (1991) and the solubility parameters of maltenes are estimated from the reported values in literatures (Lian, 1994; Altgelt and Harle, 1975). As shown in Figure 17, the solubility parameters of solvents do not solely determine the CMC. However, in general, the CMC is low in poor solvents. Figure 17 also shows that the estimated CMC for materials studied are in good agreement with the trend shown by Andersen and Birdi (1991).

The size distribution greatly affects the physical properties of many polydispersed materials. In the case of asphaltic materials, the polydispersity of asphaltenes has been shown to have significant influence on the rheological properties of asphalts (Reerink and Lijzenga, 1973). The polydispersity of asphaltenes has been studied extensively using GPC (Reerink and Lijzenga, 1973; Davison et al., 1995), SANS (Sheu et al., 1991b), and SAXS (Senglet et al.,1990). However, based on the proposed association model, the weight fraction of the aggregate of size N can be calculated using Equation (48) and (49).

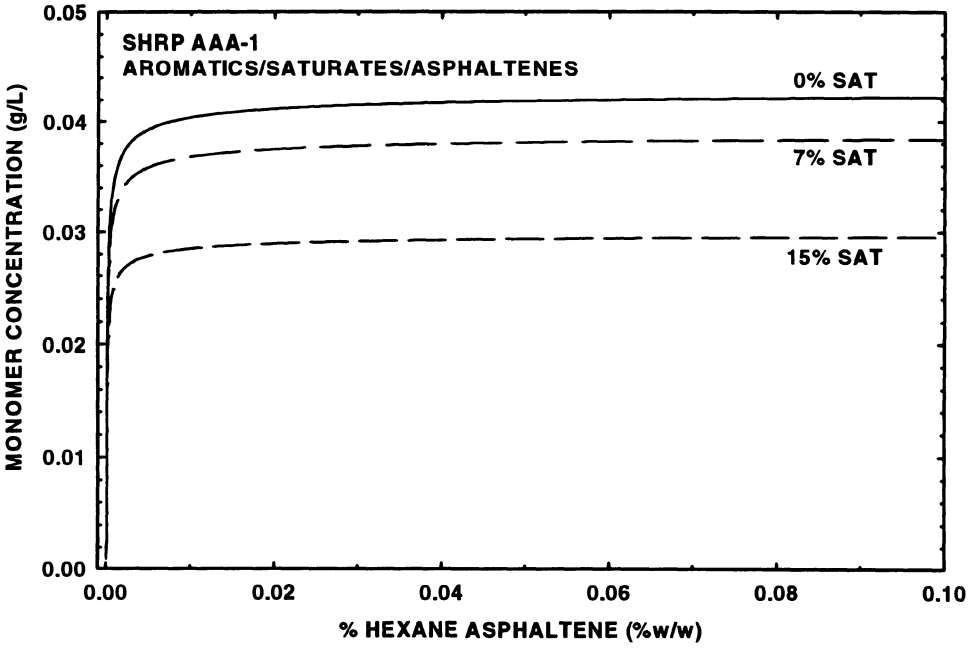

Figure 14. The effect of saturates on CMC for SHRP AAA-1 blends.

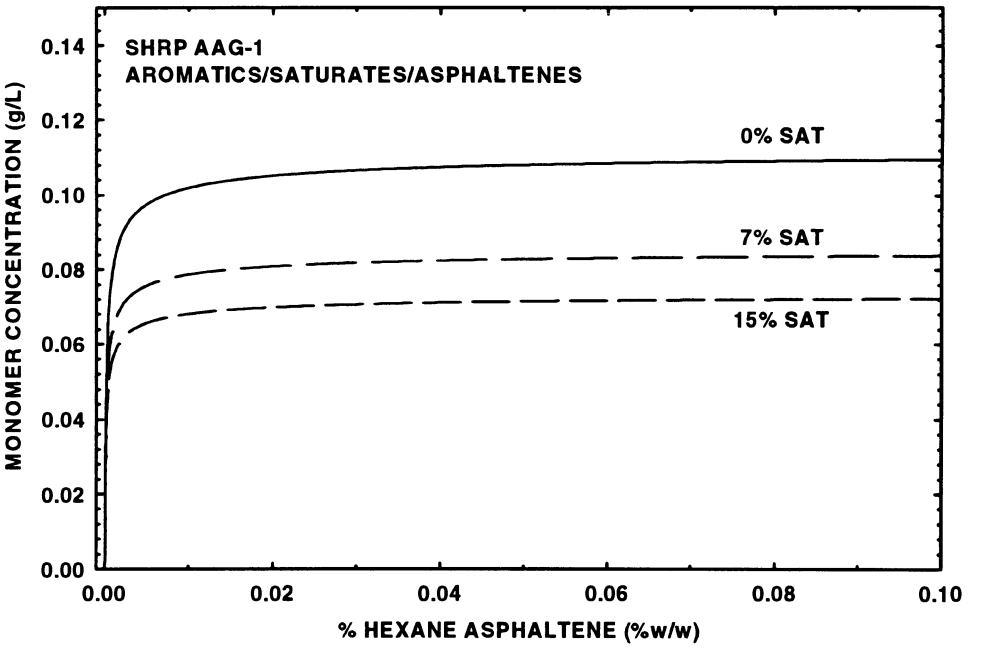

Figure 15. The effect of saturates on CMC for SHRP AAG-1 blends.

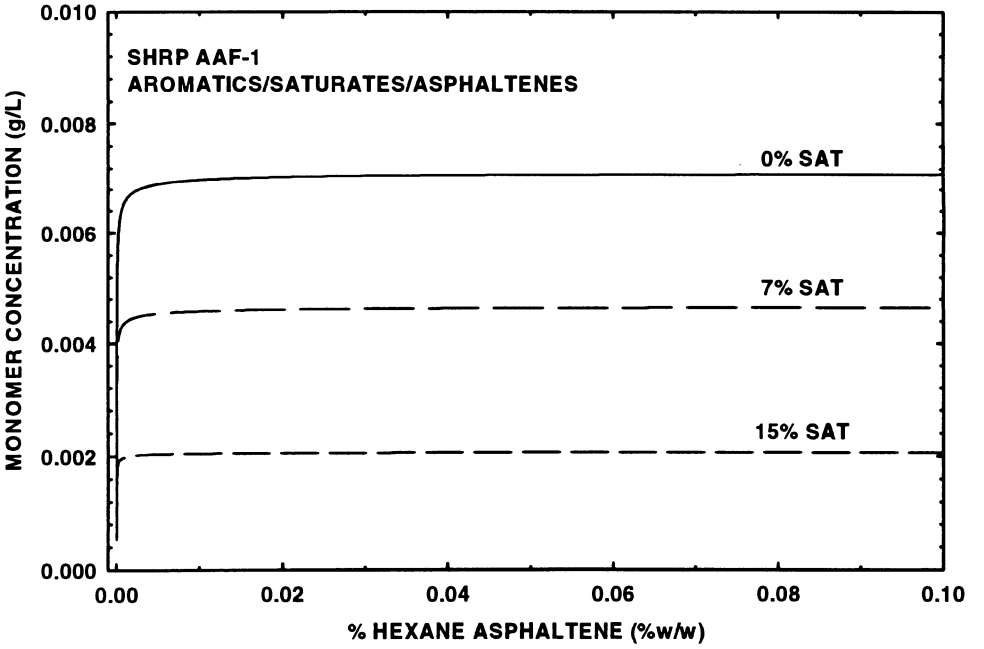

Figure 16. The effect of saturates on CMC for SHRP AAF-1 blends.

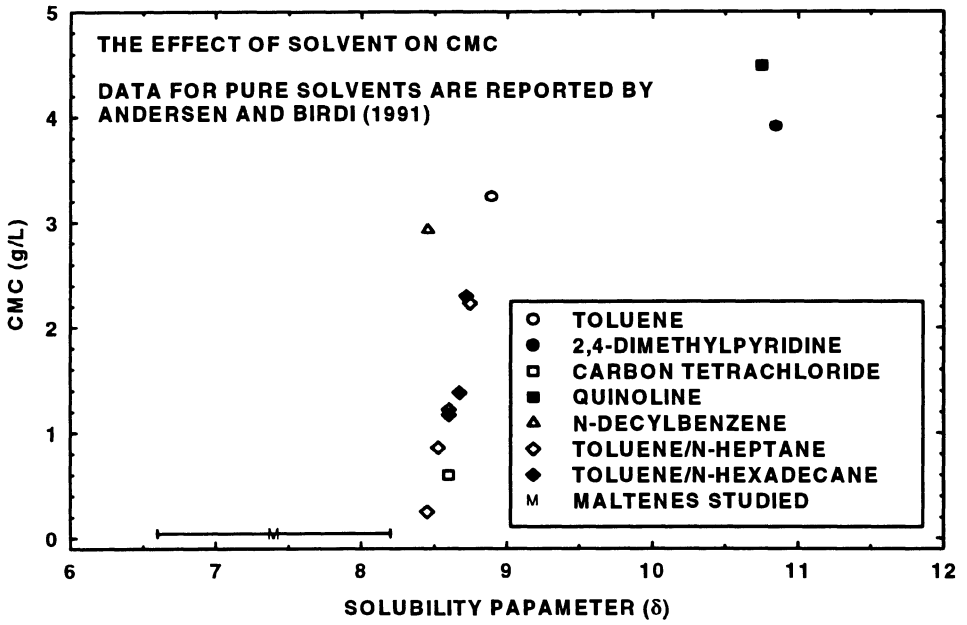

Figure 17. The effect of solubility parameter on CMC of asphaltenes in maltenes studied and pure solvents.

$$P'(N) = \frac{N[A_N]}{\sum_{N=1}^{\infty} N[A_N]} = \frac{N}{K_e c_p}\left(1 + \frac{1 - \sqrt{1 + 4K_e c_p}}{2K_e c_p}\right)^N \tag{48}$$

$$c_p = \frac{1000\rho}{M_n}\phi \tag{49}$$

Figure 18 shows the effect of asphaltene concentration on the size distribution of asphaltene aggregates for SHRP AAA-1 0% saturates asphaltene/maltene. At a concentration of 0.01 wt%, SHRP AAA-1 asphaltenes in maltenes containing no saturates shows a very narrow distribution. As asphaltene concentration increases, the width of the distribution increases. In reality, the distribution, especially at 10 wt%, may not be so wide as shown in Figure 18. This wide distribution may be due to the assumption that all equilibrium constants are equal and independent of the size of asphaltene aggregate (Equation 18). Figure 19 shows the effect of saturate content on the size distribution of asphaltene aggregates for SHRP AAA-1. As shown in Figure 19, at the same concentration, saturates move the size distribution to the right hand side of Figure 19 indicating the increase in the average size of asphaltene aggregates. The increase in average aggregate size with increasing saturates for SHRP AAA-1 is shown in Figure 20. Again, the increase in average aggregate size is due to the reduction in the solvent power of maltenes by saturates.

The geometry information of asphaltene aggregates can be obtained from the optimal model parameters ν and f_D. Many studies (Hinch and Leal,1972; Kuhn and Kuhn, 1945; Kuhn et al., 1951; Brodnyan, 1959) showed that the value of ν is a function of particle shape and shear rate. Figure 21 shows ν as a function of aspect ratio (b/a), where a and

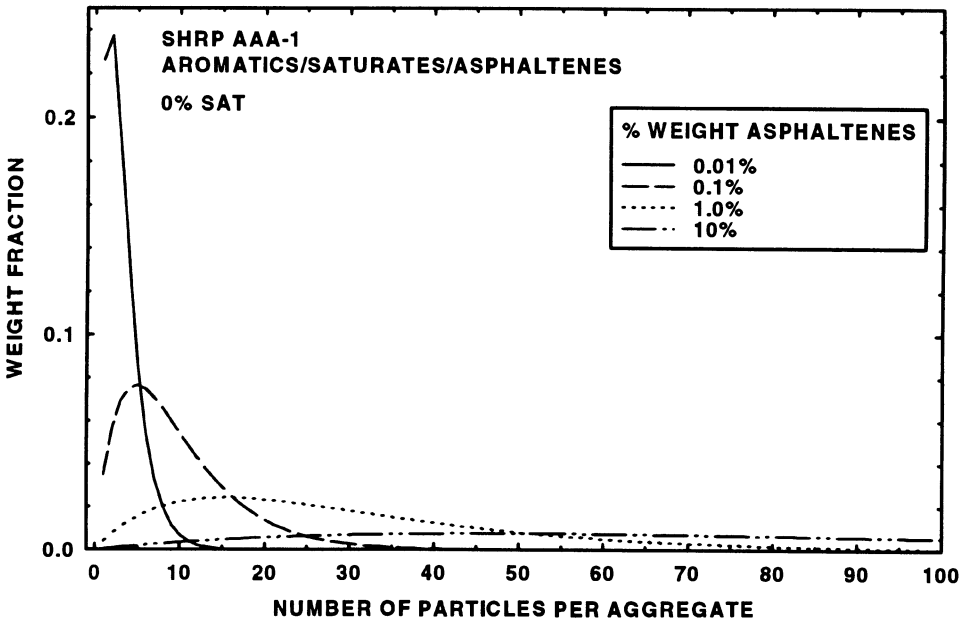

Figure 18. The effect of $\%AS$ on the distribution of asphaltene aggregates for SHRP AAA-1 containing 0% saturates.

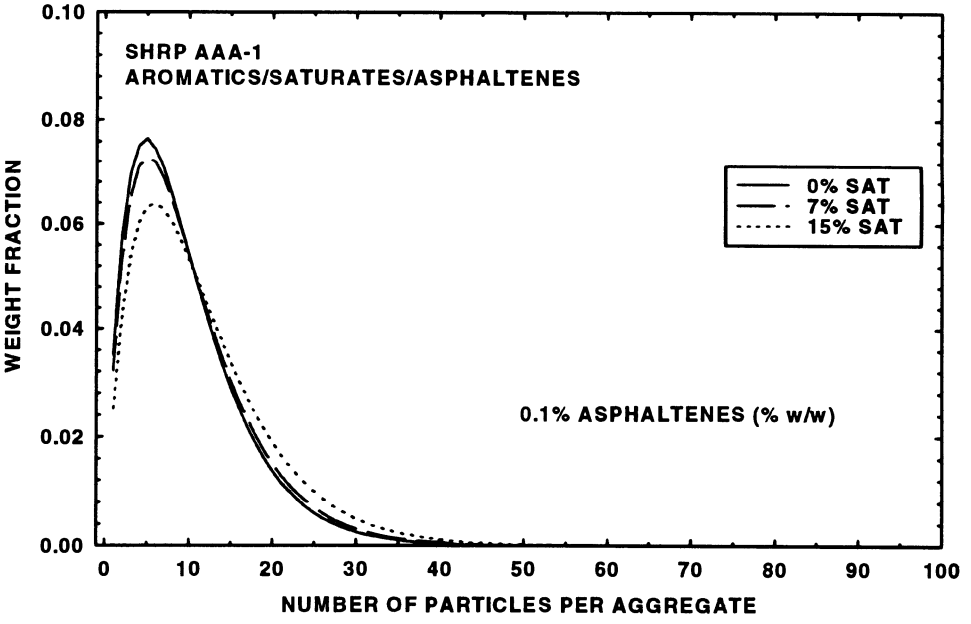

Figure 19. The effect of saturates on the distribution of asphaltene aggregates for SHRP AAA-1 at 0.1 wt% asphaltenes.

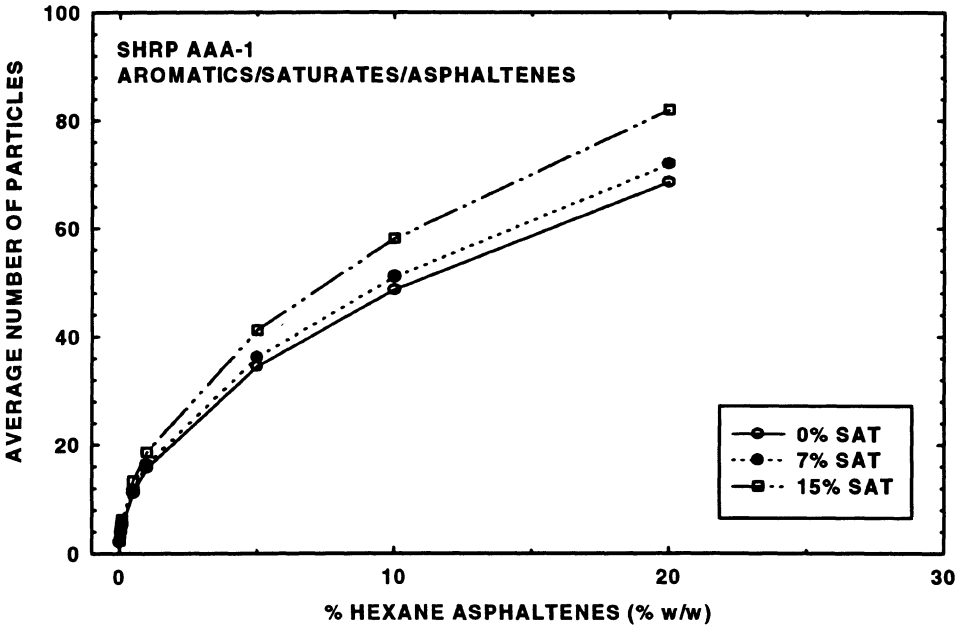

Figure 20. The effect of saturates on the average size of asphaltene aggregates for SHRP AAA-1 blends.

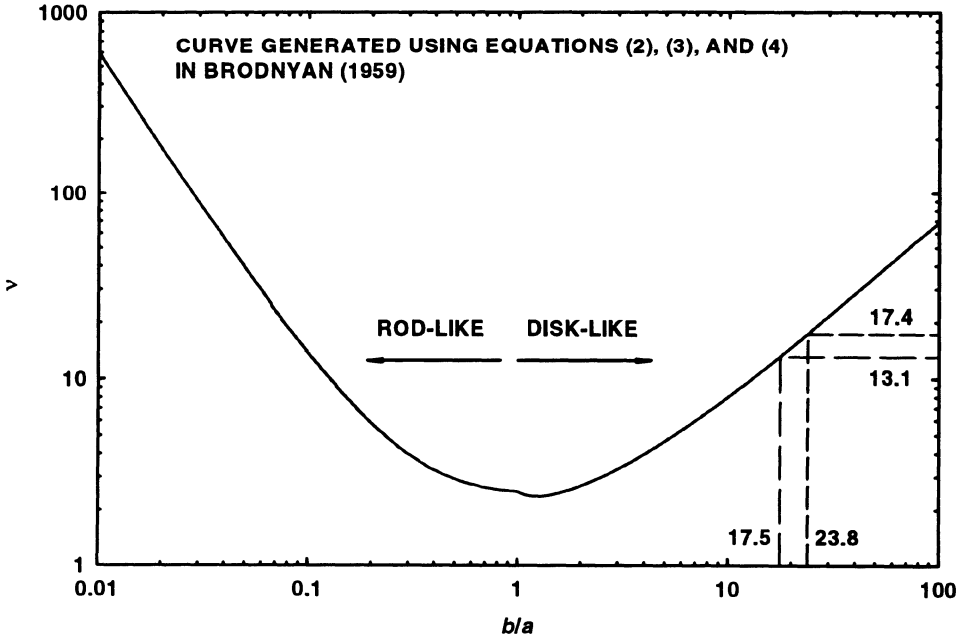

Figure 21. The effect of particle aspect ratio, *b/a*, on the shape factor, v.

b are the short and long axis of an ellipsoid, at low shear rate laminar flow conditions. The curve in Figure 21 is generated using equations reported by Brodnyan (1959). The values of ν obtained from the three asphalts studied ranges from 13.1 to 17.4, and Figure 21 also shows that this yields a range of aspect ratio from 17.5 to 23.8 for disc-like particles. These values of the aspect ratio for asphaltene particles in maltene media are not unreasonable. Reerink and Lijzenga (1973) reported a range of aspect ratios from 4 to 10 for various asphaltenes in toluene using rheological measurement at infinite dilution and an ultracentrifugation technique. More interestingly, Ravey et al. (1988) used SANS to measure the macrostructure of various asphaltenes in a number of solvents and obtained a range of aspect ratios from 10 to 25. That the result of this study and two previous studies (Reerink and Lijzenga, 1973; Ravey et al., 1988) give very similar results using three different techniques suggests that the geometry of asphaltene particles in maltenes or organic solvents may be disc-like.

It may seem unlikely that a disk shaped particle with an aspect ratio greater than 17 would be formed from spherical molecules. However, this only produces a small error in K_e from any error in D_0^3, Equation (31), resulting from the assumed packing factor in Equation (42). This is likely a smaller factor than the necessary assumption that K_e is the same for all particle sizes. The fractal dimension, f_D, of asphaltene aggregates has been studied using SANS (Overfield et al., 1989). Overfield et al. (1989) showed that the f_D for asphaltene particles in toluene is between 2.0 and 3.0. Ravey et al. (1988) fractionated n-heptane asphaltene from Safanya Crude Oil into 4 fractions using GPC. They conducted SANS experiments to determine the size and molecular weight of those asphaltene fractions in tetrahydrofuran. The effect of asphaltene concentration on the size and molecular weight of asphaltenes was investigated in their study. Although they did not actually report the value of the fractal dimension for their asphaltene fractions, it can be estimated to be from 1.5 to 2.8 from the dependency of the molecular weight on the size. For various associating particles, Tsenoglou (1990) reported a range of values of the fractal dimension from 1.7 to 2.0. Witten and Sander (1981) reported a fractal dimension of 1.78 for metal-particle aggregates and a fractal dimension of 2.1 for percolation. Compared to the previously reported results in the literature, the fractal dimensions obtained in this study, which range from 1.5 to 2.3, are quite reasonable.

Table 6 summarizes the comparison of the results from the present study to the results from several previous studies. The thermodynamic and structural parameters obtained by regression of the model developed in this study were in good agreement with those measured values reported in previous literature studies using independent techniques. The good agreement between the results in the present and previous studies indicates that this new suspension viscosity model adequately relates the microstructure of asphaltic materials to their macroscopic properties and provides a better understanding of the effect of composition on the physical properties of asphalts.

7. CONCLUSIONS

The suspension viscosity model developed in this work is relatively complicated compared to other models. However, for complex systems such as asphaltenes/maltenes, this model actually is fairly simplified. Despite its approximate nature, this suspension viscosity model is capable of describing the viscosity of asphalt as a function of asphaltene content and temperature and of relating the $\eta_r/\%AS$ relationship to the thermodynamic properties of asphaltene association and the structural information of asphaltene

Table 6. Comparison of ΔG^0, ΔH^0, f_d, v, and *b/a* obtained from this work with other works

	$-\Delta G^0$(kJ/mol)	$-\Delta H^0$(kJ/mol, 25°C)	f_D	v	*b/a*
This work	22.0–33.0	17.0–26.2	1.5–2.3	13.1–17.4	18–24
Tsenoglou (1990)	–	–	1.7–2.0	–	–
Ravey et. al. (1988)[1]	–	–	1.5–2.8	–	10–25 (25–36)[1]
Sander et. al. (1981)[2]	–	–	1.78–2.1	–	–
Overfield et. al. (1989)[3]	–	–	2.0–2.4	–	–
Reerink and Lijzenga (1973)[4]	–	–	–	–	4–10
Petersen et. al. (1971)[5]	20.3–25.6	36.4–46.5[5]	–	–	–
Petersen (1971)[6]	24.2–26.6	43.1–51.0[6]	–	–	–

[1] f_D is calculated from size and molecular weight data obtained from using small angle neutron scattering (SANS). values in parenthesis represent *b/a* for disk shape.
[2] f_D is obtained using computer simulation.
[3] f_D is obtained using SANS.
[4] Aspect ratio, *b/a*, is obtained using viscosity measurement.
[5] ΔH^0 is measured using infrared spectroscopy technique for 2-quinolones and carboxylic acids in CCl_4 at 22°C.
[6] ΔH^0 is measured using infrared spectroscopy technique for 2-quinolones and carboxylic acids in CCl_4 at 22°C.

aggregates. The physical properties obtained from this work are in good agreement with several previous studies reported in the literature. In addition, for multiple $\eta_r/\%AS$ curves from the same asphalt (crude source) this model can obtain more information with fewer fitting parameters compared to a two-parameter version of the Pal-Rhodes model. Several conclusions can be drawn from this study:

1. Association of asphaltene molecules into aggregates is aggravated by the presence of saturates in the maltene media as indicated by lower ΔG^0.
2. Association is much stronger at low temperature than at higher temperature in that K_e increases exponentially with $1/T$.
3. The present study indicates that the shape of asphaltene aggregates is disc-like.

ACKNOWLEDGMENTS

Support for this work by the U.S. Department of Energy (DOE), Assistant Secretary for Energy Efficiency and Renewable Energy under DOE Albuquerque Operations Office Cooperative Agreement DE-FC04–93AL94460, the Texas Department of Transportation (TxDOT), and the U.S. Department of Transportation is gratefully acknowledged. Also, the technical contributions of Ms. Ann Ferry are greatly appreciated.

DISCLAIMER

The contents of the report reflect the views of the authors who are responsible for the facts and the accuracy of the data presented herein. The contents do not necessarily reflect the official views or policies of the Federal Highway Administration, the Texas Department of Transportation, or the U.S. Department of Energy. This report does not constitute a standard, specification, or regulation. This report is not intended for construction, bidding, or permit purposes.

REFERENCES

ASTM, *Standard Test Methods for Separation of Asphalt into Four Fractions*, ASTM D 4124–91 (1994).

Altgelt, K.H. and O.L. Harle, "The Effect of Asphaltenes on Asphalt Viscosity," Ind. Eng. Chem. Prod. Res. Dev., **14**, 240 (1975).

Andersen, S.I. and K.S. Birdi, "Aggregation of Asphaltenes as Determined by Calorimetry," *Journal of Colloid and Interface Science*, **142**, 497 (1991).

Brodnyan, J.G., "The Concentration Dependence of the Newtonian Viscosity of Prolate Ellipsoids," *Trans. Soc. Rheol.*, **3**, 61 (1959).

Burr, B.L., R.R. Davison, C.J. Glover, and J.A. Bullin, "Solvent Removal from Asphalt," *Trans. Res. Rec.*, **1269**, 1 (1990).

Burr, B.L., R.R. Davison, C.J. Glover, and J.A. Bullin, "Softening of Asphalts in Dilute Solutions at Primary Distillation Conditions," *Trans. Res. Rec.*, **1436**, 47 (1994).

Dabak, T. and O. Yucel, "Modeling of the Concentration and Particle Size Distribution Effects on the Rheology of Highly Concentrated Suspensions," *Powder Technology*, **52**, 193 (1987).

Davison, R.R., C.J. Glover, B.L. Burr, and J.A. Bullin, "Size Exclusion Chromatography of Asphalts", Handbook of Size Exclusion Chromatography, Wu, Chi-San (ed.), 211 (1995).

Dickie, J.P. and T.F. Yen, "Macrostructures of the Asphaltic Fractions by Various Instrumental Methods," *Analytical Chemistry*, **39**, 1847 (1967).

Dwiggins, C.W., Jr, "A Small Angle X-Ray Scattering Study of the Colloidal Nature of Petroleum," *Journal of Physical Chemistry*, **69**, 3500 (1965).

Eilers, H.J., "The Colloidal Structure of Asphalt," *J. Phys. Colloid Chem.*, **53**, 1195 (1948).

Einstein, A.,"Eine Neue Bestimmung der Moleküldimensionen" *Ann. Phys.*, **19**, 289 (1906).

Farris, R.J., "Prediction of the Viscosity of Multimodal Suspensions form Unimodal Viscosity Data," *Trans. Soc. Rheol.*, **12**, 281 (1968).

Ferry, J.D., *Viscoelastic Properties of Polymers*. 3rd Edition, John Wiley and Sons, New York, NY (1980).

Frankel, N.A. and A. Acrivos, "On the Viscosity of a Concentrated Suspension of Solid System," *Chem. Eng. Sci.*, **22**, 847 (1967).

Furnas, C.C., "Grading Aggregates," *Industrial and Engineering Chemistry*, **23**, 1052 (1931).

Grimson, M.J. and G.C. Barker, "Interaction Corrections to the Viscosity of Concentrated Colloidal Dispersions," *Europhysica Letters*, **3**, 511 (1987).

Heukelom, W. and P.W.O. Wijga, "Viscosity of Dispersions as Governed by Concentration and Rate of Shear," *Proceeding of AAPT*, **40**, 418 (1971).

Hinch, E.J. and L.G. Leal, "Rheological Properties of A Suspension," *J. Fluid Mech.*, **52** 683 (1972).

Hunter, R.J., *Foundations of Colloid Science* **I**, Oxford University Press, New York, NY (1986).

Kuhn, W. and H. Kuhn, "Die Abhängigkeit der Viskosität vom Strömungsgefälle Beihochverdünnten Suspensionen und Lösungen," *Helv. Chim. Acta.*, **28**, 97 (1945).

Kuhn, W., H. Huhn, and P. Buchner, "Hydrodynamisches Verhalten von Makromolekülen in Lösung," *Ergeb. Exakt. Naturw.*, **25**, 1 (1951).

Kim, H.G. and R.B. Long, "Characterization of Heavy Residuum by a Small Angle X-Ray Scattering Technique," *Ind. Eng. Chem. Fundam.*, **18**, 60 (1979).

Krieger I.M. and T.J. Dougherty, "A Mechanism of Non-Newtonian Flow in Suspensions of Rigid Spheres," *Trans. Soc. Rheol.*, **3**, 137. (1959).

Lee, D.I., "Packing of Spheres and Its Effect on the Viscosity of Suspensions," *Journal of Paint Technology*, **42**, 579 (1970).

Lian, H., J.R. Lin, and T.F. Yen, "Peptization Studies of Asphaltene and Solubility Parameter Spectra," *Fuel*, **73**, 423 (1994).

Lin, M.S., K.M. Lunsford, C.J. Glover, R.R. Davison, and J.A. Bullin, "The Effects of Asphaltenes on the Chemical and Physical Characteristics of Asphalts," In *Asphaltenes: Fundamentals and Applications*. Ed. E.Y. Sheu and O.C. Mullins, Plenum Press, New York, NY, 155–176 (1995a).

Lin, M.S., C.J. Glover, R.R. Davison, and J.A. Bullin. 1995. The Effects of Asphaltenes on Asphalt Recycling and Aging," *Trans. Res. Rec.*, **1507**, 86–95 (1995b).

Lin, M.S., J.M. Chaffin, M. Liu, C.J. Glover, R.R. Davison, and J.A. Bullin, "The Effect of Asphalt Composition on the Formation of Asphaltenes and Their Contribution to Asphalt Viscosity," *Fuel Sci. and Technol. Int'l*, **14**(1&2), 139–162 (1996).

Mandelbrot, B.M ., *The Fractal Geometry of Nature*, W. H. Freeman, San Francisco (1982).

McGeary, R.K., "Mechanical Packing of Spherical Particles," *Journal of the American Ceramic Society*, **44**, 513 (1961).

Mercer, H.N., A.H. Boyer, and M.C. Deviney, "3-D Carbon Black Primary Structure Characterization Via a New Electron Microscopy-Photogeommetry Technique," *Ruber Chem. Technol.*, **57**, 377 (1979).

Milton, J.C. and J.C. Arnold, Introduction to Probability and Statistics, 2nd Edition, McGraw Hill, Inc., New York, NY (1990).

Mooney, M., "The Viscosity of A Concentrated Suspension of Spherical Particles," *Journal of Colloid Science*, **6**, 162 (1951).

Oono, R., "Distribution of Carbon Black in SBR," *Ruber Chem. Technol.*, **51**, 278 (1978).

Ouchiyama, N., "Porosity Estimation for Random Packings of Spherical Particles," *Ind. Eng. Chem. Fundam.*, **23**, 490 (1984).

Overfield, R.E., E.Y. Sheu, and K.S. Liang, "SANS Study of Asphaltene Aggregation," *Fuel Science and Technology International*, **7**, 611 (1989).

Pal R. and E. Rhodes, "Viscosity/Concentration Relationships for Emulsions," *J. Rheology*, **33**, 1021–1045 (1989).

Pearson, C.D., G.S. Huff, and S.G. Gharfeh, "Technique for the Determination of Asphaltenes in Crude Oil Residues," *Analytical Chemistry*, **58**, 3266 (1986).

Petersen, J.C., " A Thermodynamic Study by Infrared Spectroscopy of the Association of 2-Quinolones, Some Carboxylic Acid, and the Corresponding 2-Quinolone-Acid Mixed Dimers," *Journal of Physical Chemistry*, **43**, 1491 (1971).

Petersen, J.C., R.V. Barbour, S.M. Dorrence, F.A. Barbour, and R.V. Helm, "Molecular Interaction of Asphalt," *Analytical Chemistry*, **75**, 1129 (1971).

Peterson G.D., R.R. Davison, G.J. Glover, and J.A. Bullin, "Effect of Composition on Asphalt Recycling Agent Performance," *Trans. Res. Rec.*, **1436**, 38 (1994).

Pollack, S.S. and T.F. Yen, "Structural Studies of Asphaltics by X-Ray Small Angle Scattering," *Analytical Chemistry*, **42**, 623 (1970).

Rao, B.M.L. and J.E. Serrano, "Viscometric Study of Aggregation Interactions in Heavy Oil," *Fuel Science and Technology International*, **4**, 483 (1986).

Ravey, J.C., G. Ducouret, and D. Espinat, "Asphaltene Macrostructure by Small Angle Neutron Scattering,". *Fuel*, **67**, 1560 (1988).

Reerink, H. and J. Lijzenga, "Molecular Weight Distributions of Kuwati Asphaltenes as Determined by Ultracentrifugation. Relation with Viscosity of Solutions," *J. Inst. Pet.*, 59, 211 (1973).

Rutgers, I.R., "Relative Viscosity of Suspensions of Rigid Spheres in Newtonian Liquids," *Rheologica Acta*, **2**, 202 (1962a).

Rutgers, I.R., "Relative Viscosity and Concentration," *Rheologica Acta*, **2**, 305 (1962b).

Sander, L.M., H.B. Shore, and J.H. Rose, "Self-Consistent Bond Structure Theory of the Metal-Insulator Transition," *Physical Review B—Condensed Matter*, **24**, 4879 (1981).

Senglet, N., C. Williams, D. Faure, T. D. Courières, and R. Guilard, "Microheterogeneity Study of Heavy Crude Petroleum by U.V.-Visible Spectroscopy and Small Angle X-Ray Scattering," *Fuel*, **69**, 73 (1990).

Sheu E.Y., M.M. De Tar, and D.A. Storm, "Rheological Properties of Vacuum Residue Fractions in Organic Solvents," *Fuel*, **70**, 1151–1156 (1991a).

Sheu E.Y., D.A. Storm, and M.M. De Tar, "Asphaltenes in Polar Solvents," *Journal of Non-Cryst. Solids*, **131–133**, 341 (1991b).

Storm D.A., E.Y. Sheu, "Rheological Studies of Ratawi Vacuum Residue at 366K," *Fuel*, **72**, 233–237 (1993).

Sudduth, R.D., "A Generalized Model to Predict the Viscosity of Solutions with Suspended Particles. I," *Journal of Applied Polymer Science*, **48**, 25(1993a).

Sudduth, R.D., "A New Method to Predict the Maximum Packing Fraction and the Viscosity of Solutions with a Size Distribution of Suspended Particles. II," *Journal of Applied Polymer Science*, **48**, 37(1993b).

Sudduth, R.D., "A Generalized Model to Predict the Viscosity of Solutions with Suspended Particles. III Effects of Particle Interaction and Particle Size Distribution," *Journal of Applied Polymer Science*, **50**, 123(1993c).

Tsenoglou, C., "Scaling Concepts in Suspension Rheology," *Journal of Rheology*, **34**, 15 (1990).

Witten, T.A. and L.M. Sander, "Diffusion-Limited Aggregation, a Kinetic Critical Phenomenon," *Phys. Rev. Lett.*, **47**, 1400 (1981).

Zimm, H.B., "Apparatus and Methods for Measurement and Interpretation of the Angular Variation of Light Scattering; Preliminary Results on Polystyrene Solutions," *Journal of Chemical Physics*, **16**, 1099 (1948).

Chapter X

CHARACTERIZATION OF ASPHALTENES AND HEAVY OILS USING HYDRODYNAMIC PROPERTY MEASUREMENTS

Ruth E. Baltus

Department of Chemical Engineering
Clarkson University
Potsdam, New York 13699-5705

1. INTRODUCTION

Heavy oils and residua are characteristically more difficult to process catalytically than lighter petroleum fractions because of their large molecular size, polarity and heteroatom and metals content. The component of these materials which is generally accepted to be the most refractory is the asphaltenes, which are defined as a solubility class, typically the n-pentane or n-heptane insoluble fraction. There have been extensive efforts focused on developing an understanding of the chemical and the physical characteristics of entire resids as well as the asphaltene fraction.

An understanding of the diffusional resistances influencing catalytic upgrading reactions with heavy feedstocks requires knowledge of the transport and equilibrium properties of these materials in small pores. These properties are dependent on the size and conformation of the constituents of the material. Therefore, a fundamental understanding of the macroscopic structure of these materials is essential for the development of effective catalysts and catalytic processes for treating heavy feedstocks.

The size and shape (often referred to as the macrostructure) of heavy oils and residua also influence their elution characteristics in gel permeation chromatography (gpc), an analytical technique that is commonly used to determine the molecular weight or the molecular weight distribution of petroleum-derived materials. In gpc, the principle of separation involves the distribution of molecules between the solution contained within a porous packing and in the interstitial area surrounding the packing. The general procedure involves the preparation of a calibration plot which relates molecular weight to elution volume. This calibration is usually performed using monodisperse standards of known molecular weight. However, the partitioning of molecules between pore and bulk phases is

dependent upon the shape of the molecules.[1,2] Therefore, errors will be introduced if a calibration prepared using a flexible macromolecule such as polystyrene is used to determine the molecular weight of a sample containing more rigid molecules such as those comprising many petroleum-derived materials. In order to establish accurate calibration procedures for gpc separations of petroleum-derived materials, a fundamental understanding of the structure of these materials and their equilibrium and transport properties in small pores is necessary.

Another issue which arises when attempting to understand and quantify the macroscopic structure of asphaltenes and heavy oils is the tendency of these materials to associate in solution. The association of smaller entities into larger structures (considered by some to be micellar in nature) has been proposed as the explanation for molecular weight values that depend on temperature, solvent and the method of determination.[3,4] The ability to quantify changes in macroscopic size that result from changes in environmental conditions is an important element in the development of our understanding of the nature, and therefore the processability, of these materials.

Intrinsic viscosity, bulk phase diffusivity and sedimentation velocity measurements have been used extensively to characterize the macromolecular structure of well-defined macromolecules such as proteins and synthetic polymers. In this chapter, the use of these hydrodynamic property measurements to determine the macroscopic characteristics of asphaltenes and heavy oils will be discussed. A comparison of observations performed with different solvents, at different concentrations and different temperatures and the interpretation of these differences in terms of changes in macromolecular structure will be discussed. The principles governing these measurements will be presented and results from measurements performed in a number of different laboratores will be reviewed.

2. INTRINSIC VISCOSITY

2.1. Background and Theory

2.1.1. Einstein's Equation of Viscosity of Dispersions. When a macromolecular or colloidal sized molecule or particle is added to a liquid, the viscosity of the liquid increases. The solution viscosity is dependent on the concentration of added solute and that dependence can be described by a power series expansion in solute concentration, c:

$$\eta = A + Bc + Cc^2 + \ldots \tag{1}$$

where η is the solution viscosity and A, B, C etc. are constants.[5] As the solute concentration approaches zero, the solution viscosity approaches the viscosity of pure solvent. Therefore, the constant A must equal the solvent viscosity, η_o. The constants B, C etc. are expected to depend upon the size and shape of the solutes or particles in the solution. It is this dependence of solution viscosity on solute characteristics that is exploited when one uses measurements of solution viscosity to determine the macroscopic structure of asphaltenes and heavy oils in solution.

Einstein was the first to theoretically examine the dependence of solution viscosity on solute characteristics by considering the laminar flow of a fluid containing rigid, noninteracting spherical particles with size sufficiently larger than the solvent molecules so that the fluid surrounding each sphere can be regarded as a continuum. The analysis

yielded an expression, commonly called Einstein's equation of viscosity of dispersions, that relates the solution viscosity to the volume fraction of spheres, ϕ:

$$\frac{\eta}{\eta_o} = 1 + 2.5\,\phi \tag{2}$$

In Eq. (2), the expansion in concentration is limited to the $O(\phi)$ term because in Einstein's derivation, the spheres are assumed to be independent. When particle-particle interactions are considered, an additional term of $O(\phi^2)$ is included and the value of the coefficient of that term is dependent on the approach one uses to model those interactions. For this discussion, the value of that coefficient is not important and we will simply use the variable k_1 for it. When this $O(\phi^2)$ term is included, Eq. (2) can be rearranged to:

$$\frac{1}{\phi}\left(\frac{\eta}{\eta_o} - 1\right) = 2.5 + k_1\phi \tag{3}$$

The expression in parenthesis on the left hand side is called the specific viscosity, η_{sp} and η_{sp}/ϕ (the entire left hand side of Eq. 3) is called the reduced viscosity, η_{red}. Eq. (3) predicts that a plot of η_{red} versus ϕ should yield a straight line with slope = k_1 and intercept = 2.5. At higher solute concentrations, additional terms in the expansion become important and a non-linear relationship between η_{red} and ϕ is expected. The limiting value of the reduced viscosity as concentration approaches zero is defined as the intrinsic viscosity, $[\eta]$, and is predicted by Einstein's analysis to have a value of 2.5. Eq. (3) can therefore be written in more general form as

$$\eta_{red,\phi} = \frac{1}{\phi}\left(\frac{\eta}{\eta_o} - 1\right) = [\eta]_\phi + k_1\phi + k_2\phi^2 + \ldots \tag{4}$$

where the subscript ϕ is included with η_{red} and $[\eta]$ to indicate that volume fraction is the concentration unit used to describe the concentration dependence of η.

Although volume fraction is the concentration unit that arises naturally in the Einstein derivation, it is not the most convenient concentration unit from a practical standpoint. If one replaces the volume fraction by a mass/volume concentration, c, Eq. (4) becomes

$$\eta_{red,c} = \frac{1}{c}\left(\frac{\eta}{\eta_o} - 1\right) = [\eta]_c + k_1\left(\frac{\overline{V}_2}{M}\right)^2 c + k_2\left(\frac{\overline{V}_2}{M}\right)^3 c^2 + \ldots \tag{5}$$

where is $\overline{V}_2$ is the partial molar volume of the solute and M is the solute molecular weight. The two viscosities, $\eta_{red,\phi}$ and $\eta_{red,c}$, as defined in Eqs. (4) and (5), are related by $\eta_{red,c} = \eta_{red,\phi}\ \overline{V}_2/M$ and a similar relationship holds between $[\eta]_c$ and $[\eta]_\phi$. Eq. (5) shows that one can determine the intrinsic viscosity of a solute/solvent system by measuring the solution viscosity at several solute concentrations, plotting reduced viscosity versus c and determining the limit as $c \rightarrow 0$.

An alternative expression for the concentration dependence of solution viscosity can be written by using weight fraction as the concentration unit:

$$\eta_{red,w} = \frac{1}{w}\left(\frac{\eta}{\eta_o} - 1\right) = [\eta]_w + k_1\left(\frac{\rho\overline{V_2}}{M}\right)^2 w + k_2\left(\frac{\rho\overline{V_2}}{M}\right)^3 w^2 + \ldots \tag{6}$$

where w is the weight fraction of solute and ρ is the solution density. The reduced viscosity based on a weight fraction concentration, $\eta_{red,w}$, is related to $\eta_{red,\phi}$ by $\eta_{red,w} = \eta_{red,\phi}\,\rho\,\overline{V}_2$ /M with a similar relationship between $[\eta]_w$ and $[\eta]_\phi$. The intrinsic viscosity based on a volume fraction concentration, $[\eta]_\phi$, and the intrinsic viscosity based on weight fraction concentration, $[\eta]_w$, are both dimensionless; the intrinsic viscosity based on a mass/volume concentration, $[\eta]_c$, has dimensions of *1/c*.

As noted earlier, the intrinsic viscosity is related to the size and conformation as well as other characteristics of the solute in solution. If the solute is spherical with radius a_v, then

$$[\eta]_c = 2.5\,\frac{\overline{V_2}}{M} = 2.5\,\frac{N_A}{M}\,\frac{4}{3}\pi a_v^3 \tag{7}$$

where N_A is Avogadro's number. Eq. (7) shows that, if one wishes to use a measured value of $[\eta]_c$ to determine if the solute is spherical, additional measurements are necessary. The solute molecular weight must be known as well as solute size from another measurement such as sedimentation or diffusion. With this information, one can compare the measured intrinsic viscosity to that predicted using Eq. (7). If the values are in agreement, the rigid spherical model is appropriate; if the values are not in agreement, it can mean that the solute is not spherical. However, as discussed below, other phenomena can also lead to deviations from the Einstein prediction and it is often difficult to identify which of these phenomena are important for a particular system.

Several alternative approaches have been used to interpret measured intrinsic viscosity values using Eq. (7) or a similar equation for $[\eta]_w$ (where one must also know the solution density). If the solute molecular weight is known, one can use a measured intrinsic viscosity value to determine an effective solute radius, which is simply the radius of a sphere with similar rheological characteristics as the solute. Alternatively, if something is known about the solute size, one can determine an effective molecular weight. Neither of these approaches, however, provides any information about the macroscopic shape or conformation of the solute.

Eq. (7) is valid for solute systems which are consistent with the assumptions made in Einstein's analysis. There are a number of phenomena that can lead to deviations from the rigid sphere description which is the basis of the Einstein derivation. These include solvation of the solute particles, non-spherical solute shape, high solute concentrations and polydisperse solutions. These corrections have all been considered by investigators using intrinsic viscosity to characterize asphaltenes and heavy oils because the rigid sphere model is at best a crude approximation for these materials.

2.1.2. Deviations from Einstein's Prediction. When a solute becomes solvated in solution, it's effective size will be larger than predicted from it's dry mass which is presumably used when determining solution concentration. Therefore, the intrinsic viscosity of a solvated solute will be greater than predicted from Eq. (7) when c is determined from the dry mass of solute. One can define a solvation constant, K, as the ratio of solvated solute volume to the unsolvated, 'dry' volume. If ϕ is defined as the volume fraction of un-

solvated solute, then the effective volume fraction with solvation is $K\phi$ and the intrinsic viscosity is $2.5K$ if the solvated particles are spherical in shape.

Another type of solvation constant has been defined by considering ϕ to be the volume fraction of solvated particles in solution.[6] This solvation constant, typically also given the symbol K, has been defined as the proportionality constant between this volume fraction and the weight fraction concentration, w, which is based on the relative mass of 'dry' solute to solution mass:

$$\phi = Kw \tag{8}$$

This solvation constant is often also defined as the ratio of solvated to unsolvated solute volumes. However, one can show using dimensional arguments that this definition is valid only if the dry solute density is equal to the solution density, an assumption whose validity with asphaltene solutions depends upon the solvent used.

A solute particle which is rigid but non-spherical will also appear larger in solution than a sphere of equal mass because Brownian motion causes the rotating solute particle to exclude a sphere of radius greater than the radius of a sphere of equal mass. A reasonably simple model for a rigid asymetrical solute is an ellipsoid of revolution. A rod shaped solute can be described using a prolate ellipsoid of revolution and this model has been used to describe particles such as the tobacco mosaic virus.[5] A disc like solute can be described using an oblate ellipsoid of revolution and this model has been used by a number of workers to describe asphaltenes and heavy oils.[2,7,8] The intrinsic viscosity of a solution containing prolate or oblate ellipsoids was investigated by Scheraga[9] who tabulated values of the shape factor, υ, which is the coefficient of $\bar{V}_2 / M_2$ in the first equality in Eq. (7). The shape factor has a value of 2.5 for spherical solutes and is larger than 2.5 and is dependent upon the axial ratio for both prolate and oblate ellipsoids. The relationship between the shape factor, υ (normalized by the shape factor for a sphere, 2.5) and the axial ratio, ε, of oblate ellipsoids is shown in Figure 1. It should be noted that both particle solvation and non-spherical solutes yield intrinsic viscosity values larger than predicted from Einstein's analysis (i.e., shape factors larger than 2.5). When using Eq. (7), it is not possible to distinguish between these two effects from intrinsic viscosity measurements alone and it is likely that both are contributing to deviations from Einstein's prediction for many systems.

Another type of model structure that has been proposed to describe the macroscopic characteristics of asphaltenes and heavy oils is a series of multisubunit complexes.[10,11] These models are structures assembled from identical spherical subunits. The position of each subunit in a particle fixed coordinate system is fixed; i.e., the molecule is rigid and the distance between adjoining spheres is twice the sphere radius. Garcia de la Torre and Bloomfield[10] calculated the intrinsic viscosity of a number of different model structures containing 2–8 spheres positioned in either a polygon or polyhedron shape. The intrinsic viscosity of multilayer polygon structures containing up to 24 spheres was calculated by Nortz *et al.*[11] When the results are put in the form of Eq. (7) with a shape factor replacing the coefficient 2.5, one finds a shape factor of 2.18 for a single layer polygon containing three spheres, a shape factor of 3.5 for a single layer polygon containing six spheres and a shape factor of 4.0 for a three layer structure with each layer containing eight spheres (24 spheres total). The intrinsic viscosity of these structures deviate less from the Einstein prediction than do ellipsoids of revolution because the multisubunit structures are open and therefore less energy is dissipated when they are placed in a shearing flow when compared to rigid impermeable solutes of equal volume.

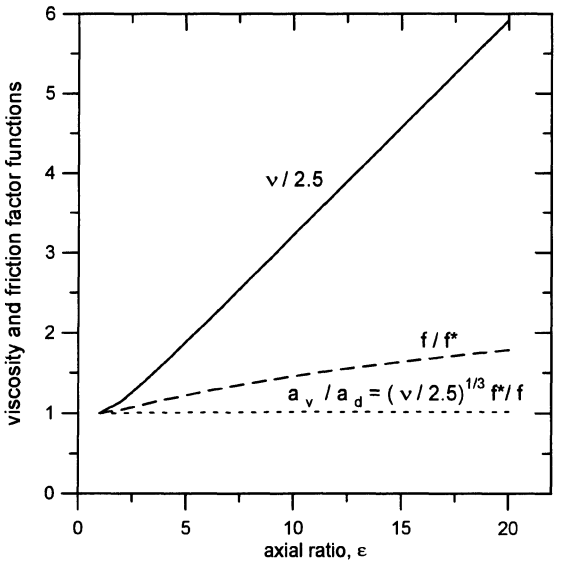

Figure 1. Viscosity and friction factor functions as a function of the axial ratio of an oblate ellipsoidal shaped solute. —— Intrinsic viscosity shape factor for an ellipsoid relative to that for a sphere,[9] – – – Friction factor for an ellipsoid relative to that for a sphere with the same volume (Eq. 25), - - - - Ratio of viscosity determined radius to diffusion or sedimentation determined radius. The axial ratio is defined as the ratio of the major to minor axis of the ellipsoid.

Another phenomenon that can yield deviations from Einstein's prediction of intrinsic viscosity is solute concentration. As solute concentration increases, it becomes necessary to add additional terms to the series expansion of η/η_0 versus c, w or ϕ and one must determine theoretically the coefficients of the added terms in order to describe solution viscosity. An alternative approach was proposed by Roscoe who considered the incremental increase in viscosity that arises when a small amount of additional solute is added to a solution that already contains solute particles at volume fraction ϕ.[12] The volume available to the added solute is $(1-\phi)$ of the total volume of the system. The change in volume fraction of the solution is then $d\phi/(1-\phi)$ and the change in viscosity resulting from the added solute $d\eta$ is $2.5\ \eta\ d\phi/(1-\phi)$. Integrating from $\phi = 0$ (where $\eta = \eta_0$) to volume fraction ϕ yields

$$\frac{\eta}{\eta_o} = (1 - \phi)^{-2.5} \tag{9}$$

which predicts the non-linear dependence of η on ϕ that is observed as concentration increases. Eq. (9) predicts $\eta/\eta_0 \rightarrow 1 + 2.5\ \phi$ for small ϕ, which is consistent with Einstein's prediction for dilute solutions.

The exponent of -2.5 in Eq. (9) arises because of the assumption of spherical solutes. If the shape is non-spherical, an exponent greater than 2.5 is expected. To illustrate the sensitivity of η/η_0 to spherical shape, a comparison of Eq. (9) to similar expressions with different exponents is shown in Figure 2. Exponents ranging from 2.5 to 8 were chosen because these values are expected for oblate ellipsoids with axial ratio up to 10 as shown in Figure 1. This comparison shows that deviations from the Roscoe equation that arise because of a non-spherical shape do not significantly affect measured viscosity values for solutions with volume fraction less than 0.3 when the exponent (i.e., the shape factor) is 4 or less. Increasing deviations are seen for more asymmetric particles but again these deviations are not distinguishable for solutions with concentration less than 10% by volume. This figure illustrates that one must be careful when interpreting agreement with Eq. (9) as an indication that the solute particles are spherical in shape.

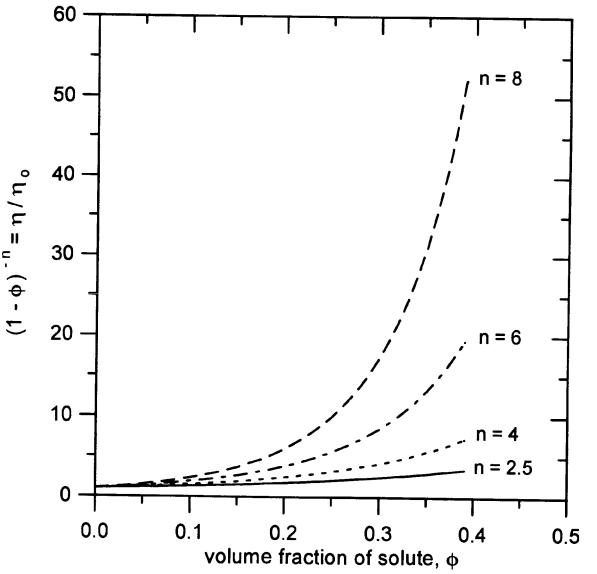

Figure 2. Solution viscosity relative to pure solvent viscosity as a function of volume fraction of solute for different viscosity shape factors (i.e., the exponent in the Roscoe equation (Eq. 9)).

The analysis leading to Eq. (9) was derived by assuming that the upper limit on ϕ is unity, and predicts $\eta \rightarrow \infty$ as $\phi \rightarrow 1$. For a system containing spherical solutes of finite size, it is expected that the particles will lock into a rigid structure (where the solution will have infinite viscosity) at some volume fraction less than 1.

Krieger derived an alternative expression which accounts for the fact that the upper limit on the volume fraction of spherical solutes in a solution is less than 1.[13] Following an exercise similar to that used by Roscoe of adding a small amount of solute to a system with volume fraction of spheres ϕ, Krieger derived the following expression:

$$\frac{\eta}{\eta_o} = \left(1 - \frac{\phi}{\phi_{max}}\right)^{-[\eta]_\phi \phi_{max}} \tag{10}$$

where ϕ_{max} is the maximum volume fraction (where $\eta \rightarrow \infty$) whose value might range from 0.52 for a simple cubic packing to 0.74 for face-centered cubic packing.

Following mathematical arguments, Mooney derived an alternative expression for the concentration dependence of η/η_0 that involves an exponential function.[14] Solution polydispersity was also explicitly included in his analysis which yielded the following equation:

$$\frac{\eta}{\eta_o} = \exp\left(\frac{[\eta]_\phi \, \phi}{1 - k\dfrac{\phi}{\phi_{max}}}\right) \tag{11}$$

where ϕ_{max} is defined again as the maximum volume fraction and k is a factor which accounts for polydispersity and has a value of 1 for a monodisperse solution. The functional form of Eq. (11) is consistent with the Einstein prediction for small ϕ and predicts $\eta \rightarrow \infty$ as $\phi \rightarrow \phi_{max}$ when $k = 1$.

The exercise considered by Roscoe[12] that led to the development of Eq. (9) also considers the effect of solution polydispersity although there is no parameter in the expression which quantitatively characterizes polydispersity. Eq. (9) is therefore valid for both monodisperse as well as polydisperse systems. To understand that this is the case, one must first recognize that Einstein's result for dilute solutions (Eq. (2)) is valid for monodisperse as well as polydisperse systems because each sphere is assumed to independently influence the flow of solvent. The interpretation of a measured intrinsic viscosity in terms of effective solute size will therefore yield an average size or average molecular weight when the system is polydisperse.

We now consider a polydisperse mixture containing particles of different sizes, each with volume fraction ϕ_i. The solution is assumed to be sufficiently dilute in each component so that the Einstein equation holds for each solute size. Additional solute with volume fraction $d\phi_i$ is now added to the solution, yielding an increase in viscosity $d\eta$. We can again note that $d\phi_i = d\phi/(1 - \phi)$ where ϕ is the total volume fraction of spheres in the system. Integration again yields Eq. (9). This analysis shows that positive deviations from Einstein's prediction can also result from solution polydispersity as well as solute concentration effects. The simplicity of Eq. (9) can be considered fortunate or unfortunate depending upon one's objective when interpreting an intrinsic viscosity measurement. The fact that Eq. (9) holds for both monodisperse as well as polydisperse systems means that one does not need to know anything about the distribution of particle sizes when using Eq. (9). The unfortunate side of the picture is that interpretation of a measured intrinsic viscosity using Eq. (9) will also not yield any explicit information about the extent of polydispersity in the mixture of interest.

Pal and Rhodes developed an empirical expression to relate solution viscosity to concentration by fitting a large body of data for oil in water and water in oil emulsions.[15] Using theoretical arguments along the lines used by Roscoe[12] in developing Eq. (9), an alternative expression which is consistent with their empirical relationship was developed. This expression simultaneously accounts for solvation, polydispersity and concentration effects:

$$\frac{\eta}{\eta_o} = (1 - K\phi)^{-2.5} \tag{12}$$

where ϕ is the volume fraction of unsolvated particles, K is the solvation constant and $K\phi$ is the volume fraction of solvated particles. Eq. (12) reduces to the Roscoe equation (Eq. 9) when $K = 1$. In developing Eq. (12), it is assumed that K is a constant for all solutes (independent of size) and that all solutes are spherical in shape, providing the exponent of 2.5. If there is a deviation from spherical shape, one expects the exponent to deviate from 2.5. Eq. (12) can be rearranged to provide an expression that allows one to determine whether viscosity data collected for a particular system are consistent with the assumptions made in the derivation:

$$\left(\frac{\eta}{\eta_o}\right)^{-0.4} = 1 - K\phi \tag{13}$$

A plot of $(\eta/\eta_o)^{-0.4}$ versus ϕ is predicted to yield a straight line with intercept = 1. The slope of the line is negative, with value equal to the solvation constant, K. One can assess

the shape of the solute particles by determining the exponent value that provides the best fit of the data. However, as noted with the discussion of the Roscoe equation and as illustrated in Figure 2, η/η_0 is not particularly sensitive to the exponent unless solution concentrations are large. Therefore, one must also be careful when interpreting agreement with Eq. (13) as an indication that the solutes can be modeled as spheres.

Eq. (13) predicts $\eta \rightarrow \infty$ as $\phi \rightarrow 1$; therefore, deviations between observations and predictions based on Eq. (13) are expected because one expects viscosity to approach infinity at volume fractions less than unity. One can correct the Pal and Rhodes expression for order at some volume fraction $\phi_{max} < 1$ by introducing corrections similar to the Krieger[13] expression (Eq. (10)) where now K will account for both solvation as well as the maximum packing factor.

Another empirical expression was developed by Eiler[16] who proposed the following:

$$\frac{\eta}{\eta_o} = \left(1 + \frac{[\eta]_\phi \, \phi/2}{1 + \phi/\phi_{max}}\right)^2 \tag{14}$$

which can be rearranged to

$$\frac{\sqrt{\eta/\eta_o} - 1}{\phi} = \frac{[\eta]_\phi}{2} - \frac{\sqrt{\eta/\eta_o} - 1}{\phi_{max}} \tag{15}$$

Eq. (15) predicts that a plot of $((\eta/\eta_o)^{1/2} - 1)/\phi$ versus $((\eta/\eta_o)^{1/2} - 1)$ should yield a straight line with slope = $-1/\phi_{max}$ and intercept = $[\eta]_\phi/2$. Plotting the data in this manner allows one to determine the intrinsic viscosity without any *a priori* knowledge of ϕ_{max}.

The final theory that will be presented has been proposed for concentrated suspensions and is not valid for dilute suspensions. Campbell and Forgacs[17] developed an expression that was based on percolation theory and is appropriate for suspensions of hard spheres whose concentration is above the percolation threshold yet below the maximum packing fraction. Below the percolation threshold, the suspension is assumed to contain free particles and freely moving clusters. At the percolation threshold, the suspended particles form infinite clusters and the viscosity is now dependent upon the number of holes in the infinite cluster. The following equation was derived for the viscosity of the suspension above the percolation threshold:

$$\frac{\eta}{\eta_o} = \exp\left(\frac{\phi_{max} - \phi_c}{\phi_{max} - \phi}\right) - 1 \tag{16}$$

where ϕ_c is the volume fraction at the percolation threshold, which is equal to *0.16* for many colloidal systems. Because Eq. (16) is valid only for concentrated suspensions where $\phi > \phi_c$, it cannot be used to predict the intrinsic viscosity.

2.1.3. Staudinger-Houwink Equation. As a final note in this background discussion, the Staudinger-Houwink equation will be introduced:

$$\eta = k M^a \tag{17}$$

which is commonly used with synthetic polymers.[5] The exponent a provides an indication of the conformation of the polymer or solute in solution, i.e., how the solution viscosity responds to changes in molecular size. For a free draining polymer chain where each monomer or bead along the chain experiences the same flow field, $a = 1$. For a random coil polymer, which is a tightly coiled chain approximately spherical in shape, $a = 1/2$. These two models bracket the observed behavior of most synthetic polymers and Eq. (17) enables one to determine polymer molecular weight from a measurement of intrinsic viscosity once k and a are known for the particular polymer. For rigid solutes, $a = 0$, 0.5, and 2 for spherical, disc-like and rod-like molecules, respectively.[18] These exponent values were determined for a series of macromolecules whose configuration does not change as molecular size increases. If the system of interest follows this assumption and one can measure intrinsic viscosity and molecular weight, one can qualitatively characterize the comformation of the solutes in solution by determining the value of the exponent a that provides the best fit to the data.

2.2. Experimental Measurement of Solution Viscosity

The two most commonly used viscometers for measuring the viscosity of solutions containing asphaltenes or heavy oils are the capillary viscometer (of which the Canon-Fenske and Ubbelohde are two types) and the concentric cylinder viscometer (also called a Couette viscometer). Because viscosity is strongly dependent on temperature, regulation of solution temperature is critical for the accurate determination of viscosity.

As it's name implies, a capillary viscometer contains a precision bore capillary with large bulbs at both ends. The volume of the upper bulb is indicated by two etched lines at the top and bottom of the bulb. The velocity of fluid through the capillary (which is proportional to the fluid viscosity) is determined by measuring the time required for the liquid level in the upper bulb to pass from one etched line to the other. The only driving force for flow is gravity. The solution viscosity is then related to flow times by the following expression:

$$\eta = constant \times time \times \rho \tag{18}$$

which was derived by considering laminar flow through a capillary.[5] The constant in Eq. (18) incorporates the characteristics of the viscometer as well as kinetic energy corrections for end effects in the capillary. When the objective is to determine intrinsic viscosity, absolute viscosity values are not needed, just the ratio of solution to pure solvent viscosity. If solution concentration is low, one can typically assume that solution and solvent densities are equal. Therefore, the ratio of viscosities is simply the ratio of flow times, corrected for end effects. Values for the end effect corrections are provided by the viscometer manufacturer. Capillary viscometers are relatively inexpensive and easy to use. The disadvantage of capillary viscometers is that they do not allow one to vary shear rates except by comparing results obtained using viscometers with different sized capillaries.

In a concentric cylinder viscometer, the solution is placed between two concentric cylinders and one cylinder is rotated (usually the inner cylinder). The torque on the other cylinder is measured and can be related to the viscosity of the solution through suitable calibration of the instrument. The advantage of a concentric cylinder device over a capillary viscometer is that one can easily vary shear rates by changing the rate of rotation.

2.3. Intrinsic Viscosity of Asphaltenes and Heavy Oils

The rheological properties of petroleum-derived materials have been of interest for many years. However, the number of reports in which the measured solution viscosity was interpreted in terms of the macroscopic structure of the constituents of these materials has been rather limited. A comparison of results obtained from different studies is often difficult because samples from a variety of different sources have been investigated and different sample preparation procedures are often utilized. Also, some studies focused solely on asphaltenes whereas others included the soluble resins (sometimes called maltenes) as well. In addition, the objectives of these studies, and therefore the approaches used to interpret results, were often quite different. In this section, results from a number of different studies will be reviewed and compared.

One of the first investigations of solution viscosity measurements with asphaltenes was reported in 1932 by Mack.[19] In this work, viscosities of solutions containing asphaltenes as solute with the parent oil as solvent were measured. Solution viscosities were found to be up to several hundred times larger than the viscosity of the deasphalted parent oil for solutions containing up to 20 volume % asphaltenes. The results were not interpreted in terms of the macromolecular structure of the asphaltenes although it was noted in a later publication by Reerink[7] that the Einstein equation of viscosity (Eq. (2)) only predicts a 50% increase in viscosity for a solution containing spheres with a volume fraction of 20%. The Roscoe equation (Eq. (9)) predicts a 75% increase in viscosity for a suspension with this concentration, a value which is still considerably smaller than the reported observations.

Lorenz *et al.*[20] reported results from viscosity measurements with asphaltene solutions in several different solvents (kerosene, gas oil, benzene and decalin) as well as with different fractions collected following ultracentrifugation of four different crude oils. Asphaltene concentrations ranged from 1 to 2 wt%, considerably more dilute than the solutions investigated by Mack. The shape factors determined by measuring the viscosity of asphaltene solutions in various organic solvents yielded shape factors reasonably close to 2.5, indicating that the asphaltenes appear to be nearly spherical and nonsolvated under these conditions. For the asphaltene solutions in the ultracentrifuged samples, shape factors ranging from 8–40 were observed. These solutions were prepared by collecting various fractions following ultracentrifugation. The 'solvent' viscosity, needed when determining the reduced viscosity, was the viscosity of the lighter fractions that contained no asphaltenes. But the 'solvent' for each of the fractions was not the same and the viscosity of each was undoubtedly larger than the viscosity of the lighter fractions. This can lead to erroneous results when interpreting measured viscosities using Einstein's equation of viscosity.

In a more recent study, Reerink measured the intrinsic viscosity and sedimentation coefficients of asphaltene fractions obtained by dialysis and fractional precipitation.[7] Several different organic solvents—toluene, cyclohexane, benzene and tetrahydrofuran—were used. Asphaltene molecular weight values were also measured using vapor pressure osmometry. The measured intrinsic viscosities (based on a volume fraction concentration) were in the range 5–8 indicating deviation from Einstein's prediction for rigid nonsolvated spheres. A Staudinger-Houwink plot of $[\eta]_\phi$ versus M yielded good agreement with the power law relationship (Eq. (17)) with an exponent $a = 0.16$ which lies between the values of 0 predicted for a spherical solute and 0.5 predicted for a disk-like planar solute. By combining the viscosity results with information obtained from the sedimentation measurements, Reerink argued that these asphaltenes could be modeled as oblate ellipsoids

with minor axis about 10A and major axis 50–90A. These results and the interpretation of them will be discussed in more detail later in this chapter.

In a similar study with petroleum pitch fractions, Sakai *et al.* [8] reported intrinsic viscosity of pitch fractions with molecular weight (as determined by vapor pressure osmometry) ranging from 400–900, values which are considerably smaller than typically observed for petroleum-derived asphaltenes. When the intrinsic viscosity was plotted as a function of molecular weight, values were in general agreement with the Staudinger-Houwink equation (Eq. (17)) with the exponent $a = 0.12$ for the smaller molecular sized fractions and $a = 0.21$ for the higher molecular weight fractions, values that are in good agreement with the exponent of 0.16 found for the data of Reerink[7] and that again lie between the prediction for a rigid spherical solute and a rigid planar or disc-like solute. The increase in a that is observed as molecular size increases indicates that the shape of the pitch fractions becomes less spherical and more disc-like as molecular size increases. It was also observed that the value of a did not change as temperature was increased from 15°C to 40°C. These observations indicate that the configuration of the components of these pitch fractions does not appear to be influenced by temperature. Measurements were performed in benzene and chloroform as solvent and little difference in the value of a was observed although the polarity of these solvents is similar. The diffusion coefficients of these fractions were also measured.[21] The information gleaned by combining diffusion results with these viscosity results will be presented later in this chapter.

Similar measurements have been performed in the author's laboratory with a number of vacuum bottoms in several different organic solvents. In the first study, the intrinsic viscosity of bitumen fractions (obtained using preparative gel permeation chromatography) from Cold Lake vacuum bottoms was measured at 10°C and 20°C in tetrahydrofuran solvent (THF) and at 50°C in 1-methylnaphthalene solvent.[22] The molecular weight of each fraction was determined using both vapor pressure osmometry (VPO) and field ionization mass spectrometry (f.i.m.s.), which yields both a number average as well as a weight average molecular weight. There was a reasonable difference in the molecular weight values determined by the two methods and there are several plausible explanations for these differences. The samples were contaminated with a stabilizer, BHT, which was present in the tetrahydrofuran used as the solvent for the chromatographic separation. The f.i.ms. molecular weight values were corrected for the BHT but it was not possible to correct the VPO molecular weight values for the presence of BHT. Determination of molecular weight by f.i.m.s. requires volatilization of the samples and there was inevitably incomplete volatilization, particularly with the heavier fractions. The molecular weight measured by VPO should provide an indication of the molecular size of constituents in solution, which for these measurements were performed in benzene at 40°C. It would not be surprising that the molecular size indicated by f.i.m.s. would be different than that indicated by VPO because of the different environmental conditions used for each measurement.

There was little difference between the intrinsic viscosity values for each fraction in THF at the two temperatures and the difference between the intrinsic viscosity measured in 1-methylnaphthalene was slightly, but not significantly, larger than in THF. This is an indication that the configuration or conformation of these materials at the three experimental conditions is quite similar. A fit of the data to the Staudinger-Houwink equation (Eq. 17) using the VPO molecular weight shows reasonable agreement when $a = 1.1–1.2$. Recall that an exponent of *1* is predicted for a free draining linear polymer and an exponent of *2* is predicted for a rod-like solute. Neither of these models is intuitively consistent with the rigid, spherical or planar structure that is expected for resid materials. However,

four of the nine fractions examined covered a narrow range of VPO molecular weight values (1000–1500), indicating that there was perhaps some error in the determination of these values which may be due to the presence of BHT. It should also be noted that Thiyagarajan *et al.* [23] found that the small angle neutron scattering of asphaltenes in 1-methylnaphthalene at 20° C suggested a rodlike morphology for the asphaltenes. These results illustrate the challenge, and the importance, of obtaining accurate molecular weight values when interpreting intrinsic viscosity results. The diffusion coefficients of these materials were also measured and these results will be discussed later in this chapter.

A subsequent study involved fractions from Athabasca tar sand bitumen vacuum bottoms as well as from a vacuum resid blend from Western Canadian crudes.[11] In this study, the molecular weight of each fraction was determined using VPO only but there was no stabilizer contaminating the samples. The VPO measurements were performed in toluene at 40° C. The intrinsic viscosity of each fraction was measured with 1-methylnaphthalene as solvent at 50°C and 70°C. It was observed that temperature did not have a strong influence on the intrinsic viscosity of these materials indicating that the materials did not appear to undergo any structural changes over the limited temperature range that was investigated. The intrinsic viscosity of fractions from both materials of similar molecular weight were approximately the same indicating that the structural characteristics of these materials are similar. When fractions from this study are compared to fractions from the earlier study with similar VPO molecular weight, similar intrinsic viscosity values were observed for the smaller fractions ($M < 900$). However, for the fractions with larger molecular sized entities, there was an increasing discrepancy between the two studies with the Cold Lake material showing larger intrinsic viscosity values when compared to the Athabasca and Western crudes fractions. This difference is illustrated by comparing the exponent a in a Staudinger-Houwink plot from the two studies. For the Athabasca and Western crudes fractions, $a = 0.44$, a value less than half of that observed with the Cold Lake material. The exponent of 0.44 is close to the prediction of $a = 0.5$ for a disc-like, planar solute, a model which is consistent with the flat, layered structure that was proposed by Dickie and Yen in 1967.[24] The results from these measurements were interpreted with results from diffusion measurements and these results will be discussed later in this chapter.

In a slightly different approach to examining the molecular size dependence of the intrinsic viscosity, Al-Jarrah and Al-Dujaili measured the intrinsic viscosity and VPO molecular weight of asphaltenes that were isolated from asphalt samples of a Northern Iraq crude oil.[25] These measurements were made at different temperatures using a number of different solvents with different polarity. The smallest entities, as indicated by VPO molecular weight as well as intrinsic viscosity, were found in nitrobenzene (the most polar solvent used) at 120°C, which was the highest temperature examined. The authors considered the asphaltenes at this set of conditions to represent a 'base' unit and the larger entities observed at other solvent or temperature conditions were assumed to be formed by association of these base units into larger structures. The degree of association was introduced to quantitatively describe the differences between results obtained at different environmental conditions and was defined as the ratio of molecular weight at the conditions of interest relative to the molecular weight determined in nitrobenzene at 120°C. An analogous definition utilized the ratio of intrinsic viscosities. At each set of conditions, there was reasonable agreement between the degree of association determined using the two definitions, indicating that VPO molecular weight and intrinsic viscosity are capturing similar changes in molecular structure that occur as environmental conditions are changed. A strong correlation between the degree of association and the dielectric constant of the solvent was also observed.

A replot of the results reported from this study in the form of a Staudinger-Houwink plot (Eq. 17) shows excellent agreement between experiment and Eq. (17) when $a = 0.82$. This value lies between the two extremes of $a = 0.44$ and $a = 1.2$ reported by Kyriacou *et al.*[11,22] and is considerably larger than the exponent of *0.1–0.2* reported by Reerink[7] and Sakai *et al.*[8] An attempt to explain these differences in results provides a good illustration of the difficulty that arises when comparing results from different laboratories. There were many differences in the samples themselves (sources as well as asphaltenes versus vacuum bottoms that contain resins in addition to asphaltenes). The work of Al-Jarrah and Al-Dujaili[25] involved a polydisperse mixture and molecular size was 'changed' by changing environmental conditions whereas the work reported by the author[11,22] as well as the study by Sakai *et al.*[8] involved reasonably monodisperse fractions. Given these differences in experimental conditions, it is difficult to determine if the observed differences arise from true differences in the structure of the different materials or simply due to differences in sample preparation and conditions of the measurements.

The results from all of these studies have been compiled and are plotted on log-log coordinates in Figure 3 as $[\eta]_c$ versus VPO molecular weight. In preparing this plot, the data of Reerink,[7] that was reported as $[\eta]_\phi$ was converted to $[\eta]_c$ using asphaltene density ($\overline{V}_2$/M) that was determined in this same study by measuring solution densities. Included in this plot is a line with $[\eta]_c \propto M^{0.5}$, the relationship predicted for planar, disk-like solutes. This comparison shows that, with a few exceptions, the data are reasonably consistent and follows the general trend indicated by the 0.5 exponent. Given the fact that this

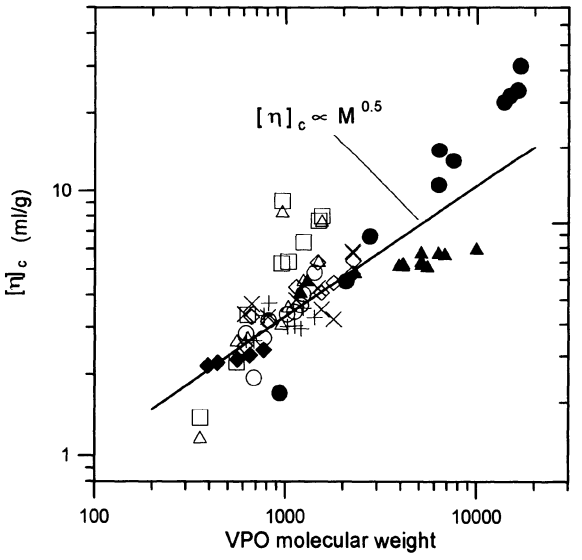

Figure 3. Experimental values of intrinsic viscosity as a function of VPO molecular weight. △ Cold Lake bitumen fractions in THF at 20°C [22], □ Cold Lake bitumen fractions in 1-methylnaphthalene at 50°C,[22] ▲ Kuwait asphaltene fractions in toluene at 25°C,[7] ● Northern Iraq asphaltenes in benzene, chlorobenzene and THF at 37°C, 45°C, 60 °C and 90°C,[25] ○ Western Canada crude vacuum resid blend fractions in 1-methylnaphthalene at 50°C,[11] + Western Canada crude vacuum resid blend fractions in 1-methylnaphthalene at 70°C,[11] ◊ Athabasca tar sand bitumen vacuum bottom fraction in 1-methylnaphthalene at 50°C,[11] × Athabasca tar sand bitumen vacuum bottom fraction in 1-methylnaphthalene at 70°C,[11] ♦ Petroleum pitch fractions in chloroform at 25°C,[8] line showing $[\eta]_c \propto M^{0.5}$.

data was collected in four different laboratories, using different solvent and temperature conditions for both the viscosity as well as the VPO measurements, the agreement is encouraging and seems to indicate that the structure of these different materials is approximately the same under a wide variety of conditions.

The studies discussed above were all performed with relatively dilute solutions. The concentration of solutions used by Reerink,[7] Nortz *et al.*[11] and Kyriacou *et al.*[22] were less than 0.02 g/ml and those used by Sakai *et al.*[8] had concentration less than 0.07 g/ml. The concentrations used by Al-Jarrah and Al-Dujaili[25] were not explicitly stated although it was noted that low concentrations were used for both VPO and viscosity measurements in order to minimize the possibility of concentration induced association or aggregation. However, the reported concentrations are larger than the values of .001 to 0.01 g/ml that have been reported for the critical micelle concentration of asphaltenes.[26] In a series of studies carried out at the Texaco Research Center,[6,27,29,30,32,33] the viscosity of asphaltene solutions in organic solvents as well as in deasphalted oil with concentrations up to volume fractions of 50% were measured. Because of the high concentrations used and because molecular weights were not measured, these viscosity measurements were interpreted using a different approach than has been discussed with the other studies.

In the first report from Texaco, asphaltenes from five different vacuum residues were investigated.[27] The residues varied considerably in their asphaltene content (3.5–23.9 wt%) and the asphaltenes varied considerably in their heteroatom and metals content. The asphaltene solutions were prepared by redissolving asphaltenes in deasphalted oil. No size fractionation was performed. Solution viscosities were measured at 93°C using a Couette viscometer for solutions with concentration up to 16 wt% asphaltenes. A plot of specific viscosity (η/η_o - *1*) versus concentration yielded a straight line for solutions with concentration less than 8 wt% with slope essentially the same for all asphaltenes investigated. Within experimental uncertainty, the line intercepted the origin, as predicted from Einstein's equation (Eq. (2)). With the data plotted in this manner, the intrinsic viscosity is equal to the slope of the line and with concentration expressed as wt%, the intrinsic viscosity is $[\eta]_w$ (Eq. (6)). Experimental data deviated from the linear Einstein prediction for solutions with concentration greater than 8 wt%.

For one of the materials, the viscosity of the native residue was also measured and when the viscosity of this solution was compared to the viscosities of 'synthetic' residues, the viscosity of the native residue fell along the line which describes the η_{sp} vs w data from the synthetic residues. This shows that the asphaltenes in the native and synthetic mixtures are essentially the same. The fact that the asphaltenes from all five sources yielded very similar rheological behavior ($[\eta]_w$ = 7–9) shows that the effect of shape and extent of solvation for these materials are quite similar, despite the fact that their heteroatom and metals contents vary considerably. This indicates that the components of the asphaltenes do not appear to influence their configuration nor their interactions with solvent or deasphalted oil.

In this study, no attempt was made to determine $[\eta]_\phi$ nor to relate the measured $[\eta]_w$ values to the effective size or configuration of the dissolved asphaltenes. In the work reported by Kyriacou *et al.*,[22] values of $[\eta]_c$ ranged from 1.2–9 cm^3/g for asphaltenes in tetrahydrofuran at 20°C and in 1-methylnaphthalene at 50°C. If we consider the density of the asphaltene solutions to be of order 1 g/cm^3, we can convert $[\eta]_w$ to $[\eta]_c$ and see that results from the two studies are reasonably consistent.

Subsequent studies from this group focused on a single source material—Ratawi vacuum resid. In these studies, attempts were made to interpret measured viscosities using a number of different theories that have been presented in this chapter. In order to use

these theories, it is necessary to establish a relationship between a volume fraction concentration (used in the theories) and a weight fraction concentration which was used experimentally. In doing this, it was recognized that the factor $M/\overline{V}_2$ needed in Eq. (6) to relate $[\eta]_w$ to $[\eta]_\phi$ can be expressed as ρ_p, the density of the solute in solution. Knowing the density of the Ratawi asphaltenes (1.13 g/cm^3), it was possible to relate w to ϕ without determining the molecular weight of the solute.[28]

In one report, the rheological properties of two different solubility fractions (pentane soluble and heptane insoluble) from Ratawi vacuum residue were reported.[29] Solutions of the lighter fraction were prepared in four different n-alkane solvents ranging from C_7 to C_{16}; solutions of the heavier fraction were prepared in toluene. Concentrations up to 45 wt% were investigated. The temperature dependence of the viscosity of solutions of the heavier fraction was also investigated.

At room temperature, the results for both fractions followed Einstein's prediction for spherical solutes for solutions with concentration $\phi < 0.1$ with increasing deviation as concentration was increased. A plot of the data following the Pal and Rhodes analysis (Eq. (13)) showed good linearity with an intercept through *1* when an exponent of 0.4 was used. The exponent of 0.4 indicates that the solutes are approximately spherical over the entire range of concentration investigated, not just in the dilute solution regime. The data for the pentane soluble material yielded lines with different slope in each solvent, with slope increasing as the length of the carbon chain of the solvent increased. The slope for the heptane insoluble material in toluene was over four times larger than for the pentane solubles in heptane. Recall that with Eq. (13), ϕ is defined as the volume fraction of unsolvated solute so that $K\phi$ is the volume fraction of solvated solute and the slope of the line resulting from the Pal and Rhodes analysis is equal to K. The observations indicate an increasing solvation effect as the length of the carbon chain of the solvent increases. However, difficulties arose when attempts were made to directly relate the K values derived from the slope to the ratio of solvated to unsolvated solute volume because $K < 1$ was found for the pentane soluble material in n-heptane solvent. The authors attributed this anomalous behavior to a lubrication effect or to some other colloidal effect that is not accounted for in the analysis of Pal and Rhodes.

A plot of the viscosity data following Eiler's equation (Eq. (15)) showed good agreement with different slopes (i.e., different ϕ_{max}) in each solvent. For the pentane soluble material, $\phi_{max} \approx 0.64$, independent of solvent; for the heptane insoluble material in toluene, $\phi_{max} = 0.43$. The authors attributed the differences between these values and the volume fraction at maximum packing for a face centered cubic arrangement ($\phi_{max} = 0.74$) to be due solvation of the material. The degree of solvation was defined as the ratio of 0.74 to ϕ_{max} determined from the viscosity measurements.

A comparison of the degree of solvation information collected by analyzing the data using the Pal and Rhodes equation to the analysis provided from Eiler's equation shows some qualitative differences and as well as some similarities between the conclusions drawn from each analysis. Both analyses indicate that the degree of solvation is greater for the heptane insoluble fraction in toluene than for the pentane soluble material in n-alkane solvents. It might have been interesting to have collected data for both materials in one solvent in order to determine how much of the observed differences can be attributed to the nature of the solute and how much to the solvent. The Pal and Rhodes analysis indicates that there is a solvent effect with the n-pentane soluble material but no such effect was observed from the Eiler analysis. The authors postulate that this difference may simply be due to the low sensitivity of Eiler's equation to the degree of solvation.

Finally, the measured solution viscosities were compared to those predicted from the Campbell-Forgacs equation (Eq. (16)) where the volume fraction at maximum packing derived from the Eiler analysis was used in making the Campbell-Forgacs prediction. Good agreement was observed for both materials for concentrations between the percolation threshold $\phi_c = 0.16$, and $\phi = 0.5$ for the pentane soluble material and $\phi = 0.35$ for the heptane insoluble material. In this range of concentration, these materials can apparently be modeled as hard spheres.

In another publication from this group, viscosity results from synthetic and natural Ratawi vacuum residue were analyzed using a number of different theories.[30] The 'synthetic' solutions were again prepared by redissolving asphaltenes in deasphalted oil. The intrinsic viscosity based on a weight fraction concentration was the same as previously reported with this material, 7.3.[27]

Using Eq. (8) to relate volume fraction and weight fraction concentrations, the Roscoe equation (Eq. (9)) was rearranged to show that a straight line is predicted from a plot of $(\eta/\eta_o)^{-0.4}$ versus w if the asphaltenes are spherical. Good linearity was observed, indicating that the asphaltenes are reasonably spherical under these conditions. With that assumption verified, the authors then went back to the observed intrinsic viscosity value to determine one value for the solvation constant, K. Now, K is simply the ratio of $[\eta]_w$ to $[\eta]_\phi$ where $[\eta]_\phi = 2.5$ for a sphere and K was determined to be $7.3/2.5 = 2.9$. As noted by the authors, however, the agreement with the Roscoe equation does not unequivocally rule out other solute shapes because similar agreement between theory and experiment was observed when the exponent was 3.0 rather than 2.5. This insensitivity to the exponent (i.e., solute shape) is illustrated in Figure 2. Using a value of 3 for the exponent, the solvation constant then reduces to 2.4.

A comparison of the data to the Eiler equation (Eq. (14)) also showed good agreement. When ϕ and ϕ_{max} are replaced by w and w_{max}, the intrinsic viscosity determined from the intercept is now $[\eta]_w$ and the value was found to be 6.9, which is consistent with the value of 7.3 which was determined from the Einstein plot. The solvation constant determined using $[\eta]_w = 6.9$ was found to be 2.8. Determination of w_{max} from the slope provided another value for K if one assumes that $\phi_{max} = 0.74$, the prediction for a face centered cubic system. The solvation constant determined in this manner was 2.5, which is again consistent with the values determined from the Roscoe and Einstein equations.

The data were compared to the prediction of Campbell and Forgacs and another solvation constant was determined by evaluating the weight fraction concentration below which the data deviate from their model. The Campbell and Forgacs model is only valid for concentrations above the percolation threshold which was assumed to occur at volume fractions of 0.16. A comparison of this volume fraction concentration to the weight fraction concentration where deviations occur ($w = 0.06$) provided another value for the solvation constant $K = 0.16/0.06 = 2.7$ again consistent with the other theories.

Finally, the viscosity results were also analyzed using a theory proposed by Grimson and Barker[31] who included an interparticle potential in addition to the hydrodynamic effects considered by all the other theories that have been discussed. The effect of solvation is included by two parameters that arise in the term accounting for interparticle interactions. These two parameters were determined by fitting the data to the Grimson-Barker equation. An examination of the potential function using these fitted parameters shows a solvation shell which extends 1.3–1.4 times the radius of the unsolvated sphere. By treating the solvation constant K as the ratio of solvated to unsolvated volumes, an estimate of K in the range $(1.3)^3 - (1.4)^3 = 2.4–2.7$ is obtained. These values are consistent with values determined from the other models. But it should again be noted that describing K, as de-

fined in Eq. (8), as a ratio of volumes is based on the assumption that solute and solution densities are the same. The agreement between these various descriptions of the rheology of this mixture indicates that the repulsive interparticle interactions which are accounted for in the Grimson-Barker analysis cover essentially the same range as the solvation shell which is accounted for in the other analyses.

The extent of interparticle interactions was further examined by measuring solution viscosity for Ratawi asphaltenes dissolved in toluene and mixed with various solutions containing different NaOH concentrations (0 N, 1N, 3N and 6N).[32] The results showed the expected increase in viscosity as asphaltene concentration increased and that for $\phi > 0.13$, the viscosity at a given asphaltene concentration increased as NaOH concentration increased. A plot of the data using the Pal-Rhodes equation (Eq. (13)) showed the expected linearity only for the asphaltene solution that had not been exposed to base solution but non-linearity for solutions exposed to NaOH.

The results were also fit to the Krieger equation (Eq. (10)) and the Mooney equation (Eq. (11)) where random packing was assumed (i.e., $\phi_{max} = 0.68$). For comparison with the Kreiger equation, $[\eta]_\phi$ was treated as an adjustable parameter for each set of data (i.e., each NaOH concentration). Good agreement was observed for the asphaltene solutions that were not exposed to base solution but increasing deviation between experiment and theory was observed as NaOH concentration increased. For comparison with the Mooney equation, both $[\eta]_\phi$ and the polydispersity factor k were used as fitted parameters. The fit to this equation was much improved relative to the Krieger equation, which the authors attribute to the fact that polydispersity is explicitly accounted for in the Mooney equation. Good agreement was also observed when the data were compared to the Grimson-Barker equation where ϕ_{max} as well as the two parameters that characterize the interparticle potential were used as fitting parameters. The volume fraction at maximum packing, ϕ_{max}, was found to be 0.61 for the untreated asphaltene solutions, which is reasonably close to the value of 0.68 predicted for a random packing. However, ϕ_{max} was found to decrease substantially as NaOH concentration increased, indicating interparticle interactions become longer range as NaOH concentration is increased.

A comparison of viscosity results to information obtained from small-angle X-ray scattering (SAXS) and small-angle neutron scattering (SANS) was used in another publication to derive information about the micellar nature of asphaltenes in solution.[6] Measurements were again performed with Ratawi asphaltenes in both native and synthetic residue mixtures with asphaltene concentrations up to 21 wt% which is the asphaltene concentration in the native residue. The small-angle X-ray results indicated that the asphaltenes appeared to be present in solution with effective radii ranging from 20–50 Å distributed according to the Schultz distribution. The viscosity data showed good agreement with the Roscoe equation, results that are consistent with earlier measurements with this same material.

Small-angle neutron scattering of asphaltene solutions were measured in deuterated toluene and solvent mixtures of toluene and pyridine. These measurements indicate that the average radii were 31.2 Å, independent of solvent mixture and the polydispersity was consistent with the Schultz distribution that provided good agreement with the SAXS results. Finally, surface tension of asphaltenes in pyridine was also measured and results indicated a sharp change in behavior at $w = 0.025$ *wt %* which the authors attributed to the critical micelle concentration. This value for the CMC is two orders of magnitude smaller than has been reported by others.[26]

The consistency of the SANS and SAXS results which were performed in different solvents indicates that the effective size of the asphaltenes are not apparently influenced by the nature of the surrounding solvent, an observation which is consistent with results

from other studies that have already been discussed here.[22] An estimate of the average molecular weight of an asphaltene particle was made by determining the average effective volume from the average particle radius (determined from SANS and SAXS) and assuming a density of 1.1 g/cm^3 for the asphaltenes. The average molecular weight was found to be around 100,000, a value which is generally higher than has been reported in most studies of asphaltene molecular weight,[4] particularly when one recognizes that this molecular weight value of 100,000 represents an estimate of the molecular weight of an unsolvated asphaltene. Using the results from the surface tension measurements, the authors also estimated a molecule weight value for an asphaltene molecule at an interface and found a value of around 1000. A comparison of these two values indicates that there appears to be an average of 100 asphaltene molecules in each 'particle' or micelle seen by SANS and SAXS. This value is considerably larger than the picture of 5–10 asphaltene molecules associated together in an asphaltene micelle that was proposed by Dickie and Yen.[24]

The temperature dependence of the viscosity of synthetic residue mixtures of Ratawi asphaltenes were measured and interpreted in terms of phase transitions that occur with these mixtures.[33] Viscosities were measured at temperatures ranging from 25°C to 300°C. The results were plotted following the Roscoe equation (Eq. (9)) where again the volume fraction concentration was replaced by the weight fraction concentration using Eq. (8). Good linearity was observed at each temperature. The proportionality constant or solvation constant, K, was determined from the slope of each line and K was found to decrease as temperature increased. An Arrhenius plot of K versus $1/T$ showed good linearity for the data collected between 65°C and 300°C. Assuming K to represent the ratio of solvated to unsolvated volume, the authors also determined the ratio of the solvent layer to the unsolvated particle radius and found that, even at 300°C, there is still a thin layer of solvent (2–4 Å thick) surrounding the asphaltenes. At temperatures below 65°C, it was found that the average interparticle spacing was less than twice the thickness of the solvation layer, providing an explanation for why the Arrhenius plot describing activation energies for removal of the solvation layer does not adequately describe behavior below this temperature. The authors attributed this to a liquid to solid like transition that occurs below 65°C. An examination of the effect of shear rate on measured viscosity showed shear thickening behavior above 150°C, an indication that there is different change in structure that sets in at this temperature. At these temperatures, the thickness of the solvation layer is only several Å thick, a thickness that may be too thin to inhibit flocculation due to van der Waals forces. This flocculation was found to be reversible by measuring behavior of a system below 150°C then above 150°C and then again at the cooler temperature where it was found that the system returned to its earlier structure.

One can categorize the viscosity results discussed here into two groups. In the first group, the asphaltene or heavy oil samples were fractionated, either by solvent fractionation, dialysis or by gel permeation chromatography and the characteristics of individual fractions were examined.[7,8,11,22] For these studies, solute molecular weight was measured, providing a reasonably straightforward means to relate volume fraction concentrations to either weight fraction or mass/volume concentrations. For all systems examined, the material was dissolved in organic solvent and measurements were made at conditions at or near ambient. In general, results from these studies indicated that the constituents of the solutions investigated were non-spherical in shape and a planar or disc like shape provided a reasonable picture of the solutes. Solution concentrations in these studies were quite low. The work by Al-Jarrah and Al-Dujaili [25] was performed with low concentration polydisperse solutions and therefore is slightly different than the others. However, the results were reasonably consistent with those from other studies in this group.

In the second group, the asphaltenes were not fractionated.[6,27,29,30,32,33] Therefore, a polydisperse mixture was examined. Solution concentrations were high relative to those used in the first group of studies. Asphaltene molecular weight values were not measured. Therefore, weight fraction concentrations were related to volume fractions by defining a factor K which characterizes solvation of the asphaltenes. In most of the experiments, the solvent used was a deasphalted oil. Results from these studies indicated that the aphaltenes could be reasonably modeled as spheres and results were found to be in general agreement with various theories that account for the effect of solute concentration and solvation on solution viscosity.

It is difficult to identify why the two groups of studies seem to arrive at considerably different results regarding solute shape. The difference may be due to the different solvents used although this explanation seems unlikely because, with the exception of Al-Jarrah and Al-Dujaili's work,[25] little effect of solvent on solute characteristics was observed. It may be possible that it is more difficult to derive solute shape characteristics from a polydisperse mixture that may contain a range of solute shapes in addition to a range of solute sizes. The results reported in the first group of studies were interpreted using an approach that requires a molecular weight value of the solute. As already noted, there are two problems with this. One is simply the experimental uncertainty that arises with this measurement. The other arises because the conditions under which the molecular weight is determined can be quite different than the conditions of the viscosity measurements and therefore the measured molecular weight may not be representative of the molecular size of the solute that is affecting the solution viscosity. One might also argue that the studies performed with dilute solutions were examining individual 'molecules' whereas the latter studies performed with solutions of larger concentration were examining aggregates or micellar structures. It is certainly plausible that non-spherical molecules could aggregate into structures that resembled spheres. However, as already noted, all the studies discussed here, with both dilute and concentrated solutions, were performed at solution concentrations above previously reported values for the CMC. Without further experiments in which the same results are interpreted using both approaches, it is difficult to identify the differences between these two groups of studies.

3. SEDIMENTATION AND DIFFUSION

3.1. Background and Theory

The principles that govern sedimentation and diffusion measurements with macromolecular or colloidal sized solutes are similar and therefore the background discussion for both can be combined. The interpretation of both measurements in terms of solute characteristics involves an examination of the velocity of a particle moving through a fluid because of external forces acting on the sphere which are balanced by viscous forces between the particle and the surrounding fluid. For sedimentation, the external forces arise from the net gravitational or centrifugal forces. For diffusion, the forces arise from a concentration or chemical potential gradient in solution.

Sedimentation measurements are typically made under steady state conditions where the net gravitational or centrifugal forces are equal to the viscous forces. For a solute of volume, V, the following expression relates this balance of forces:[5]

$$V(\rho_p - \rho_o)a = fv \tag{19}$$

where ρ_p is the density of the particle, ρ_o is the density of the solvent, a is the acceleration, f is the friction factor and v is the velocity of the particle. When sedimentation is due to gravity, $a = g$. When sedimentation is enhanced by using a centrifuge, $a = \omega^2 r$ where ω is the angular velocity and r is the radius of the circular path. For reasonably small solutes in heavy oil mixtures, sedimentation velocities are typically measured using an ultracentrifuge and results are reported in terms of a sedimentation coefficient, s which is defined as the ratio of the sedimentation velocity to the centrifugal acceleration. Rearranging Eq. (19) using this definition of s yields

$$s = \frac{v}{a} = \frac{V}{f}(\rho_p - \rho_o) \tag{20}$$

If one uses the same arguments as were used in developing Eq. (5) from Eq. (4), the particle density, ρ_p, can be replaced by $M/\overline{V}_2$.

The complementarity between sedimentation and diffusion can be seen by examining the diffusion velocity that results when the force for diffusion is expressed as a gradient of concentration or chemical potential.[5] Relating the diffusion velocity, or flux, to the flux given by Fick's Law of Diffusion yields

$$D = \frac{k_B T}{f} \tag{21}$$

where D is the solute diffusion coefficient and k_B is Boltzmann's constant. Eqs. (20) and (21) show that the measurement of either a sedimentation coefficient or a diffusion coefficient can yield a value for the friction factor which is related to the effective size and shape of the solute.

For a spherical, unsolvated solute with radius a_d:

$$f = 6\pi\eta_o a_d \tag{22}$$

For a solvated or asymmetrical particle with friction factor f, a_d can be considered to be an effective radius, i.e., the radius of an unsolvated sphere that has the same frictional characteristics (the same s or D) as the solvated particle. For a solvated sphere, a_d is larger than the radius of the unsolvated sphere. The volume of a sphere with radius a_d will be larger than the volume of an asymmetrical particle with the same frictional characteristics. In order to quantitatively predict the effect of solvation and particle asymmetry on f, we define two other friction factors, f_o and f^* which enable us to independently account for solvation and asymmetry. The factor f_o is the friction factor for an unsolvated sphere with the same mass as the solvated particle. The factor f^* is the friction factor for a spherical particle with the same volume and mass as the solvated particle. Therefore, the ratio f/f_o describes the effect of either solvation, asymmetry or both and can be separated into two contributions:

$$\frac{f}{f_o} = \frac{f}{f^*}\frac{f^*}{f_o} \tag{23}$$

The ratio f/f^* accounts for particle asymmetry and the ratio f^*/f_o accounts for solvation. If the solvation constant K is defined to be the ratio of the volume of the solvated particle to the volume of the unsolvated particle,

$$\frac{f^*}{f_o} = K^{1/3} \tag{24}$$

Eq. (24) shows that $f^*/f_o \geq 1$.

One must have a model for the asymmetric particle in order to predict f/f^*. As noted with the earlier discussion of viscosity, oblate ellipsoids of revolution are one model structure that have been proposed to describe the characteristics of asphaltenes and heavy oils. Perrin[34] developed the relationship between f/f^* and the axial ratio of an oblate ellipsoid, ε:

$$\frac{f}{f^*} = \frac{\sqrt{\varepsilon^2 - 1}}{\varepsilon^{2/3} \tan^{-1}\sqrt{\varepsilon^2 - 1}} \tag{25}$$

Eq. (25) is plotted in Figure 1 where the sensitivity of f/f^* to ε can be compared to the sensitivity of the viscosity shape factor to ε. This comparison shows that viscosity is more sensitive to solute asymmetry than is sedimentation or diffusion.

Another model that has been proposed for asphaltenes and heavy oils is a series of multisubunit complexes which are complexes comprised of identical spheres connected in various rigid structures. The theoretical predictions of Garcia de la Torre and Bloomfield[11] and Nortz *et al.*[10] can be put into the form of f/f^* in order to compare predictions for the oblate ellipsoids to some multisubunit complexes. For a solute with 6 spheres arranged as a hexagon, $f/f^* = 1.172$. This is slightly larger than the value of 1.105 predicted for an oblate ellipsoid with $\varepsilon = 3$ which is the ratio of longest to shortest dimension of the hexagon. The multisubunit hexagon is expected to have a larger friction factor than the ellipsoid with the same volume because it has more surface area exposed to solvent. The ratio f/f^* for a 6 unit structure formed from two layers with 3 spheres in each layer is predicted to be 1.048. The smaller value for this structure when compared to the hexagon is expected because this two layer structure is more symmetric than the hexagon.

3.2. Combination of Viscosity and Sedimentation-Diffusion Data

As noted in the discussion following Eq. (7), one cannot determine both an effective solute size as well as the shape or configuration of the solute by measuring only intrinsic viscosity. Similarly, one cannot determine size and shape by measuring only sedimentation or diffusion coefficients. But if one assumes that the characteristics of the solute are the same under both types of measurements, one can determine both size and shape by combining results from viscosity and sedimentation or diffusion measurements. This approach still requires one to make some assumptions about an appropriate model structure. There are several approaches that have been used to do this if one assumes the solutes are unsolvated. This discussion will first focus on oblate ellipsoids of revolution because these model structures have been proposed by a number of researchers investigating the characteristics of heavy oils and asphaltenes. The combination of viscosity and sedimentation-diffusion results as applied to multisubunit model structures will then be discussed.

If the solute under consideration is spherical and unsolvated, one expects the shape factor in Eq. (7) to be *2.5* and the effective radius from viscosity, a_v to be the same as the effective radius from sedimentation or diffusion, a_d. For ellipsoidal shaped solutes, a_v is the radius of a sphere with the same volume as the ellipsoid which, in terms of friction factors is $f_o/6\pi\eta_o$. One can express the measured friction factor, f, as the product of f_o and the ratio f/f_o. Expressing a_v in terms of these friction factors gives

$$a_v = \frac{f}{f/f_o\, 6\pi\eta_o} \tag{26}$$

Replacing a_v in Eq. (7) with the expression in Eq. (26) and rearranging yields the following expression for the shape factor, υ:

$$\nu = [\eta]_c \frac{M}{N_A} \frac{3}{4\pi} \left(\frac{f/f_o\, 6\pi\eta_o}{f} \right)^3 \tag{27}$$

If one measures $[\eta]_c$ from viscosity measurements, f from either sedimentation or diffusion measurements and the solute molecular weight, Eq.(27) is, in essence an equation with only one unknown, the axial ratio of the ellipsoid. One can use the tabulated values presented by Scheraga[9] (shown in Figure 1) to relate υ to ε. It is assumed in this analysis that the particles are unsolvated so that $f/f_o = f/f^*$. Therefore, Eq. (25) can be used to relate f/f_o to ε. This approach was used by Reerink[7] to relate information from viscosity and sedimentation measurements with asphaltenes.

An alternative approach was used by Sakai *et al.*[21] in their investigations of petroleum pitch fractions. In this approach, the two radii, a_v and a_d are defined using Eqs (7) and Eq. (22) and one can determine values for each by measuring the intrinsic viscosity, the solute molecular weight and the friction factor from either a sedimentation or a diffusion measurement. Note that a_v is defined by using *2.5* for the shape factor in Eq. (7). If the solute is spherical, these two radii will be equal. However, when the solute is asymmetrical, $a_v \neq a_d$ and their ratio can be expressed as

$$\frac{a_v}{a_d} = \left(\frac{\nu}{2.5} \right)^{1/3} \frac{f^*}{f} \tag{28}$$

For an oblate ellipsoid, one can predict the right hand side of Eq. (28) for a given value of the axial ratio by using the tabulated values of υ[9] and Eq. (25) for f/f^*. One can then determine the axial ratio that best represents the solute of interest by comparing the measured value of a_v/a_d to that predicted using Eq. (28). Unfortunately, calculations show that this ratio is not particularly sensitive to ε because the dependence of $(\upsilon/2.5)^{1/3}$ on ε is very similar to the dependence of f/f^* on ε. This insensitivity of a_v/a_d to ε is illustrated in Figure 1. It should be noted that the results in Figure 1 show that the ratio a_v/a_d is predicted to be close to, but always greater than unity for oblate ellipsoids.

The predictions of Garcia de la Torre and Bloomfield[10] and Nortz *et al.*[11] for multisubunit model structures can also be cast in the form of a_v/a_d. For multisubunit complexes assembled from identical spheres, the ratio a_v/a_d is predicted to be less than unity although again the variation of a_v/a_d with the arrangement of the spheres was not significant. For the structures examined, which contained from 2 to 24 spheres, the ratio a_v/a_d ranged from 0.974 to 0.99.

3.3. Experimental Measurement of Sedimentation Coefficients

Because of the relatively small solute sizes of asphaltenes and heavy oils, sedimentation rates are typically measured in an ultracentrifuge where accelerations of 10^4–10^5 times the gravitational acceleration are possible.[5] Sedimentation velocities are measured using an

optical system that enables one to use methods such as schlieren refractometry, interferometry or spectrophotometry to track the distribution of material along the sedimentation path. The number of reports where ultracentrifugation has been used to measure friction factors of asphaltenes has been very limited and these studies were performed at least 20 years ago. Therefore, further details of these experimental measurements will not be discussed.

3.4. Experimental Measurement of Diffusion Coefficients

A more common method of determining friction factors of asphaltenes and heavy oils involves the measurement of rates of diffusion. There are two different experimental approaches that have been reported and both will be discussed here.

The first method involves the use of a porous film that provides a well-defined geometry for establishment of a concentration gradient. In the study by Sakai *et al.*,[21] a porous glass diaphragm with average pore size of 5 μm was used. In the study by Kyriacou *et al.*,[35] porous polyester membranes with pore sizes of 0.07–0.08 μm were used. Diffusion of asphaltenes through porous membranes have also been investigated by others;[36–40] however, the objective of these studies was not to relate the measured diffusivities to macroscopic characteristics of the asphaltenes.

In this method, a porous film is placed in a cell and separates two chambers. Typically, one chamber initially contains solvent while the opposite chamber contains asphaltene or heavy oil solution of known concentration. The concentration of solute in the downstream (low concentration) chamber is monitored as a function of time, usually by measuring ultraviolet absorbance. The change in concentration with time is then related to the rate of diffusion by writing an appropriate mass balance for the diffusion/sampling process on the chamber. In order to relate the measured diffusion rate to the solute diffusivity, it is necessary to know the total area for diffusion as well as the effective path length (thickness) of the film. These can be determined by measuring the rate of diffusion of a solute of known diffusivity[21] or by measuring the hydraulic permeability of the film.[35]

In the experiments performed by Kyriacou *et al.*,[35] the measured diffusion coefficients were corrected for hindrance because the size of the pores in the polyester membranes were not significantly larger than the size of the diffusing solutes. The Renkin equation was used to determine the bulk phase diffusivity (which is related to the friction factor by Eq. (21)) from the measured diffusion coefficients.[41] This correction is not necessary when the porous film has pores ~ 20 times larger than the solute.

The second method used to determine asphaltene diffusion coefficients takes advantage of the band broadening that occurs as a solute peak flows through a capillary under laminar flow conditions.[11,42] In this experiment, solvent flow is established in a long, thin capillary tube and a solute slug is introduced. As the slug flows with the liquid, it disperses because of convective effects caused by the flow and by diffusion brought about by the concentration gradient between the sample slug and the surrounding solvent. Using the analysis originally presented by Taylor,[43] one can show that, with appropriate assumptions, the concentration profile downstream is predicted to be a normal distribution with variance related to the solute diffusivity:

$$variance = \frac{R^2 L}{24\, Du} \tag{29}$$

where R is the radius of the capillary, L is its length and u is the average linear velocity of fluid through the capillary. Eq. (29) shows that one can easily determine the solute diffusivity by monitoring the concentration profile at position L downstream from the injection point. The experimental apparatus needed for these measurements can be assembled from HPLC equipment with a long empty capillary replacing the column.

It is important to note that, unless one knows something about the nature of the size distribution for a polydisperse mixture, it is essentially impossible to 'correct' measured diffusivities for sample polydispersity. If one measures a diffusion coefficient for a polydisperse sample using one of the above techniques, the value that is obtained will be biased towards the smaller molecular weight species in the solution, i.e., the measured diffusivity will be larger than is representative of the average sized species in the sample. Therefore, in order to collect diffusion data which is representative of the range of molecular sizes in a particular crude or resid sample, it is important to carry out some sort of size fractionation prior to the diffusion measurement.

3.5. Experimental Results

3.5.1. Sedimentation. Studies that have used ultracentrifugation as a tool to study characteristics of asphaltenes and heavy oils were generally conducted several decades ago and can be categorized into two groups. In one group, ultracentrifugation was used as a separation tool to fractionate an oil or aphaltene sample into fractions with varying density. The characteristics of each fraction were then examined using a variety of analytical tools. In the second group, sedimentation rates were measured and interpreted in terms of molecular size or configuration using the principles presented in this chapter and these studies fit more closely with the objectives of this chapter.

In an early study by Ray *et al.*,[44] samples from three different crude oils were separated into four different fractions, the most dense having asphaltene character. Sedimentation rates of the heaviest fraction dispersed in heptane or petroleum ether were measured. Analysis of these rates indicated that the size of the constituents of this fraction were approximately the same for material collected from each crude oil with size in the range 30–40 Å. The authors proposed that the asphaltenes are micellar in nature when dispersed in the lighter maltene fractions.

In a later study by Weeks and McBride[45] ten different crude oils were separated using ultracentrifugation and three different fractions were collected from each crude—a top, lightly colored material, a bottom, dark precipitate fraction and a middle fraction between these two. The precipitate fraction was then examined for heteroatom and metals content as well as asphaltene content and paraffin content. The ease of processability of each crude was then compared to the chemical nature of the precipitate formed upon ultracentrifugation. It was observed that the most refractory crudes yielded the largest fraction of precipitate and that the precipitates from these materials contained the highest levels of heteroatoms and metals, factors that are generally recognized today as being major players in the processability of a particular crude.

The final study that can be classified within this first group was performed by Lorenz *et al.*[20] In this study, ultracentrifugation was used to collect several fractions that were then examined by measuring solution viscosity. The results from this study were discussed earlier in this chapter in the discussion of viscosity results.

In another early study, sedimentation rates of three different solubility fractions from an asphaltene sample were measured and interpreted in terms of the molecular weight of each fraction using a rigid ellipsoid model for the asphaltenes.[46] The intrinsic viscosity of

each fraction was also measured. In addition, diffusion coefficients were measured using an electrophoresis-diffusion apparatus, a system which yields fairly uncertain diffusivities even if the solute samples are monodisperse, which they were not.

Examination of Eq. (27) as applied to oblate ellipsoidal particles reveals four unknowns—the axial ratio of the ellipsoid, which is embedded in the shape factor υ and the ratio f/f_o, the intrinsic viscosity, the solute molecular weight and the friction factor, f. In this study, three of these unknowns were eliminated because three measurements were made, leaving one unknown, the axial ratio of the ellipsoid. This was done by combining Eq. (20) and (21) to eliminate f, recognizing that $M = N_A V \rho_p$, which enables one to solve the resulting equation for M, knowing s and D. By combining these results with those from the intrinsic viscosity measurements, it was determined that the asphaltenes could be represented by spheres with a radius of 34 Å. However, there is considerable uncertainty in these results because of the uncertainty in the diffusivity values used. Results did not change when solvent was changed from benzene to carbon tetrachloride, which is not unexpected because both solvents are non-polar.

Another study that involved the combination of information from viscosity and sedimentation has already been discussed with the viscosity results. Reerink[7] measured sedimentation and intrinsic viscosity of asphaltene fractions in a number of different organic solvents. The results were interpreted by considering the asphaltenes to be modeled as oblate ellipsoids using an equation analogous to Eq. (27). By assuming the asphaltenes are unsolvated, the axial ratio of the ellipsoid that best represented each fraction was determined and was found to range from 5–9. These values were in reasonable agreement with dimensions obtained from electron micrographs. Such agreement is not necessarily expected because the sedimentation and viscosity measurements are made in solution but the electron micrographs provide a picture of the material deposited on a surface.

3.5.2. Diffusion. There have been a large number of experimental investigations that have involved the measurement of diffusion of asphaltenes or heavy oils in porous media, either porous membranes or porous catalysts.[36–40] The objective of these studies was generally to examine the effect of solute and pore size on effective diffusivities and results were typically not examined in terms of the macroscopic structure of the diffusing solute. Because the discussion in this chapter is focused on the interpretation of experimental measurements such as diffusion in terms of the effective size and shape of asphaltenes, results from these studies, while providing worthwhile information, will not be discussed here.

Most of the studies involving the interpretation of measured diffusion rates in terms of size and configuration of the diffusing solutes have already been mentioned in this chapter in the discussion of viscosity results. The one exception to this is a study by Jost *et al.* [42] who measured the diffusivity of crude oil fractions (obtained using preparative gpc) using the Taylor dispersion technique. These measurements were performed in a 9:1 (vol/vol) THF/methanol mixture at room temperature. The molecular weight of each fraction was also measured using vapor pressure osmometry with methylene chloride solvent. A log-log plot of D versus M yielded a good correlation given by the following expression:

$$D = 2.67 \times 10^{-4} M^{-0.54} \qquad cm^2 / \text{sec} \tag{30}$$

The authors argued that Eq. (30) could be used to determine a "diffusion-averaged" molecular weight from a diffusion measurement. In an earlier publication, the authors showed

that this "diffusion-averaged" molecular weight lies between the number and weight averaged molecular weight for a polydisperse sample and that the determination of two different molecular weight values should enable one to determine the polydispersity (M_w/M_n) of a particular sample. The validity of this approach was determined by predicting the diffusion averaged molecular weight by measuring M_n with VPO and the polydispersity using gpc and comparing the predicted value to that measured with a polydisperse resid sample. The two values agreed to within 10%.

An issue that the authors did not address was the recognition that the exponent in relationships like Eq. (30) provide an indication of the configuration of the diffusing solutes just as the exponent in the Staudinger-Houwink equation (Eq. (17)) involving intrinsic viscosity provides some information about solute structure. For a rigid, impermeable sphere, one expects $D \propto M^{-1/3}$. For a random coil polymer, one expects an exponent of -0.5 between D and M. For an oblate ellipsoid with a large axial ratio, the Stokes radius, a_d is proportional to the length of the major axis.[2] If larger ellipsoids are formed by extending the major axis while keeping the minor axis constant (i.e., keeping the thickness of the disc constant), one also expects $D \propto M^{-0.5}$. However, if the major axis remains constant while the thickness of the disc increases with increasing M, one expects D to be independent of molecular weight. The -0.5 power dependence observed in this study is probably an indication that these crudes are consistent with the disc like structure that has been postulated from other types of observations and not due to a random coil structure which is not intuitively consistent with previously accepted pictures of these materials.

In a study undertaken by Sakai *et al.*,[21] the diffusion coefficients of petroleum pitch fractions were measured using a porous glass diaphragm. The measurements were performed at 25° C using chloroform as solvent. An examination of the power law dependence of D on M shows that an exponent of -0.62 provides a good fit to the data. This is in reasonable agreement with the -0.5 dependence that is predicted for disk-like solutes.

As noted earlier, the intrinsic viscosity of these materials was also measured[8] and results from both measurements were combined to determine the axial ratio of oblate ellipsoids that fit the data. This was done by determining a_v from the viscosity results and a_d from the diffusion results. The ratio a_v/a_d ranged from 0.88–1.02 and the authors attempted to use Eq. (28) to relate this ratio to the axial ratio of the ellipsoids. However, in their analysis, it was assumed that the shape factor $\upsilon = 2.5$, arguing that this does not introduce significant error when $\varepsilon \leq 3$. This assumption can introduce an 11% error in the predicted value of a_v/a_d because $(\upsilon/2.5)^{1/3} = 1.11$ when $\varepsilon = 3$. With the given assumption, the axial ratio of ellipsoids that represent the data was found to range from 1–3. However, if one uses Eq. (28) as given here, without making any assumptions about υ, essentially any axial ratio can explain the data for $a_v/a_d > 1$ whereas the results with $a_v/a_d < 1$ cannot be explained with any oblate ellipsoid model.

The final studies to be presented were performed in the author's laboratory and have also already been discussed along with the intrinsic viscosity results. In the first study, the diffusion coefficients from fractions from Cold Lake vacuum bottoms were measured using porous polyester membranes.[35] When the ratio a_v/a_d was calculated by combining the intrinsic viscosity results (using the VPO molecular weight) with the diffusion results, the ratio was found to range from 0.2–0.4 in THF at 20°C while the range in 1-methylnaphthalene at 50°C was found to be 0.4–0.77. These differences could be due to a different macrostructure for this material at the two conditions. Because the determination of a_v requires a molecular weight value, it is also possible that the VPO molecular weight better represents the material under one set of experimental conditions when compared to the other. But, if this is the case, it is impossible to identify which condition is better repre-

sented by the VPO molecular weight value. A comparison of these values of a_v/a_d to those predicted for oblate ellipsoidal solutes (Figure 1) shows that these results cannot be explained using an oblate ellipsoid model.

A log-log plot of D versus M shows an exponent of -0.74 for the data in THF and an exponent of -1.0 for the data in 1-methylnaphthalene. These exponents are not in agreement with the exponent of -0.5 that is predicted for a disk shaped solute. For a rod-shaped solute which increases in length at constant cross sectional area as molecular weight increases, one predicts an exponent of -1. This model is not consistent with the generally accepted models of these materials but it is consistent with the model found to provide reasonable agreement with the viscosity results with this material. As noted earlier, there was believed to be considerable uncertainty in the VPO molecular weight values determined in this study because of the presence of a low molecular stabilizer that was used with the solvent during gpc fractionation and this may be responsible for the anomalous results obtained when the intrinsic viscosity and diffusion values were interpreted using the VPO molecular weight values.

In a later study, the diffusion coefficients of fractions from Athabasa tar sand bitumen vacuum bottoms as well as fractions from a blend of vacuum resids from Western Canadian crudes were measured using the Taylor dispersion technique.[11] These measurements were performed in 1-methylnaphthalene solvent at 50° C and 70° C. The small differences in diffusivity at each temperature can be attributed solely to the difference in solvent viscosity at each temperature, because the effective size, a_d, was found to be independent of temperature. Combining these results with the intrinsic viscosity results with these same fractions yielded a_v/a_d ratios that ranged from 0.55–0.81, values that again cannot be explained using an oblate ellipsoid solute model.

A log-log plot of D versus M yielded agreement with a power law relationship with an exponent of -0.5, a value that is consistent with a disk-like shape for these materials. Recall that the dependence of $[\eta]_c$ on M was also consistent with this structure. It is puzzling that intrinsic viscosity and diffusivity measurements are independently in agreement with a planar conformation for these materials but the same conclusion does not arise when the measurements are combined and the ratio a_v/a_d is examined.

The intrinsic viscosity and diffusion results collected from both of these studies were also interpreted in terms of the multisubunit models that have been previously presented. These were chosen because the idea that larger asphaltene or resid entities can be represented by collections of attached smaller entities appeared to be consistent with the micellar character that has been proposed for these materials. In addition, the ratio a_v/a_d for these model structures is predicted to be less than unity, which is consistent with experimental observations. In determining the structures that best describe the experimental observations, it was assumed that the spherical units comprising each structure were the same, i.e., the larger entities were formed by adding additional spheres rather than increasing the size of the spherical subunits.

In the first study,[35] the size of the smallest 'base' unit was assumed to be equal to the size of the smallest fraction examined. Therefore, the size of the spherical subunits making up the larger fractions was assumed to be a_d (= a_v) from the smallest fraction. This value was 4.5 Å for the data in THF and 4.7 Å for the data in 1-methylnaphthalene. Using these values with the experimental molecular weight values determined for the larger fractions, the arrangement that provided the best fit between predicted and observed intrinsic viscosity values was then determined. The structures that were found to be in good agreement with the viscosity results were generally planar in nature, containing 2–8 spherical units. The diffusion coefficients predicted for these model structures were then compared

to the measured diffusivity values and it was found that the measured diffusivity values were 2–5 times smaller than those predicted for the model structures that provided good agreement with the viscosity values. This discrepancy may be due to experimental uncertainty with the molecular weight values or to the fact that the structure of the material changes with the experimental conditions of each measurement. This may be due to the fact that the shear experienced during the viscosity measurements is sufficient to disassociate some of the larger entities that are present during the diffusion measurements.

In the second study,[11] results were also interpreted using multisubunit structures but the approach was somewhat different than that used in the first study. Here, it was assumed that the molecular weight of the spherical base unit was 100. Therefore, structures comprised of 6–24 subunits were needed to obtain models with molecular weights spanning the measured molecular weights of the investigated fractions. In order to determine the radius of the spherical base unit, a series of 4–7 structures covering a range of arrangements was considered. The radius of the base unit that provided the best agreement with the predicted diffusivity values and the power law correlation that provided a good fit to the experimental results was determined (i.e., the -0.5 power dependence of D on M). A number of different series were examined and the series that provided the best agreement between prediction and observation was found to be a series of multilayer structures containing two or three layers with 3–8 spheres of radius 5.1 Å. However, a comparison of the predictions for $[\eta]_c$ to the experimental results for intrinsic viscosity again showed some discrepancy, with the discrepancy again indicating that the size determined by diffusion was smaller than the size determined by viscosity. This discrepancy was also illustrated by determining the size of the base unit needed to describe the intrinsic viscosity results, using the same series of structures that was found to represent the diffusion results. A base unit with radius of 3.5 Å was needed to provide a good fit to the viscosity results. This discrepancy again indicates that the effective size appears to be larger during a diffusion measurement than during a viscosity measurement. If one attributes this difference in the base unit size to a solvent layer on each spherical unit, a layer of thickness 1.6 Å is needed to explain the observations. This value is reasonably consistent with the solvation layer of 2–4 Å that was found to explain the viscosity results of Storm *et al.*[6] with Ratawi asphaltenes. It should be noted, however, when making this comparison, that the value of 2–4 Å was reported by Storm *et al.* for data at 300° C and was reflective of a layer of solvent on a spherical solute, not a collection of spheres as was considered in this study.

The diffusivity versus molecular weight values reported from each of these cited studies were compiled and a log-log plot of the results are shown in Figure 4. A line with $D \propto M^{-0.5}$ is also shown which is the relationship predicted for a disk-like solute. A comparison of the results shows that, in general, the results are in reasonable agreement with the prediction for a disk-like solute. The diffusivity values span over an order of magnitude but it should be noted that solute diffusivity is dependent on solute size as well as temperature and solvent viscosity. To separate temperature and viscosity effects from solute size, the effective solute radius, a_d, was determined by combining Eqs. (21) and (22) and solving for a_d using the measured diffusivity values.

A log-log plot of a_d versus M is shown in Figure 5. A comparison of the results plotted in this manner shows that much of the differences in diffusivity seen in Figure 4 can be attributed to different temperature and solvent conditions used for the measurements. The exception to this is the data reported by Kyriacou *et al.*[22] for the Cold Lake bitumen fractions in THF at 20°C as well as the higher molecular weight fractions for this same material in 1-methylnaphthalene at 50°C. The molecular weight values reported for these materials are likely to be anomalously low due to the presence of BHT in the samples and

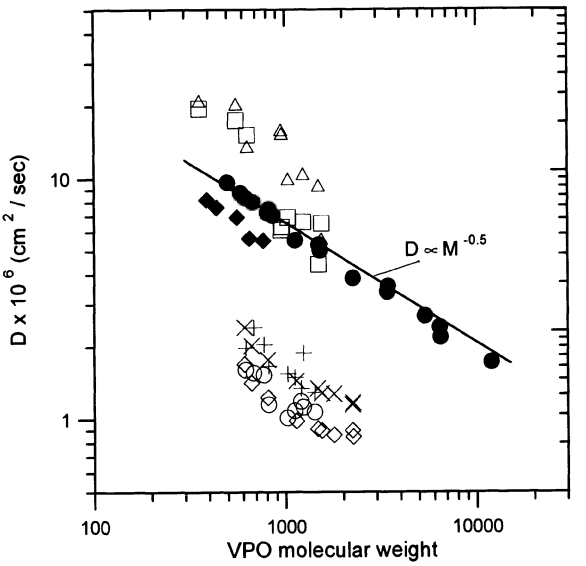

Figure 4. Experimental values of diffusivity as a function of VPO molecular weight. △ Cold Lake bitumen fractions in THF at 20°C,[22] □ Cold Lake bitumen fractions in 1-methylnaphthalene at 50°C,[22] ▲ Vacuum oil residue fractions in 9:1 (vol/vol) THF/methanol,[42] O Western Canada crude vacuum resid blend fractions in 1-methylnaphthalene at 50oC,[11] + Western Canada crude vacuum resid blend fractions in 1-methylnaphthalene at 70°C,[11] ◊ Athabasca tar sand bitumen vacuum bottom fraction in 1-methylnaphthalene at 50°C,[11] × Athabasca tar sand bitumen vacuum bottom fraction in 1-methylnaphthalene at 70°C,[11] ♦ Petroleum pitch fractions in chloroform at 25°C,[8] line showing $D \propto M^{-0.5}$.

this could provide a partial explanation for the discrepancy between these results and the others. However, the reported molecular weight values would need to be 50–100% larger in order to explain the observed differences in a_d values. It is unlikely that the molecular weight values were in err by this much. The largest discrepancy between results and the general trend shown by the rest of the data is seen for the data collected in THF at 20° C. One might postulate that these environmental conditions lead to association or aggregation yielding larger solutes. However, these conditions are very similar to those used by Jost *et al.*[42] whose results seem to provide a lower bound on the compiled results. In addition, the intrinsic viscosity results with these same materials in THF were in general agreement with results collected in other studies, as shown in Figure 3. Another possible explanation is that the determination of diffusivity values by measuring solute flux through polyester membranes yields anomalously low diffusivities, possibly due to solute adsorption onto the membrane surface. Although effective pore sizes did not appear to change appreciably upon contact with the bitumen material, it is possible that adsorption could be sufficient to affect the observed diffusivities but still not cause a detectable change in pore size.

4. SUMMARY

In this chapter, the utility of using intrinsic viscosity, diffusion and sedimentation velocity measurements to determine macroscopic characteristics of heavy oils and asphal-

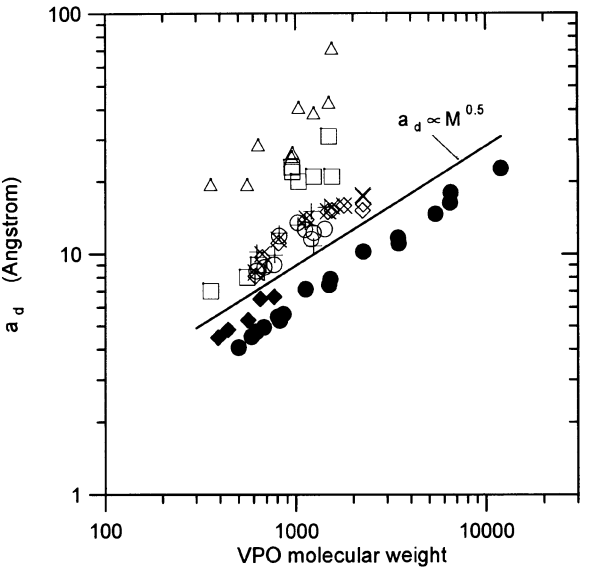

Figure 5. Effective radius, a_d, determined from diffusion as a function of VPO molecular weight. △ Cold Lake bitumen fractions in THF at 20°C,[22] □ Cold Lake bitumen fractions in 1-methylnaphthalene at 50°C,[22] ▲ Vacuum oil residue fractions in 9:1 (vol/vol) THF/methanol,[42] O Western Canada crude vacuum resid blend fractions in 1-methylnaphthalene at 50°C,[11] + Western Canada crude vacuum resid blend fractions in 1-methylnaphthalene at 70°C,[11] ◊ Athabasca tar sand bitumen vacuum bottom fraction in 1-methylnaphthalene at 50°C,[11] × Athabasca tar sand bitumen vacuum bottom fraction in 1-methylnaphthalene at 70°C,[11] ♦ Petroleum pitch fractions in chloroform at 25°C,[8] line showing $a_d \propto M^{0.5}$.

tenes has been demonstrated. Results from measurements with a variety of source materials from a number of different labs has yielded some consistent as well as some inconsistent results. Solution viscosity measurements collected from solutions with a relatively large asphaltene concentration indicate that the asphaltenes are generally spherical in shape and followed behavior predicted from a number of theories for concentrated solutions.[6,27,29,30,32,33] In contrast, results from intrinsic viscosity measurements with quite dilute solutions indicate that asphaltenes and heavy oils can be modeled as planar, disk-like structures, as shown by the 0.5 power dependence between $[\eta]_c$ and M shown in Figure 3.[7,8,11,22,25] This inconsistency between the low concentration and high concentration results may be due to different extents of association or aggregation, although both sets of data were presumably collected at concentrations above those reported for the CMC of asphaltenes.[26] With one exception,[25] the low concentration viscosity measurements were performed using fractionated materials that are reasonably monodisperse whereas the high concentration measurements were performed with a polydisperse mixture. If the high concentration solutions were polydisperse both with respect to size as well as shape, it is possible that the shape effects might be clouded by the range of solute sizes present in the mixtures.

Diffusion measurements with some of the same material used for the low concentration viscosity measurements, again collected at low concentrations yielded results that are also consistent with results expected for planar solutes, as shown by the -0.5 power dependence between D and M shown in Figure 4 and by the 0.5 power dependence between

a_d and M shown in Figure 5.[11,21,35,42] However, several attempts to model these materials as oblate ellipsoids by combining information from viscosity and diffusion measurements to determine the ratio a_v/a_d yielded results which could not be explained by an oblate ellipsoidal model.[11,21,35] One possible explanation for this inconsistency is that the materials have different characteristics (perhaps different levels of solvation or different extents of aggregation) during each type of measurement.

There have been no reported studies in which the same material has been investigated under a wide range of conditions—fractionated as well as unfractionated samples, low concentration as well as high concentration, in organic solvents as well as in deasphalted oil and where diffusion, viscosity and molecular weight have been measured under all of these conditions. A systematic, comprehensive study such as this might aid in understanding the source of the inconsistencies in the results reported here. Finally, if one wishes to use hydrodynamic property measurements to ascertain the physical characteristics of these materials under reactive conditions, it is important that these measurements be performed under higher temperatures and pressures than have generally been used for the studies reported here.

REFERENCES

1. J.C. Giddings, E. Kucera, C.P. Russel, M.N. Myers, J. Phys. Chem. 72, 4397 (1968).
2. R.E. Baltus, J.L. Anderson, Fuel 63, 530 (1984).
3. J.G. Speight, ACS Div. Pet. Chem., New York, 825 (1981).
4. J.G. Speight, D.L. Wernick, K.A. Gould, R.E. Overfield, B.M.L. Rao, D.W. Savage, Rev. Inst. Franc. Petrole. 40, 51 (1985).
5. P.C. Hiemenz, R. Rajagopalan, "Principles of Colloid and Surface Chemistry," Marcel Dekker, Inc. New York (1997).
6. D.A. Storm, E.Y. Sheu, M.M. DeTar, R.J. Barresi, Energy & Fuels, 8, 567 (1994).
7. H. Reerink, Ind. Eng. Chem. Prod. Res. Develop., 12, 82 (1973).
8. M. Sakai, T. Sogabe, H. Kitagawa, M. Inagaki, Carbon, 21, 601 (1983).
9. H.A. Scheraga, J. Chem. Phys., 23, 1526 (1955).
10. J. Garcia de la Torre, V.A. Bloomfield, Biopolymers, 17, 1605 (1978).
11. R.L. Nortz, R.E. Baltus, P. Rahimi, I&EC Research, 29, 1968 (1990).
12. R. Roscoe, Br. J. Appl. Phys. 3, 267 (1952).
13. I.M. Krieger, Adv. Colloid Interface Sci. 3, 111 (1972).
14. M. Mooney, J. Colloid Interface Sci. 6, 162 (1951).
15. R. Pal, E. Rhodes, J. Rheol. 33, 1021 (1989).
16. H. Eiler, Kolloid - Z. Z. Polym., 97, 313 (1941).
17. G.A. Campbell, G. Forgacs, Phys. Rev. A., 41, 8 (1990).
18. J.G. Kirkwood, "John Gamble Kirkwood Collected Works - Macromolecules," P.L. Auer, Ed., Gordon & Breach, New York (1967).
19. C. Mack, J. Phys. Chem., 36, 2901 (1932).
20. P.B. Lorenz, R.J. Bolen, H.J. Dunning, I.A. Eldib, J. Colloid Sci., 16, 493 (1961).
21. M. Sakai, K. Sasaki, M. Inagaki, Carbon, 21, 593 (1983).
22. K.C. Kyriacou, R.E. Baltus, P. Rahimi, Fuel, 67, 109 (1988).
23. P. Thiyagarajan, J.E. Hunt, R.E. Winans, K.B. Anderson, J.T. Miller, Energy & Fuels, 9, 829 (1995).
24. J.P. Dickie, T.F. Yen, Anal. Chem., 39, 1847 (1967).
25. M.M.E. Al-Jarrah, A.H. Al-Dujaili, Fuel Sci. & Tech. Int'l, 7, 69 (1989).
26. S.I. Andersen, J.G. Speight, Fuel, 72, 1343 (1993).
27. D. A. Storm, R.J. Barresi, S.J. DeCanio, Fuel, 70, 779 (1991).
28. E.Y. Sheu, personal communication.
29. E.Y. Sheu, M.M. DeTar, D.A. Storm, Fuel, 70, 1151 (1991).
30. D.A. Storm, E.Y. Sheu, Fuel, 72, 233 (1993).
31. M.J. Grimson, G.C. Barker, Europhys. Lett., 3, 511 (1987).
32. E.Y. Sheu, M.B. Shields, D.A. Storm, Fuel, 73, 1766 (1994).

33. D.A. Storm, R.J. Barresi, E.Y. Sheu, Energy & Fuels, 9, 168 (1995).
34. P.F. Perrin, J. de Phys. Radium, 7, 1 (1936).
35. K.C. Kyriacou, V.V. Sivaramakrishna, R.E. Baltus, P. Rahimi, Fuel, 67, 15 (1988).
36. R.E. Baltus, J.L. Anderson, Chem. Eng. Sci., 38, 1959 (1983).
37. R.L. Mieville, D.M. Trauth, K.K. Robinson, ACS Div. Pet. Chem., 34, 635 (1989).
38. R.C. Sane, T.T. Tsotsis, I.A. Webster, ACS Div. Fuel Chem. 33, 237 (1988).
39. R.C. Sane, T.T. Tsotsis, I.A. Webster, V.S. Ravi-Kumar, Chem. Eng. Sci., 47, 2683 (1992).
40. R.C. Sane, T.T. Tsotsis, I.A. Webster, V.S. Ravi-Kumar, in "Asphaltenes and Asphalts. 1. Developments in Petroleum Science", T.F. Yen, G.V. Chilingar (Ed.), 40, 365 (1994).
41. J.L. Anderson, J.A. Quinn, Biophys. J., 14, 130 (1974).
42. K. Jost, W. Steuer, I. Halász, Chromatographia, 20, 700 (1985).
43. G. Taylor, Proc. R. Soc. London, Ser. A, A219, 186 (1953).
44. B. R. Ray, P.A. Witherspoon, R.E. Grim, J. Phys. Chem., 61, 1296 (1957).
45. R.W. Weeks, W.L. McBride, ACS Div. Pet. Chem., 990 (1979).
46. M. Wales, M. van der Waarden, ACS Div. Pet. Chem., B-21 (1964).

Chapter XI

ASPHALTENE AND RESIN STABILIZED CRUDE OIL EMULSIONS

Experimental Characterization and Destabilization

Johan Sjöblom,[1] Øystein Sæther,[1] Øivind Midttun,[1] Marit-Helen Ese,[1] Olav Urdahl,[2] and Harald Førdedal

[1]Department of Chemistry
University of Bergen
Allegt. 41, N-5007 Bergen, Norway
[2]Statoil Research Centre
Field Development Technology
N-7005 Trondheim, Norway

1. INTRODUCTION

Asphaltenes can have crucial impact on several stages of production of crude oils. First of all, asphaltenes can precipitate in the well or in the formation and cause severe formation damage, and in the worst case the well might be shut down. Second, asphaltenes cause problems if they deposit on the steel walls in the production line. They can also be transported along the production line and accumulate in separators or in other fluid processing units.

In this chapter we will focus on the role of the asphaltenes in stabilizing formation water in crude oils, and thus preventing coalescence of the water droplets from taking place. In the offshore production of crude oil the problem of crude oil emulsions is encountered at an early stage. In the planning and construction of the production unit, platform or production ship, enough space must be reserved for emulsion destabilization equipment, such as separators, water treaters and coalescers. With reliable information about the crude oil and its tendency to form emulsions, this space could be reserved for other equipment with other purposes, or the production unit could be made smaller.

The hydrocarbon reserves in the North Sea include several marginal fields, which are either small or deep water fields. Feasible economic exploitation of these reserves will require a shift towards lower cost options in subsea production, or the use of minimum-

processing platforms tied to centralized or land-based processing facilities. This will require the transportation of unprocessed or minimum processed fluids over long distances. Multiphase flow in pipelines has taken place on the Norwegian Continental Shelf for several years. Connection of wellhead platforms and subsea production plants to processing platforms by means of multiphase transportation is also available technology. However, these solutions have hitherto been restricted to transportation of unprocessed well stream over short distances. In the case of a multiphase transport from platforms offshore to land-based process plants there will be possibilities for formation of water-in-crude oil emulsions due to turbulence in the flow, joints and valves in the pipeline, etc.

These emulsions are of interest in the offshore production of crude oils from two different points of view. As the production time of the oil wells increases, there will be an increased coproduction of oil and water in the form of an emulsion. Secondly, as mentioned above, in establishing multiphase transport systems, large quantities of the water will be in an emulsified form during transportation. This colloidal state can, due to extreme stability and high viscosity, create substantial transport problems. There are obvious needs for an increased understanding of the mechanisms underlying the formation of stable emulsions and for predictions of the problems created by these.

At an ongoing Statoil field development in the North Sea it is recommended that an electrical coalescer unit is not installed. Based on laboratory experiments of the emulsion stability of water and oil from the fields, the quality of the oil was satisfactory and no electrical coalescer was necessary to improve the quality of the oil. This is a direct saving of \$2.5 million in direct coalescer investments, and a total saving in the order of \$7 million due to savings in space and weight. If a "correct" fluid/emulsion characterization is possible, there are better possibilities of designing more compact coalescers and compact separation processes and separators. At another Statoil field development in the North Sea it was estimated that a weight reduction of 20–40% of the separation equipment gave a saving in the weight of the order of 600 ton and in the order order of \$20–30 million in equipment investments. The crucial step in field development evaluations will be to predict emulsion stability from measured analytical and physico-chemical properties of crude oil samples and/or prepared synthetic crude oil emulsions.

Crude oil emulsions have been the subject of intense debate and research during the last eighty years.[1-10] There has been a lack of fundamental understanding of the mechanisms governing the stability of oil-continuous emulsions. The reason for this is that the most important stabilizing mechanisms are different from those of water-continuous emulsions. For crude oil emulsions the importance of a rigid and protective film surrounding the water droplets is usually pointed out.[11-14] The detailed properties of this film together with a fundamental knowledge about the chemistry of the interfacially active components in the crude oil are far from completely understood. However, empirical studies have shown the importance of components like asphaltenes and resins for the stabilization.[15-20] They are believed to have surface active properties and hence to accumulate at the interface of water and oil. Formation of an interfacial film possessing certain surface-rheological properties, in combination with a particle and/or steric stabilization, is obviously of fundamental importance for the stability of crude oil emulsions.

In order to understand the properties of the interfacially active components in true crude oil systems it is of great chemical interest to build up model systems with chemical properties equal or similar to that of the original crude oil.

Crude oils are mixtures of numerous aliphatic and aromatic hydrocarbons, and oxygen, nitrogen and sulphur compounds. Some of these compounds are surface-active in nature, and can adsorb to water-crude oil interfaces. Two such classes of compounds are

asphaltenes and resins. They are both polymeric in nature and have structural similarities, as observed from infrared spectroscopy. There are different definitions of asphaltenes as they are not one compound, but a solubility-class of compounds. Part of the heterocyclic molecules in a crude oil is dissolved in a molecular state and the rest is in an undissolved colloidal state. The asphaltenes are stabilized in the crude oil by the lighter resins. It is commonly known that the asphaltenes precipitate when the crude oil is treated with a light aliphatic hydrocarbon. For practical approaches in the laboratory a commonly used flocculant is n-pentane. Since the resins are soluble in n-pentane they will be removed from the asphaltene aggregate to the bulk of the crude, and hence the heavy asphaltene aggregates can flocculate and precipitate.

To stabilize an emulsified system is to control four fundamental processes, i.e. sedimentation (creaming), flocculation, coalescence and Ostwald ripening. The first process is the formation of a droplet concentration gradient within the emulsion. Flocculation is the process where interparticular distances between the droplets are strongly diminished due to a net attraction between the droplets. In this process the individual droplets maintain their identity. Coalescence means the formation of large droplets with a concomitant phase separation. Coalescence as a process involves the elimination of the thin liquid films separating the dispersed droplets in a close-packed array. Ostwald ripening is a phenomenon in polydisperse emulsions where large droplets will form at the expense of small ones.[21-23]

In order to counteract the destabilization processes above, some common stability mechanisms have been developed. Electrostatic stabilization is based on a double-layer repulsion between two adjacent droplets with equal charges. Steric stabilization is due to the overlap of polymeric interfaces on the emulsion droplets. Particle stabilization is due to the incorporation of solid particles in the interfacial zone of the emulsion droplets, and a distinct change in the mechanical properties of the interfacial film.[24-32] The formation of multilayer surfactant structures (lamellar lyotropic liquid crystalline phases) at the water/oil interface will also drastically increase the stability against coalescence.[33-36]

When the stability of an emulsified system is discussed there are two different approaches to be considered. The first approach deals with the overall behaviour of the system. This may include bulk viscosity, droplet size and the total composition of the system.[37-39] The second approach deals with the interfacial properties of the system.[40] The combined information from these two approaches will therefore give a total description of the emulsified system.

The properties of different crude oils from the Norwegian Continental Shelf and their ability to create stable water-in-crude oil emulsions have recently been focused on in a series of publications.[39,41-48] This paper tries to update recent findings in the field.

2. EXPERIMENTAL TECHNIQUES FOR DETERMINATION OF DROPLET SIZES AND SIZE DISTRIBUTIONS

This chapter summarizes some of the most important and frequently used methods for characterization of water-in-crude oil emulsions.

The most common way to determine the emulsion stability is to record the separated volume of water from a crude oil and water mixture. This technique gives a good measure of the separability of crude oil and water. However, often a few percent of water remains dispersed in the crude oil, and these last amounts of water can be stable in the crude oil for a very long period of time. In the oil industry, electrical coalescers are widely used to remove the last remaining dispersed water droplets.

In order to understand the emulsified state and to predict the stability of the emulsions at different stages in the processing of the crude oil, the determination of the droplet size and their distribution is crucial. In the following we view some useful techniques to do this.

2.1. Video Enhanced Microscopy

The microscope is traditionally used in the measurement of particle size and has been so for many years. It is relatively inexpensive and simple to operate, but the method is less attractive when used in the determination of size for a large number of objects, as manual measurement techniques[49] are both laborious and time consuming. Video microscopy, or video enhanced microscopy, markedly represents an improvement as computer assisted analysis offers substantially improved efficiency of measurement.

The basic apparatus of the videomicroscopic technique (Figure 1 gives a schematic view) is a videocamera connected to an ordinary compound microscope. The camera transfers the image to a computer which in turn can be used for image treatment and analysis. As an obvious consequence, the data which can be produced from VM emulsion study is based on information contained within the images. Therefore, the images must truly represent the actual sample, which in turn puts great demand on sample preparation. A useful preparative technique in this respect is the utilization of flat, rectangular microcapillaries of glass. These allow the seclusion of a pseudo bulk sample volume (governed by the inner diameter or height of the capillary), limiting contamination and sample distortion by evaporation. In such fashion an emulsion sample can remain intact for observation over a period of time. Obviously, sedimentation of droplets and the possibility for droplet/glass wall interaction must be taken into account when considering this method of sample preparation. Figure 2 shows two image segments (1/6 of the complete images) of emulsions in microslides. On the left is a freshly prepared w/crude oil emulsion wherein the droplets are still in the process of sedimenting to the lower glass wall. On the right is an example of a most readily analysable image, where the droplets can be measured automatically through application of functions built into current image analysis software (see below). The system depicted is w/model oil containing asphaltenes precipitated from a crude oil.

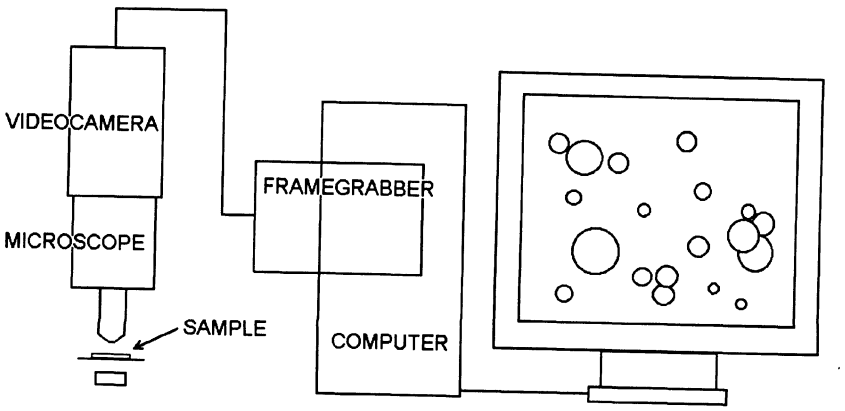

Figure 1. Schematic of typical VM setup.

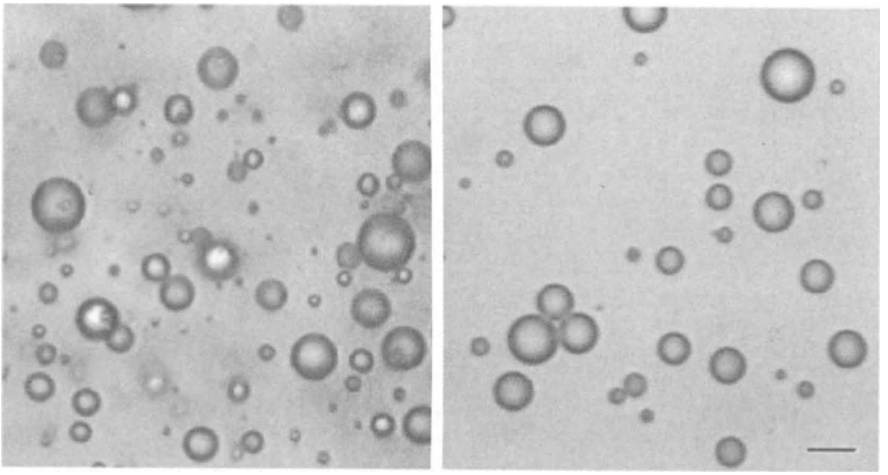

Figure 2. Image segments from two different emulsions; on the left a freshly prepared w/crude oil emulsion with a large part of the population not yet sedimented to the lower glass wall (the focal plane); on the right readily measureable water droplets in a model oil containing asphaltenes. Microslide inner diameter 100 μm. The scale on the lower right marks 10 μm.

The foremost advantage of videomicroscopy lies in the directness of the sample observation. The operator may see if droplets interact to produce flocs or if they remain as single droplets, if there are other particles present, and so on. Also, depending on the preparative method chosen, even quite opaque samples can be studied, as the sample thickness is not very high. This includes the study of crude oil emulsions. Important objections towards the technique may be a quite high time consumption, as automation of data analysis cannot be easily achieved on complex systems, leaving much of the work to the operator. Further, it is vulnerable to error in sample preparation and data acquisition as, in a statistical sense, only a rather small number of objects (droplets) is observed and measured. The role of the operator is then obvious, as the operators skill and decisions can greatly influence the data.

In the determination of droplet size, the technique can be used effectively on droplet sizes down to the 1 micron region. The optical resolution limit is, according to Miller et al.,[50] about 0.25 microns for typical microscope optics, while Shaw[51] states that oil immersion objectives may set the limit down at about 200 nm due to high numerical apertures. On the question of measurement error, Allen[52] warns that even though the optical resolution limit may be as low as 0.2 microns, the error in the visual estimate may be much higher, e.g. +13% for 1 micron droplets and +36% for 0.5 micron droplets.

The width of the drop size distribution (d.s.d.) also influences the correctness of the data. If a distribution has a long tail towards higher diameters and a moderate number of droplets are counted, the importance of each larger droplet on the cumulative volume will be significant. A miscalculation of only a few or even one droplet may result in serious misplacement of the volume/size distribution; e.g. as the radius increases by a factor of 10 the volume increases by a factor of 1000: one 20 micron diameter droplet contains the volume of a thousand 2 micron droplets.

To some extent, image analysis programs can assist the measurement and sometimes provide some degree of automation. Basically, image enhancement comprises a wide

range of image operations designed to prepare the image for analysis and measurement, e.g. noise reduction, contrast enhancement, etc. For the program to automatically measure the droplets, it must be able to distinguish the droplets from the background and from one another. Droplets are defined by a range of grey levels characteristic to them. The degree of automation is a function of image complexity, e.g. droplet flocculation. Droplet sizes in heavily flocculated systems, a situation not uncommon in the study of crude oil emulsions or asphaltene stabilized model emulsions, are by nature not easily quantified as droplets tend to hide other droplets in the vertical direction (viewing path).

To obtain a statistically reliable size distribution a rather large number of droplets must be measured.[53] A large number of droplets per image means that a moderate number of images are needed. However, if the droplet concentration is high, the analysis may be complicated by droplets overlapping, typically resulting in an underestimation of smaller droplets. For the microcapillary technique, problems resulting from high droplet concentration manifest themselves at even rather low disperse fractions, as droplets usually sediment to and accumulate along the capillary wall. The effect increases with the thickness of the viewing path (which corresponds to the inner diameter, i.d., of the capillary), as the bulk volume providing the droplets increases. For i.d.s of about 50 microns and a size distribution in the range of 1–10 microns, sample concentrations of more than 1% disperse phase may prove difficult to analyze. This can however be countered. For example, by using a non-destructive form of dilution of the original concentrated emulsion, taking into account the risk of changing the d.s.d. by changing the system chemically. Also, the use of a flow cell may be useful as the droplets distribute themselves through the entire volume of the cell[54]. The use of video enhanced microscopy in determination of polystyrene particle size has been examined. Also the water droplet size in crude oil emulsions has been tested and it was found that the technique performed well compared to laser diffraction and Coulter counting. Mason et al.[55] found the d.s.d. photomicroscopically in emulsions destabilized by addition of a demulsifier. The d.s.d. was studied as a function of several parameters, e.g. emulsion age, demulsifier concentration and mixing after addition of demulsifiers. VM has also proven valuable in the study of kinetic properties of emulsions. The flocculation and coalescence processes in dilute o/w emulsions were investigated through determination of the d.s.d. as a function of time and by direct study of droplet-droplet interaction.[56,57] The methods described may provide a tool for improving the understanding of these fundamental processes of destabilization.

Two examples show the d.s.d. as function of the oil phase for w/o emulsions. The microscope used is a Nikon Optiphot 2 with 20X and 40X DIC optics connected to a Hitachi KP-160 CCD camera. The images are grabbed by an Integral Technologies Flashpoint PCI card in a Pentium 166 MHz PC. Media Cybernetics Image-Pro Plus for Windows 95 is used for image enhancement and measurement. Figure 3 shows the normalized d.s.d. of a water-in-crude oil emulsion and of a model emulsion with 10% of the asphaltene content of the crude (about 0.07 g/ml). The model oil is 30/70 v/v toluene/decane. Both emulsions 40% v/v 3.5% NaCl solution in oil were mixed at 50°C, since the importance of wax particles increases at lower temperatures. The number of droplets decreases from the crude oil emulsion to the model emulsion by a factor of 18, while the dispersed area is about 6.5 times lower. The effect of combining a hydrophilic resin fraction and asphaltenes in the oil phase is shown in Figure 4. Both emulsions are 40% v/v 3.5% NaCl solution in oil and both emulsions have 1.53 w% asphaltene relative to the disperse phase. The asphaltene/resin emulsion has a hydrophilic resin fraction (adsorbed on silica from the de-asphalted oil/pentane eluate and desorbed with a 7% methanol in dichloromethane solvent after washing with benzene) at 1/4 the mass of the asphaltene. The oil phase is a 30/70 v/v

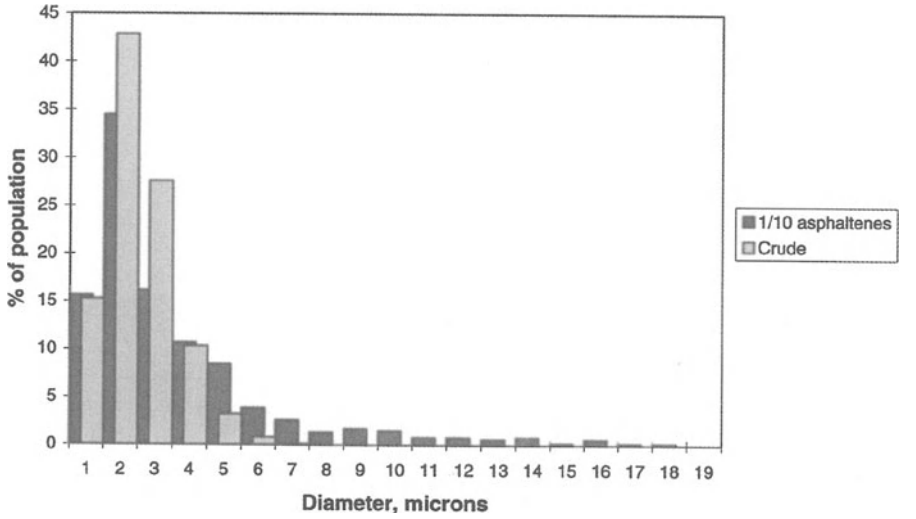

Figure 3. Normalized droplet size distributions of w/crude oil vs. w/model oil with 1/10 of the asphaltene content of the crude.

toluene/decane mixture. Aromatic toluene is an effective asphaltene solvent, contrary to decane. The oil phase is thus expected to contain both monomeric and aggregated asphaltenes as well as particles. Resins are expected to disperse the asphaltenes in the oil, which, up to a certain resin/asphaltene ratio, will increase the ability of the oil phase to stabilize water droplets. Indeed, Figure 4 shows a 30% increase in the number of droplets as well as a shift in the d.s.d. towards smaller droplets.

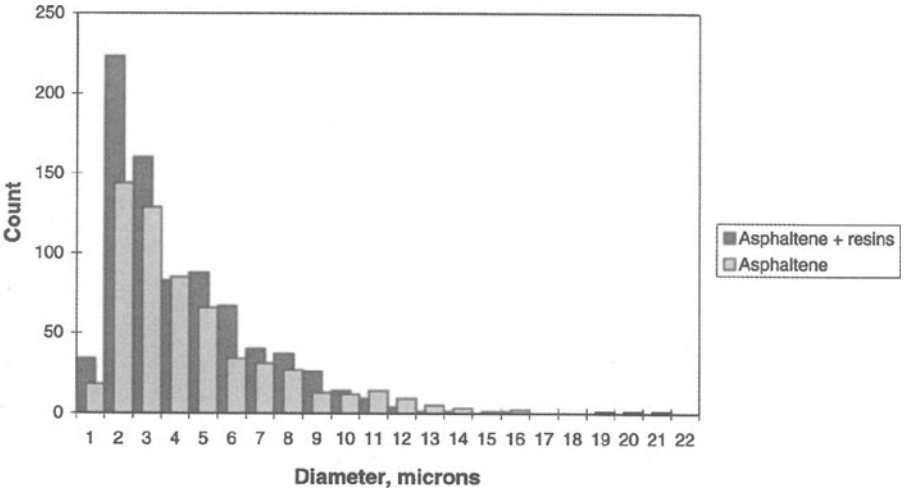

Figure 4. *Droplet size distributions of crude oil based model emulsions stabilized by asphaltenes and asphaltenes/resins extracted from an asphaltene rich crude.*

2.2. NMR Self Diffusion

The pulsed field gradient NMR-method has been used to determine the droplet size in different emulsified systems.[58-61] This technique is based on measuring the restricted self-diffusion of molecules within the droplets where the NMR spin echo signal is highly sensitive to droplet size. The method is rapid, nonperturbing and independent of the physical state of the sample and may be used without additional processing of the emulsion. The method should be very applicable for characterization of water-in-crude oil emulsions.

The measurement of size-distribution functions by means of NMR has been applied for a number of years to systems where the diffusion of the molecules is free, i.e. with no diffusion barriers on the length scale of the experiments. The simplest version of the NMR self-diffusion experiment is based on a spin-echo experiment, where in addition to the radio frequency pulses generating the spin echo there is also included two pulsed-field gradients. The first gradient pulse tags the spin by inducing a spatially dependent phase angle to them, while the second pulse determines their relative position at time D later. The result of the experiment is therefore the translational displacement of the molecules during the time-interval D. The echo attenuation for free diffusion measured by the experiment described above is exponential and defines the diffusion coefficient D. When the molecules experience barriers to their diffusion and the distance between the barriers is of the same order of magnitude as the distance travelled during D, the outcome of the experiment will be affected. For such a situation the echo attenuation will depend on the geometry of the barriers. It has to be stressed that the exact relation for the echo attenuation for an arbitrary geometry has not yet been derived, so one has to resort to different levels of approximation. In the case of molecules confined to a spherical cavity, emulsions, the droplet size is found using a Gaussian Phase Distribution (GPD) approximation[62] containing the radius of the spherical cavity (droplet). The assumption underlying the approximation has recently been tested by computer simulations, and it was found that the deviation in describing the diffusion within the spheres was below 5%.[63] In the case of emulsions where the droplets are polydisperse with respect to their sizes the situation will be more complicated. If the exchange of molecules between droplets is slow on the NMR time-scale (D) then droplets of each size will follow the echo attenuation and the measured NMR echo intensity will be a sum of the contributions from the different droplets weighed by the volume fraction of each droplet size. According to this the echo intensity can be rewritten to contain a size distribution function P(r).[59] It is not possible to determine the functional form of P(R) from the NMR experiments, but given a functional form of the distribution function the different parameters of that particular function can be calculated. Generally the results obtained from NMR studies have been verified by the use of optical microscopy.

In Figure 5 the droplet size and size distribution of a crude oil emulsion obtained by optical microscopy and NMR measurements are given. It is interesting to note that both methods indicate that the size distribution of water droplets in crude oil can be described by a log-normal size distribution.

2.3. Ultrasound Measurements

Acoustic methods have some advantages when analyzing emulsified systems. By means of accurate acoustic methods both particle size and concentration of the dispersed phase can be determined. These methods can be applied for optically opaque systems. The methods are non-intrusive, and low intensity acoustic waves will not affect the systems.[64]

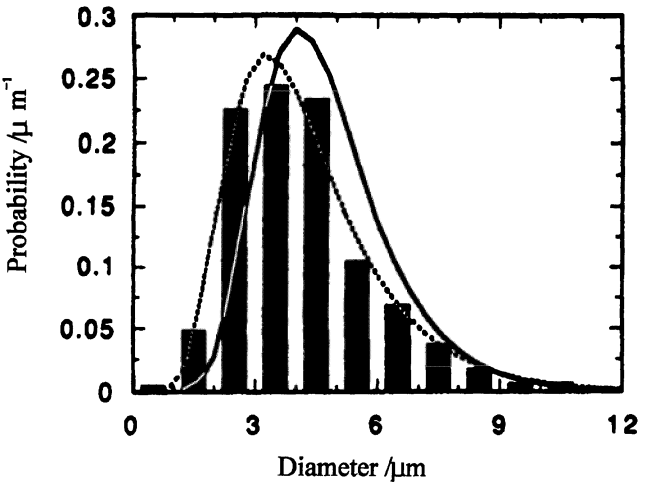

Figure 5. Size distribution curves obtained by microscope for an emulsion containing 10% water after measuring 2250 droplets (12 images covering different sizes). The broken line is the best fit of the microscope data with a log-normal size distribution of d_0=3.9 μm and σ=0.42. The solid line represents the size distribution obtained by NMR which gave d_0=4.5 μm and σ=0.32.

For a detailed evaluation of acoustic methods in emulsion research we refer the reviews by Pal,[65] McClements,[66] Frøysa and Nesse,[64] and Dukhin et al.[67-69] In the following we shall restrict ourselves to the ultrasonic aspects, i.e., the sonic wave frequencies in the range from 20 kHz to approximately 100 MHz.

Pal described the sound-scattering technique based on the sound scattering properties of the emulsion droplets. The intensity of the scattering depends on the amount and sizes of the dispersed droplets. By measuring the intensity of the scattered field in several directions, an average radius and the concentration of the droplets may be extracted. This method, however, will probably require very high frequencies in the range from 100 MHz up to as high as 1 GHz.

Pal also mentioned the ultrasound vibration potential (UVP). In this technique the incident ultrasound wave will cause the droplet to oscillate. If the droplets are charged this oscillation will produce an electric field generating a UVP-signal. The signal depends on the number of droplets in the emulsion. However, other parameters may also influence the UVP-signal, thus raising the uncertainty when applied to disperse systems.

Pal and McClements described the measurement of the speed of sound. Frøysa and Nesse also described this method in detail, since they regard the method as the best applicable to emulsified systems. This assessment is due to its simplicity in use, and the great number of studies on the method. The measurement of speed of sound is considered to be well suited for the determination of concentrations and droplet size distributions in emulsions.[64]

A mixture of oil and water will have a speed of sound which is somewhere between those of the pure components. Hence from these measurements at a well-defined temperature it should be possible to calculate the volume fraction of water and oil. For a disperse system such as an emulsion one has both a group velocity and a phase velocity at a fixed frequency. The frequency dependence of the phase velocity together with its absolute level will provide useful information about the droplet sizes and the amount of the phases present.

Models predicting the concentration from measured speeds of sound are obviously needed. To start with, simple models giving the concentration (without any droplet size dependence) from a frequency-independent phase velocity can be applied, using Wood's[70] equation (also denoted Ulrich's[71] equation). This equation is based on the expression of the speed of sound (C) in a fluid characterized by a density ρ:

$$C = \sqrt{\frac{1}{\kappa_c \rho}} \tag{2.3-1}$$

where κ_c is the adiabatic compressibility of the liquid. For a two-phase system with the volume fractions ϕ_1 and ϕ_2, $\rho_s = \phi_1\rho_1 + \phi_2\rho_2$ holds for the average density. A similar expression is also valid for the average compressibility.

For a mixture we have

$$C_{mix} = \sqrt{\frac{1}{\kappa_s \rho_s}} = \sqrt{\frac{1}{\left(\frac{\phi_1}{\rho_1 C_1^2} + \frac{\phi_2}{\rho_2 C_2^2}\right)\left(\phi_1\rho_1 + \phi_2\rho_2\right)}} \tag{2.3-2}$$

which is the Wood's equation.

An alternative model, Wyllie and Gregory's equation,[72] is a two-layer approach (similar to a series coupling of capacitances) where

$$\frac{1}{C_{mix}} = \frac{\phi_1}{C_1} + \frac{\phi_2}{C_2} \tag{2.3-3}$$

In this equation the density has disappeared, which of course sets some limitations on the use of the equation, especially with regard to frequencies.

A third model, which in a simple way just averages the effect of the two media, is

$$C_{mix} = \phi_1 C_1 + \phi_2 C_2 \tag{2.3-4}$$

for the speed of sound.

When applying Eqs. (2.3-2)–(2.3-4) any information about the frequency dependence together with the alternation in the emulsion will be lacking. Frøysa and Nesse[64] gave a complete treatment of these phenomena in their review based on the Waterman-Truell multiple scattering theories.[73,74] Those interested in details should consult Ref. (64). In order to carry out precise computations, detailed knowledge on the physical properties of the liquids (oil/water) is needed. The drawback of using multiple scattering theories is the limitation in validity to higher concentrations of the dispersed phase. For example, for $\phi_2 > 50\%$ the adopted Waterman-Truell theory will no longer be valid.

3. CHARACTERIZATION OF INTERFACIALLY ACTIVE CRUDE OIL COMPONENTS

With the intention of creating a fundamental understanding of the mechanisms responsible for stable water-in-crude oil emulsions, much effort has been directed towards

the chemistry of the chemical constituents in the crude oils. When analyzing the influence of asphaltenes, waxes, porphyrins and nonspecified polar compounds it is very striking how rough the separation techniques are. Asphaltenes are precipitated in hexane or pentane, waxes in acetone or at low temperatures, for instance. As a result of this it is rather difficult to obtain unambiguous experimental results from stabilization/destabilization tests with these operationally defined fractions. This is the background for the improved separation procedure described below for the resin fraction.

3.1. Chromatographic Separation of Resins from Crude Oils

Resins can be separated from deasphaltened crude oil by chromatographic methods, and the particle type most commonly used is silica.[75-77] By using different combinations of surfaces and solvents one can obtain resins that have different interfacial properties.[78] In Ref. (78) the resins were separated by adsorbing molecules from deasphaltened crude onto silanol, siloxane, CaO and talc particles, washing these with a solvent (solvent 1) and then desorbing the resins using a second solvent (solvent 2). All possible two-step permutations of two of the three solvents benzene, dichloromethane (DCM) and a mixture consisting of 7% methanol in DCM were used in combination with each of the three particle types. The procedure was used to extract resins from three different crudes. The resins are named using four letters: the first indicates the crude, the second the particle type, the third solvent 1 and the last gives solvent 2. A complete description of the extraction procedure can be found in Ref. (78), and the letters used to designate the resins are given in Table 1. The crude, asphaltene and the resin fractions were analyzed using diffuse reflectance infrared spectroscopy to study the relative concentrations of IR-active functional groups,[79-83,95] and the Kubelka-Munk transformed IR-spectra of the region 1800 - 600 cm^{-1} of these fractions from three different crudes are shown in Figure 6. It is seen that significant differences are present, both between the crudes and internally in the crudes. Peak assignments are given in Table 2, and show that in addition to the aliphatic and aromatic absorption bands ketone, aldehyde, amide, nitro, ester and ether and/or sulfoxide bands are present in one or more spectra. The crude and asphaltene spectra show only minor peaks in other bands than the aliphatic and aromatic. The only resin separation procedure which gave relatively similar spectra of the obtained resins from all three crudes are the Talc-MeOH/DCM-DCM sequence.

The analysis of the three groups of spectra is facilitated by the use of principal component analysis (PCA),[84] the resulting scores of which are seen in Figure 7 and loadings in Figure 8. Principal component analysis (PCA) explains most of the original variation in a dataset through a few linear combinations of the original variables called principal components (PC). In the present dataset, the principal component analysis extracts the directions

Table 1. Abbreviations used in coding the resin fractions ABCD. For example, the FSBD fraction were obtained from deasphaltened crude F fractions which were adsorbed on Silanol particles that were not desorbed by Benzene but by Dichloromethane to obtain the resin

Crude (A)	Particle (B)	Solvent (C and D)
F = France	C = CaO	B = Benzene
N =North Sea	S = Silanol	D = DCM
V = Venezuela	T = Talc	M = 7%MeOH in DCM
	X = Siloxane	

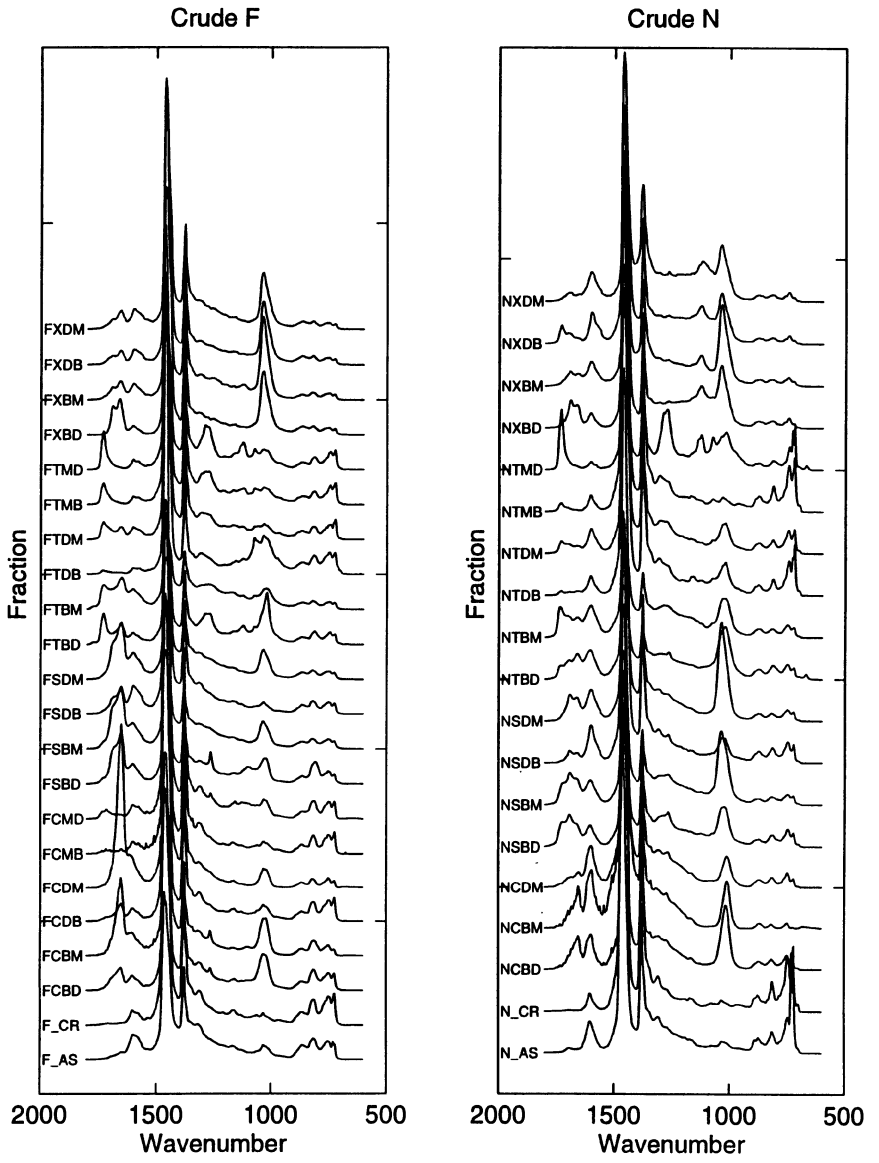

Figure 6. (Above and facing page) DRIFT spectra (in Kubelka-Munk units) for the studied region (1800–600 cm^{-1}) for all the studied fractions from crudes F, N and V. F_CR is the spectrum of crude F, F_AS the spectrum from the asphaltene fraction of crude F. Prefix N and V signifies the other crudes.

in the multidimensional space represented by the ir-spectra which, under the constraint of orthogonality between the extracted components, displays the largest variation in the dataset analysed. This is illustrated for two-dimensional data in Figure 9, and can easily be extended to any number of dimensions. This makes it possible to reduce the number of variables, often facilitating the interpretation of large datasets. The value of a sample on a principal component is called the score of that sample on that particular PC, and the con-

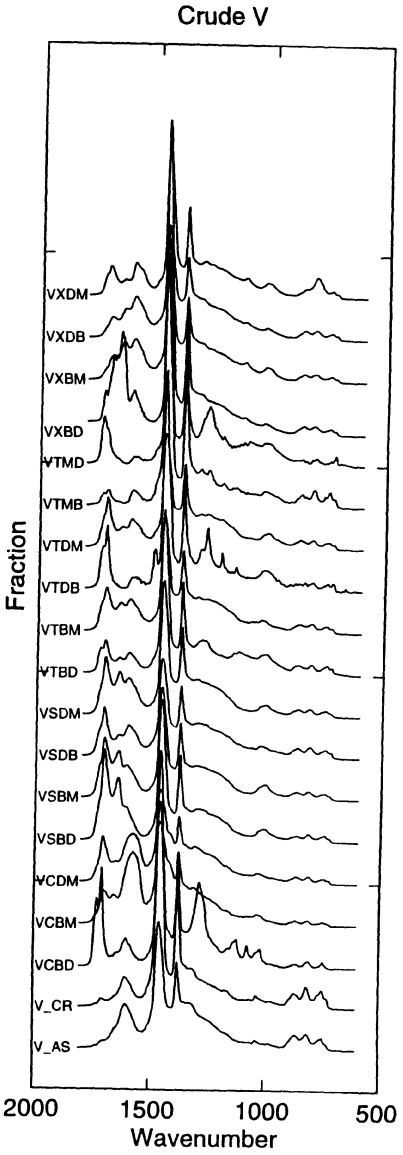

tribution of a variable to a PC is called the loading of that variable on that PC. The variance explained by the four first principal components is given in Table 3. It is seen from the loadings on PC1 that these are dominated by the aliphatic bands for all three crudes showing that most of the variation in the datasets are in these bands, and that the fraction of variation in these bands are lower in the Venezuelan crude V than in the other two crudes. From the scores and loadings on PC1 it is seen that from crude F the FCMB resin is the most aliphatic fraction. PCA of the spectra from crude N fractions reveals that the crude itself has the most aliphatic spectrum, while for crude V the resin fractions VTMB and VXBD have the highest aliphatic IR-spectra. For all three crudes the combinations of

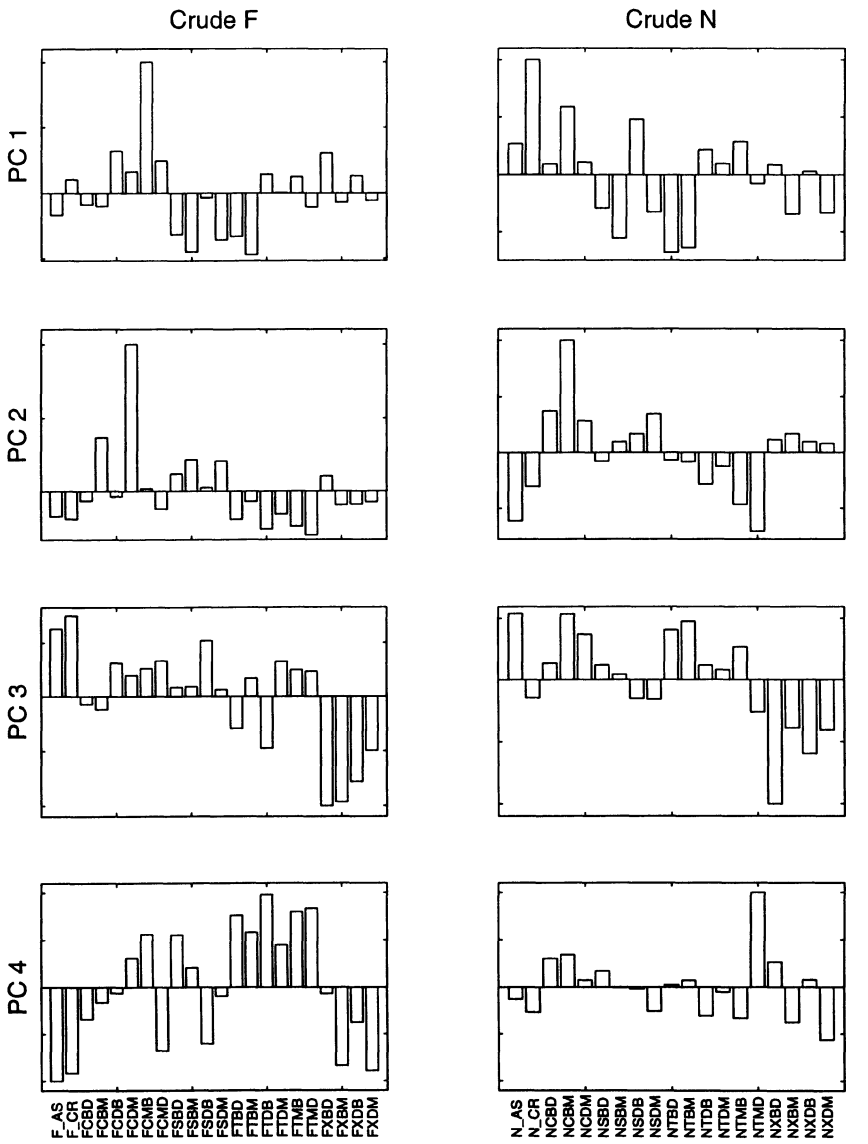

Figure 7. (Above and facing page) Scores on the first four principal components from PCA of the matrix of spectra of fractions from crudes F, N and V. F_CR is the spectrum of crude F, F_AS the spectrum from the asphaltene fraction of crude F. Prefix N and V signifies the other crudes.

silanol, siloxane or talc particles and MeOH/DCM as solvent 2 gave resins with relatively low intensity in the aliphatic bands (low score on PC1). When adsorbing onto CaO particles and using MeOH/DCM as solvent 2 a similar trend is the case only for resins from crude V. The structure of the scores and loadings on PC2 - PC4 is unique to each crude, reflecting the different distribution of functional groups in the resin fractions separated from them. Because of this the scores and loadings for each crude on these PC's are treated separately.

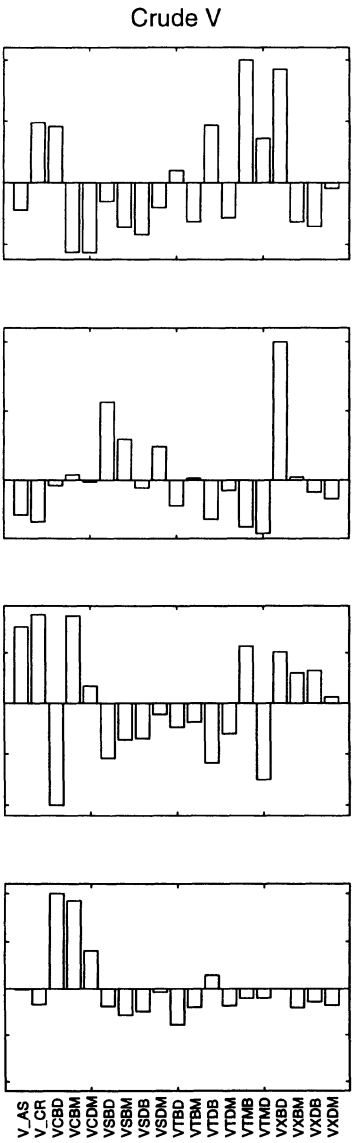

For crude F the fraction with the largest score on PC2 is FCDM, seen from the loadings to be caused by its high intensity in the amide peak at 1650 cm^{-1}. The FCBM fraction also has a large score on this PC, and is similar with respect to both experimental procedure and spectrum. On PC3 it is seen that all the siloxane resins have low scores. They all have high intensity in the band at 1030 cm^{-1}. Both ether and the sulfoxide groups absorb in this region. The 1030 cm^{-1} band dominates the loadings on PC3. On PC4 all the talc resins have a high score and several resins desorbed from all the other particle surfaces plus the crude and asphaltenes score low. The loading pattern on this PC is complex: the ester and amide bands have positive loadings, the ether/sulfoxide and aromatic C=C stretching

Table 2. Band assignments for DRIFT spectra. The assignments are taken from Ref. (78)

Functional groups	Absorption bands (cm^{-1})
OH (stretch, free)	3650–3600
O-H, N-H (stretch, H-bonded)	3500–3200
C-H (stretch, C=C and aromatics)	3050–3000
CH_3, CH_2 (stretch in aliphatics)	2950–2850
Ester (C=O stretch)	1750–1710
Ketones (C=O stretch)	1730–1700
Aldehydes (C=O stretch)	1730–1690
Amide (C=O stretch)	1670–1620
C=C (conjugated and aromatic)	1600
Nitro (N=O symmetric stretch)	1600–1480
C-CH3, C-CH2 (asymmetric bending)	1465
Nitro (N=O antisymmetric stretch)	1400–1300
C-CH3 (symmetric bending)	1377
Ester (C - O stretch)	1320–1100
Aromatic ether (C - O stretch)	1300–1200
ROH (C - O stretch or O - H def. (coupled))	1210–1000
Aliphatic ether (C - O stretch)	1150–1050
Sulfoxide (C_2S=O)	1060–1020
Aromatic C - H def.	900–700

bands low loadings. Several other regions not containing prominent bands also contribute to this PC.

No single bands dominate the loadings on PC's 2–4 from PCA of crude N spectra. The NCBM has the highest loading on PC2 and NTMD the lowest. The high score of NCBM can be explained by the loading of the amide and the aromatic bands, while the low score of NTMD is a result of the low intensity in the amide and aromatic bands together with the contributions from the ester bands and the bands around 720 cm^{-1}. All the siloxane spectra have low scores on PC3. This is explained by the loadings of the bands from 1200 - 1000 cm^{-1}, which are assigned to ether and/or sulfoxide functionalities. The NTMD resin dominates the scores on PC4 because of its high intensity in the ester bands.

The resin fraction VXBD has the highest scores on PC2 from PCA of crude V. The reason for this is seen from the high intensity in the bands at 1700 and 1650 cm^{-1} attributed to carbonyl and amide functionalities, respectively. These bands also cause VSBD to score high on this PC. No single spectrum dominates the scores on PC3. The VCBD and VTMD resins score low because of their high intensity in the ester bands at 1730 and 1280 cm^{-1}. The positive scores of the VCBM and VCDM resins are caused by their high intensity in the nitro bands located around 1580 and 1400 cm^{-1}, the VCBM fraction having the highest intensity in these bands. The resins desorbed from CaO particles dominate the scores on PC4 because of their high intensity in the ester and nitro bands.

From the IR-spectra it is seen that the functionalities present in the resins separated using this procedure depend on the crude oil, particle surface and solvent used. It is also seen that that the distribution of the functional groups is different for each of the three crudes, and the PCA quantifies and describes the spectral similarities and differences.

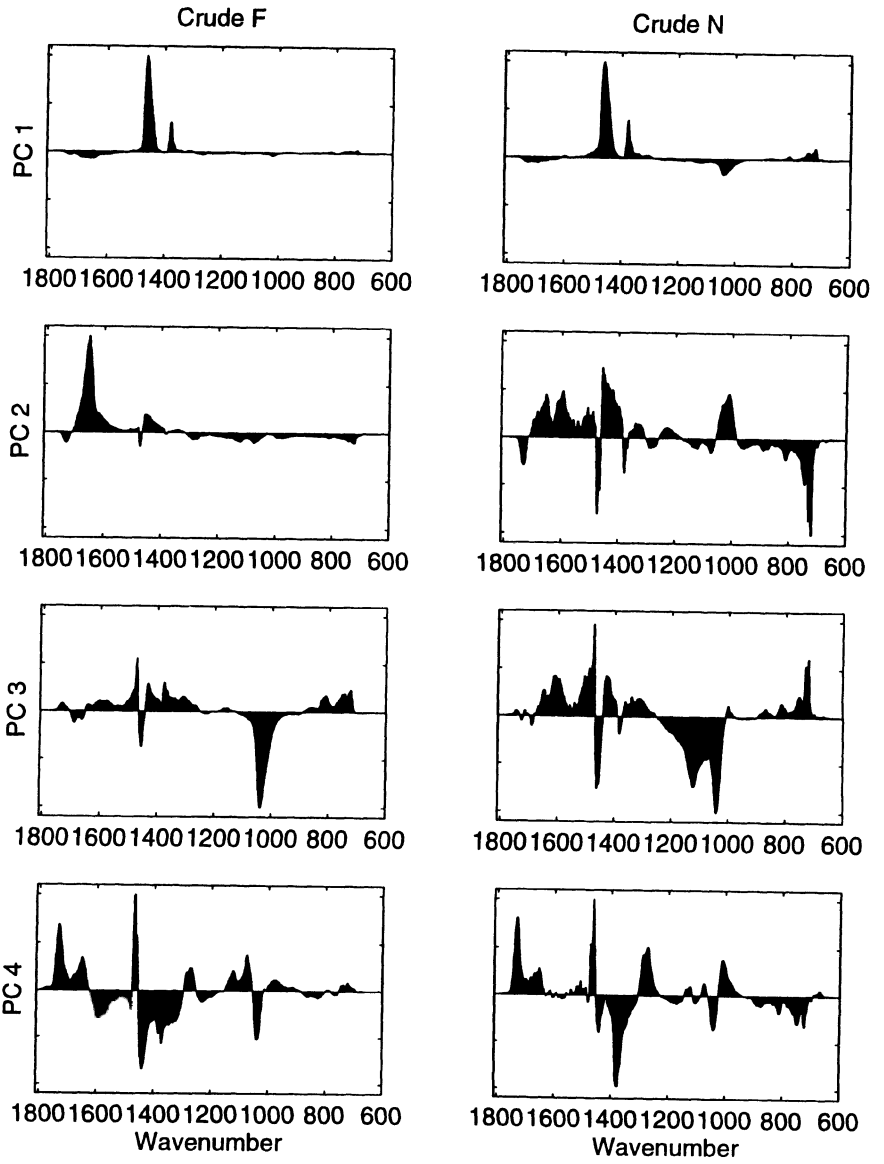

Figure 8. Loadings for the first four principal components from PCA of the matrix of spectra of fractions from crudes F, N and V. F_CR is the spectrum of crude F, F_AS the spectrum from the asphaltene fraction of crude F. Prefix N and V signifies the other crudes.

3.2. Experimental Techniques for Characterization of the Interfacially Active Components

In order to understand the stabilizing mechanisms in water-in-crude oil emulsions and to follow the destabilization by means of chemical inhibitors, it is essential to characterize the interfacial film between the water droplet and the crude oil bulk phase. The most trivial

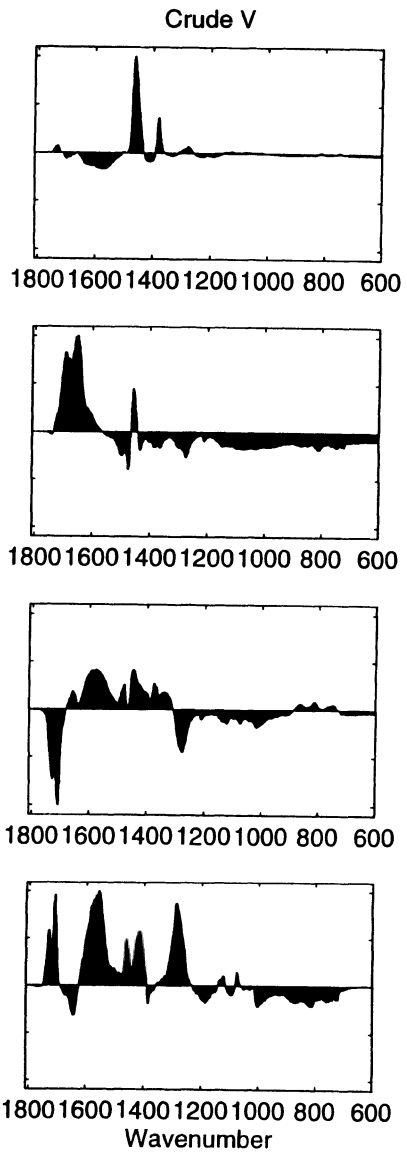

Figure 8. (*Continued*)

way of doing so is to measure the interfacial tension for extracted asphaltene and resin additives between a synthetic oil phase and an aqueous phase. Recent results are reported in 3.2.1. Essential for the emulsion stability are the rheological properties of the stabilizing film. These are determined by means of interfacial rheology which is a sophisticated way to analyze emulsion stability. Since this technique is covered in another chapter in this book we leave it out here. Finally, a very direct way to monitor fundamental properties of asphaltene/resin films is the Langmuir-Blodgett technique (Section 3.2.2). Fundamental properties, like compressibility and packing, can be determined by means of this technique.

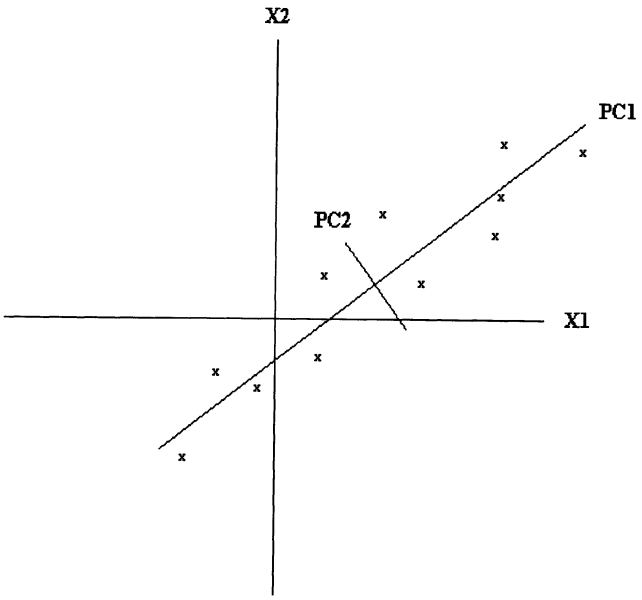

Figure 9. Illustration of principal component analysis. The variation in the dataset described by the measured variables X1 and X2 can be explained totally by the two new variables PC1 and PC2. It is seen that most of the variation in this dataset can be explained by one variable only (PC1) that is a linear combination of the two original variables. This makes a data reduction possible.

3.2.1. Interfacial Tension and Pressure. The interfacially active fractions are less well-defined mixtures of chemical compounds. However, from the characterization one can conclude that they consist of relatively low molecular weight, highly polydisperse hydrocarbon polymers. These contain small amounts of polar groups, and are swollen with 10–15% aliphatic hydrocarbons. The carbon/hydrogen ratio and IR data indicate that the polymers contain considerable amounts of aromatic groups. They are soluble in non-polar solvents but completely insoluble in water.

Interfacial tension[85] and monolayer studies[42] from North Sea crudes have shown that the fractions are not strongly surface active. Their surface pressures do not exceed 15 mN/m before film fracture and the minimum oil/water tension observed is 25–30 mN/m. In a previous study when only asphaltenes were analyzed, we concluded that high inter-

Table 3. Variation of data sets described by each of the first 4 principal components for the three crudes

	Crude F		Crude N		Crude V	
PC	% variation	Cum. variation	% variation	Cum. variation	% variation	Cum. variation
1	78.7	78.7	79.3	79.3	57.1	57.1
2	12.1	90.8	7.9	87.2	18.2	75.2
3	4.9	95.7	4.9	92.2	13.2	88.4
4	1.9	97.6	2.8	95.0	5.5	93.9

facial pressure was a necessity for stabilizing model water-in-oil emulsions by means of an asphaltenic fraction. The interfacial pressure, π, is defined as:

$$\pi = \gamma_0 - \gamma \qquad (3.2.1\text{-}1)$$

where γ_0 is the interfacial tension of the pure components and γ is the interfacial tension after addition of chemicals. A value of π of the order of 10 mN m^{-1} or less is insufficient in order to achieve stable emulsions. However, our previous studies also reveal that the nature of the organic phase is very decisive for the solution chemistry of these fractions. When benzene is added in sufficient quantities, the interfacial tension between the oil and the water phase is depressed and hence the originally interfacially active fractions will no longer accumulate at the w/o interface. Hence, the whole emulsified system loses its stability.

Interfacial tensions of aqueous/organic phases where the latter contains the asphaltenes has been investigated by several groups. Sheu et al.[86] measured the dynamic interfacial tensions between alkaline aqueous phases and asphaltene/toluene organic phases. The asphaltene fraction was precipitated from a heptane solution. The interfacial tension was found to follow an exponential law where the level of the equilibrium data depended on the alkalinity. For 2 M NaOH, γ_{eq} was close to 10 mN m^{-1} for 0.01% of asphaltene. When the amount of asphaltene was raised to 0.1% in 1 M NaOH, similar γ_{eq} values were obtained. The authors found that the dynamic interfacial tensions reflected the diffusion-controlled adsorption/desorption of asphaltene molecules. Equilibrium values reflect more a reaction-controlled situation with rearrangements of the asphaltene molecules.

Singh and Pandey[87] characterized the interfacially active fractions in Indian crudes. They also concluded that a high interfacial pressure correlated very well with a high w/o emulsion stability.

A well known phenomenon is that ageing is substantially changing the emulsion stability and also the interfacial properties of the stabilizing components. In the following we show an example on changes in interfacial activity upon ageing. For three North Sea crudes the surface tension was determined to 23.1–23.3 mN m^{-1} at 50 °C. The ageing had no influence on the surface tension of model systems based on decane:toluene (90:10) mixtures containing indiginous surfactants. For the interfacial tension towards brine the situation is completely different. The value of $\gamma_{o/w}$ is depressed from an initial value of 25–30 mN m^{-1} down to values around 10 mN m^{-1} within 1 week of oxidation in atmospheric conditions. It should be mentioned that an additional UV treatment did not accelerate the trend in $\gamma_{o/w}$. Table 4 summarizes the effect of ageing on $\gamma_{o/w}$ and the influence on the corresponding emulsion stability.

The ageing process is associated with chain-breaking mechanisms due to autoxidation. In this reaction scheme initiation, propagation and termination processes are involved. IR-spectra show that due to oxidation both the intensity of the carbonyl group at 1704 cm^{-1} and the C-O bond at 1060 cm^{-1} will increase considerably for most samples. As a consequence the polar molecules will undergo different condensation reactions. Obviously, this process is combined with a substantial increase in the interfacial activity for the oxidized species. Similar results are found in Refs. (88-91).

3.2.2. Langmuir-Blodgett Films. On the surface between air and water amphiphilic molecules will orient with the polar part in the water phase, while the unpolar chains reach out from the water surface. The structure in a monolayer of such components stabilizes through; alkylgroup-alkylgroup, polargroup-subphase and polargroup-polargroup interac-

Table 4. Separation of the aqueous phase (synthetic formation water) from model emulsions consisting of decane/toluene (90:10 by volume) stabilized[a] by the interfacially active components from a crude oil

Time	γ^b (mN m^{-1})	π (mN m^{-1})	Separation time (h) 1	2	3	4	8	24	48
			Separation water (%)						
Without UV light									
0 h	30.9	5.3	No stable emulsions						
24 h	11.5	24.7	No stable emulsions						
48 h	11.0	25.2	No stable emulsions						
72 h	9.6	26.6	No stable emulsions						
1 week	9.6	26.6	–	20	40	50	80	80	80
2 weeks	9.7	26.5	–	–	10	30	60	70	80
3 weeks	10.0	26.2	–	–	–	10	40	70	80
4 weeks	10.4	25.8	–	–	–	20	60	80	90
2 months	9.5	26.7	–	–	–	10	50	80	80
With UV light									
0 h	30.9	5.3	No stable emulsions						
24 h	16.1	20.1	No stable emulsions						
48 h	14.8	21.4	No stable emulsions						
72 h	14.5	21.7	No stable emulsions						
1 week	11.7	24.5	–	–	–	–	0	60	60
2 weeks	11.4	24.8	–	–	–	–	10	60	70
3 weeks	11.8	24.3	–	–	–	–	10	60	70
4 weeks	11.5	24.7	–	–	–	–	10	30	50
2 months	10.4	25.8	–	–	–	–	–	–	0

The stabilizing fraction was oxidized under atmospheric conditions with and without UV light. The separation was undertaken at 50°C.

[a]The amount of stabilizer was 1% before 72 h and 2% after 72 h.

[b]Referred to the system decane/toluene and synthetic formation water with the oxidized crude oil fraction present.

tions. Using the Langmuir technique, the surface pressure against reduced surface area is measured, giving surface pressure-area (Π-A) isotherms. The interaction forces will change related to the packing of the molecules. As in three dimensions, the state of the film is related to the free space between the molecules on the surface. If the surface area is so large that there are no interactions between the molecules the phase is called a two-dimensional gas. Some interaction gives a two-dimensional liquid, while a monolayer of close packed molecules is called a solid phase.[92]

The Langmuir-Blodgett technique makes it possible to monitor the monolayer stability. This is done by compressing the film to a certain pressure, which is held constant. The film area-loss is then measured as a function of time. An observed loss of film material may be a result of rearrangements of the film molecules, dissolution of film molecules into the subphase and/or collapse by nucleation[93] and a subsequent growth of solid bulk fragments.

3.2.2.1. Langmuir-Films of Asphaltenes and Resins. Figure 10 shows Langmuir-isotherms of asphaltenes and resins. The graph provides information about the ability of the fractions to pack into a two dimensional film on a water surface. The asphaltene isotherm shows no variation in surface pressure at high surface areas, until a sharp increase is observed. Here the asphaltene molecules/aggregates start to interact, and after this the film

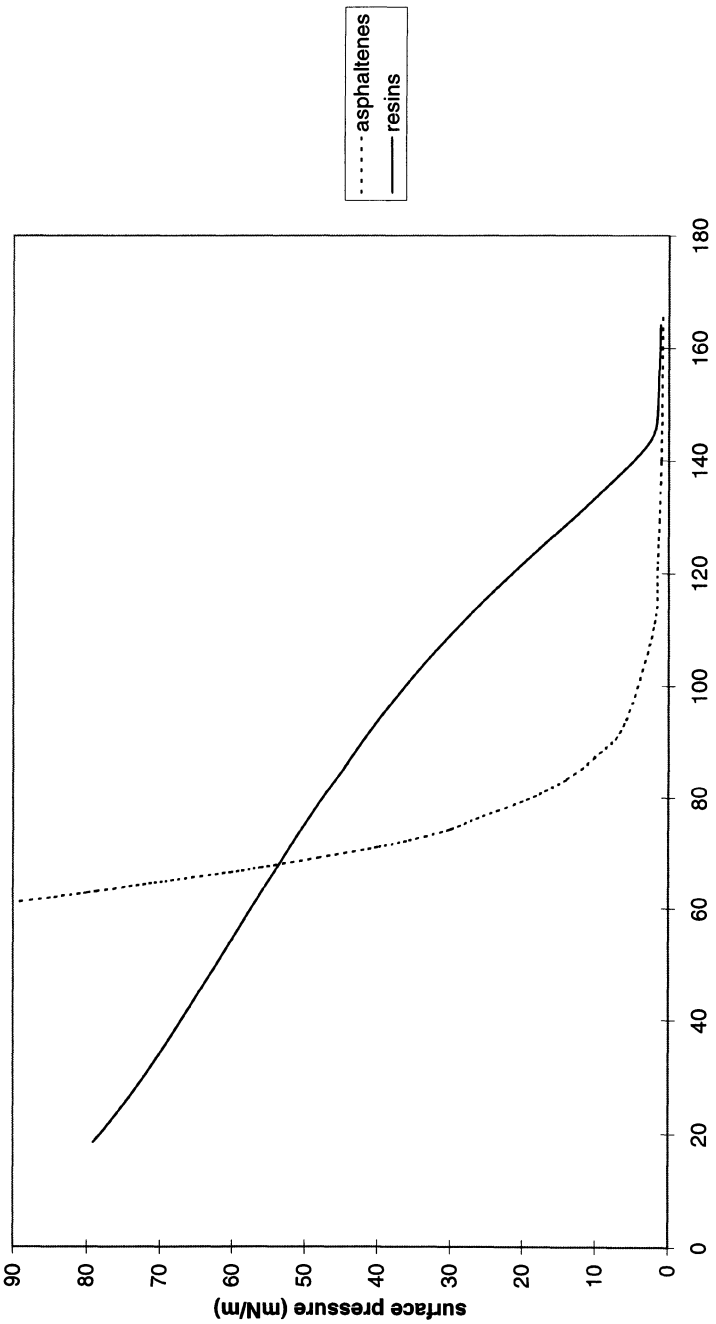

Figure 10. Langmuir-isotherms of asphaltenes and resins on pure water.

has a low compressibility. The rise in surface pressure is likely due to interactions between the rigid aromatic hydrocarbon parts of the asphaltenes. The relatively few polar groups are probably still so far apart that an interaction between these does not play any significant role. In contrast to this the film of resins shows a high degree of compressibility at high surface pressures. This phenomenon indicates that other processes than a straight forward compression of the hydrocarbon chains is taking place. This process, involving higher compressibility and enabling the units to pack into very small areas, is probably a reversible collapse of the segments, which pass out of the surface plane gradually building up an overfilm. So the increase in surface pressure, which describes the energy needed to compress the film is partly used to overcome repulsions between the molecules, and partly to force some of the residues away from the surface. As the pressure rises, more and more energy is dissipated in forcing groups into the overfilm. These properties resembles those for films of polymers as reported in Group I[94], which consists of amorphous, usually soft polymers giving stable fluid films gelating at high surface pressures (20–30 dynes/cm.). Compared with asphaltenes, smaller amounts of resins are needed on the surface to achieve increased surface pressure. This is probably a consequence of higher polarity of the resin fraction than of the asphaltene fraction.

Figure 11 shows a monolayer stability isotherm (loss of monolayer area) at constant surface pressure (10 mN/m) for an asphaltene-film. This figure indicates a small area loss in the beginning of the measurement before it stabilizes at constant pressure, which verifies the stability of the investigated monolayer. The small area loss is due to rearrangements of the film molecules, observed because of turbulence in the film immediately after the compression.

A constant surface pressure investigation of the resin-film shows that the pressure will continue to increase above 10 mN/m even when the position of the barriers is fixed. This is in accordance with a multilayer formation at the surface. In addition the effect may be due to oxidation of the surface layer, which would result in higher polarity of the film. This process entails increased affinity of the film material towards the surface, giving increased pressure.

Mixtures of asphaltenes and resins give the isotherms in Figure 12, where a gradual increase in repulsion for an increased amount of resin in the film is observed. This is a consequence of increased polarity in the film. When the resin content exceeds 40% a distinct increase in compressibility at high surface pressures is observed. So for these amounts, the more polar fraction starts to predominate the film properties due to the higher affinity of the resins towards the surface (water/air).[95] Stability isotherms for the combinations of asphaltenes/resins gave the same result as for the pure resin fractions. The increase in surface pressure with fixed barrier positions became more prominent as the resin content increased.

4. STABILIZATION AND DESTABILIZATION OF MODEL AND CRUDE OIL BASED EMULSIONS

Stability mechanisms for water-continuous emulsions have been mapped and classified long ago. A central mechanism in this respect is the electrostatic stabilization which has an origin in adsorption of charged surfactants onto the surface of the oil droplets. Stabilization by means of polymers and nonionic surfactants is usually classified as steric stabilization. In addition to these mechanisms particle stabilization is also frequently encountered. Special features of surfatcant association into lamellar lyotropic liquid crys-

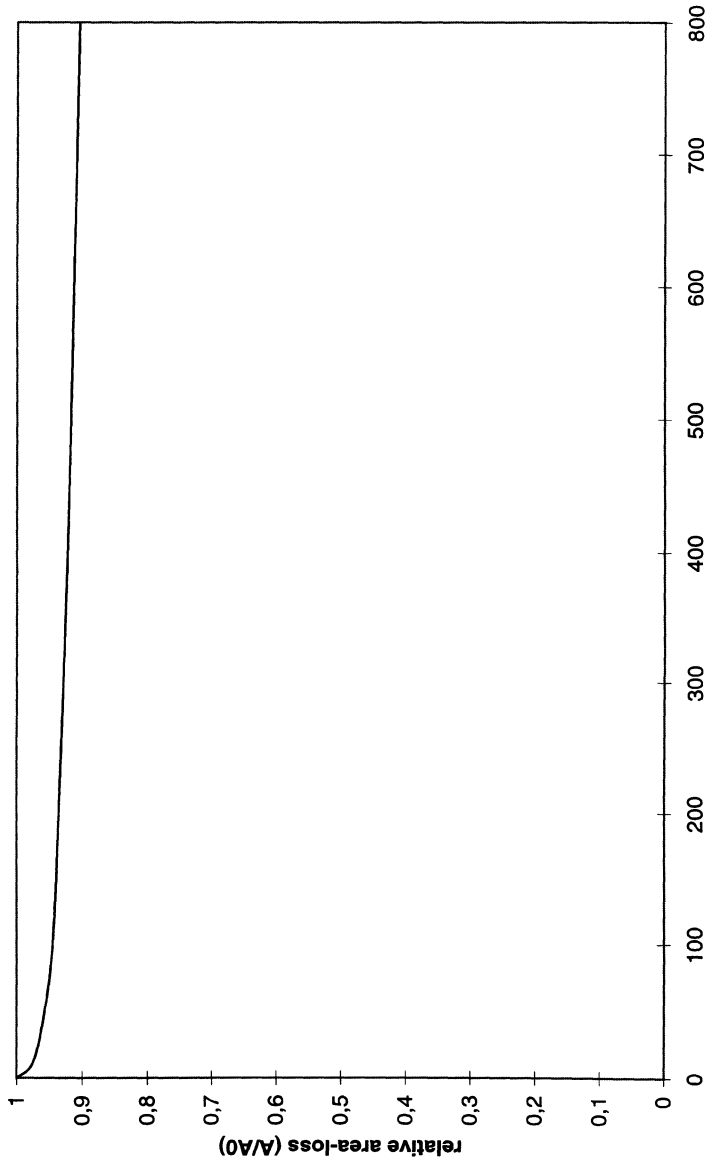

Figure 11. Monolayer stability of asphaltenes at $\Pi = 10$ mN/m on sub-solution of pure water.

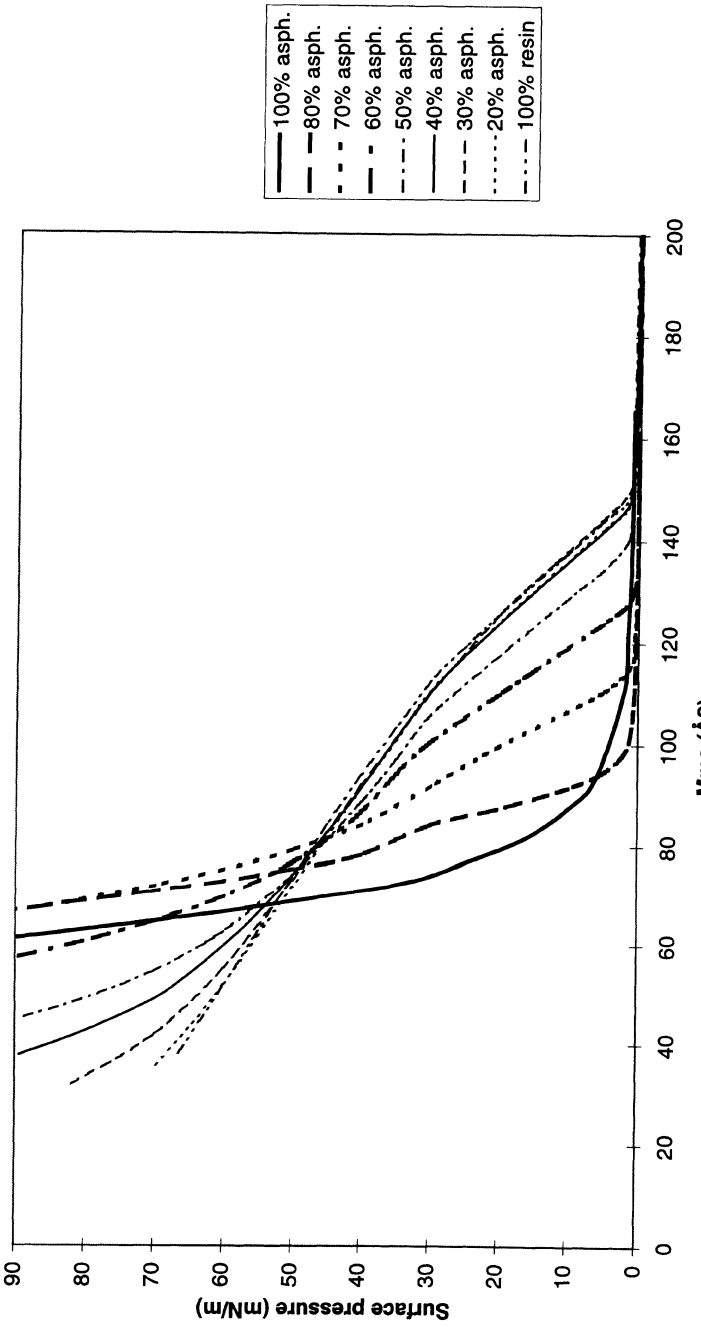

Figure 12. Langmuir-isotherms of asphaltene/resin mixtures on pure water.

talline phases is important for the formation of multilayer structures at the surfaces. For w/o emulsions the electrostatic stabilization seems to be of less importance leaving the other three as predominating.

4.1. Stabilization of Water-in-Crude Oil Emulsions

It is by now rather well recognized that the stability of these emulsions is an interplay between the heavy components and waxes. By heavy components we mean asphaltenes, resins, porphyrins, etc. Normally, in a crude oil without water the asphaltenes are dispersed by the lighter components and are hence prevented from precipitation. When water is mixed into the crude oil a new interface is created and there will occur a new distribution of the heavy components. It has been shown that resins are more interfacially active than the asphaltenes, which means that these molecules will initially cover the fresh w/o interface. As a consequence of this the solubility conditions of the asphaltenes will drastically change and a precipitation will take place. With a lot of aqueous droplets present the asphaltene particles will accumulate at the surface of these droplets with a very high total surface area. In this way there are possibilities to rigidify the "monolayer" of resins initially adsorbed at the interface. Central mechanisms will hence be both steric and particle stabilization.

The mechanical properties of the interfacial film are essential for the stabilization of the w/o emulsions. Concentrated polymer films at interfaces may show elastic or viscous properties that make it difficult to break the corresponding emulsions, either because insufficient energies are involved in collisions between droplets, or because the kinetics of breaking is slow compared to the times involved in the collisions. Aromatic molecules like asphaltenes will stack into a sandwich-like structure when they associate.[96] The presence of solid particles (waxes or inorganic clays) at the interface will further increase the rigidity of the film and hence make it even more difficult to break the emulsions.

Results of Sjöblom et al.[48] have shown the existence of a direct correlation between interfacial pressure (see Eq. 3.2.1-1) and emulsion stability when well-defined asphaltene components are used as stabilizers. Values of π in the range 10–14 mN/m showed the first signs of instability, while for $\pi < 10$ mN/m the emulsions were completely unstable. Addition of benzene to the oil phase (n-decane) reduced the interfacial tension and therefore also the interfacial pressure. As a consequence the above mentioned fractions could no longer reduce the interfacial tension. Hence, they were only dissolved into the oil continuous phase and gave no stability of the emulsions.

Christenson et al.[97,98] investigated the interaction forces between mica sheets immersed in crude oils. They found that a surface active fraction from the crude oil was adsorbed on the mica, and that the force/distance dependence of the interactions between these mica sheets did not indicate a typical steric stabilization. The results indicated a "hard wall" repulsion occurring at short distances. However, one should be careful when comparing crude oils of different origins due to the large differences in properties that can be present. The crude oils used by Christenson et al. were from Australian reservoirs, while ours are from the North Sea. This study confirms our results with regard to the mechanical properties of the interfacial film, probably combined with some steric contribution, as the main mechanism responsible for the stabilization of water-in-crude oil emulsions.

4.2. Destabilization of Water-in-Oil Emulsions

The breaking of an emulsion can broadly be divided into three different processes; creaming/sedimentation, inversion and coalescence.

4.2.1. Coalescence. Coalescence is defined as the combination of two or more droplets to form a larger drop. When these droplets approach each other a thin film of the continuous phase will therefore be trapped between the droplets, and it is obvious that the properties of this film will determine the stability of the emulsion.[99] Based on this it is clear that the mechanism of coalescence occurs in two stages; film thinning and film rupture. In order to have film thinning there must be a flow of fluid in the film, and a pressure gradient present. The rate of film thinning is dependent on the rate at which the interface moves the film. It is obvious that this process is affected by the properties of the colloidal system present, and some of the most important parameters are defined as[100] viscosity and density of the two phases present, interfacial tension and its gradient, interfacial shear and dilational viscosities and elasticities, drop size, concentration and type of surfactant present at the interface and forces acting between the interfaces. Considerable effort has been made to develop models for prediction of the rate of film thinning and critical film thickness. In most of these models it is assumed that the film thickness is large enough for the van der Waals-London forces and electrostatic forces to be ignored. Reynolds[101] made the first mathematical analysis of parallel disks. He assumed the bounding interfaces to be solid and the film to be of uniform thickness. Frank and Mysels[102] investigated dimple formation and drainage through the dimple. Later models of film thinning are those of Zapryanov[103] and Lin and Slattery.[104,105] Zapryanov investigated surfactant partitioning at the interface using the parallel disk model. This model has later been extended to account for the adsorption/desorption kinetics of surfactants.[106] Film rupture is a non-equilibrium process that may occur due to flow instabilities, temperature fluctuations, electric fields or Marangoni effects.[107] Investigations by De Vries[108] and Lang[109] showed that there exists a critical film thickness. Above this thickness the probability of rupture is zero, and below it the probability of rupture increases with decreasing film thickness. Scheludko[110] investigated the rupture of thin liquid films between two droplets in relation to fluctuations at the interface. He also developed an expression for the critical film thickness which is valid for films where only the van der Waals forces are acting: $d_c = [A\,\pi/32\,K^2\,\gamma_0]^{0.25}$, where A is the Hamaker, γ_0 is the interfacial tension between the continuous and dispersed phase when they create an interface and not a film and K is the wave number of the surface fluctuations. Vrij[111] has derived an alternative expression for d_c; for large thicknesses: $d_c = 0.268[A^2R^2/\gamma_0\,\pi\,f]^{0.14}$, where R is the droplet radius and f is dependent on d. For small thicknesses: $d_c = 0.22[A\,R^2/\gamma_0\,f)]^{0.25}$. According to the first equation $d_c \rightarrow \infty$ when $\gamma \rightarrow 0$, i.e. the film should spontaneously rupture at large d values. However, this is not the fact since emulsion droplets become highly stable when $\gamma \rightarrow 0$ (as in microemulsions). Also, the first equation predicts that as $R \rightarrow 0$, $d_c \rightarrow 0$, i.e. small emulsion droplets would never rupture. Sonntag and Strenge[112] showed that d_c will not change when the contact area is varied. This is due to the fact that the lamella formed between two droplets, at non-equilibrium separations, does not have an idealized planar interface between them. Sonntag and Strenge[112] also showed that emulsion films of octane/water droplets stabilized by a nonylphenol ethoxylated surfactant plus an oil soluble surfactant, had a d_c independent of γ_0.

4.3. Demulsification of Water-in-Crude Oil Emulsion

The most common methods for demulsification of water-in-crude oil emulsions can be divided into three different categories; electrical, mechanical and chemical. Chemical demulsification is today the most common method for treating crude oil emulsions. The resolution of crude oil emulsions by electrical methods is possible because most oil field

emulsions are oil-continuous and, in consequence, the systems are relatively non-conducting. Electrical dehydrating techniques are based on the principle that external electric fields will induce a charge on the surface of the water droplets. One must distinguish between the mechanism of electrically induced coalescence in a low-conductivity and a high-conductivity continuous phase, respectively. Media with a low conductivity, such as distillate fuel, have low relaxation times and, hence, the suspended droplets can keep their charge for quite some time. In this case the droplets have time to travel from one electrode to the other under the influence of the applied field and, as they move, collide with each other and coalesce. On the other hand, in a medium with higher electrical conductivity, such as crude oils, charges acquired by the droplets are dissipated before the droplets can move any appreciable distance. The coalescence in such a medium is caused by inducing polarization charges on the droplets, thus creating weak interdroplet forces which attract neighboring droplets.[113] The electrical coalescence in high conductivity media is generally slower than in low-conductivity media.

Walton[114] has found that coalescence of droplets is difficult if their size distribution is very narrow and the amount of dispersed phase is low. This is due to the large distance between the droplets. If the amount of dispersed phase exceeds 3 vol% the results are generally satisfactory. A variety of mechanical methods to resolve crude oil emulsions are available. Examples of these techniques include ultrafiltration, reverse osmosis, centrifugal coalescence, filtration coalescence, etc. For further details Menon and Wasan[115] is recommended. It is very important to clarify the different parameters of importance when chemical demulsification is considered. How will compounds of specific chemical functionality destabilize these emulsions? What are the mechanisms responsible for the emulsion stability, and what are the mechanisms behind the destabilization? Most chemical agents used for demulsification are preferentially oil soluble blends consisting of high molecular weight polymers. These blends commonly consist of: 1) flocculants (large, slow acting polymers). 2) coalescers (low molecular weight polyethers). 3) wetting agents. 4) solvents/cosolvents. Some chemical structures of demulsifiers used for breaking crude oil emulsions have been listed by Jones et al.[14] Much work has been carried out in order to identify and understand the mechanisms behind chemical demulsification. Fiocco[116] concluded that the interfacial viscosity was kept at a low level when demulsifiers were present. Later on it has been realized that the interfacial shear viscosity of crude oil emulsions does not have to be very low in order to ensure accelerated water separation.[117]

Wasan et al.[118,119] investigated the coalescence of systems containing petroleum sulfonates. They concluded that the coalescence rates correlated well with the interfacial shear viscosity, while no correlation was observed with the interfacial tension. Sjöblom et al.[48] investigated the influence of simple, well defined solvent molecules on the stability of water-in-crude oil emulsions from the Norwegian Continental Shelf. Based on the different effectiveness of the chemical additives, medium chain alcohols and fatty amines, two different destabilization mechanisms were proposed. The alcohols seemed to modify the rigidity of the interfacial film by a diffusion/partitioning process, while the amines showed a strong and specific interaction with the interfacial groups, hence hydrophilizing the whole film. Aveyard et al.[120,121] investigated the correlation between surfactant interfacial behaviour, surfactant association and the destabilization efficiency. They observed a clear correlation between the demulsifier concentration at optimal demulsification efficiency and the critical micellization concentration (CMC) of the demulsifier in the crude oil system as long as simple surfactants were used. This means that the monomer activity of the surfactants is crucial for the destabilization of the emulsion system. They also showed that for crude oil systems with a demulsifier present the o/w interfacial tension

passed through a minimum when the NaCl concentration varied between zero and 1 M. They further showed that the emulsion type could invert from o/w to w/o for salt concentrations in the same range. Obviously the hydrophilic-lipophilic balance (HLB) of the demulsifier could be balanced by these other conditions. Wasan et al.[122,123] investigated in detail the processes taking place at the o/w interface during a destabilization process with a low molecular weight amphiphilic compound. From studies of different additives they concluded that oil-soluble destabilizers should be able to partition into the aqueous droplets in order to act as destabilizers. The concentration of the demulsifier inside the droplets should be high enough to ensure a diffusion flux to the o/w interface. In order to be efficient as destabilizers the additives must show a high rate of adsorption to the interface. Wasan also emphasized the importance of sufficiently high interfacial activity of the demulsifier to suppress the interfacial tension gradient. In this way the film drainage will be accelerated and droplet coalescence will be promoted. Little[124] suggested that the sequence of steps leading to demulsification of petroleum emulsions involves the displacement of asphaltic material from the interface by the demulsifier followed by the formation of demulsifier micelles which solubilize and/or stabilize the asphaltic compounds in the oil. Studies by Berger et al.[125] suggested a method for prediction and characterization of different demulsifiers. This method is based on the relationship between the equivalent alkane number (EACN) of the crude oil and the preferred alkane number (PACN) of the demulsifier. They concluded that the lowering of the interfacial tension itself is not indicative of demulsifier performance, and that lowering of the interfacial viscosity may be a possible mechanism for demulsification. Furthermore, they concluded that no correlation between HLB and demulsifier effectiveness could be expected when the demulsifier was equally soluble in both the aqueous and the oil phase.

The destabilization of emulsions is dependent on the coalescence rate of the dispersed droplets. This rate can be greatly enhanced by the addition of chemicals. Among the single solvents two different categories were shown to be most efficient as destabilizers. These were medium-chain alcohols and fatty amines, and for these two types a qualitative destabilization mechanism has been proposed. An important parameter for alcohols when acting as destabilizers seems to be their ability to dissolve into the different regions in the emulsified system. Hence, medium chain alcohols (n-butanol, n-pentanol and benzyl alcohol) readily dissolve in the aqueous, the interface and the bulk (oil) phase. This partitioning of the molecules between the phases will create disadvantageous conditions for the stability of the water-in-crude oil emulsions. Krawczyk[117] investigated the influence of different demulsifiers on the stability of water-in-crude oil emulsions. He defined a partitioning coefficient, $KP = c_a/c_o$, where c_a refers to the demulsifier concentration in the aqueous phase and c_o to the concentration in the oil phase. He concluded that demulsifiers with K=1 gives the best results. This implies that the demulsifier should be equally soluble in both the aqueous and the oil phase. He also concluded that the interfacial activity and adsorption kinetics of the demulsifier are important parameters. Based on these observations and the fact that medium chain alcohols are soluble both in water and oil, it is clear that the interfacial region will become less rigid and structured as a result of the extensive partitioning. The interfacial region can be expected to be more dynamic, and considerable interfacial fluctuations may occur in the presence of medium-chain alcohols. Furthermore, if multilayers are present at the interface it is interesting to know that medium chain alcohols like n-butanol have a characteristic tendency to reduce the existing regimes of the lamellar liquid crystalline D phase as viewed by means of phase diagrams.[126-128] It seems likely that a similar mechanism can influence the stability of water-in-crude oil emulsions. Since the adsorbed and stabilizing film has been shown to contain some fatty acids (palmi-

tic acid) an interaction with added amines will result in polar (charged) complexes.[129] These charged sites will create a lateral electrostatic repulsion and, hence, alter the molecular packing in the interfacial film. With these hydrophilic groups present, the film can no longer stabilize the water-in-crude oil emulsion against coalescence. With no fatty acids present in the interfacial film, the amines can just replace the interfacial film due to a higher interfacial activity. Sjöblom et al.[48] have shown that hexylamine is capable of lowering the interfacial tension between crude oil and water from 30 mN/m to 10 mN/m with the concentrations used in the destabilization tests, while Nordli et al.[42] have shown that hexylamine is capable of replacing a film consisting of the interfacially active crude oil fraction in Langmuir-Blodgett experiments.

The mechanism behind a destabilization with surfactants is probably an interfacial competition. In this situation the indigenous crude oil film will be replaced by a surfactant layer which cannot stabilize the crude oil emulsion. Two main categories of surfactants are hydrophobic and hydrophilic ones. When comparing two different hydrophobic surfactants, tetraoxyethylene-nonylphenol ether (Triton N-42) and sodium(bis-2-ethylhexyl)-sulfosuccinate (AOT), it was found that the hydrophobic ionic surfactant, AOT, was more efficient than the nonionic analogue. Three different hydrophilic, fluorinated surfactants were also investigated in Ref. (130). They were all very efficient as destabilizers, probably due to their high interfacial activity. In the destabilization process the nature of the crude oil film and the added surfactant will be very important for their internal interactions. If an interfacial complexation between these two species occurs, the efficiency of the surfactant may be changed. Complexation between the anionic AOT and the species present in the interfacial film may create charged complexes that will further disfavour a close packing of stabilizing molecules at the interface. This might be the explanation behind the differences between the two hydrophobic surfactants. The fluorinated surfactants are very efficient in lowering the interfacial tension[131,132] and, hence, their destabilization mechanism can be easily comprehended. As mentioned earlier Wasan et al.[122,123] have analyzed in detail the processes taking place at the o/w interface during destabilization. The results for the hydrophobic surfactants are in direct agreement with their conclusions. Also, in the case of common solvents where we found medium chain alcohols to be efficient as destabilizers, the results also correspond with their conclusions. The medium chain alcohols are soluble in all three pseudophases and will therefore partition between these. The hydrophobic surfactant AOT is soluble in water up to a few percent, and will therefore also be present in the aqueous phase, whereas Triton N-42 is completely water insoluble. This will most likely contribute to the differences between the surfactants.

Aveyard et al.[120,121] have stressed the importance of monomer activity when simple surfactants are used as demulsifiers. For a commercial demulsifier the interfacial tension between oil/water seems to pass through a minimum for NaCl concentrations between zero and 1 M. According to Menon and Wasan,[24] AOT has been found to have a CMC at approximately 300 ppm in a water/oil system with asphaltenes present. This means that in our destabilization tests, where the concentration of AOT is up to 100 ppm, the results correspond with the conclusions from Aveyard.[120,121] Fluorinated surfactants have been investigated for systems containing both distilled water and synthetic formation water.[130] The results showed that the resolution of water was faster when synthetic formation water was used as the dispersed phase. The explanation for this might be in accordance with Aveyards conclusions.[120,121] In the case of Triton N-42 the influence of salt is not believed to be significant since this is a nonionic surfactant, and its phase behaviour is not so sensitive to the addition of salt.

The mechanism behind destabilization with macromolecules is very dependent on the size of the molecule. Polymers of lower molecular mass can show a strong affinity to the oil/water interface, adsorb irreversibly and destabilize in this way. Another route of destabilization is flocculation. Flocculation is an aggregation process in which droplets form three-dimensional clusters, each droplet retaining its individual identity. In order to model the importance of the flocculation in destabilization of our model systems, we have chosen to investigate α-alumina dispersions. In this case we have dispersed 0.2 wt% hydrophilic Al_2O_3 in decane and tested the influence of the polymeric additives on the stability of these dispersions. The particle size of the Al_2O_3 was 40 μm. This solid particle is representative of the water droplets in the water-in-crude oil emulsions with respect to size and hydrophilicity. Hence, the adsorption onto these particles will be governed by similar mechanisms as the adsorption onto the water droplets in the true crude oil systems. However, in addition there might be contributions caused by specific interactions between the polar part of the polymers and the alumina particles. The highest flocculation efficiency at these concentrations is shown by the Agefloc polymers. It should be mentioned that the flocculation tendency at 30 seconds is reproduced after 60 and 90 seconds. Hence, there is no observed time dependence after 30 seconds. The observed flocculation is rapid and followed by sedimentation. The recorded adsorbance will consequently decrease upon this process. These findings correspond with the destabilization tests within reasonable limits. The Agefloc polymers were shown to be very efficient both as flocculants and destabilizers. They reduced the interfacial tension to some degree from the level of the indigenous crude oil system. Obviously they can adsorb at the oil/water interface and in this way reduce the stability by complete or partial replacement of the film. It is of course difficult to verify that the same kind of driving forces responsible for the adsorption of the Agefloc polymers in the system containing alumina particles (in decane) also apply to the system of water droplets (in crude oil). With interfacial tensions available for the solid/liquid interface in the case of the particles, a qualitative comparison with the emulsified system would hence be possible. Most likely it is not a direct affinity to the interface that is the driving force, but an entropy effect originating from polymer/solvent interactions that will account for the adsorption in both systems.

4.4. Electrocoalescence by Means of Dielectric Spectroscopy

The group in Bergen has during the last years developed a technique for determination of stability of emulsions. The method is based on dielectric spectroscopy, which is a very fast measuring technique, and which is sensitive to the amount of water in the system as well as the interaction between/among droplets. This makes it suitable tool for investigation of time dependent processes, like destabilization processes in emulsions.[146,154-156]

4.4.1. Dielectric Spectroscopy. The permittivity of a substance is defined as $\varepsilon^* = 1 + P/\varepsilon_0 E$, where P is the polarization due to the applied electric field E and ε_0 is the permittivity of free space. Depending on the origin the polarization, at higher frequencies, may not be able to follow the applied ac field $E = E_0^{i\omega\tau}$ and a phase lag will appear between the polarization and the field E. This can be expressed by means of complex permittivities as

$$\varepsilon^*(\omega) = \varepsilon'(\omega) - i\varepsilon''(\omega) \qquad (4.4\text{-}1)$$

where the imaginary part ε" is also called the loss factor.

Normally the decay in polarization due to relaxation of the system is following an exponential law $P(t) = P_0 (1 - e^{-t/\tau})$. Inserting this into Eq. (4.4-1) one obtains the Debye equations

$$\varepsilon^*(\omega) = \varepsilon_\infty + \frac{\varepsilon_s - \varepsilon_\infty}{1 + i\omega\tau} \tag{4.4-2}$$

or

$$\varepsilon'(\omega) = \varepsilon_\infty + \frac{\varepsilon_s - \varepsilon_\infty}{1 + \omega^2\tau^2}, \quad \varepsilon''(\omega) = \varepsilon_\infty + \frac{\varepsilon_s - \varepsilon_\infty\, \omega\tau}{1 + \omega^2\tau^2} \tag{4.4-3}$$

where ε_S is the static permittivity, ε_∞ the limiting permittivity at high frequencies and τ the dielectric relaxation time. The maximum in the dielectric dispersion occurs at $\omega = 1/\tau$.

In order to fit the dielectric spectrum different kinds of model functions can be used. Normally a simple Debye function or a sum of several Debye functions, or a Cole-Cole function can be used.[133-137]

Contrary to traditional spot frequency measurements the time domain technique makes it possible to cover a large frequency range in one single measurement. The Dielectric Time Domain Spectroscopy (TDS) is based on the study of the change in the shape of a fast-rising pulse propagating in a coaxial line when the sample is inserted into the line. From Fourier analysis it is known that the response pulse will contain information on the influence of the dielectric (i.e., its permittivity) over the entire frequency range up to some limiting frequency determined by the rise time of the step pulse. A necessary criterion for the characterization of a dielectric dispersion by means of this technique is that the pulse shapes are monitored in a time window longer than the relaxation time of the system under study.

Figure 13 shows the principle of a TDS spectrometer based on the total reflection method.[138] The pulse generator generates step pulses with a short rise time, <25 ps, which propagates in a coaxial line. The pulse is reflected from a sample placed at the end of an open–ended coaxial line. The sampling oscilloscope registers the influence of a dielectric sample on the shape of the reflected pulse. Finally a computer calculates the Fourier transforms and solves the reflection coefficient equations. From the reflection coefficient the permittivity as a function of frequency can be calculated and the whole spectrum presented. Figure 14 shows the permittivity spectrum of a w/o emulsion.

Instead of utilizing the reflection method also transmission methods can be used. Corresponding equations must be solved also in this case.

We have recently extended the dielectric set-up to include measurements of systems that are exposed to high external electric fields, in order to monitor the electrocoalescence mechanism of w/o emulsions. In addition to the fast-rising ac step pulse, an external electric dc field is applied through a bias tee (Picoseconds Pulse Labs, 5530A), as shown in Figure 13. The bias tee includes a dc block which allows the application of a voltage over the sample cell while it passes the fast-rising step pulse used to measure the permittivity without appreciably degrading the pulse.

The pioneering impact in the field of high electric fields and emulsified systems was done by Cottrell, who also had the first patents as well as the first electrical coalescers in

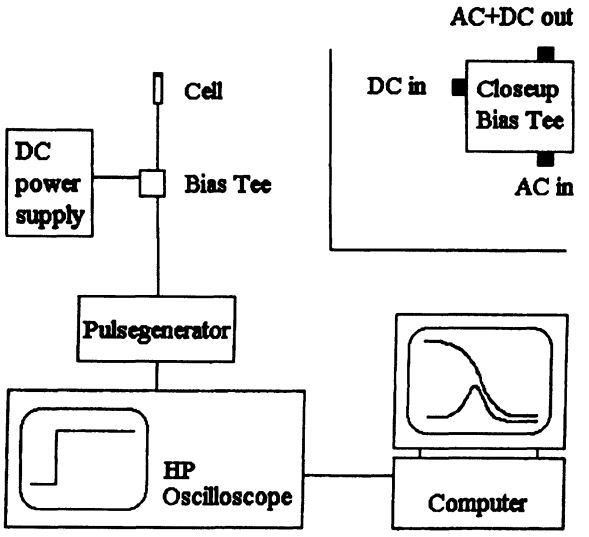

Figure 13. Experimental setup for dielectric measurements according to the time-domain principle. For emulsion stability measurements (electrocoalescence) the external DC power supply is used.

an oil field.[1,3] In recent years electrocoalescence has been combined with a lot of experimental techniques.[139-145]

Dielectric spectroscopy has proven to be an appropriate experimental technique for investigating w/o emulsions. The conducting water droplets dispersed in an oil resemble dipoles. The time domain dielectric spectroscopy technique is fast, and hence suitable for investigations of systems that change with time, such as w/o emulsions. In order to study

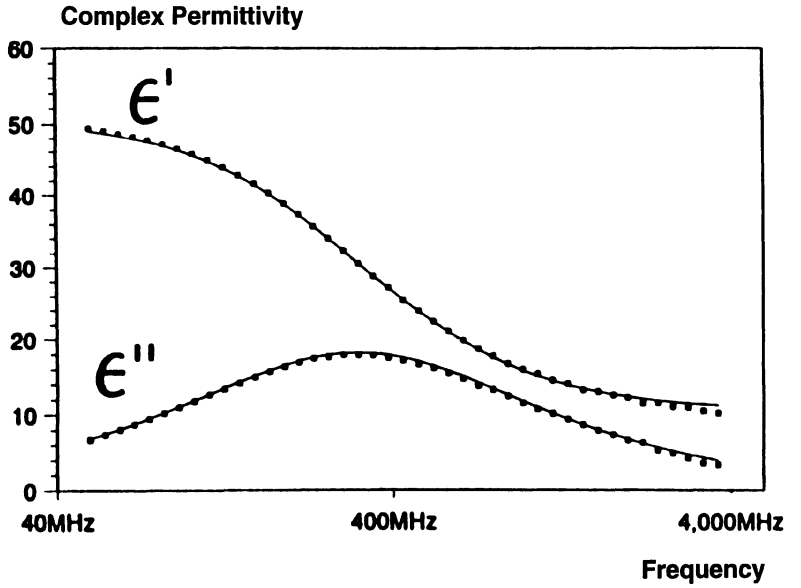

Figure 14. Permittivity spectrum of a water-in-oil emulsion (water content, 40 vol%; salt concentration 5 w% NaCl). The squares are experimental points and the solid line represents a fit to Eq. 4.4-2.

such effects we have equipped our spectrometer with an external power supply (Figure 13). This instrumentation enables us to study electrocoalescence in w/o emulsions.

When a high electric field is applied to a w/o emulsion the ions inside the emulsion droplets tend to orient themselves in the direction of the electric field. The maximum value of the potential decrease over the separating films will be found if the droplets orient themselves parallel to the electric field. At low field strengths, the applied field is not high enough to induce coalescence. Hence, when the electric field is switched off the system returns to a random distribution of the aqueous droplets, and the system shows a reversibility of the dielectric parameters. However, when the external electric field exceeds a critical value, E_{cr}, the membrane protecting the aqueous droplets ruptures and a coalescence of droplets takes place.[146]

The emulsions studied include w/o model emulsions stabilized by nonionic surfactants as well as interfacially active crude oil compounds and true water-in-crude oil systems.

In Bergen we have during the past years developed procedures to separate and isolate interfacially active components from crude oils. The basic idea behind the separation of the interfacially active fractions is to simulate interfacial conditions of relevance for true crude oil systems. In order to undertake more detailed studies of the stabilizing film, we have separated the components responsible for the emulsion stability into asphaltenes and resins[147] and undertaken chemical characterizations of these fractions.[148–153]

In order to visualize the importance of different parameters on the stability of model emulsions and crude oil emulsions, we undertook reduced factorial designs on these systems.[154-156] A reduced factorial design is an experimental design used to get a maximum of information about a system with as few experiments as possible. The two studies show that for a typical model system with parameters given in Figure 15 the volume fraction, conductivity and surfactant concentration are crucial parameters. Also cross terms including these variables are essential. For model crude oil systems (Figure 16) essentially two parameters are of importance, i.e., the level of asphaltenes and the nature of the continuous phase. This is further explored in the next figure where the stability is plotted vs. concentration of toluene in the oil phase. The reason for this behaviour is that the asphaltenes exist as small stabilizing particles in paraffinic hydrocarbons while they disaggregate in toluene. Hence they loose their stabilizing role (Figure 17).

5. CONCLUSIONS

Experimental characterizations of water-in-oil emulsions stabilized by asphaltenes and/or resins are reviewed. Several experimental techniques represent good alternatives for study of droplets and droplet size distributions in such systems, i.e. video enhanced microscopy, NMR self-diffusion and ultrasound measurements. The pros and cons of these techniques are briefly discussed. In order to understand the stabilizing mechanisms of water-in-crude oil emulsions new methods to isolate and separate the indigenous compounds are reported. By utilizing these separation techniques and dielectric spectroscopy to characterize the corresponding w/o emulsions valuable new information can be gathered. Also the Langmuir technique provides a good opportunity to directly investigate surface films of asphaltenes/resins and the compressibility of these films, which is essential for emulsion stabilization.

		Levels		
		-	+	centerpoints
Disperse phase (wt%)	X_1	40	80	60
Salinity (wt% NaCl)	X_2	1	4	2.5
Temperature (°C)	X_3	4	23	13.5
Time (h)	X_4	0.25	24	12
Surfactant (wt%)	X_5	2	4	3
Ratio, surfactants	X_6	0.25	0.75	0.5
Laponite (wt% of Φ_2)	X_7	0.5	2	1.25

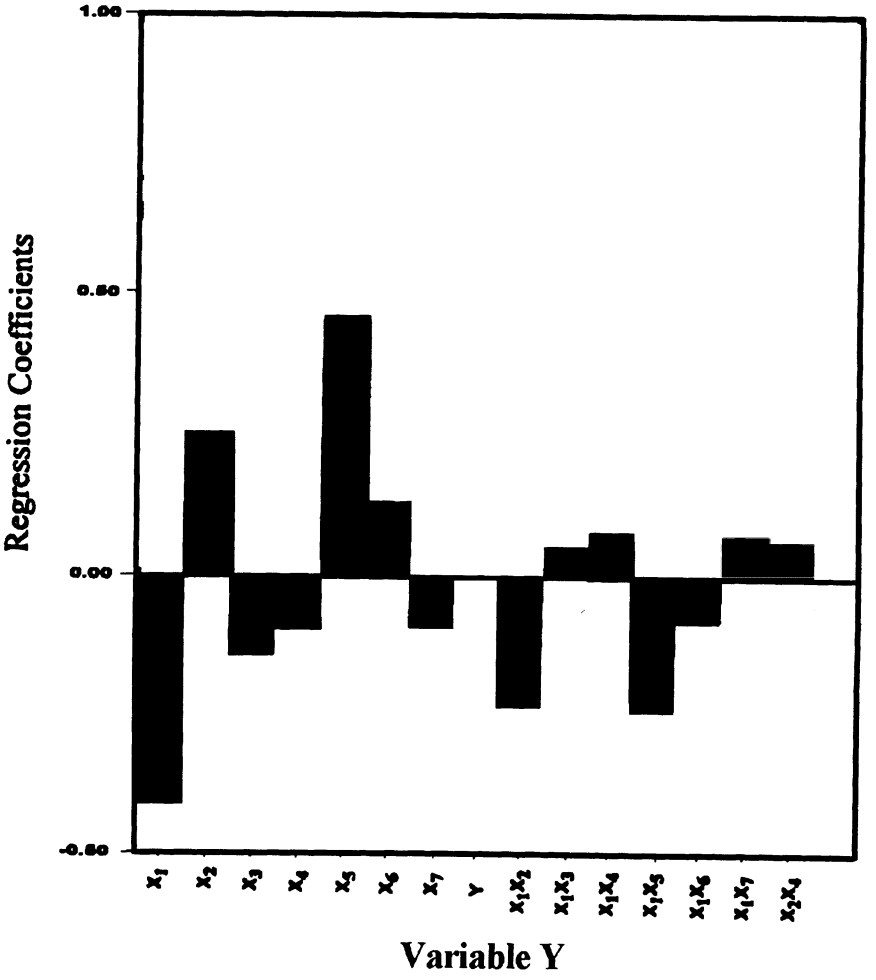

Figure 15. Definition of variables and their levels together with regression coefficients for electrocoalescence of model nonionic w/o emulsions based on reduced factorial design.

		Levels		
		-	+	centerpoints
Flocculation solvent	X_1	pentane	isooctane	50:50 mix.
Continuous phase	X_2	decane	toluene	50:50 mix.
Disperse phase (wt%)	X_3	30	60	45
Asphaltenes (wt%)	X_4	1	5	3
Salinity (wt%)	X_5	1	4	2.5
Temperature (°C)	X_6	4	23	13.5
Emulsification time (min.)	X_7	0.5	3	1.75

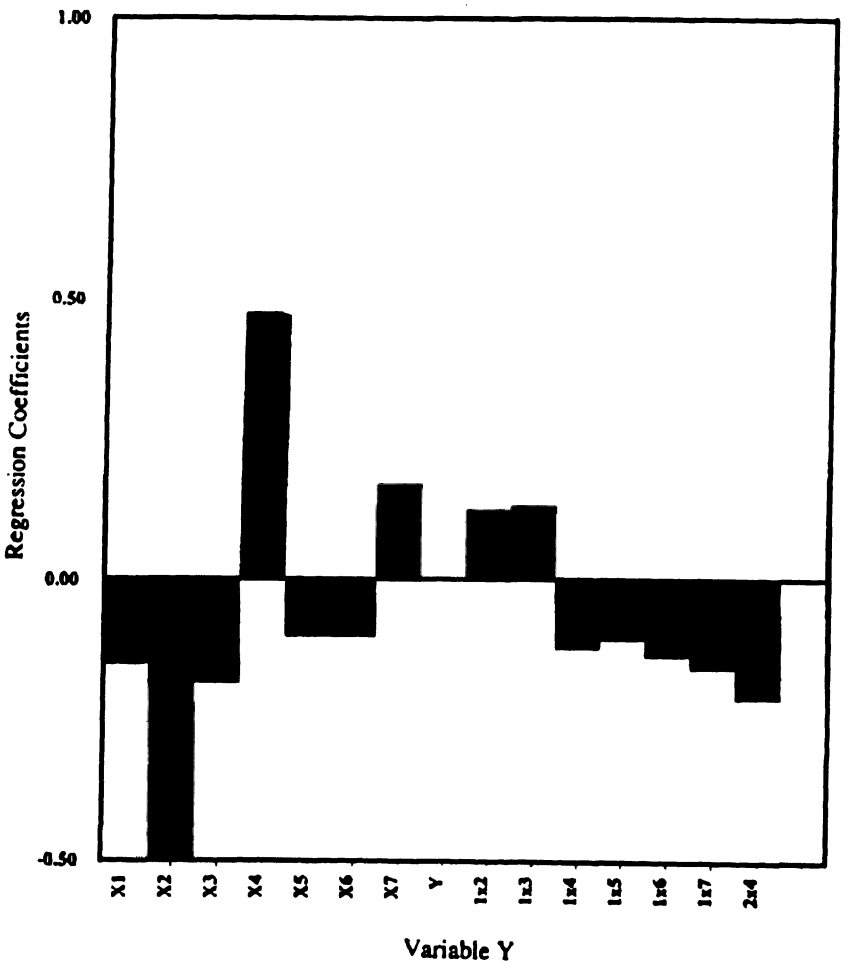

Figure 16. Definition of variables and their levels together with regression coefficients for electrocoalescence of model crude oil emulsions based on reduced factorial design.

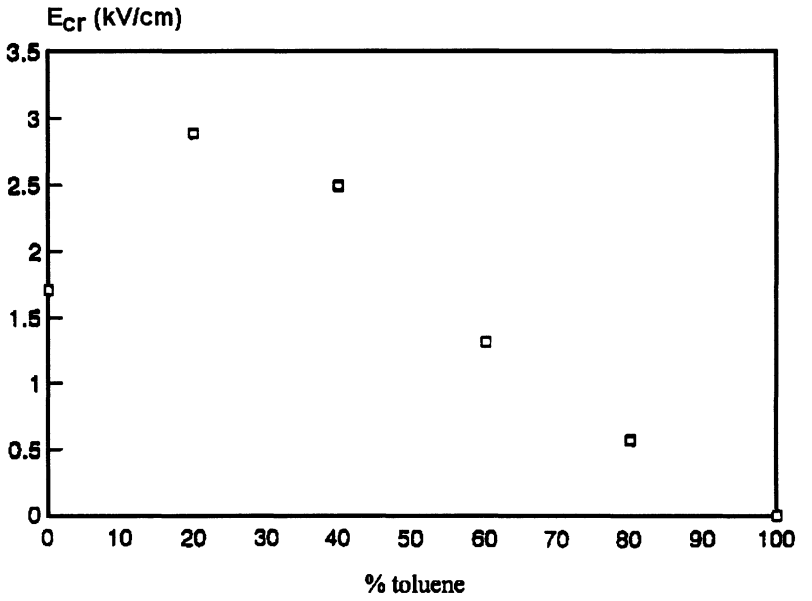

Figure 17. Emulsion stability (expressed as E_{cr}) of asphaltene stabilized (2%) model systems consisting of brine and a toluene/decane oil phase at varying tol/dec ratios.

ACKNOWLEDGMENTS

The technology programme FLUCHA financed by the Norwegian Research Council and oil industry is thanked for financial support to the Ph D candidates.

REFERENCES

1. F.G. Cottrell, *U.S. Patent 987,114*, (1911).
2. F.G. Cottrell and A. Cheever, *U.S. Patent 987,117*, (1911).
3. F.G. Cottrell and J.B. Speed, *U.S. Patent 987,115*, (1911).
4. F.G. Cottrell and J.B. Speed, *U.S. Patent 987,116*, (1911).
5. D.B. Dow, *U.S. Dep. Comm. Bull.*, 250, (1926).
6. G.B. Shea, *U.S. Bur. Mines Bull.*, 417, (1939).
7. A.S.C. Lawrence, *Chem. Ind. (London)*, **39**, 615, (1948).
8. J.L. Wiggins, *Pet. Eng. Int.*, **29B**, 47, (1957).
9. F. Steinhauff, *Petroleum (London)*, **25**, 294, (1962).
10. P.L. Bansbach, *Oil Gas J.*, **52**, 87, (1970).
11. C.M. Blair, *Chem. Ind. (London)*, 538, (1960).
12. J. E. Strassner, *J. Pet. Technol,*. **20**, 303, (1968).
13. A.A. Petrov and S.S. Blatova, *Technol. Toplio, Masel*, **17**, 32, (1974).
14. T.J. Jones, E.L. Neustadter and K.P. Whittingham, *J. Can. Pet. Tech.*, **17**, 100, (1978).
15. G.D.M. MacKay, A.B. McLean, O.J. Betancourt and B.D Johnson, *I. Inst. Pet.(London)*, **59**, 164, (1973).
16. E. Papirer, C. Bourgeois, B. Siffert and H. Balard, *Fuel*, **61**, 732, (1982).
17. H.N. Dunning, J. W. Moore and M. O. Denekas, *In. Eng. Chem.*, **45**, 1759, (1953).
18. H.N. Dunning, *J. Colloid Int. Sci.*, **8**, 279, (1953).
19. G.P. Canevari, *Proceedings of Joint Conference on Prevention and Control of Oil Spills*, API, New York, (1969).

20. A.L. Birdie, T.H. Wanders, W. Zegveld and H.B. van der Heide, *Marine Pollut. Bull.*, **11**, 343, (1980).
21. P. Becker (Ed.), "*Encyclopedia of emulsion technology. Vol. 1*", Marcel Dekker, New York, (1983).
22. L. Lissant (Ed.), "*Emulsions and emulsion technology. 2 & 3*", Marcel Dekker, New York, (1976 & 1984).
23. J. Sjöblom (Ed.), "*Emulsions- A fundamental and practical approach*", NATO ASI Series, Kluwer Academic Publishers, Dordrect, (1992).
24. V.B. Menon and D.T. Wasan, *Colloids Surfaces*, **19**, 89, (1986).
25. V.B. Menon and D.T. Wasan, *Colloids Surfaces*, **19**, 107, (1986).
26. V.B. Menon and D.T. Wasan, *Colloids Surfaces*, **23**, 353, (1987).
27. V.B. Menon, A.D. Nikolov and D.T. Wasan, *J. Colloid Int. Sci.*, **124**, 317, (1988).
28. V.B. Menon and D.T. Wasan, *Colloids Surfaces*, **29**, 7, (1988).
29. H. Hassander, B. Johansson and B. Tørnell, *Colloids Surfaces*, **40**, 93, (1989).
30. S. Levine and E. Sanford, *Can. J. Chem. Eng.*, **62**, 258, (1985).
31. S. Levine, B. Bowen and S.J. Partridge, *Colloids Surfaces*, **38**, 325, (1989).
32. S. Levine, B. Bowen and S.J. Partridge, *Colloids Surfaces*, **38**, 345, (1989).
33. S. Friberg, P.O. Jansson and E. Cederberg, *J. Colloid Int. Sci.*, **55**, 614, (1976).
34. S. Friberg, *J. Colloid Int. Sci.*, **37**, 291, (1971).
35. S. Friberg, L. Mandell and M. Larsson, *J. Colloid Int. Sci.*, **29**, 155, (1969).
36. S. Friberg and C. Solans, *Langmuir*, **2**, 121, (1986).
37. D.D. Eley, M.J. Hey and J.D. Symonds, *Colloids Surfaces*, 32, 103, (1988).
38. D.G. Thompson, A.S. Taylor and D.E. Graham, *Colloids Surfaces*, 15, 175, (1985).
39. E.J. Johansen, I.M. Skjærvø, T. Lund, J. Sjöblom, H. Söderlund and G. Boström, *Colloids Surfaces*, **34**, 353, (1988).
40. A.K. Mahlorta and D.T. Wasan in (I. B. Ivanov (Ed.)) "*Thin liquid films, Fundamentals and Applications*", Surfactant Sci. Series, Vol.29, Marcel Dekker, New York, p. 829, (1988).
41. J. Sjöblom, L. Mingyuan, H. Høiland and E.J. Johansen, *Colloids Surfaces*, **46**, 127, (1990).
42. K.G. Nordli, J. Sjöblom, J. Kizling and P. Stenius, *Colloids Surfaces*, **57**, 241, (1991).
43. L. Mingyuan and J. Sjöblom, *J. Disp. Sci. and Tech.*, **12**, 303, (1991).
44. K.G. Nordli Børve, J. Sjöblom and P. Stenius, *Colloids Surfaces*, **63**, 241, (1992).
45. L. Mingyuan, J. Sjöblom and A.A. Christy, in (J. Sjøblom (Ed.)),"*Emulsions- A Fundamental and Practical Approach*",. NATO ASI Series, Kluwer Academic Publishing, Dordrecht, p. 157, (1992).
46. J. Sjöblom, L. Mingyuan, A.A. Christy and T. Gu, *Colloids Surfaces*, **66**, 55, (1992).
47. H. Ebeltoft, K.G. Nordli Børve, J. Sjöblom and P. Stenius, *Progress in Coll. Pol. Sci.*, **88**, 131, (1992).
48. J. Sjöblom, H. Söderlund, S. Lindblad, E.J. Johansen and I.M. Skjærvø, *Colloid Polym. Sci.*, **268**, 389, (1990).
49. Bradbury, S., Microscopy and Analysis, May 1990.
50. Miller, D.D., Bellare, J.R., Evans, D.F., Talmon, Y., Ninham, B.W., J. Phys. Chem. 1987, 91, p. 681.
51. Shaw, D.J.: Introduction to Colloid and Surface Chemistry, 4th Ed, (1992) Butterworth-Heinemann Ltd.
52. Allen, T.: Particle Size Measurement, (1968) Chapman and Hall.
53. Orr, C., in *Encyclopedia of emulsion technology. Vol.3: Basic theory, measurement, applications*; Becher, P., Ed.; Marcel Dekker: New York, 1988; Vol. 3, pp 137–169.
54. Jokela, P., Fletcher, P.D.I., Aveyard, R., Lu, J.-R., J. Coll. Interf. Sci., 1990, Vol. 134, No. 2, p. 417.
55. Mason, S.L., May, K., Hartland, S., Colloids and Surfaces A, 1995, Vol 96, p. 85.
56. Holt, Ø., Saether, Ø., Sjöblom, J., Dukhin, S.S., and Mishchuk, N.A., Coll. Surf. A, 123–124 (1997) 195–207.
57. Videomicroscopic Investigation of the Coupling of Reversible Flocculation and Coalescence. Sjöblom, J., Saether, Ø., Verbich, S., Mishchuk, N., and Dukhin, S., Coll. Surf., submitted.
58. P.T. Callahan, K.W. Jolley and R.J. Humphrey, J. Coll. Int. Sci., 93, 521, (1983).
59. K. Packer and C.J. Rees, J. Coll. Int. Sci., 40, 206, (1971).
60. I. Lönnquist, A. Khan and O. Söderman, J. Coll. Int. Sci., 144, 401, (1991).
61. O. Söderman, I. Lönnquist and B. Balinov, in (J. Sjöblom, Ed.) "Emulsions - A Fundamental and Practical Approach", NATO ASI Series, Kluwer Academic Publishing, Dordrect, p.239, (1992).
62. D.C. Douglas and D.W. McCall J. Phys. Chem, 62, 1102, (1958).
63. B.Balinov, B. Jönsson, P. Linse and O. Söderman, J. Magnetic Resonance, Vol. 104, No. 1 (1993) p. 17.
64. K-.E. Frøysa and Ø. Nesse, "*Ultrasonic Characterization of Emulsions*", in "*Emulsions and Emulsion Stability*" (J. Sjöblom, ed.), Surfactant Science Series, Volume 61, Marcel Dekker, Inc. New York (1996).
65. R. Pal, Colloids Surfaces A: Physicochem. Eng. Aspects, 84, 141 (1994).
66. D.J. McClements, Adv. Colloid Interface Sci. 37, 33 (1991).
67. Dukhin, A.S., Goetz, P.J., Langmuir, **12**, 18 (1996), pp. 4336–4344.
68. Dukhin, A.S., Goetz, P.J., Langmuir, **12**, 21 (1996), pp. 4987–4997.

69. Dukhin, A.S., Goetz, P.J., Hamlet, C.W., Langmuir, **12**, 21 (1996), pp. 4998–5003.
70. A.W. Wood, "A textbook of Sound", Bell, London, (1911).
71. R.J. Ulrich, J. Appl. Phys. 18, 983 (1947).
72. M.R.J. Wyllie, A.R. Gregory and G.H.F. Gardner, Geophysics 23, 459 (1957).
73. P.C. Waterman and R. Truell, *J. Math. Phys.* **2,** 512 (1961).
74. R.J. Ulrich and W.S. Ament, *J. Acoust. Soc. Am.* **21,** 115, (1949).
75. Speight, J.G., (1991) The Chemistry and Technology of Petroleum, Marcel Dekker, New York, pp 329–340.
76. Schildberg, Y., Sjöblom, J., Christy, A.A., (1995) *J. Dispersion Sci. Technol.* 16 (7):575–605.
77. Koots, J.A., Speight, J.G., (1975) *Fuel* 54:179–184.
78. Midttun, Ø., Sjöblom, J., Kvalheim, O.M., A Multivariate Study of Diffuse Reflectance Infrared Profiles of Resin Fractions From Crude Oils. Submitted to *Progress in Colloid and Polymer Science* (1997).
79. Koots, J.A., Speight, J.G., (1975) *Fuel* 54:179–184.
80. Mingyuan, L., Christy, A.A., Sjöblom, J. (1992) In: Sjöblom, J. (ed) Emulsions - a fundamental and practical approach. Kluwer, NATO ASI series, C 363:157–172.
81. Christy, A.A., Dahl, B., Kvalheim, O.M., (1989) *Fuel* 68:430–435.
82. Christy, A.A., Kvalheim, O.M., Høiland, H., (1994) *Chemometrics and Intelligent Laboratory Systems* 23:197–204.
83. Yen, T.F., Wu, W.H., Chilingar, G.V., (1984) *Energy Sources*, 7:203–235.
84. Johnson, R.A., Wichern, D.W., (1992) Applied multivariate statistical analysis. Prentice Hall, New Jersey, pp 356–395.
85. J. Sjöblom, H. Söderlund, S. Lindblad, E.J. Johansen and I.M. Skjærvø, Colloid Polym. Sci., 268, 389, (1990).
86. Sheu, E.Y., De Tar, M.M., Storm, D.A., Fuel, **71** (1992) 277.
87. Singh, B.P., Pandey, B.P., Indian J. Technol., **29** (1991) 443.
88. Ronvaux-Vankeerbergen A., Thyrion, F.C., Fuel, **68** (1989) 793.
89. Moschopedis, S.E., Speight, J.G., Fuel, **54** (1975) 210.
90. Moschopedis, S.E., Speight, J.G., Fuel, **57** (1978) 235.
91. Tort, F., Andersen, S.I., Proc. 1st World Conference on Emulsions, Paris, 1993.
92. G.L. Gains Jr. (ed.)"Insoluble Monolayers at Liquid-Gas Interfaces", Wiley, NY, 1966.
93. R.H. Doremus, B.W. Roberts and D. Turnbull (eds.), Growth and Perfection of Crystals", Wiley, NY, 1958.
94. D.J. Crisp, J. Colloid Sci., **1** (1946) 49.
95. Y. Schildberg, J. Sjöblom, A.A. Christy, Volle, J-L. and Rambeu, O., J. Disp. Sci. and Technology **16(7)** (1995) 575.
96. B. Siffert, I. Bourgeois and E. Papierer, Fuel, 63, 834, (1984).
97. H.K. Christenson and J.N. Israelachvilli, J. Coll. Int. Sci., 119, 194, (1987).
98. J. Fang and H.K. Christenson, J. Disp. Sci. and Technology, 11, 97, (1990).
99. A.H. Brown, Chem. Ind., 30, 990, (1968).
100. A.J.S. Liem and D.R. Woods, "Review of Coalescence Phenomena", AIChE Symp. Ser., 70, 8, (1974).
101. O. Reynolds, Phil. Trans. R. Soc. (London), A177, 157, (1886).
102. S.P. Frank and K.J. Mysles, J. Phys. Chem., 66, 190, (1960).
103. Z. Zapryanov, A.K. Malhorta, N. Aderangi and D.T. Wasan, Int. J. Multiphase Flow, 9(2), 105, (1983).
104. C.Y. Lin and J.C. Slattery, AIChE J., 28(1), 147, (1982).
105. C.Y. Lin and J.C. Slattery, AIChE J., 28(5), 786, (1982).
106. A.K. Malhorta, Ph.D. Thesis, Illinois Institute of Technology, Chicago, (1984).
107. C.V. Sternling and L.E. Scriven, AIChE J., 5, 514, (1959).
108. A.J. de Vries, Recl. Trav. Chim., 77, 383, 441, (1958).
109. S.S. Lang, Ph.D. Thesis, University of California, (1962).
110. A. Schedluko and E. Manner, Trans. faraday Soc., 64, 1123, (1968).
111. A. Vrij, Disc. Faraday Soc., 42, 23, (1966).
112. H. Sonntag and K. Strenge, "Coagulation and Stability of Disperse Systems", Halstead-Wiley, New York, (1969).
113. S.E. Sadek and C.D. Hendrick, Ind. Eng. Chem. Fundam., 13(2), 139, (1979).
114. A.E. Walton, Filtr. Sep., 15(1), 68, (1974).
115. V.B. Menon and D.T. Wasan in (P. Becker, (Ed.)), "Encyclopedia of emulsion technology. Vol. 2: Applications", Marcel Dekker, New York, p. 1, (1985).
116. R. Fiocco, U.S. Patent 3,536,529, (1970).
117. M.A. Krawczyk, Ph.D. Thesis, Illinois Institute of Technology, Chicago, (1990).
118. D.T. Wasan, K. Sampath and N. Aderangi, AIChE Symp. Ser., 76, 93, (1980).

119. D.T. Wasan, N.F. Djabbarah, M.K. Vora and S.T. Shah, Lect. Notes Phys., 105, 205, (1979).
120. R. Aveyard, P.B. Binks, P.D.I. Fletscher and J.R. Lu, J. Colloid Interface Sci., 139, 128 (1990).
121. R. Aveyard, P.B. Binks, P.D.I. Fletscher, R. Ye and J.R. Lu, in (J. Sjöblom (Ed.)), "Emulsions A Fundamental and Practical Approach", NATO ASI Series, Kluwer Academic Publishing, Dordrecht, p. 97, (1992).
122. M.A. Krawczyk, D.T. Wasan and S S. Chandrashekar. Ind. Eng. Chem. Res., 30, 367 (1991).
123. D.T. Wasan, in (J. Sjöblom (Ed.)), "Emulsions - A Fundamental and Practical Approach", NATO ASI Series, Kluwer Academic Publishing, Dordrecht, p. 283, (1992).
124. R.C. Little, Environ. Sci. Technol., 15, 1184, (1981).
125. P.D. Berger, C.Hsu and J.P. Arendell, Paper presented at the SPE International Symposium on Oilfield Chemistry, San Antonio, February, (1987).
126. P. Ekwall, in (G. H. Brown, Ed.) "Advances in Liquid Crystals", 1:1, Academic Press, New York, (1975).
127. J. Sjöblom, Thesis, Åbo Akademi, Åbo, Finland, (1982).
128. T. Wörnheim, Thesis, The Royal Institue of Technology, Stockholm, Sweden, (1986).
129. J.O. Saeten, J. Sjöblom and B. Gestblom, J. Phys. Chem., 95, 1449, (1991).
130. O. Urdahl, A.E. Møvik and J. Sjöblom, Coll. Surf. A, 74 (1993) 293.
131. H.B. Clark, M.T. Pike and G.L. Rengel, Pet. Tech., 7, 1565, (1982).
132. H.B. Clark, M.T. Pike and G.L. Rengel, SPE Paper 7894, Presented at the AIME International Symposium on Oilfield and Geothermal Chemistry, Houston, Texas, (1979).
133. N.E. Hill, W.E. Vaughan, A.H. Price and M.Davies, "Dielectric Properties and Molecular Behaviour" Van Norstrand, London, 1969.
134. J.B. Hasted, "Aqueous Dielectrics" Chapman & Hall, London, 1973.
135. E.H. Grant, R.J. Sheppard and G.P. South, "Dielectric Behaviour and Biological Molecules in Solution" Clarendon Press, Oxford, 1978.
136. P. Debye, "Polar Molecules", Reinhold New York, 1929.
137. K.S. Cole and R.H. Cole, J. Phys. Chem. 9 (1941) 341.
138. B. Gestblom and E. Noreland, J. Chem. Phys. 81 (1977) 782.
139. S.E. Taylor, Inst. Phys. Conf. Ser. 118, 185 (1991).
140. T.J. Williams and A.G. Bailey, IEEE Trans. Ind. Appl. IA-22, 536 (1986).
141. S.E. Taylor, Colloids Surfaces 29, 29 (1988).
142. C.A.R. Pearce, British J. Appl. Phys. 5, 136 (1954).
143. U. Zimmermann, G. Pilwat and F. Riemann, Biophys. J. 14, 881 (1981).
144. U. Zimmermann, Biochim. Biophys. Acta, 694, 227 (1982).
145. A.H. Brown and C. Hanson, Trans. Faraday Soc. 61, 1754 (1965).
146. B. Gestblom, H. Førdedal and J. Sjöblom, J. Dispersion Sci. Technol. 15, 449 (1994).
147. J. Sjöblom, O. Urdahl, H. Høiland, A.A. Christy and J. Johansen, Progr. Colloid Polym. Sci. 82, 131 (1990).
148. J. Sjöblom, Li Mingyuan, T. Gu and A.A. Christy, Colloids Surfaces, 66, 55 (1992).
149. K.G. Nordli, J. Sjöblom, J. Kizling and P. Stenius, Colloids Surfaces, 57, 83 (1991).
150. K.G. Nordli, J. Sjöblom and P. Stenius, Colloids Surfaces, 63, 241 (1992).
151. J. Sjöblom, Li Mingyuan, A.A. Christy and H.P. Rønningsen, Colloids Surfaces A, 96, 261 (1995).
152. H.P. Rønningsen, J. Sjöblom and Li Mingyuan, Colloids Surfaces A, 97, 119 (1995).
153. S.E. Friberg, in J. Sjöblom (Ed.), Emulsions - A Fundamental and Practical Approach, NATO ASI Series C 363, Kluwer, Dordrecht, 1992, p.1.
154. H. Førdedal, E. Nodland, J. Sjöblom and O.M. Kvalheim, J. Colloid Interface Sci. 173, 396, (1995).
155. H. Førdedal, Y. Schildberg, J. Sjöblom and J-L. Volle, Colloids Surfaces A, 106, 33 (1996).
156. H. Førdedal, Ø. Midttun, J. Sjöblom, O.M. Kvalheim, Y. Schildberg and J-L. Volle, J. Colloid Interface Sci. 182, 117 (1996).

Chapter XII

THE ROLE OF PETROLEUM ASPHALTENES IN THE STABILIZATION OF WATER-IN-OIL EMULSIONS

Joseph D. McLean, P. Matthew Spiecker, Andrew P. Sullivan, and Peter K. Kilpatrick*

Department of Chemical Engineering
North Carolina State University
Raleigh, North Carolina 27695-7905

1. INTRODUCTION

An emulsion is a thermodynamically unstable dispersion of two immiscible liquids, the droplets of which, when stable, are slow to flocculate and coalesce. Emulsions are formed quite often in industrial processes and can be both desirable and undesirable. Examples of useful emulsions occur in foods, cosmetics, pharmaceuticals, and agricultural products. Emulsions are also found in the petroleum industry where they are typically undesirable and result in high pumping costs, reduced throughput, and special handling equipment.[1] Crude oil is found in reservoirs along with water or brine. During oil production, water is often coproduced.[2–5] Water is also injected into the crude to wash out contaminants or is used as steam to improve fractionation.[6] While contamination of water when processing crude oil frequently leads to emulsions of the oil-in-water type,[7] water-in-crude oil emulsions are much more prevalent in the petroleum industry.[8–11] Figure 1 illustrates the various types of water-crude oil emulsion systems. Crude oil is typically and is produced as a water-in-crude oil (w/o) emulsion. When crude oil is spilled on the sea and agitated, high viscosity, stable w/o emulsions are formed. During the refining of crude oil, emulsions of all types are formed, although the mechanisms of stabilizing o/w emulsions are very different from those responsible for w/o emulsion stability.

The location of several emulsions in the refinery are depicted schematically in Figure 2. The desalter reduces the amount of emulsified water in the bulk of the crude and

* To whom correspondence should be addressed. Phone: (919) 515-7121; Fax: (919) 515-3465; peterk@eos.ncsu.edu

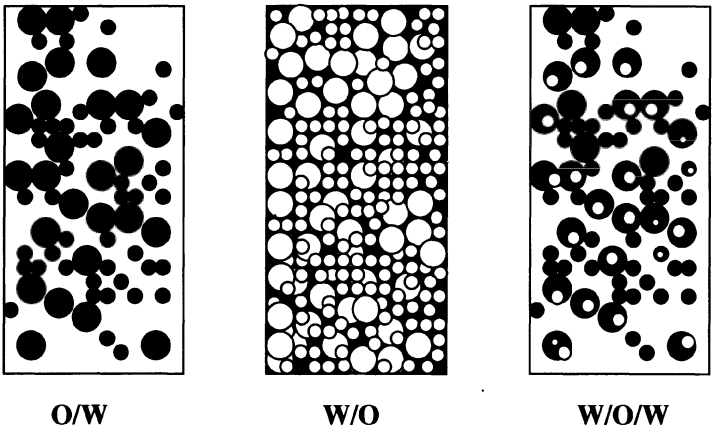

Figure 1. Schematic illustration of emulsion types encountered in crude oil-water systems.

generates a stable emulsion rag layer with a small inventory of the processed crude. As a preliminary step during refinery treatment, crude oils are normally desalted to remove species such as chloride salts which poison refinery catalysts and promote corrosion of processing units. In this process, typically 5–10% of fresh water ('wash water') is deliberately emulsified into the oil to contact hydrophilic solids, which then partition into the aqueous droplets.[11,12] These desalter emulsions are typically of the w/o variety and must subsequently be broken down to recover the "clean" crude oil. Also, whenever these mixtures pass through pipes with bends, valves, and chokes, emulsification of the aqueous phase

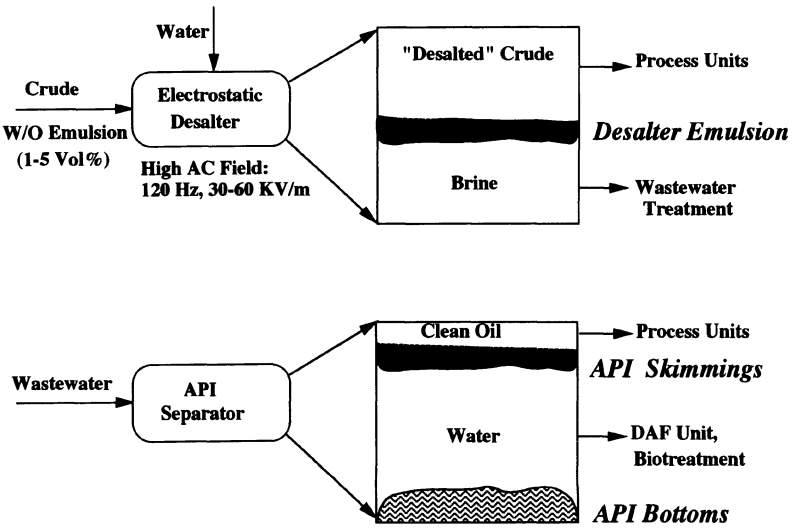

Figure 2. Schematic of the locations in refineries in which emulsions and sludges are observed. Top panel shows the desalter operation; bottom panel shows the API gravity separator, in which heavy sludges (API bottoms) and lighter emulsions (API skimmings) occur.

into the crude oil occurs due to turbulence.[5,13,14] These emulsions increase pumping and transportation expenses (owing to the higher viscosity and additional water present), cause corrosion of pipes, pumps, production equipment and distillation columns, and poison downstream refinery catalysts.[13] It is evident that crude oils have differing abilities to stabilize water-in-crude oil emulsions, but a considerable proportion of these petroleum emulsions are characterized by a rather remarkable stability and lead to significant sludge generation.[10] The space required to demulsify, the costs associated with additional equipment, the oil loss due to entrainment in the emulsion, and the problems associated with waste disposal, make emulsions a major problem for the petroleum industry.[5,14–18]

As mentioned, petroleum emulsions can also form subsequent to ocean borne oil spills.[19] The *Torrey Canyon* incident in 1967 (and many other crude spills over the years) was highlighted by the formation of a highly viscous and stable "chocolate mousse" emulsion, containing nearly 70% sea water by volume. The presence of wave action provided the necessary energy to generate an emulsion. Viscosity measurements showed that at a 70–30 water-oil ratio, sea water mousses may even solidify upon transfer to storage vessels or tanks. After a spill in Chedabucto Bay, viscosity increased from 700 poise for the crude oil, to 30,000 poise for a 40% water-in-oil emulsion. These emulsions are not responsive to the usual methods of oil clean up such as the use of sorbents or dispersants, burning, and pumping.[20]

The formation of stable emulsions and sludges in petroleum refineries comprised of water, crude oil, and solid particles has become a serious environmental concern. The magnitude of the problem has been documented in a 1982 API survey in which it was estimated that 830,000 tons of API separator sludge (see Figure 2), 718,000 tons of DAF float and 260,000 tons of slop oil emulsion solids were generated by the American petroleum refining industry each year. As the EPA continues to redefine specific petroleum-derived components which will be targeted as listed wastes, the need to minimize the formation of emulsions and the impetus to develop new methods for effective treatment of them have become more acute.

The mechanisms whereby emulsions are stabilized has been an active area of study this century. Ramsden,[21] Pickering,[22] Newman,[23] and Finkle et al.[24] reported on a variety of differing types of emulsions and speculated on the causes. This early work focused on establishing the presence of emulsions and investigating the factors which determine the type of emulsion formed (w/o or o/w). Despite years of research, there is still considerable uncertainty regarding the mechanisms governing the stability of oil-continuous emulsions. With crude oil emulsions, the importance of long-term stability of a rigid and protective film surrounding the water droplets is clear. The detailed properties of this film, together with a fundamental knowledge of the chemistry of the interfacially active components in the crude oil, are far from understood. In this chapter we will show the role that asphaltenes play in the formation and stability of water-in-crude oil emulsions. We will begin with an overview of the petroleum emulsion problem and what motivates research in this area. Next, we will examine possible mechanisms of stabilization of these petroleum emulsions. From this examination we will conclude that stabilization is brought about by the formation of an interfacial skin at the water droplet interface which prevents disperse phase coalescence. A review of the literature on the chemistry of asphaltenes and their interactions will suggest the concept of asphaltene aggregation. With this concept in mind, an analysis of experimental observations on the formation of crude oil emulsions and the interfacial films formed will support the idea that asphaltenic aggregates are important for stabilization through the formation of an interfacial skin. This idea will be shown more clearly in the next section, when experimental evidence of model oil systems is reviewed. In model oil systems all possible contributors to emulsion stabilization have been eliminated except

for the presence of asphaltenes and resins. The observation of stable emulsions in these cases and the similarity of these results with those of crude oil emulsions proves the importance of asphaltenes to water-in-crude oil emulsion stability through the formation of an interfacial skin composed of asphaltene aggregates.

2. MECHANISMS OF EMULSION STABILIZATION

Emulsions are stable when the disperse phase droplets do not coalesce. The coalescence process occurs in three steps. The first step begins with movement of the droplets toward each other through the continuous phase. Subsequently, droplets deform as they approach one another, forming a thin plane parallel film between them. Finally, this film thins to a critical thickness, below which the droplets coalesce.[25] At least four distinct mechanisms can be clearly identified for emulsion stabilization, or halting of this coalescence process, of oil-in-water (o/w) and water-in-oil (w/o) emulsions: (1) electrical double layer repulsion, (2) steric repulsion, (3) the Marangoni-Gibbs effect, and (4) rigid, cross-linked network formation of the adsorbed interfacial layers (see Figures 3 and 4).

The approach of emulsion droplets to one another may be resisted by electrostatic forces. Electrostatic forces consist of coulombic repulsion between two like charged objects and attractive van der Waals forces. These two forces are accounted for by the Derjaguin, Landau, Verwey, and Overbeek (DLVO) theory. A third force, Born repulsion, occurs at very small separation distances when electron clouds overlap.[1] In emulsion systems an electric double layer may form around the disperse phase droplets. While electric double layer repulsion is certainly important in o/w emulsions (Figure 3a), it does not play a large role in the stabilization of w/o systems due to the low dielectric constant of oil.[4,26] Evidence that the w/o emulsions reported here and elsewhere are not electrostatically stabilized is apparent from data for the amount of resolved water upon centrifugation of water-in-crude oil emulsions versus NaCl concentration in the aqueous phase (Figure 5). Increasing the salinity of the aqueous phase affects the formation of the double layer by dramatically reducing the Debye length. The resolved water data show insensitivity to the concentration of NaCl, except for an initial stabilizing effect at very low NaCl concentrations (< 0.5 %). This initial stabilizing effect with added salt is precisely the opposite effect one would expect if the emulsions were stabilized electrostatically. With double layer repulsion, one would expect destabilization upon addition of electrolyte and screening of Coulombic repulsion. The effect of added salt at low electrolyte concentrations is likely a screening of lateral repulsion between surface-active species adsorbed in the interface. This screening enables a higher density of surface-active species to pack in the interface which increases film rigidity and mechanical strength, and stabilizes the emulsions. At very high salt concentrations (>20%) the emulsions appear to destabilize to a small extent, but this effect is probably due to a restructuring of the solvent at the interface, not a changing double layer interaction.

Steric repulsion is a result of strong interactions between solvent and material adsorbed at the droplet interface. Due to this strong interaction, there are both enthalpic and entropic penalties brought about by the approach of one droplet to another.[27] The adsorbed species favor interaction with solvent rather than lateral interaction with other adsorbed species (Figure 3b). Mackor and van der Waals modeled the adsorption of molecules onto a pair of adsorbing planes, and based on comparisons with experimental data, concluded that steric stabilization must be responsible for the stabilization of some dispersions.[28] This phenomenon is common with emulsion droplets stabilized by nonionic polymers.

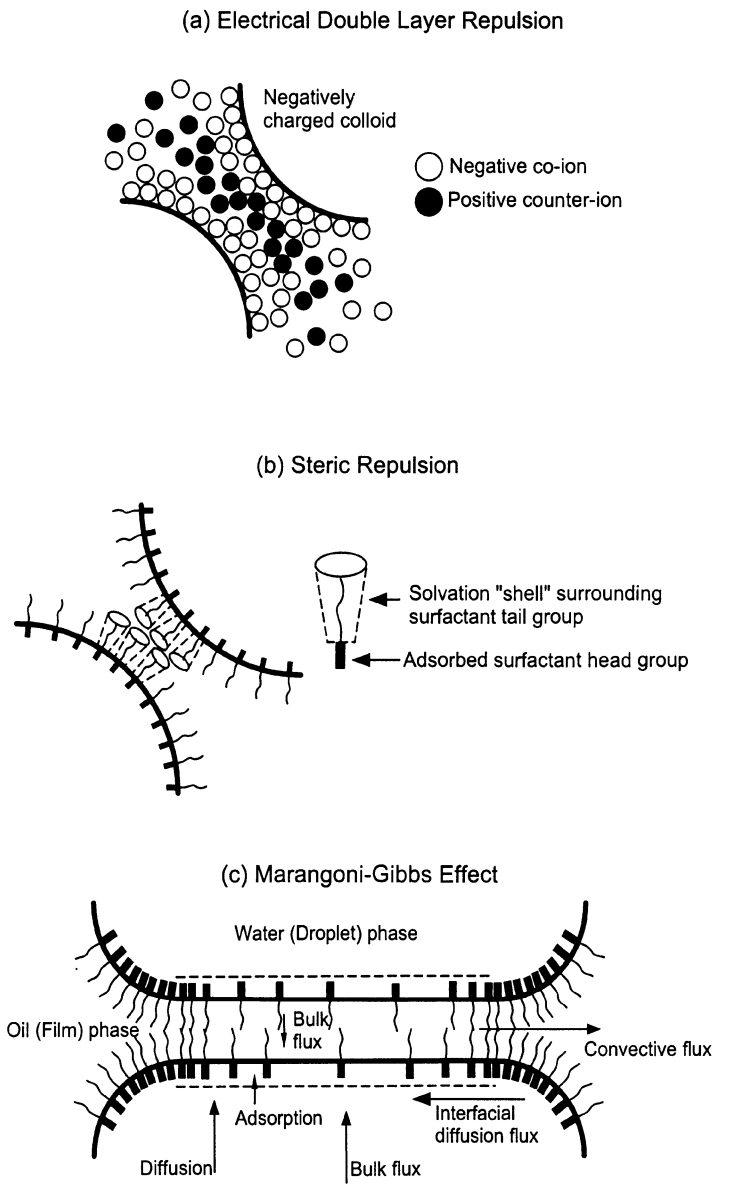

Figure 3. Depiction of emulsion stabilization mechanisms related to (a) electrostatic repulsion, (b) steric repulsion, and (c) Marangoni-Gibbs effects (after Wasan[31]).

Typically, the solvation energies required are high and reflective of hydrogen bonding. With asphaltene and resin adsorption to water droplets, it seems unlikely that the van der Waals energies or dispersion energies associated with saturated and aromatic hydrocarbon solvation would be adequate to produce significant stabilization.

A third mechanism of emulsion stabilization is the Marangoni-Gibbs effect.[13,29,30] As two droplets approach one another, the continuous phase drains out from between them,

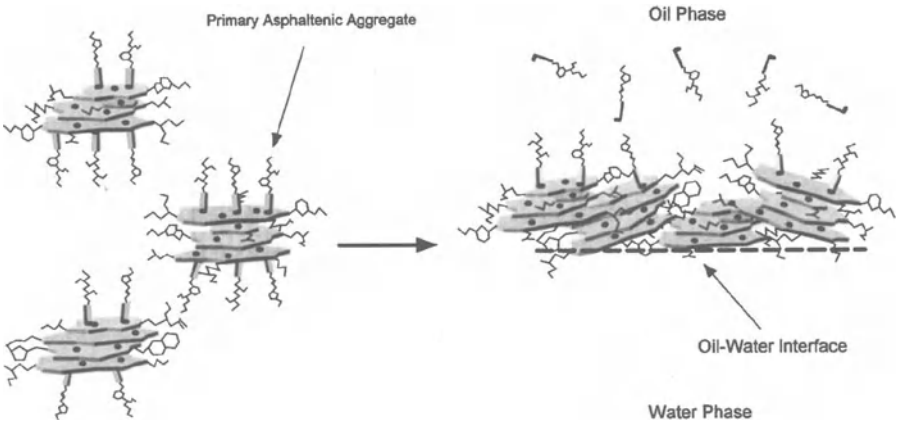

Figure 4. Depiction of emulsion stabilization mechanism in crude oil-water systems governed by adsorption of asphaltenic aggregates and organization into a third phase comprised of a rigid, viscoelastic, three-dimensional cross-linked network. The left portion of the picture shows primary asphaltenic aggregates comprised of individual asphaltene molecules aggregating through lateral stacking interactions and capped on the faces of the aggregates by resin molecules. The right portion depicts flocculation of asphaltenic aggregates through inter-aggregate interactions to form a cross-linked three-dimensional film.

creating an interfacial tension gradient at the droplet interface as the surfactants are dragged with the liquid. Due to the depletion of surfactant at the center of the thin film interface, a diffusion flux is generated opposing the drainage in order to restore the equilibrium distribution. This diffusion flux increases the rigidity of the interface and slows fluid drainage (Figure 3c). In order to enhance coalescence in systems stabilized by the Marangoni-Gibbs effect, the interfacial activity of the surfactant must be high enough to account for the interfacial tension gradient created.[30–34] Increased coalescence is observed with increased interfacial activity and diffusivity of the surfactant. Mukherjee and Kushnick[29] found that in order to increase the coalescence rate in Marangoni-Gibbs stabilized systems, the interfacial shear viscosity and dynamic tension gradient must be lowered. As we will show later, the stable interfaces created in water-in-crude oil emulsions are not only rigid and solid-like, they have strong elastic components and relatively high interfacial tensions as well. In a decane-water system with asphaltenes and resins present, Førdedal et al.[35] found the interfacial tension to be 24–32 mN/m compared with 0.3–0.5 mN/m when commercial surfactants were added. It thus seems unlikely that these interfacial materials are sufficiently mobile to exhibit the Marangoni-Gibbs effect.

The formation of an interfacial layer consisting of surface active material present in crude oil (asphaltenes and resins) may provide a physical barrier for droplet-droplet coalescence. Numerous researchers have noted the presence of an interfacial "skin" in oil-water systems with these surface active components present.[3,9,31,35–41] Mohammed et al.,[36] using a Langmuir film balance, found the interfacial dilational modulus to be dependent on the presence of asphaltenes and resins. Førdedal et al.[35] have shown that these components are responsible for stabilizing emulsions. From observations of interfacial tension measurements, they reasoned that the ratio of resins to asphaltenes is an important factor for determining emulsion stability. As we will show, the evidence is compelling that the primary mechanism of asphaltene stabilization of water-in-crude oil emulsions is through

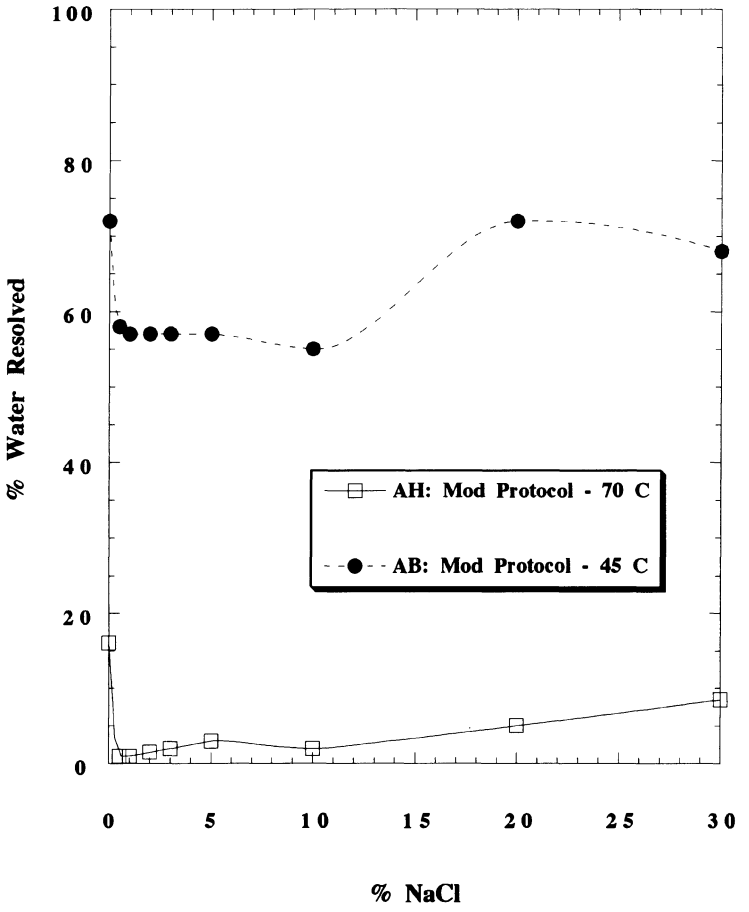

Figure 5. Effect of NaCl concentration (0–30 % w/w) on emulsion stability of Arab Berri-aqueous phase and Arab Heavy-aqueous phase emulsions. The crudes, emulsion making procedure, and emulsion stability protocol are described in the Experimental Scetion. Arab Berri crude emulsions were prepared using the so-called modified protocol (MP) with an intermediate heating step at 45°C and Arab Heavy crude emulsions were prepared with a similar protocol and an intermediate heating step at 70°C (See Figure 6).

the formation of a viscous, cross-linked three-dimensional network with high mechanical rigidity (Figure 4). Shown on the left side of Figure 4 is a schematic depiction of asphaltenic aggregates interacting through donor-acceptor interactions (either of the proton or electron type) and solvated on edge by resins. On the right side of the Figure is shown the adsorption of these aggregates at an oil-water interface and accompanied by inter-aggregate interactions to form a viscous, mechanically rigid film. While the schematic of Figure 4 is obviously oversimplified, there are several salient features illustrated which likely capture the essence of asphaltene-stabilized films. First, surface adsorption of asphaltene molecules is probably driven by hydration of polar functional groups in the aromatic core of an individual asphaltene molecule. Secondly, resin molecules probably serve to solvate primary aggregates (asphaltene micelles) in the bulk phase but these resins are likely shed

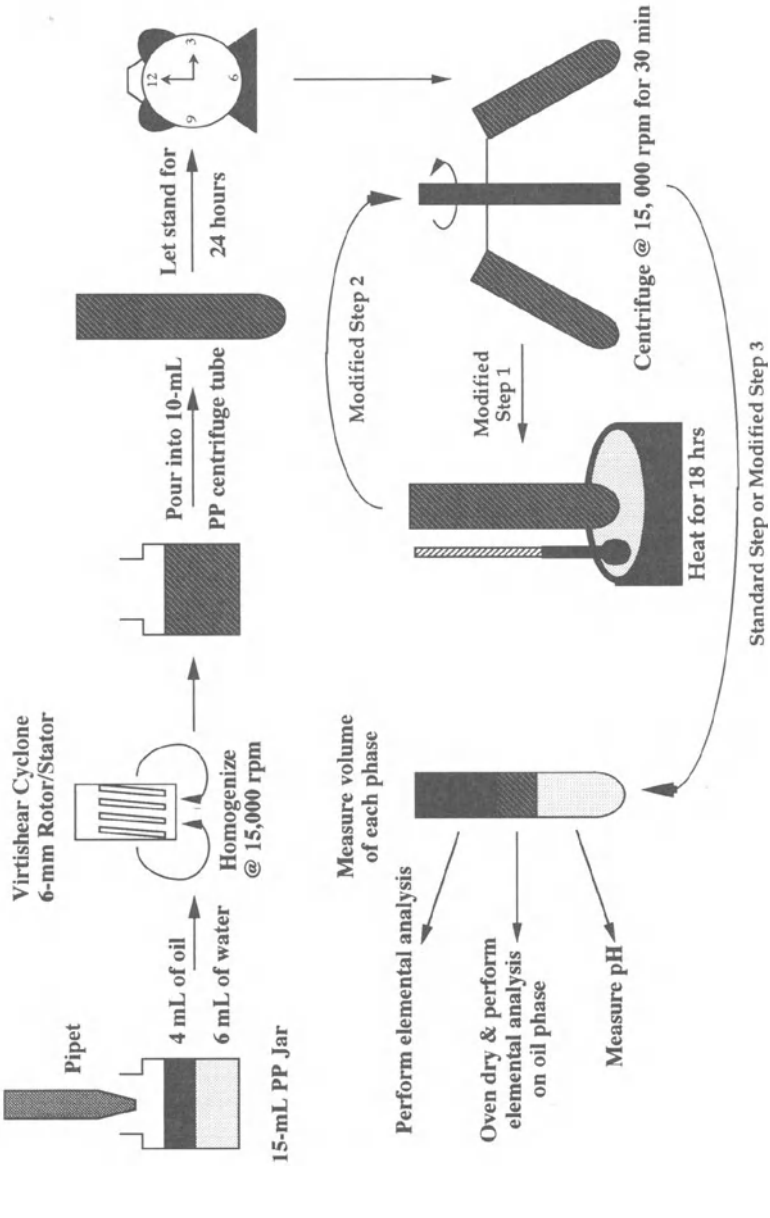

Figure 6. Schematic depiction of emulsion-making and stability protocols (both standard and modified). The standard protocol entails phase observation immediately following centrifugation. The modified protocol entails a heating step and a second centrifugation step before phase observation.

and do not appreciably participate in the actual stabilizing film. In fact, as we will show later, resins are totally unnecessary in the stabilization of asphaltenic films. A missing detail in Figure 4 is the means whereby individual asphaltene molecules crosslink to form a networked interfacial film. In the schematic, the aliphatic side-chains on the aromatic core are shown to intimately commingle. The specific forces which crosslink asphaltenic molecules at oil-water interfaces are likely much stronger than simple dispersion forces and the likeliest candidates are H-bonds or electron donor-acceptor interactions. A contributory element in the stabilization of water-in-crude oil emulsions may be the presence of organic (wax) or inorganic solid particles or aggregates in the thinning films between water droplets which raise film viscosity and reduce film drainage. We will, however, not be able to review these solids-based contributions to emulsion stability here.

3. REVIEW OF ASPHALTENE CHEMISTRY AND ITS ROLE IN MOLECULAR AGGREGATION

3.1. Introduction

Deducing the mechanisms by which emulsions are stabilized requires an intimate knowledge of crude oil composition. Characterization begins with the separation of crude oil into more distinct fractions. The general procedure for crude oil fractionation involves removal of asphaltenes by precipitation with a light aliphatic solvent (typically n-heptane or n-pentane) followed by sequential elution chromatography of the remaining fraction—called maltenes or petrolenes—to generate saturated hydrocarbons, aromatics, and resins. The asphaltene fraction is defined by its insolubility in a particular solvent, namely n-pentane or n-heptane. N-pentane will generally precipitate more heavy end components with a wider variety of molecular weights and polarities than will n-heptane. Asphaltenes driven from solution with n-heptane have higher average molecular weights and polarities within a more narrow distribution and contain no free hydrocarbons. The very definition of asphaltenes as insolubility classes of compounds dictates a very broad distribution of molecular types, weights, functional groups, and physical properties in asphaltenes derived from different sources. Tremendous bodies of literature have been developed by outstanding physical and analytical chemists such as Boduszynski, Long, McKay, Yen, Strausz, Speight, Bestougeff, and a host of others. With respect to function, and more specifically colloid and surface-adsorption properties of asphaltenes, there are a number of concepts and rules which have been developed to explain the experimental evidence.

Since Pfeiffer and Saal[42] and Nellensteyn's[43] work early this century, there is broad consensus that asphaltenes aggregate in solution to form supramolecular, colloidal species with emulsion-stabilizing properties which are almost certainly governed by their size and structural integrity, as we will discuss below. Based on a large body of x-ray and neutron scattering evidence, these colloidal aggregates—known variously as asphaltene "micelles", liquid crystallites, discotic mesophases, "particules", and supramolecular aggregates—associate through a stacking interaction based on the rigid disk-like nature of the fused aromatic ring functional groups (See Figure 7). An analogue of this type of molecular aggregation in monodisperse solute-solvent systems would be the stacking of anthraquinone dye molecules through non-cooperative association.[44] Pfeiffer and Saal's early picture of asphaltene aggregation was less clear, as might be expected without the benefit of x-ray or neutron scattering information. Due to the polydispersity, variability, and relative lack of certainty in asphaltene molecular structure, many researchers still prefer a somewhat vague view of asphaltene aggregate structure.

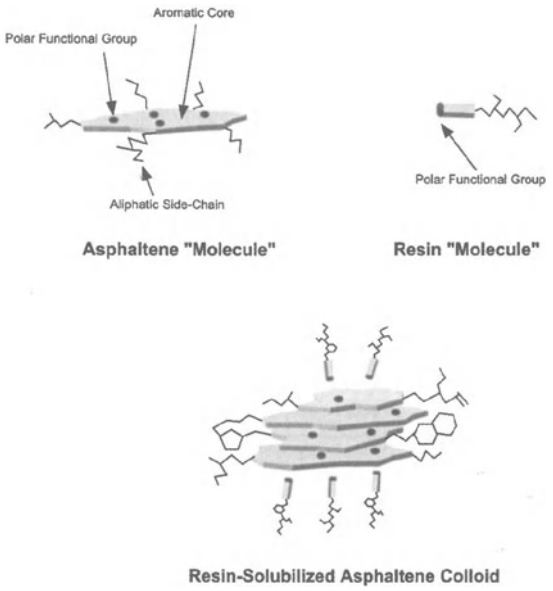

Figure 7. Schematic illustration of putative mechanism of asphaltene aggregation through lateral π-bonding and dipolar, H-bond, and electron donor-acceptor interactions between adjacent asphaltene molecules. Resin molecules, which are amphiphilic, solvate the edges of the lamellar asphaltene aggregates.

What ultimately limits the size of these aggregates are (1) entropic effects, which tend to favor dissociation, (2) smaller amphiphilic molecules which solvate the faces of these disks (two examples being resins and naphthenic acids, which may not be mutually exclusive), and (3) mismatch of the asphaltenic molecules due to polydispersity in size, chemistry, and functional groups. The molecular interactions which likely drive this aggregation are (1) π-bond overlap of fused aromatic rings in adjacent asphaltene molecules, (2) hydrogen bonding between proton donors (carboxylic, pyrrolic, phenolic) and proton acceptors (carbonyl, pyridinic, sulfoxidic), or (3) Lewis acid-base interactions among electron donors (oxygen, nitrogen, sulfur, aromatic functional groups) and electron acceptors (metallic species such as vanadyl, porphyrins, nickel-containing moieties). It is the thesis of this chapter that the molecular chemistry and the intermolecular interactions summarized in the above statements dictate the surface adsorptive properties of asphaltenes at air-oil, water-oil, and solid-oil interfaces, thus controlling foam and emulsion stability, as well as the extent of asphaltene adsorption to solids and the resulting effects on emulsion stabilization. Moreover, these intermolecular interactions also influence the properties of the viscoelastic film of interconnected asphaltenic functional groups which forms following surface adsorption and which governs the long-term stability of emulsions and their ability to be destabilized by chemical and physical means.

3.2. The Composition of Asphaltenes

Boduszynski, McKay, and coworkers have shown convincingly[45–48] that the composition of "asphaltenes" is very much dependent on the asphalt chosen for study and the solvent used to perform the precipitation. Despite this well-known and well-recognized fact, most researchers in the last 20 years have performed compositional, structural, and functional tests of all types on one or a handful of different types of asphaltenes. What we

Table 1. Range and typical values of elemental composition in asphaltene fractions

	Range	Typical
Carbon (%)	78–90	82–84
Hydrogen (%)	6.1–10.3	6.5–7.5
Nitrogen (%)	0.5–3.0	1.0–2.0
Sulfur (%)	1.9–10.8	2.0–6.0
Oxygen (%)	0.7–6.6	0.8–2.0
Vanadium (ppm)	0–1200	100–300
H/C	0.8–1.5	1.0–1.2

will overview here briefly are the salient features of asphaltenes related to colloid function, adsorptive properties, and emulsion stabilization. We will also attempt to provide a coherent picture of the range of properties which can be expected.

3.2.1. Elemental Analysis. The elemental profile of asphaltenes has been discussed by most investigators.[45,47,49–60] The range and typical values seem to be those given in Table 1. One of the most useful descriptions of asphaltene structure is the degree of "condensation" or aromaticity as gauged by H/C ratio. This has been shown to directly correlate with aromaticity.[61] As has been pointed out by several investigators, an even more revealing indicator of asphaltene structure is the distribution of H/C ratio, or equivalently Jurkiewicz N factor,[62,63] over the range of molecular weights which characterizes the polydispersity of asphaltenes.

3.2.2. Molecular Weight. The molecular weight of "monomolecular" asphaltenes is a hotly contested topic. Most investigators would agree that a large molecular weight of 2,000–5,000 daltons or more for a typical asphaltene fraction is probably in error due to the extent of molecular aggregation observed experimentally. Most measurements are performed by either mass spectrometry, vapor pressure osmometry (VPO), size exclusion chromatography (SEC), or cryoscopy.[45,59,64–66] The challenge with the mass spectrometric methods has always been whether the sample is completely volatilized intact with no fragmenting, polymerization, or pairing. Early careful work in this area on a crude from the Soviet Union indicates a rather low value of the monomolecular weight of 500–1500 daltons with a number-average of around 900–1000 daltons.[45] This result has been independently observed by Al-Jarrah and Al-Dujaili[58] on a different system—northern Iraqi heavy crude—using a different experimental approach, i.e., VPO in a variety of solvents: toluene, benzene, chlorobenzene, tetrahydrofuran, and nitrobenzene. In their study, Al-Jarrah and Al-Dujaili obtained a low number-average molecular weight of 935 daltons but only in extreme conditions (120°C) with an extreme solvent—nitrobenzene. This suggests that under most conditions, i.e. low temperature and common aromatic solvents, asphaltenes are highly aggregated to form micelles or aggregates. Bunger[64] reached a similar conclusion with a variety of methods. Cryoscopic work by Filimonova et al.[59,65] on a large number of Siberian crudes of vastly different properties yielded a range of number average monomolecular asphaltene weights of 900–2100 daltons. Vapor pressure osmometry, when performed in room temperature solvents of low dissociating power, such as toluene, yields high molecular weights. By performing the experiments at elevated temperatures (130°C) in strong polar dissociating solvents, such as o-dichlorobenzene, Wiehe[67,68] ob-

tained values ranging from ca. 500–4000 daltons for monomolecular asphaltene weights. Again, caution is warranted as even in these strong solvents and high temperatures, strongly associated oligomers may be present for which multiple sites of H-bonding or aromatic π-bonding are possible.

3.2.3. Hydrocarbon Skeleton. Based on some elegant mapping of asphaltene distribution Jurkiewicz graphs, Bestougeff[60] concluded that asphaltenes were comprised of "polycondensed" oligomers of small clusters of 5–7 fused aromatic rings in which the linkages were heteroatomic or aliphatic. If this picture is accurate and generalizable, the rigidity of these fundamental building blocks is sufficient to confer a preferred local orientation on the molecules in aggregates. Molecular packing of similarly shaped and structured asphaltene monomers would lead one to conclude that the "micelle" or aggregate structure must resemble the picture in Figure 7. However, small angle neutron scattering data suggest that asphaltenic aggregates in toluene/pyridine mixtures are relatively spherical, with a radius of about 30 Å.[69] Thus, it is still unclear to what degree asphaltenes orient themselves in aggregates and whether this orientation is important in emulsion stability.

3.2.4. Functional Group Analysis and Speciation. The detailed chemistry of heteroatom speciation, polar functional group determination, and hydrogen and carbon types in asphaltenes has been probed primarily by infrared spectroscopy, nmr spectroscopy, x-ray methods such as x-ray absorption near-edge structure spectroscopy (XANES), and esr spectroscopy. The picture which emerges has become clearer with time and seems to indicate that most asphaltene molecules have 1–3 heteroatoms (S, N, O) per molecule. Sulfur exists predominantly as thiophenic heterocycles (typically 65–85%) with the remainder as sulfidic groups.[70,71] Only in highly biodegraded crudes does there appear to be a large amount of sulfoxide. Nitrogen occurs as pyrrolic, pyridinic, and quinolinic groups, the dominant portion being pyrrolic. Interestingly, relatively small amounts of porphyrin complexes appear to exist in asphaltenes. However, when asphaltenes are extracted with warm acetone, what little porphyrin material present is extracted. The film-forming capability of the asphaltene fraction, and the shear strength of that film, appear to be diminished when the porphyrin fraction is removed.[72] This suggests that porphyrin groups may play an important role in crosslinking asphaltenic species at the oil-water interface and creating a sufficiently strong film to stabilize emulsions. Oxygen species are predominantly hydroxylic, carbonyl, and ether.[63,73] Acidic functional groups appear to play a critical role in asphaltenic films which stabilize emulsions.[74] By fractionating asphaltenes and resins from North Sea crudes using a solvent extraction procedure, Sjöblom's group has shown that model emulsions were strongest when stabilized by asphaltene fractions richest in open-chain carbonyl functional groups. They hypothesized that the hydrogen bonding afforded by flexible carboxyl groups in asphaltenes yields a rigid mechanical barrier film to water droplet coalescence.

Gated spin echo ^{13}C nmr methods have been applied to asphaltenes to gauge the degree of aromatic ring condensation.[57] This fused ring character is also reflected in H/C ratio and aromaticity, and could play an important role in the aggregation properties of asphaltenes.[75] The implication is that more "mature" asphaltenes—i.e. more highly biodegraded—with lower molecular weight, smaller aliphatic substituents, greater aromatic condensation, and more fused ring character, could potentially associate through lateral stacking interactions mediated by π-bonding. Whether this type of intermolecular interaction engenders stronger viscoelastic films at oil-water interfaces has not been studied to date.

3.3. Emerging Picture of Asphaltene Aggregation

While there is a great deal of experimental data detailing a variety of structural properties of asphaltenes, much of the molecular chemical picture as it relates to film-forming structure remains unclear. The early Nellensteyn and Pfeiffer and Saal models of a locally structured solution comprised of a graded interfacial zone between asphaltenic species and the crude solvent (saturated and aromatic hydrocarbons) seems to have some legitimacy in the light of detailed scattering data suggesting spherical aggregates. Moreover, the molecular structural distribution data of Bestougeff and coworkers suggests polycondensed structures connected by flexible linkers which further implies a relatively disordered aggregate interior. On a very local level (O[10 Å]), the interaction of fused aromatic ring systems suggests a local director axis similar to discotic mesogens. Specific scattering evidence of sedimented asphaltenic films indicates discotic lamellar structures.[76] Thus, a balanced picture of the literature suggests that asphaltenes may aggregate to form locally directed anisotropic structures connected through space to form a three-dimensional network. This picture is in fact very close to Yen's model.[77,78] It seems clear that strong, directed intermolecular forces must hold asphaltene molecules together in supramolecular aggregates and the likeliest forces are π-bonds, hydrogen bonds, and electron donor-acceptor bonds. We also know that primary aggregates of asphaltenes agglomerate further in "poor" solvents, i.e. n-alkanes, to form larger colloidal particles. This subsequent agglomeration may also be attributable to the aforementioned types of forces as it is driven by increasingly aliphatic solvents which would promote all three types of interactions. In "good" solvents, such as toluene and pyridine, asphaltenes are known to micellize or aggregate,[69] but the extent of aggregation is modest (small spherical aggregates of 30 Å). Thus, it is the subsequent larger scale aggregation or agglomeration which ultimately gives rise to three-dimensional network formation, viscoelastic film formation, and emulsion stabilization, as we will describe below.

4. STUDIES OF CRUDE OIL EMULSIFICATION AND INTERFACIAL FILM FORMATION

4.1. Introduction

Motivated primarily by the challenges associated with transport and clean-up of viscous emulsions formed subsequent to marine spills of crude oils and residual fuel oils and by the need to demulsify production emulsions at the wellhead, water-in-crude oil emulsions and interfacial films at oil-water interfaces have been studied extensively over the last 50 years.[3–5,38,79–85] A chronological summary of these studies is provided in Table 2, which collects the references, crude oils, and techniques used in many of these publications. The recurring themes in these studies aimed at understanding mechanisms of and agents responsible for emulsification are (1) asphaltenes are the key agent in crudes responsible for emulsification, (2) the role of resins is unclear, sometimes facilitating emulsion formation and sometimes serving to demulsify, (3) the natural emulsion-forming materials accumulate at the oil-water interface to form a viscous interfacial film with viscoelastic properties which governs emulsion stability, and (4) other "bulking" agents, such as wax particles or inorganic solids, seem to contribute to the opacity and potentially the strength of the film. In this section, we will review the evidence for these conclusions related to water-in-crude emulsions and present our studies on crude oils and "doped"

Table 2. Summary of studies conducted on crude oil-water interfaces, either emulsion, pendant drop, or planar interface studies

Investigators	Ref #	Crude oil	Method of study	Key findings
Lawrence et al.	79	Venezuela, Borneo, Trinidad, Sumatra, Mexico, Iran, and Texas	water separation; visual observations of emulsion	emulsion stabilization requires lowering of IFT and a mechanical barrier to coalescence
Denekas et al.	93	Oklahoma	water spray extraction to separate film forming constituents from the crude	analysis of crude forming material
Dodd et al.	94	California	water spray extraction of surface active components and fractionation of the resulting benzene solubles; IFT: pendant drop	surface active and film forming material is present in crude oil
Blair	5	Angola, Venezuela, Texas, Germany, Kuwait, Canada, Mexico, and Arkansas	IFT, spreading coefficients: du Nuoy ring	rigid, highly condensed interfacial skin can be replaced with demulsifier
Dodd	39	Illinois	IF rheology	asphaltene and resin structures in the interfacial film stabilize emulsions; R and A have specific roles
Mardanenko et al.	86	Uzen and Zhetybai fields	water spray extraction of "foam-forming" components with petroleum ether; surface tension; water separation	
Kimbler et al.	3	Texas, Venezuela, New Mexico, Louisiana	film pressure: float at interface	
Strassner	4	unspecified	IFT: pendant drop	resin and asphaltene effects are important
Cairns et al.	114	Zakum, Tia Juana, Murban	IF rheology: bob at interface; IFT: du Nuoy ring, pendant drop	
Jones et al.	96	Ninian, Kuwait, Iranian Heavy, Murban, Forties, Magnus	IF rheology: bob at interface; film compressibility: Wilhelmy plate	
Pasquarelli et al.	37	California	IFT: spinning drop; IF shear viscosity: viscous traction shear viscometer	resins may increase emulsion stability by preventing asphaltene precipitation
Menon et al.	115	Australia	photomicrography; IF shear viscosity: deep channel viscous traction surface viscometer; IFT: spinning drop	IF viscosity correlates with coalescence rate
Siffert et al.	112	unspecified	small angle x-ray scattering	lamellar structure at interface similar to model oil systems with asphaltenes
Thompson et al.	116	North Sea	IFT: Wilhelmy plate	
Eley et al.	117	Brega, Kuwait, Tia Juana	IF rheology: bob at interface; IF compressibility: pendant drop	correlation between amount of demulsifier required and asphaltene content; thick films of asphaltenes at interface

Mukherjee et al.	29	unspecified	IF rheology: du Nuoy ring, maximum bubble pressure shear, viscous traction shear viscometer, pulsed oil drop	shear viscosity and dynamic IFT gradient need to be lowered for demulsification
Johansen et al.	17	North Sea	IFT: du Nuoy ring	
Aveyard et al.	118	North Sea	water separation; IFT: spinning drop	demulsification rate increases with surfactant concentration up to aggregation point
Isaacs et al.	40	Leduc field	ultrasonic field to measure extent of coalescence; photomicrography	demulsifier and surfactant are more effective together than individually at demulsification
Sjöblom et al.	18	North Sea	IFT: pendant drop	
Wasan	31	California	water separation; drop size distribution; IF activity: maximum droplet pressure	demulsifier performance correlates with interfacial activity
Acevedo et al.	113	Cerro Negro	IF rheology: bob at interface	rheological differences found when resins are present (from model studies)
Bhardwaj et al.	119	Germany	IFT: drop volume method; water separation	effective demulsifiers require sufficient surface pressure and partitioning between phases
Mohammed et al.	14	North Sea Buchan	IF rheology: bob at interface	build up of asphaltenes at interface
Mohammed et al.	36	North Sea Buchan	IFT: Wilhelmy plate	resin-asphaltene interactions are important for strong films
Urdahl et al.	120	North Sea	IFT: du Nuoy ring	
Bhardwaj et al.	121	Germany	IFT: drop volume method; water separation	interface toughens due to slow adsorption of natural surfactants, correlation with demulsifier adsorption and rate of demulsification
Mohammed et al.	15	North Sea Buchan	IF rheology: bob at interface	asphaltene structure builds up with time
Skodvin et al.	122	unspecified	time domain dielectric spectroscopy	information on relaxation times and static permitivities
Kim et al.	32	Mississippi	water separation; dynamic film tension, stress-relaxation performed with a film tensiometer	correlation between film dilational modulus and demulsifier performance; rapidly diffusing, low MW components lower IFT for demulsification
Førdedal et al.	35	France, North Sea	IFT: du Nuoy ring; time domain dielectric spectroscopy	resin and asphaltene interactions are important for emulsion stability
Kim et al.	123	Louisiana	film rheometer	lowering of IFT gradients is required for demulsification
McLean et al.	107	Alaska, Saudi Arabia, California	water separation	asphaltene concentration and R/A are important for asphaltene aggregation and resulting emulsion stability

Abbreviations include IF (interface); IFT (interfacial tension); R (resins); and A (asphaltenes).

crudes, i.e. crudes which have been selectively modified by the addition of specific components. In the following section, we will review the evidence from "model" systems, i.e. oils comprised of pure heptane, toluene, xylene, and the like to which have been added asphaltenes, resins, and other materials, in order to isolate the individual effects of these components.

4.2. Film-Forming Agents in Crude Oils

A variety of components, functional groups, and fractions of crude have been implicated as containing the agents primarily responsible for viscous film formation and emulsion stabilization. Much of the evidence is somewhat confusing and seemingly contradictory. This confusion is likely due to the remarkably broad distribution of physical properties in crude as well as the variety of agents which can participate in emulsion film stabilization. Many studies have independently confirmed that the emulsifying and film-forming agents are present in the atmospheric residua,[79] the asphaltene fraction,[38,86–89] and the fraction which adsorbs most strongly to polar solid adsorbents, such as activated silica.[74,90] Mackay carefully diluted water-xylene-asphalt emulsions with xylene and then filtered the water droplets to concentrate them, whereupon they evaporated the water and analyzed the residual emulsifying material. Only the emulsion-stabilizing material which formed a rigid, mechanically stable film remained upon dilution in xylene and filtration. The residual film-forming material, which was called Compound X, had an H/C ratio of 1.09, a nitrogen content of 1.3 %, and was virtually identical in elemental composition to the asphaltene fraction in the crude oil they studied. We have performed similar studies in which we formed emulsions of water, toluene, heptane, and asphaltenes isolated from Safaniya (Arab Heavy crude oil) and then centrifuged the emulsions at high speed to form a residual film.[91] The fraction of the asphaltenes which we isolated at the interface had an H/C ratio of about 1.09, slightly lower than the bulk asphaltene H/C ratio of 1.11. Thus, there appears to be a sub-fraction of asphaltenes of possibly lower H/C ratio than whole asphaltenes which is more stable at the interface or participates to a greater extent than the entire fraction in the formation of a rigid interfacial film. We have indirectly verified this recently in experiments performed with acidic, basic, and neutral fractions of asphaltenes isolated by ion exchange chromatography.[92]

Denekas et al.[93] and Dodd et al.[94] had previously performed similar experiments with an Oklahoma crude and with a Rio Bravo, California crude, respectively. In their experiments, the film-forming material was isolated by water-spray extraction and isolation. From their analyses, they concluded that resins, waxes, and porphyrin-containing compounds were all present in the interfacially active and film-forming fraction. Moreover, by extracting the interfacial residual material with benzene and analyzing, they obtained H/C ratios of about 1.00–1.19 for the benzene extract, which is in the range for asphaltenic material. The importance of porphyrin-containing material in asphaltenes in strengthening interfacial films at oil-water interfaces has been independently confirmed by Mansurov et al.[72] They found that the shear strength of the asphaltenic films formed in mineral oil-xylene-water-0.1% asphaltene mixtures, as measured by a torsion pendulum rheometer, was reduced by as much as 50% upon removal of the porphyrins by acetone extraction. Potentially, other materials were also extracted in their experiments. However, their results do support the notion that porphyrin functional groups play a role in enhancing the strength of asphaltene interfacial films.

Many studies mention anecdotally the presumed role of resins in stabilizing water-in-crude oil emulsions. The role of resins in the stabilization of oil-water interfacial films

has not been precisely elucidated for a variety of reasons. In many of the experiments performed to probe emulsion stability, the strength of emulsions studied has varied greatly, with some emulsions simply being stable to gravity settling while others were stable towards centrifugal fields. While petroleum resins by themselves can, in some instances, stabilize emulsions against gravity settling, they tend to be much weaker than those stabilized by asphaltenic films.[91] What additionally has confused the literature on this point is that the combination of resins with asphaltenes, which is what occurs in whole crude emulsions, can produce more stable emulsions or stronger interfacial films than asphaltenes alone, under certain solvency conditions.[72] The role of resins, as we will describe in detail below, seems to be to solvate large colloidal aggregates of asphaltenes, creating smaller aggregates which are more mobile and can organize in the oil-water interface more effectively. Thus the resins seem to serve to produce a state of aggregation of asphaltenes most conducive to interface adsorption and film generation. Whether the resins actually participate in forming the interfacial film and contributing to its rheological strength has not been determined.

4.3. Emulsion and Interfacial Film Studies on Crude Oils

In this section, we will attempt to summarize and review the literature on water-in-crude oil emulsions and the studies of the interfacial films formed at water-crude oil interfaces. No effort is made to be exhaustive but we will attempt to provide a comprehensive view of our current understanding of this issue.

In 1960, Blair[5] and Dodd[39] published key studies on water-in-crude emulsions and their films. Using a film balance to study the water-oil interface, Blair showed that the nature of the interfacial film was not at all akin to the classical picture of emulsion stabilization by an adsorbed monolayer yielding low interfacial tension values. Rather, a thick mechanically rigid film was observed to form when the film pressure was increased by compression beyond 15–17 dyne/cm. Careful photomicroscopic examination of these films revealed some very unusual phenomena. When the interface was observed from below through the water phase, it was seen to acquire a greyish, opalescent appearance. When probed, the film was observed to be elastic. Upon gross deformation, the films developed wrinkles and thick striations, but many recovered to assume the uniform grey opalescence. Blair concluded that the films were likely polymolecular (see Figure 4). The film opacity was observed to be greatly reduced upon filtering all particles larger than 0.5 μm. It thus appeared that a primary adsorbed layer is initially formed, almost certainly comprised of asphaltenes, and a secondary layer superimposes on this primary layer and is likely comprised of asphaltenes, wax particles, and possibly inorganic particulates. Resins and polyaromatics may also be associated with the film as asphaltene-solvating species.

Dodd[39] employed an interfacial shear rotational viscometer to study crude-water interfaces with NaCl, acid, and basic additives in the water phase. He observed high elasticity and rigidity when the interface was aged for 18–70 hours. NaCl did not affect rigidity but basic solutions of as little as 0.01% NaOH destroyed film rigidity. Dodd concluded that the film must be comprised of naphthenic acids in combination with resins, asphaltenes, and waxes. Furthermore, the acidic species must desorb from the interface under basic conditions and partition into the aqueous phase, rendering the interface considerably less rigid. Dodd did not explore whether these acidic species were in fact part of the asphaltene fraction, but subsequent researchers have shown that acidic asphaltenes are more effective at emulsion stabilization than their neutral counterparts.[74,92]

Strassner[4] explored the effects of pH on interfacial film properties and the stability of crude oil-water emulsions utilizing a pendant drop method to measure so-called film ratio. In this experiment, a droplet of water is extruded through a capillary into crude oil, aged for 20 seconds to allow adsorption of components at the oil-water interface, then contracted to a smaller drop size by changing the pressure in the capillary until a "sharp" change is observed in the drop geometry. While this latter point is obviously somewhat arbitrary, Strassner observed very distinct "wrinkling" of the interface and clear evidence of film rigidity as evidenced by a "crinkly or prune-skin appearance". The ratio of the cross sectional area of the contracted droplet to the original droplet is defined as the "film ratio". Strassner observed that when the film ratio was greater than 20% with bulk crude viscosities of 6 cP or greater, the crude always produced stable emulsions with water relative to gravitational settling. Thus, there was a clear relationship established between film rigidity and emulsion stability. Strassner observed that the films formed were of three distinct types: (1) solid, rigid films that under compression form relatively insoluble skins and possess high interfacial shear viscosity, (2) highly mobile films that pack under compression to give a momentary distortion but rapidly redistribute and return the drop to a symmetrical shape when contraction is stopped (these films have low interfacial shear viscosity), and (3) transitional films that show no distortion under compression and whose presence can only be detected by relatively low interfacial tension. Both rigid and mobile films can possess high film ratios, but the rigid films are obviously considerably more effective in creating stable emulsions. Moreover, Strassner was able to show, by performing experiments on a de-asphalted Venezuelan oil to which asphaltene was added in varying amounts that, with high R/A of 8 or greater, only mobile films were obtained while with R/A of less than 5–6, rigid films were obtained. Strassner concluded that asphaltenes form more rigid films than do resins. Also, by varying the pH of the aqueous phase, Strassner showed that at acidic pH with low gravity Venezuelan crude, the most rigid films were formed with the highest emulsion stability. A tentative conclusion which may be drawn is that acidic functional groups (which are protonated) are present in asphaltene fractions and confer the cross-linking required for rigid asphaltenic films to form.

A number of other early studies of crude oil-water interfaces identified rigid oil-water interfacial films generated by the adsorption of natural crude surfactants.[3,85,95] Space here does not allow us to summarize these papers but their publication adds to the evidence of mechanically rigid films as the primary mechanism of water-in-crude oil emulsion stabilization.

Jones et al.[96] and Neustadter et al.[97] performed some critically important studies of crude oil film formation at oil-water interfaces utilizing experimental probes of interfacial tension, surface pressure, and interfacial rheology. Differing crudes exhibited radically different pressure-area (π-A) curves as probed by a Langmuir film balance with a hydrophobic Wilhelmy plate. Four types of interfacial film behavior were observed: (1) compressible relaxing, (2) incompressible relaxing, (3) incompressible relaxing with L_1-L_2 phase transition, and (4) incompressible non-relaxing (i.e. mechanically rigid elastic film formation). The last category of film (of which Ninian crude was an exemplar) produced the most stable emulsions and the films of greatest surface shear viscosity (> 200 mN/s-m for a 4+ hour aged interface), elasticity, and compressed film pressure (> 10–12 mN/m). These films could be induced to relax by elevation of temperature to > 60°C, although the film relaxation was observed to be a kinetically slower process than for the other types of films formed at lower temperature. Thus, the specific physico-chemical interactions whereby these films are formed at lower temperatures can be weakened by elevation of

temperature. This certainly would be expected with hydrogen bonding, electron donor-acceptor interactions, π-bonding, or partial paraffin crystallization.

Sjöblom and his research team have probed the causes of emulsion stability in a series of North Sea crudes and observed that emulsion stability correlates with asphaltene, wax, and resin/asphaltene ratio.[18,74,90,98,99] In their early work, they theorized that asphaltenes may aggregate through stacking interactions mediated by aromatic π-bond overlap to form discotic lamellar structures which stabilize the emulsions, similar to lamellar liquid crystalline stabilization of emulsions in ternary surfactant-oil-water mixtures.[100–103] Moreover, they further observe that the interfacially active fractions of crude oils which give rise to emulsion stability are rich in acidic functional groups.[74,90] These observations are fully consistent with the earlier studies of Dodd, Blair, and Strassner. Nordli et al.[98] have studied the surface pressure–specific area isotherms of the interfacially active fractions of North Sea crude and discovered that once the surface pressure exceeds 15–20 dyne/cm, the interfacial films are observed to become rigid. The strongest films are formed under the most acidic conditions. Finally, the films least able to relax under reduced surface stress conditions were observed to form the most stable emulsions. The molecular picture that seems to emerge is that of self-assembling asphaltenic films which, with the proper functional groups for cross-linking, form rigid solid-like interfacial films to stabilize emulsions. The most stable emulsions form with the most rigid films. It is also clear, however, that components other than asphaltenes, such as alkanes (paraffin waxes), resins, and aged interfacially active components of relatively high H/C ratio (1.5), can also contribute to the stabilization of water-in-crude oil emulsions.[104]

Mohammed et al.[14,15,36,105,106] published a series of papers in which they probed the rheology, interfacial tension, surface pressure, and compressional modulus of Buchan crude oil -water interfaces with and without added demulsifiers under thermal and electrical fields. Their rheological method was the biconical bob technique described above.[97] In their rheological study,[14] they observed that with short aging times of the crude-water interface (< 2–3 hours), the interface rheology could be characterized as substantially viscous but with very little elastic character. The values of shear viscosity measured at relatively short times were of the order of 1–10 mN/s-m.

4.4. Effects of Resins and Aromatic Solvent Addition on Emulsion Stabilization in Crude Oils

McLean et al.[91,107] have investigated the effects of crude oil solvency and resin-asphaltene interactions on the stability of both water-in-crude oil emulsions and model systems.

4.4.1. Experimental Section

4.4.1.1. Materials. The crude oils chosen for this study (Arab Berri, Arab Heavy, Alaskan North Slope, and San Joaquin Valley) have been selected based on their extensive use in oil refineries and because they represent extremes in gravity, resin and asphaltene content, and emulsion-forming tendencies. The general properties of the crude oils selected for this study are presented in Table 3. Arab Heavy is a high sulfur crude produced from Safaniya, the world's largest off-shore field.[108,109] Arab Berri (i.e. Arab Extra Light) is a high °API gravity, low sulfur crude produced from Upper Jurassic Arab zone reservoirs in Berri, Saudi Arabia.[109,110] The nitrogen-rich San Joaquin Valley crude oil (a blend of crudes from San Joaquin Valley, California) is a crude of low °API gravity and unusu-

Table 3. Properties of crude oils used in this study

Property	Test methods	SJV	ANS	AB	AH
Gravity,°API	ASTM-D 287	12.2	27.5	38.6	27.4
Viscosity*, SUS @ 100°F	ASTM-D 445	15,025	71	41	118
Nitrogen, wt %	GC Combustion	0.90	0.31	0.07	0.25
Sulfur,wt %	"	1.20	1.42	1.52	3.16
Asphaltenes, wt %	n-C7 Insolubles	4.57	3.35	0.68	8.27
Resins, wt %	Elution Chromatography	20.26	9.47	3.49	9.56
R/A		4.43	2.83	5.13	1.16
Arom. Oil:Arom. Asphaltenes	C-13 NMR Spectroscopy	0.45	0.45	0.31	0.43
Arom. Resins:Arom. Asphaltenes	C-13 NMR Spectroscopy	0.84	0.73	0.71	0.77
% Polar Functional Groups**	FTIR Spectroscopy	4.44	1.64	1.98	1.21

*Viscosity of distilled water @ 68°F is 31 SUS.
**Wt % of total asphaltenes and resins

ally high viscosity.[111] Alaskan North Slope (ANS) is produced from fields in the North Slope of Alaska, predominantly in the Prudhoe Bay region.

4.4.1.2. Methods: Crude Emulsion Studies. In order to ensure homogeneity of the oil samples, the whole crudes were mixed thoroughly with the use of a Harbil GQM high-speed paint mixer for 3 min. The aqueous phase (i.e. deionized water) was prepared by adjusting the pH using diluted NaOH and HCl. The emulsions were produced according to a standard protocol outlined in schematic form in Figure 6. Six mL of deionized water (@ specified pH) and four mL of the whole crude oil were pipetted into a 15 mL polypropylene jar. This mixture was then processed with the use of a Virtishear Cyclone IQ homogenizer with a 6-mm rotor/stator configuration (gap width = 0.127 mm) at 15,000 rpm for 3 min at the oil/water interface, for 2 min at the bottom of the jar, and for 1 min just below the oil/air interface. Immediately after homogenizing, the emulsions were transferred to 10 mL polypropylene centrifuge tubes; most emulsions poured readily immediately following emulsification. The amounts of oil and water to be emulsified (including the W/O ratio), the geometry of emulsifying equipment (e.g. 15 mL jar, 6-mm rotor/stator configuration, etc.), and the amount of energy input to the system specified in the emulsification protocol were determined in preliminary experiments to ensure reproducibility, complete emulsification of materials, and droplet size distributions typical of emulsions produced in the refineries (5–50 μm).

Referring again to Figure 6, after a period of 24 hours, the amount of separated water was determined since a period of rapid coalescence is known to immediately follow the formation of an emulsion.[38] The volume of oil and water resolved was measured via visual inspection by placing the emulsion samples next to a graduated centrifuge tube. The emulsions were then centrifuged using a RC5C refrigerated centrifuge from Sorvall Instruments at 15,000 rpm (28,700 g) and 30°C for 30 min. The volumes of water and oil separated due to centrifugation were determined by decanting the oil and pipetting the water into separate graduated tubes. The amount of resolved water is the most appropriate gauge of emulsion stability in water-in-crude oil emulsions since coalescence of the droplet phase is the limiting step in the demulsification process.[99]

In order to study the effects of changes in system variables (e.g. crude oil types, added resins, added solvents of varying aromatic carbon content, etc.), a modified stability protocol was employed which resolved approximately half the water from the whole

crudes (i.e. base cases). As shown in Figure 6, the modified stability protocol simply adds heating and re-centrifugation steps to the standard stability protocol in order to attain the desired water resolution. When using the modified protocol, the emulsion samples were heated in a water bath to a specified temperature for ~18 hours after the initial centrifugation and then re-centrifuged at the previously-noted specifications. By changing the amount of heat input into the system between centrifugations, one can control and determine the amount of water resolved for each of the base cases in a particular study. This enables the investigator to broaden the window of observed trends in relative emulsion stability. Preliminary results indicated the standard protocol was sufficient to obtain the desired water resolution (~50%) for Alaskan North Slope crude, while Arab Berri and Arab Heavy crudes required heating to 45°C and 70°C, respectively.

The crude oils under investigation were fractionated into resins and asphaltenes and subsequently characterized with respect to their elemental, functional group, and aromatic carbon contents in a prior study. The instruments and techniques used to obtain the compositional analyses of these crudes are described in a previous paper.[61]

4.4.1.3. Methods: Model Emulsion Studies. The model crudes were constructed using the resin and asphaltene fractions derived from a fractionation method applied to the four different crudes mentioned previously.[61] Briefly, the asphaltenes were precipitated from the crude oil in an excess of n-heptane at room temperature. Resins were then isolated after adsorption of the heptane-soluble portion on activated silica gel.

The resin and asphaltene fractions from these crudes were typically dissolved in 4.4 mL of heptol (7:3 heptane:toluene, unless otherwise noted), both as separate entities and in various combinations to study the possible synergistic effects of these fractions. In order to enhance dissolution of these polar materials, the asphaltenes were first crushed into fine particulates with the use of a metal spatula. Appropriate amounts of these fractions were weighed on a Mettler AE 166 Deltarange Balance. The resins and asphaltenes were dissolved separately in 3.1 mL of n-heptane and 1.3 mL of toluene, respectively, in 15 mL polypropylene jars. The solvents used were the purest HPLC grade available. Both jars were shaken at the lowest setting on a Fisher Genie 2 Vortex mixer for at least 5 min. The resin solution was then added to the asphaltene solution, and the mixture was shaken for another 5 min before emulsification with 6.6 mL of DI water adjusted to pH 6.

The formation of these model emulsions was carried out in the same manner as previously described above for the whole crude oils. All of the emulsions formed in this study were of the w/o type. Their stability was determined by the amount of water resolved after 24 hours and then again after centrifugation at various field strengths for 30 min. Most emulsions were centrifuged at 15,000 rpm (28,700 g).

The interfacially active components remaining in the unresolved emulsion phase as well as those found in the creamed oil phase were isolated by carefully decanting the oily, organic phase before evaporating the water and/or heptol from each of the phases in a nitrogen-flushed vacuum oven at 70°C for 24 hrs. Elemental and neutron activation analyses were then utilized to obtain C, H, N, S, V, and Ni contents in these isolated polar components. Details of these characterization techniques were presented previously.[61]

4.4.2. Molecular Model of Role of Resins in Asphaltene Aggregation. Before we can attempt to relate the observed trends in the stability of the emulsions produced from the crude oils in this study to certain characteristics of these crudes, we must consider how the polar, surface-active constituents of the crude (e.g. resins and asphaltenes) interact with each other and with the surrounding crude medium and how these interactions could affect

the resultant emulsion stability. As mentioned previously, resins help to solubilize the asphaltenes by forming a resin-solvated asphaltenic aggregate (Figure 7) and thus tend to diminish the surface-active nature of the asphaltenes. However these resin-solvated asphaltenic aggregates may lower their free energy by 'shedding' the solvating resins on one side to form a partially-solvated aggregate which is interfacially-active and adsorbs at the water-oil interface. As pointed out in the literature review, the extent to which the asphaltenes are solvated is one of the controlling factors in determining the surface-active nature of these colloidal aggregates. Strongly solvated asphaltenic aggregates, either by the aromatic portion of the crude solvent or by the resin fraction, are relatively surface-inactive as gauged by emulsion stability. Asphaltenes which prefer inter-asphaltene interaction to solvation are strongly surface-active. In addition, based on the vast amount of evidence in the literature, one might expect structural reorganizations at the oil-water interface of these asphaltenic aggregates to engender more intimate association and, apparently, extensive crosslinking to produce rigid elastic films.

With this in mind, what are the dominant contributors to the state of asphaltene solubility? If we consider, for example, a crude oil which is rich in solvating resins relative to its asphaltene content (i.e. a crude oil which has a high resin-to-asphaltene ratio), we would expect the asphaltenes in this particular crude oil to be strongly solvated as small (O[30–40Å]) aggregates and therefore unable to stabilize emulsions. This was apparent in Strassner's study with R/A greater than 8.[4] Aside from R/A, there are at least two other characteristics that merit consideration: (1) asphaltenes are known to be the most aromatic portion of the crude oil, therefore we would expect that as the aromaticity of the resins and surrounding oil medium increased with respect to the aromaticity of the asphaltenes, the asphaltenes would become more molecularly dissolved and less able to stabilize emulsions; (2) the hydrogen-bonding interactions of the polar functional groups would help determine the strength of solvation between the resins and asphaltenes. It stands to reason that if the asphaltenes from a particular crude oil contain high concentrations (relatively speaking) of C=O groups and if the corresponding resin fraction is rich in carboxylic acid functional groups, then intermolecular hydrogen bonding could lead to strong solvation of asphaltenes by resin molecules. The higher the concentration and polarity of these functional groups, the stronger the interactions between them thus diminishing the ability of these colloidal aggregates to shed their sheath of solvating resins in order to become surface-active.

Apparently, then, there are clearly identifiable molecular properties which should control the solubility of asphaltenes in crude oil, their tendency to aggregate, and their tendency to adsorb at oil-water interfaces. These are (1) the ratio of resins to asphaltenes (R/A), (2) the concentration of the functional groups (e.g. carbonyls, carboxylic acids, pyrroles, amides, and phenols) contained in the resin and asphaltene fractions, and (3) the aromaticity ratios of the resins and the crude medium to the asphaltenes (i.e. the aromatic carbon content of the resin fraction divided by the aromatic carbon content of the asphaltenes and the aromatic carbon content of the saturate/aromatic fraction divided by the aromatic carbon content of the asphaltenes, respectively).

The different modes and extents of asphaltene solvation are illustrated in Figure 8. This figure highlights the different properties which determine the extent of asphaltene solvation and the proposed resultant effects on the surface activity of the asphaltenes within a given crude oil. These assertions also suggest possible means for emulsion minimization and/or resolution. The top path (in going from a colloidal aggregate which is weakly solvated and strongly surface-active to an aggregate which becomes strongly solvated and weakly surface-active) shows the expected effect of increasing the concentration of resins (i.e. the R/A value) in a given crude oil. The asphaltenes would become less

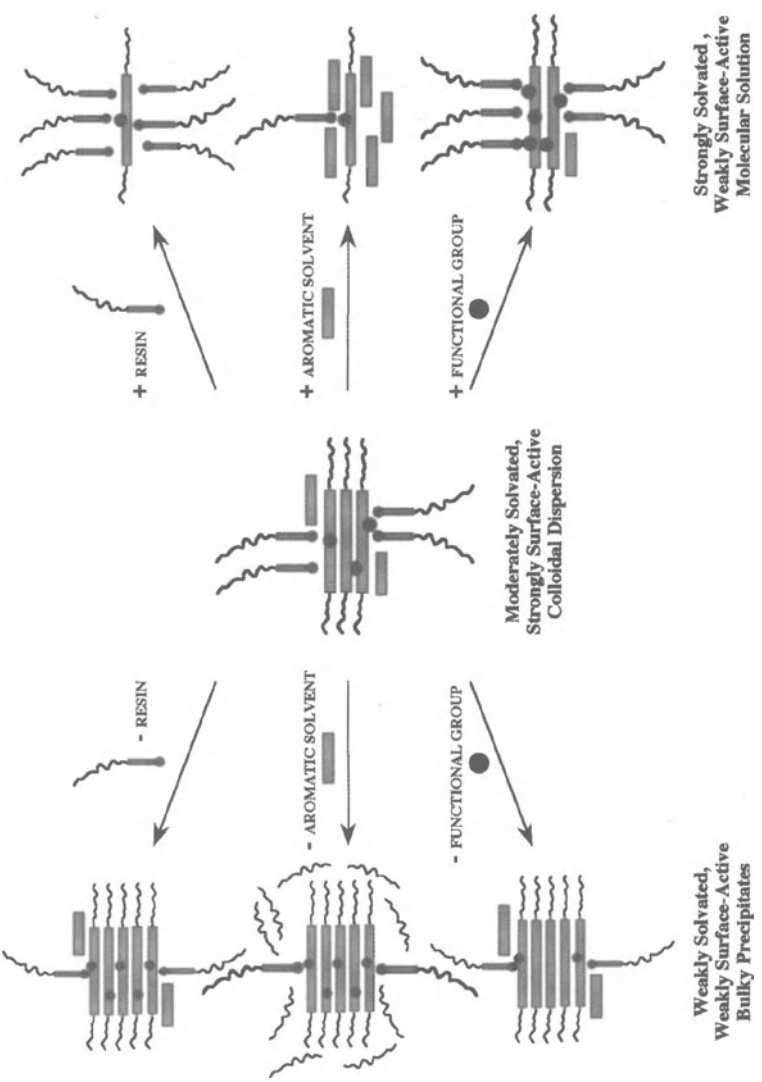

Figure 8. Molecular schematic illustrating the modes through which asphaltene aggregation can be mediated by resins, aromatic solvent, and polar functional group density. Addition of resins, aromatic solvent, and polar functionality to the asphaltenes is expected to promote solvation and reduce surface activity. A decrease in resin-to-asphaltene ratio, aromatic solvent character, or polar functionality in the asphaltene molecules is expected to increase the relative strength of asphaltene-asphaltene interactions, diminish solvation, and hence increase surface activity.

surface active with the increasing availability of solvating resins. Also, as shown in the middle path, increasing the aromaticity (i.e. aromatic carbon content) of the crude medium through the addition of aromatic solvents would help to deactivate strongly surface-active asphaltenes by creating an environment that is more 'like' the nature of the condensed, polyaromatic asphaltene molecules. This in effect is increasing the aromaticity ratio of the crude medium with respect to the asphaltenes. Finally, the bottom path shows that a crude oil which has a high functionality (i.e. high concentration of functional groups) in its resin and asphaltene molecules would tend to create asphaltenic colloidal aggregates which are more strongly solvated through the increased number of H-bond interactions with the resin molecules than a crude oil of lower functional group content. Thus, the crude oil composed of resins and asphaltenes of high polar functionality would contain asphaltenic aggregates that find it difficult to shed their solvating resins and are consequently *less* surface active and have a lower propensity to form stable emulsions. Of course, each of these contributions are not isolated from each other in determining the solubility state of the asphaltenes within a given crude oil. In fact, one could envision combining some or all of these ideas such as the addition of resin molecules which are both very aromatic and highly functional into a particular crude in order to molecularly dissolve the indigenous asphaltenes and minimize the formation of stable emulsions during processing.

4.4.3. Emulsion Stability of Whole Crudes with Water at Various pH. The emulsion stability results for the crude oils in this study which formed emulsions stable to gravity sedimentation are presented both as a function of crude type and aqueous phase pH in Figure 9. It should be noted that emulsion stability, according to this operational definition, increases as the amount of resolved water decreases (i.e. they are inversely related). It is apparent that Arab Heavy forms the most stable emulsions (0–5 % water resolved, except at basic pHs 10 & 12) and that Arab Berri and Alaska North Slope form considerably weaker emulsions (50–90% water resolved). San Joaquin Valley crude formed emulsions which were totally unstable to gravity sedimentation (i.e. all of the water resolved after gravity settling for 24 hrs). This was thought to be due to its high viscosity at room temperature which inhibits the shearing of water droplets to the micron-level sizes necessary to form a stable emulsion. Attempts to form an emulsion with SJV at a temperature of 100°C were successful to some extent. The heating of the SJV crude oil to 100°C would be sufficient to melt any paraffinic and/or microcrystalline waxes present in the crude and consequently lower the viscosity of the continuous oil phase enough to allow intimate mixing of the oil and water. However, these emulsions were still not very stable (approximately half the water resolved after settling under gravity for 24 hours) compared to the emulsions formed from the other crudes in this study at room temperature. The stability of emulsions produced from these crudes in order of decreasing rank are as follows:

Arab Heavy » Arab Berri = Alaska North Slope > San Joaquin Valley

An emulsion formation and stability protocol which allows analysis at higher temperatures and pressures is currently being developed.

4.4.4. Correlation of R/A and Asphaltene Contents with Emulsion Stability. The R/A and asphaltene contents of the four crudes in this study (in order of increasing emulsion stability) are presented graphically in Figure 10. It is evident that Arab Heavy has the lowest R/A and is also richest in asphaltenes as would be expected from the proposed stabilization mechanism. However, AB has the highest R/A but forms the second most stable

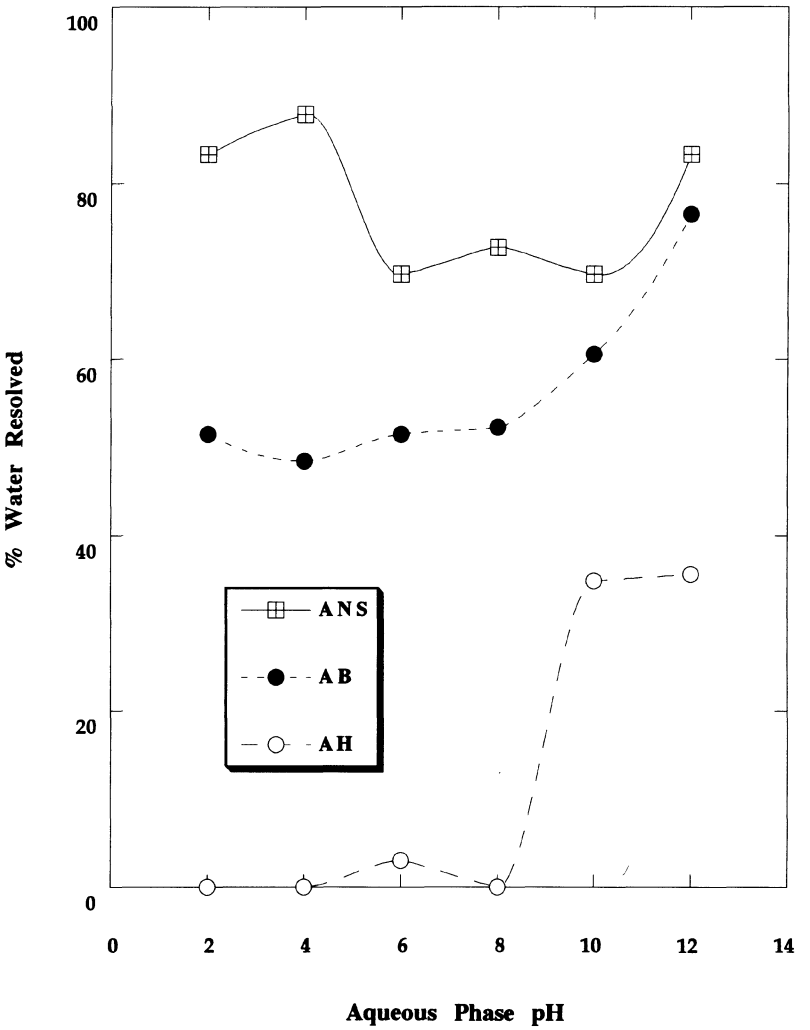

Figure 9. Effect of crude type (AH, AB, and ANS) and aqueous phase pH on % water resolved in standard emulsion stability protocol (see Figure 6 and Experimental Section for details).

emulsion. The R/A definitely tells us part of the 'story', but it is obvious that one cannot depend solely on this parameter as a predictor of relative emulsion stability. As we will show in the section on model emulsions later, the specific chemical effects of the asphaltenes and resins—i.e. the relative polarity and density of specific H-bonding functional groups such as carbonyls and pyrroles— is an important secondary determinant of emulsion stability.

4.4.5. Effect of Addition of Resins on Emulsion Stability. In order to see a more direct and comprehensive effect of the R/A on emulsion stability, we explored the option of adding or "doping" resins to the crude oil. This study has been performed with most combinations of crude types and resins from different crude types dissolved in heptol (in order

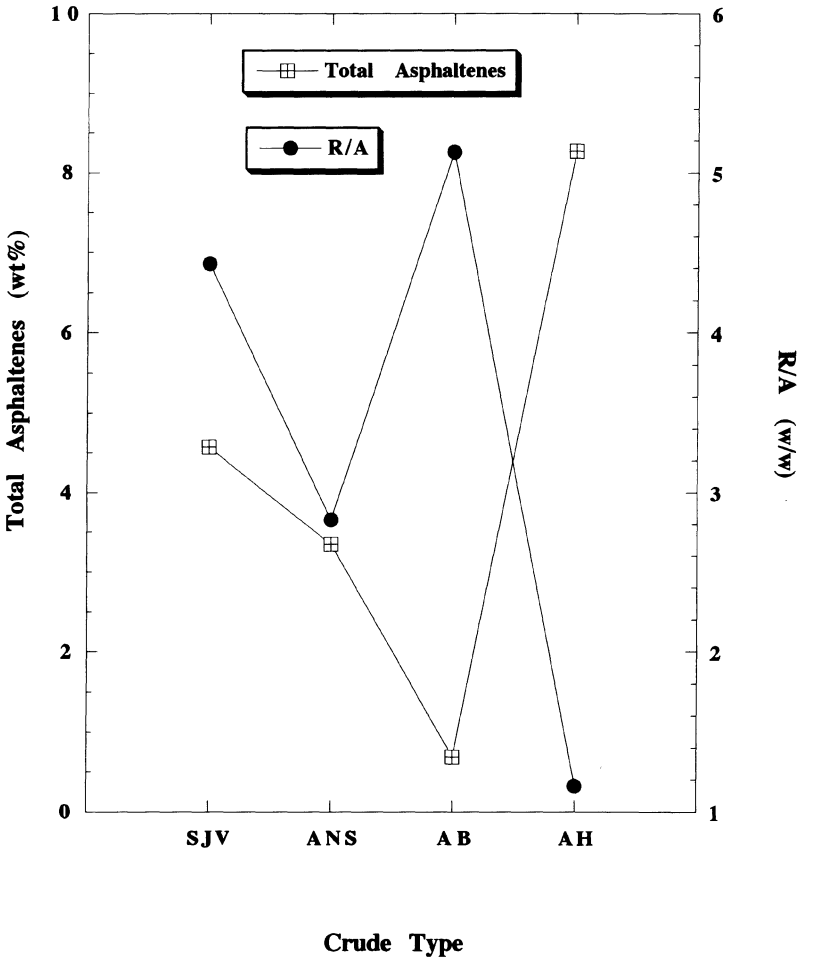

Figure 10. Total asphaltene content (as measured by n-heptane insolubles) and resin-to-asphaltene ratio (R/A) for the four crudes in this study (SJV, ANS, AB, AH). The results are plotted in order of increasing water-in-crude oil emulsion stability at neutral pH.

to ensure complete dissolution of the resin fraction within the crude oil) to gain further insight into the interactions between these interfacially-active constituents in the presence of the indigenous crude oil. The effect of adding resins from AH, AB, and SJV to solvent-modified AH crude oil (30% v/v heptol in crude oil) using the modified protocol at 50°C as a function of R/A is presented in Figure 11. The added AH resins destabilize the emulsion appreciably as the R/A is raised from 2.1 to 3.8 and then appear to have little effect thereafter. However, the addition of AB resins, which are relatively higher in sulfoxide content, appears to have a more dramatic and consistent destabilizing effect over the entire range of R/A up to 6.6. Adding SJV resins, which are rich in pyrrolic and carboxylic functional groups, has the most dramatic destabilizing effect upon raising the R/A from 2.1 to 3.9. It's obvious that resins isolated from different crude types have varying impacts on the resultant emulsion stability based on specific chemical effects as discussed above.

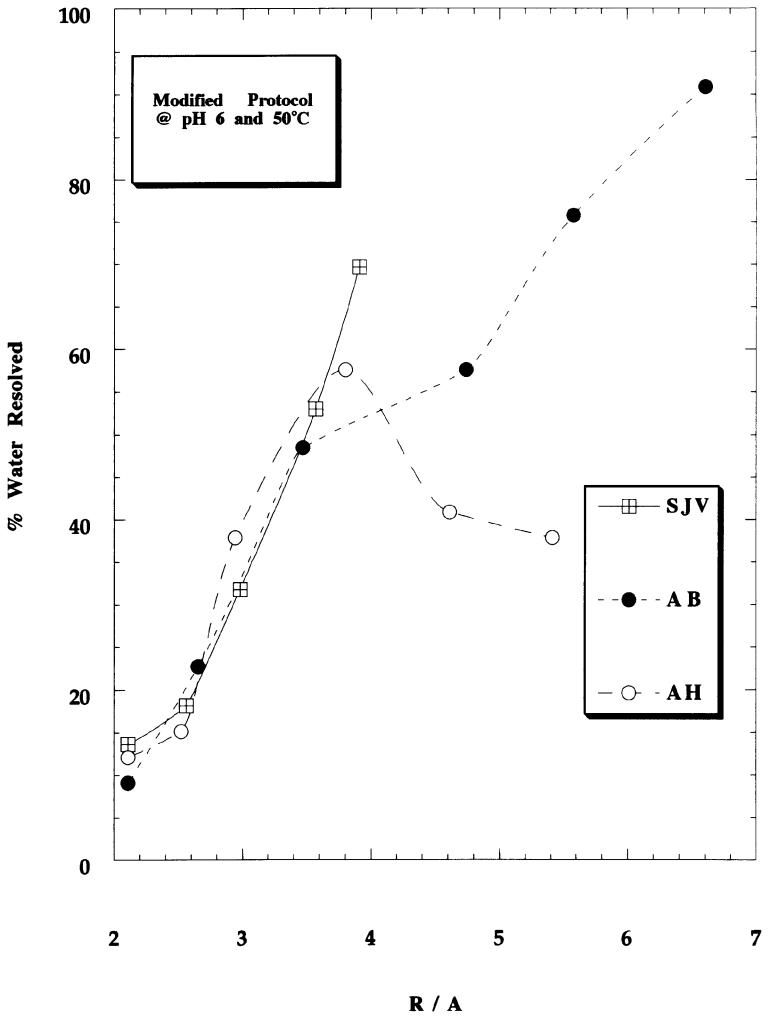

Figure 11. Effect of adding resins (SJV, AB, and AH) to AH crude oil on % water resolved in the modified protocol for gauging emulsion stability (see Figure 6 and Experimental Section for details). The trend with increasing R/A clearly illustrates the destabilizing effect of R/A > 4–5.

Moreover, it appears that the more polar resins destabilize the emulsions more effectively, as suggested by the solvation mechanism mentioned in Figure 8. This theme will be illustrated in more depth in the section on model emulsions.

4.4.6. Effect of Addition of Organic Solvents on Emulsion Stability. The hypothesis that the solvation of asphaltenes is the primary determinant of emulsion stability led to another study aimed at measuring the effect of changing the aromatic nature of the crude medium by blending solvents of varying amounts and aromaticity with the whole crude oils. In our first experiment, crudes were systematically modified by addition of either a purely aliphatic solvent (n-heptane), an aromatic solvent (toluene), or a mixture of the two

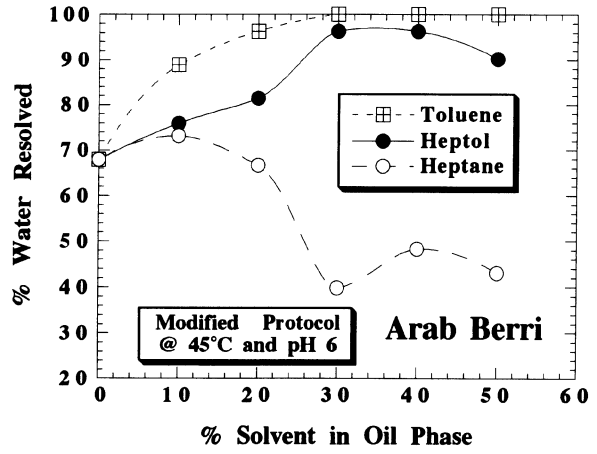

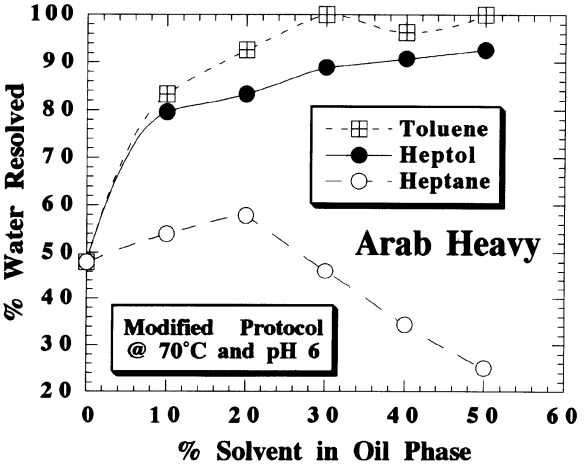

Figure 12. Effect of solvent addition (n-heptane, heptol -- 30% toluene, 70% n-heptane (v/v), toluene) to AH crude oil on % water resolved using modified protocol (see Figure 6 and Experimental Section for details).

(70% n-heptane and 30% toluene, so-called heptol) in increasing amounts (10–50%). Figure 12 shows the effects of blending the three different solvents with AB and AH (prior to homogenization) on emulsion stability as a function of the solvent content in the oil phase. It is clear that addition of toluene and heptol destabilizes the emulsions while with sufficient addition of n-heptane (30–50%), the emulsions are stabilized. This is fully consistent with the notion that increased aromaticity of the crude medium helps to further solubilize the asphaltenes. Moreover, with heptol and toluene, there may be a viscosity reduction effect. With n-heptane, however, it is clear that the stabilization of the emulsion must be due to increased agglomeration or flocculation of the asphaltene fraction of the crude. Despite the fact that 30% added n-heptane is clearly not sufficient to precipitate the asphaltenes, there must be reduced molecular solubilization resulting in aggregation and surface activity.

4.4.7. Effects of Solvent Aromaticity and Molecular Structure on Emulsion Stability. Solvents of varying molecular structure and aromaticities—benzene, toluene, xylene, ethyl benzene, tert-butylbenzene, cumene, cymene, naphthalene, and phenanthrene—were also utilized to further gauge the influence of the solvent "power" on emulsion stability as mediated by the state of dispersion of the asphaltenes in the crude medium. The results from this study are plotted in Figure 13 as a function of the % of oleic phase comprised by added aromatic solvent prior to homogenization. It is evident that all of the solvents are sufficiently aromatic to destabilize the emulsions and that the most aromatic solvents (i.e. solvents of highest aromatic carbon content) are more effective in resolving the emulsions. Since asphaltenes are known to be condensed polyaromatic-ringed compounds, naphthalene and phenanthrene were dissolved in benzene (at concentrations just under their solubility limits of 0.37 and 0.35 g/mL of benzene, respectively) to see if this would effect any

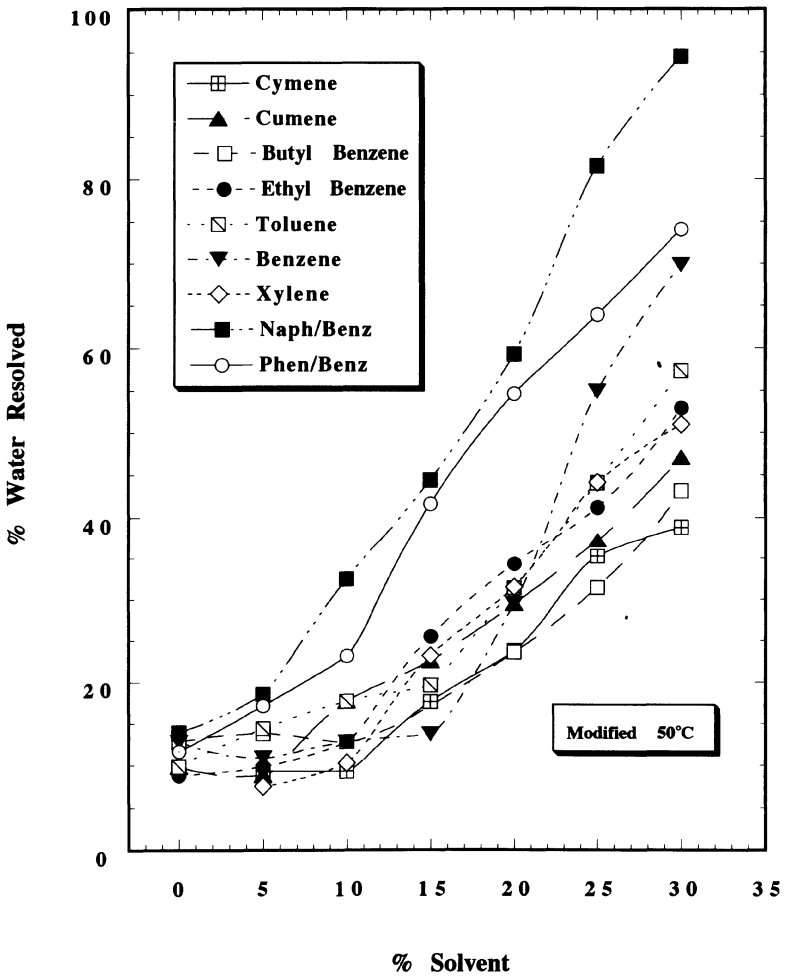

Figure 13. Effect of solvent molecular structure and aromaticity (% aromatic carbon in the solvent) on emulsion stability of selectively doped Arab Heavy crude oil using the modified protocol.

further destabilization of the emulsions produced with these solvent-modified crudes. This was indeed found to be the case as Figure 13 shows a considerable destabilization with naphthalene-benzene and phenanthrene-benzene mixtures over and above what was observed with pure benzene over the entire range of added solvent.

5. MODEL SYSTEMS OF ASPHALTENES, PURE OILS, AND WATER

In addition to the wealth of studies performed on crude oil-water interfaces, a number of researchers have probed the oil-water interface in which isolated fractions of asphaltenes and/or resins have been adsorbed. In the majority of these studies, the oil phase was carefully controlled by using either pure solvents, such as xylene, heptane, or toluene, or was a blend of an aliphatic and an aromatic solvent in an effort to simulate the solvent properties of crude oil. These studies are collected chronologically in Table 4, in which the citation, the model oil and asphaltene fractions, and the key techniques are identified.

5.1. Interfacial Films and Water-in-Oil Emulsions of Model Oils and Asphaltenes

Lawrence and Killner[79] were among the first to probe the properties of asphalt diluted in mixtures of toluene and hexane adsorbed at the oil-water interface. They observed that, under hexane-rich solvent conditions leading to the aggregation of asphaltenes, the interfacial films of asphalt were highly elastic. They described the film encapsulating the water droplets in the w/o emulsion as "plastic bags". Using a simple rheological device, they measured interfacial viscosities greater than 2×10^4 surface poise. No elastic moduli were measured or reported, probably due to the limitations of their technique.

Van der Waarden[41] reported emulsions of water and clean oil—i.e. low-viscosity, wax- and resin-free hydrocarbons—stabilized by asphaltenes isolated from crudes. The oleic phase in his study was a mixture of kerex, an aromatic fraction from crude oil, and an aromatic-free kerosene fraction. Van der Waarden studied the aggregation properties of asphaltenes as a function of the aliphatic-aromatic ratio by blending kerex and kerosene. Strongly polar asphaltenes, obtained by thermally cracking atmospheric residue, were flocculated with modest amounts (20%) of an aromatic-free kerosene while less polar asphaltenes required larger concentrations (60%) of aliphatic kerosene to induce flocculation. Emulsions prepared with 0.1 % asphaltenes in the oleic phase were very stable to gravity separation when the solvent conditions were such that the asphaltenes were flocculated. Resins added at a 5:1 weight ratio were observed to diminish considerably the emulsion stability at solvent conditions in which the asphaltenes were strongly flocculated. Finally, a simple rheological test of the interface using an oscillating disc revealed that the strongly flocculated asphaltenes exhibited large values (5–40) of a parameter "d" which essentially gauges the damping of the oscillations of the disc due to interfacial shear viscosity. As we will describe below, this experiment is very similar to the oscillating biconical bob method developed and applied by Neustadter et al.[97] and Mohammed et al.[14,15,36,105,106] Presumably, this "d" value is reflective of high interfacial shear viscosity and/or elasticity and is likely attributable to physical cross-linking of primary asphaltene aggregates at the oil-water interface through specific proton and electron donor-acceptor interactions. Very modest amounts (0.01 wt%) of sodium and calcium petroleum sulfon-

Table 4. Summary of studies conducted on model oil-water interfaces with adsorbed asphaltenes and/or resins, either emulsion, pendant drop, or planar interface studies

		System studied			
Investigators	Ref #	Oil phase	Crude fractions	Method of study	Key findings
van der Waarden	41	kerex/kerosene	A: benzene ppt mineral oil distillate, R: butane ppt bitumen	IF rheology: bob at interface	resins decrease stabilizing effect of asphaltenes
Mardanenko et al.	86	vaseline oil/toluene	pet ether extraction Uzen and Zhetybai field crudes	surface tension of extracted fractions	
MacKay et al.	38	xylene	A: heptane ppt Venezuela crude	Optical microscopy; physical isolation of collapsed "skin"	
Rogacheva et al.	124	toluene	A: isooctane ppt tar, cracking residue, crude, distillate of Kotu-Tepinsk crude	IFT: maximal bubble pressure	asphaltenes aggregate and have surface activity
Pasquarelli et al.	37	benzene	A: pentane ppt, R: silica ads. California crude	IFT: spinning drop; IF shear viscosity: viscous traction shear viscometer	resins may increase emulsion stability by preventing asphaltene precipitation
Papirer et al.	76	decalin, pet ether	A: heptane ppt Boscan, Aquila, Zubair crudes	Absorbance measurement (H-bonding); NMR; water separation	hydrogen bonding is important for asphaltene stacking
Siffert et al.	112	decalin, pet ether	A: heptane ppt Boscan, Aquila, Zubair crudes	GPC; IFT: interaction of asph. adsorbed on glass with oil and water phases	organization of asphaltenes at interface is responsible for emulsion stability
Mansurov et al.	72	min oil/xylene-1/1, xylene	A: pet ether ppt Sergeevsk crude R: silica ads. Sergeevsk, Chutyrsk crudes	IFT: torsion pendulum	resin-asphaltene interaction is important, increase in IF strength with R/A up to 1/3 then decrease
Sjöblom et al.	90	decane/ dodecane	hexane ppt and silica ads. North Sea crudes	FTIR; GC	stacking of material at interface is inferred
Krawczyk et al.	30	heptane/toluene -7/3	A: pentane ppt East Texas crude	IFT: Wilhelmy plate; IF viscosity: deep channel viscous traction viscometer; water separation	demulsifier effectiveness increases with adsorption rate, IF activity must be high enough to suppress IFT gradient
Nordli et al.	98	toluene/hexane-1/1	silica ads.	Surface pressure: Langmuir trough	aromatics strongly interact with and modify the interfacial film
Mingyuan et al.	74	decane	A: pentane ppt, R: silica ads. North Sea crudes	FTIR	emulsion stabilizing components are found in both resins and asphaltenes (more in A)

Table 4. (*Continued*)

Investigators	Ref #	System studied: Oil phase	System studied: Crude fractions	Method of study	Key findings
Shetty et al.	13	heptane/toluene -7/3	A: pentane ppt East Texas crude	water separation	water soluble surfactants can destabilize emulsions
Sjöblom et al.	125	decane, benzene, heptanol	A: pentane ppt, R: silica ads. North Sea crudes	IFT: drop volume	resin-asphaltene interactions are important
Wasan	31	heptane/toluene -7/3	A: pentane ppt California crude	IF viscosity: deep channel viscous traction viscometer; IF activity; max. droplet pressure; water separation	demulsifier performance correlates with interfacial activity
Acevedo et al.	113	xylene	A: hexane ppt, R: hexane soxhlet extraction Cerro Negro crude	IF rheology: bob at interface	rheological differences when resins are present
Mohammed et al.	36	xylene/heptane -1/3	A: heptane ppt R: xylene extraction North Sea Buchan crude	IFT: Wilhelmy plate; surface pressure: Langmuir film balance	resin-asphaltene interactions important for strong films
Urdahl et al.	120	decane	hexane ppt and silica ads. North Sea crudes	IFT: du Nuoy ring	surfactants destabilize emulsions by replacing surface active material at interface
Bhardwaj et al.	121	toluene	A: heptane ppt Germany crude	IFT: drop volume method; water separation	interface toughens due to slow adsorption of natural surfactants, correlation with demulsifier adsorption and rate of demulsification
Skodvin et al.	122	decane	hexane ppt and silica ads. North Sea crudes	time domain dielectric spectroscopy	information on relaxation times and static permitivities
Førdedal et al.	35	decane	A: heptane ppt, R: silica ads. France crude	IFT: du Nuoy ring	resin-asphaltene interaction is important
Ese et al.	126	toluene/decane -1/9	A: pentane ppt, R: silica ads. North Sea crude	time domain dielectric spectroscopy; water separation	emulsion stability depends on asphaltene concentration, degree of A and R aging, and R/A
McLean et al.	91	heptane/toluene	A: heptane ppt, R: silica ads. Alaska, Saudi Arabia, California crudes	water separation	asphaltene concentration and R/A are important for asphaltene aggregation and resulting emulsion stability

Abbreviations include IF (interface); IFT (interfacial tension); GPC (gel permeation chromatography); GC (gas chromatography); NMR (nuclear magnetic resonance spectroscopy); FTIR (Fourier transform infrared spectroscopy); R (resins); and A (asphaltenes).

ates, as well as higher amounts (0.5 wt %) of resins, were observed to reduce this rheological "d" parameter from >5–10 to 1, thus indicating either the break-up of these physical cross-links at the interface due to selective solvation or due to displacement of the cross-linked films from the interface by the additive.

Mackay et al.[38] isolated a sub-fraction of asphaltenes from Venezuelan crude oil—identified as "Compound X"—and generated emulsions of compound X in xylene with water at concentrations as low as 0.03 wt%. Compound X was indistinguishable from the bulk asphaltene fraction in terms of its elemental composition, but was clearly more effective at creating strong emulsions at lower concentrations than the whole asphaltene fraction. Mackay et al. isolated the interfacial "skin" of compound X-stabilized xylene-water emulsions and found it to be quite comparable in appearance to Lawrence and Killner's[79] "plastic bag". They argue that the mechanism of stabilization is *not* repulsive forces between droplets but rather the "considerable elasticity and mechanical strength" of the films encapsulating the droplets. Their evidence suggests that the strongest film formers are a sub-fraction of asphaltenes and that, under appropriate solvent conditions, resins and other components of the crude are not necessary for the formation of a strong, mechanically stable interfacial film.

Papirer et al.[76] and Siffert et al.[112] published studies of the emulsifying properties of three different asphaltene fractions isolated from Aquila and Boscan vacuum distillation residues and from a Zubair distillation residue which had been air blown at 280°C. The Zubair asphaltenes were observed to have the lowest H/C ratio of the three (1.05), the highest contact angle with water (95.6°), the greatest acid-base imbalance (acid-base ratio of 5:1), and the lowest H-bonding ability as measured by phenol interaction value or PIV (28 versus 31 and 37 for the others). This Zubair asphaltene fraction also formed the most stable w/o emulsions when mixed at 1–5 wt% in water (70%), decalin (15%) and petroleum ether (10–15%). Papirer et al. concluded that the Zubair asphaltenes must be more easily deformed on a molecular level (less intermolecular cohesion) but still possess strong acidic groups to adopt the ideal conformation for the formation of oriented layers at the water-oil interface. Thus, they seem to argue that there are competing effects which suggest that cohesion is important for mechanically rigid films but the molecular aggregates must possess sufficient flexibility to adopt the appropriate orientation. This latter point seems somewhat tenuous as the difference in PIVs among the three asphaltenes is modest. Moreover, other investigators have observed that the presence of carbonyls, carboxylic acids, and other H-bonding groups is essential for stable asphaltenic films.[74] Siffert et al.[112] performed x-ray diffraction studies of the asphaltenic films and observed that the Zubair asphaltenes formed a discotic lamellar phase upon sedimentation of the asphaltenes in solvent. They argue that the ability of these asphaltenes to stack and form lamellar mesophases may be enhanced by air blowing, which may crosslink the aromatic cores of the individual asphaltene molecules.

Mansurov et al.[72] studied the shear strength of interfacial films of asphaltenes adsorbed from a 1:1 (v/v) mixture of white mineral oil and m-xylene at an oil-water interface with distilled water. The asphaltenes were isolated from a variety of Russian crudes and added to the oil mixture at a concentration of 0.1% (w/w). The interfaces were aged for 20 hours at room temperature. The shear strength of the films was measured with a rheological device of the "torsion pendulum type." The value of shear strength σ_t, which is presumably closely related to either the shear or elastic modulus as measured by a biconical bob experiment, varied from 0.8–4.0 mN/m. This shear strength parameter was also observed to be a strong function of the concentration of asphaltenic species containing metal porphyrin complexes, as deduced by extracting these materials with acetone while monitoring the shear strength. Mansurov et al. thus concluded that these metal porphyrin-containing materials re-inforce the film-forming properties of the asphaltenes and increase

their shear strength. We might further speculate that this occurs through electron donor-acceptor cross-linking of primary asphaltenic aggregates to form stable, flocculated three-dimensional networks which confer film rigidity and elasticity.

Mansurov et al.[72] also probed the effects of blending resins isolated from Sergeevsk and Chutyrsk crudes with varying concentrations of Sergeevsk asphaltenes. The shear strength of pure 0.2% (w/w) asphaltenes was observed to be 1.16 mN/m when adsorbed to the water-oil interface of a distilled water/mineral oil-m-xylene (1:1 v/v) system. This shear strength was doubled by adding small amounts of resins such that the ratio of resins to asphaltenes was 1:3 (w/w). At higher ratios of resins to asphaltenes (> 0.5), the shear strength was observed to fall and at R/A > 4, the shear strength fell below that of pure asphaltenes and continued to fall with increasing R/A. Pure resins were not observed to form strong films. As we will discuss later, what is likely occurring relates to the state of aggregation of the asphaltenes in the oleic medium and how this is affected by solvating resins. Apparently, Sergeevsk asphaltenes are partially flocculated in 1:1 mineral oil:m-xylene and are thus not totally surface-active or able to organize into strong three-dimensional films. Addition of modest amounts of resins apparently either (1) solvates the asphaltenes and facilitates their compact adsorption at the interface or (2) functions to cross-link the asphaltenes by providing functionality to assist in this cross-linking (i.e. complementary H-bond or electron donor-acceptor sites). However, as we will show below, resins are certainly not always required nor are they always desirable. Under proper solvent conditions (i.e. proportion of aromatic versus aliphatic solvent character), asphaltenes alone form more stable films (as indicated by w/o emulsion stability) and addition of resins simply destabilizes the emulsions. The extent to which resins are advantageous or desirable in assisting in strong film formation also seems to be a very strong function of crude chemistry, which has been a hidden dimension in most previous studies in the literature.

Acevedo et al.[113] utilized the biconical bob rheometer (model SR-14) developed by the British Petroleum group[97,114] to study the rheology of Cerro Negro asphaltenes adsorbed at a xylene-water interface. They also studied the whole crude oil diluted (30 % v/v) in xylene in contact with water and aged for 36 hours. Both shear viscoelasticity and creep compliance measurements were performed. The aqueous phase was either pure distilled water or 2% NaCl and then pH-adjusted between 1.8 and 9.0. The surface creep compliance curves were fit to either two- or four-body rheological models comprised of Maxwell and Voigt units. With the most viscoelastic films, the value of the instantaneous interfacial elastic modulus E_o was estimated from the early stages of the creep compliance curve. This modulus varied from 2–45 mN/m. With the xylene-diluted crude, the maximum modulus was observed at nearly neutral pH (6.6) against distilled water, and was observed over a pH range of 3.5–6.5 against 2% NaCl in water. With the asphaltene-xylene system, the film rigidity as gauged by E_o, is maximized at lower pHs and is somewhat less sensitive to pH than the diluted crude. The authors conclude that the lower sensitivity of film rigidity in the asphaltene system may be attributable to the absence of resins in the model system. As we have shown in our crude emulsion studies, in which the crude was selectively doped with solvents and/or added resins, the effects of resins on asphaltene aggregation and film formation cannot be de-coupled from the aromaticity of the solvent phase used in solubilizing the asphaltenes. We will further illustrate this below.

5.2. Effect of Resins on Asphaltene-Stabilized Emulsions in Model Toluene-Heptane-Water Mixtures

As described in McLean and Kilpatrick,[91] we have performed an extensive series of experiments on the relative emulsion stability of asphaltene-stabilized emulsions in mix-

tures of heptane, toluene, and water. In particular, we have studied in detail the effects of a variety of resin types on the stability of these emulsions as gauged by the standard emulsion protocol schematized in Figure 6 and described in the Experimental Section. In what follows, we will describe the sequence of experiments and discuss the implications of these experiments with respect to our current molecular-level understanding of the mechanism of asphaltene stabilization of water-in-oil emulsions.

5.2.1. Emulsions Stabilized Purely by Asphaltenes or Resins. Our initial experiments on model emulsions focused on establishing that asphaltenes in the absence of resins were capable of stabilizing water-in-oil emulsions. Accordingly, we dissolved asphaltenes from

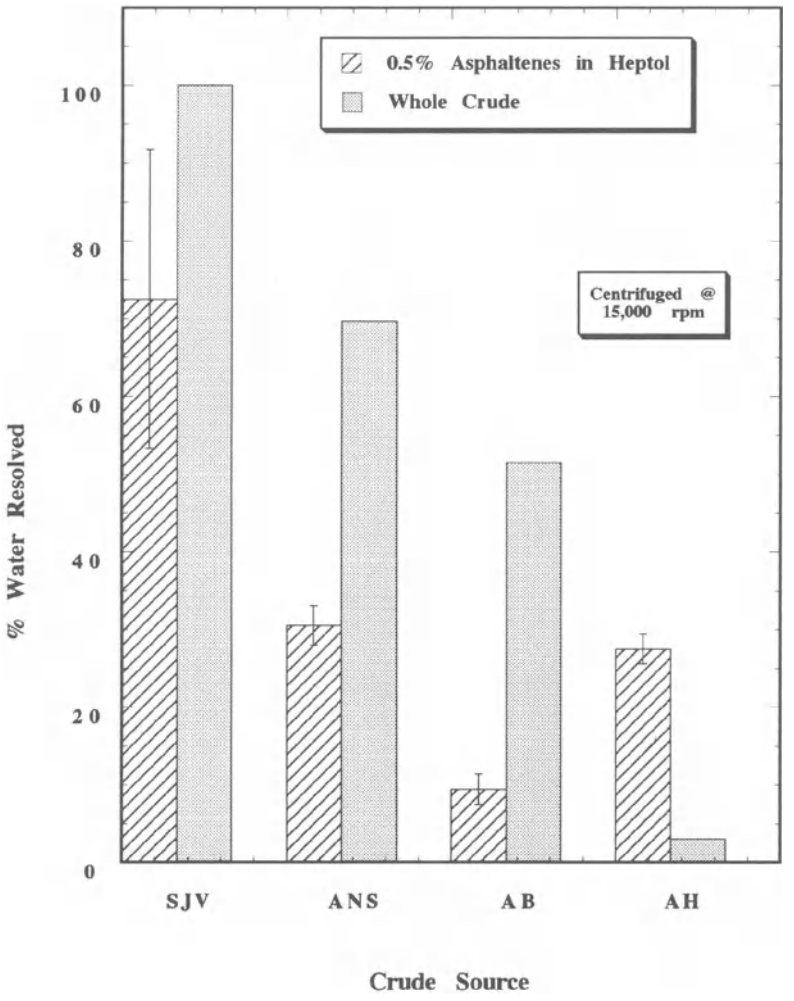

Figure 14. Comparison of emulsion stability, as gauged by % water resolved, of water-in-whole crude emulsions versus model n-heptane-toluene (70:30 v/v)-water-0.5 wt% asphaltenes. The standard emulsion protocol was used with centrifugation at 15,000 rpm.

the four crudes (SJV, ANS, AB, AH) in toluene and added sufficient heptane to generate 0.5 % asphaltenes in a mixture of 30% toluene and 70% n-heptane. This mixture was emulsified with water at pH 6 and centrifuged at 15,000 rpm according to the standard protocol. These results are compared with experiments on whole crudes in Figure 14. It is interesting to note that the model emulsions are nearly as stable or more stable than the whole crudes in all cases except AH, despite the fact that the asphaltene levels in the model experiments (0.5%) are considerably lower than the corresponding levels in the whole crudes. Thus, it is clearly the asphaltenes which dominate emulsion stability. The other materials in the crude (resins, waxes, di- and polyaromatics) primarily serve to solvate the asphaltenes and reduce their ability to stabilize emulsions.

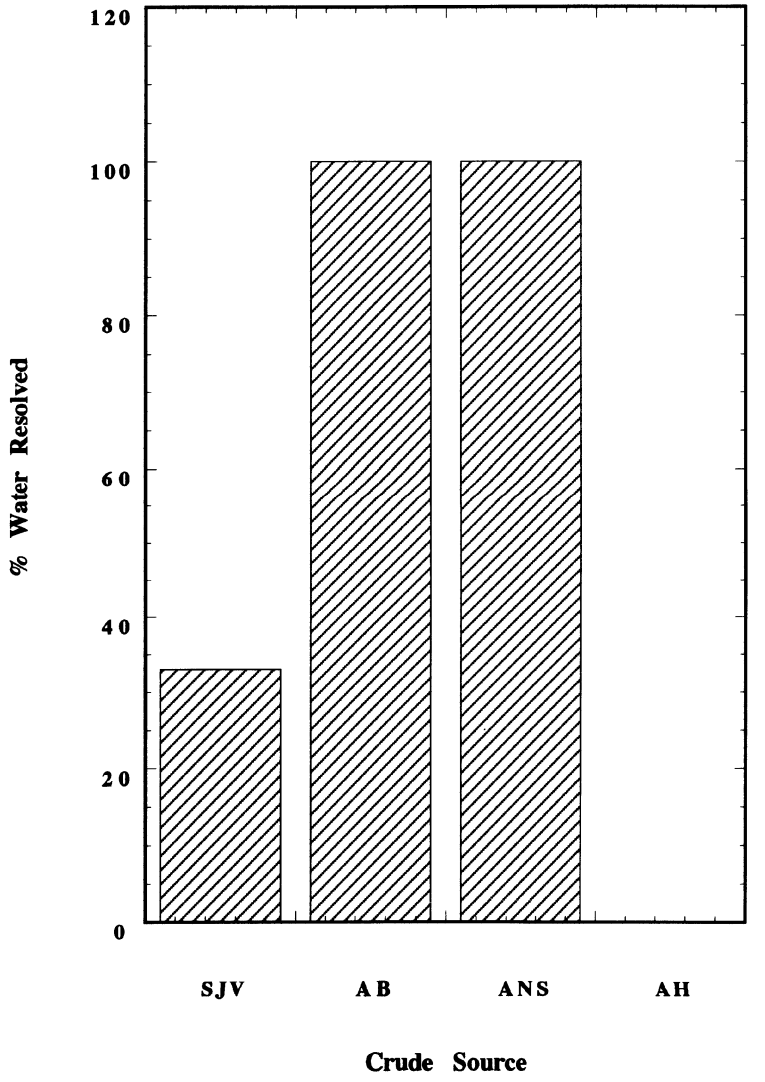

Figure 15. Relative emulsion stability to gravity settling of n-heptane-water-0.5 wt% resins.

We also performed experiments in which 0.5 % resins in n-heptane were added to water, emulsified according to the standard protocol, and observed with simply gravity settling (see Figure 15). Emulsions prepared with ANS and AB resins were totally unstable, emulsions prepared with SJV resins were partially stable, and emulsions prepared with AH resins were stable to gravity settling. However, the slightest amount of centrifugation at any speed was observed to totally break the emulsions and resolve all of the water. We infer from this experiment that there must certainly be specific chemical and structural differences between the differing resins. However, a simple functional group and elemental analysis (see McLean and Kilpatrick[61]) does not readily reveal the differences in resins. Nonetheless, one can conclude that resins are not effective at stabilizing emulsions to the degree that asphaltenes can.

5.2.2. Effect of Varying Toluene-Heptane Ratio on Asphaltene-Stabilized Emulsions. Based on our experience with the addition of aromatic solvents to whole crude oils (see Figures 12 and 13), we devised a series of experiments in which we probed the effects of varying aromaticity on emulsion stability of 0.5 % asphaltenes in heptane-toluene mixtures. The results are all collected in Figure 16, in which four separate series of experiments are superimposed. In two sets (AH-1 and ANS), AH and ANS asphaltenes were dissolved in pure toluene and diluted with n-heptane to generate 0.5 wt% asphaltenes in heptol mixtures of varying % toluene. These mixtures were then emulsified with water and centrifuged at 15,000 rpm according to the standard protocol. In the latter two sets (AH-2 and SJV), the same procedure was employed except the samples were centrifuged at 10,000 rpm. What is remarkable about these four sets of experiments is the degree of reproducibility given the differing sources of asphaltenes and the variation in stability protocol. All four experiments display optima—maximum emulsion stability—at 40% toluene in heptol. All four experiments also show significant instabilities in the emulsions at higher toluene content (> 60%) and at low toluene content (< 10–15 %). The emulsion instabilities at high toluene content is consistent with our doped crude studies described above in which increased solvation by aromatic solvent leads to decreased aggregation of asphaltenes and decreased surface activity. What is intriguing is the diminished stability at low toluene content. Apparently, sufficiently aliphatic solvent conditions precipitate asphaltenes and the precipitates are either not sufficiently surface-active or have a low surface-to-volume ratio relative to smaller agglomerates. The effect seems to be universal regardless of the source of asphaltenes.

5.2.3. Effect of Resin Addition to Model Emulsions of Asphaltenes, Heptol, and Water. In analogy with the resin doping experiments performed with whole crudes (see Figure 11), we have also performed a series of experiments in which resins of all four crude types (AH, SJV, AB, and ANS) were added to solutions of 0.5 % asphaltenes in 30% toluene, 70% n-heptane and then emulsified with water according to the standard protocol. The emulsion stabilities as gauged by % water resolved are very revealing with respect to universal trends as well as specific chemical effects. The experiments with AH asphaltenes are shown in Figure 17. All four types of resins are observed to inhibit emulsion stability. However, AB and ANS resins seem to be somewhat more effective than SJV and AH resins, achieving total instability at R/A = 4. Emulsions stabilized by ANS asphaltenes are similar in stability trends to AH asphaltenes (see Figure 18); AB and ANS resins are more effective at destabilizing ANS asphaltene emulsions while SJV and AH resins are somewhat less effective. The comparable results with SJV asphaltene-stabilized emulsions are displayed in Figure 19. The emulsions in this last set of experiments were centrifuged at a

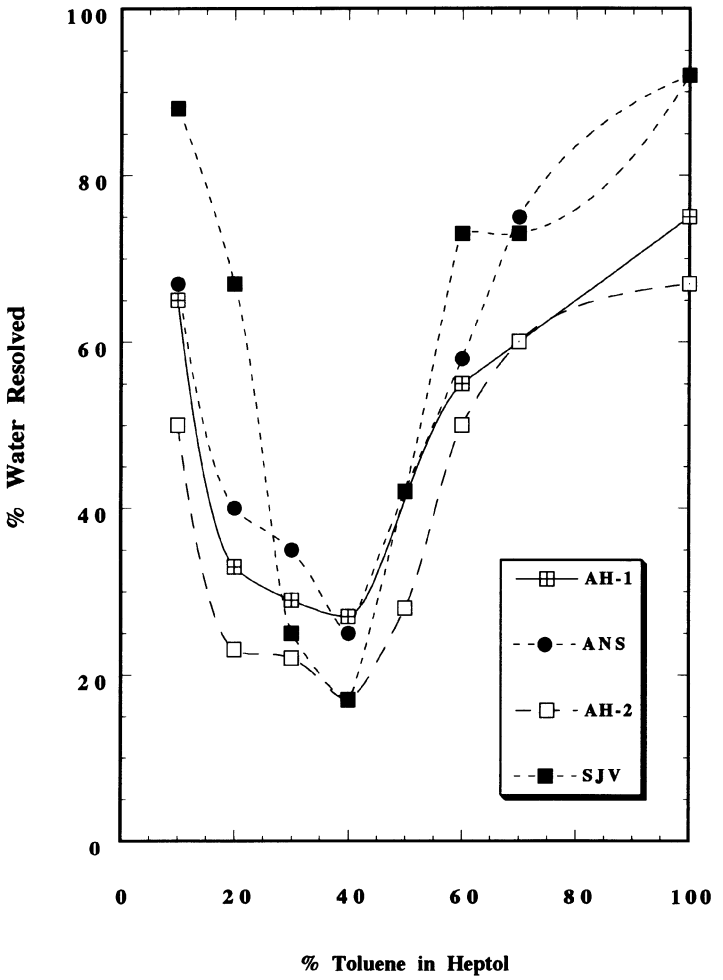

Figure 16. Emulsion stability, as gauged by % water resolved, of model emulsions comprised of n-heptane, toluene, water, and 0.5 wt% asphaltenes in the oleic phase. The oleic phase varied from 10% (v/v) toluene to 100% toluene with the complement being n-heptane. Relative proportions of the materials were 6 mLs oleic phase and 4 mLs water. The differing asphaltenes used were Arab Heavy (AH-1, AH-2), Alaska North Slope (ANS), and San Joaquin Valley (SJV). Experiments were performed using the standard emulsion protocol with centrifugation at either 15,000 rpm (AH-1 and ANS) or 10,000 rpm (AH-2 and SJV). It is clear that the trends with varying aromaticity are nearly universal.

slightly lower field strength (10,000 rpm) than in the previous two sets of experiments and hence the relative emulsion stability as indicated by % water resolved here is somewhat lower. More interesting is the effect of resin addition. While AB and ANS resins were most effective at destabilizing AH and ANS asphaltene-solubilized emulsions, they are least effective here. Conversely, AH and SJV resins—which were less effective at destabilizing AH and ANS asphaltenes—are more effective with SJV asphaltenes. Clearly, some very specific chemical functional effects are responsible for these inferred solvating

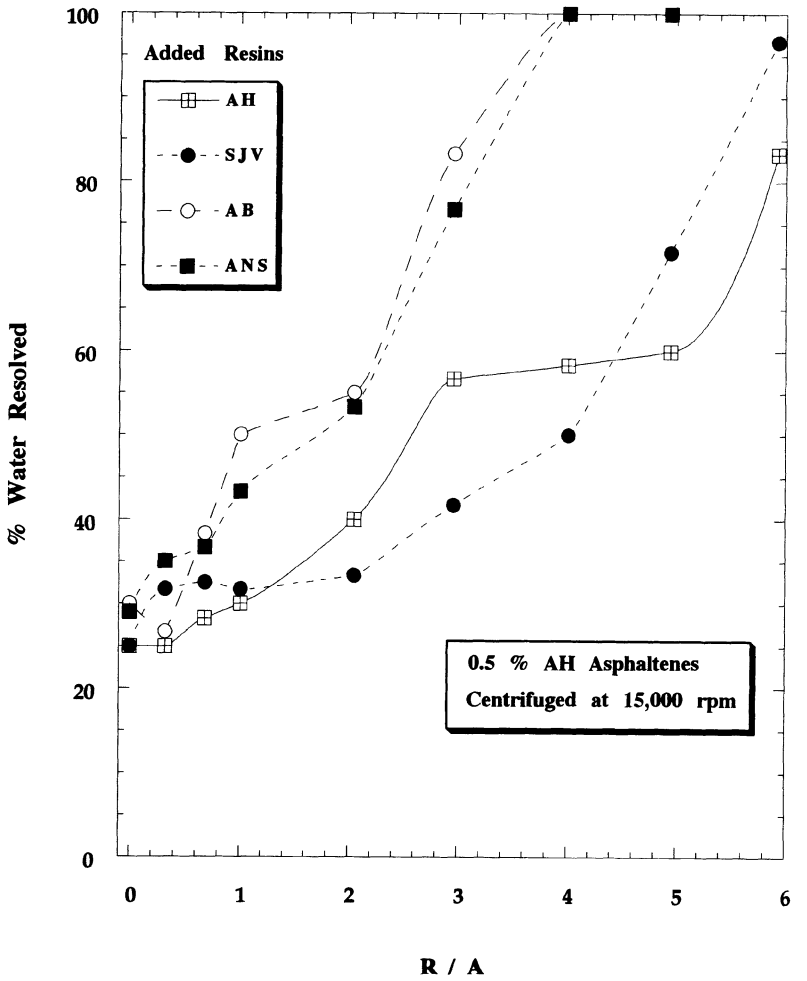

Figure 17. Emulsion stability, as gauged by % water resolved, of model emulsions comprised of 6 mLs n-heptane and toluene (70:30 v/v), 4 mLs water, 0.5 wt% AH asphaltenes in the oleic phase, and varying amounts of four different resins (AH, SJV, AB, and ANS). The standard emulsion protocol was used with centrifugation at 15,000 rpm.

trends. These effects cannot be resolved without careful fractionation of these resin and asphaltene fractions into sub-classes of acidic, basic, and neutral materials and then probing the colloid-forming and emulsion-stabilizing properties of these better defined subfractions. We are currently exploring these specific chemical effects.[92]

6. CONCLUSIONS

We have reviewed the literature on the role of asphaltenes in stabilizing water-in-oil emulsions and in generating rigid, mechanically strong films at oil-water interfaces. In the

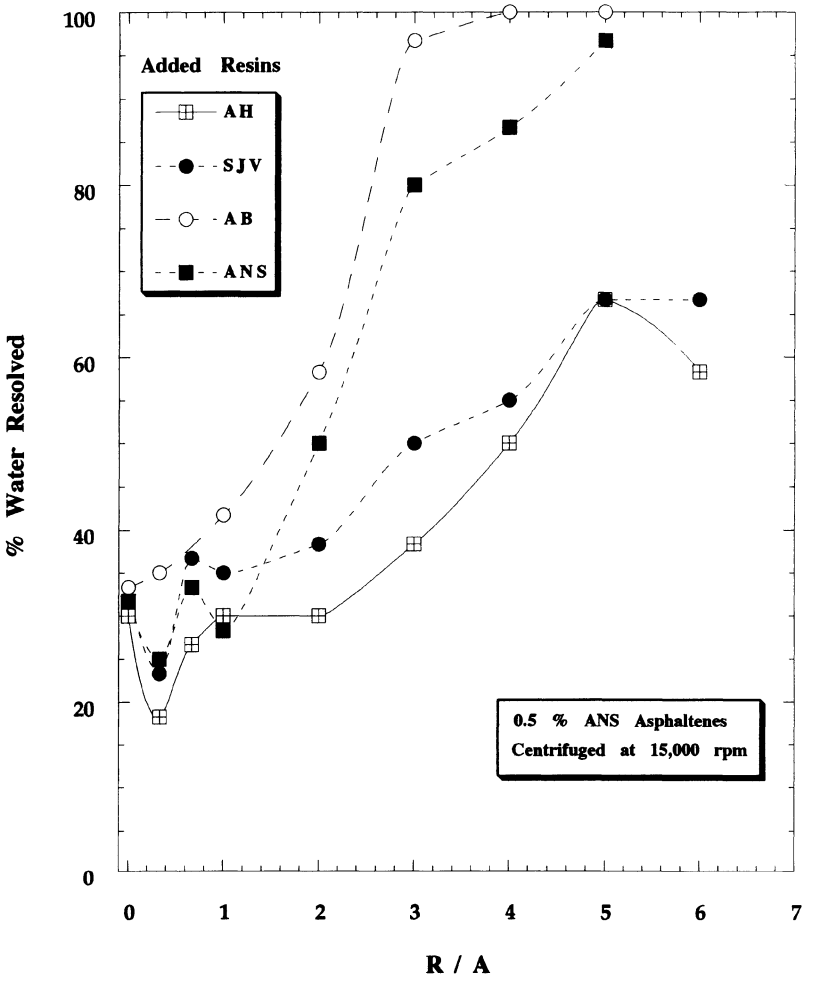

Figure 18. Emulsion stability, as gauged by % water resolved, of model emulsions comprised of 6 mLs n-heptane and toluene (70:30 v/v), 4 mLs water, 0.5 wt% ANS asphaltenes in the oleic phase, and varying amounts of four different resins (AH, SJV, AB, and ANS). The standard emulsion protocol was used with centrifugation at 15,000 rpm.

absence of any other crude oil components—i.e. resins, waxes, and aromatics—asphaltenes appear to be capable of forming rigid, cross-linked, elastic films which are the primary agents in stabilizing water-in-crude oil emulsions. The precise conformations in which asphaltenes organize at oil-water interfaces and the specific intermolecular interactions which facilitate crosslinking in these films has still not been elucidated. However, one can speculate based on a large body of literature that these intermolecular interactions must either be π-bonds between fused aromatic sheets, H-bonds mediated by carboxyl, pyrrolic, and sulfoxide functional groups, or electron donor-acceptor interactions mediated by porphyrin rings, heavy metals, or heteroatomic functional groups. Specific experimental designs to test these concepts are needed to understand the phenomenon at the molecular

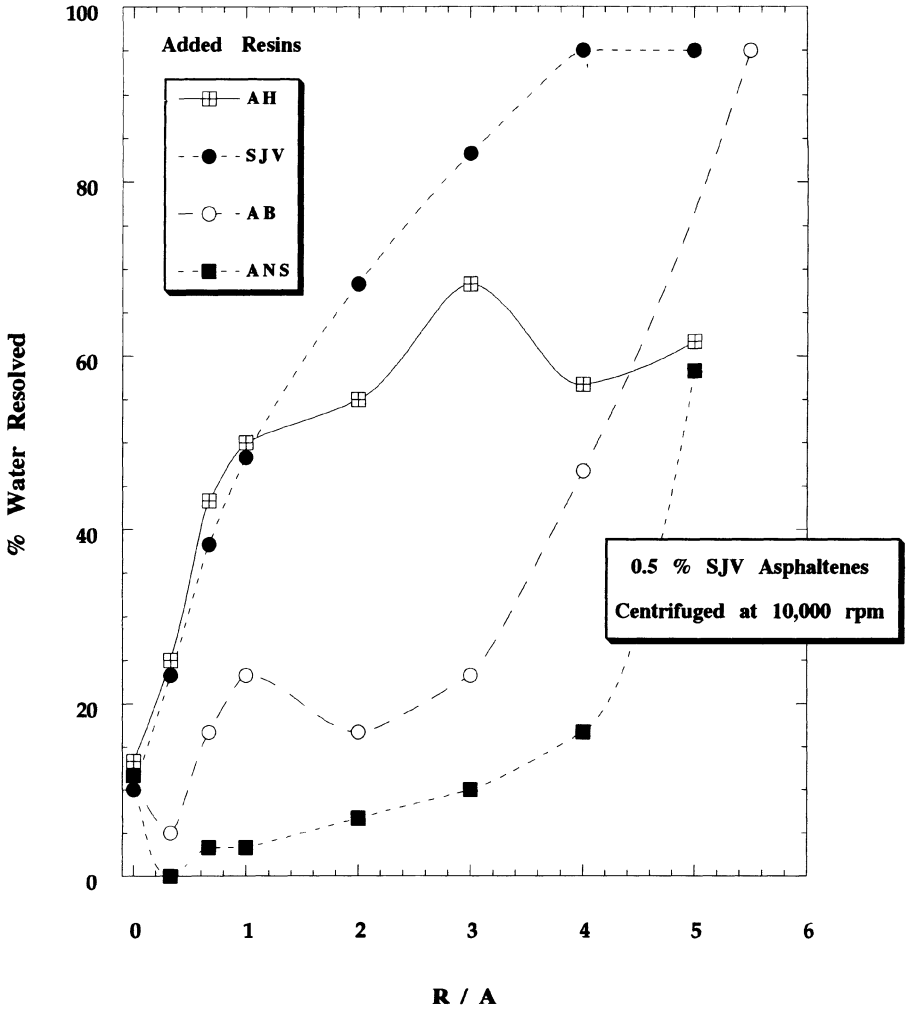

Figure 19. Emulsion stability, as gauged by % water resolved, of model emulsions comprised of 6 mLs n-heptane and toluene (70:30 v/v), 4 mLs water, 0.5 wt% SJV asphaltenes in the oleic phase, and varying amounts of four different resins (AH, SJV, AB, and ANS). The standard emulsion protocol was used with centrifugation at 10,000 rpm.

level and this knowledge would facilitate the design of chemical demulsifiers. We have shown that the solvating capacity of the oleic medium plays a large role in the surface activity of asphaltenic aggregates as well as in the resulting emulsion stability. What still eludes emulsion scientists is the precise role played by waxes and inorganic solids in either enhancing or destabilizing emulsions which are primarily stabilized by rigid, elastic asphaltenic films.

ACKNOWLEDGMENTS

This research has been supported by contracts from the Petroleum Environmental Research Forum (grants 88-07, 91-05, 95-02, and 97-05) and by discretionary grants from

Mobil Oil Company, Chevron Oil Field Research Company, ARCO Chemicals Company, and Exxon Production Research Company.

REFERENCES

1. Schramm, L.L., Petroleum Emulsions: Basic Principles, in Emulsions: Fundamentals and Applications in the Petroleum Industry. 1992, American Chemical Society: Washington, D.C. p. 1–49.
2. Stalss, F., R. Bohm, and R. Kupfer, "Improved Demulsifier Chemistry: A Novel Approach in the Dehydration of Crude Oil." Society of Petroleum Engineers—Production Engineering, 1991(August): p. 334–338.
3. Kimbler, O.K., R.L. Reed, and I.H. Silberberg, "Physical Characteristics of Natural Films Formed at Crude Oil-Water Interfaces." Society of Petroleum Engineers Journal, 1966(6): p. 153–165.
4. Strassner, J.E., "Effect of pH on Interfacial Films and Stability of Crude Oil-Water Emulsions." Journal of Petroleum Technology, 1968. **20**: p. 303–312.
5. Blair, C.M., "Interfacial Films Affecting the Stability of Petroleum Emulsions." Chemistry and Industry, 1960: p. 538–544.
6. Grace, R., Commercial Emulsion Breaking, in Emulsions: Fundamentals and Applications in the Petroleum Industry, L.L. Schramm, Editor. 1992, American Chemical Society: Washington, D.C. p. 313–339.
7. Jackson, G.E., "Oily Wastewater Treatment in the Production of Crude Oil." Chemicals in the Oil Industry, 1983. **45**: p. 92–107.
8. Neumann, H., "Investigations Regarding the Separation of Crude Oil Emulsions." Petrochemie, 1965. **18**: p. 776–779.
9. Eley, D.D., M.J. Hey, J.D. Symonds, and J.H.M. Willison, "Electron Micrography of Emulsions of Water in Crude Petroleum." Journal of Colloid and Interface Science, 1976. **54**(3): p. 462–466.
10. Obah, B., "The Chemical Demulsification of Crude Oil Emulsion." Erdohl, Kohle, Erdgas Petrochemie, 1988. **41**(2): p. 71–74.
11. Taylor, S.E., "Resolving Crude Oil Emulsions." Chemistry and Industry, 1992. **20**: p. 770–773.
12. Menon, V.B. and D.T. Wasan, "A Review of the Factors Affecting the Stability of Solids-Stabilized Emulsions." Separation Science and Technology, 1988. **23**(12 & 13): p. 2131–2142.
13. Shetty, C.S., A.D. Nikolov, and D.T. Wasan, "Demulsification of Water in Oil Emulsions Using Water Soluble Demulsifiers." Journal of Dispersion Science and Technology, 1992. **13**(2): p. 121–133.
14. Mohammed, R.A., A.I. Bailey, P.F. Luckham, and S.E. Taylor, "Dewatering of Crude Oil Emulsions 1. Rheological Behavior of the Crude Oil-Water Interface." Colloids and Surfaces A: Physicochemical and Engineering Aspects, 1993. **80**: p. 223–235.
15. Mohammed, R.A., A.I. Bailey, P.F. Luckham, and S.E. Taylor, "The Effect of Demulsifiers On the Interfacial Rheology and Emulsion Stability of Water-in-Crude Oil Emulsions." Colloids and Surfaces A: Physicochemical and Engineering Aspects, 1994. **91**: p. 129–139.
16. Liem, A.J.S. and D.R. Woods, "Review of Coalescence Phenomena." AIChE Symposium Series, 1974. **70**(144): p. 8–23.
17. Johansen, E.J., I.M. Skjarvo, T. Lund, J. Sjoblom, H. Soderlund, and G. Bostrom, "Water-in-Crude Oil Emulsions from the Norwegian Continental Shelf Part I. Formation, Characterization and Stability Correlations." Colloids and Surfaces, 1989. **34**: p. 353–370.
18. Sjöblom, J., H. Soderlund, S. Lindblad, E.J. Johansen, and I.M. Skjarvo, "Water-in-Crude Oil Emulsions from the Norwegian Continental Shelf Part II. Chemical Destabilization and Interfacial Tensions." Colloid and Polymer Science, 1990. **268**: p. 389–398.
19. Bridie, A.L., T.H. Wanders, W. Zegveld, and H.B.v.d. Heijde, "Formation, Prevention, and Breaking of Sea Water in Crude Oil Emulsions 'Chocolate Mousses'." Marine Pollution Bulletin, 1980. **11**: p. 343–348.
20. Bobra, M., M. Fingas, and E. Tennyson, "When Oil Spill Emulsify." Chemtech, 1992(April): p. 236–241.
21. Ramsden, W., "Separation of Solids in the Surface-Layers of Solutions and'Suspensions'." Proceedings of the Royal Society (London), 1903. **72**: p. 156–164.
22. Pickering, S.U., "Emulsions." Journal of the Chemical Society, 1907. **91**: p. 2001–2021.
23. Newman, F.R., "Experiments on Emulsions." Journal of Physical Chemistry, 1914. **18**: p. 34–54.
24. Finkle, P., H.D. Draper, and J.H. Hildebrand, Journal of the American Chemical Society, 1923. **45**: p. 2780.
25. Zapryanov, Z., A.K. Malhotra, N. Aderangi, and D.T. Wasan, "Emulsion Stability: An Analysis of the Effects of Bulk and Interfacial Properties On Film Mobility and Drainage Rate." International Journal of Multiphase Flow, 1983. **9**(2): p. 105–129.
26. Carroll, B.J., "The Stability of Emulsions and Mechanisms of Emulsion Breakdown." Surface and Colloid Science, 1976. **9**(1): p. 1–65.

27. Mackor, E.L., Journal of Colloid Science, 1951. **6**: p. 492.
28. Mackor, E.L. and J.H.van der Waals, "The Statistics of the Adsorption of Rod-Shaped Molecules in Connection with the Stability of Certain Colloidal Dispersions." Journal of Colloid Science, 1952. **7**: p. 535–550.
29. Mukherjee, S. and A.P. Kushnick. Effect of Demulsifiers on Interfacial Properties Governing Crude Oil Demulsification. in Symposium On Advances in Oil Field Chemistry Presented Before the Division of Petroleum Chemistry, Inc. 1988. Toronto: American Chemical Society.
30. Krawczyk, M.A., D.T. Wasan, and C.S. Shetty, "Chemical Demulsification of Petroleum Emulsions Using Oil-Soluble Demulsifiers." Industrial and Engineering Chemistry Research, 1991. **30**(2): p. 367–375.
31. Wasan, D.T., Destabilization of Water-in-Oil Emulsions, in Emulsions - A Fundamental and Practical Approach, J. Sjöblom, Editor. 1992, Kluwer Academic Publishers: Netherlands. p. 283–295.
32. Kim, Y.H., D.T. Wasan, and P.J. Breen, "A Study of Dynamic Interfacial Mechanisms for Demulsification of Water-in-Oil Emulsions." Colloids and Surfaces A: Physicochemical and Engineering Aspects, 1995. **95**: p. 235–247.
33. Hirato, T., K. Koyama, T. Tanaka, Y. Awakura, and H. Majima, "Demulsification of Water-in-Oil Emulsion by an Electrostatic Coalescence Method." Materials Transactions, 1991. **52**(5): p. 257–263.
34. Malhotra, A.K. and D.T. Wasan, "Stability of Foam and Emulsion Films: Effects of the Drainage and Film Size on Critical Thickness of Rupture." Chemical Engineering Communications, 1986. **48**: p. 35–56.
35. Førdedal, H., Y. Schildberg, J. Sjöblom, and J.-L. Volle, "Crude Oil Emulsions in High Electric Fields as Studied by Dielectric Spectroscopy. Influence of Interaction Between Commercial and Indigenous Surfactants." Colloids and Surfaces A: Physicochemical and Engineering Aspects, 1996. **106**: p. 33–47.
36. Mohammed, R.A., A.I. Bailey, P.F. Luckham, and S.E. Taylor, "Dewatering of Crude Oil Emulsions 2. Interfacial Properties of the Asphaltic Constituents of Crude Oil." Colloids and Surfaces A: Physicochemical and Engineering Aspects, 1993. **80**: p. 237–242.
37. Pasquarelli, C.H. and D.T. Wasan, The Effect of Film-Forming Materials On the Dynamic Interfacial Properties In Crude Oil-Aqueous Systems, in Surface Phenomena in Enhanced Oil Recovery, D.O. Shah, Editor. 1981, Plenum Press: New York. p. 237–248.
38. Mackay, G.D.M., A.Y. McLean, O.J. Betancourt, and B.D. Johnson, "The Formation of Water-in-Oil Emulsions Subsequent to an Oil Spill." Journal of the Institute of Petroleum, 1973. **59**(568): p. 164–172.
39. Dodd, C.G., "The Rheological Properties of Films at Crude Petroleum-Water Interfaces." Journal of Physical Chemistry, 1960. **64**(5): p. 544–550.
40. Isaacs, E.E., H. Huang, A.J. Babchin, and R.S. Chow, "Electroacoustic Method for Monitoring the Coalescence of Water-in-Oil Emulsions." Colloids and Surfaces, 1990. **46**: p. 177–192.
41. van der Waarden, M., "Stability of Emulsions of Water in Mineral Oils Containing Asphaltenes." Kolloid Z. Z. Polymer, 1958. **156**(2): p. 116–122.
42. Pfeiffer, J.P. and R.N.J. Saal, "Asphaltic Bitumen as Colloid System." Journal of Physical Chemistry, 1940. **44**: p. 139–149.
43. Nellensteyn, F.J., "The Constitution of Asphalt." Journal of the Institute of Petroleum Technologists, 1924. **10**: p. 311–325.
44. Mukerjee, P. and A.K. Ghosh, "Multiple Association Equilibria in the Self Association of Methylene Blue and Other Dyes." Journal of the American Chemical Society, 1970. **92**: p. 6408–6412.
45. Boduszynski, M.M., J.F. McKay, and D.R. Latham, "Asphaltenes, Where Are You?" Proceedings of the Association of Asphalt Paving Technologists, 1980. **49**: p. 123–143.
46. Boduszynski, M., B.R. Chadha, and T. Szkuta-Pochopien, Fuel, 1977. **56**: p. 432.
47. McKay, J.F., P.J. Amend, T.E. Cogswell, P.M. Harnsberger, R.B. Erickson, and D.R. Latham, Petroleum Asphaltenes: Chemistry and Composition, in Analytical Chemistry of Liquid Fuel Sources, Tar Sands, Oil Shale, Coal and Petroleum, P.C. Uden, S. Siggia, and H.B. Jensen, Editors. 1978, American Chemical Society: Washington D.C. p. 128–142.
48. Boduszynski, M., in Preprints Division of Petroleum Chemistry. 1979, American Chemical Society. p. 935.
49. Speight, J.G., "Latest Thoughts on the Molecular Nature of Petroleum Asphaltenes." Preprints—ACS Division of Petroleum Chemistry, 1989. **34**(2): p. 321–328.
50. Kiselev, V., "Acid and Basic Components of Native Asphaltenes of Petroleum and Coal." Petroleum Chemistry, USSR, 1979. **19**: p. 714.
51. Bestougeff, M.A. and P. Gendrel. Study on the Structure of Asphaltenic Constituents by Combined Physical and Chemical Methods. in 147th American Chemical Society Meeting. 1964. Philadelphia, PA: ACS, Division of Petroleum Chemistry.
52. Acevedo, S., G. Escobar, L. Gutierrez, and H. Rivas, "Isolation and Characterization of Natural Surfactants *from Extra Heavy Crude Oils, Asphaltenes*, and Maltenes. Interpretation of Their Interfacial Tension-pH Behaviour in Terms of Ion Pair Formation." Fuel, 1992. **71**(6): p. 619–623.

53. Acevedo, S., B. Mendez, A. Rojas, I. Layrisse, and H. Rivas, "Asphaltenes and Resins From the Orinoco Basin." Fuel, 1985. **64**: p. 1741–1747.
54. Andersen, S., "Effect of Precipitation Temperature on the Composition of n-Heptane Asphaltenes." Fuel Science and Technology International, 1994. **12**(1): p. 51–74.
55. Ali, M.F. and A. Bukhari, "Residue Fractions from Saudi Arabian Crude Oils Characterization and Analysis." Preprints ACS Division of Petroleum Chemistry, 1989. **34**(2): p. 306–309.
56. Sarowha, S.L.S. and I.D. Singh, "Compositional and Structural Studies of Petroleum Asphaltenes Employing Spectroscopic Techniques." Fuel, 1988. **67**(1): p. 145–146.
57. Calemma, V., P. Iwanski, M. Nali, R. Scotti, and L. Montanari, "Structural Characterization of Asphaltenes of Different Origins." Energy & Fuels, 1995. **9**: p. 225–230.
58. Al-Jarrah, M.M.H. and A.H. Al-Dujaili, "Characterization of Some Iraqi Asphalts II. New Findings on the Physical Nature of Asphaltenes." Fuel Science and Technology International, 1989. **7**(1): p. 69–88.
59. Filimonova, T.A., L.V. Gorbunova, and V.F. Kam'yanov, "Asphaltenes of West Siberian Crude Oils." Petroleum Chemistry, USSR, 1987. **27**(3): p. 210–220.
60. Bestougeff, M.A., "Composition Chimique et Structure des Asphaltenes et leur Place Parmi les Substances Organiques Naturelles." Bulletin of the Chemical Society of France, 1967. **12**: p. 4773.
61. McLean, J.D. and P.K. Kilpatrick, "Comparison of Precipitation and Extrography in the Fractionation of Crude Oil Residua." Energy and Fuels, 1997. **11**: p. 570–585.
62. Jurkiewicz, J. and S. Rosinski, "Coal Tar Compounds." Koks, Smola, Gaz, 1956. **1**(4): p. 143–152.
63. Bestougeff, M.A. and R.J. Byramjee, Chemical Constitution of Asphaltenes, in Asphaltenes and Asphalts, 1. Developments in Petroleum Science, 40, T.F. Yen and G.V. Chiliingarian, Editors. 1994, Elsevier Science. p. 67–94.
64. Bunger, J.W., K.P. Thomas, and S.M. Dorrence, "Compound Types and Properties of Utah and Athabasca Tar Sand Bitumens." Fuel, 1979. **58**(3): p. 183–195.
65. Filimonova, T.A., L.V. Gorbunova, and V.F. Kam'yanov, "Structural Characteristics of Asphaltenes of Typical West Siberian Crude Oils." Petroleum Chemistry, USSR, 1987. **27**(4): p. 257–265.
66. Speight, J.G. and S.E. Moschopedis, On the Molecular Nature of Asphaltenes, in Chemistry of Asphaltenes, J.W. Bunger and N.C. Li, Editors. 1981, American Chemical Society: Washington D. C. p. 1–15.
67. Wiehe, I.A., "The Pendant-Core Building Block Model of Petroleum Residua." Energy & Fuels, 1994. **8**: p. 536–544.
68. Wiehe, I.A. and K.S. Liang, "Asphaltenes, Resins, and other petroleum macromolecules." Fluid Phase Equilibria, In press.
69. Sheu, E.Y. and D.A. Storm, Colloidal Properties of Asphaltenes in Organic Solvents, in Asphaltenes: Fundamentals and Applications, E.Y. Sheu and O.C. Mullins, Editors. 1995, Plenum Press: New York. p. 1–52.
70. Lamathe, J., "Dosage Potentiometrique des Fonctions Soufrees non Thiopheniques. Application aux Produits d'Origine Petrioliere." Comptes Rendus des Seances, Academie des Sciences, Series C, 1966. **2663**: p. 862–874.
71. Mullins, O.C., Sulfur and Nitrogen Molecular Structures in Asphaltenes and Related Materials Quantified by XANES Spectroscopy, in Asphaltenes: Fundamentals and Applications, E.Y. Sheu and O.C. Mullins, Editors. 1995, Plenum Press: New York. p. 53–96.
72. Mansurov, I.R., E.Z. Il'yasova, and V.P. Vygovskoi, "Shear Strength of Interfacial Films of Asphaltenes." Chemistry and Technology of Fuels and Oils, 1987. **23**(1–2): p. 96–98.
73. Yen, T.F., "Structure of Petroleum Asphaltene and its Significance." Energy Sources, 1974. **1**(4): p. 447–463.
74. Mingyuan, L., A. Christy, and J. Sjöblom, Water-in-Crude Oil Emulsions from the Norwegian Continental Shelf Part VI—Diffuse Reflectance Fourier Transform Infrared Characterization of Interfacially Active Fractions from North Sea Crude Oil, in Emulsions—A Fundamental and Practical Approach, J. Sjöblom, Editor. 1992, Kluwer Academic Publishers: The Netherlands. p. 157–172.
75. Khryashchev, A.N., N.A. Popov, N.A. Posadov, and D.A. Rosendal, Petroleum Chemistry, USSR, 1991. **31**: p. 601–604.
76. Papirer, E., C. Bourgeois, B. Siffert, and H. Balard, "Chemical Nature and Water/Oil Emulsifying Properties of Asphaltenes." Fuel, 1982. **61**(8): p. 732–734.
77. Dickie, J.P. and T.F. Yen, "Macrostructures of the Asphaltic Fractions by Various Instrumental Methods." Analytical Chemistry, 1967. **39**(14): p. 1847–1852.
78. Yen, T.F., Meso-Scaled Structure and Membrane Mimetic Chemistry, in Advances in the Applications of Membrane-Mimetic Chemistry, T.F. Yen, R.D. Gilbert, and J.H. Fendler, Editors. 1994, Plenum Press: New York. p. 255–279.
79. Lawrence, A.S.C. and W. Killner, "Emulsions of Seawater in Admiralty Fuel Oil with Special Reference to their Demulsification." Journal of the Institute of Petroleum, 1948. **34**: p. 281.

80. Dunning, H.N., J.W. Moore, and M.O. Denekas, "Interfacial Activities and Porphyrin Contents of Petroleum Extracts." Industrial and Engineering Chemistry, 1953. **45**(August): p. 1759–1765.
81. Love, F.E., "Oilfield Emulsions... How to Make and Break Them. Part 1." Oil and Gas International, 1962. **2**(9): p. 56.
82. Albers, W. and J.T.G. Overbeek, "Stability of Emulsions of Water in Oil. I. The Correlation Between Electrokinetic Potential and Stability." Journal of Colloid Science, 1959. **14**: p. 501–509.
83. Harvey, R.R., "Theoretical Approach to the Investigation of Films Occurring at Crude Oil-Water Interfaces." Transactions of the American Institute of Mining, Metallurgical, and Petroleum Engineers, 1960. **219**: p. 350–353.
84. Bartell, F.E. and D.O. Neiderhauser, Film Forming Constituents of Crude Petroleum Oils, in Fundamental Research on Occurrence and Recovery of Petroleum, 1946–47. 1949, API. p. 57.
85. Reisberg, J. and T.M. Doscher, "Interfacial Phenomena in Crude Oil-Water Systems." Prod. Monthly, 1956. **21**: p. 43.
86. Mardanenko, V.P. and V.G. Benkovskii, Chemistry and Technology of Fuels and Oils, 1965(July): p. 41–45.
87. Petrov, A.A. and G.N. Pozdnyzhev, Chemistry and Technology of Fuels and Oils, 1969(March): p. 11–14.
88. Berridge, S.A., M.T. Thew, and A.G. Loriston-Clarke in Symposium on Scientific Aspects of Pollution of the Sea by Oil. 1969. London: Institute of Petroleum.
89. Levchenko, D.N., A.D. Khudyakova, and L.I. Ratich, Chemistry and Technology of Fuels and Oils, 1970(October): p. 21–25.
90. Sjöblom, J., O. Urdahl, H. Hoiland, A.A. Christy, and E.J. Johansen, "Water-in-Crude Oil Emulsions. Formation, Characterization, and Destabilization." Progress in Colloid and Polymer Science, 1990. **82**: p. 131–139.
91. McLean, J.D. and P.K. Kilpatrick, "Effects of Asphaltene Aggregation in Model Heptane-Toluene Mixtures on Stability of Water-in-Oil Emulsions." Journal of Colloid and Interface Science, 1997. **196**: p. 23–34.
92. Spiecker, P.M. and P.K. Kilpatrick, "Fractionation of Crude Oil Residua into Acid, Base and Neutral Components by Ion Exchange Chromatography." in preparation, 1998.
93. Denekas, M.O., F.T. Carlson, J.W. Moore, and C.G. Dodd, "Materials Adsorbed at Crude Petroleum-Water Interfaces." Industrial and Engineering Chemistry, 1951. **43**(5): p. 1165–1168.
94. Dodd, C.G., J.W. Moore, and M.O. Denekas, "Metalliferous Substances Adsorbed at Crude Petroleum-Water Interfaces." Industrial and Engineering Chemistry, 1952. **44**(11): p. 2585–2590.
95. Hassiba, H.H. and F.W. Jessen, "Film-Forming Compounds From Crude Oils, Interfacial Films and Paraffin Deposition." The Journal of Canadian Petroleum Technology, 1968. **7**(1): p. 1–12.
96. Jones, T.J., E.L. Neustadter, and K.P. Whittingham, "Water-in-Crude Oil Emulsion Stability and Emulsion Destabilization by Chemical Demulsifiers." Journal of Canadian Petroleum Technology, 1978. **17**(2): p. 100–108.
97. Neustadter, E.L., K.P. Whittingham, and D.E. Graham, Interfacial Rheological Properties of Crude Oil/Water Systems, in Surface Phenomena in Enhanced Oil Recovery, D.O. Shah, Editor. 1981, Plenum Press: New York. p. 307–326.
98. Nordli, K.G., J. Sjöblom, J. Kizling, and P. Stenius, "Water-in-Crude Oil Emulsions from the Norwegian Continental Shelf 4. Monolayer Properties of the Interfacially Active Crude Oil Fraction." Colloids and Surfaces, 1991. **57**: p. 83–98.
99. Sjöblom, J., O. Urdahl, K.G.N. Borve, L. Mingyuan, J.O. Saeten, A.A. Christy, and T. Gu, "Stabilization and Destabilization of Water-in-Crude Oil Emulsions from the Norwegian Continental Shelf. Correlation with Model Systems." Advances in Colloid and Interface Science, 1992. **41**: p. 241–271.
100. Friberg, S., L. Mandell, and M. Larsson, "Mesomorphous Phases, a Factor of Importance for the Properties of Emulsions." Journal of Colloid and Interface Science, 1969. **29**(1): p. 155–156.
101. Friberg, S. and L. Rydhag, "The System: Water-p-Xylene-1-Aminooctane-Octanoic Acid II: The Stability of Emulsions in Different Regions." Kolloid Z., 1971. **244**(1): p. 233–239.
102. Friberg, S., P.O. Jansson, and E. Cederberg, Journal of Colloid and Interface Science, 1976. **55**: p. 614.
103. Friberg, S. and C. Solans, Langmuir, 1986. **2**: p. 121.
104. Sjöblom, J., L. Mingyuan, A.A. Christy, and H.P. Ronningsen, "Water-in-Crude Oil Emulsions from the Norwegian Continental Shelf 10. Ageing of the Interfacially Active Components and the Influence on the Emulsion Stability." Colloids and Surfaces A: Physicochemical and Engineering Aspects, 1995. **96**: p. 261–272.
105. Mohammed, R.A., A.I. Bailey, P.F. Luckham, and S.E. Taylor, "Dewatering of Crude Oil Emulsions 3. *Emulsion Resolution by Chemical Means*." Colloids and Surfaces A: Physicochemical and Engineering Aspects, 1994. **83**: p. 261–271.

106. Chen, T.Y., R.A. Mohammed, A.I. Bailey, P.F. Luckham, and S.E. Taylor, "Dewatering of Crude Oil Emulsions 4. Emulsion Resolution by the Application of an Electric Field." Colloids and Surfaces A: Physicochemical and Engineering Aspects, 1994. **83**: p. 273–284.
107. McLean, J.D. and P.K. Kilpatrick, "Effects of Asphaltene Solvency on Stability of Water-in-Crude Oil Emulsions." Journal of Colloid and Interface Science, 1997. **189**: p. 242–253.
108. Ali, M.F. and M.A. Ali, "Investigation of Nitrogen Compound Types in High-Boiling Petroleum Distillates From Saudi Arabian Crude Oils." Fuel Science and Technology International, 1988. **6**(3): p. 259–290.
109. Ali, M.F., M.U. Hasan, A.M. Bukhari, and M. Saleem, "Arabian Crude Fractions Analyzed." Hydrocarbon Processing, 1985. **64**(2): p. 83–86.
110. Hasan, M.U., M.F. Ali, and M. Arab, "Structural Characterization of Saudi Arabian Extra Light and Light Crudes by 1-H and 13-C NMR Spectroscopy." Fuel, 1989. **68**(6): p. 801–803.
111. Boduszynski, M.M., "Characterization of "Heavy" Crude Components." Preprints ACS Division of Petroleum Chemistry, 1985. **30**: p. 626–640.
112. Siffert, B., C. Bourgeois, and E. Papirer, "Structure and Water-Oil Emulsifying Properties of Asphaltenes." Fuel, 1984. **63**(6): p. 834–837.
113. Acevedo, S., G. Escobar, L.B. Gutierrez, H. Rivas, and X. Gutierrez, "Interfacial Rheological Studies of Extra-Heavy Crude Oils and Asphaltenes: Role of the Dispersion Effect of Resins in the Adsorption of Asphaltenes at the Interface of Water-in-Crude Oil Emulsions." Colloids and Surfaces A: Physicochemical and Engineering Aspects, 1993. **71**: p. 65–71.
114. Cairns, R.J.R., D.M. Grist, and E.L. Neustadter. The Effect of Crude Oil-Water Interfacial Properies on Water-Crude Oil Emulsion Stability. 1974. Brunel University: Academic Press.
115. Menon, V.B. and D.T. Wasan, "Coalescence of Water-in-Shale Oil Emulsions." Separation Science and Technology, 1984. **19**(8 & 9): p. 555–574.
116. Thompson, D.G., A.S. Taylor, and D.E. Graham, "Emulsification and Demulsification Related to Crude Oil Production." Colloids and Surfaces, 1985. **15**: p. 175–189.
117. Eley, D.D., M.J. Hey, and M.A. Lee, "Rheological Studies of Asphaltene Films Adsorbed at the Oil/Water Interface." Colloids and Surfaces, 1987. **24**: p. 173–182.
118. Aveyard, R., B.P. Binks, P.D.I. Fletcher, and J.R. Lu, "The Resolution of Water-in-Crude Oil Emulsions by the Addition of Low Molar Mass Demulsifiers." Journal of Colloid and Interface Science, 1990. **139**(1): p. 128–138.
119. Bhardwaj, A. and S. Hartland, "Study of Demulsification of Water-in-Crude Oil Emulsion." Journal of Dispersion Science and Technology, 1993. **14**(5): p. 541–557.
120. Urdahl, O., A.E. Movik, and J. Sjöblom, "Water-in-Crude Oil Emulsions from the Norwegian Continental Shelf 8. Surfactant and Macromolecular Destabilization." Colloids and Surfaces A: Physicochemical and Engineering Aspects, 1993. **74**: p. 293–302.
121. Bhardwaj, A. and S. Hartland, "Dynamics of Emulsification and Demulsification of Water in Crude Oil Emulsions." Industrial and Engineering Chemistry Research, 1994. **33**: p. 1271–1279.
122. Skodvin, T., J. Sjöblom, J.O. Saeten, O. Urdahl, and B. Gestblom, "Water-in-Crude Oil Emulsions from the Norwegian Continental Shelf IX. A Dielectric Spectroscopic Characterization of Authentic as Well as Model Systems." Journal of Colloid and Interface Science, 1994. **166**: p. 43–50.
123. Kim, Y.H., A.D. Nikolov, D.T. Wasan, H. Diaz-Arauzo, and C.S. Shetty, "Demulsification of Water-in-Crude Oil Emulsions: Effects of Film Tension, Elasticity, Diffusivity, and Interfacial Activity of Demulsifier Individual Components and their Blends." Journal of Dispersion Science and Technology, 1996. **17**(1): p. 33–53.
124. Rogacheva, O.V., R.N. Rimaev, and V.Z. Gubaidullin, "Investigation of the Surface Activity of the Asphaltenes of Petroleum Residues." Colloid Journal of USSR, 1980: p. 490–493.
125. Sjöblom, J., L. Mingyuan, A.A. Christy, and T. Gu, "Water-in-crude-oil Emulsions From the Norwegian Continental Shelf 7. Interfacial Pressure and Emulsion Stability." Colloids and Surfaces, 1992. **66**: p. 55–62.
126. Ese, M-H., J. Sjoblom, H. Førdedal, O. Urdahl, and H.P. Rønningsen, "Ageing of Interfacially Active Components and Its Effect On Emulsion Stability As Studied By Means of High Voltage Dielectric Spectroscopy Measurements." Colloids and Surfaces, 1997. **123–124**: p. 225–232.

INDEX

Abraham's scheme, 9
Absorption spectroscopy, 24, 32–44
  large chromophores, population distribution in crude oil and asphaltenes, 41–44
  Urbach tail, 35–41
Acetone
  coal asphaltenes and extracts, 207, 208, 220
  crude oil DRIFT spectra, 352
Acid-affins, 5
Acid-base reactions, 12, 386
Acidic hydrogen-bearing molecules, 7
Acidic/neutral components, coal asphaltenes, 214
Acids
  emulsion preparation, self-association studies, 116
  refining catalysts, 146
Adsorption, 386
  crude oil emulsions, 365
  emulsion stabilization, 383
  heavy crudes, 145
  resins and, 393
Adsorption/desorption, selective, 1
Agefloc polymers, 365
Aggregation, 13; *see also* Self-association, structure and molecular packing
  crude oil, 154, 386
  crude oil emulsions
    interfacial film studies, 395
    resins and, 393
  intermolecular interactions, 179
  Safaniya VR asphaltenes, 175
  structure of, 129–132, 388
  water-in-oil emulsions, 386–388
Airblowing, 11–12
Alaskan North Slope, 395–405, 410–415, 416, 417
Albertite, 10
Alcohols, 7, 364–365
Aldehydes, 347, 352
Aliphatic ether, 352
Aliphatic linkages, 6, 93
Aliphatics, 147
  coal versus petroleum asphaltenes, 213, 214
  crude oil, 227, 338
    heavy crude asphaltenes, 154
    resin separation, 347, 349
Alkane number, crude oil emulsion stabilization, 364
Alkanes
  aggregation in solvents, 389
  conductivity studies, 259
Alkylation, coal asphaltenes, 216
Alkylporphyrin-DPEP ratio, 9–10
Alkyl side chains
  methyl groups, 91
  NMR, 87, 88, 89
Alkyl substituents, 7
Alkyl sulfoxides, 74
Alumina, 365
Amides, 347; *see also* Nitrogen
Amphoteric polymers, 14
Anthracene, 29–32
Anthracite, 203
Anthraxolite, 10
AOT (sodium (bis-2-ethylhexyl)-sulfosuccinate), 365, 366
Appalachian Shale, 19
Aquila, 409
Arab Berri, 395–405, 410–415, 416, 417; *see also* Spectroscopy, molecular structure and intermolecular interactions
Arab Heavy, 395–405, 410–415, 416, 417
Argon, 103, 104, 108

Aromaticity
coal extracts, 208, 209–210
coal-liquid vs. petroleum asphaltenes, 17–19
coal versus petroleum asphaltenes, 213
and colloid stability, 7
comparisons of asphaltenes from different sources, 19
crude oil, 227, 230
gas oils, 7
NMR studies, 23
optical spectroscopy studies, 21–75; *see also* Optical spectroscopy, aromatic moieties
source of asphaltenes and, 16, 17
Aromatics, 6
coal, 206
crude oil, 239, 338
DRIFT spectra, 352
heavy crude, 153
NMR, 87, 88, 90, 92–93
solubility parameters, 4
spectroscopy, 67–75, 99
aromatic ring size, 73–75
short-wavelength emission, 67–73
Aromatic sheets, defect centers, 7
Arrhenius plot, 321
Aspect ratio, 298, 299
Asphalt, distribution of asphaltic fractions, 10
Asphaltenes
distribution of asphaltic fractions, 9, 10
solvent fractionation, 6
types and sources: *see* Types and sources of asphaltenes
Asphaltene stabilized crude oil emulsions, 337–372; *see also* Crude oil emulsions, asphaltene and resin stabilized
Asphaltics/allied substances, 4–7
gas oils, 7
resins, 6–7
Asphaltides, 16
Asphaltites, 1, 10, 213
Asphaltoids, 1, 9, 10, 16
Assemblages, 13
Association
coal asphaltenes, 220
coal-liquid vs. petroleum asphaltenes, 17–19
heavy oils, dielectric constant of solvents and, 316
and viscosity, 268; *see also* Suspension viscosity model
Athabasca
asphaltene structure, 149
bitumen, 11, 213
comparisons of asphaltenes from different sources, 18
distribution of asphaltic fractions, 10
Atmospheric residues, refining process, 146
Atomic force spectroscopy, 154
Attapulgus clay, 232
Aurabon process, 8
Auto-oxidation, crude oil emulsion stabilization, 356
Axial ratio, 324
Bachaquero, 18
Barium sulfate, 16
Basic (alkali) components, coal asphaltenes, 214
Baxterville, 18
Beehive-like networks, heavy crude asphaltenes, 154
Belayim, spectroscopy: *see* Spectroscopy, molecular structure and intermolecular interactions
Belridge, 18
Benzene, 3
coal, 203, 212, 213, 217
crude oil
chromatography, 346
colloidal structural evolution, 175, 177
conductivity measurements, 254, 255, 257
heavy oil viscometry, 313
molecular weight determination, 387
oil-in-water emulsion stability, 404, 405
solubility fractions
insoluble fraction, 6, 9, 10
soluble fraction, 4, 6
Benzoic acid, 288
Biconial bob rheometer, 395, 410
Biodegradation of crude oil, 23
Bitumen, 1, 9
heavy oil sedimentation-diffusion measurements, 332
hydrocracking products, 11
rheology, polymer addition and, 156
structure, macroscopic organization, 146
viscosity measurements, 316
Bituminous coal, 203, 208; *see also* Coal; Coal asphaltenes
Blokker constants, 15
Blue-green algae, 8
Boiling point, 151, 216
Boltzmann factor, 105
Born–Oppenheimer approximation, 28
Boscan, 228
comparisons of asphaltenes from different sources, 18
water-in-oil emulsions, 409
Brent, spectroscopy: *see* Spectroscopy, molecular structure and intermolecular interactions
Brooks–Taylor spherules, 14, 15
Brown–Ladner structural parameters, 205–213
Brunei, 58–63
Bulk analysis, asphaltenes, 23
Bulk phase, heavy oil partitioning, 303–304
Bulk properties, self-association processes, 116
Burgan, comparisons of asphaltenes from different sources, 18

Caged molecule, 12
Calcium oxide, 347, 349
Calorimetry, self-association studies, 117
Campbell–Forgacs equation, 319
Capillary pressure, 9
Capillary viscometer, 312
Carbazoles, 147

Carbene
solubility parameters, 4
solvent fractionation, 6
weathering and oxidation of spills, 15
Carboids
solubility parameters, 4
solvent fractionation, 6
weathering and oxidation of spills, 15
Carbon disulfide, 6
coal component solubility classes, 203
coal extracts, 207, 208, 212, 217
Carbon fibers, improved recovery systems, 15
Carbon tetrachloride, 6, 288
Carbonyl groups
aggregation mechanisms, 386
crude oil DRIFT spectra, 352
crude oil emulsion stabilization, 356
Carboxyl groups, coal versus petroleum asphaltenes, 214
Carboxylic acids, 7, 147, 248, 386
Catalytic cracking, 146
Catalytic cracking bottoms, 249
Catalytic Inc.–SRC asphaltenes, 15
Centrifugal TLC, 6
Centrifugation, 393; *see also* Sedimentation and diffusion measurements
Cerro Negro, 395, 410
Ceylon, 9
Chain breaking, crude oil emulsion stabilization, 356
Charge transfer processes
coal asphaltenes, 216
coal-liquid vs. petroleum asphaltenes, 18
heavy crude, 153
Chattanooga Shale, 19
Chelates, 7, 81
Chemical composition, 1, 386–388
and crude oil asphaltene deposition/flocculation, 228
vacuum residues for colloidal structure studies, 167, 168
Chemical precipitation, 1
Chemical reactions, optical spectroscopy, 12, 21
Chemical shift data, 80
Chemistry, water-in-oil emulsions, 386–388
aggregation, 386–388
composition of asphaltenes, 386–388
p-Chloranil, 218
Chloroform, 3
Chocolate mousse, 146, 379
Chromatography, 1, 2–3, 6, 81, 147–148; *see also* Gel permeation chromatography; Size exclusion chromatography
coal asphaltenes, 218
crude oils, 23, 152–153
asphaltene and resin stabilized emulsions, 347–352
characterization and phase behavior, 229–232
Chromophores, 24, 41–44
Chutyrsk crude, 409–410
Classical model of colloidal aggregation, 154
Cluster, 13
Coal
coal liquids, 1, 17–19
macerals, EPR, 107
pyrolysis tar fluorescence, 74
Coal asphaltenes, 203–223
colloidal structure, 214–223
computer simulation, 222–223
interactions, 214–216
molecular weight, 218–219
SANS, 221–222
surface tension, 219–220
true solutions or suspensions, 216–217
viscosity, 219
X-ray analysis, 220–221
comparisons of asphaltenes from different sources, 19
hydrogenation, 11
metals, 7
molecular structure, 204–214
comparison with petroleum asphaltenes, 213–214
preparation of materials, 204
structural parameters and model, 203–213
optical spectroscopy, 22
separation processes, 16
structural parameters, 2
Coalescence, crude oil emulsions, 339
destabilization, 362–363
stabilization, 382
Coal oil, 205
COED process, 16
Coking, 146, 148
Cold Lake
bitumen, 236–244, 315, 316
heavy oil sedimentation-diffusion measurements, 329, 332
Colloidal structure, 12–13
Colloidal structure (coal extracts and asphaltenes), 214–223
computer simulation, 222–223
interactions, 214–216
molecular weight, 218–219
SANS, 221–222
surface tension, 219–220
true solutions or suspensions, 216–217
viscosity, 219
X-ray analysis, 220–221
Colloidal structure (heavy crude and asphaltene solutions), 145–197
experimental methods, 159–167
cryo-SEM, 166
small-angle scattering methods, 159–166
viscosimetry, 166–167
n-heptane addition to asphaltene solutions, 183–188
cryo-SEM, 185–188
SANS, 183, 184, 185
viscosity, 183, 184

Colloidal structure (*cont.*)
macrostructure, asphaltene solutions
cryo-SEM, 181–182
small-angle scattering methods, 167–181
natural systems, 190–196
overview, 147–159
resin solutions, 188–190
sample preparation, 167
Colloids, 8
aggregation in solvents, 389
stability of, 7
Complex ions, 7
Compound X, 406, 409
Computer simulation
coal asphaltenes, 222–223
self association and molecular packing, 141–142
Concentration effects, SANS and SAXS, 182
Concentric cylinder viscometer, 312
Conductivity, 247–265
aggregation and, 118–119, 123–126, 132–136
experimental, 252–254
heavy crude, 153
as indicator of precipitation, 257–261
literature summary, 249–252
purified asphaltenes in organic solvents, 254–257
reversibility of precipitation, 261–265
Cone penetrometers, 22
Constituents of asphaltenes, 1
Coordination compounds, 7
Coordination to transition metals, 6
Coorongite, 9, 10, 18
Corbett's scheme, 5
Covalent bonds, coal, 204, 207
Cracking, 11
metals and, spectroscopic studies, 81
refining process, 146
Creaming, crude oil emulsions, 339
Critical micelle concentration, 293–296
crude oil emulsion stabilization, 364
heavy oil viscosity, 317, 322
improved recovery, 13–14
Cross linking
colloidal structural evolution, 195
emulsion stabilization, 380
heavy crude asphaltenes, 154
water-in-oil emulsions, 406
Crowding factor, and viscosity, 270
Crude oil(s)
emulsion stabilization: *see* Water-in-oil emulsion stabilization, petroleum asphaltenes
optical spectroscopy, 22, 23, 38–39
viscosity measurements, 315, 316
Crude oil(s), characterization and phase behavior, 227–245
behavior, 232–236
particle size distribution, 232–234
precipitation onset measurements, 234–236
characterization, 229–232
field desorption MS, 232
Crude oil(s) (*cont.*)
characterization (*cont.*)
gel permeation chromatography, 229–232
phase behavior, 240–244
asphaltene precipitation onset behavior, 242–244
particle size distribution, 240–242
results
field desorption MS, 237–240
gel permeation chromatography, 236–237
Crude oil emulsions, asphaltene and resin stabilized, 337–332
droplet sizes and size distribution methods, 339–346
NMR, pulsed field gradient, 344, 345
ultrasound, 344–346
video enhanced microscopy, 340–343
interfacially active compounds, characterization of, 346–361
chromatography of resins, 347–352
experimental technique, 352–361
stabilization and destabilization of model emulsions, 361–372
demulsification of water-in-crude oil emulsions, 363–367
destabilization of water-in-oil emulsions, 361–362
electrocoalescence, 367–369, 370, 371, 372
stabilization with crude oil emulsions, 361–362
Cryoscopy, 387
Cryo-SEM
colloidal structural evolution, 166
flocculation process, *n*-heptane addition, 185–188
toluene solutions, 181–182
heavy crudes, 158
Crystallization, 1
Cumene, 404, 405
Curie law, 105, 106, 107
Curie–Weiss law, 103, 15
Cyclohexane, 3
Cyclohexanecarboxylic acid, 288
4-Cyclohexylbutanoic acid, 288
Cymene, 404, 405

Dead oil particle size distribution, 240–241
Debye correlation function, 121
Debye–Huckel constant, 254
Decalin, 313
Defect centers, 7
Density fluctuations, 174
Depolarization, fluorescence, 24
Depolymerization, coal extracts, 205
Deposition during transportation, 16
Derjaguin, Landau, Verwey, and Overbeek (DLVO) theory, 380
Dialysis, 321
o-Dichlorobenzene, 387
Dichlorodicyano-p-benzoquinone (DDQ), 218
Dichloromethane, 346, 347, 349
Dickinson's equations, 87
Dielectric constants, 248, 315
Diels–Alder reaction, 12

Diffusion, 24; *see also* Sedimentation and diffusion measurements
Diffusion-limited colloid aggregation (DLCA), 154, 164, 165
Diffusion velocity, heavy oil sedimentation-diffusion measurements, 323
Dilute suspension viscosity, 311
N,N-Dimethylacetoamide, 207, 208
Dipole-dipole forces
  aggregation mechanisms, 140
  heavy crude, 153
Discotic lamellar structures
  aggregation, 389
  interfacial film studies, 395
Distillation, 1, 2
Distortionless Enhancement by Polarization Transfer (DEPT), 80–81
Donor-acceptor mechanisms: *see* Electron donor-acceptor interactions
Doublets, 80, 105
DPEP (deoxophyllo-erythroetioporphyrin) to alkylporphyrin ratio, 9–10
Drag-reduction polymers, flow property modification, 15
DRIFT spectra, crude oil resin separation, 349, 352
Droplet sizes, 339–346
  NMR, pulsed field gradient, 344, 345
  ultrasound, 344–346
  video enhanced microscopy, 340–343
Dupré equation, 16

Eiler equation, 311, 318, 319
Einstein equation, 128, 304–311, 318
Elasticity, 394
  interfacial film studies, 394
  water-in-oil emulsions, 406
Electrical double-layer repulsion, emulsion stabilization, 380
Electrocoalescence of crude oil emulsions, asphaltene and resin stabilized, 367–369, 370, 371, 372
Electrokinetic effects, and crude oil asphaltene deposition/flocculation, 228
Electron donor-acceptor interactions, 12, 18
  aggregation, 389
  interfacial film studies, 394
Electronic photoexcitation, 46
Electron paramagnetic resonance (EPR) spectroscopy, 23, 81, 84, 148
Electrons
  π: *see* Pi bonding/pi electrons
  unpaired, 97, 105
Electron spin resonance (ESR), 8, 95–108
  free radical concentration, 99
  g-value, 97–99
  linewidth and lineshape, 96–97
  saturation, 99–102
  temperature and oxygen partial pressure, 102–108
Elemental composition, 81, 387
Emulsion stabilization: *see* Crude oil emulsions, asphaltene and resin stabilized; Water-in-oil emulsion stabilization, petroleum asphaltenes
Energy Gap Law, 25, 31, 32, 55–58
Energy Transfer Law, 67
Entropy effect
  aggregation mechanisms, 386
  crude oil emulsions, 365
Environmental monitoring, 22
Equivalence alkane carbon number (EACN), 14, 364
ESR: *see* Electron spin resonance
Esters, 147, 347, 352
Ethane, 262–263
Ethanol insoluble-benzene soluble fraction, 4
Ethers, 3
  coal asphaltenes, 214
  coal-liquid vs. petroleum asphaltenes, 18
  crude oil DRIFT spectra, 352
  crude oil resin separation, 347, 350
Ethyl benzene, 404, 405
EVA (polymer), 146
Evolution of colloids: *see* Colloidal structure
EXAFS/XANES, 147, 148
Extraction, fluorescent materials, 22

Fiber optic remote sensing, 22
Fick's law of diffusion, 323
Field desorption MS, 227, 232, 236–237
Field ionization MS, 218, 314
Films
  film-forming agents in crude oils, 392–393
  heavy oil diffusion measurements, 326
  interface, crude oil emulsions, 338
  interfacial, water-in-oil emulsions, 393–395
Flash pyrolysis, 81
Flat ellipsoid model, 152
Flexibility, heavy oil macrostructure, 304
Flocculation, *see also* Colloidal structure
  crude oil emulsions, 339
  heavy crudes, 145, 153–154
  n-heptane addition and, 183–188
  and optical properties, 22
  self-association: *see* Self-association, structure and molecular packing
  during transportation, 16
Flow properties, 15
  crude oil asphaltene deposition/flocculation, 228
  heavy crudes, 145
  multiphase, 338
  self-association and: *see* Self-association, structure and molecular packing
Fluid-bed catalytic cracking, 146
Fluorescence depolarization, 24
Fluorescence detection, 21
Fluorescence lifetime data, 25
Fluorescence microscopy, 154

Fluorescence spectroscopy, 24, 44–67, 81
intermolecular interactions, 44–67
fluorescence spectra, 58–67
quantum yields, 52–58
unifying model of molecular interactions, 45–52
Urbach tails, 38, 40
instrumentation, 25–27, 84
quantum yields, 52–58
unifying model of molecular interactions, 45–52
FMC-COED asphaltene, improved recovery systems, 15
Form factors, colloidal structure evolution models, 160, 161–166
Fourier-transform IR spectroscopy, 84, 85–87
Fractal dimension
aggregates
colloidal, 164–165
crude oil, 193
structure, 275
and percolation, 299
Fractal objects, polydiverse, 165
Fractionation
for heavy oil viscosity measurements, 321
solvent: *see* Solvent fractionation; Solvents
techniques, 1
France crude, 347–348
Franck–Condon principle, 29
Free radicals, 6, 95–96, 99
Freezing point depression, 151
Friction factors
heavy oil sedimentation-diffusion measurements, 323, 324, 325
heavy oil viscosity measurements, 308
Friedel–Craft's reaction, 12
Fuller's earth, 232
Functional group analysis, 388
Functional groups, *see also specific groups*
coal versus petroleum asphaltenes, 214
crude oil resin separation, 352

Gaggiano: *see* Spectroscopy, molecular structure and intermolecular interactions
Gaps, 7
Gas chromatography, 81, 209
Gas condensate optical properties, 22
Gas oil, 7
heavy oil viscometry, 313
solubility parameters, 4
solvent fractionation, 6
spills, 15
Gas-oil ratios, crude oil, 236
Gated Spin Echo (GASPE), 81, 83, 90, 91
Gaussian phase distribution (GPD) approximation, 344
Gela: *see* Spectroscopy, molecular structure and intermolecular interactions
Gel permeation chromatography, 6, 81, 84
coal asphaltenes, 218
Gel permeation chromatography (*cont.*)
crude oil
asphaltene characterization, 229–232, 236–237
heavy crude, 152–153, 303
viscosity measurements, 321
Geochemical studies, heavy crude, 154
Geological clock, 9–10, 11
Geological maturation indicator, asphaltenes as, 8–9
Geometry: *see* Macrostructure
Geoporphyrin, 8
Gilsonite, 10, 18
Grahamite, 9, 10, 18
Graphite, 9, 15
Gravitational forces: *see* Sedimentation and diffusion measurements
Green River asphaltenes, 9, 19
Grimson–Barker equation, 319, 320
g-tensor, 8
Guinier's law, 163, 164
Gulf of Mexico crude, 242–244
Gunflint Shale, 19
Gyration radius, 170, 173, 275

Halogenation, 12
Hartley micelles, 12
Heat of mixing, 3–4
Heat treatment
flow property modification, 15
mesophase generation, 4–5
Heavy crude
colloidal structure: *see* Colloidal structure
conductivity, 153
Heavy metals, 227
Heavy oils: *see* Hydrodynamic property measurements, heavy oils
n-Heptane, 299
colloidal structure of heavy crude and asphaltene solutions, 183–188
cryo-SEM, 185–188
SANS, 183, 184, 185
viscosity, 183, 184
crude oil
film forming agents, 392
flocculation process, 158, 183–188
as heavy crude flocculant, 158
oil-in-water emulsion stability, 403, 404, 405
solubility classes, 227, 303, 385
n-Heptane asphaltenes, spectroscopy, 25, 82–83
Heptol, 403, 404, 405
Heterocyclic compounds, 1, 6, 147
Hexadecane, 259
Hexane, 3, 6
coal extracts, 212, 213
peptidization by, 13
Hildebrand and Scott and Scatchard theory, 3–4
Hildebrands, 3–4
Holes, 7
HO-LU gap, 32, 38–39, 40, 44, 45, 49, 51, 52, 53, 54, 55, 58, 67

HPLC
coal extracts, 212–213
crude oil, 231
crude oil asphaltenes, 229
Hunt, 38–39, 40
Huntington Beach Oilfield, improved recovery, 13–14
Hydraulic permeability, heavy oil diffusion measurements, 326
Hydrocarbons, 1; *see also* Aliphatics; Aromaticity; *specific classes of hydrocarbons*
Hydrocarbon skeleton, 388
Hydrochloric acid
emulsion preparation, self-association studies, 116
improved recovery, 13–14
self-association processes, 116
Hydrocracking, 11, 81, 146
Hydrodynamic flow, 9
Hydrodynamic property measurements, heavy oils, 303–334
intrinsic viscosity, 304–322
asphaltenes and heavy oils, 313–322
background and theory, 304–312
experimental measurement, 312
sedimentation-diffusion data with, 324–325
sedimentation-diffusion, 322–334
background and theory, 322–324
diffusion coefficient measurement, 326–327
diffusion results, 328–332, 333
experimental measurement of, 325–326
sedimentation results, 327–328
Hydrogen
chemical composition, 387
hydrocracking, 146
Hydrogenation, 11
coal extracts, 209, 212
Hydrogen bonding, 12, 80, 150
aggregation mechanisms, 386, 389
coal asphaltenes, 214
colloidal structural evolution, 179
heavy crude, 153
molecular weight determination, 388
Hydrogen-carbon ratio
asphaltenes from different sources, 18
chemical composition, 387
interfacial film studies, 395
Hydrogen-donor solvent liquefaction (HDS), 210
Hydrophile-lipophile balance, improved recovery, 13–14
Hydrophobically modified polymers, 14
Hydrophobic Wilhelmy plate, 394
Hydroxyl groups
coal asphaltenes, 214, 217
coal-liquid vs. petroleum asphaltenes, 18
coal versus petroleum asphaltenes, 214
crude oil DRIFT spectra, 352

Improved oil recovery (IOR), 13–14
Infra-red spectroscopy, 22, 23, 81, 84–87, 147
crude oil emulsion stabilization, 356
Infra-red spectroscopy (*cont.*)
crude oil resin separation, 347
instrumentation, 84
Ingramite, 10
Inorganic salts, 7
Interchain distance, coal asphaltenes, 215
Interface properties, self-association processes, 116–117
Interfacial films
crude oil emulsions, 338
water-in-oil emulsions, 393–395, 406, 409–410
Interfacial layers, emulsion stabilization, 380, 382–383
Interfacialllly active agents, 7
Interfacially active components
chromatography of resins, 347–352
crude oil emulsions, asphaltene and resin stabilized, 346–361
crude oil emulsion stabilization
interfacial tension and pressure, 353–356
Langmuir–Blodgett films, 356–361
experimental technique, 352–361
Interfacial shear viscosity, water-in-oil emulsions, 406
Interlamellar distance, 150
Intermolecular interactions, 44–67
coal asphaltenes, 216
colloidal structural evolution, 179, 195
fluorescence spectra, 58–67
heavy crude, 153
quantum yields, 52–58
temperature effects, 195
unifying model of, 45–52
Interparticle interactions, viscosity measurements, 320
Intrinsic viscosity, 304–322
asphaltenes and heavy oils, 313–322
background and theory, 304–312
experimental measurement, 312
sedimentation-diffusion data with, 324–325, 328
Ion pairing constant, 257
Iron, 6
Iron sulfide, 7
Isopentane, 6

Katacondensed systems, 80
Kerogens, 9
comparisons of asphaltenes from different sources, 19
geochemical investigations of, 154, 155
geological maturation, 8–9
heavy crude, 154
spectroscopy
EPR, 107
fluorescence, 22
Kerosene, 313
Ketones, 147
crude oil DRIFT spectra, 352
crude oil resin separation, 347
Kinetic models, crude oils, 227
Kuwait, 18, 316

Lagunillas, 18
Lamellar structure
  aggregation, 389
  interfacial film studies, 395
  liquid crystalline D phase, 365
Langmuir–Blodgett film, 353, 356–361
Langmuir film balance, 394
Laser sources
  crude oil particle size distribution, 233–234
  optical spectroscopy, 25–26
Lewis acid-base interactions, aggregation mechanisms, 386
Lewis acid-type metal halides, airblowing, 12
Libya, 18
Light scattering studies
  heavy crude, 153, 154
  molecular weight determination, 151
Lignite, 203, 213, 214
Limestone, 22
Linewidth and lineshape, ESR, 96–97
Liquefaction products, coal, 205
Liquid chromatography, heavy crude, 152
Liquid crystals
  D phase, 365
  interfacial film studies, 395
Liquid-solid chromatography, crude oil, 231–232
Lithium salts, 153

Macrostructure
  colloidal structure of heavy crude and asphaltene solutions
    cryo-SEM, 181–182
    small-angle scattering methods, 167–181
  flow property modification, 15
  heavy oils
    hydrodynamic property measurement: *see* Hydrodynamic property measurements, heavy oils
    sedimentation-diffusion measurements, 324; *see also* Sedimentation and diffusion measurements
Magnetic field, 16
Maltenes, 5, 194, 195
Manjak, 10
Marangoni–Gibbs effect, 380, 381–382
Mass spectrometry, 147
  coal extracts and asphaltenes, 209, 212, 218
  crude oil asphaltenes, 227
  molecular weight determination, 387
Mass transfer, 8
Maturation, 8–9
  and fluorescence, 22
  methyl groups in alkyl side chains, 91
Mavjak, 18
Mercaptans, 7
Mesogens, 389
Mesophase, 4–5, 6, 14–15
Metal halides, airblowing, 12
Metallochelates, 7
Metalloporphyrins, 7
Metals, 147–148
  coordinated compounds, 6
  particle aggregates, fractal dimension, 299
  spectroscopic studies, 81
  tar ball (coastal spill) constituents, 15–16
Meteoric retigens, 19
Methane, 9
Methanol, 347, 349
N-Methyl-2-pyrrolidinone, 203, 208, 212, 217, 220, 222
Methylcyclohexane, 6
Methyl ethyl ketone, 3
Methyl groups
  alkyl side chains, 91
  crude oil DRIFT spectra, 352
  heavy crude hydrogen bonding, 153
1-Methylnaphthalene, 314, 316, 330, 332
Micelles, 8, 150–151, 388
  coal asphaltenes, 219–220
  oil-external, 12
Micro-calorimetry, 117
Microcapillary technique, 342
Migration, 9, 10
Mildrel Lake Athabasca, 10
Mineral oil, 409
Mineral wax, 10
Minimum particle packing fraction, 270, 287
Mixing, heat of, 3–4
Models of colloidal structure, 152
Model systems, 406–417
  crude oil emulsions, asphaltene and resin stabilized, 361–372
    demulsification of water-in-crude oil emulsions, 363–367
    destabilization of water-in-oil emulsions, 361–362
    electrocoalescence, 367–369, 370, 371, 372
    stabilization with crude oil emulsions, 361–362
  interfacial films and W-O emulsions of model oils and asphaltenes, 406, 409–410
  resin effects on asphalt-stabilised emulsions in toluene-heptane-water systems, 410–415, 416, 417
Molar conductivity, 257–258
Molar enthalpy, coal asphaltenes, 215
Molecular association: *see* Association; Suspension viscosity model
Molecular dynamics
  optical spectroscopy, 21
  self association and molecular packing, 128–129, 139–140
  self-association studies, 118
Molecular interactions: *see* Intermolecular interactions
Molecular packing of aggregates, 123–126, 140–141, 388
  conductivity, 132–135
  self-association: *see* Self-association, structure and molecular packing

Molecular structure, *see also* Macrostructure
coal extracts and asphaltenes, 204–214
comparison with petroleum asphaltenes, 213–214
preparation of materials, 204
structural parameters and model, 203–213
Molecular weight, 6, 24
coal extracts and asphaltenes, 218–219
coal-liquid vs. petroleum asphaltenes, 17–19
coal versus petroleum asphaltenes, 213, 214
colloidal structural evolution, 175, 177
composition of asphaltenes, 387–388
crude oil, 230, 236–237, 238
vs. depth, 10, 11
heavy crude, 153
heavy oil sedimentation-diffusion measurements, 327, 328–330, 331
techniques, 151
Mono-cylindrical model, 131
Monodisperse fraction, viscometry, 315, 316
Morphology: *see* Macrostructure
Mousse, 146, 379
Mud diapirs, 9
Multiphase flow, 9, 338
Multiplets, 84, 105
Multisubunit structures, heavy oil sedimentation-diffusion measurements, 325, 330

Naphthalene, 404, 405
Naphthas, 6
Naphthenic acids, agregation mechanisms, 386
Naphthenic rings, 6, 147, 148
Natural gas, 22
Natural systems, colloidal structure of heavy crude and asphaltene solutions, 190–196
Near-IR spectroscopy, 22, 24, 33, 214
Nellenstein, Pfeiffer, and Saal model, 389
Networked interfacial film, emulsion stabilization, 385
Neutron scattering methods, 152; *see also* Small angle spectroscopy (SANS and SAXS)
Newtonian behavior, heavy crude, 156
Nickel, 6, 8, 147, 148
crude oils, 227
tar ball (coastal spill) constituents, 15–16
Ninian crude, 394
Nitration, 12
Nitrobenzene, 293, 387
Nitrogen, 1, 8
chemical composition, 387
coal asphaltenes, 214
crude oil, 227, 338
crude oil DRIFT spectra, 352
crude oil resin separation, 347
functional group analysis, 388
heterocyclic species, 147
spectroscopic analysis, 99
vanadyl chelate model characterization with ligands, 81
NMR, 23, 81, 85, 87–95
C13, 23, 80–81, 83, 87–95, 147
coal, 204, 205–213, 214
proton, 80, 83, 87, 230
pulsed field gradient, 344, 345
2-D, 81
Nonesuch Shale, 19
Non-newtonian behavior, heavy crude, 156
Northern Iraq asphaltenes, 316
North Sea crude, *see also* Crude oil emulsions, asphaltene and resin stabilized
fluorescence lifetime, 48, 49, 54
optical spectroscopy, 63–66
resin separation, 347–348

Oblate ellipsoids, 325
Oil, coal, 205
Oil-internal colloids, 12
Oil sand, distribution of asphaltic fractions, 10
Oil shale, 1
comparisons of asphaltenes from different sources, 18, 19
nitrogen, 8
Oil spills, 15; *see also* Water-in-oil emulsion stabilization, petroleum asphaltenes
Oil transportation and spills, 15–16
Oklahoma crude, 392
Olefins, 146, 156
Optical spectroscopy, aromatic moieties, 21–75
absorption spectra, 32–44
large chromophores, population distribution in crude oil and asphaltenes, 41–44
Urbach tail, 35–41
experimental methods, 25–27
fluorescence and intermolecular interactions, 44–67
fluorescence spectra, 58–67
quantum yields, 52–58
unifying model of molecular interactions, 45–52
methods, 21–24
optical transitions of molecules, 28–32
simple aromatics, 29–32
theory, 28–29
small aromatics and asphaltenes, 67–75
aromatic ring size, 73–75
short-wavelength emission, 67–73
Organic free radicals, ESR, 95–96
Organic solvents: *see* Solvents
Osmometry, 151
coal asphaltenes, 218
heavy crude, 153
Osmotic pressure, 151
Ostwald ripening, crude oil emulsions, 339
Oxidation
asphalt, 267
spills, 15
Oxidized species, crude oil emulsion stabilization, 356
Oxidizing agents, analytic techniques, 81

Oxygen-containing functional groups, 1, 8, 80, 147
chemical composition, 387
coal asphaltenes, 214
coal-liquid vs. petroleum asphaltenes, 18
crude oil resin separation, 347
crude oils, 227, 338
ESR studies, 97
functional group analysis, 388
vanadyl chelate model characterization with ligands, 81
Oxygen partial pressure, ESR, 102–108
Ozokerite, 10

Packing: *see* Self-association, structure and molecular packing
Packing condition, aggregates, 123–126
Packing fraction, minimum particle, 270, 287
Pal–Rhodes model, 268, 310, 318
Paraffins, *see also* Aliphatics
crude oil, 230, 242
crystallization, interfacial film studies, 394
Parallel disk model, 362
Paramagnetic molecules, 103
Particle asymmetry, heavy oil sedimentation-diffusion measurements, 323
Particle interaction coefficient, 270
Particle size distribution
crude oil, 232–234
crude oil asphaltene phase behavior, 232–234, 240–242
viscosity models, 269
Particulates, crude oil resin separation, 347, 349
Paving asphalts, 16
Pendant drop method, 393–394
n-Pentane, 6
conductivity studies, 258
crude oil chromatography, 231–232
peptidization by, 13
solubility classes, 4, 6, 227, 303, 385
Peptidization, 13
Peptized micelles, 156
PERC, 16
Percolation
aggregates, 140–141
conductivity, 135–136
mechanism, 126
fractal dimension and, 299
Permeability, heavy oil diffusion measurements, 326
Petrolene, 5
Petroleum, *see also* Water-in-oil emulsion stabilization, petroleum asphaltenes
improved oil recovery, 13–14
structural parameters, 2
Petroleum ether, 6
Petroleum pitch: *see* Pitch
Petroleum shale, 8
pH, crude oil-in-water emulsion, 400
Phase change, reversibility of precipitation, conductivity studies, 261–265
Phase partitioning, heavy oils, 303–304
Phase separation, improved recovery, 14
Phenanthrene, 404, 405
Phenolic OH, coal asphaltenes, 214
Phenols
aggregation mechanisms, 386
coal depolymerization, 205
o-Phenylphenol (OPP), 214
Photoexcitation, 46
π bonding/ electrons
aggregation, 386, 389
aromatic molecules, 28
delocalized, 97
interfacial film studies, 394, 395
molecular weight determination, 388
pi-pi association, 150, 214
Picot–Benoit effect, 178–179, 181
p-inhibitors, flow property modification, 15
Pipelines, 15–16, 338
Pitch, 18
heavy oil sedimentation-diffusion measurements, 329
improved recovery systems, 15
viscometry, 314, 316
Plasma desorption mass spectrometry, 218
Polar constituents
aromatic constituent, 5
coal-liquid vs. petroleum asphaltenes, 17–19
coal vs. petroleum asphaltenes, 213, 214
crude oil, 154, 239
emulsion stabilization, 383
Polydisperse fractal objects, 165
Polydispersity, 151; *see also* Self-association, structure and molecular packing
Einstein's analysis, 306
heavy oil sedimentation-diffusion measurements, 329
heavy oil viscosity measurements, 309, 310, 322
Ostwald ripening, 339
scattering contribution at small Q, 179
Polyelectrolytes, 14
Polymers, 14
bitumen, 146, 156
flow property modification, 15
Polynuclear aromatic hydrocarbons, 93–94, 148
Pores
colloidal structural evolution, 182
heavy crude asphaltenes, 154
heavy oil partitioning, 303–304
Porod plot, 122, 132
Porous films, heavy oil diffusion measurements, 326
Porphyrins, 7, 8, 81, 147–148
aggregation mechanisms, 386
crude oil film forming agents, 392
ESR, 95–96
Portis plot, 103
Powder XRD, 81
Power law, 185, 193
Preasphaltenes
coal, 203, 205
distribution of asphaltic fractions, 9, 10

Precipitation, 1
conductivity, 257–265
crude oil asphaltene phase behavior, 234–236, 242–244
optical spectroscopy, 23–24
reversibility of, conductivity studies, 261–265
self-association: *see* Self-association, structure and molecular packing
Preferred alkane number, 364
Pressure, and crude oil asphaltene deposition/flocculation, 228
Principal component analysis
crude oil emulsion stabilization, 353, 354–356
crude oil resin separation, 347–352
Propane deasphalting, 6
Propane insoluble fraction, 6
Proportionality constant, 321
Purified asphaltenes in organic solvents, conductivity, 254–257
Pyridine, 147
aggregation in, 389
chromatography of heavy crude, 153
coal asphaltenes, 214, 217, 220
coal component solubility classes, 203
coal extracts, 207, 208, 212, 213
colloidal structural evolution, 175, 177
conductivity measurements in, 254, 256, 257
critical micellization concentration in, 293
solubility fractions, 6
spectroscopic analysis, 99
Pyrobitumen, 9, 10
Pyrolysis, 81, 147
Pyrroles, 147
aggregation mechanisms, 386
coal asphaltenes, 214
coal-liquid vs. petroleum asphaltenes, 18
spectroscopic analysis, 99

Q
and aggregation, 175
resin suspensions at, 188
Quantum yield, 25, 27, 45, 52–58, 67
Quartet multiplicity, 80
Quasi-elastic scattering, heavy crude flocculation, 153–154
Quenching, 24, 45, 46, 51–52, 67
Quinoline, 207, 215
2-Quinolone, 288, 293
Quinone-type oxygen, 80

Radical pairs formation, 106
Radius of gyration, 170, 173, 275
Ragusa, 10, 18
Ratawi
critical micellization concentration, 293
self-aggregation studies, 129–130, 135–136, 137, 138, 139, 140
viscosity measurements, 317–318, 319, 310, 321
Raudhatain, 18
Reaction-limited colloidal aggregation (RLCA), 154, 164, 165
Recovery of oil, improved, 13–14
Red shifts, 22, 41
Refinery asphalt, comparisons of asphaltenes from different sources, 18
Refinery products, 16
Refining, heavy crudes, 146
Refining bottoms, 1, 19
Refractive index, 229
Remote sensing, fiber optic, 22
Reservoir crude, 248
Resid viscometry, 314, 316, 317–318
Resin and solvent effects, 395–405
Resins, 6–7, 7
acid components, 5
aggregation mechanisms, 386
asphalt-stabilised water-in-oil emulsions in toluene-heptane-water systems, 410–415, 416, 417
colloidal structural evolution, 188–190
and crude oil asphaltene deposition/flocculation, 228
distribution of asphaltic fractions, 9, 10
emulsion stabilization, 383, 395–405; *see also* Crude oil emulsions, asphaltene and resin stabilized
oxygen functional groups, 80
solubility parameters, 4
solvent fractionation, 6
spills, 15
stabilization of interfacial films, 392–393
Resonance multiplicity, 80
Retigens, 19
Reversed-phase chromatography, 148
Rheology, *see also* Colloidal structure
bitumen, polymer addition and, 156
colloidal structural evolution, crude oil, 193
crude oil emulsion interfacially active components, 352
heavy crude, 156
interfacial film studies, 395
water-in-oil emulsions, 406, 410
Rheometer, biconical bob, 395, 410
Rigidity, heavy oil macrostructure, 304
Ring size, 73–75, 213, 214
Ring structures
coal extracts, 209–210
coal vs. petroleum asphaltenes, 214
Ring systems, coal-liquid vs. petroleum asphaltenes, 17–19
Rio Bravo crude, 392
Roscoe equation, 309–310, 311, 321
Rostler's test, 5
Rozel Point, 10, 18
Russian crudes, 409

Safaniya, 299
colloidal structural evolution
natural systems, crude oils, VR, and maltenes, 190–192
in solution, 168–182
crude oil film forming agents, 392
spectroscopy: *see* Spectroscopy, molecular structure and intermolecular interactions

Sales, optical spectroscopy, 48, 49, 50, 51, 52, 53, 54, 58–66
Salt domes, 9
Sample preparation, heavy oil viscometry, 316
Sampling, subsurface, 22
San Joaquin Valley crude, 395–405, 410–415, 416, 417
Santiago, 18
SANS: *see* Small angle scattering
SARA (saturated, aromatic, resin, asphaltene) column, 3, 230–231
SAS: *see* Small angle scattering
Saturates
  and colloid stability, 7
  crude oil, 239
  solubility parameters, 4
Saturation, ESR studies, 99–102
SAXS: *see* Small angle scattering
SBS, 146
Scanning electron microscopy, 154
  coal asphaltenes, 216–217
  cryo-: *see* Cryo-SEM
Schroedinger equation, 28
Schultz distribution, 130, 131
Sedimentation, crude oil emulsions, 339
Sedimentation and diffusion measurements, 322–334
  background and theory, 322–324
  combined with viscosity measurements, 324–325
  diffusion coefficient measurement, 326–327
  diffusion results, 328–332, 333
  experimental measurement of, 325–326
  sedimentation results, 327–328
Seeps, distribution of asphaltic fractions, 10
Selective adsorption/desorption, 1
Self-association, structure and molecular packing, 115–143, 153
  aggregates, structure of, 129–132
  conductivity, 118–119, 123–126, 132–136
  future prospects, 142
  percolation, molecular packing and, 140–141
  SANS, 118, 119–123
  simulation
    computer, 141–142
    molecular dynamics, 128–129, 139–140
  viscosity, 119, 126–128, 136–138
Semi-cokes, 15
Sergeevsk crude, 409–410
Shale
  comparisons of asphaltenes from different sources, 19
  structural parameters, 2
Shale extracts, 1
Shale oils, 1
Shape: *see* Macrostructure
Shape factor, 298, 325
Shear flow, heavy oil viscosity measurements, 307
Shear-induced association, 273
Shear rotational viscometry, 393
Shear strength, water-in-oil emulsions, 409
Shear viscosity
  interfacial film studies, 394, 395
  water-in-oil emulsions, 406
Siberian crude, 387
Silanol, 347, 349
Siloxane, 347, 349, 350
Silylation
  coal asphaltenes, 215, 217
  heavy crude hydrogen bonding, 153
Single Frequency Off-resonance Decoupling (SFORD), 90
Singlet multiplicity, 80
Single-triplet states, 105
Size: *see* Macrostructure
Size distribution methods, 339–346
  NMR, pulsed field gradient, 344, 345
  ultrasound, 344–346
  video enhanced microscopy, 340–343
Size exclusion chromatography, 147–148
  heavy crude, 152–153, 152
  molecular weight determination, 387
Small-angle scattering (SANS and SAXS), 81, 268, 299
  coal asphaltenes, 220–222
  colloidal structural evolution
    flocculation process, *n*-heptane addition, 183–185, 186
    natural systems, crude oils, VR, and maltenes, 190–192
    natural systems, distillation products, atmospheric and VR, 192–194
    resin solutions, 188–190
    temperature effects, 195–196
  colloidal structural evolution in solution
    comparison of SANS and SAXS, 172, 175, 176
    concentration effects, 172, 173, 174
    solvent and temperature effects, 175, 177
    techniques, 168–169
    treatment of data, 169–172
    upturn of I(Q) at very low (Q), 177–181
  colloidal structure, evolution of, 159–166, 167–181
    form and structure factors for models, 161–166
    principles, 160
    scattering contrast, 160–161
  heavy crude, 152, 154, 158
    heavy oil viscosity measurement comparisons, 320–321
    particle size distribution, 233–234
  self-association studies, *see also* Self-association, structure and molecular packing
    aggregate models, 139–140
    instrumentation, 118
    model analysis, 129–130
    theory, 119–123
Sodium (bis-2-ethylhexyl)-sulfosuccinate (AOT), 365, 366
Solids detection system, crude oil phase behavior, 234, 235

Solubility
coal versus petroleum asphaltenes, 214
self-association: *see* Self-association, structure and molecular packing
Solubility parameter, 6
asphaltenes from various sources, 16
mesophase generation, 4–5
solvent fractionation, 3, 4
Solute solvation: *see* Solvation
Solution concentrations, heavy oil viscosity measurements, 322
Solution viscosity, 304, 305
Solvated sphere model, 152
Solvation
aggregation mechanisms, 386
Einstein's analysis, 306, 307
heavy oil sedimentation-diffusion measurements, 323
heavy oil viscosity, 318, 321
Solvation constant, 321
Solvent extraction, 1
coal, 204, 206
Solvent fractionation, 3–4; *see also* Solvents; *specific solvents*
coal, 205
heavy crude, 152
solubility parameters, 6
Solvent partitioning, 1
Solvent polarizability, 24
Solvent refined coal, 210
Solvents, 6
aggregation, 389
chromatography, 6
coal component solubility classes, 203
colloidal structural evolution, 175, 177, 181–182
conductivity in, 254–257
crude oil chromatography, 346
crude oil film forming agents, 392
crude oil flow property modification, 15
crude oil-in-water emulsion stability, 403–405
crude oil resin separation, 347, 349
heavy oil sedimentation-diffusion measurements, 328, 330
heavy oil viscometry, 313, 314, 315, 316
molecular weight determination, 387
self-association: *see* Self-association, structure and molecular packing
Sources of asphaltenes, 16–19; *see also* Types and sources of asphaltenes; *specific geographic regions*
Speciation, 388
Spectroscopy
optical, 21–75; *see also* Optical spectroscopy, aromatic moieties
SAS: *see* Small angle scattering
self-association studies: *see* Self-association, structure and molecular packing
Spectroscopy, molecular structure and intermolecular interactions, 79–109
ESR, 95–108
free radical concentration, 99
g-value, 97–99
linewidth and lineshape, 96–97
saturation, 99–102
temperature and oxygen partial pressure, 102–108
FTIR, 85–87
methods, 82–84
NMR, 87–95
Spectroscopy, optical
absorption spectra, 32–44
large chromophores, population distribution in crude oil and asphaltenes, 41–44
Urbach tail, 35–41
experimental methods, 25–27
fluorescence and intermolecular interactions, 44–67
fluorescence spectra, 58–67
quantum yields, 52–58
unifying model of molecular interactions, 45–52
methods, 21–24
optical transitions of molecules, 28–32
simple aromatics, 29–32
theory, 28–29
small aromatics and asphaltenes, 67–75
aromatic ring size, 73–75
short-wavelength emission, 67–73
Spherical Schultz model, 131
Stabilization of emulsions: *see* Crude oil emulsions, asphaltene and resin stabilized; Water-in-oil emulsion stabilization, petroleum asphaltenes
Stacking order, coal asphaltenes, 215
Stacks, 13
Statistical mechanics, self-association processes, 116
Staudinger–Houwink equation, 311–312, 313, 314, 315, 316
Steric repulsion, emulsion stabilization, 380–381
Stern–Volmer analysis, 49, 50, 51, 53, 54, 55
Stokes–Einstein equation, 124
Stokes radius, 329
Streaming potential, 228
Structural evolution: *see* Colloidal structure
Structure, *see also* Colloidal structure; Macrostructure
coal extracts and asphaltenes, 203–213
colloidal structure evolution, models of, 160, 161–166
heavy oil sedimentation-diffusion measurements: *see* Sedimentation and diffusion measurements
self-association: *see* Self-association, structure and molecular packing
Sublimation, 182
Substituents
coal-liquid vs. petroleum asphaltenes, 17–19
coal versus petroleum asphaltenes, 213
Subsurface sampling, 22
Sulfidic sulfur, spectroscopic findings, 23

Sulfonation, improved recovery, 14
Sulfoxides
  aggregation mechanisms, 386
  crude oil resin separation, 347, 350, 352
  spectroscopic findings, 23
Sulfur, 1, 7–8, 147
  crude oil, 227, 338
    chemical composition, 387
    functional group analysis, 388
    heavy crude chromatographic fractions, 153
    resin separation, 347
  spectroscopic analysis, 23, 99
  vanadyl chelate model characterization with ligands, 81
Supramolecular aggregates, 385, 389
Surface properties, self-association processes, 116
Surface tension
  coal asphaltenes, 219–220
  self-association studies, 117
Surface-to-volume ratio, self-association studies, 122, 131–132
Surfactants, 7
  crude oil components, natural, 394
  crude oil emulsion coalescence, 362
  crude oil emulsion destabilization, 365–366
  crude oil emulsion stabilization, 382
  improved recovery, 13–14
Suspension viscosity model, 267–300
  application of model, 279–282
    parameter reduction, 281–282
    solvation constant approximation, 279–281
  development of, 272–276
    aged and unaged materials, 278
    blend preparation, 277
    experiments, 276–279
    methodology, 276
    molecular weight determination, 278–279
    oxidative aging, 277–278
    separation into asphaltenes, aromatics, and saturates, 277
  existing models, 269–272
    monodispersed non-associating suspensions, 269–271
    particle size distribution, 271–272
Synthetic residues, viscosity measurements, 317
Synthoil, 15, 215

Tabbyite, 10, 18
Talc, 347, 349, 350
Tars
  coal, 205
  optical properties, 22
Tar sands, 1, 316
Taylor dispersion technique, 328
Temperature, 6
  coal extracts, 207–208
  colloidal structural evolution, 175, 177
    cryo-SEM studies, 181–182
    SAXS investigation, 194–196
Temperature (*cont.*)
  crude oil asphaltenes
    deposition/flocculation, 228
    interfacial film studies, 394
    and viscosity, 152, 321
  ESR, 102–108
  improved recovery systems, 15
Tert-butylbenzene, 404, 405
Tetracyanoethylene (TCNE), 216, 217, 218
Tetracyanoquinodimethane (TCNQ), 217
Tetrahydrofuran
  coal asphaltene VPO, 218
  coal component solubility classes, 203
  conductivity measurements in, 254, 255
  crude oil asphaltene chromatography, 229
  heavy oil viscometry, 314
  molecular weight determination, 387
Tetraoxyethylene-nonylphenol ether (Triton N-42), 365
Texaco, 38–39, 40
Thermal cracking, 11, 81, 146
Thermal diffusion, 1
Thermodynamics
  crude oils, 227
  heavy crude flocculation, 153–154
  suspension viscosity model: *see* Suspension viscosity model
Thioethers, 8
Thiophenes, 23, 99, 147
Thixotropic pseudo-plastic flow, 15
Time domain spectroscopy (TDS), 367
Toluene, 299
  coal component solubility classes, 203
  coal extracts, 207
  colloidal structural evolution in, cryo-SEM studies, 181–182
  crude oil aggregation in, 389
  crude oil emulsions
    molecular weight determination, 387
    oil-in-water, stability of, 403, 404, 405
    preparation, self-association studies, 116
  crude oil film forming agents, 392
Toluene-heptane-water systems, 410–415, 416, 417
Torrey Canyon incident, 379
Transition metals, 6, 7; *see also* Vanadium
Transport, 15–16
Triplet state, 105
Triton N-42, 365
Turkish asphaltite, 213
Types and sources of asphaltenes, 1–19
  asphaltics/allied substances, 4–7
    gas oils, 7
    resins, 6–7
  chemical reactivity, 12
  colloidal nature, 12–13
  as geological clock, 9–10, 11
  geological maturation indicator, asphaltenes as, 8–9
  improved oil recovery, 13–14
  mesophase material, 14–15

Types and sources of asphaltenes (*cont.*)
oil transportation and spills, 15–16
separation from source material, 2–4, 5, 6t
sources, 16–19
sources, migration and occurrence, 9, 10
sulfur, 7–8
upgrading, 11–12

UG8 crude oil, 55, 57, 67, 68, 75
Ulrich's equation, 346
Ultracentrifugation, 151
colloidal structural studies, 180
heavy crude, 152, 153
heavy oil sedimentation-diffusion measurements, 326
Ultrafiltration, 151
Ultrasound, 344–346
Unit sheet, 13
Unpaired electrons, 97
Upgrading of oils, 11–12
Urbach tail, 35–41, 74
UV detectors, chromatography, 229, 231
UV exposure, 16
UV spectroscopy, 21–22, 24, 209

Vacuum distillation, 1, 146
Vacuum residues
colloidal structural evolution studies, 167, 168
macrostructure, 156
refining process, 146
Vacuum UV spectra, 24
Valence electrons, 21
Vanadium/vanadyl complexes, 6, 7, 8, 147
aggregation mechanisms, 386
chemical composition, 387
crude oils, 227
EPR spectroscopy, 81, 82
ESR, 95–96
tar ball (coastal spill) constituents, 15–16
Vanadyl chelate models, 81
Van der Waals forces
colloidal structural evolution, 179
crude oil emulsion coalescence, 362
heavy crude, 153
Vapor-liquid equilibria, crude oils, 227
Vapor pressure osmometry, 81, 151
coal asphaltenes, 218, 219
crude oil asphaltenes, 230
heavy crude, 153
heavy oils, 314
intrinsic viscosity measurements, 315
sedimentation-diffusion measurements, 329–330
molecular weight determination, 387
Venezuelan crude
resin separation, 347–348
structure, 149
water-in-oil emulsions, 406, 409
Video enhanced microscopy, 340–343
Villafortuna crude: *see* Spectroscopy, molecular structure and intermolecular interactions
Virgin heavy crudes, 2
Visbreaking, 146, 152
Viscosimetry, *see also* Vapor pressure osmometry
colloidal structural evolution, 166–167
crude oil interfacial films, 393
heavy crudes, 156, 158
molecular weight determination, 151–152
Viscosity, 12
coal extracts and asphaltenes, 219
colloidal structural evolution, 197
flocculation process, *n*-heptane addition, 186
natural systems, crude oil, 193
colloidal structure of heavy crude and asphaltene solutions, 183, 184
heavy oil sedimentation measurements, 322–333
interfacial film studies, 394, 395
models of, 268–269; *see also* Suspension viscosity model
Safaniya VR, 183–185, 186
self association and molecular packing, 119, 126–128, 136–138
water-in-oil emulsions, 406
Visible spectra, 24
Vixburg oil, 55, 56
Volume fractions, heavy oil viscosity measurements, 305, 307, 308, 309, 322
VPO: *see* Vapor pressure osmometry

Wafra, 18
Water, crude oil film forming agents, 392
Water-alternating-gas injection, 259
Water bed transport, 15
Water cut, 228
Water-external colloids, 12
Water-in-oil emulsions
asphaltene and resin stabilized, 361–362, 363–367
heavy crude, 146
self-association studies, 125
Water-in-oil emulsion stabilization, petroleum asphaltenes
chemistry, 386–388
aggregation, 386–388
composition of asphaltenes, 386–388
model systems, 406–417
interfacial films and W-O emulsions of model oils and asphaltenes, 406, 409–410
resin effects on asphalt-stabilised emulsions in toluene-heptane-water systems, 410–415, 416, 417
summary table, 407–408
studies, 389–405
emulsion and interfacial films, 393–395
film forming agents in crude oils, 392–393
resin and solvent effects, 395–405
Waxes, 7, 10, 16
Weathering, in spills, 15
Weight fraction concentrations, heavy oil viscosity measurements, 322
West Texas intemediate-West Sour, 5

White mineral oil, 409
Wide angle X-ray scattering, 148, 150
Wilhelmy plate method
  coal asphaltenes, 220
  oil emulsions, 394
Wood's equation, 346
Wurtzilite, 10
Wyllie and Gregory's equation, 346

X-ray absorption near-edge structure spectroscopy (XANES), 8, 23, 147, 148, 388
X-ray analysis, 80, 81, 84
  coal extracts and asphaltenes, 215, 220–221
  structural evolution, 148, 150
X-ray diffraction, 80, 81, 84
Xylene, 392
  conductivity studies, 257, 258
  crude oil-in-water emulsion stability 404, 405

Yen model, 389
Yorba Linda, 18
Young's equation, 16

Z-average radius of gyration, 170
Zeta potential, 249
Zimm plot, 173
Zimm's equation, 163, 165
Zinc chloride coal conversion process, 11
Zubair, 409